Bernard Simon

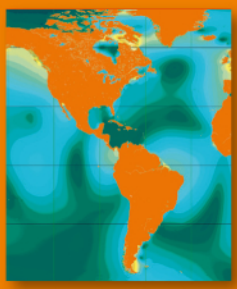

Coastal Tides

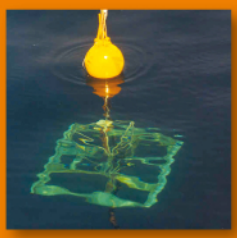

Institut océanographique
Fondation Albert Ier, Prince de Monaco

943-MOC

Coastal Tides

ISBN 978-2-903581-83-1

Copyright deposit: May 2013

Bernard Simon

with the participation of Joseph Gonella
Professor at the Muséum national d'histoire naturelle, Paris

Translation by David Manley

Steven Shipman MBE of the International Hydrographic Bureau is thanked for his valuable support during the translation process.

COASTAL TIDES

Collection Synthèses

Contents

I
General

1 • Introduction

The tide[1] refers to the alternate rising and falling of the surface of the ocean due to gravitational forces of the Moon and Sun, stellar bodies whose movements can be precisely calculated for periods of several hundreds or even thousands of years. Tides are often studied with the aim of drawing up tide prediction formulas on the basis of established relationships between stellar body movements and the response of oceans to gravitational forces. Meteorologically induced changes in water level, which essentially have to be accounted for by statistical methods, must be added to or subracted from these otherwise regular movements. One problem is that this meteorological influence is not entirely random. There can, for instance, be seasonal cycles due to annual fluctuations in atmospheric pressure fields or in diurnal thermal wind cycles. These signals are often hard to distinguish from gravitational signals since their periods may be identical. In practice, the tide is taken as the predictable portion of height variations, including predictable atmospheric-driven variations, i.e. the 'radiational tide'.

Differences between observed and predicted tidal heights are not considered as part of the tide per-se. But they are still worth investigating to obtain key information in various other fields (navigation, hydrography, harbour development, climate studies, etc.).

1. The term tide is currently considered to embody low amplitude movements of any fluid or solid element within our geosphere (nucleus, magma, lithosphere, ocean and atmosphere), associated with gravitational attraction forces of the Moon and Sun. This book focuses only on oceanic tides.

Tidal currents represent another (yet sometimes poorly understood) aspect of tides. This phenomenon is still very important for navigation, and studies on biological, sedimentological and ecological parameters.

2 • Description of the tidal phenomenon

The tide, or the ceaseless rise and fall of ocean waters along most maritime coasts, is a familiar phenomenon for anyone living or visiting a coastal area. This tempo markedly influences the lives of people earning their livelihood from ocean-related activities. It may seem surprising that such an important phenomenon has yet to be satisfactorily and rationally explained, but it is even more astonishing that it is still the focus of ongoing studies.

Beyond the scientific interest, a rational explanation is urgently needed to enhance tide prediction accuracy and thus facilitate coastal navigation. Hydrographers, whose job it is to fulfil sailors' nautical information needs, were likely amongst the first to become aware of this issue and have since contributed substantially to finding a solution. But maritime navigation is not the only field concerned, others include harbour development, flood control, tidal energy use, military amphibian operations, offshore petroleum engineering and, more recently, geodesy, satellite altimetry and climate change research. These latter applications largely explain the scientific community's renewed interest in studying tides in the world ocean.

For Laplace, this is the "trickiest problem in celestial mechanics". The complexity of the phenomenon is immediately evident in its description. As one tries to dig deeper to gain greater insight, the clearer it becomes that certain empirical prediction rules that should be obtained from observations can only be approximated. Despite these drawbacks and long before the advent of modern techniques, tide tables were drawn up according to these rules to help navagators. They are based on simple observed relationships between the apparent movement of the Moon (lunar day) and time series of tidal heights (high and low tide), and between lunations and amplitudes of the phenomenon. Peak amplitudes, which are reached around the spring and autumn equinoxes along the Atlantic coast, or around the summer and winter solstices in some parts of Asia, were also noted, but it was impossible to draw up empirical laws that could be used to achieve accurate predictions. It is indeed very hard to document the rhythm of this phenomenon. It is even theoretically impossible because, contrary to popular belief, the tide is not periodic, it is the sum of periodic constituents, most of which have undefinable frequencies – so there is no period at the end of which tidal

height variations are duplicated identically. However, these conditions were found to be largely fulfilled at the end of certain periods. The saros, or Chaldean, period is the most famous and regulates the eclipse cycle – it corresponds to around 6,585 days, or 18 years and 11 days (see Appendix A). At the end of this period, the Moon, Sun and elements in their apparent orbits return to close to their same relative positions and, in turn, the tide-generating forces slip back to within the range of the initial values. This does not, however, mean that saros is a tidal period since the resemblance with the initial tide markedly declines after several saros periods.

Describing spatial aspects of the tide is just as problematic as the temporal description. In terms of tidal heights, the geographical distribution of oceanic tidal amplitudes (figure 1.1) does not, *a priori*, seem to follow any obvious rule.

Note, however, that the highest values are mainly noted on the continental shelf fringing the continents, or in shallow areas like the English Channel. These amplitudes are very low in small semi-enclosed seas (Japan, Caribbean, Baltic, Mediterranean). No other general rules can be established apart from these mainly qualitative findings on the effects of depths and water body sizes.

We will see that the tidal cycle is mainly the result of the overlap of a diurnal constituent (one daily maximum and minimum) and a semidiurnal constituent (two daily maximums and minimums). The relative importance of these two constituents, which is highly geographically variable, determines the different basic tidal patterns, and the tide classifications are relatively arbitrary and vary between countries. The following classification was adopted in France (criteria defined in Chapter VIII):

- semidiurnal type: two daily high and low tides with substantially the same respective tidal heights
- mixed semidiurnal type: two daily high and low tides, but the high and low tides differ markedly in height
- mixed type: sometimes two daily high and low tides, sometimes just one
- diurnal type: only one high and one low tide each day.

The distribution of these four basic tidal patterns in the world ocean (figure 1.2) also shows that no general rule applies, apart from the fact that semidiurnal tides prevail in the Atlantic and other types occur only when the semidiurnal tidal amplitude is low. The regional distribution of the semidiurnal term of the tide-generating potential (see Chapter III) is likely related to the predominance of this constituent in the Atlantic, which is the only ocean that stretches practically from the northern polar basin to the

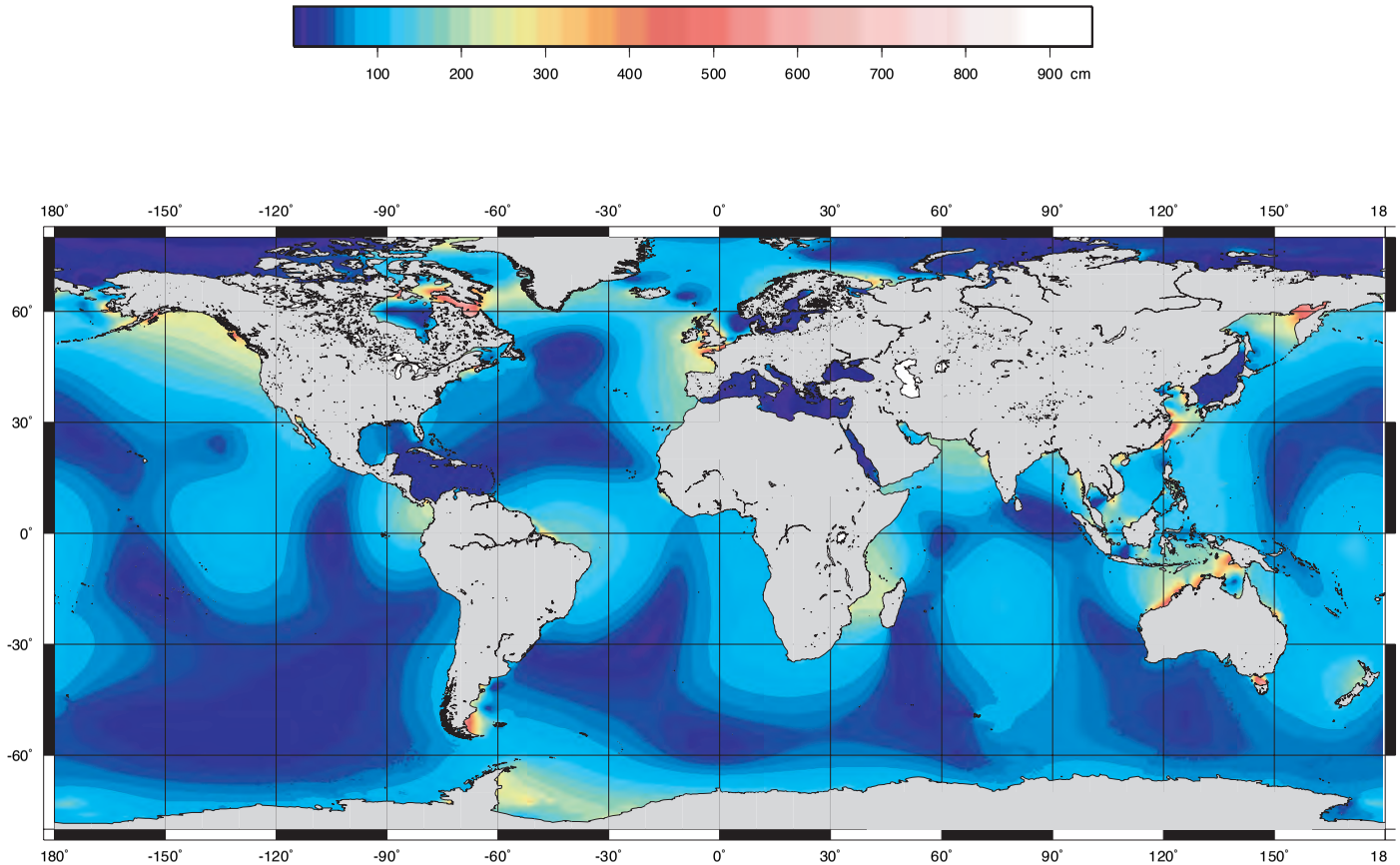

Figure 1.1: Tidal amplitudes in the three oceans.

Southern Ocean.

Another feature of the tide – as an ocean wave – is its propagation mode. Peaks of each constituent wave propagate around so-called amphidromic points where the tidal amplitude is nil.

In the example presented (figure 1.3) concerning the propagation of an average semidiurnal tidal wave in the Atlantic, each so-called cotidal line represents the position of the wave peak at a given time. The indicated phases are referenced relative to the Greenwich meridian crossing time of the Moon. Note, for instance, that the line gyrating in the clockwise direction around the amphidromic point located around 50° N propagates from south to north along the African and European coastlines but from north to south along the Greenland and American coastlines. In the southern Atlantic, the two main networks have common cotidal lines but they inevitably gyrate around the two amphidromic points in opposite directions. No systematic rules apply to this rotation direction, which is governed only by hydrodynamic laws.

These cotidal lines are representative of an average semidiurnal tide and do not entirely reflect the real situation. Amphidromic points corresponding to real tides are not always immobile, so 'amphidromic zones' would be a more accurate term. Moreover, the diurnal constituent propagates much differently, i.e. its amphidromic points are not located in the same positions and there are around twofold fewer as compared to those of the semidiurnal constituent (around 20 throughout the world ocean).

All of these tidal aspects – discovered as increasingly accurate and geographically extensive observations have been obtained – have over the centuries been the focus of queries, more or less relevant hypotheses, theories and scientific studies conducted using increasingly precise techniques, up to the most recent satellite and computer based technology.

3 • Historical background

This historical review is by no means exhaustive. The history of progress in understanding tides has been covered by several authors, with the most recent and complete being that of David E. Cartwright (1999). Only the main steps in tidal observation and measurement that gave rise to successive tidal theories and that in turn led to the development of current tide prediction methods are presented here.

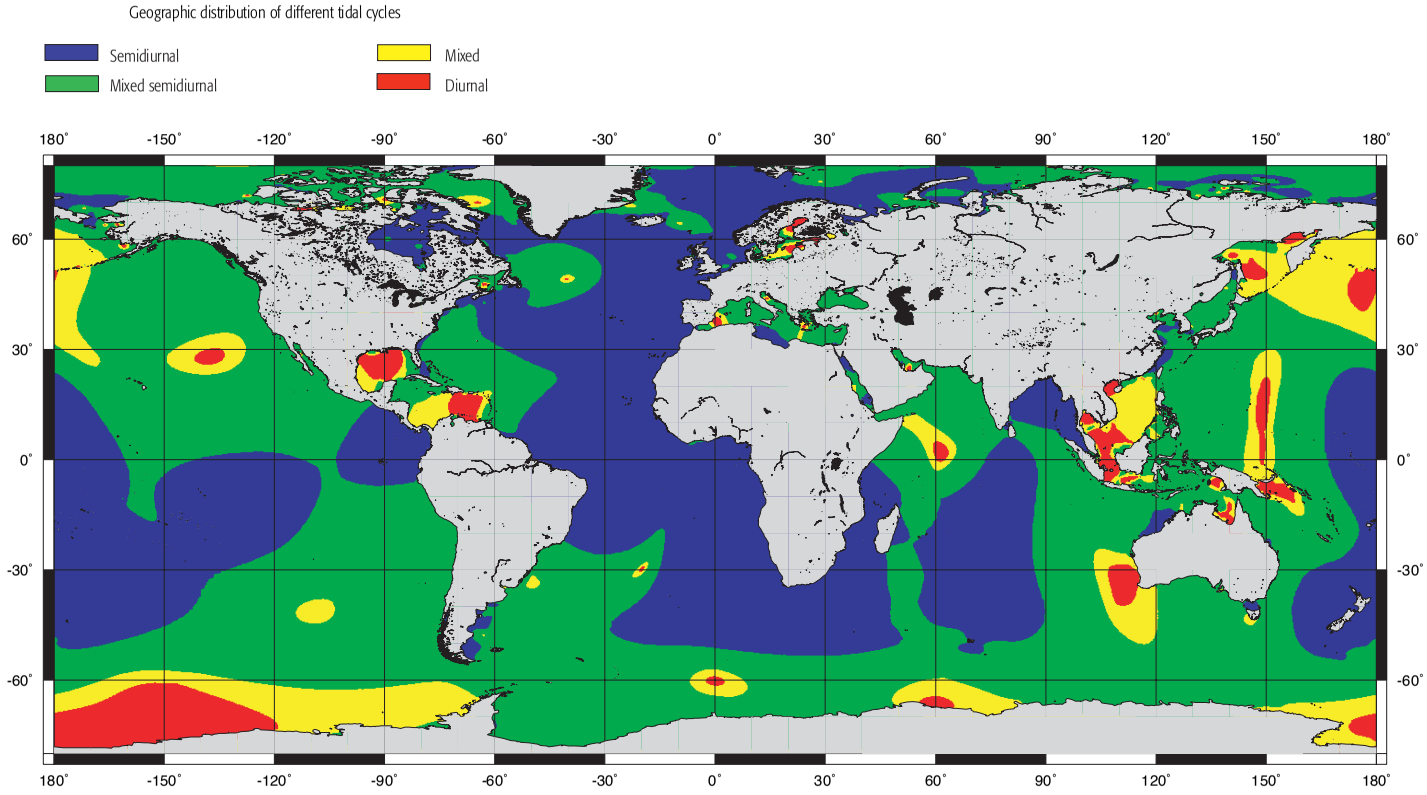

FIGURE 1.2: Distribution of the four basic tidal patterns in the three oceans. Note that semidiurnal tides prevail in the Atlantic.

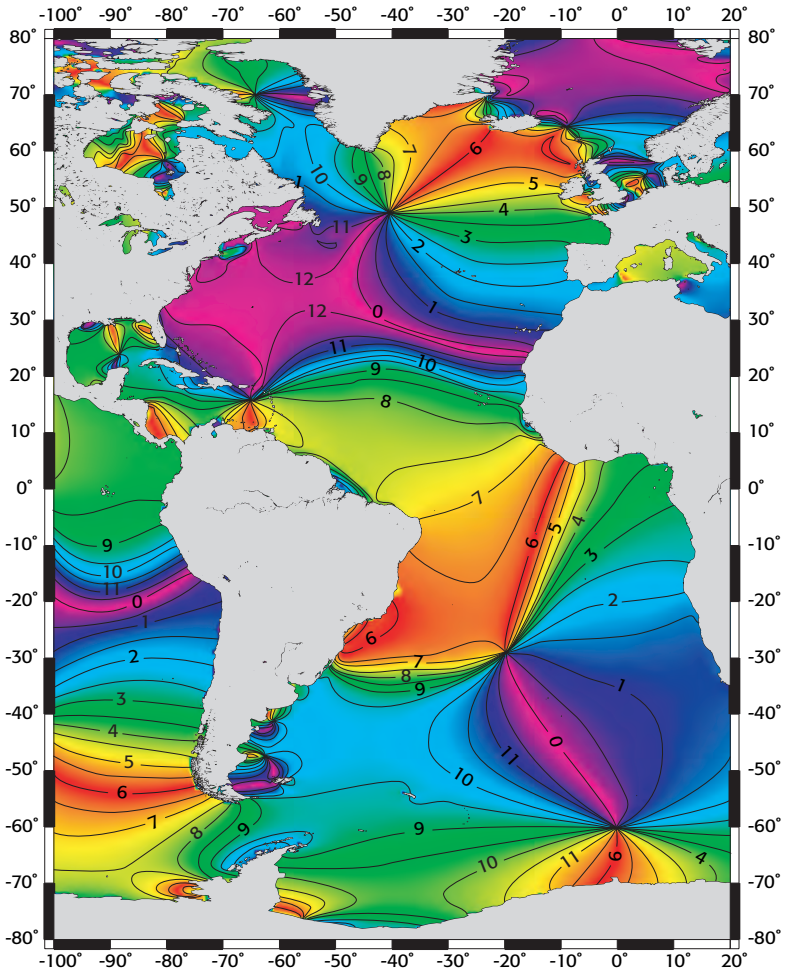

FIGURE 1.3: Cotidal lines of an average semidiurnal tide in the Atlantic – wave peak lines gyrating around amphidromic points, with the phase expressed in hours relative to the Greenwich meridian crossing time of the Moon.

3.1 • From Aristotle to Newton

At the end of Aristotle's life, his interest in tides was sparked by watching tidal current changes in Euripus Strait, between Euboea Island and the mainland coast of Boeotia, but he was unable to explain this phenomenon. His frustration prompted him to throw himself into the channel and drown.

Around 330 BC, the Greek geographer and explorer Pytheas left from Marseille, which was a Greek colony at the time, for a long voyage to the

British Isles. He observed tides of unimagined amplitude for someone only familiar with the Mediterranean Basin, and he made a fundamental discovery – the tide was in some way linked with the movement of the Moon. He noted that there were two low and high tides each lunar day, but also that the tidal amplitude was dependent on the phase of the Moon. The discovery of these relationships could be considered as the beginning point of tidal theory research.

At around the same time, when observing tides in the Persian Gulf, Selerrens of Babylonia noted that declinations of stellar bodies affected the tidal amplitude.

Some 150 years later, the Greek astronomer Selukos discovered diurnal irregularities when observing Red Sea tides and related their amplitude to the lunar declination.

During the first century BC, the Rhodes philosopher and physicist Posidonius drew up a table for tides along the Spanish coasts, correlating their diurnal, semidiurnal and monthly variations with movements of the Moon and Sun. At the beginning of the Christian era, the Greek geographer Strabon described tides in Portugal, England, Denmark, Italy and the Persian Gulf. Around the same time, the Roman naturalist Pliny the Elder mentioned the 'establishment', the 'age of tide' and annual variations in the amplitude of 'spring tides'.

Hence, the most important tidal characteristics were already known more than two millennia ago thanks especially to the observations of Greek explorers around the British Isles and in the Red Sea. But it was not until the late 17th century that the first satisfactory rational explanation for this phenomenon was found.

Meanwhile a number of bizarre hypotheses were put forward, sometimes even by distinguished scientific minds.

Venerable Bede (673-735), the British scholarly priest, thought that ebb currents were due to 'breathings of the Moon' on the water and that flood currents occurred when the Moon moved away.

Zakariya al-Qwazwini (1203-1283), an Arab wise man, put forward the first tentative scientific explanation. According to him, the flood tide was due to thermal expansion of water heated by the Moon and Sun. But his hypothesis could clearly not explain why the Moon had the more important role.

The German astronomer Johannes Kepler (1571-1630), foreseeing the origin of the phenomenon, was convinced that the explanation could be found in the action of an attractive force of the Moon and Sun, i.e. a kind of magnetism. He was likely inspired by the recent discovery of terrestrial

magnetism by the English doctor and physicist William Gilbert (1540-1603).

The Italian physicist and astronomer Galileo (1564-1642) was apparently surprised by Kepler's interest in the action of the Moon on water and in concealed phenomena and other trifling matters. In support of the theory of Copernicus (1473-1543) that the Earth rotates around its axis, Galileo believed that tides were induced by a combined effect of this rotation and the Earth's orbital movement around the Sun. These movements supposedly triggered oscillations of oceanic masses to generate tides.

Descartes (1596-1650) thought that tides were induced by the Moon. According to him, the Moon and Earth were surrounded by a great turbulence and the pressure exerted by the Moon's turbulence on that of the Earth produced global tides.

In 1666, the English mathematician Wallis (1642-1727) proposed an amended version of Galileo's theory whereby he sought to include the Moon's influence. He explained tidal oscillations by the movement of the Earth around the Sun, as well as by its movement around the Earth-Moon centre of gravity.

3.2 • Newton's static theory

In 1687, Isaac Newton (1642-1727) published the theory of universal gravitation in his *Philisophiae naturalis principia mathematica*, thus providing the first really credible explanation on the origin of tides.

He showed that this involved the attraction exerted on water molecules in the oceans by the Moon due to its proximity, and also by the Sun on account of its mass, with the planets having very little influence. A simple celestial mechanics calculation indicates that, for a specific celestial body (Moon or Sun), the tide-generating force is the difference between the force of attraction exerted on an isolated body on the Earth's surface and that which the same body would be subjected to if it were located at the Earth's core.

Newton could explain three fundamental tide properties with this theory: the principle 12-lunar hour period, the relationship between tide amplitudes and phases of the Moon, and finally the diurnal inequality of the tide. He also determined the values of tide-generating forces exerted by the Sun and Moon, respectively. He used the Sun's perturbation of the lunar orbit to assess the mean distance between the Earth and Moon as equivalent to 60.5 Earth's radii. This estimate then enabled him to calculate the generating force of the Sun at its zenith or nadir and at its average distance. He thus evaluated this constituent as equal to "$0.259 \cdot 10^{-7} g$", i.e. 386,049 million-

fold less than the gravity *g*. This value was remarkably close (less than 2% error) to the currently accepted value. However, by analysing the spring tide/neap tide amplitude ratio on the basis of observations along the English coast, he found that the force exerted by the Moon was 4.5-fold that of the Sun, whereas the real value is around 2.2 – so he had overestimated the Moon's influence by around twofold.

Knowledge of fluid mechanics was too rudimentary in Newton's day to enable him to propose a more accurate theory of tides. The static theory Newton developed is based on the notion that waters covering the face of the Earth instantly respond to the gravitational attraction of stellar bodies to form a surface of equilibrium according to the position of these bodies. This model is unworkable, however, because it disregards the inertia of water masses and the rate of movement of the stellar bodies. It is especially unsuitable for explaining the so-called age of tide, i.e. the interval between syzygy (full moon or new moon) and the next spring tide, or the tidal amplitude range along coastlines. In 1740, Bernoulli (1700-1782) published a study based on Newton's theory, but the only really interesting finding, in an analysis of tidal observations recorded in Brest from 1714 to 1717, was a ratio of 2.5 between lunar and solar tides – close to the theoretical value (2.18).

Newton's fundamental discoveries were unsatisfactory for tide forecasting, but they still provided a basis for the development of subsequent theories.

3.3 • Laplace's dynamic theory of tides

It took more than a century before further progress was made in explaining the tidal phenomenon. Laplace (1749-1827) introduced the 'tide-generating potential' concept in a theory he presented before the French Académie Royale des Sciences in 1775. Later he developed this theory considerably and included it in his celestial mechanics treatise. He was the first to deal with the tide in terms of water mass dynamics rather than as a static problem.

According to this dynamic theory, which has yet to be challenged, the marine response to the tide-generating force is in the form of diffuse waves that propagate through the oceans at a depth-dependent velocity. Like all undulating phenomena, these waves are reflected, refracted and dissipated according to the nature of the propagation medium and shape of the oceanic basins. The tide that occurs at one point is thus the result of the convergence of all of these elementary waves originating from different oceanic points, each of which has encountered different propagation conditions on its path.

All of these constituents can obviously interfere with one another, thus boosting or, conversely, diminishing the amplitudes at certain frequencies.

The hydrodynamic equations proposed by Laplace could not be solved with the calculation methods of the time, but they have never been challenged. They gave rise to Laplace's formula, which can be used for tidal predictions, based on two key principles:

- the forced oscillation principle: water masses subjected to a periodic force induce oscillations of the same period
- the overlapping submovement principle: the total movement of a system subjected to small forces equals the sum of the elementary movements.

These two principles express the postulated linearity of oceanic responses to the tide-generating force. Laplace monitored the tide at Brest to test his theory and the findings closely confirmed this linearity hypothesis. As the tide-generating force is the sum of elementary periodic forces, Laplace's formula implies that the tide can be broken down into oscillations of the same period. The linearity hypothesis is not out of line with the fact that two parameters, i.e. the proportionality factor and the phase difference between a constituent tide and the corresponding tide-generating force, could be frequency dependent. These two parameters, which also depend on the hydraulic conditions at the location (tidal wave propagation varies with depth), should in practice be determined experimentally through analyses of available tidal height data.

A key aspect of Laplace's formula is that it can be applied to highlight, for tides generated by each stellar body (Moon and Sun), three distinct terms that each correspond to oscillation period groups, which Laplace called 'species'. The first so-called 'long-lived' species correspond to periods ranging from 7 days to over 18 years; the second 'diurnal' species have frequencies of roughly one cycle per lunar day (cpld); while the third 'semidiurnal' species have frequencies of around 2 cpld.

This species classification is the foundation of Laplace's dynamic theory of tides. Based especially on the findings of his studies carried out at Brest between 1771 and 1776 and published by J.-J. de Lalande, Laplace calculated monitoring site dependent coefficients that enabled him to develop a method for predicting high and low tide times with the corresponding tide heights at the tide-monitoring port. The main advantage of Laplace's formula is that it provided a practical method for predicting high and low tides – this is referred to as the Laplace method. In 1839, the hydrographical engineer Chazallon published the first scientifically calculated tide table. High and low tide times for Brest were determined using this method, while tide heights for other ports were calculated based on the levels at Brest. Following

some initial reluctance to change habits, this table was quickly adopted by navigators to replace their previous tables published in different almanacs that were empirically drawn up (and likely quite inaccurate).

Laplace's formula was used for tide table calculations for the French *Annuaire des marées des côtes de France* for over 150 years. Prior to the advent of computers, no other method was developed that could provide more accurate tide calculations at Brest. However, due to the linearity hypothesis upon which it is based, this formula could not be reliably applied elsewhere. Indeed, it has only been used to calculate tide tables for Brest. The linearity hypothesis was fully confirmed for this port, but a few adjustments were necessary to correct certain systematic errors, especially those associated with radiational tides.

Subsequently, the two Englishmen Whewell and Airy focused studies on the propagation of tidal waves – these waves rank first in oceans and second in channels and rivers when friction is taken into account.

It was not until the late 19th century that further progress in tidal prediction calculations was made, especially through the work of Sir William Thomson (Lord Kelvin).

3.4 • The harmonic method of Kelvin-Darwin-Doodson

Thomas Young (1773-1829) had already stressed the importance of analysing ocean level data overall, rather than just low and high tide data as Laplace did. Airy contributed by laying the foundations for harmonic analysis. However, merit goes especially to Kelvin for developing a practical tide data analysis method. In 1867, the British Association for the Advancement of Science (BAAS) formed a committee to promote the enhancement and widespread application of tidal harmonic analysis. The first report of this committee was written by Kelvin himself and published the next year. Further similar reports were subsequently published on this topic. However, the most significant contribution was G.H. Darwin's report published in 1883. Concerning the tide-generating potential, this latter document presented a harmonic constituent expansion that has been widely used and provided a basis for all tidal studies carried out since then.

These harmonic constituents are still referred to by Darwin's initial names. The calculation methods, which were developed and adapted using means available at the time, are often used on computers without modification. However, their expansion is based on an ancient lunar theory whereby all elements are related to the orbit, which is somewhat unsatisfactory since it is not completely harmonic. In fact, corrective factors had to be introduced to

account for slow variations in the expansion constituents. With these long-term variations, the corrective factors can be taken as constants for annual durations. These factors are calculated for several years and available in table form. These tables are not suitable for computer predictions, but they are not problematic for manual calculations.

This is probably why Darwin's method has been used for such a long time, even though a strictly harmonic expansion was available as early as 1921. This advance was due to another Englishman, A.T. Doodson. He published an expansion in the *Proceedings of the Royal Society* that was more accurate with respect to lunar latitudes and longitudes. These coordinates are based on the ecliptic for here and were determined by Brown in a new lunar theory (1905). This new numeric harmonic expansion gives a much greater number of terms than Darwin's expansion and, moreover, it does not require corrective factors. Tables are therefore no longer required and automatic processing is substantially improved.

Other more complete or accurate expansions have been proposed since then. However, for practical tide calculation applications, these new expansions did not bring any significant progress and Doodson's expansion is still the international benchmark.

3.5 • The models

The harmonic method was developed on the basis of the work of Darwin and Doodson and then fully exploited in order to come up with a practical, accurate, and potentially widely applicable tidal prediction method. This latter procedure does not markedly differ from Laplace's method as it is also based on a theoretical formulation, and a number of parameters have to be determined experimentally by analysing available data. The timeframe must be long enough to achieve maximal accuracy. For instance, for tidal height variations in the range of those occurring along the coasts of France, the English Channel and the Atlantic, a year of top quality measurements are required to generate tidal predictions that are sufficiently accurate to meet navigation needs. Then the results can only be used to predict tides at the site where the initial data were recorded.

A more far-reaching approach, whereby the physical problem of tidal wave formation and propagation is solved directly in its environment, has long been a focus of interest, pioneered by Bernoulli, Whewell, Poincaré and Harris. However it was not possible to come up with an accurate solution to this issue without using powerful calculation tools because of the bathymetric complexity and highly irregular coastlines fringing ocean

basins. It was still possible, through analytical solutions, to qualitatively explain overall trends concerning tidal propagation in ocean basins like the Atlantic. In particular, amphidromic points where the tidal amplitude is nil and around which cotidal lines gyrate (figure 1.3) could be determined analytically.

With the advent of computers, the development of new numeric methods enabled real progress in this direction. Studies by the German scientist Hansen (1949) sparked renewed interest in solving Laplace's equations for real tidal conditions. Deviations and some incoherence in results generated by different models (Bogdanov and Magarik, 1967; Pekeris and Accad, 1969; Hendershott, 1972; Zahel, 1977; Schwiderski, 1981) indicated that, over and above boosting environmental knowledge, it was essential to gain greater insight into the form and bathymetry of ocean basins, but also to refine the equations. In fact, major physical and mathematical problems, associated with tidal energy dissipation (bottom friction and internal tidal wave formation) and also numeric methods adopted for modelling, are still at issue.

Finally, it should be mentioned that accurate offshore tide data are now essential to fulfil current spatial altimetry, trajectography and geodesy needs, and there is renewed interest in modelling offshore tides on a global scale. The advent of spatial altimetry, which generates centimetre-accuracy water level recordings in the world ocean, has led to the development of more realistic tide models that incorporate abundant spatial altimetry data.

4 • Various tidal features and definitions

4.1 • Tidal curves

Tidal curves are plotted on graphs that give ocean height measurements or predicted tide heights over a period of time. For example, the curve shown in figure 1.4 was plotted for a 24 h semidiurnal tide prediction for Brest.

This graph shows four extremes (two minima and two maxima), with each minimum representing low water (LW) and each maximum being high water (HW). The short period at high or low water during which there are no appreciable height variations is called stand. This is, however, a somewhat subjective definition because there is generally no plateau at high or low water. From low to high water, the height rises during the flood or rise phase, and it declines from high to low water during the ebb or fall phase.

The difference in height between the two consecutive extremes is called the tidal range, which should not be confused with amplitude, which refers

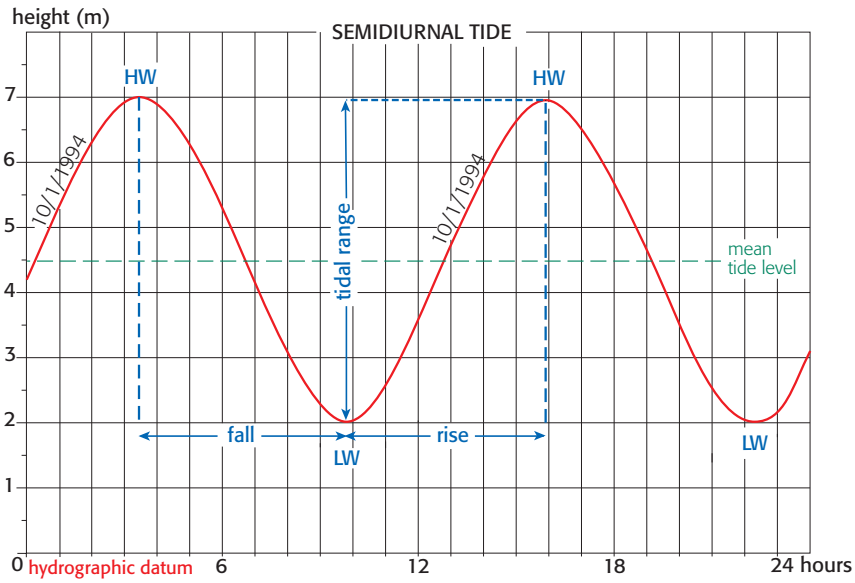

FIGURE 1.4: Tidal curve (prediction) for a semidurnal tide, with two high tides (HT) and two low tides (LT) daily with practically equal tidal ranges – 24 h prediction for Brest, France.

to a sinusoidal function such as that of a constituent tide – when amplitude is used in reference to tides, it means half of the tidal range.

The 'hydrographic datum', or what is still called the 'chart datum', is used for referencing tidal heights.

Figure 1.5 presents another example of a semidiurnal tide curve over a lunation cycle of around 30 days. The tidal range variations are very typical, going from a minimum during the neap tide (NT) to a maximum during the spring tide (ST). The tidal range increases during the priming phase and declines during the lagging phase.

The age of tide is the time interval between phases of the moon and the tidal minima or maxima that immediately follows. The full and new moons (FM and NM) are followed by spring tides, while the first and last quarter moons (FQ and LQ) are followed by neap tides.

4.2 • Types of tide

At the beginning of this chapter, the different tidal types, and the arbitrary basis for such classifications, were described (figure 1.2). The British often classify tides into three categories, whereas a four-type classification is practiced in France, as illustrated in the following examples:

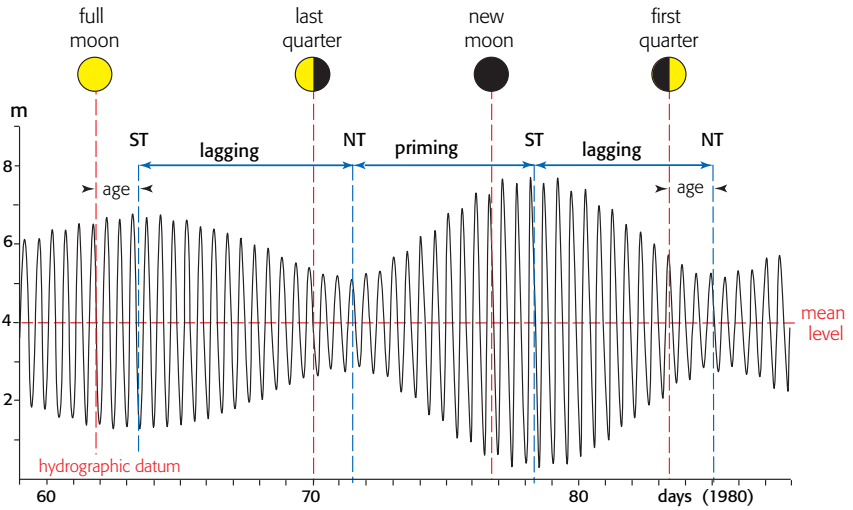

Figure 1.5: Semidiurnal tide prediction curve over one lunation cycle (29 days) showing tidal range variations according to phases of the Moon (Brest, France).

a. Semidiurnal tide. — Brest, France, figures 1.4 and 1.5; Casablanca, Morocco, figure 1.6A. The curves for this type of tide, as already discussed for Brest, clearly show two daily high and low waters with almost identical respective heights, corresponding to almost identical tidal ranges. Semidiurnal tides prevail in the Atlantic, especially along the African and European coasts.

b. Mixed semidiurnal tide. — Mui-Vung-Tau, Vietnam (southern coast), figure 1.6B. The tidal range varies markedly over one lunar day. The diurnal inequality, i.e. the difference between the high and low tidal ranges, is greatest when the declinations of the stellar bodies are reaching their maxima.

Diurnal inequality may also be noted along the European coasts, but the tide is classified as semidiurnal since this inequality is slight. However, the inequality is very high in many ports in the Pacific and Indian Ocean regions.

c. Mixed tide. — Qui-Nhon, Vietnam (eastern coast), figure 1.6C. In ports with a mixed tide, a semidiurnal tidal period is succeeded by a diurnal tidal period over one lunation cycle. This type of tide is also noted along the coasts of Indonesia, Siberia and Alaska, as well as in some ports in the Atlantic and Caribbean (Fort-de-France).

d. Diurnal tide. — Do Son, Vietnam (northern coast), figure 1.6D. There is only one high and low tide per lunar day along coasts where diurnal tides prevail. The associated tidal range varies with the declination of stellar bodies. This uncommon tidal type occurs especially in the Pacific Ocean,

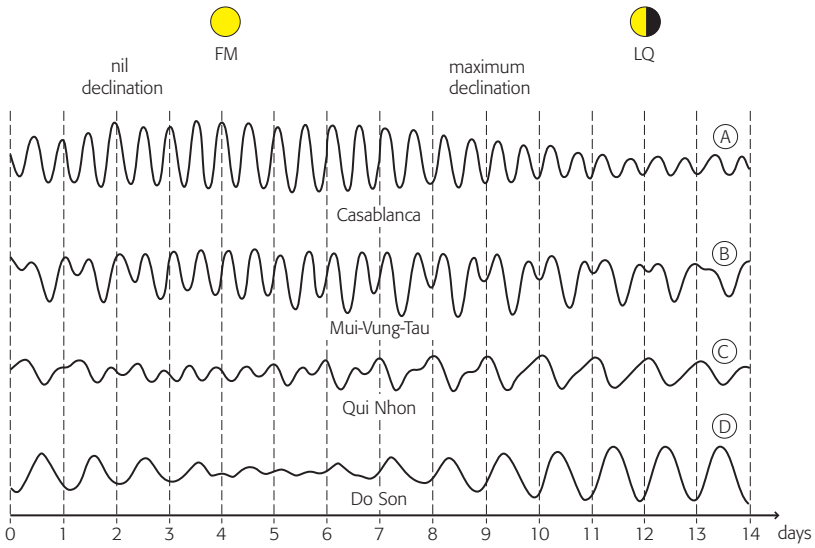

FIGURE 1.6: The French four-type tidal classification illustrated with a half-lunation tidal prediction curve (14 days). A: semidiurnal tide, B: mixed semidiurnal tide, C: mixed tide, D: diurnal tide.

along the Siberian coasts where the tidal range is very high, in Alaska and Southeast Asia.

It is interesting to note that the latter three tidal types often occur in neighbouring regions.

4.3 • Shallow-water tides

Sinusoidal tidal waves propagate through deep open ocean waters until they reach a continental shelf. The wave shape changes markedly close to coasts and shallow estuaries. This can be explained by the fact that the periodic tidal constituents derived from the tide-generating force overlap in these shallow-water areas, thus creating harmonics that can propagate independently. Tidal curves plotted for coasts along the English Channel (Portsmouth, UK, figure 1.7A) and the North Sea (Hoek van Holland, Netherlands, figure 1.7B) are typical examples for points reached by the wave after a long passage over a shallow continental shelf.

Tide propagation patterns up the Gironde estuary provide another typical example of shallow-water wave distortion (figure 1.8). This modification could be explained by hydrodynamic laws according to which the wave velocity c of a hydraulic wave is a function of the square root of the depth,

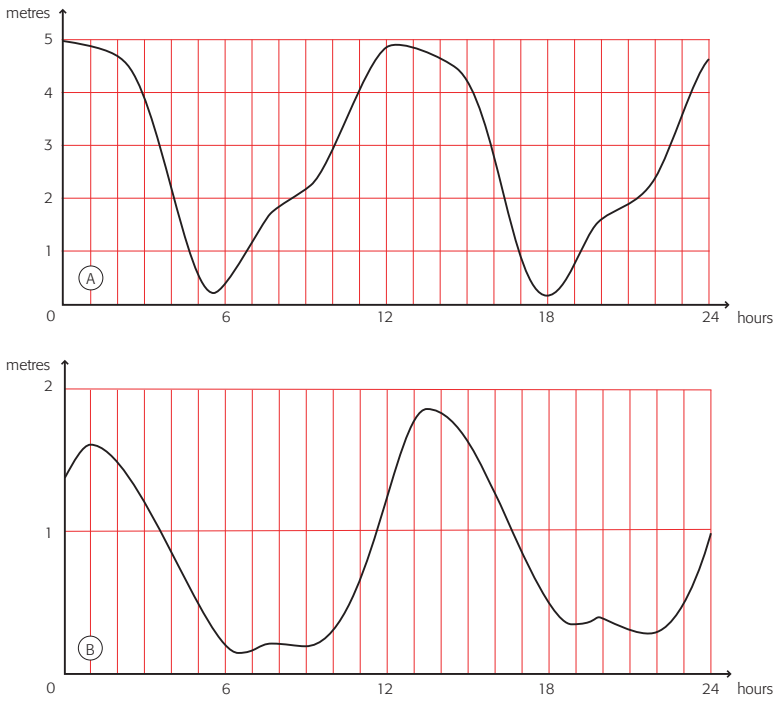

Figure 1.7: Tidal prediction curves for shallow-water areas over a 24 h period. A: Portsmouth, UK; B: Hoek Van Holland, Netherlands. Tidal curves for sinusoidal waves propagating through deep ocean waters are distorted as the waves propagate through shallow waters.

or:

$$c = \sqrt{g(\mathrm{H} + h)}$$

where H is the mean depth at the site and h is the time dependant wave height (with mean = ϕ).

When the depth H is great, differences in amplitude $\delta h = h_{max} - h_{min}$ do not appreciably modify the propagation velocity, whereas they do when H is shallow. Wave crests thus progress faster than the troughs, i.e. a wave crest tends to overtake the previous trough. This phenomenon is especially clearcut in estuaries, as shown in the Gironde example (France, figure 1.8). A tidal bore, or wall-like wave, may form in extreme cases – a phenomenon that occurs in many large river estuaries. Bore heights can reach several metres, especially in Qiantang-Jian (China; almost 9 m during equinox periods) and Amazon (Brazil) estuaries.

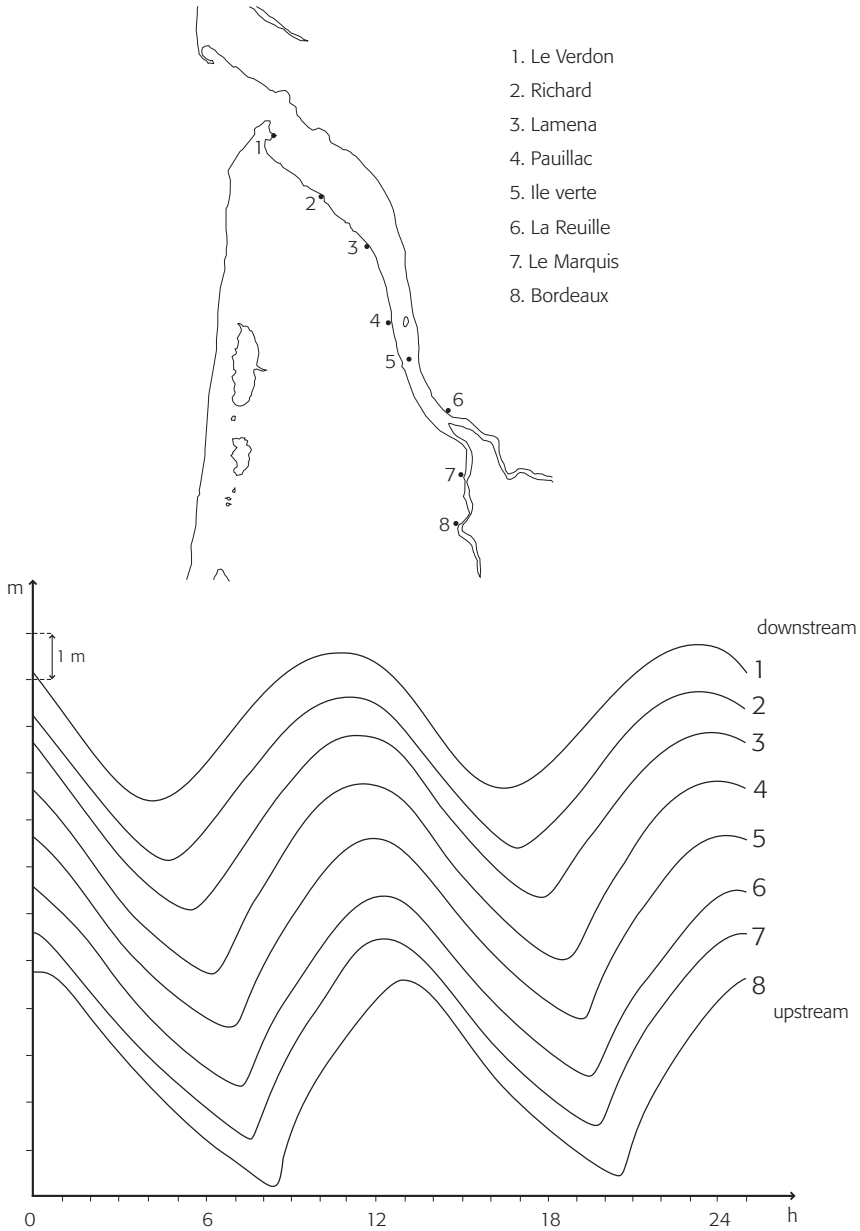

FIGURE 1.8: Tidal prediction curves for eight points located along the Gironde estuary (France) over a 24 h period. Note how the curve distorts as the tidal wave propagates upstream from Verdon to Bordeaux.

4.4 • Spectral features of tides

The tidal spectrum is an objective representation of the phenomenon obtained by calculation, and is independent of all tidal theories. It is especially suitable for representing the observed signal (ocean level variations), so it is worth acquainting ourselves with this mode of representation as it will be referred to regularly hereafter. We will not propose a precise definition for spectrum apart from the fact that it represents the amplitude, or energy, according to the frequency or period of the analysed signal.

This type of low resolution spectral representation (adjacent frequencies are poorly resolved) highlights changes in tide structure upstream from the mouth of a large river (Seine River, France: figures 1.9A and 1.9B). This change in tide structure is linked with tidal wave propagation through shallow waters. These examples show that the main feature of tidal spectra is the distribution of spectral lines in clearly distinct groups separated by relatively broad but regular frequency intervals. The semidiurnal tide group, which corresponds to two cycles per lunar day (cpld), is the largest. It appears wider than the others, but is actually an artefact due to the relatively short time series analysed.

Note the high energy values at low frequencies in both of these examples, especially for those below 4 cpld. Part of this energy is derived from variations in tide heights induced by weather disturbances.

These two spectra (figures 1.9A and 1.9B) clearly show the increase in harmonic number when the tidal wave propagates upstream from the river mouth. The upstream spectrum gives an energy distribution up to very high frequencies. In fact, tidal interaction harmonic constituents formed because this is a spectrum of tidal levels recorded in a river (shallow waters). Most of the astronomical tide directly generated by attractions of the Moon and Sun are simply represented by the first three tide groups (diurnal, semidiurnal and mixed diurnal). The increase in the number of between-wave interactions gives rise to the other groups (so-called hydraulic waves) during tide propagation upstream from the mouth.

The high-resolution spectral signature for a semidiurnal group at Brest obtained through an analysis of more than 120 years of almost continuous recordings gave a multiple-line spectrum (figure 1.10). A large number of clearly identified constituents appear in this latter spectrum (see Chapter V and Annex C for a definition of the alphanumeric characters on each line of the graph). These results confirm the advantages of representing tides in harmonic series.

An enlarged view of the part of the spectrum in the vicinity of the M2

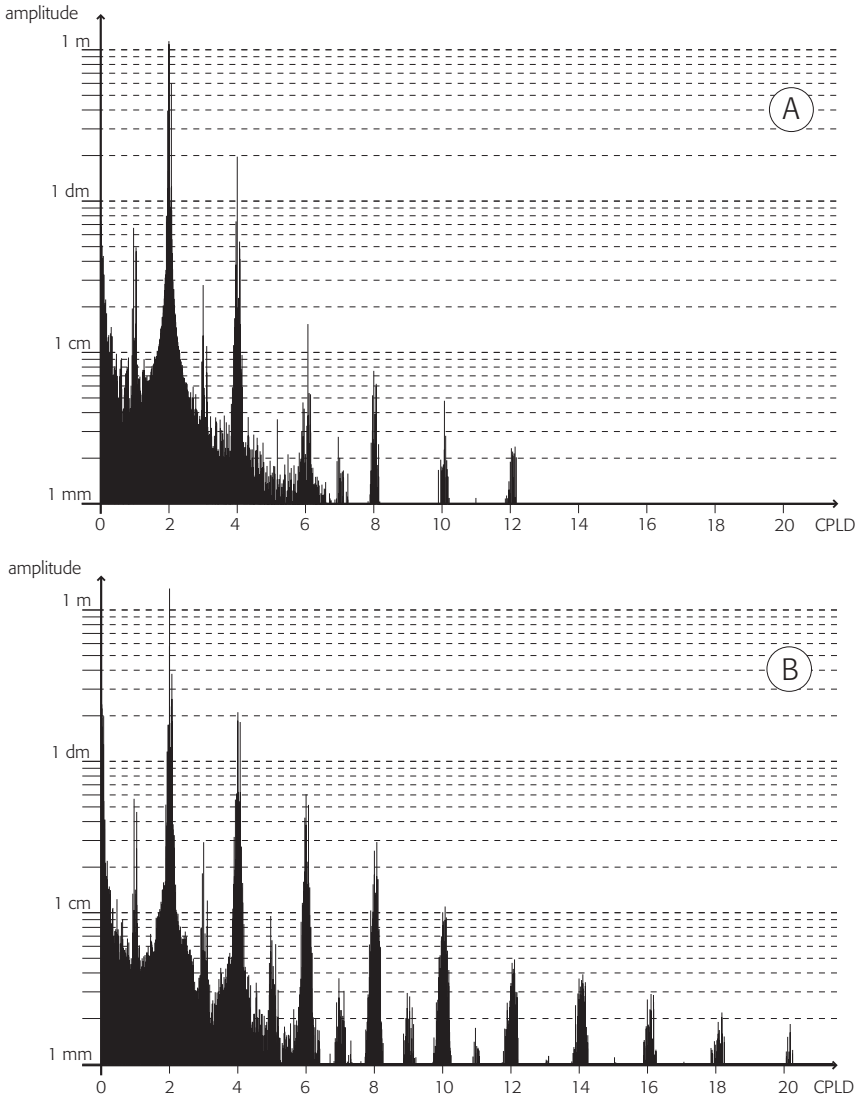

FIGURE 1.9: Low resolution tidal spectra in shallow waters (Seine River, France). A: Beacon A at the river mouth, B: at Rouen, about 100 km upstream. This type of representation highlights the energy distribution around frequencies close to integer numbers of cycles per lunar day (cpld).

spectral line, i.e. the main lunar wave, provides a more detailed illustration of this structure (figure 1.11). Most of these are low amplitude constituents, some of which one might be tempted to disregard.

It is, however, essential to avoid eliminating any of these small constituents

as they could be crucial for reconstructing the tide. There are actually just six degrees of freedom in the three-body system (Sun, Earth, Moon). Hence, all of these small constituents are derived from this system and are interdependent. Taken individually, each of these constituents could be disregarded but their cumulated energy is quite substantial due to their number.

4.5 • Tidal currents

The tide oscillates like swell movements in the ocean surface layers. In both cases, and at first approximation, water molecules have a closed vertical path with specific wave frequencies and lengths. Contrary to swells, however, the tide always has a much longer wavelength with depth. In a uniform deep ocean, tidal movements affect the entire water column. All molecules within the same vertical plane have virtually the same extremely flat orbits. These vertical movements make up the actual tide, while the horizontal movements are incomparably greater and form tidal currents. These currents are generally more intense on the continental shelf (shallow waters) than offshore (deep waters).

In a density-stratified ocean, internal tidal waves occur, especially near continental slopes, and modify the vertical structure of currents. In extreme

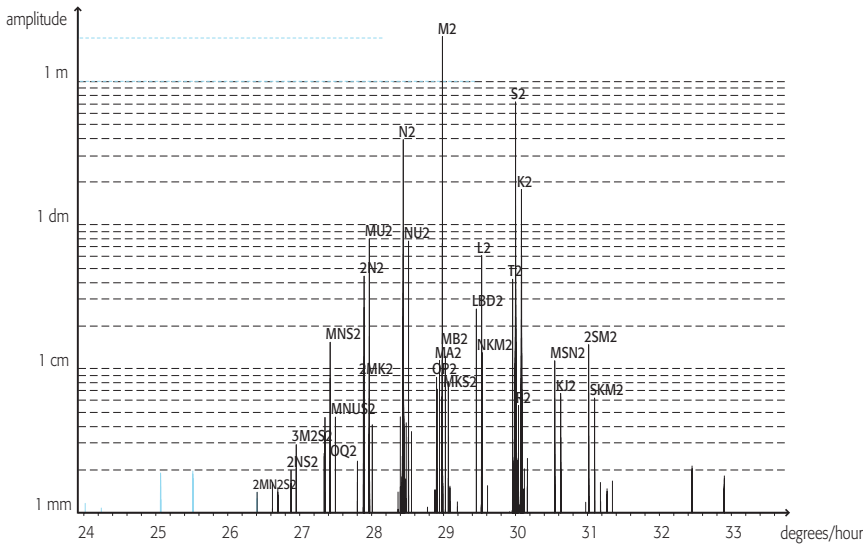

Figure 1.10: 'High resolution' spectrum of a 'semidiurnal group' at Brest, showing spectral lines typical of astronomical tides.

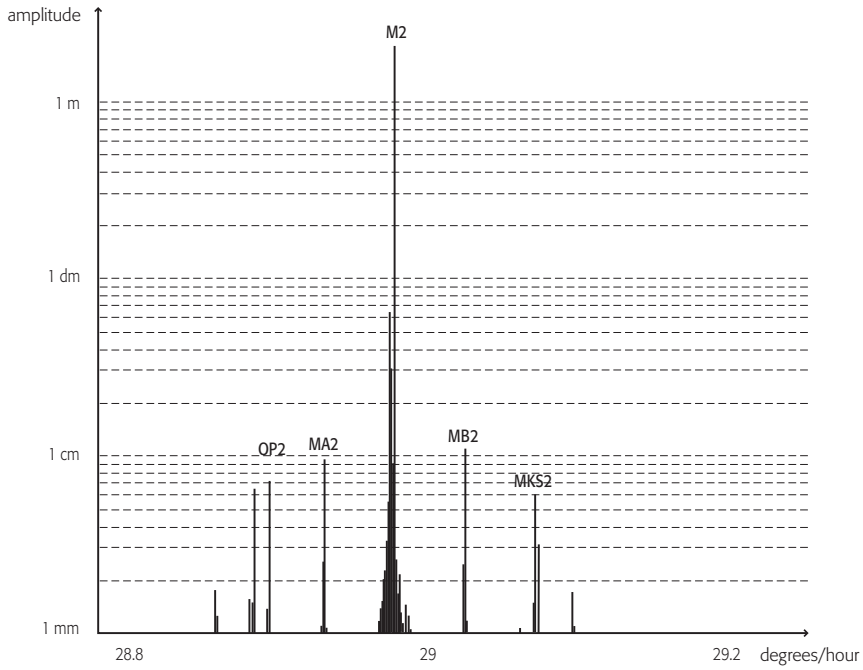

FIGURE 1.11: Spectrum within the vicinity of the main semidiurnal M2 constituent at Brest, showing a very fine structure responsible for long-term modulations.

cases, e.g. in Gibraltar Strait, currents induced by these mainly semidiurnal internal waves sometimes move in opposite directions between the surface and the bottom. Like bottom friction, these internal waves contribute to tidal energy dissipation.

Tidal currents are studied to some extent with the same tools as those used for tidal analysis, but there are more problems for two main reasons, i.e. the high spatial variability in current features, and also the lower temporal regularity of currents under the influence of meteorological factors. Because of the very high intensity of tidal currents in certain areas (close to coasts and in straits), it is essential to study the mechanisms so as to be able to draw up navigational aids, which is a key task of hydrographic services.

Current calculation methods enable detailed modelling of tidal currents. Such modelling is used to an increasing extent for the purposes of drawing up current charts according to tide times. The example shown in figure 1.12, which represents currents around Ile de Batz 3 h after full tide at Roscoff (Brittany, France), is extracted from a navigation handbook, which is especially useful in zones where tidal currents are sometimes violent.

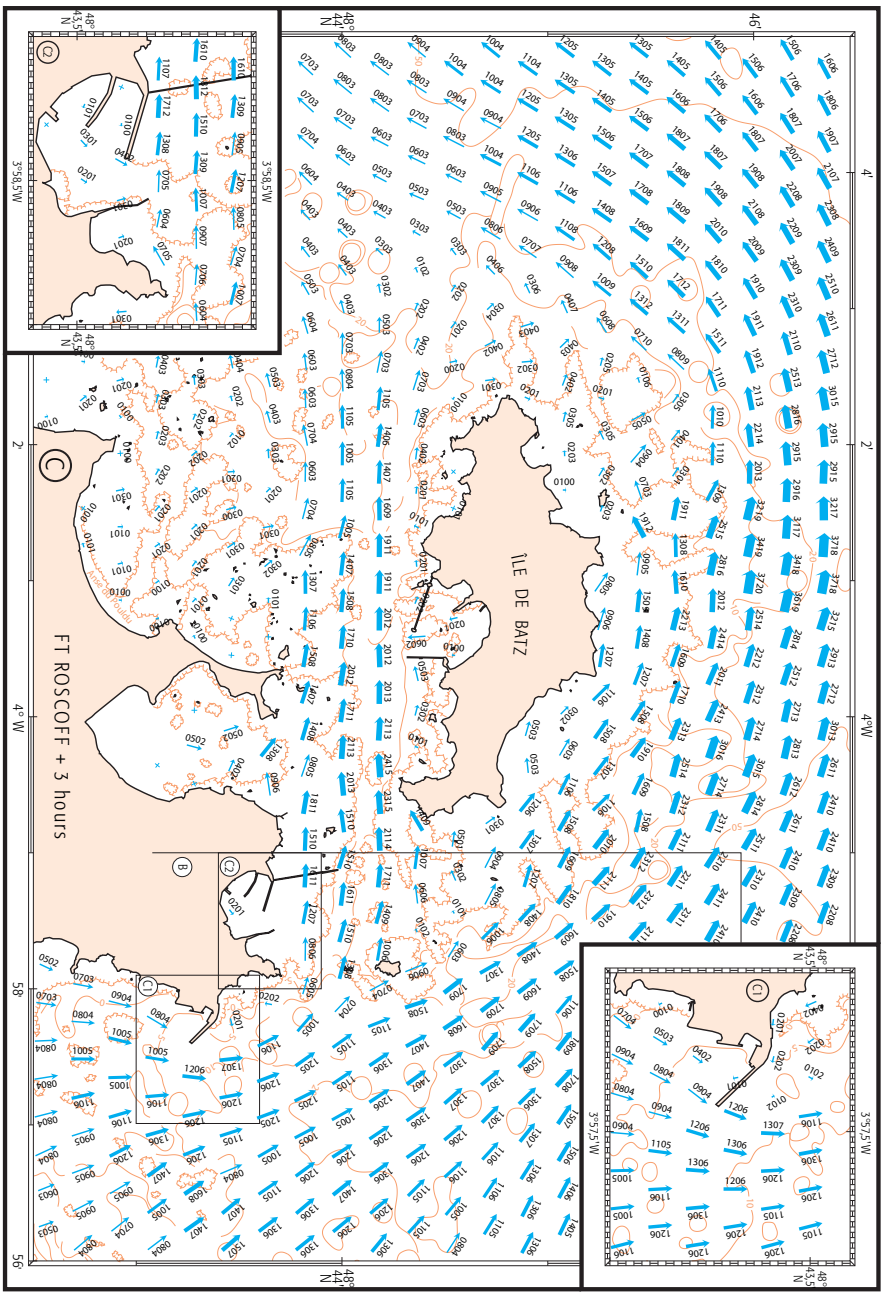

FIGURE 1.12: Results of modelling tidal currants around Ile de Batz, Brittany, France, 3 h after high tide at Roscoff: arrows (by their length and thickness) indicate current velocities. Numbers above the arrows indicate current velocities in tenths of knots for a mean spring tide (first two figures) and mean neap tide (last two figures).

The last chapter of this book focuses especially on these tidal currents and their modelling.

II

Tides and their measurement

Tides and their measurement refers to the description of the tidal phenomenon and measuring instruments that are used to measure the tides and thereby understand them. In this chapter, the needs of this discipline are reviewed and the focus is then placed on 'stilling wells', which are somewhat cumbersome structures but necessary to achieve high quality water level measurements with conventional tide gauges. The main calibration and monitoring systems are then described, ranging from the standard tide staff, which is still a mainstay, to radar altimetry derived from spatial techniques.

1 • Aims of sea level measurement

Accurate information on sea level variations, especially in coastal areas, is crucial for tide measurement, navigation and studies on the oceanic environment. The information needed thus varies depending on the accuracy required, measurement timeframe and processing conditions.

There is a rising demand for highly accurate measurements, especially from the scientific community, whereas the network of existing tide stations was set up chiefly to fulfil the requirements of marine navigation needs.

This network is virtually the exclusive source of data for tidal prediction and chart sounding correction.

Difficulties associated with various measurement and processing conditions hamper the use of these measurements for other scientific applications

(studies on coastal and offshore works, etc.). Issues concerning the streamlining of these measurement systems to fulfil a broad range of alternative needs are technical, but also both structural and financial.

1.1 • Coastal marine navigation

Information on sea levels was first collected to facilitate navigation along coasts and to allow safe access to harbours with a broad tidal range. It was essential that these measurements be available in real or almost real time.

Users generally obtained information by direct observation to fulfil their navigational needs:

- from a tide staff at the entrance to harbours or along channels in maritime sections of rivers,
- or in large harbours via buoyage markers and signals, i.e. cones and cylinders during the day and green, red and white lights at night.

Highly advanced systems have been developed in some estuaries, with water levels at different observatories being transmitted to ships via radio relay, VHF, etc.

It is important to keep in mind that the uncertainty in water height measurement makes it difficult to accurately determine the under keel clearance, i.e. the margin of safety between the seabed and the ship's keel. Moreover, there is increasing demand from sea transport services and pilots for high quality water height records due to the high operating costs for large vessels (harbour layover is very costly), and also to the fact that harbour infrastructures must remain cost-effective. The data precision currently required is around ± 5 cm.

1.2 • Navigational chart bathymetry

Tidal correction of chart sounding data is necessary do establish the navigational chart bathymetry. This so-called sounding reduction operation will be discussed in Chapter IX.

Measurements required for sounding reduction have long been obtained from portable float gauges located near the coast. The drawback is that they require fixed vertical structures, which may not be available near the survey area. Moreover, the quality of the data obtained from these devices is often poor.

Pneumatic bubbler tide gauges are sometimes used and then the choice of site is less restrictive. However, tide measuring operations using these gauges are not always conducted carefully enough to obtain accurate high quality measurements.

So-called 'deep-sea tide gauge' pressure sensor systems (moored on the seabed) are used to an increasing extent for this application. Their connection to the levelling network is achieved by simultaneous readings from a tide staff within the vicinity. These tide gauges can also be used for sounding in offshore areas. However, atmospheric pressure and sea water density corrections are required to determine water levels on the basis of readings from these sensors. Moreover, real-time readings would be useful for processing sounding data while facilitating sensor monitoring, but unfortunately this is not possible with these devices. Some prototypes have been developed to enable data transmission in response to remote requests, but there is a greater need for an instrument that would be robust (easy to transport and install) and generate real-time measurements, in addition to having a remote transmission potential, while of course being equipped with a high quality sensor.

1.3 • Tidal prediction

High quality tide data are required to accurately calculate tide tables. Systematic errors, due for instance to discrepancies in tidal time or height measurements of recording systems, are detrimental to the prediction accuracy.

A 1-year record of hourly water level measurements is generally sufficient to generate predictions that are accurate enough for navigational needs. However, wherever the tidal wave flows over broad shallow expanses (continental plate or estuaries), a record of more than 4 years is required to enable calculation of certain harmonic constituents of nonlinear interactions. It is generally recognized that the best predictions require a 19-year water level record, but such long-term high quality tide data are seldom available.

A record of less than 1-year may be acceptable for some sites, e.g. when there is such a low tidal amplitude that even an imprecise prediction is sufficient, or when the use of tidal constants is possible due to the presence of a nearby port where accurate predictions are readily achieved. A 1-month record may be sufficient if high quality measurements are available. In such cases, it is preferable to obtain measurements in summer when the sea level is least likely to be disturbed by meteorological effects.

Series of hourly recordings are used to assess the frequency spectrum for up to 1/12th diurnal tides, which is generally sufficient. However, for some river tides, a faster recording rate may be required because energy could be detected beyond the 1/30th diurnal tide in some estuaries (e.g. see the tidal spectrum for the Seine River at Rouen, figure 1.9B).

1.4 • Miscellaneous studies

Tidal height data are also used for nonhydrographic purposes. Measurements used for such applications differ mainly with respect to their accuracy, logging rate and duration requirements.

1.4.1 • Meteo-oceanic and climatic studies

In all coastal and offshore parts of the ocean, the sea level is affected by highly interdependent physical processes such as the water density (dependent on temperature and salinity), other local nontidal currents, ocean circulation, waves, atmospheric pressure and wind. Sea level measurements thus bear the mark of each of these phenomena and could consequently contribute to their study.

1.4.2 • Extreme levels

Information on maximum and minimum tidal levels over very long periods (a century if possible) is required for all project studies (harbour infrastructures, coastal structures or oil rigs). When the tide heights are considered to be known, only the probability of positive and negative surges has to be assessed. Long series of high quality measurements are also required for such studies.

1.4.3 • Coastal wave propagation models

Tide records are required to determine the boundary conditions when calibrating and validating tide propagation and storm surge models. It is hard to obtain sea level measurements for water depths of several hundreds of metres under open offshore boundary conditions.

As noted above, this measurement technique is achieved for bathymetric studies of continental shelves at depths of less than 200 m. However, for modelling on an ocean basin scale, considerable expertise and financial resources are often required to obtain accurate water height measurements in very deep water areas, and cooperation between several organizations is generally necessary.

1.4.4 • Mean sea level

Studies of relatively long-term changes in mean sea level could, for instance, provide essential information on the impact of the ocean on climate and global ocean circulation. For such studies, however, the standard world network of tide stations has major shortcomings – it is not uniform (concentrated in the Northern Hemisphere) or suitable for monitoring global ocean dynamics. Tide gauges specifically designed to generate such readings would therefore have to be installed to meet this need.

It is generally acknowledged that the sea level rises by around 1-2 mm a year worldwide, but estimates on the rate of increase vary markedly between authors. Hence, the exact causes of this rise are unknown, especially the extent of involvement of the greenhouse effect, due to the increase in industrial carbon dioxide release into the atmosphere. However, TOPEX-Poseidon satellite ocean surface measurement data indicated a mean increase of around 2 mm/year between 1993 and 2000, but this increase was not uniform throughout the world's oceans, i.e. regional differences of ± 20 mm/year were noted.

The problem of measuring sea level increases could be overcome by positioning tide gauges with reference to a single vertical reference level, e.g. the International Ellipsoid of Reference. Moreover, an increasing number of tide stations are now equipped with geodetic positioning systems involving spatial technology.

In 1984, the joint IOC/WMO committee for the Integrated Global Ocean Services System (IGOSS) launched the pilot IGOSS Sea Level Project in the Pacific (ISLPP) to promote operational exchange of mean sea level data for the Pacific Ocean region. The ISLPP data center is based at the University of Hawaii and is responsible for rapid dissemination (within 4 weeks) of monthly mean sea level maps.

It is also important to mention the Global Sea Level Observing System (GLOSS), i.e. an international programme under the aegis of the Joint Technical Commission on Oceanography and Marine Meteorology (JCOMM) of the World Meteorological Organization (WMO) and the Intergovernmental Oceanic Commission (IOC). GLOSS has overcome the shortcomings of conventional tide monitoring networks by promoting the development of a top quality joint global/regional network to fulfil the needs of oceanographic and climatological research. The Global Core Network (GCN) is the mainstay of GLOSS, with almost 300 tide stations located worldwide to monitor climatic and sea level variations. These stations are designed to supply sea level measurements with centimetre accuracy and are referenced in a global geodetic system. These data are available online from the University of Hawaii Sea Level Center, the Permanent Service for Mean Sea Level(PSMSL) or the World Ocean Circulation Experiment (WOCE).

1.4.5 • Improvement of tidal predictions in shallow waters

Traditional analysis and prediction methods are unreliable when the tidal wave is highly deformed by nonlinear processes such as bottom friction and advection. These processes have a substantial effect when tidal height variations are comparable to the mean ocean depth variations.

Tidal prediction methods tailored for and used in estuarine regions take variations in stream discharge into account. This requires series of good quality sea level measurements obtained at 10 min intervals.

1.4.6 • Warning systems

Some sea level monitoring networks are coordinated to forewarn coastal inhabitants who are vulnerable in cases of natural catastrophes such as storm surges and tsunamis. The two most famous systems are located in the North Sea, to issue warnings on especially dangerous storm surges along the eastern coasts of Great Britain and the Netherlands, and in the Pacific where the University of Hawaii issues tsunami warnings.

1.4.7 • Spatial altimetry calibration

The development of spatial monitoring techniques has given rise to an increased need for sea level data. As we noted in the introductory chapter, satellite-borne radar altimetry equipment currently provides sea level data with centimetre accuracy. However, due to the altimeter sampling conditions and the fact that little information is available on the geoid aspects of coastal waters, the satellite readings have to be calibrated via a tide recorder located on the vertical axis of the satellite's orbit. The geodetic positioning of the tide recorder is thus absolutely crucial, as is also true for long-term studies on sea level variations.

2 • Stilling wells

Most tide stations have a so-called 'stilling well' installed. It consists of a pipe, chamber or compartment that communicates with the sea via a small intake opening located at the bottom, below the lowest water level. It is sometimes fitted with a pipe extension whose length depends on the topography of the site. This device is cumbersome but also essential for several reasons. It mainly serves to dampen variations in level due to waves, swells and seiches (sea level variations in harbour basins and bays) in order to obtain a horizontal surface whose height is identical to the external level, averaged over a time span equal to the measurement sampling time. The stilling well housing also provides weatherproof protection for the recording systems. Without this protection, even the sturdiest instruments would quickly break down, especially at exposed sites.

However, the stilling well hydraulic system has the drawback of not providing linear damping. Errors associated with the internal response of this

system should also be examined with respect to external sea level variations. This issue is discussed in Appendix B.

2.1 • Other errors associated with stilling wells

In addition to the intrinsic error (not related to the measurement system) associated with the nature of the response of the stilling well hydraulic system, various other errors (also independent of the measurement system) can bias measurements.

For instance, the errors mentioned in Appendix B, which are not related to the stilling well but rather to the characteristics of the medium in which it is submerged. Siltation and concretion (due to the growth of marine organisms) are two factors that should be carefully monitored around both the intake opening and within the pipe. Partial plugging is often not noticed at first and may cause a phase lag without markedly altering the amplitude. This problem, however, often seriously degrades the quality of the readings over time. The stilling well pipe should thus be inspected and cleaned on a yearly basis.

2.1.1 • Errors due to density differences

The difference in water density between the internal and external sides of the stilling well is another source of error that has to be accounted for to ensure that high accuracy measurements are obtained. During a tidal cycle, the temperature and salinity of coastal waters may vary widely, especially during the summer months and near river mouths. The water within the well is never completely renewed since the exchange takes place only via the small intake opening at the bottom of the well. Hence, the water that flows into the well as the tide rises is often denser than the external water at equal depth. The result is that the water level is lower within the well than outside it. This effect is reversed when water of lower density flows into the well and remains there (with no possibility of being renewed), i.e. the water in the well is less dense and the level is higher than outside the pipe. Using the notations given in Appendix B (figure C.1), let $\delta h = h_p - h$ and $\delta\rho = \overline{\rho}_p - \overline{\rho}$ be the density error (mean determined for the water height from the well intake) between the water in the stilling well and the external sea water. The difference in level according to the hydrostatic hypothesis is

$$\delta h = (z_0 + h)\frac{\delta\rho}{\overline{\rho}_p} \approx (z_0 + h)\frac{\delta\rho}{\overline{\rho}}. \tag{2.1}$$

For a stilling well of around 10 m depth (with a broad tidal range), a

one part in a thousand error in density would cause a centimetre height difference.

Another often overlooked source of error associated with density differences is atmospheric water vapour condensation on the walls of large diameter deep wells. The resulting condensation runoff creates a surface layer of fresh water within the well that tends to increase over time if there is not sufficient evaporation. The relative error in density between the sea water and the fresh water is around $3 \cdot 10^{-2}$, so a cumulated fresh water layer of 1 m in a deep well would induce a 3 cm overprediction error relative to the external sea level.

It is not common practice to measure the vertical distribution of water densities on the internal and external sides of stilling wells. Easy advanced techniques are nevertheless available for such measurements. In wells designed to provide accurate readings for scientific applications, these techniques could be useful – at least for verification purposes – if only to supplement conventional tide pole and light probe readings.

In estuaries, water level errors due to density variations are almost systematically encountered. In tidal rivers, for instance, the water density within the well is lower than the external water density and water level errors of over 6 cm for a 2 m tidal amplitude may occur.

2.1.2 • Errors due to currents around the intake opening

Water movements around the intake opening of the well (permanent or tidal currents, orbital speed of swells and waves) can, by the Venturi effect (vacuum created by streamline bottlenecking around the stilling well), induce unwanted pressure variations that affect the water level reading inside the well (Appendix B). This Venturi effect could be accounted for in the well equation, but would substantially boost the complexity of the calculation.

This vacuum created at the intake opening is maximum when the intake plane is parallel to the flow upstream from the well, thus inducing a decrease in the internal water level, e.g. 20 cm with an upstream current of 1.5 m/s $\approx$ 3 knots (figure 2.1). The different curves in this figure show that the measurement error can be reduced by gradually introducing appropriate improvements. A reduction in the corresponding error of over an order of magnitude is thus possible by changing the shape and location of the input opening, whose characteristics may be seen on the small icons at the ends of the curves on the graph. The best solution for a well with an intake opening (without pipe) is represented by the icon at the end of the *g* curve in figure 2.1. This configuration has been adopted in particular for Australian stilling wells in the Pacific tide station network (figure 2.2).

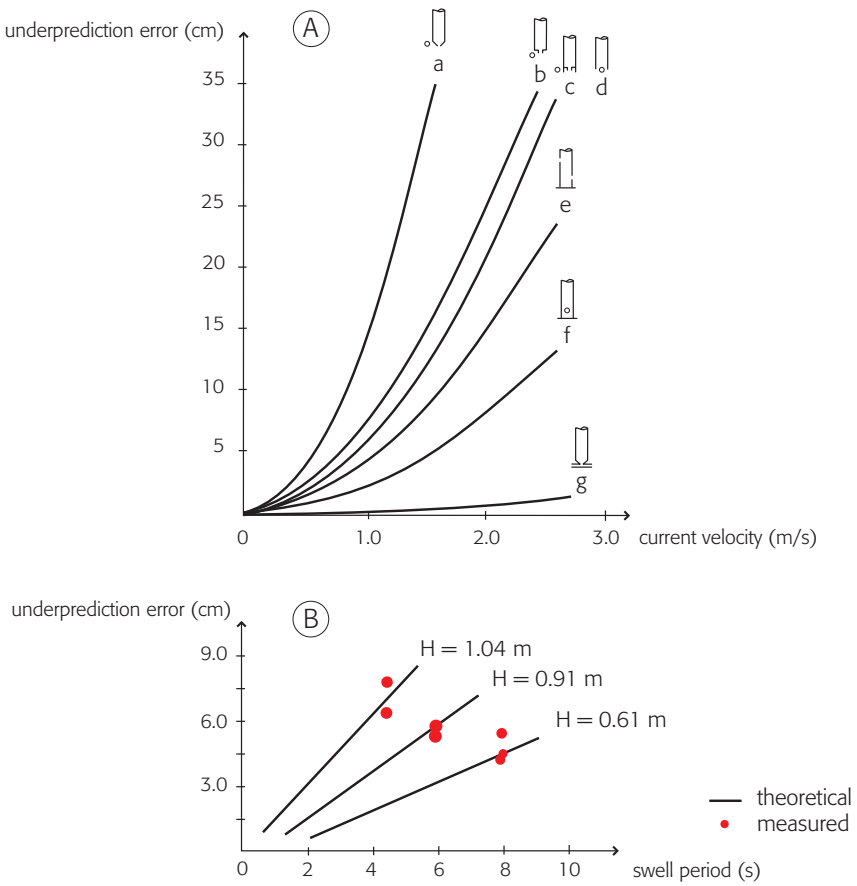

FIGURE 2.1: Decrease in water levels in a stilling well due to currents (Source: G. W. Lennon, 1967).

Note also that there may be discrepancies in atmospheric pressure between the inside and outside of the tide station (where the stilling well is installed) – vacuums created by strong winds (Venturi effect around the housing) or excess pressure due to warming of the air within the housing if it is too air- and water-tight. These variations generally induce errors of the order of centimetres.

Fortunately, all of the faults noted above are extreme cases. They are generally not a problem at harbour sites with very marked tidal falls or where tide recorders are protected from swells, currents and siltation. Internal/external stilling well water level differences can be systematic, but they are generally of minor consequence. It would therefore be untimely to try to overcome

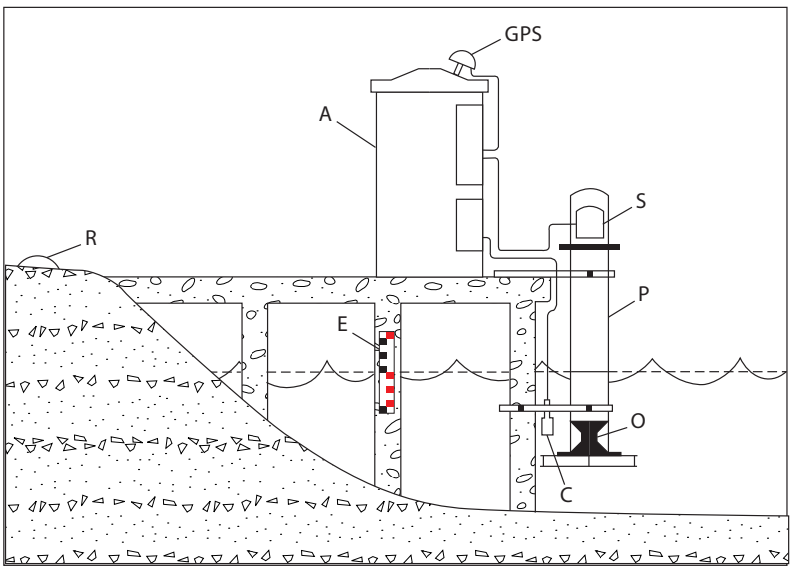

Figure 2.2: Diagram of a Seaframe-type tide station (Australia). A: protective housing for the recorder and transmitter; C: pressure sensor; E: tide staff; GPS: antenna for GPS positioning of the station; O: stilling well intake opening (note the Venturi tube and wave protection plate); P: protective housing for the stilling well; R: control mark (geodetic point); S: ultrasonic depth finder (Source: IOC Manuals and Guides).

this fault by renovating a tide station that has been operating for decades as such modifications could upset long-term monitoring of tidal phenomena. This fault actually induces differences in water level caused by factors similar to those that induce systematic water level differences that may be observed between the internal and external sections of a port, roadstead or bay.

3 • Conventional tide recording systems

A stilling well is essential when setting up a permanent tide station along a coast. Many permanent tide gauges managed by hydrographic services are located in harbour areas or along navigable estuaries. Data from temporary stations are generally processed for short-term hydrographic purposes.

Several techniques are used for sea level measurement. The most long-standing techniques remain important and widely used, such as tide staffs (or poles). Float gauges are still used, whereas so-called analogic graphic recording systems are gradually being replaced by automatic digital data logging systems.

As this new tide recording technology has only been introduced in recent decades, long time-series sea level data (required to determine long-term patterns) are still mainly obtained with conventional recording instruments such as tide staffs and float gauges.

These latter two instruments will first be presented while assessing the quality and accuracy of the respective data they generate, and more recent systems will be discussed in section 4 of this chapter.

3.1 • Tide staff–the mainstay

The first tide data were obtained from direct tide staff readings. Some of the oldest known tide data were logged at Brest (France). From 1711 to 1717, tide staff low water and high water readings were obtained during daylight hours and subsequently used by Laplace to develop his dynamic theory of tides.

As noted at the beginning of this chapter (1.1.Coastal marine navigation), direct tide staff readings can facilitate navigation. Readings from this instrument are now mainly used to calibrate and monitor levels determined via other tide-measuring systems.

In compliance with hydrographic sea level measurement standards (set by the International Hydrographic Organization, IHO), all permanent tide stations should be equipped with a tide staff. This is the only instrument that provides direct water level readings outside a stilling well, so it is a mainstay for overall monitoring of levels measured within the well (to ensure that the well is functioning properly and to validate the resulting data logs). For accurate monitoring, the tide staff should be installed within the immediate vicinity of the tide station.

The material that the tide staff is made of and its location should be dictated by common sense. The material should be rust resistant and easy to clean so that the scale can be read correctly. When deciding on where to install the staff, hazardous sites (i.e. risk of destruction or deterioration) or places that might be hidden by berthed vessels should be avoided. The staff must also be mounted vertically. If this is impossible (slightly leaning wharves or jetties), the graduated scale must be adjusted to indicate real water heights.

Although not absolutely required, it is recommended that the tide staff be installed such that its zero is at the hydrographic datum so as to avoid misinterpretations by uninformed users.

Figure 2.3 shows an example of a tide staff. The scale is graduated in 10 cm intervals with a series of red and black blocks separated by a blank of the

Figure 2.3: Tide staff: the red and black blocks are 10 cm squares.

same size. The grouping of alternating sets of three blocks of the same colour makes it easy for an observer to quickly determine the height in the metric range. Although 10 cm may seem to be a very rough scale measurement unit, an observer can quite easily estimate a quarter of a block ($\pm$2.5 cm) by eye– waves and ripples are almost constantly present, so higher precision is not unfeasible. Several tide staff readings are required to calibrate tide gauges for vertical water level measurement.

In some cases, especially in areas with a substantial tidal range, it may be impossible to install just one tide staff to span the entire vertical tidal range. Two or more staffs are required in such situations: a high water staff may be mounted on a wharf, for instance, with a low water staff installed where it can be used at LW but is submerged at HW.

It is sometimes hard to get a tide staff reading, especially when it is being hit by waves, so successive maximum high and low readings are usually just averaged in such cases. However, as waves have a trochoidal (the crest height is greater than the trough depth) rather than a sinusoidal profile, it should be kept in mind that values obtained by this method will be higher than the real level.

The tide staff zero mark is determined with respect to at least three fixed onshore benchmarks. These control marks must be sufficiently far apart to reduce the risk that they could all be destroyed at once, e.g. during harbour work. One of them is selected to serve as the fundamental benchmark–it is generally recommended that this be a terrestrial benchmark. Their respec-

tive zero marks with respect to the hydrographic datum and the terrestrial benchmark (if there is one) are recorded on a data sheet with maps and photographs provided to make it easy to find them.

3.2 • Floating tide gauge

The English engineer Henry Palmer is usually given credit for inventing the first float tide gauge equipped for graphic recording (figure 2.4) in 1831, but his prototype was never used to record tide levels over a long term. In France, the hydrographic engineer Rémi Chazallon, who published a list of tide tables for the coasts of France in 1839, devised one of the first operational float gauges in 1842. In 1859, around 10 of these gauges were operational along the French coasts.

This gauge can thus be considered as a conventional recorder, and it is still widely used despite the ongoing technological advances achieved in this domain. The float is located in the stilling well and the graphic recorder is

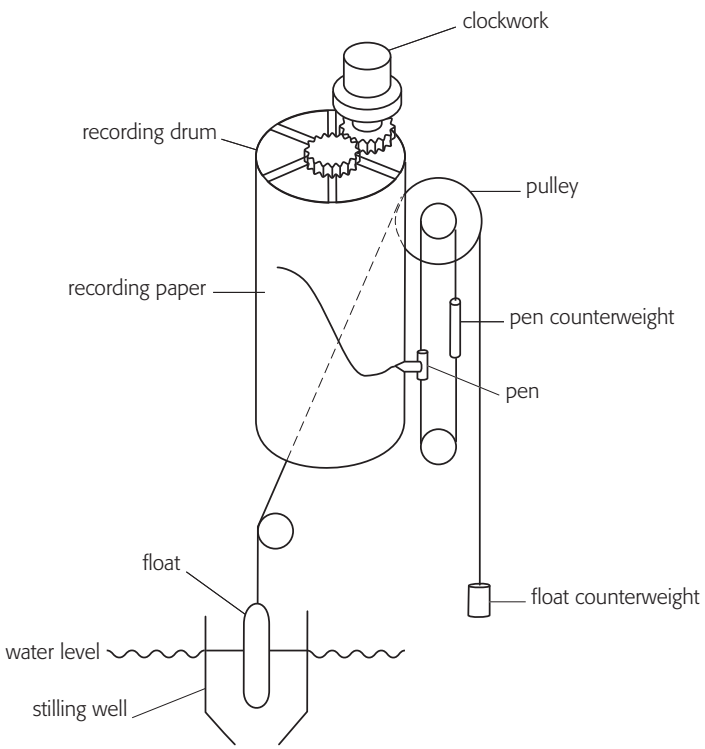

FIGURE 2.4: Diagram of a floating tide gauge with a graphic recorder.

usually located in a housing above, thus providing efficient weather protection. These instruments are reliable and easy to manage. When high accuracy is not essential, maintenance and operation of these tide gauges does not require highly trained personnel.

The data logs obtained with these devices – despite the fact that they are hampered by a number of faults associated with the stilling well, the mechanism and tide graph digitization – represent the almost exclusive source of historical sea level data currently available worldwide. The recording system has now been upgraded to generate computerized digital data.

3.2.1 • Tide graphs

Float tide gauges mainly generate time-based graphs of sea levels. Data are plotted with a pen on a chart attached to a recording drum whose rotation is controlled by clock. A so-called tide curve is thus traced on the tide chart. Despite the fact that the name 'tide graph' is widely used, it actually represents variations in sea level with tide generally being the main component.

A complete recording drum rotation takes 24 h, but water height data may be plotted continuously on the same chart for several days. The curves are staggered because the tide is mainly affected by movements of the Moon and a lunar day is around 50 min longer than a solar day (figure 2.5). For a semidiurnal tide, the chart can be left on the recording drum for 2 weeks, but thereafter the curves may partially overlap, thus causing errors when the chart is digitized, often resulting in considerable data loss (i.e. recordings cannot be processed).

Several sources of error can affect this type of recording:

- for the height measurement: poor vertical registration of the chart paper on the recording drum when it is changed; variations in the water height scale on the chart paper due to humidity or temperature variations
- for the time measurement: poor horizontal registration of the chart paper on the recording drum when it is changed, often associated with take up of slack on the recording drum; chart paper is not compatible with the drum diameter, thus inducing cyclical variations in the time scale; irregular clock functioning; and variations in drum rotation due to drive gear defects.

None of these faults are very important, but they should all be monitored through regular careful checks.

Time measurement errors can sometimes be corrected by taking movements of the Moon and Sun into account since very accurate information on their cycles is available.

Height registration errors are harder to correct and may sometimes go

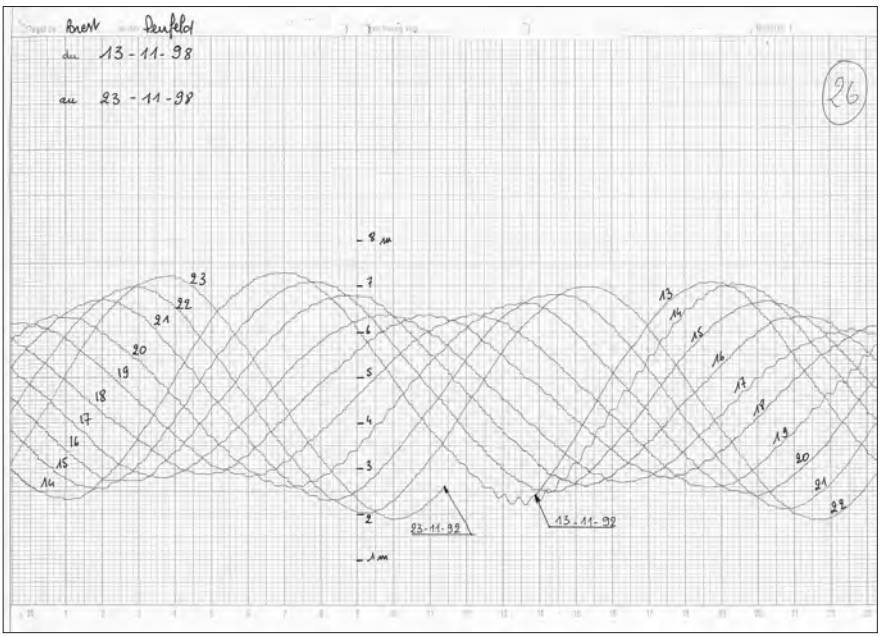

FIGURE 2.5: Tide chart obtained on a recording drum with a 24 h rotation time. Because of the 50 min difference between lunar and solar days, the chart paper can be left on the drum for a few days without any problem of curve overlap (records from 13/11/1998 to 23/11/1998, Brest, France).

unnoticed. In fact, they can only be detected through comparisons with data from nearby tide stations or by detection of obvious discontinuities on the tide charts.

3.2.2 • Tide chart digitization

Direct data recording systems have been developed to overcome drawbacks associated with manual digitization of tide charts, which is done to fulfil the need for computerized digital data. Data digitization involves coding of the analog signal, which can be carried out in several ways. One of the most accurate involves optical coding of the rotation of a disk attached to the pulley, which rotates as the float moves. Another system that is also widely used, but which is probably less reliable, uses a potentiometer where the voltage measured on the contact is transformed into a frequency.

These systems are backed up by a magnetic tape recording (punched paper tape was once used but has now been abandoned) or by radio transmission or telephone transmission of sea level data to a remote recorder. All of these refinements require special skills, and experience has shown that

hardcopy graph paper recording is essential for data recovery following a breakdown.

Tide chart digitization generally involves hourly water height data logging, which is usually sufficient for tide analysis. In centres where many tide charts are processed, a digitizer may be used to enable direct logging of sea level data onto a computer.

The recordings should be accompanied by a tide chart monitoring sheet (figure 2.6) upon which the operator's tide staff or light probe water level readings obtained at given times are recorded.

Poor interpretation of these monitoring sheets, especially when they have not been carefully filled in, is a relatively important source of error.

The fact that manual or semiautomatic digitization of tide charts is generally a tedious routine task is another shortcoming, i.e. errors may be generated as the operator's motivation wanes.

3.2.3 • Functional control

The measurement accuracy mainly depends on how carefully the different functional control tests at the tide gauge site have been carried out. As already noted, considerable negligence in this field can be detrimental to the data quality and may even lead to substantial data loss.

A 2 to 3 day inspection rate is recommended. Weekly inspections, which is common practice, should be considered as a second-best option.

The inspection operation simply involves comparing the tide chart data with recognized accurate independent indicators. Any timekeeping unit (usually the operator's watch) can be used as reference for the time checks.

Special care should be taken when changing the chart paper. After installing and adjusting a new chart sheet on the recording drum and setting the pen at the exact required height, the operator should initiate the tracing prior to noting the respective watch and tide chart times so as to avoid time setting errors associated with any play in the recording drum drive gear.

During intermediary verifications, the tide gauge will only be adjusted when there is an obvious malfunction, other than for time and height setting adjustments.

The height setting is normally checked by comparison with tide staff readings. The light probe is a graduated metallic tape fitted with an electric contact at the base which closes when it comes in contact with water and illuminating a light.

These two checks are complementary and recommended. The light probe enhances the accuracy, but it only tests part of the set-up as it is only used in the stilling well. The tide staff provides direct measurements and is thus an

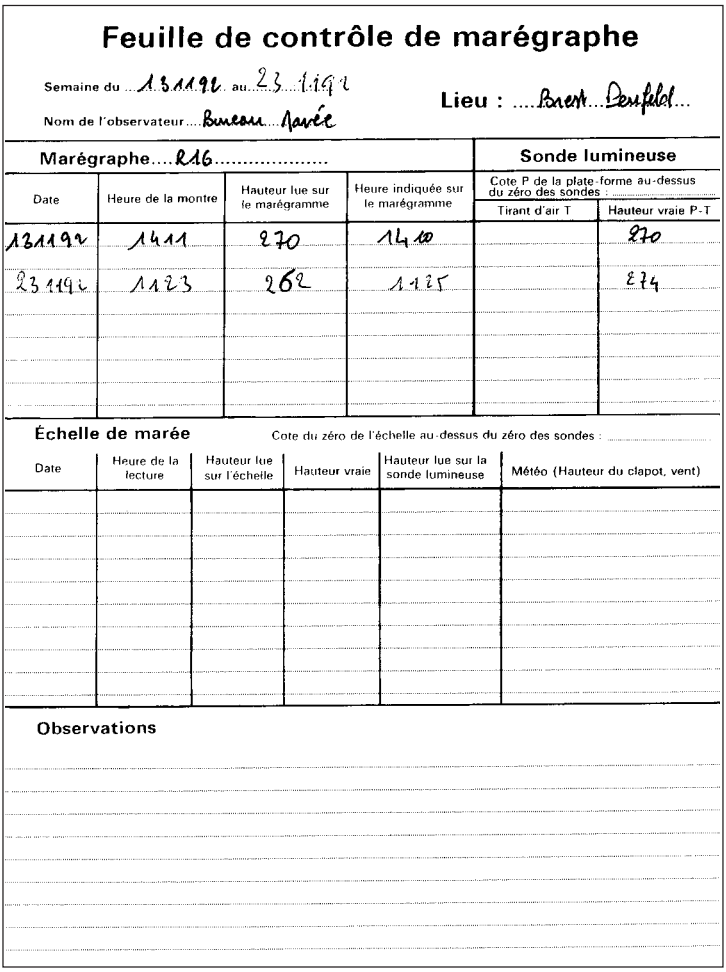

Feuille de contrôle de marégraphe

Semaine du 13/11/92 au 23/11/92 Lieu : Brest Penfeld

Nom de l'observateur : Bureau Navée

Marégraphe R16

Date	Heure de la montre	Hauteur lue sur le marégramme	Heure indiquée sur le marégramme
13/11/92	1411	270	1410
23/11/92	1123	262	1125

Sonde lumineuse

Cote P de la plate-forme au-dessus du zéro des sondes :

Tirant d'air T	Hauteur vraie P-T
	270
	274

Échelle de marée Cote du zéro de l'échelle au-dessus du zéro des sondes :

Date	Heure de la lecture	Hauteur lue sur l'échelle	Hauteur vraie	Hauteur lue sur la sonde lumineuse	Météo (Hauteur du clapot, vent)

Observations

FIGURE 2.6: An example of a tide chart monitoring sheet (from 13/11/1992 to 23/11/1992, Brest, France).

ideal reference. However, as noted above, the best achievable accuracy for a single reading is ± 2.5 cm due to the presence of waves and ripples.

The results of all of these checks are listed on the tide gauge monitoring sheet (figure 2.6).

3.2.4 • Detection of measurement errors

Measurement errors can be avoided by preventive maintenance and regular monitoring, but tide logs may sometimes be obtained from stations

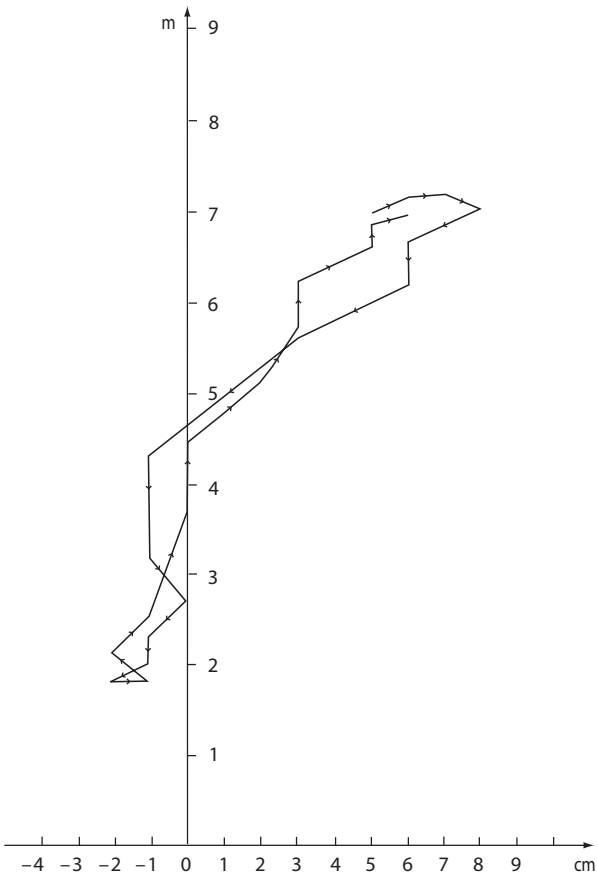

Figure 2.7: Van de Casteele test: for a tidal cycle, the curve illustrates variations in the deviation (X-axis) between an MCN ultrasonic sensor measurement and a float tide gauge (OTT 20030) measurement plotted against the water height measured by MCN (Y-axis). The difference would be nil if there was no fault.

that are not in compliance with required standards. Some errors are hard to detect (stability of the vertical control datum), but other floating tide gauge malfunction faults can be identified by different tests, including the Van de Casteele test (figure 2.7).

The vertical control datum stability warrants special attention because errors in the corresponding measurements are hard if not impossible to detect, especially if they are permanent or cyclical and where there is not regular monitoring. The main causes are poor height adjustment of the chart paper on the recording drum and vertical movements in the system support (e.g. wharf) or in the attachment fixtures. Obviously we will not get into an indepth discussion on the fact that ground movements due to seismic or tectonic activity could be responsible for measurement errors. Indeed, it is understood that the accuracy of a tidal reading is dependent on the stability of the tide gauge support, but on condition that this support does not undergo modifications due to human activities or inclement weather conditions (storms, flooding). It is crucial to focus on modifications that cause vertical movement in the benchmarks, especially those located in the vicinity of recent harbour structures. It is thus essential to have several benchmarks in the area that are reasonably separated.

The Van de Casteele test identifies most other floating tide gauge errors and faults. A light probe is required for this operation. The test involves monitoring freeboard in the stilling well throughout a tidal cycle and comparing the resulting series of freeboard values with data from the tide gauge that is being checked. The sum of the two measurements should remain constant if the tide gauge is functioning properly.

This test can also be carried out with two tide gauges of the same type or different types, with one serving as reference, and with both gauges measuring the water level in the same well (if it is large enough), or levels in two neighbouring wells. The measurement difference should remain constant in this comparison, i.e. nil when the recorders have datums representing the same reference. A comparison of readings from two tide gauges (figure 2.7), i.e. an OTT float gauge and an MCN ultrasonic probe (reference), provides an example of a common float tide gauge fault. A scale factor change occurs after a certain height, which is likely due to an overlapping coil on a cable reel. In this example, the float tide gauge gives a reading that is lower than that of the ultrasonic probe after around 4.5 m height, with the modulus of this deviation increasing by about 2.5 cm/m.

The Van de Casteele test can also be used to detect:

- slack in the mechanism
- a wrong scale factor: a graphic scale that differs from the reduction factor
- something attached to the float cable or pen cable
- interference or blockage of the float movement at a certain water level in the stilling well

• cable slippage on the pulley.

The source of a potential tide gauge fault can often be readily identified by interpretation of a Van de Casteele test graph.

4 • Modern measuring systems

Few physics disciplines benefit from such a broad range of measuring systems, several of which have been the focus of development and applications for tide measurement. The system to be used is selected on the basis of various factors, including the overall cost (material and maintenance) is often the decisive factor, sometimes to the detriment of the performances required.

The nature of the site where the device is to be installed is another factor to consider. A sensor and recorder suitable for coastal sites – where a stilling well may be installed (harbours, estuaries, shallow water areas) to provide weather protection for these new systems – will differ from those suitable for offshore sites (continental shelf and deep oceanic waters) for which additional equipment is required to allow tide gauge immersion and recovery.

4.1 • Tide pressure gauge

Pressure gauges appeared with the advent of pneumatic tide gauges, i.e. mercury differential pressure gauges, which measure the difference between the pressure of air released at specific depths and atmospheric pressure measured on land.

However, it was not until technological advances gave rise to the development of small-scale pressure gauges – especially strain gauges and piezoelectric quartz crystal sensors – that these devices were widely adopted. It thus became possible to design deep-sea tide gauges (so-called bottom-mounted tide gauges) with enough energy self-sufficiency to enable digital data logging for periods extending up to and even beyond one year. These devices are widely used in hydrography for measuring tide heights around sounding sites or for determining boundary conditions of digital tide and current models in specific areas on continental shelves (for depths of generally less than 100 m).

4.1.1 • Measurement principle

Let us consider a bottom-mounted tide pressure gauge, where:

• H: is the depth at the measured site (mean gauge depth)

• $h(t)$: is the sea level variation, as a function of time t and zero mean $\overline{h(t)} = 0$

• $\mathrm{H} + h(t)$: is the water height above the gauge

• $p(t)$: is the pressure measured by the gauge

• $p_a(t)$: is the atmospheric pressure at sea level

• $\overline{\rho}$: is the mean sea water density (as a function of the temperature and salinity, with the pressure ignored for depths of less than a few hundred metres) over the height $\mathrm{H} + h(t)$

• g: is the acceleration due to gravity.

The pressure given by the gauge is thus equal to the sum of the atmospheric pressure and the hydrostatic pressure, or:

$$p(t) = p_a(t) + \overline{\rho} g[\mathrm{H} + h(t)]$$

The water height above the bottom-mounted tide pressure gauge is therefore:

$$\mathrm{H} + h(t) = [p(t) - p_a(t)]/\overline{\rho} g \tag{2.2}$$

Some gauges measure the differential pressure $p(t) - p_a(t)$, which is equal to the hydrostatic pressure of the water column. The differential sensor requires atmospheric pressure data, as determined through an air intake, but this is difficult when the gauge is submerged offshore. Moreover, the pressure $p(t)$ is the key factor for some applications, especially in the physical oceanography field. Information on the three parameters g, $\overline{\rho}$ and $p_a(t)$ is required for studies of offshore sea level variations $h(t)$ on the basis of the seafloor pressure $p(t)$.

The gravitational acceleration g varies with the latitude L according to the following formula (in $\mathrm{m/s^2}$):

$$g = 9.7803185(1 + 0.005302357 \sin^2 \mathrm{L} - 0.0000059 \sin^2 2\mathrm{L}) \ \mathrm{m/s^2}$$

Its intensity thus increases by approximately 0.5 % from the Equator to the Pole. For the same hydrostatic pressure variation amplitude, this corresponds to a relative tidal fall of 5 mm/m. If we take a g value corresponding to a mean latitude, the maximum possible error is 2.5 mm/m tidal fall. This is quite substantial, especially as it has a marked effect on the accuracy of the depth H determination, which is a crucial factor in climate change studies (pending corrections to account for potential tectonic movements).

The mean density $\overline{\rho}$ of sea water is around $1.028 \cdot 10^3$ $\mathrm{kg/m^3}$, and is a function of the temperature, salinity and pressure. As high pressures are involved, the compressibility of sea water should be taken into account in deep sea areas, whereas the pressure has little effect on ρ in the surface layers.

Figure 2.8 shows curves plotted at different salinity levels, while not accounting for the adiabatic compression of sea water, with a gravity value of $g = 9.81$ m/s^2. For example, a hydrostatic pressure of 10^4 Pa for a water column at 4°C corresponds to a height of 101.94 cm for fresh water (S = 0) and 99.34 cm for sea water at S = 37 salinity, i.e. an error of 2.6 cm. Note that the same type of error arises when assessing sea levels on the basis of water heights in a stilling well.

4.1.2 • Pneumatic or bubbler tide gauges

This is one of the first types of tide gauge that takes the relationship between the water height and the corresponding hydrostatic pressure into account. With this system (figure 2.9), a low controlled flow of air or nitrogen is maintained in a small diameter tube (restricted flow with little pressure loss) until the selected level is reached, i.e. must be below the lowest LW. At this level, the tube is connected to the upper section of a cylinder that is sealed on top and open at the bottom, and that also has a very small diameter opening at mid-height. The low constant flow of gas in the tube ensures a continuous release of bubbles from this small opening. Gas is released from a supply cylinder whose discharge pressure equalizes that associated with the water height and the atmospheric pressure.

The gas pressure is measured relative to the atmospheric pressure in the tide station using a mercury differential pressure gauge, and then transformed into water heights and recorded on a chart.

Bubbler tide gauges have major advantages, i.e. they are easy to maintain and do not require a stilling well. The main shortcoming is that waves upset their performance. Waves induce pressure surges, causing a rise in the water level in the cylinder, thus hampering air bubble release. Moreover, as noted with respect to tide staff readings, the skewed wave patterns, between crests and troughs, lead to errors in water height deduced from this pressure measurement. This problem can be overcome by increasing the air flow, but there is a risk of flow turbulence in the tube. When this happens, there may be pressure loss in the supply pipe, thus increasing the measurement error. A compromise must be found between the two types of errors induced by surface disturbance and pressure loss. Flow through the tube is harder to regulate when the pipe is long. In practice, it is thus recommended that the pipes be no longer than 200 m.

These tide gauges are often used in estuaries because they are easy to install. However, river flow can induce substantial vertical density variations. These data, without simultaneous vertical density distribution measurements, are clearly unsuitable for applications requiring high accuracy.

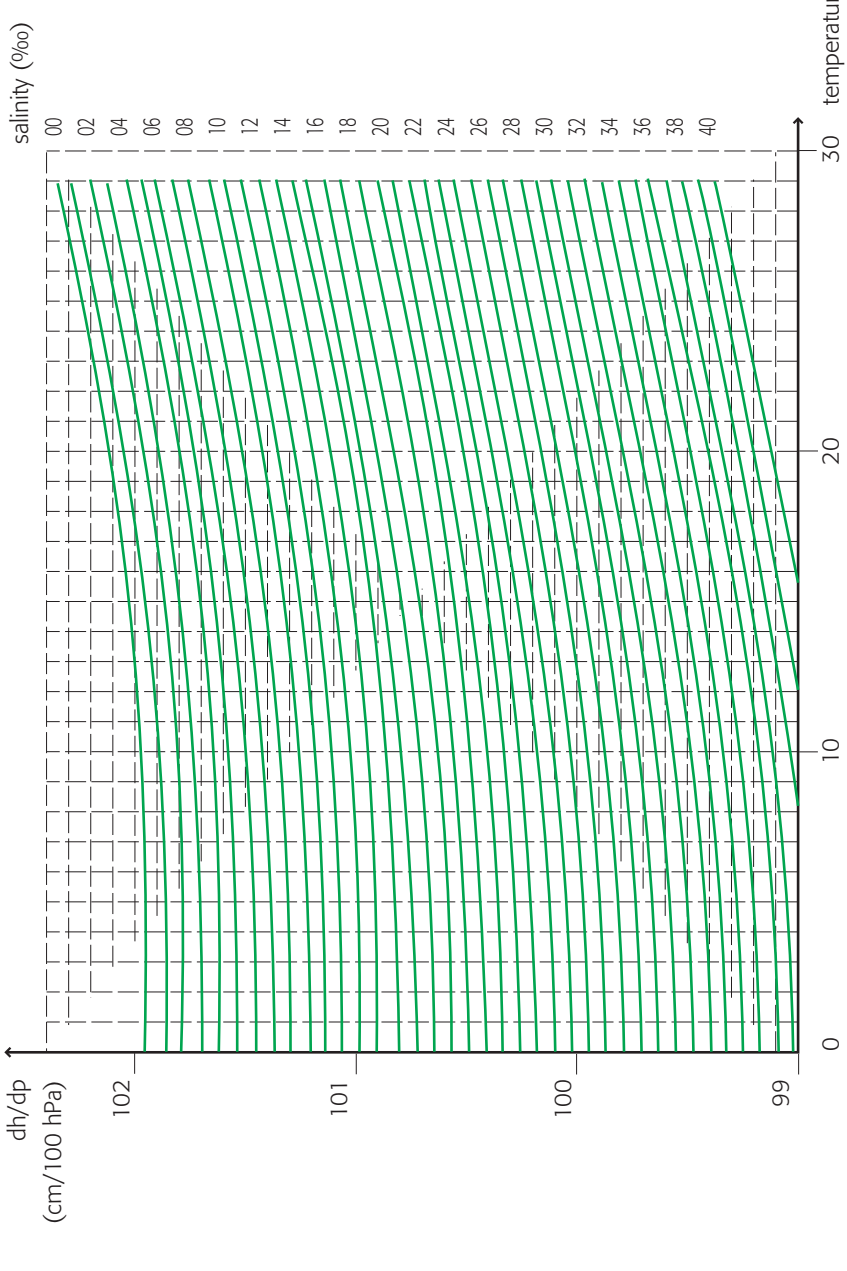

FIGURE 2.8: Nomogram showing water level variations (h in cm) relative to a hydrostatic pressure of 100 hPa (10^4 Pa) as a function of the temperature (T°C) and salinity (S), while considering sea water as incompressible and $g = 9.81$ m/s^2.

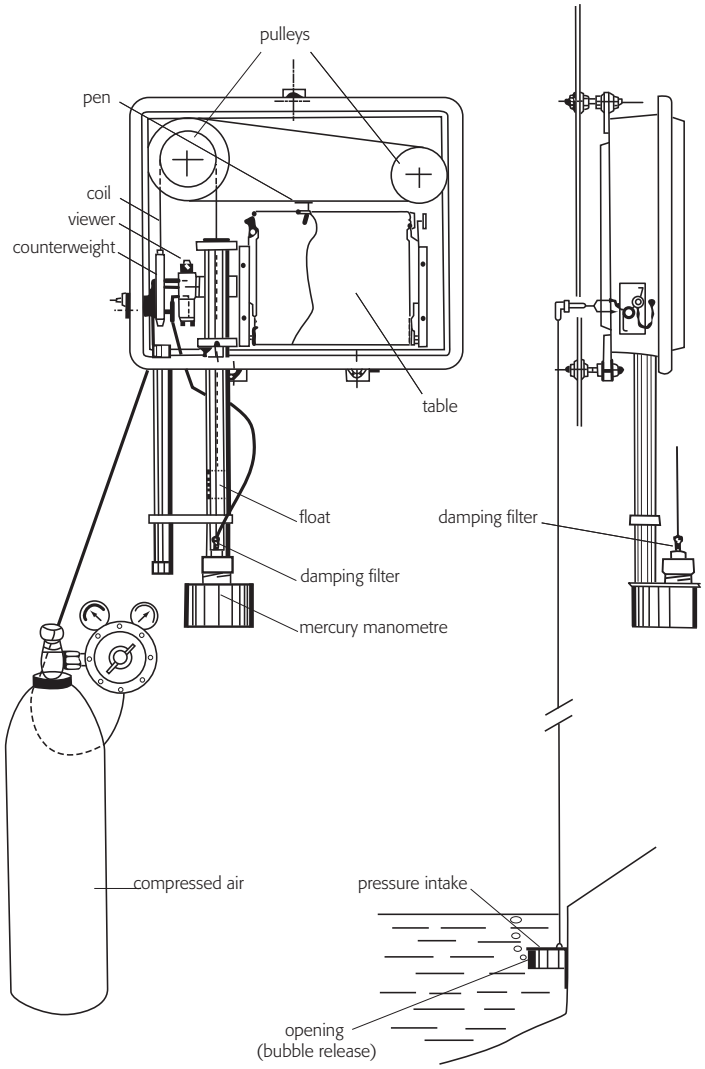

Figure 2.9: Bubbler tide gauge: easy to use, but very careful monitoring is required to obtain accurate data.

Apart from these operating restrictions (estuaries and sites with rough sea conditions), these tide gauges can supply high quality data when appropriately calibrated.

4.1.3 • Tide gauges with a strain gauge or piezoelectric quartz crystal sensor

Strain gauges and piezoelectric quartz crystal sensors are products of technological progress and are the main instruments currently used to measure pressure in deep ocean waters.

Electrical resistors of strain gauges function with both pressure and temperature, and their key feature is that they are inexpensive. These gauges are temperature sensitive and a supply voltage is required to measure their electrical resistance, so they have to be carefully calibrated and monitored and have a fully regulated electrical supply in order to be able to provide accurate pressure readings. These gauges can thus generate high quality measurement data only if they are managed by qualified organizations, otherwise this data may be useful for some applications but not for hydrographic or oceanographic purposes.

The most accurate tide gauges use a quartz crystal measurement sensor whose resonant frequency varies with the pressure applied. These sensors are used in bottom-mounted tide gauges as they provide millimetric resolution at depths of several hundreds of metres. They are also temperature sensitive, but to a lesser extent than strain gauges, and the temperature-dependent calibration coefficients can be considered to remain constant for several years. However, this correction being necessary, it is recommended that the gauge be used to record pressure directly. This is done by integrating a temperature sensor in tide gauges with a piezoelectric quartz crystal sensor, and an onboard software program corrects for the effects of temperature on the signal frequency.

Note, however, that with these sensors there is a slight calibration drift associated with the mean operational pressure, which is especially marked when the gauges are submerged in very deep waters. This fault cannot be modelled because it differs between sensors and depends on their deployment history. In practice, this slowly evolving defect does not impact height fluctuation measurements, but it hampers studies on very long-term variations in mean levels. This drift can be detected by performing a pre- and post-data recording calibration, but this defect cannot be corrected since it is not linear.

Advanced computer systems provide considerable data acquisition, logging and processing flexibility, so tide gauges submerged far offshore can thus remain completely self sufficient for several months or even years. This type of tide gauge is also quite easy to use. The instrument is integrated in a structure (figure 2.10) that includes ballast for submersion, a 'release-transponder' and a buoy which is large enough for the gauge to float without

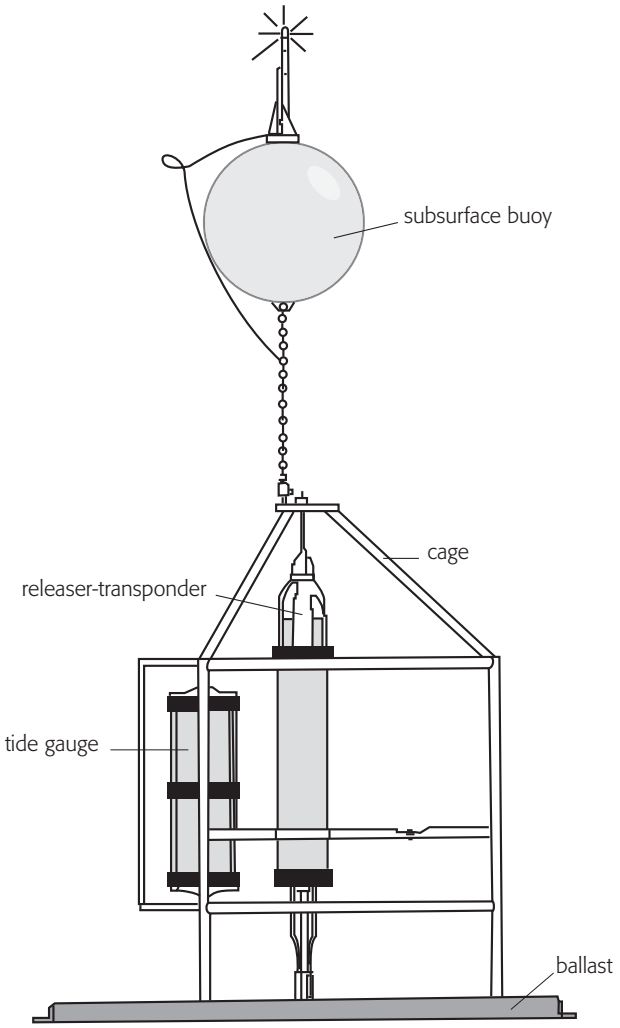

Figure 2.10: Bottom-mounted tide gauge: mooring structure with a release and recovery system. This self-sufficient tide gauge is very reliable and generates highly accurate data on deep sea pressure variations.

ballast. The buoy cannot be deformed by the pressure and is equipped with a light beacon and sometimes a radar reflector for surface tracking. The transponder facilitates tracking of the tide gauge offshore. The ballast is left on the sea bed after remote acoustic controlled release of the buoy supporting the cage (tide gauge and releaser) by an operator in a tide-gauge recovery vessel.

4.2 • Airborne depth sounder tide gauges

Advances in time measurement techniques and in acoustic and electromagnetic transducer design have made highly accurate distance measurement possible, but acoustic and electromagnetic wave propagation corrections are required. This progress has benefited tidal analysis and several new types of tide gauge have been developed for sea level measurement.

4.2.1 • Ultrasonic airborne depth sounder tide gauges

In the 1980s, the Naval Oceanographic Survey (NOS) carried out a study to determine ways to modernize the existing American tide-gauge network. This study revealed that remote airborne acoustic ranging possibly provided the best tradeoff between the sea level measurement quality and the overall network costs (including equipment acquisition, implementation and maintenance over a 20 year period). The accuracy requirements at the time were, however, not very demanding as compared to current requirements of the scientific community.

These ultrasonic tide gauges can be deployed without protection if there is sufficient transmission power, but they are often installed in stilling wells to provide weather protection, thus increasing their service life, while also ensuring a flat water surface to reduce sound reflection loss. Potential well wall irregularities can cause artifactual reflections. It is therefore recommended that sound beams be channelled through smooth rigid tubes, e.g. PVC. The many reflections on the walls of such tubes are not problematic as long as a careful calibration is performed, which is necessary in any case.

The measurement principle is simple, i.e. an above-surface transducer transmits a downward ultrasonic signal and then picks up the reflected signal. Given the sound velocity in air c, the measurement of the roundtrip wave transit time Δt gives the distance l, as well as the freeboard between the transducer and the surface: $l = c\Delta t/2$

Where d is the elevation of the base of an acoustic transponder in relation to a benchmark (usually the hydrographic datum), the sea level height h is expressed as:

$$h = \mathrm{d} - l = \mathrm{d} - (c \cdot \Delta t/2) \tag{2.3}$$

With sufficient accuracy for our applications, the wave velocity in air c (in m/s) is given by the following formula, where T is the temperature (°C), p_a is the atmospheric pressure (hPa) and w is the ambient relative humidity.

$$c = 331.2 \cdot [1 + 0.97 \cdot (w/p_a) + 1.9 \cdot 10^{-3}\mathrm{T}] \text{ m/s}$$

Experience has shown that relative humidity variations are negligible in a closed well as the air layer is almost completely water saturated. However, given $c_0 = 331.2$, we have:

$$\frac{\partial l}{\partial \mathrm{T}} = \frac{\partial l}{\partial c}\frac{\partial c}{\partial \mathrm{T}} = 1.9 \cdot 10^{-3}\frac{c_0}{c} l \approx 1.9.10^{-3} l \,\mathrm{m/°C}$$

As equation (2.3) gives $\partial h = -\partial l$, this corresponds to an opposite sign error on h of around 2 mm/m of the freeboard l and per °C.

Two methods are used to offset this marked temperature effect.

• The first involves setting a reflector under the probe at a known distance l_0. The wave velocity can be obtained directly on the basis of the transit time Δt_0 measurement (roundtrip of the signal between the transponder and reflector):

$$c = \frac{2\, l_0}{\Delta t_0} \quad \Rightarrow \quad l = l_0 \frac{\Delta t}{\Delta t_0}.$$

• The second involves placing a temperature sensor alongside the transducer and calculating the acoustic wave velocity as a function of the measured temperature.

Both of these methods have specific faults. The first gives the mean acoustic wave velocity between the probe and reflector, but not for the entire well freeboard. The second method is even less accurate because it only estimates the wave velocity at one level. Various experiments have shown, however, that variations in temperature and its vertical gradient in the stilling well induce substantial water level measurement errors, especially when diurnal heating of the tide gauge structure boosts the air temperature within the well. This phenomenon causes a temperature gradient that is not detected by the sensor. No really suitable solutions to this problem have been found.

Tailored tide gauges have been developed to fulfil different ocean dynamics research needs. These gauges have watertight temperature sensors at different levels, so they are not hampered by being submerged. However, these special tide gauges are not widely used because they are too expensive.

4.2.2 • Ultra-high frequency radar tide gauges

For distance measurement, these electromagnetic probes run on the same principal as the gauges discussed immediately above, except that they process electromagnetic rather than ultrasonic signals.

The advantage of using ultra-high frequency (UHF) tide gauges in coastal tide stations is that the wave velocity taken into account is constant (light

waves), so short-distance water height measurements are thus not susceptible to environmental variations. These tide gauges meet all accuracy requirements, but their installation and calibration is sometimes complicated. An above-water structure is nevertheless required to enable vertical pointing of the transducer. This structure does not have to be elaborate because the data logging and processing system may be remotely located and thus protected.

As the technology advances, these tide gauges are being developed at a fast pace to meet the rising need for accurate water height measurements, so they are being installed in many tide stations.

4.3 • Altimeters

The present book is not specifically aimed at boosting readers' insight into the tidal phenomenon worldwide, but it should still be noted that, thanks to the excellent quality of satellite-borne radar altimeters, highly accurate subdecimetre sea level measurements have now been obtained for more than two decades. The vertical distance between the satellite and the ocean surface is measured as described for the two previous systems. This involves measuring the roundtrip vertical transit time Δt of the electromagnetic pulse transmitted by the onboard radar and reflected back from the ocean surface (with the reflective surface being around 10 km^2 to 20 km^2). As this wave is transmitted over a long distance (around 2 000 km) through a heterogeneous environment – especially through the ionosphere and troposphere – its velocity c is not exactly the same as that of a light wave in a vacuum. Corrections for the ionospheric and tropospheric (water vapour) effects on the propagation of this electromagnetic pulse are therefore necessary. The vertical distance ζ between the satellite and the ocean surface is:

$$\zeta = c\Delta t/2$$

Since, by orbital satellite tracking, its altitude ζ_e (figure 2.11) can be determined in a certain geocentric reference line, the height of the ocean surface h_e in the same reference line is the difference between the two levels:

$$h_e = \zeta - \zeta_e$$

Different techniques are used for accurate satellite positioning, such as laser ranging, GPS and the DORIS system from stations located beneath the satellite track. These stations are positioned with centimetre accuracy with respect to consistent station marks within the International Terrestrial Reference System (ITRS). The sea level is determined relative to these reference marks.

The correspondence between this altimetric sea level measurement and conventional references (benchmarks, mean level, chart datum) raises the issue of the relative positions of these different references. Orbital tracking stations, especially for GPS and Doris, are thus set up in the vicinity of coastal tide stations.

The altimeter is calibrated by comparing the satellite water level reading with the tide graph reading with reference to the same datum. There is a problem, however, satellite altimetry data are only suitable beyond a certain distance from the coast (around 10-20 km), for at least two reasons. The first is technical, i.e. reflection of the altimetric signal is upset by the simultaneous presence of earth and water, while the second is associated with the rapid variation in the geoid shape at the sea-land interface. Interpretation of the error between the coastal tide graph reading and the first reliable satellite reading is not easy without prior knowledge on the local geoid shape.

Onboard satellite altimeters measure the sea height at specific points over an interval of a few days. The satellite orbit tracks cross the Equator at an angle of around 60° and form a regular network with a grid of a few hundred kilometres, which varies according to the latitude. Data for one point are thus only available at time intervals that are much longer than basic tide

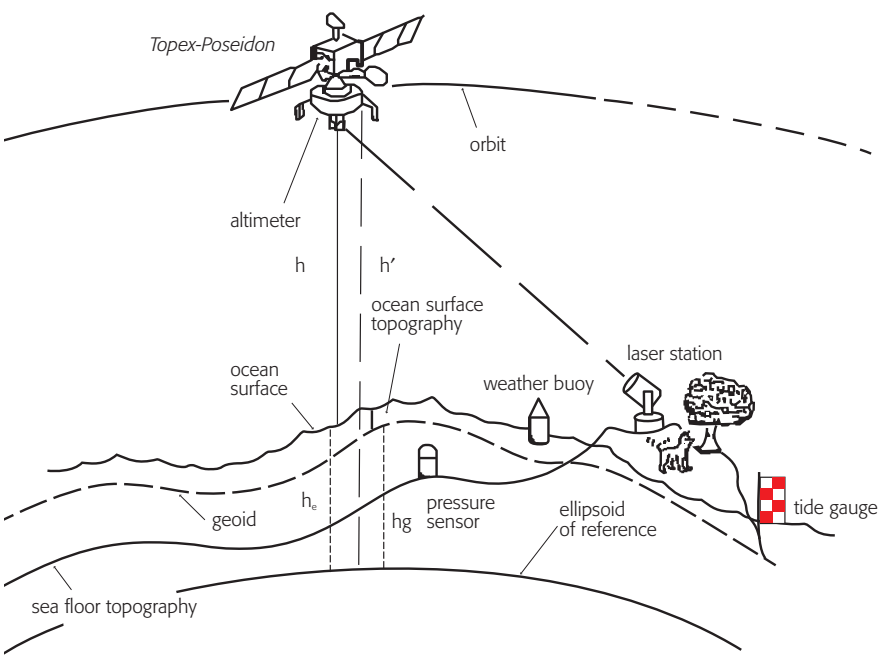

Figure 2.11: Satellite altimetry measurement of the ocean surface.

intervals. These constraints generate many data processing issues, especially the problem of multiple tidal spectrum aliasing distortion. The lack of adequate temporal sampling at a fixed point could be partially overcome by taking seamless spatial sampling throughout the orbit and readings at track intersection points into account using tailored analysis methods.

Despite these problems, this remote sensing technique generates invaluable information, with an accuracy of a few centimetres, for worldwide geophysical and meteo-oceanic research. Radar altimetry data can thus be used for the determination of several parameters such as the marine geoid, wave height and wind speed, as well as the discrepancy between the ocean surface and the geoid.

This ocean surface topography (relative to the geoid), which is especially useful for determining surface currents, is only relevant after a highly accurate tide correction, especially with respect to the altimetric variability. In the light of these advances in satellite altimetry, the scientific community has renewed its interest in tide measurement.

III

Tide-generating force and potential

The heuristic approach of Newton and Laplace to respectively describe the tide-generating force and potential is not covered in this chapter. Instead we use contemporary mathematical and mechanical formulations to quantify these factors–calculation of the tide-generating force with its geometric construction (Proctor's rule), along with expansion of the potential in Legendre polynomial series and breakdown into 'tidal species' as defined by Laplace.

1 • Tide-generating force

The term 'force' very often turns up in the proofs presented in this section. To avoid any misunderstandings, this term should be taken as meaning the acceleration of a liquid object M per unit mass. After formulating the force exerted by a celestial body A, Proctor's geometric construction provides an evaluation of the respective actions of the two tide-generating astronomical bodies (Moon and Sun), along with the magnitude of their ratio.

1.1 • Calculation of the tide-generating force exerted by a celestial body

The tide-generating force formula presented hereafter represents the action of a single celestial body, i.e. the Moon or Sun, with the total force of course being the sum of both.

Let us consider two orthonormal reference frames:

• an inertial (absolute) reference frame having the centre of mass of the Sun-Earth-Moon system as origin, e.g. an ecliptic reference frame (see Appendix A); this reference frame is not absolutely inertial, but we may

consider it as such because no dynamic events resulting from its acceleration have been detected to date with respect to any terrestrial movements;

• the second is linked with the Earth and revolves with it (relative reference frame), it has the centre of mass T as origin: or, for instance, the equatorial reference frame (having the meridian of point M as origin).

As ocean tides occur on Earth, the acceleration of object M thus has to be calculated in this relative reference frame.

Where $\overrightarrow{\omega_T}$ is the vector of the Earth's northward-oriented rotation parallel to the polar axis (clockwise west-to-east rotation). Based on standard conventions, we have:

• in the absolute reference frame (index S), the absolute velocity and acceleration vectors for points T and M, respectively defined by:

$$\frac{d_S(\overrightarrow{ST})}{dt} = \overrightarrow{v_S}(T) \qquad \text{and} \qquad \frac{d_S^2(\overrightarrow{ST})}{dt^2} = \overrightarrow{\gamma_S}(T),$$
$$\frac{d_S(\overrightarrow{SM})}{dt} = \overrightarrow{v_S}(M) \qquad \text{and} \qquad \frac{d_S^2(\overrightarrow{SM})}{dt^2} = \overrightarrow{\gamma_S}(M)\ ;$$

• and in the relative reference frame (index T), the relative velocity and acceleration vectors for point M, defined by:

$$\frac{d_T(\overrightarrow{TM})}{dt} = \overrightarrow{v_T}(M) \qquad \text{and} \qquad \frac{d_T^2(\overrightarrow{TM})}{dt^2} = \overrightarrow{\gamma_T}(M).$$

Derivation of the vectorial relation $\overrightarrow{TM} = \overrightarrow{SM} - \overrightarrow{ST}$ with respect to time t in the absolute reference frame, gives:

$$d_S(\overrightarrow{TM})/dt = \overrightarrow{v_S}(M) - \overrightarrow{v_S}(T) \tag{3.1a}$$

Based on the velocity law in the relative reference frame, this relation (3.1a) becomes:

$$d_S(\overrightarrow{TM})/dt = \overrightarrow{v_T}(M) + \overrightarrow{\omega_T} \wedge \overrightarrow{TM} \tag{3.1b}$$

Considering that $\overrightarrow{\omega_T}$ is constant, thus not time-dependent, and by deriving the previous equation (3.1b) with respect to time t, we obtain:

$$d_S\overrightarrow{v_T}(M)/dt = \overrightarrow{\gamma_T}(M) + \overrightarrow{\omega_T} \wedge \overrightarrow{v_T}(M) \tag{3.2}$$
$$= \overrightarrow{\gamma_T}(M) + \overrightarrow{\omega_T} \wedge [\overrightarrow{v_T}(M) + \overrightarrow{\omega_T} \wedge \overrightarrow{TM}] \tag{3.3}$$

By deriving the same equation (3.1a) as a function of time t, and taking relation (3.3) into account, we get:

$$\overrightarrow{\gamma_S}(M) - \overrightarrow{\gamma_S}(T) = \overrightarrow{\gamma_T}(M) + \overrightarrow{\omega_T} \wedge \overrightarrow{v_T}(M) + \overrightarrow{\omega_T} \wedge [\overrightarrow{v_T}(M) + \overrightarrow{\omega_T} \wedge \overrightarrow{TM}]$$

The acceleration $\overrightarrow{\gamma_T}(M)$ of object M in the terrestrial reference frame could thus be expressed as:

$$\overrightarrow{\gamma_T}(M) = \overrightarrow{\gamma_S}(M) - \overrightarrow{\gamma_S}(T) - 2\overrightarrow{\omega_T} \wedge \overrightarrow{v_T}(M) - |\overrightarrow{\omega_T}|^2\overrightarrow{RM} \qquad (3.4)$$

where point R represents the projection of point M on the polar axis (figure 3.1).

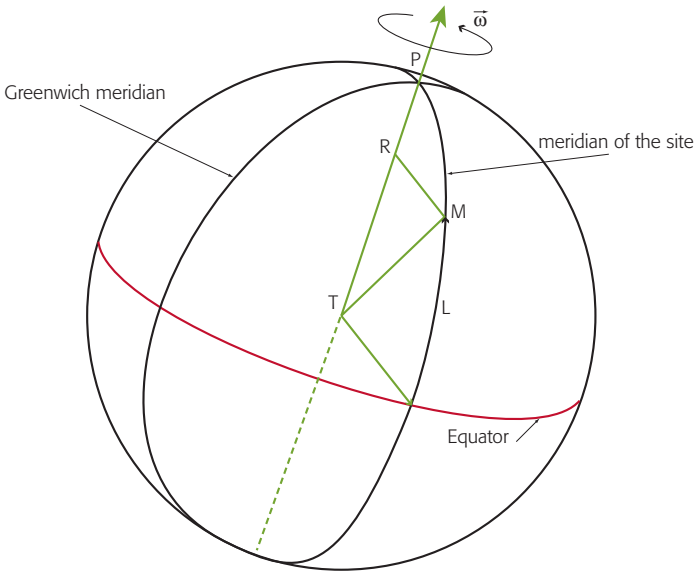

FIGURE 3.1: The terrestrial reference frame (relative reference frame), where T is the Earth's centre, M is the object of unit mass at latitude L, and R is the projection of M on the polar axis.

In relation (3.4):

• the term $\overrightarrow{\omega_T} \wedge (\overrightarrow{\omega_T} \wedge \overrightarrow{TM}) = |\overrightarrow{\omega_T}|^2\overrightarrow{RM}$ is the centrifugal force due to the Earth's rotation applied at point M;

• component $2\overrightarrow{\omega_T} \wedge \overrightarrow{v_T}(M)$ represents the so-called acceleration of Coriolis which deviates (to the right in the Northern Hemisphere and to the left in the South) particle M at velocity $\overrightarrow{v_T}(M)$;

• acceleration $\overrightarrow{\gamma_S}(T)$ is the result of the sum of external forces applied on T–with the only significant ones being the gravitational forces exerted by each tide-generating celestial body. We will first investigate the action of a single celestial body, so acceleration $\overrightarrow{\gamma_S}(T)$ will here be assimilated to the force $\overrightarrow{F}_{A/T}$ exerted by celestial body A on the unit mass object in T.

According to the law of gravitational attraction:

$$\overrightarrow{\gamma}_{S}(T) \equiv \overrightarrow{F}_{A/T} = k\frac{m_A}{r_A^2}\overrightarrow{u} \tag{3.5}$$

where:

k is the universal gravitational constant

m_A is the mass of celestial body A

r_A is the distance TA of the centres (Earth-celestial body)

$\overrightarrow{u}$ is the unit vector of axis $\overrightarrow{TA}$.

Finally, the term $\overrightarrow{\gamma_S}(M)$ is the sum of external forces applied to object M of unit mass. By adopting the acceleration-force assimilation, these forces are:

$\overrightarrow{\nabla}\, p(M)/\rho$: is the pressure gradient per mass unit, where ρ is the density and $p(M)$ is the pressure in M, with $\overrightarrow{\nabla}$ representing the 'gradient' vectorial operator of components $(\partial/\partial x, \partial/\partial y, \partial/\partial z)$ in a Cartesian system;

$\overrightarrow{F}_f(M)$: represents friction forces that are cancelled out at $\overrightarrow{v_T}(M)$;

$\overrightarrow{g}(M) = -g\,\overrightarrow{\zeta}(M)$: is the gravitational force exerted by the Earth, where $\overrightarrow{\zeta}$ is the unit vector of the ascending vertical in M ($\overrightarrow{TM} = a_T\overrightarrow{\zeta}$, with a_T being the Earth's radius); where m_T is the mass of the Earth, and the value of gravity g expressed by:

$$g = k\frac{m_T}{a_T^2}; \tag{3.6}$$

$\overrightarrow{F}_{A/M}$: is the gravitational force exerted by celestial body A on M.

The sum of forces in M is thus expressed by:

$$\overrightarrow{\gamma}_{S}(M) = \frac{\overrightarrow{\nabla}\, p(M)}{\rho} + \overrightarrow{F}_f(M) + \overrightarrow{g}(M) + \overrightarrow{F}_{A/M}$$

Considering an object of unit mass M at rest, we obtain velocity $\overrightarrow{v_T}(M)$, which is of course nil, thus voiding the Coriolis force $2\overrightarrow{\omega_T} \wedge \overrightarrow{v_T}(M)$ and the friction forces $\overrightarrow{F}_f(M)$, as well as the horizontal constituents of the fluid pressure gradient. According to Archimedes principle (hydrostatic pressure), the vertical constituent of the pressure gradient is balanced by 'ordinary gravity' $\overrightarrow{g}(M) - |\overrightarrow{\omega}_T|^2\overrightarrow{RM}$, including the centrifugal force associated with the Earth's rotation.

By assimilating the acceleration $\overrightarrow{\gamma_T}(M)$ with the force $\overrightarrow{F_A}(M)$ on object M of unit mass, equation (3.4) becomes:

$$\overrightarrow{F_A}(M) = \overrightarrow{F}_{A/M} - \overrightarrow{F}_{A/T} \tag{3.7}$$

Equation (3.7) expresses the 'tide-generating force' $\overrightarrow{F}_A(M)$ exerted by celestial body A at point M–it is the difference in gravitational attractions exerted by the celestial body at point M (constituent $\overrightarrow{F}_{A/M}$) and at the Earth's centre T (constituent $\overrightarrow{F}_{A/T}$).

Note that each of these two constituents defines a force field of a different nature:

• Force $\overrightarrow{F}_{A/T}$, the tractive force in the Earth reference frame, is identical at all points M and thus defines a force field of constant intensity in the direction of axis $\overrightarrow{TA}$ of unit vector $\overrightarrow{u}$.

• However, $\overrightarrow{F}_{A/M}$, which is the attractive force exerted by celestial body A at all points M on Earth, is a function of the position of the point. This constituent which, for each point, is directed towards axis $\overrightarrow{MA}$ of unit vector $\overrightarrow{v}$, thus defines a radial force field of variable intensity. Where Δ represents the distance MA, this force is expressed according to the law of gravitational attraction by a relation equivalent to (3.5) for point T:

$$\overrightarrow{F}_{A/M} = \frac{km_A}{\Delta^2}\overrightarrow{v}.$$

Equation (3.7), which gives the tide-generating force exerted by a celestial body, can thus be expressed by:

$$\overrightarrow{F}_A(M) = km_A\left(\frac{\overrightarrow{v}}{\Delta^2} - \frac{\overrightarrow{u}}{r_A^2}\right) \tag{3.8}$$

Note that by this formulation the force field accepts $\overrightarrow{TA}$ as axis of revolution. Hereafter we will look at how a very simple geometric construction, known as 'Proctor's rule' (after the English astronomer, 1837-1888), can be implemented to come up with a vector that is proportional to the force, and to thus deduce the magnitude that will be expressed when gravity g is set at unity.

1.2 • Geometric construction of force–Proctor's rule

Where point T is the Earth's centre, let us consider the vertical plane of celestial body A at point M with θ being the geocentric zenithal distance (figure 3.2).

Figure 3.3 clearly illustrates Proctor's construction in the same plane as shown in figure 3.2.

B is the intercept of axis $\overrightarrow{TA}$ with circumference centre point A and radius AM. The line parallel to TM from point B intersects AM at C.

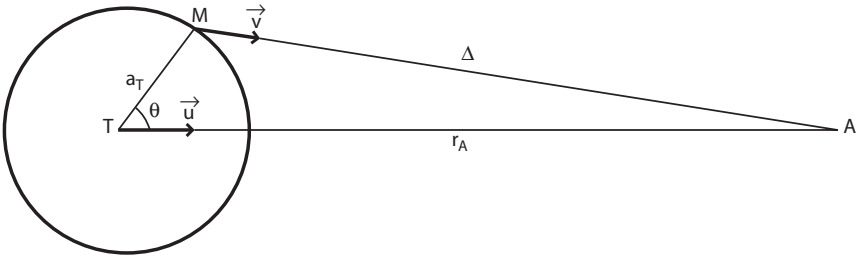

Figure 3.2: Vertical plane of celestial body A at point M, where a_T is the Earth's radius and θ is the geocentric zenithal distance of the celestial body.

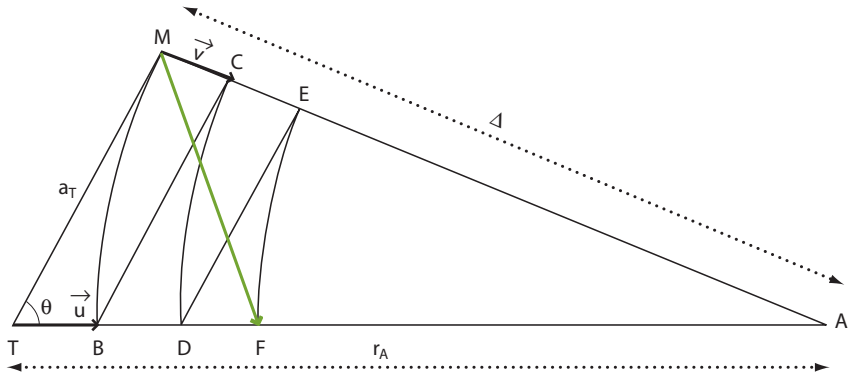

Figure 3.3: Proctor's construction: the tide-generating force is proportional to vector $\overrightarrow{MF}$.

Let us use the same method to construct the two successive figures BCD and DEF homothetic to TMB. This gives the following equalities: $r_A = AT$; $\Delta = AM = AB$; $AC = AD$; and $AE = AF$.

When Thales' theorem is applied while taking these equalities into account, we get:

- for triangles ATM and ABC:

$$\frac{AC}{AB} = \frac{AM}{AT} \Rightarrow AC = \frac{\Delta^2}{r_A};$$

- for triangles ATM and ADE:

$$\frac{AE}{AD} = \frac{AM}{AT} \Rightarrow AE = \frac{\Delta^3}{r_A^2}.$$

Since AF = AE, vector $\overrightarrow{\mathrm{FA}}$ is expressed by:

$$\overrightarrow{\mathrm{FA}} = \frac{\Delta^3}{r_\mathrm{A}^2}\overrightarrow{u}\,.$$

The vectorial relation $\overrightarrow{\mathrm{MF}} = \overrightarrow{\mathrm{MA}} - \overrightarrow{\mathrm{FA}}$ gives rise to:

$$\overrightarrow{\mathrm{MF}} = \Delta^3\left(\frac{\overrightarrow{v}}{\Delta^2} - \frac{\overrightarrow{u}}{r_\mathrm{A}^2}\right).$$

Vector $\overrightarrow{\mathrm{MF}}$ is thus proportional to the tide-generating force $\overrightarrow{\mathrm{F}}_\mathrm{A}(\mathrm{M})$ given by (3.8). This force can also be expressed by the so-called Proctor's rule equation:

$$\overrightarrow{\mathrm{F}}_\mathrm{A}(\mathrm{M}) = \frac{km_\mathrm{A}}{\Delta^3}\overrightarrow{\mathrm{MF}}. \tag{3.9}$$

When celestial body A is considered at infinity, directions TA and MA become parallel, thus simplifying this construction (figure 3.4). In this vertical plane of the celestial body, let us consider an orthonormal system with T as origin and $\overrightarrow{\mathrm{TA}}$ as x-axis, then the x-axis of point F, i.e. the projection of M on this axis, is equal to threefold that of point B. This approximation, which is often accepted for the Moon, also *a fortiori* applies for the Sun.

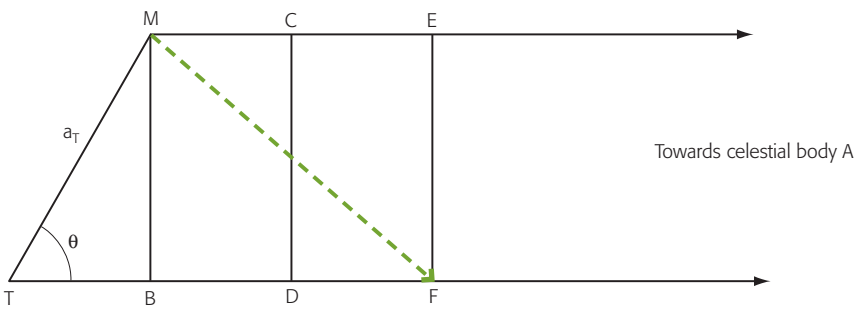

FIGURE 3.4: Simplification of the construction of vector $\overrightarrow{\mathrm{MF}}$ where the celestial body is at infinity: vector $\overrightarrow{\mathrm{TF}}$ is threefold greater than $\overrightarrow{\mathrm{TB}}$, and B is the projection of point M on $\overrightarrow{\mathrm{TA}}$.

In the orthonormal reference frame described above, the matrix representations of constituents of $\overrightarrow{\mathrm{TM}}$ and $\overrightarrow{\mathrm{MF}}$ are respectively defined in equation 3.10:

$$\overrightarrow{\mathrm{TM}} \Rightarrow \begin{bmatrix} a_\mathrm{T} \cos\theta \\ a_\mathrm{T} \sin\theta \end{bmatrix} \qquad \overrightarrow{\mathrm{MF}} \Rightarrow \begin{bmatrix} 2a_\mathrm{T} \cos\theta \\ -a_\mathrm{T} \sin\theta \end{bmatrix} \tag{3.10}$$

The modulus of $\overrightarrow{\mathrm{MF}}$ is readily determined, and is equal to:

$$\mathrm{MF} = a_\mathrm{T}\sqrt{1 + 3\cos^2\theta}.$$

In an orthonormal reference frame, let ξ_{MF} be the vertical constituent (positively oriented towards the zenith) and η_{MF} the horizontal constituent of the $\overrightarrow{\mathrm{MF}}$ vector:

$$\begin{aligned} \xi_{\mathrm{MF}} &= |\mathrm{TF}| \cos\theta - a_\mathrm{T} = a_\mathrm{T}\left(3\cos^2\theta - 1\right) \\ \eta_{\mathrm{MF}} &= |\mathrm{TF}| \sin\theta = \frac{3}{2} a_\mathrm{T} \sin 2\theta \end{aligned} \tag{3.11}$$

With approximation $\Delta \approx r_\mathrm{A}[1 - (a_\mathrm{T}\cos\theta / r_\mathrm{A})] \approx r_\mathrm{A}$ and with equation (3.6) representing g, Proctor's rule (3.9) may be applied to evaluate modulus $\mathrm{F_A(M)}$ of the tide-generating force of celestial body A at point M, or:

$$\mathrm{F_A(M)} \approx g \frac{m_\mathrm{A}}{m_\mathrm{T}} \left(\frac{a_\mathrm{T}}{r_\mathrm{A}}\right)^3 \sqrt{1 + 3\cos^2\theta} \tag{3.12}$$

The distance r_A from the Earth-celestial body centre points is not constant since the orbit is elliptical. The mean distance r_0 can be introduced in order to determine the parallax i_A of celestial body A, whose value is around unity:

$$i_\mathrm{A} = \frac{r_0}{r_\mathrm{A}} \tag{3.13}$$

Then:

$$\chi_\mathrm{A} = \frac{m_\mathrm{A}}{m_\mathrm{T}} \left(\frac{a_\mathrm{T}}{r_0}\right)^3 \tag{3.14}$$

Modulus $\mathrm{F_A(M)}$ of the tide-generating force could first be formulated as:

$$\mathrm{F_A(M)} \approx g \chi_\mathrm{A} i_\mathrm{A}^3 \sqrt{1 + 3\cos^2\theta} \tag{3.15}$$

The same result (see Appendix B) could be obtained from the tide-generating potential, expressed in Legendre polynomial series and restricted to its first term in $\mathrm{P_2}(\cos\theta)$.

The characteristics of this force may also be assessed through equations (3.12) and (3.15).

1.3 • Main features of the tide-generating force

These relations, which are obtained by Proctor's rule (3.9), show:

1. that the tide-generating force is proportional to the mass of celestial body m_A and the reciprocal of the cube of its distance r_A;

2. that its spatial distribution at a given time revolves around axis $\overrightarrow{TA}$ as it is a function of the geocentric zenithal distance θ of celestial body A with the term $\sqrt{1 + 3\cos^2\theta}$, which is never cancelled out at the Earth's surface and whose value ranges from 1 to 2.

Note also that the modulus of the horizontal constituent of this force is proportional to the η_{MF} modulus given by (3.11). This modulus varies as $\sin 2\theta$ and is maximal for θ values of 45° and 135° and nil for $\theta = 0°$ and 90°, i.e. on the $\overrightarrow{TA}$ axis and on the entire great circle upon which the celestial body is visible on the horizon.

At a given time, this rotational force field (around $\overrightarrow{TA}$) gives a distribution on the Earth's surface that may be studied along a parallel of latitude L where rising and setting of the celestial body (on the horizon) can be observed during the day (figure 3.5). On this parallel, points M and M′ are respectively on the upper and lower meridians of the celestial body. The corresponding moduli $\overrightarrow{F}$ and $\overrightarrow{F'}$ reach relative maxima. In figure 3.5, latitude L is the same sign as the declination δ, so the upper force maximum is obtained in M. The maximum force is in M′ if the L and δ values have opposite signs. When the Equator is the considered parallel, or when the declination of the celestial body is nil, the two forces $\overrightarrow{F}$ and $\overrightarrow{F'}$ have identical moduli.

On the 'celestial body on the horizon' great circle, the horizontal constituent is nil, so the corresponding tide-generating force is directed towards the Earth's centre and the minimum absolute amplitude for the considered celestial body is reached. This is the case for force $\overrightarrow{F''}$ applied in M″, at the intersection of this circle and the visible part of the parallel of latitude L in figure 3.5.

Point P′, at the intersection of the meridian of the celestial body and the great circle of the 'celestial body on the horizon', defines latitude L_N of the northern polar circle of celestial body A for declination δ. In figure 3.5, the northern polar circle is at $\delta + L_N = 90°$ whereas latitude L_S of the southern polar circle is $\delta - |L_S| = 90°$ (southern latitudes are negative numbers). At all parallels whose latitude L fulfils condition $|\delta| + |L| > 90°$, the celestial body can no longer be seen on the horizon. The minimum absolute force is no longer reached, and the secondary maximum force dissipates to merge with the relative minimum on this parallel.

The terms $\sqrt{1+3\cos^2\theta}$ and $(i_A)^3$ are around unity. When gravity g is taken for the unit of force, expression (3.15) shows that the magnitude of the tide-generating force of each celestial body is represented by its parameter χ_A defined by relation (3.14), where r_0 is the mean Earth-celestial body distance. Where the Earth's mass is $m_T = 5.98 \times 10^{24}$ kg and its equatorial radius is $a_T = 6.378 \cdot 10^3$ km, we obtain the following table:

Celestial body	m_A/m_T	a_T/r_0	$(a_T/r_0)^3$	χ_A
Moon	$1.23 \cdot 10^{-2}$	$1.66 \cdot 10^{-2}$	$4.57 \cdot 10^{-6}$	$5.62 \cdot 10^{-8}$
Sun	$3{,}33 \cdot 10^{5}$	$4.26 \cdot 10^{-5}$	$7.75 \cdot 10^{-14}$	$2.58 \cdot 10^{-8}$

The fraction of the tide-generating force due to the Moon is thus slightly more than twofold greater (exactly 2.18-fold) than that due to the Sun. Despite its small mass, the Moon has a greater tide-generating influence because of its close relative proximity to the Earth, with a power law index of 3 according to the a_T/r_A ratio.

The lunisolar impact on a particle of unit mass is thus very slight relative to the gravity $g \approx 10\ \mathrm{m \cdot s^{-2}}$, with a maximum of around:

$$10^{-7} \cdot g \approx 10^{-6}\ \mathrm{m \cdot s^{-2}} = 1\ \mu\mathrm{m \cdot s^{-2}}$$

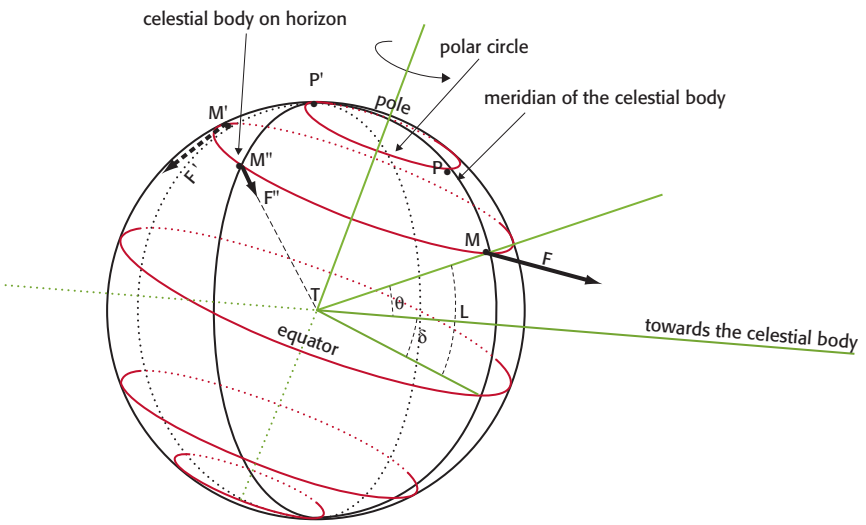

Figure 3.5: Spatial distribution of the tide-generating force associated with celestial body A at a given time on the parallel of latitude L, at points M, M′ and M″ (see explanations in text).

The vertical constituent of this force is therefore negligible with respect to g. Only the horizontal constituent can set liquid particles in motion. It is quite astonishing that such low acceleration has been noted to have a major role in the oceanic tidal phenomenon.

2 • Tide-generating potential

For many problems involving vector fields, substantial simplifications are possible and greater physical insight may be gained into the phenomenon when there is a likelihood that a potential exists (see Appendix B). In the previous section, we analysed the spatial distribution of the tide-generating force over the Earth's surface for a given time and celestial body. This distribution was shown to be representative of a force field where the direction $\overrightarrow{TA}$ is the axis of rotation of the system.

For each celestial body, the tide-generating force is clearly described by the difference between two elementary forces, i.e. a radial force that is dependent on the application point and a force of constant direction and intensity. We will see that these elementary constituents stem from so-called 'meridian' potential fields (see Appendix B) of axis $\overrightarrow{TA}$. These fields are expressed in Legendre polynomial series as a function of the cosine of angle θ. For a given celestial body, the difference between these two elementary fields, which have the same axis of revolution, defines the tide-generating potential.

2.1 • Elementary force potentials associated with celestial bodies

Oceanic tides occur on Earth so an associated reference frame is required. This includes the Txyz orthonormal frame (figure 3.6) with the Earth's centre T as origin and the vertical plane of celestial body A at point $M_0(x_0, y_0, 0)$ serving as the Txy plane. The axis of revolution of force field $\overrightarrow{TA}$ is selected as the x-axis (unit vector $\overrightarrow{u}$), with point B here being the projection of M_0 on this axis.

When $\alpha = a_T/r_A$, coordinates of M_0 and the matrix representation of the constituents of vector $\overrightarrow{M_0A}$ can be formulated as:

$$M_0 \left| \begin{array}{l} x_0 = r_A \alpha \cos\theta \\ y_0 = r_A \alpha \sin\theta \\ z_0 = 0 \end{array} \right.$$

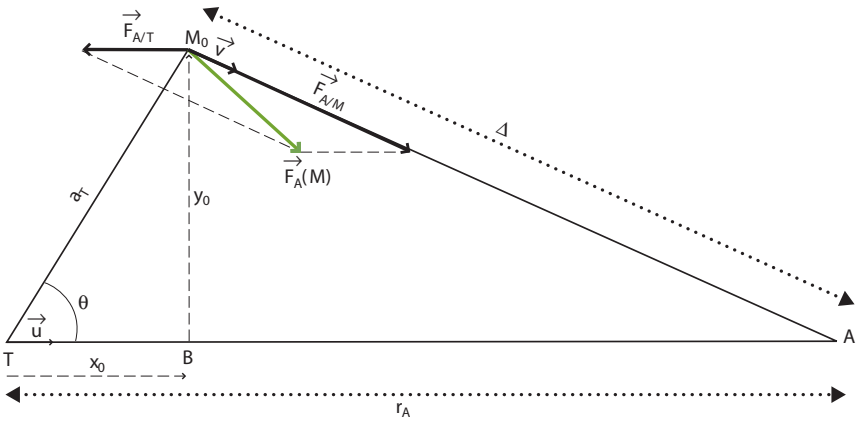

Figure 3.6: Orthonormal reference frame Txyz, where Txy is the TAM$_0$ plane of the vertical of celestial body A at point M$_0(x_0, y_0, 0)$, with Tx according to $\overrightarrow{\text{TA}}$; the T$z$ axis is not shown.

and

$$\overrightarrow{\text{M}_0\text{A}} \Rightarrow \begin{bmatrix} (r_\text{A} - x_0) \\ (0 - y_0) \\ 0 \end{bmatrix} = \begin{bmatrix} r_\text{A}(1 - \alpha\cos\theta) \\ -r_\text{A}\alpha\sin\theta \\ 0 \end{bmatrix} \tag{3.16}$$

In the Txyz reference frame, modulus Δ of $\overrightarrow{\text{M}_0\text{A}}$ can be expressed by:

$$\Delta = r_\text{A}\sqrt{1 - 2\alpha\cos\theta + \alpha^2} \tag{3.17}$$

This expression (3.17) obviously applies for all points M(x, y, z) of the Earth's intersection with a sphere of radius Δ, i.e. the circumference of radius $y_0 = a_\text{T}\sin\theta$, centre B and where the $\overrightarrow{\text{TA}}$ axis is taken as the axis of revolution.

Recall that the tide-generating force $\overrightarrow{\text{F}}_\text{A}(\text{M})$ associated with celestial body A and affecting all points M(x, y, z) in the Earth's environment is the difference between two elementary constituents, i.e. the attractive force $\overrightarrow{\text{F}}_{\text{A/M}}$ of celestial body A on M and the tractive force $\overrightarrow{\text{F}}_{\text{A/T}}$ of the reference frame associated with the Earth (force equal to the attraction of celestial body A on T).

The analytical expression of both of these components is regular, i.e. definite, non-null, bounded, continuous and derivable at least once. Their spatial distribution gives rise to lines of force with a meridian structure in relation to the axis of revolution $\overrightarrow{\text{TA}}$, which in turn serves as the polar axis

for the two fields defined by these distributions. Moreover, force $\overrightarrow{F}_{A/T}$ has a constant modulus and direction and the second force $\overrightarrow{F}_{A/M}$ has a radial direction $\overrightarrow{MA}$, and its modulus is a function of θ. The rotational factor is thus nil, which is a prerequisite for all of these elementary forces to be derived from a potential. Hence there are two meridian fields with the same axis of revolution $\overrightarrow{TA}$. The difference between them defines the tide-generating potential corresponding to the considered celestial body. This potential is therefore also defined by a meridian field of the axis $\overrightarrow{TA}$.

2.1.1 • Expression of the potential of $\overrightarrow{F}_{A/M}$ – the attractive force exerted by celestial body A on all points M of unit mass

This force defines the 'sink field' (gravitational forces) created by the celestial body. All spheres centred on A are equipotential surfaces. We can verify that the flux Φ of this radial force through each of these spheres is constant (null divergence) by:

$$\Phi = 4\pi\Delta^2 F_{A/M}$$

with

$$F_{A/M} = km_A/\Delta^2 \Rightarrow \Phi = 4\pi km_A$$

where k is the universal gravitational constant and m_A is the mass of the celestial body. In a positive sense from M to A, the potential of all points M is thus:

$$U_{(r)}(M) = km_A/\Delta \tag{3.18}$$

where index (r) indicates that it is a field of radial lines of force (the celestial body is on the right side of the equation as a subscript to the mass). Considering the Δ value given by equation (3.17), equation (3.18) can be expressed in the neighbourhood of T as a function of the potential $U_{(r)}(T)$ and of a Legendre polynomial series. Since condition $|2\alpha\cos\theta - \alpha^2| < 1$ is satisfied, the expression deduced from (3.17) giving r_A/Δ represents the Legendre polynomial tide-generating function (see Appendix B), or:

$$r_A/\Delta = 1/\sqrt{1 - 2\alpha\cos\theta + \alpha^2} = \sum_{n=0}^{n\to\infty} \alpha^n P_n(\cos\theta) \tag{3.19}$$

When $U_{(r)}(T)$ designates $U_A(T)$, then:

$$U_A(T) \equiv U_{(r)}(T) = km_A/r_A \tag{3.20}$$

The meridian attractive potential $U_{(r)}(M)$ of celestial body A in M as a function of the T potential and the geocentric zenithal distance θ is thus expressed as:

$$U_{(r)}(M) = U_A(T) \sum_{n=0}^{n\to\infty} \alpha^n P_n(\cos\theta) \tag{3.21}$$

2.1.2 • Expression of the potential of $\overrightarrow{F}_{A/T}$ – the tractive force of the reference frame associated with Earth (equal to the attraction of celestial body A at the Earth's centre T

This second elementary force is identical at all M points in the Earth's environment. It is always parallel to the axis of revolution $\overrightarrow{TA}$ and thus defines a meridian field of parallel force lines. This field is represented by (p), so $U_{(p)}(M)$. In the Txyz reference frame, the matrix representation of these constituents is:

$$\overrightarrow{F}_{A/T} \Rightarrow \begin{bmatrix} F_{A/T} \\ 0 \\ 0 \end{bmatrix} = \begin{bmatrix} km_A/r_A^2 \\ 0 \\ 0 \end{bmatrix} = \begin{bmatrix} U_{AT}/r_A \\ 0 \\ 0 \end{bmatrix}$$

A force flux in any tube with generatrices parallel to $\overrightarrow{TA}$ is constant. The equipotential planes are thus perpendicular to the field axis. In the neighbourhood of T, the potential $U_{(p)}(M)$ corresponding to all points M on the plane perpendicular to $\overrightarrow{TA}$ in B(equipotential plane of M_0) can be expressed as:

$$U_{(p)}(M) = U_A(T) + x_0 F_{A/T} = U_A(T)\big(1 + \alpha\cos\theta\big) \tag{3.22}$$

with $U_A(T)$ given by (3.20) and x_0 by (3.16). The product $x_0 F_{A/T}$ represents the impact of force $\overrightarrow{F}_{A/T}$ along every pathway between T and all points M on the equipotential plane containing M_0.

As the primary Legendre polynomials are $P_0(\cos\theta) = 1$ and $P_1(\cos\theta) = \cos\theta$, equation (3.22), which gives the meridian potential corresponding to the tractive force $\overrightarrow{F}_{A/T}$, can also be expressed as:

$$U_{(p)}(M) = U_A(T)\big[1 + \alpha P_1(\cos\theta)\big] \tag{3.23}$$

2.2 • Tide potential field generated by a celestial body

The tide-generating force for a given celestial body is the difference between forces $\overrightarrow{F}_{A/M}$ and $\overrightarrow{F}_{A/T}$, so the tide potential U induced by celestial body A at point M is thus determined by the difference between the two

elementary potentials $U_{(r)}(M)$ and $U_{(p)}(M)$, which are respectively given by (3.21) and (3.23), or:

$$U = U_{(r)}(M) - U_{(p)}(M) = U_A(T) \sum_{n=2}^{n\to\infty} \alpha^n P_n(\cos\theta) \tag{3.24a}$$

We symbolised this potential simply by U since the nature of celestial body A and the coordinates of point M on the celestial body's vertical are expressed on the right side of the equation.

Considering expressions (3.6), (3.13), (3.14) and (3.20), which respectively define k as a function of g, parallax i_A, parameter χ_A and potential $U_A(T)$, and where $\alpha = (a_T/r_0)(r_0/r_A) = \alpha_0 i_A \Rightarrow \alpha_0 = a_T/r_0$, the tide-generating potential U for a specific celestial body is finally expressed by:

$$U = a_T g \chi_A \sum_{n=2}^{n\to\infty} i_A^{n+1} \alpha_0^{n-2} P_n(\cos\theta) \tag{3.24b}$$

Although the parallaxes i_A remain around unity, with a maximum of 1.067 for the Moon and 1.017 for the Sun, this is not the case for the α_0 ratios, which have lower magnitudes of around $1{,}666 \cdot 10^{-2}$ for the Moon and $0{,}427 \cdot 10^{-4}$ for the Sun, thus prompting a very rapid decline in the series terms (3.24b). We will see in Chapter IV that only the first terms are retained (three for the Moon, two for the Sun). However, expression (3.24b), which is reduced to $P_2(\cos\theta)$ in the first term, provides a very good first approximation of the lunar tide-generating potential, or:

$$U \approx a_T g \chi_A (i_A)^3 P_2(\cos\theta) \tag{3.24c}$$

where

$$P_2(\cos\theta) = (3\cos^2\theta - 1)/2 \tag{3.25}$$

The observed tide-generating potential clearly consists of the sum of potentials related to the two generating celestial bodies (Moon and Sun)–it is often called the 'lunisolar potential'. This global potential is not a meridian potential, except at equinox when the celestial body declinations are nil and the hour angles identical. At this time, the two field axes merge and the impact of the two celestial bodies on the tide is maximum.

When $C_A = 3\chi_A g a_T/4$ is a constant value, equation (3.24c) becomes:

$$U \approx 2C_A i_A^3 [\cos^2\theta - (1/3)] \tag{3.26}$$

This latter equation will enable us to resolve the potential into the three species described by Laplace.

3 • Breakdown of the potential into Laplace species

Spherical coordinate systems are outlined in Appendix A. In particular, a relation that gives the geocentric zenithal distance θ as a function of the equatorial coordinates of celestial body A (hour angle Ħ and declination δ) and latitude L at point M is expressed by the cosine relation in the PAM triangle (figure 3.7), or:

$$\cos\theta = \sin L \sin\delta + \cos L \cos\delta \cos Ħ \tag{3.27}$$

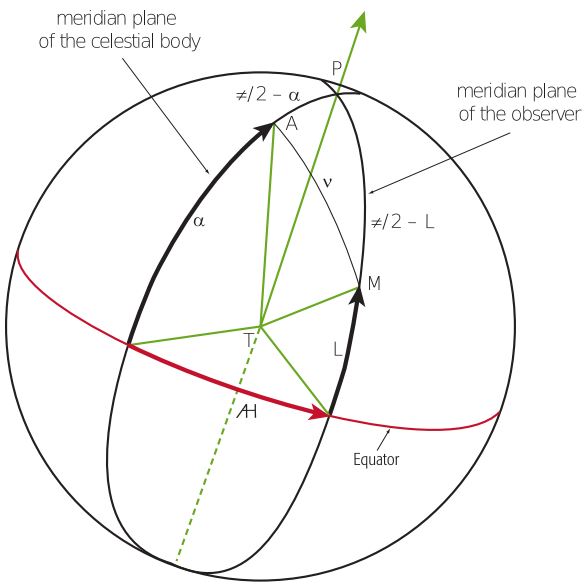

Figure 3.7: Relative positions of celestial body A, zenith M and north pole P on the local celestial sphere.

When cos θ is replaced by its value given by (3.27), expression (3.26) of the tide-generating potential U becomes:

$$U = C_A i_A^3 \left[3\left(\sin^2 L - \frac{1}{3}\right)\left(\sin^2\delta - \frac{1}{3}\right) + \sin 2L \sin 2\delta \cos Ħ + \cos^2 L \cos^2\delta \cos 2Ħ \right] \tag{3.28}$$

This relation reveals the sum of three constituents of U_i potentials ($i = 0, 1$

or 2), with each defining a very specific tide frequency domain, or:

$$U_0 = 3C_A i_A^3 \left(\sin^2 L - \frac{1}{3}\right)\left(\sin^2 \delta - \frac{1}{3}\right) \tag{3.29}$$

$$U_1 = C_A i_A^3 \sin 2L \sin 2\delta \cos \text{Æ}H \tag{3.30}$$

$$U_2 = C_A i_A^3 \cos^2 L \cos^2 \delta \cos 2\text{Æ}H \tag{3.31}$$

The hour angle ÆH coefficient value in each constituent of the U_i potential enables a species classification according to frequency domains: 0 for long periods (LP), 1 for diurnal species and 2 for semi-diurnal species.

The three U_i constituents have parameter i_A^3 in common, which in a first approximation is equivalent to $1 + 3e_A \cos(\sigma_A t)$, where σ_A is the angular velocity of celestial body A in its eccentric orbit e_A (Appendix A). In all tidal species, this parameter introduces modulations associated with the rotation rate of each celestial body (annual for the Sun, monthly for the Moon). Other factors are more informative.

Expression (3.29) for the U_0 potential (long-period and low-frequency species) does not include the hour angle (coefficient 0 for ÆH) and depends only on the other two parameters, i.e. declination δ and latitude L:

- In factor $\sin^2 \delta - 1/3$, the declination is involved via its square sine; as in $\sin^2 \delta = \frac{1 - \cos 2\delta}{2}$, temporal variations in this factor introduce a constituent with a period equivalent to half of the celestial body's rotational time, i.e. around 14 days for the Moon and 6 months for the Sun. This factor is always negative due to the extreme declination values reached by the Moon (28°30′) and Sun (23°27′).
- The second factor ($\sin^2 L - 1/3$) is cancelled out at latitudes L such as $\sin L = \pm\frac{1}{\sqrt{3}}$, i.e. at parallels 35°16′N and 35°16′S. Nodal axes (points where this long-period term is cancelled out) are thus two corresponding parallels. This feature affects the so-called 'zonal' distribution (figure 3.8) of the tidal long-period term.

As the first factor is always negative, the LP term of the potential is always positive for latitudes between 35°16′N and 35°16′S, and negative elsewhere.

Note that during one revolution of the celestial body in its orbit, the mean U_0 term is not null and solely depends on the latitude.

In equation (3.30), the U_1 of diurnal species contains the product $\sin 2L \sin 2\delta \cos \text{Æ}H$, where ÆH has a coefficient of 1. The nodal axes of this term are the Equator ($\sin 2L = 0$) and the meridian great circle orthogonal to the celestial body's meridian ($\cos \text{Æ}H = 0$). This term has a so-called 'tesseral' distribution (mosaic pattern: figure 3.9) and its sign changes with

that of the declination δ. The periodicity of the hour angle $\text{Æ}\text{H}$ is approximately 24 h for the Sun and 24 h 50 min for the Moon. However, the declination δ, like the parallax cube i_{A}^3, has a slow variation pattern (annual for the Sun, monthly for the Moon) as compared to that of the hour angle $\text{Æ}\text{H}$. The 2δ variation modulates (14 days for the Moon, 6 months for the Sun) the amplitude of this species–it is called 'diurnal' in reference to its dominant period (as dictated by the dominant period of the $\text{Æ}\text{H}$).

The modulus of the diurnal term is maximum when the celestial body crosses the meridian plane above or below the site–at this time $|\cos \text{Æ}\text{H}| = 1$. Maximum maximorum values are reached at latitudes 45°N and 45°S ($|\sin 2\text{L}| = 1$) when the declination δ has a maximum absolute value (23°27′ for the Sun and 28°30′ for the Moon). This term is nil for points on the equator and at the poles ($\sin 2\text{L} = 0$) or when the celestial body's declination is nil ($\sin 2\delta = 0$).

Finally, for U_2, i.e. a constituent of the potential of semi-diurnal species, the hour angle $\text{Æ}\text{H}$ has a coefficient of 2 in the $\cos^2 \text{L} \cos^2 \delta \cos 2\text{Æ}\text{H}$ term. As nodal axes, it accepts meridian circles located 45° on each side of the celestial body's meridian–$\cos 2\text{Æ}\text{H}$ is nil for these axes.

These nodal axes divide the Earth into four sectors with a so-called 'sectorial' distribution (figure 3.10) over the globe (4 90° sectors). This term is positive in the two opposite sectors, with the median being the celestial body's meridian, and negative in the two other sectors. It also allows two

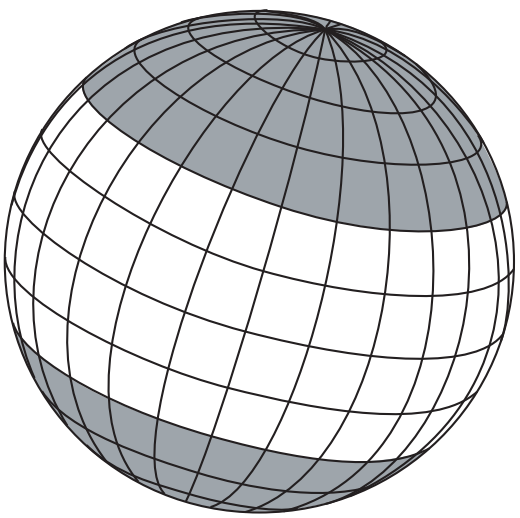

Figure 3.8: Zonal distribution of the long-period and low-frequency terms: $\text{U}_0 \propto (\sin^2 \text{L} - 1/3)(\sin^2 \delta - 1/3)$.

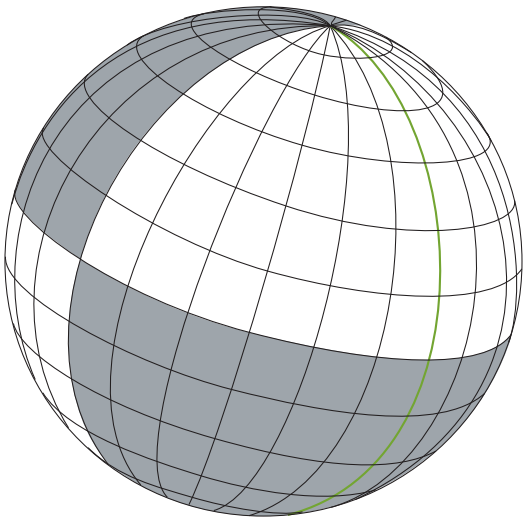

FIGURE 3.9: Tesseral distribution of the diurnal term: $U_1 \propto \sin 2L \sin 2\delta \cos \text{Ĥ}$.

maxima and two minima per day because of the $\cos 2\text{Ĥ}$ periodicity. Maximum maximorum values are reached by points on the Equator ($\cos^2 L = 1$) when crossed by the celestial body ($\cos^2 \delta = 1$). This term is nil at the poles.

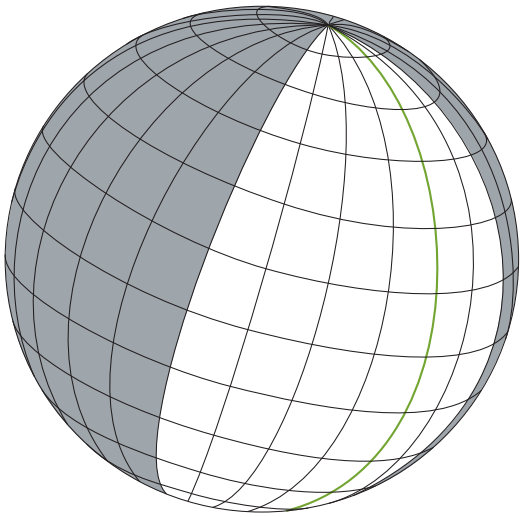

FIGURE 3.10: Sectorial distribution of the semi-diurnal term: $U_2 \propto \cos^2 L \cos^2 \delta \cos 2\text{Ĥ}$.

The next chapter describes how Laplace developed his method for predicting high and low water heights whereby the potential is considered according to three separate species.

IV

Laplace's dynamic theory of tides

Laplace was the first to consider tides as a hydrodynamic issue. His equations are hard to integrate, except in special cases, but they have not been challenged. Moreover, they provided a basis for subsequent developments after the advent of computers. Through a semiempirical analysis based on observations, Laplace used the structure of these equations to develop a formula and a prediction method that bear his name. The predictions were first used to calculate high and low waters. This method, with minor modifications, continued to be used in France until the late 20th century. It is still used to calculate the tidal coefficient, which is a very popular tide table feature in the Atlantic coastal region of France. A general definition of this coefficient is provided in the next chapter describing the harmonic analysis of tides.

1 • Laplace's equations

In 1776, Laplace formulated fundamental equations describing the response of the oceans to the tide-generating forces. We will outline the hypothesis with the same notations that have been used to date. In the absence of a tide-generating potential, the Earth is spherical and of radius a_T. It rotates uniformly around the polar axis (rotation vector $\overrightarrow{\omega_T}$), which is covered with an incompressible ocean of constant density ρ, and of depth H which is a function of position M with its geographical coordinates (G, L). In the presence of the lunisolar tide-generating potential U, the sphere becomes a spheroid covered by fluid. Laplace accounted for the modification in the

potential by the presence of this fluid covering. To simplify the presentation, this factor will not be taken into account (the corresponding correction is of the order of 10%). The major hypothesis put forward by Laplace is that the response of the ocean to the excitation of the tide-generating force is linear, so nonlinear terms are ignored in the hydrodynamic equations. The horizontal constituent of the tide-generating force induces an ocean current whose horizontal velocity $\overrightarrow{u}$ is identical at all ocean depths H. As the values of $\overrightarrow{u}$ and H vary with the position M, the continuity of the fluid volume implies variations in the elevation z of the ocean surface, which in turn generate a tide wave. Note that this elevation z is defined as an upward local vertical value (unit vector $\overrightarrow{\zeta}_{\mathrm{M}}$) measured from the initial sphere. Laplace formulated the following equations to illustrate his theory:

- the first is the continuity equation applied to an incompressible fluid assuming zero velocity divergence; in this case, the equation is as follows:

$$\overrightarrow{\nabla}_h \cdot (\mathrm{H}\overrightarrow{u}) + \partial z/\partial t = 0 \tag{4.1}$$

where $\overrightarrow{\nabla}_h \cdot (\mathrm{H}\overrightarrow{u})$ is the scalar product (symbol $\cdot$) of the vectorial horizontal gradient operator $\overrightarrow{\nabla}_h$ of constituents $(\partial/\partial x, \partial/\partial y)$ in a Cartesian system, and of vector $\mathrm{H}\overrightarrow{u}$ representing transport of the entire water column;

- the second is the horizontal fluid movement equation, or:

$$\frac{\partial \overrightarrow{u}}{\partial t} + 2\overrightarrow{\omega_{\mathrm{T}}} \wedge \overrightarrow{u} = \frac{1}{\rho}\overrightarrow{\nabla}_h(\mathrm{U} - gz). \tag{4.2a}$$

Laplace in 1776 was the first to take into account the effect of the Earth's rotation $\overrightarrow{\omega_{\mathrm{T}}}$ on marine currents, while the discovery of the inferred acceleration $2\overrightarrow{\omega_{\mathrm{T}}} \wedge \overrightarrow{u}$ is usually attributed to the mathematician Coriolis, who had rediscovered it almost half a century later, in 1835! Oceanographers and meteorologists thus refer to the projection of the vector $2\overrightarrow{\omega_{\mathrm{T}}}$ on the upward local vertical as the 'Coriolis parameter' (symbolised by f), or:

$$f = 2\overrightarrow{\omega_{\mathrm{T}}} \cdot \overrightarrow{\zeta_{\mathrm{M}}} = 2\omega_{\mathrm{T}} \sin \mathrm{L}$$

which has the same sign as the latitude (positive north, negative south). Equation (4.2a) can also be formulated with the vertical vector $f\overrightarrow{\zeta}_{\mathrm{M}}$:

$$\frac{\partial \overrightarrow{u}}{\partial t} + f\overrightarrow{\zeta}_{\mathrm{M}} \wedge \overrightarrow{u} = \frac{1}{\rho}\overrightarrow{\nabla}_h(\mathrm{U} - gz) \tag{4.2b}$$

Equations (4.1) and (4.2b), which are expressed in spherical coordinates, are the fundamental tidal equations formulated by Laplace. The tide equilibrium is obtained when the $\mathrm{U} - gz$ term is considered to be constant. The horizontal gradient is zero and the solution for (4.2b) – but which without

internal wave propagation in the ocean does not verify equation (4.1) – is the inertial current, which is also called inertial oscillation.

2 • Laplace's formula

The linearity of the response of the ocean to the applied force is shown by low amplitude movements (nonlinear terms disregarded and small movements superimposed). Laplace studied these equations and introduced a friction term that is proportional to the velocity in (4.2a) and thus shows that, because of their dissipation, the initial conditions do not have a crucial role. He concluded that the only realistic solutions are those with oscillatory characteristics (forced oscillations). Laplace presented his hypotheses as follows:

• Superimposition of minor movements (response linearity): "The total motion of a system under the influence of very small forces is the result of the combination of all partial movements generated separately by these forces."

• Forced oscillation (dissipation of initial conditions and response periodicity): "The state of a system of physical bodies in which the primary motion conditions have vanished as a result of passive resistance phenomena is periodic like the forces exciting it."

This being an extremely simple series of equations, they are not applicable in general cases. Laplace, however, demonstrated that the potential U could be resolved into the sum of three terms (corresponding to the three tidal species defined in Chapter III), and then – through a semiempirical approach – used the result to formulate an equation to describe the tide at specific locations. This method is so reliable and accurate that it was used, with a few minor modifications, by the French Hydrographic Service until 1992. In line with the semiempirical approach implemented by Laplace, hereafter we present the formulation obtained using mathematical signal processing tools (transfer function, admittance, convolution, factoring into harmonic and/or Fourier series, Dirac distribution, etc.). We first briefly review the response of linear systems to external excitation and then explain Laplace's formulation for the three tidal species relative to a given celestial body. The sum of the expressions obtained with the two tide-generating celestial bodies gives Laplace's formula for a lunisolar tide at a given point.

2.1 • Heights of three tidal species: Laplace's formula

For simplicity, the sidereal time (see Appendix A) was selected as the reference time. Fluctuations $\Delta\omega_T$ in the Earth's rotation are small enough

($\max|\Delta\omega_T/\overline{\omega}_T| \approx 10^{-7}$) for this time to be considered constant for tidal calculations. It is useful to symbolise it as t_γ in order to distinguish it from the mean time, but here we will simply refer to it as t. It is the hour angle $\text{Ħ}_\gamma(G,t)$ of the vernal equinox, or point γ, relative to a benchmark meridian, i.e. the Greenwich meridian (longitude $G = 0$): $\text{Ħ}_\gamma(0,t) = \omega_T t$.

Where α_A is the right ascension of the celestial body and δ_A is its declination (see Appendix A), at the position M(G, L) celestial body $A(\alpha_A, \delta_A)$ has an hour angle of $\text{Ħ}_A(G,t)$, symbolised hereafter by $\text{Ħ}_A(t)$, and satisfies equation:

$$\text{Ħ}_A(G,t) \equiv \text{Ħ}_A(t) = (\omega_T t + G) - \alpha_A \tag{4.3}$$

(n.b. longitude G is positive east of Greenwich and negative west of this meridian, and all angles are expressed in radians here). In addition, equation (3.28) for the tide-generating potential U_A, corresponding to celestial body A, is expressed according to three constituents relative to Laplace's tidal species:

$$U_A = U_{A,0} + U_{A,1} + U_{A,2} = \sum_{k=0}^{k=2} U_{A,k}$$

where index k in the summation represents the coefficient of the hour angle $\text{Ħ}_A(t)$ in the expression of potential $U_{A,k}$. Moreover, the terms for a celestial body and a given location are constant in (3.28). Coefficient C_A depends only on the celestial body (n.b. $r_0 = \overline{r_A}$, where the 'overline' symbol indicates the mean value), and is formulated as follows:

$$C_A = \frac{3}{4} g a_T \chi_A \text{ avec } \chi_A = \frac{m_A}{m_T}\left(\frac{a_T}{r_0}\right)^3.$$

Let $B_{A,k}(M)$ represent the terms relative to each species, which also depend on the latitude L for point M, or:

$$B_{A,0}(M) = 3C_A\frac{(1-3\sin^2 L)}{3} \tag{4.4a}$$

$$B_{A,1}(M) = C_A \sin(2L) \tag{4.4b}$$

$$B_{A,2}(M) = C_A \cos^2 L \tag{4.4c}$$

Index A is omitted below since we are dealing only with the effects of a single celestial body, but this factor will be included later when needed to understand the text. This also applies with respect to point M in the expression of B_k terms. Times t are however included for time-dependent

parameters. The three potentials can thus be expressed by:

$$U_0(t) = B_0 i^3(t) \frac{[1 - 3\sin^2 \delta(t)]}{3} \tag{4.5a}$$

$$U_1(t) = B_1 i^3(t) \sin 2\delta(t) \cos Ⱥ(t) \tag{4.5b}$$

$$U_2(t) = B_2 i^3(t) \cos^2 \delta(t) \cos 2Ⱥ(t) \tag{4.5c}$$

Parallax $i(t)$ and trigonometric functions containing coordinates of the celestial body (α, δ) are periodic terms linked mainly to the tropical period of the celestial body (365.242 days for the Sun and 27.321 days for the Moon). Taking into account equation (4.3), $U_1(t)$ and $U_2(t)$ become:

$$\begin{aligned} U_1(t) &= B_1 i^3(t) \sin 2\delta(t) [\cos \alpha(t) \cos(\omega_T t + G) + \sin \alpha(t) \sin(\omega_T t + G)] \\ U_2(t) &= B_2 i^3(t) \cos^2 \delta(t) \big[\cos 2\alpha(t) \cos 2(\omega_T t + G) \\ &\qquad + \sin 2\alpha(t) \sin 2(\omega_T t + G)\big]. \end{aligned}$$

Factors $\cos(\omega_T t + G)$ and $\sin(\omega_T t + G)$ are periodic with period $2\pi/\Omega_A$, so they can be expanded in Fourier series. Hence, the potentials of each tidal species k, including $U_0(t)$ which is expressed by (4.5a), can be expanded in an harmonic series of the type:

$$U_k(t) = \sum_{n=-N}^{n=+N} p_{kn} \cos(\nu_{kn} t - \alpha_{kn}) \tag{4.6}$$

where discrete frequencies generating multiple-line spectra are expressed by the relation:

$$\nu_{kn} = k\omega_T + n\Omega_A \tag{4.7}$$

with Ω_A representing the mean angular velocity of the celestial body in its orbit, as expressed here in radians per sidereal time unit. It should be noted that the symbol k always represents the hour angle coefficient in expressions of the corresponding potentials (n.b. LP, $k = 0$; diurnal, $k = 1$; semidiurnal, $k = 2$). Moreover, the Earth rotation velocity $\omega_T \approx 1$ cpd (cycles/day) is very high relative to Ω_A ($\Omega_L \approx 1/28$ cpd for the Moon L and $\Omega_S \approx 1/365$ cpd for the Sun S). Summations in n are thus performed in an interval $(-N, +N)$ where N is an integer of generally a few units. B_i terms associated with the celestial body characteristics and the latitude of the site (but not time dependent) are included in the value of amplitude p_{kn}. Note also that the frequency deviations in each set of species are low and that the amplitudes p_{kn} quickly drop to very low or negligeable values as the absolute n values increase. By adding the imaginary sine constituent to

each associated cosine constituent, and based on the same amplitude and argument, the $U_k(t)$ potentials become real parts of complex series:

$$\Psi_k(t) = \sum_{n=-N}^{n=N} p_{kn} e^{j(\nu_{kn} t - \alpha_{kn})} \tag{4.8}$$

The corresponding water heights $h_k(t)$ are represented by the real parts of series:

$$\eta_k(t) = \sum_{n=-N}^{n=N} h_{kn} e^{-j\phi_{kn}} e^{j(\nu_{kn} t - \alpha_{kn})} \tag{4.9a}$$

and

$$\eta_k(t) = \sum_{n=-N}^{n=N} a_{kn} p_{kn} e^{j(\nu_{kn} t - \alpha_{kn})} \tag{4.9b}$$

where the a_{kn} terms represent complex admittances of each frequency ν_{kn} :

$$a_{kn} = w_{kn} e^{-j\alpha_{kn}} \tag{4.10}$$

Laplace defined admittances on a semiempirical basis according to observations (thus dependent on the site), and also based on the fact that the frequencies of each species are concentrated in a relatively limited domain. Laplace's initial hypotheses were thus as follows. First, the amplitude factors w_{kn} maintain a constant value b_k for each species k, irrespective of the frequency but not of the celestial body, or:

$$w_{kn} \equiv b_k$$

for all n. This amplitude factor will be symbolised by $b_{A,k}$ hereafter to reflect its relationship with celestial body A. Phase differences φ_{kn} are a function of the frequencies within the species, and an increasing linear function of the frequency in the domain corresponding to each species, or:

$$d\varphi_{kn}/d\nu_{kn} = T_k$$

The three T_k parameters are time lapses that induce frequency-dependent phase lags. These are the 'ages' of the corresponding tidal species. By integration, we obtain:

$$\varphi_{kn} = \nu_{kn} T_k + k\lambda_k$$

where $k\lambda_k$ is a constant frequency independent phase difference for the considered species. Laplace also considered that the two coupled parameters $(T_k, k\lambda_k)$ were identical for the two tide-generating celestial bodies. The index corresponding to the celestial body is thus not presented in the notation for these parameters. For the long-period (LP) tidal species group,

because of the slow movement induced in the oceans, Laplace hypothesised a static phase response, i.e. zero values of T_0 and λ_0. In brief, Laplace's admittances have constant amplitude factors $b_{A,k}$ for a celestial body and a given tidal species group. However, phase differences φ_{kn} are not dependent on celestial bodies and are characterised, for each species, by an age T_k, thus introducing a lag associated with the frequency ν_{kn}, and by a constant phase difference $i\lambda_k$. If $D(t)$ represents the Dirac distribution, the translation of these hypotheses gives, for each species, the complex transfer function (with index A added for the celestial body):

$$\Phi_{A,k}(t) = b_{A,k} e^{-jk\lambda_k} D(t - T_k) \tag{4.11}$$

with zero T_0 and λ_0 for LP species ($k = 0$). Each transfer function thus pools all of the elements included in Laplace's hypotheses, i.e. gain, phase differences and age of the tidal species. Note that the convolution of $D(t-T)$ with a function $U(t)$ induces a translation in the time of $-T$:

$$D(t - T) * U(t) = \int_{-\infty}^{+\infty} D(\tau - T) * U(t - \tau) d\tau = U(t - T)$$

The response of the oceans to the complex potential given by (4.8) for a given celestial body, is thus expressed by:

$$\eta_{A,k}(t) = \Phi_{A,k}(t) * \Psi_{A,k}(t) \tag{4.12}$$

For a specific celestial body A and a given time t, the sum of real parts of each species (index and factor k), the corresponding water height $h_{A,k}(M, t)$ is expressed as:

$$h_{A,k}(M, t) = b_{A,k}(M) \sum_n u_{A,k,n} \cos\big[(k\omega_T + n\Omega_A)(t - T_k) - \varphi_{A,k,n} - k\lambda_k\big] \tag{4.13}$$

where the amplitude factor, as a function of position M, is represented by $b_{A,k}(M)$. Moreover, because of the equivalence of the harmonic series expression (4.6) of potentials $U_i(t)$ and their original relations (4.5a, 4.5b and 4.5c), equation (4.13) applies for each set of species ($k = 0$, $k = 1$ and $k = 2$) through the following expressions in which indices $t - T_k$ attributed to astronomic elements i_A, ∂_A and $\mathcal{H}_A$ indicate that they are taken at times $t - T_k$.

$$h_{A,0}(M, t) = H_{A,0}(M)\big[i_{A(t-T_0)}\big]^3 \left[1 - 3\sin^2 \delta_{A(t-T_0)}\right] \tag{4.14a}$$

with $T_0 = 0$

$$h_{A,1}(M,t) = H_{A,1}(M)\left[i_{A(t-T_1)}\right]^3 \sin\left[2\delta_{A(t-T_1)}\right] \times \cos\left[\text{Ⱨ}_{A(t-T_1)} - \lambda_1\right] \tag{4.14b}$$

$$h_{A,2}(M,t) = H_{A,2}(M)\left[i_{A(t-T_2)}\right]^3 \cos^2\delta_{A(t-T_2)} \times \cos\left(2\left[\text{Ⱨ}_{A(t-T_2)} - \lambda_2\right]\right) \tag{4.14c}$$

In the last three equations, the water heights $H_{A,k}(M)$ have constant values at the monitoring site for a given species and celestial body, as expressed by the following relation:

$$H_{A,k}(M) = b_{A,k}(M) \times B_{A,k}(M)$$

with coefficients $B_{A,k}(M)$ defined by (4.4a), (4.4b) and (4.4c). If L represents the Moon and S the Sun, the Laplace formula for a lunisolar tide at point M is thus obtained by the sum of the three tidal species generated by each celestial body, or:

$$h(M,t) = \sum_{k=0}^{k=2}\left[h_{L,k}(M,t) + h_{S,k}(M,t)\right] \tag{4.15}$$

For guidance, the range variation of the celestial body parameters (parallax i_A and declination δ_A) are:

- for the Moon:

$$\begin{aligned} 0.94 \le i_L \le 1.06 &\Rightarrow 0.83 \le i_L^3 \le 1.19 \\ -28°.57 \le \delta_L \le 28°.57 &\Rightarrow -0.84 \le \sin 2\delta_L \le 0.84 \\ &\Rightarrow 0.77 \le \cos^2\delta_L \le 1 \end{aligned}$$

- for the Sun:

$$\begin{aligned} 0.983 \le i_S \le 1.016 &\Rightarrow 0.95 \le i_S^3 \le 1.05 \\ -23°.44 \le \delta_S \le 23°.44 &\Rightarrow -0.73 \le \sin 2\delta_S \le 0.73 \\ &\Rightarrow 0.84 \le \cos^2\delta_S \le 1 \end{aligned}$$

The earliest tidal observations at Brest were limited to high and low water levels and times. Laplace used these readings to calculate all amplitude factors $b_{A,i}(M)$, which were then used to predict daily extremes and their corresponding times.

3 • High water times; tidal coefficient

Laplace formula calculations concern only high and low water determinations. These times and levels were chiefly calculated by iterative processes

tailored to the calculation resources available at the time, prior to the advent of calculators and computers. In this part, we will also limit our discussion to the calculation of high water times and Laplace's tidal coefficient definition.

3.1 • Calculation of high water times

When calculating high and low water times, in his first approximation, Laplace overlooked the influence of long-period and diurnal tidal species. He only took semidiurnal lunisolar constituents into account; in an additional approximation solar constituents were considered as a disturbance to the corresponding lunar species. With these Laplace's approximations, equation (4.15) becomes:

$$h(\mathrm{M},t) \approx h_{\mathrm{L},2}(\mathrm{M},t) + h_{\mathrm{S},2}(\mathrm{M},t) = h_2(\mathrm{M},t) \tag{4.16}$$

where $h_2(\mathrm{M},t)$ is the semidiurnal lunisolar constituent. To simplify the formulations, it should be understood hereafter that the water heights are a function of site M. Hence, when:

$$\mathrm{A}_{\mathrm{A},2} = \mathrm{H}_{\mathrm{A},2} \times i_{\mathrm{A}^3_{(t-\mathrm{T}_2)}} \times \cos^2 \delta_{\mathrm{A}_{(t-\mathrm{T}_2)}} \tag{4.17}$$

where index A = L or S, the height $h_2(t)$ can be expressed as:

$$\begin{aligned} h_2(t) = {} & \mathrm{A}_{\mathrm{L},2} \cos\left(2[\mathit{Ä}\mathrm{H}_{\mathrm{L}_{(t-\mathrm{T}_2)}} - \lambda_2]\right) \\ & + \mathrm{A}_{\mathrm{S},2} \cos\left(2[\mathit{Ä}\mathrm{H}_{\mathrm{S}_{(t-\mathrm{T}_2)}} - \lambda_2]\right) \end{aligned} \tag{4.18}$$

For extreme high or low waters, and neglecting variations in $\mathrm{A}_{\mathrm{A},2}$, we get:

$$dh_2(t)/dt = 0$$

Variations in amplitudes $\mathrm{A}_{\mathrm{S},2}$ and $\mathrm{A}_{\mathrm{L},2}$ around their means have their respective periods of 1 year (tropical year: 365.242 2 d) and about 1 month (tropical revolution of the Moon: 27.321 58 d); thus they vary slowly relative to the cosines of the hour angle, which have periods of around 24 h. Laplace ignored variations of these amplitudes, but he gave them temporal values calculated to be close to $(t_{\mathrm{hw}} - \mathrm{T}_2)$, where t_{hw} is the high water time(index hw). With these approximations, relation (4.17) is condensed into the following equation:

$$\begin{aligned} & \mathrm{A}_{\mathrm{L},2}\,(\sin[2(\mathit{Ä}\mathrm{H}_{\mathrm{L}} - \lambda_2)]) \times (\mathrm{d}\mathit{Ä}\mathrm{H}_{\mathrm{L}}/\mathrm{d}t) \\ & \qquad + \mathrm{A}_{\mathrm{S},2}\,(\sin[2(\mathit{Ä}\mathrm{H}_{\mathrm{S}} - \lambda_2)]) \times (\mathrm{d}\mathit{Ä}\mathrm{H}_{\mathrm{S}}/\mathrm{d}t) = 0 \end{aligned} \tag{4.19}$$

where the hour angles and their derivatives are taken at time $(t - T_2)$. When considering equation (4.10), the variation in $\mathcal{H}_L$ relative to that of $\mathcal{H}_S$ gives parameter $R(t)$:

$$R(t) = \frac{d\mathcal{H}_L/dt}{d\mathcal{H}_S/dt} = \frac{\omega_T - (d\alpha_L/dt)}{\omega_T - (d\alpha_S/dt)} \tag{4.20}$$

This time-dependent ratio $R(t)$ fluctuates slightly around a mean $\overline{R}$, which can be estimated by taking into account the mean angular velocity of celestial body A in its orbit ($\Omega_A = \overline{d\alpha_A/dt}$), or

$$\begin{aligned} \overline{R} &= \frac{\omega_T - \Omega_L}{\omega_T - \Omega_S} \\ \overline{R} &\approx \frac{\left[1 - \left(\frac{1}{27.32}\right)\right]}{\left[1 - \left(\frac{1}{365.24}\right)\right]} \approx 0.966. \end{aligned} \tag{4.21a}$$

Laplace adopted the approximate value:

$$\overline{R} \approx \frac{29}{30} = 0.966\,666\ldots \tag{4.21b}$$

This parameter has since been determined with more accuracy:

$$\overline{R} = \frac{24}{24.841\,202\,4} = 0.966\,136\,808 \tag{4.21c}$$

and is known as the ratio of durations of the solar day to the lunar day.

The Laplace approximation turned out to be sufficient for calculating the time of high water.

When considering the solar constituent as a disturbance to the lunar constituent, and where $\varpi(t)$ represents the deviation between the lunar and solar vertical ascensions (or hour angles), we obtain:

$$\varpi(t) = \alpha_L(t) - \alpha_S(t) \Rightarrow \mathcal{H}_S(t) = \mathcal{H}_L(t) + \varpi(t) \tag{4.22}$$

From this equation (4.22), we can deduce:

$$\begin{aligned} \sin\left(2[\mathcal{H}_S(t) - \lambda_2]\right) = \sin\left(2[\mathcal{H}_L(t) - \lambda_2]\right)\cos[2\varpi(t)] \\ + \cos\left(2[\mathcal{H}_L(t) - \lambda_2]\right)\sin[2\varpi(t)] \end{aligned}$$

Taking this last relation into account and assuming:

$$p = \mathcal{H}_L(t - T_2) - \lambda_2 \tag{4.23}$$

equation (4.19) enables us to formulate, with the Laplace approximation for $\overline{R}$, the following expression:

$$\tan(2p) = \frac{-\sin[2\varpi(t - T_2)]}{(29/30)(A_{L,2}/A_{S,2}) + \cos[2\varpi(t - T_2)]} \tag{4.24}$$

An iterative process starts from an initial approximate value for parameter p. Knowing an exact time of an extreme water level, e.g. high water (index *hw*), the following one will take place approximately 12 h 25 min later. This initial information is used to determine the corresponding p_{hw} value through equation (4.24). The fact that the deviation in right ascensions of the two celestial bodies $\varpi(t)$ slowly varies is accounted for by:

$$\varpi(t - \mathrm{T}_2) \approx \varpi(t) - \mathrm{T}_2 \frac{\mathrm{d}\varpi(t)}{\mathrm{d}t} \approx \varpi(t) - \mu_2 \tag{4.25}$$

with the angle $\mu_2 = \mathrm{T}_2 \overline{\mathrm{d}\varpi(t)/\mathrm{d}t} = (\Omega_{\mathrm{L}} - \Omega_{\mathrm{S}})\mathrm{T}_2$ being constant.

The time t_0 of the passage of the Moon across the meridian of the site is then taken as the time of origin as follows:

$$t_0 = 0 \Rightarrow \mathcal{H}_{\mathrm{L}}(t_0) = \mathcal{H}_{\mathrm{L}}(0) = 0$$

By a limited expansion of $\mathcal{H}_{\mathrm{L}}(t)$ based on this origin, we can state as a first approximation:

$$\mathcal{H}_{\mathrm{L}}(t) \approx \mathcal{H}_{\mathrm{L}}(0) + t(\mathrm{d}\mathcal{H}_{\mathrm{L}}/\mathrm{d}t)$$

or

$$\mathcal{H}_{\mathrm{L}}(t) \approx [\omega_{\mathrm{T}} - (\mathrm{d}\alpha_{\mathrm{L}}/\mathrm{d}t)]t \approx (\omega_{\mathrm{T}} - \Omega_{\mathrm{L}})t$$

The Moon's hour angle at time $(t - \mathrm{T}_2)$ is thus expressed by:

$$\mathcal{H}_{\mathrm{L}}(t - \mathrm{T}_2) \approx (t - \mathrm{T}_2) \times (\omega_{\mathrm{T}} - \Omega_{\mathrm{L}})$$

Then equation (4.23) becomes:

$$\lambda_2 + p_{\mathrm{hw}} \approx (t - \mathrm{T}_2) \times (\omega_{\mathrm{T}} - \Omega_{\mathrm{L}})$$

Considering expression (4.21b) for parameter $\overline{\mathrm{R}}$ (value used by Laplace), the high water time t_{hw} is thus obtained by equation:

$$t_{\mathrm{hw}} \approx \mathrm{T}_2 + \frac{30}{29} \times \frac{\lambda_2 + p_{\mathrm{hw}}}{\omega_{\mathrm{T}} - \Omega_{\mathrm{S}}} \tag{4.26a}$$

Note that the term $(\omega_{\mathrm{T}} - \Omega_{\mathrm{S}})$ represents the mean angular velocity of the Sun in relation to a reference meridian, or $360°/24\,\mathrm{h} \Rightarrow 15°/\mathrm{h}$, and that the Earth is divided into 24 time zones of 15° angles ($15° \Rightarrow 1$ h). As the angles λ_2 and p_{pm} are usually expressed in hours, the previous elements enable us to formulate an equation that gives the high water time t_{hw} from the Moon's passage across the meridian of the site, by the relation:

$$t_{\mathrm{hw}} \approx \mathrm{T}_2 + \frac{30}{29}(\lambda_2 + p_{\mathrm{hw}}) \tag{4.26b}$$

with λ_2 and p_{hw} expressed in hours. To assess the amplitude of the tidal range throughout the year, the elements described above can also be used to calculate the tidal coefficient.

3.2 • Tidal coefficient

The 'tidal coefficient' notion was first introduced by Laplace and included in French coastal tide tables in the late 19th century. To compare tidal ranges, Laplace allocated a height unit U to each harbour, which he defined as follows: "the height unit is the mean amplitude (half-range of tide) of the highest water height around 1.5 days after the time of the full or new Moon, around equinoctial syzygy." The tidal coefficient C is an amplitude ratio directly derived from this definition. By convention, coefficient 100 is attributed to the mean half-range of the spring tide following the syzygy closest to equinox. We thus have the formula:

$$C = 100\frac{h_{hw} - N_{mm}}{U}$$

where h_{hw} is the high water height and N_{mm} is the half-tide height; $h_{hw} - N_{mm}$ represent the half-range of tide. In practice, this coefficient is only calculated for Brest harbour, as it is based solely on the semidiurnal tidal constituents. U is evaluated assuming that, at time t_ς of a mean equinoctial syzygy, the following elements are available:

- for hour angles:

$$Æ H_S(t_\varsigma) \pm 12\,h$$

- for declinations:

$$\delta_L(t_\varsigma) = \delta_S(t_\varsigma) = 0°$$

- for mean parallaxes:

$$i_L(t_\varsigma) = 120/119 \Rightarrow i_L^3(t_\varsigma) \approx 41/40 = 1.025$$
$$i_S(t_\varsigma) = 1$$

For each celestial body, equation (4.14c) gives us the maximum spring tide (high water) T_2 hours after syzygy, or:

$$h_{A,2}(t_\varsigma + T_2) \approx H_{A,2} i_A^3(t_\varsigma)$$

A good approximation of height unit U is thus obtained with the following equation:

$$U \approx U_2 \approx (41/40)H_{L,2} + H_{S,2} \qquad (4.27)$$
$$U \approx (1.025 + m)H_{L,2}$$

where

$$m(\mathrm{M}) = \frac{\mathrm{H}_{\mathrm{S},2}(\mathrm{M})}{\mathrm{H}_{\mathrm{L},2}(\mathrm{M})} < 1 \tag{4.28}$$

The tide is reduced to its semidiurnal constituent to calculate a high water height h_{hw} for a given day. It can be evaluated by considering the complex expression η_2 of the height given by equation (4.18), which may be formulated by introducing deviation ϖ of the right ascensions (or hour angles):

$$\eta_2 = \mathrm{H}\left(\mathrm{A}_{\mathrm{L},2} + \mathrm{A}_{\mathrm{L},2}e^{2j\varpi}\right) e^{2j(\text{Ⱥ}\mathrm{H}_\mathrm{L} - \lambda_2)}$$

where $\text{Ⱥ}\mathrm{H}_\mathrm{L}$ and ϖ are obtained for the time $(t - \mathrm{T}_2)$. The complex amplitude X_2 of a semidiurnal tide is the first factor on the right side of the equation, expressed as:

$$\mathrm{X}_2 = \mathrm{A}_{\mathrm{L},2} + \mathrm{A}_{\mathrm{S},2}e^{2j\varpi} = \mathrm{P}_2 e^{-2j\theta}$$

Module P_2 of the complex amplitude X_2 is time dependent and equal to:

$$\mathrm{P}_2(t - \mathrm{T}_2) = \sqrt{\mathrm{A}_{\mathrm{L},2}^2 + \mathrm{A}_2^2 + 2\mathrm{A}_{\mathrm{L},2}\mathrm{A}_{\mathrm{S},2}\cos 2\varpi} \tag{4.29}$$

Phase θ at time $(t - \mathrm{T}_2)$ is readily deduced through the tangential equation:

$$\tan 2\theta = \frac{-\sin 2\varpi}{(\mathrm{A}_{\mathrm{L},2}/\mathrm{A}_{\mathrm{S},2}) + \cos 2\varpi}$$

This θ value is very close to parameter p defined in 4.24, where the $(\mathrm{A}_{\mathrm{L},2}/\mathrm{A}_{\mathrm{S},2})$ factor is the coefficient $\overline{\mathrm{R}} = 29/30$. The two values would be identical if the hour angle deviation were neglected over a timespan equivalent to the tidal age T_2. This can be accounted for since, in a first approximation, the initial equation (4.21a) can be formulated as:

$$\mathrm{R} \approx 1 + \frac{1}{\omega_\mathrm{T}} \frac{\mathrm{d}\varpi}{\mathrm{d}t}$$

where $\omega_\mathrm{T} \approx 1$ cpd. However, the high water time is t_{hw}, and determined from p_{hw}. Hence, by incorporating module P_2 considered at time $(t_{\mathrm{hw}} - \mathrm{T}_2)$ at the half-range of tide, the tidal coefficient may be expressed on the basis of equations (4.27) and (4.29) by:

$$\mathrm{C} \approx 100\,\mathrm{P}_2/\mathrm{U}. \tag{4.30}$$

Equations (4.18), (4.27), (4.28) and (4.29), respectively define amplitudes $\mathrm{A}_{\mathrm{L},2}$ and $\mathrm{A}_{\mathrm{S},2}$, height unit U, ratio $m(\mathrm{M})$ and module P_2 so tidal coefficient C may now be formulated as follows:

$$\frac{\mathrm{C}}{100} = \frac{\sqrt{(i_\mathrm{L}^3 \cos^2\delta_\mathrm{L})^2 + m^2(i_\mathrm{S}^3\cos^2\delta_\mathrm{S})^2 + 2m(i_\mathrm{L}^3\cos^2\delta_\mathrm{L})(i_\mathrm{S}^3\cos^2\delta_\mathrm{S})\cos 2\varpi}}{1.025 + m}$$

In this latter equation, all astronomic elements, i.e. (i_A, δ_A and ϖ), are considered at time $t_{hw} - T_2$. As defined here, coefficient C depends only on ratio m and age T_2 of a semidurnal tide. If we assume that parameter m is constant (which seems rational since it is a ratio of two contributions of close periods), the tidal coefficient would be completely identical at all points M, except for an offset due to the age of tide. However, this is not exactly the case, even though the spatial variation in m is small enough that the tidal coefficient calculated for a given point can be assigned to all nearby points, but with a time shift to account for the difference in ages T_2. Tide predictions currently provided in tide tables published for French ports are no longer based on the Laplace formula, but the tidal coefficient concept has remained so popular that the coefficient is still being used.

4 • Conclusion

In summary, the Laplace formula was found to be very satisfactory for predicting high and low waters in areas where diurnal tidal species are low to negligible as compared to semidiurnal species. This is the case at Brest and in most other European coastal regions. When there is a substantial diurnal constituent, Laplace's method is not accurate enough for predicting extreme water levels associated with tidal phenomena. Moreover, in shallow waters (particularly in estuaries), the nonlinear terms of hydrodynamic equations cannot be ignored and Laplace's hypotheses no longer apply. Nonlinear effects give rise to water level variations at composite frequencies, especially at the harmonics of the semidiurnal species. The Laplace formula cannot be universally applied and has thus been superseded by a method based on the harmonic analysis of tide. A harmonic method for calculating the tidal coefficient will be proposed.

V

Harmonic tidal equation

1 • Introduction

The harmonic tidal equation stems directly from the two fundamental principles of Laplace's dynamic theory of tides: the forced oscillation principle and the principle of superposition. It is based on development of the tide-generating potential function and the sum of strictly periodic terms and discrete clearly delineated frequencies representative of the sum of Dirac distributions. This frequency distribution involves a so-called multiple-line spectrum as opposed to a continuous spectrum (a continuous function of the frequency). Laplace had already thought of expressing the potentials of each celestial body by sine functions with arguments that varied linearly with time. Each term of the expansion could be interpreted as the potential of a hypothetical celestial body with a uniform circular motion on the equatorial plane, which generates a tidal wave of the same period, but with an amplitude and phase that are functions of the site considered and the angular velocity of this hypothetical body at the celestial equator. Based on the hypothesis of a linear response of the ocean at the celestial body's orbital period for diurnal as well as semidiurnal constituents, i.e. in sufficiently narrow frequency domains, Laplace was able to overcome the need for a complete harmonic development. He could thus express the sum of constituent tidal waves in the form of a finite development with just a few terms. He also showed how to achieve a completely harmonic development of the potential while also taking the main lunar orbit perturbations into account. He

deduced the expression corresponding to each wave irrespective of all amplitude and phase hypotheses. Kelvin (in 1867) and then Darwin (in 1883) further pursued this work of Laplace and called it harmonic development of the tidal potential.

However, the lunar theory that was popular at the time did not enable Darwin to come up with a complete development of the tide-generating potential. Correction factors (called nodal factors) had to be introduced to overcome irregularities induced by lunar nodes, which were considered as disturbances.

Doodson's tidal potential development of 1921, which is more appropriate for automatic calculation methods, remained a reference for over half a century, despite the fact that it was calculated on the basis of astronomic constants of 1900. It does not markedly differ from the computer-assisted developments proposed by many authors in the 1970s based on new astronomic constants.

2 • Darwin's development of the tide-generating potential

As the lunar orbit is substantially altered by the effect of the Sun, the development of the tide-generating potential proposed by Darwin in 1883 is not fully harmonic and may be presented as follows:

$$\mathrm{U}(t) = \sum_i f_i(t)\mathrm{A}_i \cos[\mathrm{V}_{i,0} + q_i t + u_i(t)] \tag{5.1}$$

where:

t: civil time at the site

i: number of the considered constituent

A_i and q_i: constant amplitude and angular velocity of constituent i

$\mathrm{V}_{i,0}$: argument at time zero ($t = 0$)

$f_i(t)$ and $u_i(t)$: nodal factors of constituent i.

Nodal factors are time functions (amplitude $f_i(t)$ and phase lag $u_i(t)$ factors) that must be taken into account to correct slow variations in constituent i. These variations are induced by the inclination of the lunar orbit at the Equator (see Appendix A: 'The Moon and its typical movements'). This inclination, which ranges from 28°.8 to 18°.1, may be expressed as a function of the ecliptic longitude of the ascending node (18.6 year period). These

terms are thus called nodal factors. Note also that the amplitude of a tide-generating potential constituent is also called 'coefficient' because it is usually a relative value of the amplitude, which is useful information.

Although this development is not completely harmonic, it actually turned out to be perfectly tailored for calculation methods available before the advent of computers. Darwin calculated the A_i constant coefficients with a very simplified lunar orbit equation. This avoided the problem of having to calculate a much higher number of trigonometric functions that would be required for a complete development. The corrections introduced by these nodal factors were minor and varied slowly. They were also available as tables that were compatible with the calculation methods of the time. It may be considered that most nodal factors are constant throughout the year, while also being relatively accurate. As these systematic corrections were quite easy to implement, with constant values for each constituent i over such a timespan, this method was widely used for routine applications. This approach probably helped spread the idea that the year should be the baseline period considered when performing harmonic analysis for tidal records. Despite advances in calculation methods, Darwin's development of the tide-generating potential was long considered to be the gold standard, even after publication of Doodson's more complete development in 1921. Calculation methods are no longer a stumbling block to using Doodson's tide-generating potential development. Darwin's work has still had a marked impact on modern day tide monitoring. The main tide-generating potential constituents, which are common to both developments, are now widely designated under the names attributed by Darwin. Moreover, nodal factors are still very useful, especially for predictions because they enable the user to limit the size of harmonic constituent files without subtantial loss of accuracy. The list of constituents proposed by Darwin is still usually enough to obtain a high quality prediction for navigation needs. The names of the main constituents outlined by Darwin are given in the following tables (5.1a and 5.1b). However, the coefficients are those used in Doodson's development, which differ very little from those calculated by Darwin. In practice, only their relative importance has to be considered. Note that the magnitudes of the coefficients highlight a clear hierarchy in these constituents.

A few comments should now be made on certain specific constituents. First, the potential constant terms obviously do not apply to the tide itself. LP constituents (low frequency or long period) of astronomical tides are generally very low since they pertain to static theory and are often masked by meteorological interference (action of the wind and atmospheric pressure on the tide level). They are hard to detect on tidal records. Only the S*a*

Table 5.1a: Lunar potential constituents

Symbol	**Constituent name**	**Angular velocity** degrees/hour	**Period** days or hours	**Coefficient** $u \times 10^5$
	Constant term	00.000 000 00		50 458
	Long periods		*Days*	
M*m*	monthly	00.544 374 68	27.554 551 21	8 253
M*sf*	variational	01.015 895 76	14.765 294 42	1 367
M*f*	bimonthly	01.098 033 04	13.660 791 11	15 640
	Diurnal		*Hours*	
$2Q_1$	2nd order elliptic	12.854 286 23	28.006 222 48	952
Q_1	major elliptic	13.398 660 92	26.868 356 63	7 206
ρ_1	evectional	13.471 514 52	26.723 053 25	1 368
O_1	principle lunar	13.943 035 60	25.819 341 66	37 689
M_1	minor elliptic	14.496 693 96	24.833 248 26	2 961
K_1	declinational	15.041 068 64	23.934 469 59	36 232
J_1	secondary elliptic	15.585 443 32	23.098 476 73	2 959
OO_1	2nd order lunar	16.139 101 68	22.306 074 22	1 615
	Semidiurnal		*Hours*	
$2N_2$	2nd order elliptic	27.895 354 87	12.905 374 45	2 300
μ_2	variational	27.968 208 48	12.871 757 60	2 777
N_2	major elliptic	28.439 729 56	12.658 348 21	17 391
NU_2	major evectional	28.512 583 16	12.626 004 38	3 302
M_2	medium lunar	28.984 104 24	12.420 601 20	90 812
λ_2	minor evectional	29.455 625 32	12.221 774 13	669
L_2	minor elliptic	29.528 478 92	12.191 620 20	2 567
K_2	declinational	30.082 137 28	11.967 234 80	7 852
	Third-diurnal		*Hours*	
M_3		43.476 156 36	8.280 400 80	1 188

and S*sa* constituents, which more reflect seasonal radiational tide variations (associated with the thermal effects of solar radiation on the atmosphere and ocean), can generally be highlighted. Tide-generating potential coefficients relative to S*a* and S_1 waves are under 10^{-5}. These two elements should not

TABLE 5.1B: Solar potential constituents.

Symbol	**Constituent name**	**Angular velocity** degrees/hour	**Period** days or hours	**Coefficient** $u \times 10^5$
	Constant term	00.000 000 00		23 411
	Long periods		*Days*	
S*a*	annual	00.041 068 64	365.242 189 66	$u < 10^{-5}$
S*sa*	semiannual	00.082 137 28	182.621 094 83	7 245
	Diurnal		*Hours*	
P_1	principle solar	14.958 931 36	24.065 890 22	16 817
S_1	radiational	15.000 000 00	24.000 000 00	$u < 10^{-5}$
K_1	declinational	15.041 068 64	23.934 469 59	16 124
	Semidiurnal		*Hours*	
T_2	major elliptic	29.958 933 32	12.016 449 19	2 472
S_2	medium solar	30.000 000 00	12.000 000 00	42 286
R_2	minor elliptic	30.041 066 68	11.983 595 78	437
K_2	declinational	30.082 137 28	11.967 234 80	3 643

be displayed in the table because other ones with higher coefficients are not mentioned. They are, however, presented here so as to be able to account for observed tide level variations at annual and diurnal radiational tide frequencies, respectively. Generally, the respective actions of the two celestial bodies may be better interpreted by documenting partial tides disturbed by radiational constituents. Constituents K_1 and K_2, which are called sidereal waves because their periods are equal to a sidereal day and a sidereal half-day, respectively, are present in both the lunar and solar potentials. The coefficients taken into account when studying them are the sum of coefficients from both origins. K_1, O_1, P_1 and Q_1 are the main constituents for diurnal tides, and M_2, S_2, K_2 and N_2 for semidiurnal tides. Alone they contain most of the energy of the tidal signal and are sometimes the only factors taken into account in baseline studies.

3 • Doodson's harmonic development

Note that in 1921 Doodson proposed a harmonic development of the tide-generating potential based on Brown's recent (1905) lunar theory which

corresponded to a description of the Moon's movement along ecliptic coordinates (see Appendix A). In this lunar model, Brown provides elements concerning the orbit (mean longitude and latitude) and the parallax according to a series of trigonometric functions whose arguments are linear functions of the mean time. In 1895, Newcomb provided the same elements for the apparent Sun in the ecliptic. A very good tidal prediction over several centuries may be obtained via these two orbit models. In Chapter III, it was found that the meridian field of the generating potential U of a celestial body A, of mass m_A and at distance r_A from the centre of the Earth (i.e. r_A is the mean distance), varies essentially with the cosine of the geocentric zenithal distance θ of the celestial body at point M at latitude L. We review expressions of the $\cos\theta$ function in the different celestial reference frames (see Appendix A), with the pairs (α, δ) and (β, λ) being urographic and ecliptic coordinates of the celestial body, respectively:

- in equatorial systems (A1.1):

$$\cos\theta = \sin L \sin\delta + \cos L \cos\delta \cos \text{Æ}H$$

where the $\cos\theta$ function is a linear function of $\cos$ ÆH;

- in the ecliptic system (A1.4):

$$\cos\theta = \sin L \cdot f(\beta, \lambda) + \cos L \cdot g(\beta, \lambda, \text{Æ}H)$$

with

$$f(\beta, \lambda) = \cos\epsilon \sin\beta + \sin\epsilon \cos\beta \sin\lambda$$

and

$$g(\beta, \lambda, \text{Æ}H) = \cos\beta \cos\lambda \cos(\alpha + \text{Æ}H) + (\cos\epsilon \cos\beta \sin\lambda - \sin\epsilon \sin\beta) \sin(\alpha + \text{Æ}H).$$

In this system, the $\cos\theta$ function is a linear function of $\cos$ ÆH and $\sin$ ÆH. The equivalence of the relations (A1.01) and (A1.04) gives:

$$\sin\delta = f(\beta, \lambda)$$
$$\cos\delta \cos \text{Æ}H = g(\beta, \lambda, \text{Æ}H)$$

The tide-generating potential of each celestial body can thus be expressed in a harmonic series on the basis of its ecliptic coordinates and hour angle, whose harmonic development was provided by Brown.

3.1 • Harmonic development by species

Taking expression (3.24b) of the Legendre polynomial series potential, relative to the constant potential $g a_T \chi_A$ for the considered celestial body A,

we may write:

$$\frac{\mathrm{U}}{g a_{\mathrm{T}} \chi_{\mathrm{A}}} = \sum_{n=2}^{n\to\infty} i_{\mathrm{A}}^{n+1} \left(\frac{a_{\mathrm{T}}}{r_{\mathrm{A},0}}\right)^{n-2} \mathrm{P}_n(cos\theta) \tag{5.2}$$

where the constant parameter χ_{A} depending on celestial body A (L: Moon; S: Sun) is given by:

$$\chi_{\mathrm{A}} = \frac{m_{\mathrm{A}}}{m_{\mathrm{T}}} \left(\frac{a_{\mathrm{T}}}{r_{\mathrm{A},0}}\right)^3$$

with

$$\chi_{\mathrm{L}}/\chi_{\mathrm{S}} \approx 2.2$$

and the parallax by $i_{\mathrm{A}} = r_{\mathrm{A},0}/r_{\mathrm{A}}$, which is around unity.

As the maximum absolute Legendre polynomial values are equal to unity, the magnitudes of the terms in the series are given by the values of $(a_{\mathrm{T}}/r_{\mathrm{A},0})^{n-2}$ with $n \geq 2$.

To calculate the tide-generating potential in harmonic series, Doodson restricted his development to terms with a ratio to the greatest element of over 10^{-5}, while disregarding the other terms.

For the Moon, the ratio of the Earth's radius to the mean distance of this celestial body is around 1/60, which for $n = 5$ gives maximum values of $(a_{\mathrm{T}}/r_{\mathrm{L},0})^{n-2} \approx 0.5 \cdot 10^{-5}$ (index L for the Moon). For this celestial body, Doodson thus considered its development with the first three terms of the series, i.e. up to the term containing $\mathrm{P}_4(\cos\theta)$. Doodson studied the contribution of this latter term and found that all constituents were below the threshold he had set, except for a few that were very close. Since this threshold was rather arbitrary, we only take the first two terms in the series into account.

For the Sun, we have $a_{\mathrm{T}}/r_{\mathrm{S},0} \approx 4.26 \cdot 10^{-5}$, so the corresponding development of the potential therefore only includes the $\mathrm{P}_2(\cos\theta)$ term, with the $\mathrm{P}_3(\cos\theta)$ term being around $2 \cdot 10^{-9}$.

Moreover, by disregarding the $\mathrm{P}_4(\cos\theta)$ term and ranking Doodson's development of the lunar potential according to increasing powers m of $\cos\theta$, from equation (5.2) we obtain the following equation:

$$\frac{\mathrm{U_L}}{g a_{\mathrm{T}} \chi_{\mathrm{L}}} = \sum_{m=0}^{m=3} u_{\mathrm{L},m} \cos^m \theta_{\mathrm{L}} \tag{5.3}$$

In the ecliptic coordinate system, $\cos\theta$ is a linear function of the sine and cosine of the hour angle $\mathcal{H}$ (see equations in Appendix A, and recalled above). These trigonometric functions of $\mathcal{H}$ are thus implicitely involved with the same powers m as $\cos\theta$. The series (5.3) can thus be developed as a

sum of terms that each include a sine or cosine of an argument that is a linear function of a multiple m of the hour angle Ħ; for $m = 0$, the corresponding terms are obviously independent of Ħ. Pooling these terms according to the m coefficient of the hour angle reveals a separation into frequency domains, called 'species' as in Laplace's equation:

- for $m = 0$, the hour angle is not involved; this species is the sum of long period (LP) terms, where long periods depend only on the declination δ_L and parallax ($i_L = r_{L,0}/r_L$);
- for $m = 1$, the set of terms containing Ħ is a diurnal species;
- for $m = 2$, we obtain the semidiurnal species with 2Ħ
- for $m = 3$, the third-diurnal species with 3Ħ.

Taking the $P_4(\cos\theta)$ term of (5.2) into account would obviously reveal the quarter-diurnal species with 4Ħ.

This species arrangement is the framework of Doodson's harmonic development. When only considering the first two terms of (5.2) for the Moon, the formulation is as follows:

$$U_L = g a_T \chi_L \sum_{n=2}^{n=3} i_L^{n+1} (a_T/r_{L,0})^{n-2} P_n(cos\theta) = \sum_{n=2}^{n=3} A_n \tag{5.4}$$

The elementary potential A_n corresponds to the term of the U_L development containing the $P_n(\cos\theta)$ polynomial. By grouping the terms by m species, the elementary potential can be formulated as:

$$A_n = i_L^{n+1} \sum_{m=0}^{m=4} c_{n,m} G_{n,m} H_{n,m} \tag{5.5}$$

where, for each m species, we have:

- the $H_{n,m}$ terms, including $m\text{Ħ}$, which are time functions; in an equatorial system, they consist of linear $\cos(m\text{Ħ})$ functions with factors that depend on the trigonometric function of the declination δ; Doodson used the polar distance, i.e. a declination complement that we designate as $\varpi = (\pi/2) - \delta$;
- the $G_{n,m}$ terms, called geodesic coefficients, which depend only on the L latitude of the site;
- the $c_{n,m}$ factors are constant and dimensionless, which could be considered as 'standardisation'. Doodson adjusted these factors along with the geodesic coefficients so that they would have a maximum value (as a function of the latitude) equal to the selected benchmark lunar potential, as follows:

$$C_L = 3 g a_T \chi_L / 4$$

Table 5.2 provides the contributions of the coefficient terms as a function of the m species and of the n degree of the Legendre polynomial. To simplify the formulations in the table, $H_{n,m}$ terms are expressed in the equatorial system; in the equations given in Appendix A, which are presented above (A1.1 and A1.4), $H_{n,m}$ terms are expressed as a function of the ecliptic coordinates.

TABLE 5.2: Doodson's development of the lunar potential.

n° species	n° $P_n(\cos\theta)$	Norm	Geodesic terms	Variable terms
m	n	$c_{n,m}$	$G_{n,m}/C_L$	$H_{n,m}$
0	2	1	$0.5(1-3\sin^2 L)$	$(2-6\cos^2 \varpi)/3$
0	3	0.004 947	$1.118\,03(3-5\sin^2 L)\sin L$	$(3-5\cos^2 \varpi)\cos \varpi$
1	2	1	$\sin 2L$	$\sin 2\varpi \cos \mathcal{H}$
1	3	0.011 425	$0.726\,18(1-5\sin^2 L)\cos L$	$(1-5\cos^2 \varpi)\sin \varpi \cos \mathcal{H}$
2	2	1	$\cos^2 L$	$\sin^2 \varpi \cos 2\mathcal{H}$
2	3	0.031 935	$2.598\,08 \sin L \cos^2 L$	$\sin^2 \varpi \cos \varpi \cos 2\mathcal{H}$
3	3	0.013 828	$\cos^3 L$	$\sin^3 \varpi \cos 3\mathcal{H}$

Note that Doodson forced the development as far as the Legendre polynomial $P_4(\cos\theta)$, which we have disregarded here. The $c_{n,m}$ coefficients provide relative magnitudes of the different terms of the development. However, due to the presence of latitude in the geodesic coefficient expression, terms corresponding to $c_{n,m}$ norms of the same magnitude are not directly comparable with respect to their tidal impact.

3.2 • Fundamental variables

There is no analytical solution for the movement of three bodies in a gravitational field, but this movement (and thus all phenomena that exclusively depend on it) can be described via five independent parameters. When the tide is taken into account (additional movement of water particles relative to the Earth), which is regulated by relative movements of three celestial bodies (Earth, Moon and Sun), a sixth parameter associated with the Earth's rotation around the polar axis must be added. As the orbits of these celestial bodies are elliptic, their angular velocity is not mechanically uniform. We know that the definition of the mean time (see A) is based on the 'mean Sun' concept describing the ecliptic of a uniform movement (from vernal point to vernal point) over the same timespan (tropical year) as the apparent Sun. This also holds for the mean Sun, which is defined as a hypothetical celestial

body whose orthogonal projection on the ecliptic is governed by a uniform movement with a revolution time identical to that of the real Moon. The ecliptic longitudes of these fictitious celestial bodies are called 'mean celestial body longitudes'. Although these names are inaccurate because they obviously do not designate the actual mean longitudes, they are now time-honoured terms. In any case, no confusion is possible since the mean of a cyclic variable is senseless.

Hereafter, and according to the adopted conventions, the symbols s (from *selene*, for Moon in Greek) and h (for *helios*) represent the mean longitudes of the Moon and Sun, respectively. The mean longitudes of lunar perigee p, of the ascending node N and of solar perigee p_1 are defined according to the same principle: they are angles (measured positively from the vernal point) of the corresponding mean elements. These five independent parameters are enough to describe movements related to the three celestial bodies (Earth, Moon, Sun). As noted above, for the movement of a particle on the globe (fourth mobile element in the ecliptic reference frame), it is necessary to add a sixth parameter linked with the Earth's rotation. It would seem natural to select the local hour of the mean time that accurately describes the apparent movement of the mean Sun. However, as the Moon is the main tide-generating body, it is preferable to use the mean lunar time which, for consistency, will be expressed in degrees. This is t, i.e. the parameter representing the hour in civil time (n.b. the mean local time plus 12 h). The τ variable represents the hour angle of the mean Moon, i.e. plus 180° by analogy with the civil time. This may be called the 'lunar civil time', and is expressed by equation (figure 5.1):

$$\tau^\circ = 15^{\circ/\mathrm{h}} \cdot t^\mathrm{h} + h^\circ - s^\circ \tag{5.6}$$

These six parameters (τ, s, h, p, N, p_1) are independent cyclical variables as there is no common period between any of them. All of these variables are increasing functions of time, except for the mean longitude N of the ascending node. For consistency with the other parameters, it is replaced by its opposite value $\mathrm{N}' = -\mathrm{N}$.

Where T represents the time expressed in Julian centuries of 36525 days of mean time since 1 January 2000 at midday in civil time (local), Table 5.3 gives the relations as a function of T, thus enabling calculation of the value of each of these fundamental variables with better than a hundredth of a degree accuracy over several centuries. This level of accuracy, as sought by astronomers, is by far sufficient to obtain an excellent quality tidal prediction over several centuries.

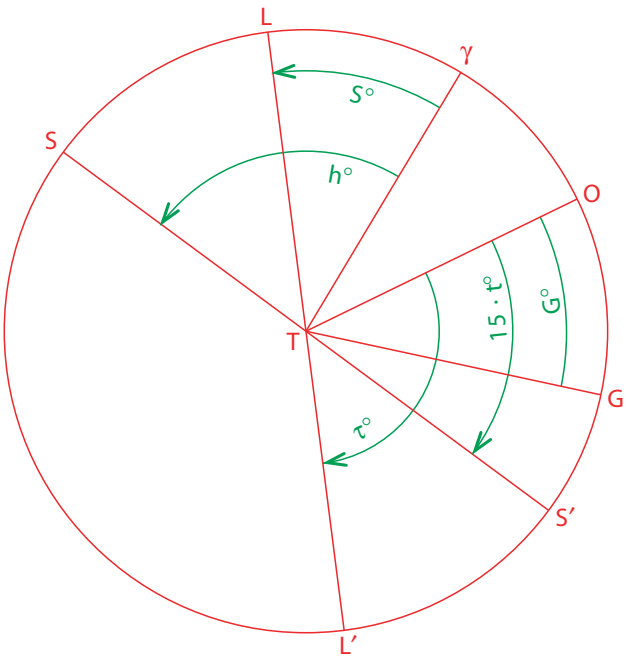

FIGURE 5.1: Relationship between the hour angles and mean longitudes of celestial bodies. Time t (expressed in h), gives the hour angle of $15 \cdot t°$ ($= 15^{°/\mathrm{h}} \cdot t^{\mathrm{h}}$). The lunar civil hour angle τ is thus given by the relation $\tau = 15t + h - s$ (angles are in degrees).

4 • Doodson's classification

Note that the lunar potential amplitudes derived from $P_4(\cos\theta)$ are all 10^{-5} fold lower than the peak amplitude of this potential (M_2 wave), apart from a few that are very close to this lower threshold arbitrarily set by Doodson. We thus disregard the latter amplitudes and the development considered here stops at the $P_3(\cos\theta)$ term.

Doodson presented all terms of the development in a single table. The proposed classification is based on the expression of the argument (each constituent of the potential) by a linear function of six fundamental variables ranked in order of decreasing angular velocities (Table 5.4). This table also shows the arguments expressed according to two types of coding (numerical or alphabetical). The numerical coding proposed by Doodson is discussed later in the text (with the corresponding literal coding).

When taking equation (5.5) for elementary potentials A_n and the argument formulations based on fundamental variables into account, Doodson's

TABLE 5.3: Relations giving fundamental variables in arc degrees as a function of the mean time T expressed in Julian centuries. The time origin is 01/01/2000 12:00:00 of the civil time t, which in turn is expressed in hours (with 1 h corresponding to 15°).

Fundamental variables (Mean longitude ML)	Value of the variable in degrees, as a function of time T in Julian centuries	Period d, days; y, years
Civil lunar hour angle	$\tau° = 15^{°/\mathrm{h}} t^{\mathrm{h}} + h° - s°$	1.035 050 d
ML of the Moon	$s° = 218.316\,5 + 481\,267.880\,4\mathrm{T} - 0.001\,6\mathrm{T}^2$	27.321 582 d
ML of the Sun	$h° = 280.466\,1 + 36\,000.769\,8\mathrm{T} + 0.000\,3\mathrm{T}^2$	365.242 199 d
ML of the lunar perigee	$p° = 83.353\,5 + 4\,069.021\,5\mathrm{T} - 0.103\mathrm{T}^2$	8.847 309 y
Point opposite the ML of the ascending lunar node	$\mathrm{N}' = -\mathrm{N}° = 234.555 + 1\,934.136\,3\mathrm{T} + 0.0021\mathrm{T}^2$	18.612 904 y
ML of the solar perigee	$p°_1 = 282.938\,4 + 1.719\,5\mathrm{T} + 0.000\,5\mathrm{T}^2$	20 940.21 y

TABLE 5.4: Classification of fundamental variables and ratio of magnitudes to the mean lunar angular velocity.

Rank	Symbol	Angular velocity Degrees/h	Angular velocity ratio	Numerical argument	Alphabetical argument
1	τ	14.492 052 121	$1.00 \cdot 10^{0}$	1 5 5 5 5 5	A Z Z Z Z Z
2	s	0.549 016 518	$3.79 \cdot 10^{-2}$	0 6 5 5 5 5	Z A Z Z Z Z
3	h	0.041 068 640	$2.83 \cdot 10^{-3}$	0 5 6 5 5 5	Z Z A Z Z Z
4	p	0.004 641 822	$3.20 \cdot 10^{-4}$	0 5 5 6 5 5	Z Z Z A Z Z
5	N'	0.002 206 407	$1.52 \cdot 10^{-4}$	0 5 5 5 6 5	Z Z Z Z A Z
6	p_1	0.000 001 962	$1.35 \cdot 10^{-7}$	0 5 5 5 5 6	Z Z Z Z Z A

development (5.4) may be expressed by equation (5.7) given in the following box, where the m_τ values define the species number:

Doodson's harmonic equation

$$\mathrm{U} = \sum_{n=2}^{n=3} \sum_{m_\tau=0}^{m_\tau=3} \mathrm{G}_{n,m_\tau}(\mathrm{L}) \times \sum_{\forall m_x=-5}^{\forall m_x=+6} \mathrm{A}_{\tau,x,\pi/2} \cos\Big[m_\tau \tau + m_s s + m_h h + m_p p + m_{\mathrm{N}'} \mathrm{N}' + m_{p_1} p_1 + m_{\pi/2} \frac{\pi}{2} \Big] \quad (5.7)$$

where

- the m_x coefficients of the five fundamental variables ($x = s, h, p, \mathrm{N}'$ or p_1) are integers ranging from -5 to $+6$;
- $\mathrm{A}_{\tau,x,\pi/2}$ is a simplification of $\mathrm{A}_{m_\tau m_s m_h m_p m_{\mathrm{N}'} m_{p_1} m_{\pi/2}}$

Summation of m_x coefficients from -5 to $+6$ leads to the harmonic series development of the lunar orbit parameters provided by Brown. Actually, constituents with a value over Doodson's threshold correspond to m_x integer coefficients within the -5 to $+6$ range. For the m_τ species, the $\mathrm{G}_{2,m_\tau}(\mathrm{L})$ geodesic coefficients are derived from the $\mathrm{P}_2(\cos\theta)$ term, and the $\mathrm{G}_{3,m_\tau}(\mathrm{L})$ geodesic coefficients are derived from the $\mathrm{P}_3(\cos\theta)$ term. Due to the presence of sines and cosines containing τ in $\mathrm{H}_{n,m}$, the $\pi/2$ angle is given in

equation (5.7) with a $m_{\pi/2}$ integer coefficient in such a way that only cosines are obtained in the development. This coefficient is even for geodesic coefficients associated with cosines ($G_{2,0}$, $G_{2,2}$, $G_{3,1}$, $G_{3,3}$), and odd for geodesic coefficients associated with sines ($G_{2,1}$, $G_{3,0}$, $G_{3,2}$).

Doodson's classification represented an extremely convenient advance in the presentation of tide-generating potential terms in a single table. Note, however, that the tide-generating force is a diffuse phenomenon in oceans and that the geodesic coefficients reflect the effect of latitude on the action of this force. The result is that when these coefficients are from different Legendre polynomials their origin is distinct, which means that it would be risky to compare their respective $A_{\tau,x,\pi/2}$ amplitudes. This remark applies especially to harmonic development elements that are linked to geodesic coefficients of the $P_3(\cos\theta)$ term of the lunar potential: presumably they are not comparable to those associated with $G_{2,m_\tau}(L)$ coefficients. Some constituents of these two origins also have identical frequencies, which could add to the confusion. They should be distinguished in the listings to ensure clarity. Because of the remoteness of the Sun, we have seen that the terms of its generating potential, derived from $P_3(\cos\theta)$, are all negligible. The problem just noted for the Moon therefore does not apply for the Sun. The nature of the gravitational pull of the Sun does not differ from that of the Moon, so it seems at first glance that their effects could be cumulated. However, there also seems to be a significant complementary action linked to the effect of solar radiation on the tide level, which thus hampers interpretation. This action, which may be direct (water dilation) or indirect (meteorological effects), leads to diurnal, seasonal and annual cycles. This results in tide level variations, i.e. the radiational tide, in addition to diurnal or seasonal variations in the gravitational tide. By this radiational action, the behaviour of the solar constituents differs from that of the lunar constituents. Although this effect is weak, it is still enough to substantially modify the solar gravitational constituents. Since their respective frequencies are identical, it is not possible to distinguish the parts associated with each of these actions. It has been proposed that a radiational potential could be introduced, which is calculated from the solar radiation that reaches the Earth's surface. However, due to the complexity of the oceanic response to this action, it is not really possible to benefit from these developments. It would be preferable to list the solar constituents separately while only maintaining the gravitational potential coefficients in order to be able to highlight constituents that could eventually be disturbed by radiational frequencies, thus enhancing interpretation of differences between the respective actions of each celestial body. Only these coefficients may be compared directly to the lunar potential coefficients.

5 • Doodson numbers, argument numbers and letters

For constituents with a non-negligible value (according to Doodson's 10^{-5} criterion), we have already pointed out that m_x integer coefficients of the five astronomic parameters ($x = s, h, p, \mathrm{N}', p_1$), which are involved in the harmonic development cosine argument, range from -5 to $+6$. To obtain a concise representation of this series of figures, by elimination of the negative signs, it is easy to add a value of 5 to each of them. Moreover, to avoid having to characterise each of the highest coefficients (5 and 6) by a two-figure number, the number 10 is usually replaced by the Roman numeral X and the number 11 is replaced by E (for eleven). For interacting tidal frequencies, it has even been proposed that a star $*$ and the letter T (for twelve) could be added for coefficients -1 and $+12$, respectively. The m_τ factor of the Moon's civil hour angle τ, which represents the species number (hence always positive or nil), remains unchanged. The thus defined series of figures or letters, including the m_τ coefficient (unchanged) and then the figures or letters, is the result of the coding of m_x coefficients that are classified in decreasing order of angular velocities of the five astronomic LP parameters ($x = s, h, p, \mathrm{N}', p_1$). In other words, here the 'Doodson number' or 'argument number' refers to the integral number (or alphanumerical expression) denoted by the $\mathrm{N_D}$ symbol, such that:

$\mathrm{N_D} = 10(10(10(10(10(m_\tau) + m_s + 5) + m_h + 5) + m_p + 5) + n_{\mathrm{N}'} + 5) + m_{p_1} + 5$

$\mathrm{N_D}$ is an integral number for all $-5 \leq m_x \leq 4$;

$\mathrm{N_D}$ is an alphanumerical expression for:

$$\begin{aligned} m_x = -6 \quad &: \quad m_x + 5 \Rightarrow * \\ m_x = 5 \quad &: \quad m_x + 5 \Rightarrow \mathrm{X} \\ m_x = 6 \quad &: \quad m_x + 5 \Rightarrow \mathrm{E} \\ m_x = 7 \quad &: \quad m_x + 5 \Rightarrow \mathrm{T} \end{aligned}$$

where $x = s, h, p, \mathrm{N}$ or p_1

Let us consider, for instance, the equlibrium argument of the mean semidiurnal solar constituent, denoted $\mathrm{S_2}$ by Darwin, whose period is exactly 12 h. Considering equation (5.6), this argument can be expressed in degrees as follows:

$$\mathrm{V_{S_2}} = 30^{\circ/\mathrm{h}} t^{\mathrm{h}} = 2\tau + 2s - 2h$$

This gives the following table for the m_x coefficients of the six fundamental variables, with n_D being the Doodson coefficient corresponding to each coefficient:

Coefficient m_x	m_τ	m_s	m_h	m_p	$m_{N'}$	m_{p_1}
Value for S_2	2	2	−2	0	0	0
Added figure	0	5	5	5	5	5
n_D	2	7	3	5	5	5

from which we deduce the Doodson number representing the S_2 constituent:

$$N_D(S_2) = 273555$$

The equilibrium argument of the mean semidiurnal lunar constituent (denoted M_2), is formulated as:

$$V_{M_2} = 2\tau$$

with the following coefficient table:

Coefficient	m_τ	m_s	m_h	m_p	m_N	m_{p_1}
Value for M_2	2	0	0	0	0	0
Added figure	0	5	5	5	5	5
n_D	2	5	5	5	5	5

The argument number for this wave is:

$$N_D(M_2) = 255555$$

This procedure developed by Doodson is still widely used. One of its advantages is that, since the argument numbers are classified in increasing order, the angular velocities of the corresponding constituents will be automatically ranked in increasing order. This procedure is often amended by adding a seventh figure $n_{D,\pi/2}$ associated with the $m_{\pi/2}$ coefficient to the Doodson number in equation (5.7). This seventh figure accounts for the fact that it is the argument of a cosine whose $m_{\pi/2}$ coefficient can be positive or negative. We have seen that this $m_{\pi/2}$ coefficient represents the factor that should be allocated to the $\pi/2$ angle so as to ensure that the argument of the considered constituent will become the argument of a positive cosine coefficient. For consistency, the number 5 is added to $m_{\pi/2}$ to form what could be called the 'extended Doodson number', which we symbolise by $N_E(i_i)$ for constituent i_i.

Hence, when $n_{D,\pi/2} = m_{\pi/2} + 5$, for a ϕ argument, we have

- for a positive sine coefficient:

$$\sin\phi = \cos[\phi - 1(\pi/2)] \Rightarrow m_{\pi/2} = -1 \Rightarrow n_{D,\pi/2} = 4$$

- for a positive cosine coefficient:

$$\cos\phi = \cos[\phi + 0(\pi/2)] \Rightarrow m_{\pi/2} = 0 \Rightarrow n_{D,\pi/2} = 5$$

- for a negative cosine coefficient:

$$-\sin\phi = \cos[\phi + 1(\pi/2)] \Rightarrow m_{\pi/2} = 1 \Rightarrow n_{\mathrm{D},\pi/2} = 6$$

- for a negative sine coefficient:

$$-\cos\phi = \cos[\phi + 2(\pi/2)] \Rightarrow m_{\pi/2} = 2 \Rightarrow n_{\mathrm{D},\pi/2} = 7$$

Another very popular alternative involves replacing the argument number figures by a completely literal codification. Harmonic development of the tide-generating potential is highly compatible with Doodson's representation since most of the constituents have a numerical codification. However, the harmonic representation of the oceanic response is more complex than that of the potential. Indeed, hydrodynamic interactions, especially in shallow areas, are not linear and new frequencies may be noted on tide level records (see Chapter I). Some of these compound waves require, for the main variable coefficients, values that are not within the $[-5, +6]$ interval taken into account for the potential. The present solution is to replace the Doodson alphanumerical characters by letters. The table below shows the correspondence between the $m_\forall$ coefficient value of each parameter (including τ and $\pi/2$), the Doodson coding n_D of the m_x and $m_{\pi/2}$ coefficients (with the m_τ coefficients remaining unchanged), and Λ, the literal codification of all $m_\forall$ (with no restrictions):

$m_\forall$	-7	-6	-5	-4	-3	-2	-1	0	1	2	3	4	5	6	7	8	9	10
$n_\mathrm{D}(m_\forall \neq m_\tau)$		*	0	1	2	3	4	5	6	7	8	9	X	E	T			
$\Lambda(m_\forall)$	S	T	U	V	W	X	Y	Z	A	B	C	D	E	F	G	H	I	J

Traditions obviously have some importance and cannot be disregarded, but the literal codification is just as easy as that of Doodson. Its use should, since it is not hampered by any restrictions, be widely adopted (not the analogy with the time zone principle). Concerning the M_2 and S_2 constituents exemplified above, their equilibrium arguments are associated with cosines whose coefficients in the development of the potential are positive ($m_{\pi/2} = 0 \Rightarrow n_7 = 5$). Recall that $\mathrm{N_E}(q_i)$ denotes the extended Doodson number for the q_i constituent, or its literal equivalent $\mathrm{N}_\Lambda(q_i)$. It thus becomes:

- for the S_2 constituent

$$\mathrm{N_E}(\mathrm{S_2}) = 2735555$$
$$\mathrm{N}_\Lambda(\mathrm{S_2}) = \mathrm{B\,BXZ\,ZZZ}$$

- for the M_2 constituent

$$N_E(M_2) = 2555555$$
$$N_\Lambda(M_2) = B\,ZZZ\,ZZZ$$

Note that waves having the same m_τ form a species. Those with the same respective m_τ and m_s coefficients form a group. Within a group, constituents having the same m_p, $m_{N'}$ and m_{p_1} represent a subgroup.

6 • Harmonic tidal equation

So far we have looked at the tide-generating potential developments successively proposed by Laplace, Kelvin, Darwin and Doodson. The harmonic development highlighted the problem of constituent listings, with the constituent numbers continuing to increase, i.e. around 20 for Kelvin, around 40 for Darwin, and over 200 for Doodson. Doodson then proposed a constituent codification, which was very convenient for the tide-generating potential. This representation ranks constituents according to increasing argument numbers with the constituent frequency. However, an analysis of tide level measurements revealed m_τ species that were not present in the potential development, as well as m_x coefficients that were not within the thresholds set by Doodson. The listing of these waves created by nonlinear hydrodynamic interactions warranted the literal coding based on the representation of a wave determined by seven alphabet letters. Moreover, two procedures were used for the harmonic tide-generating potential development. The first, which was used by Darwin and Doodson, involves solving the problem analytically on the basis of current theories concerning the Moon and Sun. The second, which is hard to apply without access to modern calculation technology, involves harmonic analysis of the potential over long periods. Several developments were proposed after Doodson's, especially by the terrestrial tide research community, but they did not provide any substantial advances with respect to the analysis of ocean tides. The development provided in the tables given in Appendix C are from the analysis of lunar and solar tide-generating potentials spanning eight orbital periods of the ascending node of the Moon, i.e. approximately 150 years. The results are similar (up to the fifth decimal) to those published elsewhere. They have been used to calculate time series, i.e. completely semidiurnal and completely diurnal, in order to be able to combine and simulate nonlinear interactions responsible for shallow water waves. These interactions have been calculated up to the fifth order for semidiurnal constituents so as to be able to reach twelfth

diurnal species constituents. Around 600 frequencies have thus been determined (see Appendix D).

6.1 • Oceanic response: compound waves

When a hydrodynamic wave generated by the tide-generating force in the oceans passes over shallow areas, the water depth influences wave propagation. High water progression is generally faster than low water retraction due to the combined effect of friction force, which has a greater impact in shallow waters, and the gravitiational wave velocity, which is proportional to the square root of the depth, especially in coastal regions where the bottom slope is very gradual. Hence, a wave, which will have the frequency of one tide potential constituent and be completely sinusoidal in the deep open ocean, will be deformed and gradually lose this sinusoidal aspect as it progresses over increasingly shallow bottoms (as in estuaries; figure 1.8). Its amplitude will increase to the point that it will no longer be negligeable over shallow bottoms close to the coast. This wave will never undergo modification in its initial period. However, as its shape will no longer be sinusoidal, its profile modification will be reflected in the spectral domain by the appearance of harmonics that are greater than the fundamental initial frequency. Actually, the tidal wave is not entirely sinusoidal and the above schematic outline of the deformation process is not completely correct, but the approach is more acceptable. We postulate that the original wave has an amplitude and phase that varies periodically, and also that the coefficients of the original harmonic development could themselves be the focus of a development considering the superior harmonics of this modulation frequency. Although no corresponding developments are required, we have noted the appearance of constituents whose frequencies are combinations of the fundamental frequency and the modulation frequency.

Other approaches, especially mathematical methods and the perturbation method, can also be applied. The perturbation method is based on equations that model the hydrodynamics of oceanic tide propagation, while clearly distinguishing between linear and nonlinear terms (considered as small perturbations). The solution of the nonlinear part, which contains only the tide-generating potential frequencies, is specifically inserted into the nonlinear terms. These terms then give rise to periodic constituents that include frequency combinations derived from the tide-generating potential.

A tidal wave undergoes spatiotemporal distortion when it propagates into shallow water areas, thus giving rise, in the spectral domain, to so-called ‘shallow water constituents’ or ‘interaction waves’ that have frequency com-

binations that derive from the tide-generating potential. Some of these are harmonic terms of the main tide-generating potential constituents. Hence, the semidiurnal M_2 and S_2 constituents give rise to higher harmonic terms, e.g. quarter-diurnal, sixth-diurnal, etc., given by the symbols M_4, M_6, …, and S_4, S_6, …, where the subscript represents the number of oscillations per lunar day (M waves) or solar day (S waves). However, most shallow water waves are the result of interactions between tide-generating potential constituents, mainly between the greatest ones, which are (see Tables 5.1a and 5.1b): M_2, S_2,N_2, K_2, K_1, O_1, P_1 and Q_1. The symbols adopted to represent each interaction wave consist of the letters of the main constituents from which they are derived and a subscript representing the species to which the wave belongs, i.e. the number of cycles per day. For instance, the constituent having an angular velocity equal to the sum of those of M_2 and S_2 represents the quarter-diurnal wave symbolised by MS_4. The examples given below should familiarise readers with these notations. Where q_i denotes the angular velocity of constituent i, we have, for instance:

$$
\begin{aligned}
q_{\mathrm{KQ_1}} &= q_{\mathrm{K_2}} - q_{\mathrm{Q_1}} \\
q_{\mathrm{2MS_2}} &= 2q_{\mathrm{M_2}} - q_{\mathrm{S_2}} \\
q_{\mathrm{MK_3}} &= q_{\mathrm{M_2}} + q_{\mathrm{K_1}} \\
q_{\mathrm{2MK_3}} &= 2q_{\mathrm{M_2}} - q_{\mathrm{K_1}} \\
q_{\mathrm{MS_4}} &= q_{\mathrm{M_2}} + q_{\mathrm{S_2}} \\
q_{\mathrm{2MKS_4}} &= 2q_{\mathrm{M_2}} + q_{\mathrm{K_2}} - q_{\mathrm{S_2}} \\
q_{\mathrm{4MK_5}} &= 4q_{\mathrm{M_1}} + q_{\mathrm{K_1}} \\
q_{\mathrm{2MK_5}} &= 2q_{\mathrm{M_2}} + q_{\mathrm{K_1}} \\
q_{\mathrm{2MS_6}} &= 2q_{\mathrm{M_2}} + q_{\mathrm{S_2}} \\
q_{\mathrm{2(MS)K_6}} &= 2(q_{\mathrm{M_2}} + q_{\mathrm{S_2}}) - q_{\mathrm{K_2}}
\end{aligned}
$$

Letters representing tide-generating potential constituents involved with negative angular velocities are placed in the last position. Some interaction waves have the same angular velocities as constituents of this potential, e.g. for the $2MS_2$ wave combined with the μ_2 variational constituent of the potential, or $2MN_2$ combined with the L_2 minor ellipsoid.

Once produced, these interaction constituents propagate autonomously, eventually beyond the zone from which they originated, e.g. quarter-diurnal waves have been noted in the middle of the Atlantic Ocean. Moreover, they may eventually be amplified or, conversely, attenuated depending on the propagation conditions. They may also interact and give rise to interactions of a higher degree.

Numerical modelling may be used to quite accurately simulate them but, because of the extremely high complexity of their interactions and propagation, which depends closely on the bathymetry (generally very chaotic), it is impossible to provide any elements that could be used to even roughly determine rules underlying their behaviour. At most, it may be stated that when the tidal amplitude is substantial it is quite likely that these interaction waves will be relatively strong in shallow areas. Estuaries with a quite simple geometry have been the focus of studies whose results have facilitated interpretation of the highly typical deformation of the tidal curve during the tide's upstream progression. Simultaneous water level measurements at several points along estuaries have thus enabled analysis of interaction tidal wave behaviour and modelling of the formation process. The curves (figure 1.8) obtained for the Gironde River basin (France), clearly show the deformation of the wave shape between Verdon (at the mouth of the estuary) and Bordeaux (≈100 km upstream) for both flood and ebb tides. The flood tide duration, which is around 7 h at the Verdon site, decreases gradually as the tide progresses upstream, i.e. it is only around 4.5 h at Bordeaux. Conversely, the ebb tide has a longer duration upstream (≈ 8.5 h at Bordeaux) than at the mouth of the estuary (≈ 6 h). The propagation velocity at high water is thus faster (≈40 km/h) than that at low water (≈25 km/h). The approximately sinusoidal wave shape at the estuary mouth is transformed to the extent that cusps may be noted on curves plotted for the most upstream sites. This feature, which is very marked around low water, denotes a discontinuity in the water height variation pattern. Tide logs obtained even further upstream revealed even more marked irregularities at high water of spring tide. Such marked irregularities give rise to a tidal bore phenomenon, i.e. a breaking wave that forms at around low water and propagates up the estuary. In the spectral domain, the tidal bore and even the turning point of the tidal curve can only be reflected by a series of spectral lines extending to infinite frequencies that are beyond reach for analysis. Excluding these extreme cases, analysis of esutuary tides generally reveals spectral lines past the twelfth diurnal. An indepth analysis of the high frequencies also revealed a proliferation of interacting waves evolving with the species degree. All of these specific features complicate harmonic analysis of this type of tide. Indeed, the harmonic analysis method is based on identification of the origin of all constituents involved in constituting the spectral line representative of the interaction wave. Experience has shown that this is a laborious task for species above the twelfth diurnals. This problem is further complicated by the fact that the discharge of streams running into estuaries interacts with the tides. With two different discharge rates, two different corresponding

spectral signatures will influence the tidal curve. Here we are reaching the limits of application of the harmonic analysis method.

6.2 • Harmonic tidal equation

As the tide level at a given site depends not only on the time, the chosen temporal reference must be specified before formulating the harmonic tidal equation. First, for convenience, the time unit used in the harmonic tidal equation is the mean time (in hours), preferentially to the legal unit (i.e. seconds). There are several temporal reference possibilities available for tide logging or forecasting. We could adopt one of the following references (expressed in hours):

• t_0, the universal time (UT), which is the civil time at the baseline meridian (Greenwich meridian);

• t_n, the time in time zone n at site M(n.b. n ranges from 0 h to 23 h eastward from Greenwich, with 1 corresponding to 15°).

• t, civil time at site M on longitude meridian G (measured positively in degrees eastward from the baseline meridian).

These temporal references are linked by the following relations:

$$\begin{aligned} t_0 &= t_n - n = t - (\mathrm{G}/15) \\ t_n &= t_0 + n = t + n - (\mathrm{G}/15) \\ t &= t_0 + (\mathrm{G}/15) = t_n + (\mathrm{G}/15) - n \end{aligned} \tag{5.8}$$

For the study of the tide-generating potential, we have used the local civil time (symbolised above by t). The oceanic response to excitation of the tide-generating force at a given site leads to a temporal variation in the tide level $h(t)$, which may be in the form of a sum of sinusoidal functions:

$$h(t) = \sum_i h_i \cos[\mathrm{V}_i(t) - \kappa_i]$$

where h_i is the amplitude of argument V_i(as a function of t), which can be an equilibrium argument or an argument of an interaction constituent (combination of equilibrium arguments):

$$\mathrm{V}_i = m_{\tau,i}\tau + m_{s,i}s + m_{h,i}h + m_{p,i}p + m_{\mathrm{N},i}\mathrm{N} + m_{p_1,i}p_1 + m_{\pi/2,i}\frac{\pi}{2}$$

where $\tau = 15t + h - s$, and the phase lag κ_i is called the phase lag of the $\mathrm{V}_i(t)$ argument.

We have seen that fundamental variables (s, h, p, N' and p_1) are linear functions of time. Hence, for each i constituent, a constant angular velocity

q_i may be determined and is generally expressed in degrees per hour. The following equation can thus be formulated:

$$h(t) = \sum_i h_i \cos(\mathrm{V}_{i,0} + q_i t - \kappa_i)$$

where $\mathrm{V}_{i,0}$ is, as in equation (5.1), the equilibrium argument at time $t = 0$ (justification of the second subscript in $\mathrm{V}_{i,0}$). With the temporal reference t, the κ_i parameter represents the absolute phase lag of constituent i. If this constituent is directly derived from the potential, the time period obtained by dividing the κ_i phase lag by the angular velocity q_i represents the lag of wave i with respect to the element corresponding to the tide-generating potential. The harmonic constants of tide relative to a site M are formed by the set of κ_i phase lags and h_i amplitudes calculated for this site.

The civil time at a site is seldom used in practice. Instead, the universal time or the time in the time zone of the site are used for routine purposes. Equations (5.8) enable us to determine the relative phase lags with respect to the Greenwich meridian by using:

- the universal time (UT), denoted here by t_0,
- or the time t_n of the local time zone n.

Note first that in the light of the third part of equation (5.8), the fundamental variable τ at site M is expressed as a function of time t_0 by:

$$\tau = 15t + h - s = 15t_0 + h - s + \mathrm{G}$$

Moreover, for $t = 0 \Rightarrow t_0 = \dfrac{-\mathrm{G}}{15}$, the equilibrium argument $\mathrm{V}_{i,0}$ of constituent i, with angular velocity q_i, can thus also be formulated as follows:

$$\mathrm{V}_{i,0} = \mathrm{V}_{i,0,0} + m_{\tau,i}\mathrm{G} - q_i \frac{\mathrm{G}}{15}$$

where $\mathrm{V}_{i,0,0}$ is the equilibrium argument of constituent i at the Greenwich meridian at time $t_0 = 0$, with $m_{\tau,i}$ being the species to which this constituent belongs.

Hence, depending on the temporal reference used, we have three equations:

$$h(t) = \sum_i h_i \cos\left(\mathrm{V}_{i,0} + q_{i.} t - \kappa_i\right)$$

$$h(t_0) = \sum_i h_i \cos\left(\mathrm{V}_{i,0,0} + q_i t_0 - g_{i,0}\right)$$

$$h(t) = \sum_i h_i \cos\left(\mathrm{V}_{i,0,0} + q_i t_n - g_{i,n}\right)$$

Recall that κ_i is the absolute phase lag of constituent i. Parameter $g_{i,0}$ is then the relative phase lag with respect to the Greenwich meridian and at universal time t_0, and $g_{i,n}$ is the relative phase lag with respect to the Greenwich meridian and at the time in the local time zone $t_n = t_0 + n$.

The relationships between these different phase lags are deduced from the previous equations concerning the temporal references:

$$g_{i,0} = \kappa_i - m_{\tau,i}\mathrm{G}$$
$$g_{i,n} = g_{i,0} + q_{in}$$

Amplitudes h_i and phase lags (κ_i, $g_{i,0}$ or $g_{i,n}$) are harmonic constants of tide, and in practice cannot be separated from the time.

In practice, only constants from Darwin's list are generally available. The others are considered with nodal corrections (amplitude f_i and phase lag u_i factors) which are assumed to be constant over a period of around a year. The harmonic equation used in current practical applications is thus as follows:

$$h(t_n) = h_{\mathrm{NM}} + \sum_i f_i h_i \cos(\mathrm{V}_{i,0,0} + q_i t_n - g_{i,n} + u_i)$$

where h_{NM} is the mean water level at the considered site.

Nodal corrections are available in table form, but they can also be calculated from Doodson's development while also taking known nonlinear interactions into account. This latter issue is studied in the next chapter.

VI
Harmonic analysis

The first analysis methods that were developed for manual tide prediction computation are not covered in this document. They are based on simple linear combinations of tidal height measurements (i.e. integer coefficients) designed to amplify a given wave while more or less eliminating other constituents and noise. Some of these analysis methods (there are many) have been adjusted to be suitable for automatic computation and are likely still being used, especially Doodson's method. However, because of their lack of flexibility, they do not always tap the full potential offered by modern computation methods.

The methods described in this chapter are highly efficient for dealing with long historical data series (up to 150 years) and are flexible enough to accept even short-term tidal data and series with gaps in the data. Like all quantifiable phenomena, temporal water level variations – with the tide being a major constituent – can be readily analysed by spectral techniques using the Fourier transform. Key elements concerning Fourier transforms and series are presented in Appendix D. However, they are briefly outlined here to highlight the impact of aliasing in the analysis of very broad spectrum tides. Then, because of the many constituents (potential and compound waves: around 600 frequencies are listed in Appendix D), we will see how a filter was tailored to deal with separate species. Meteorological effects and measurement errors give rise to spectral perturbations, which are considered as noise in tidal analysis, that must be effectively eliminated. Moreover, the focus is placed especially on the problem of poorly separated constituents and on efficiently conditioning the harmonic analysis by the least-squares method. Finally, the question of nodal corrections and interaction waves is discussed.

1 • Spectral analysis

Spectral analysis involves locating, on a frequency scale, amplitudes that are 'significant' relative to temporal variations in the studied phenomenon, i.e. tide level in our case. Considering its periodic pattern, the tide would clearly seem to be amenable to this type of analysis. The general spectral features of tides were already discussed in Chapter I (figures 1.9, 1.10 and 1.11). The tide has amplitudes that are much higher than the noise at typical clearly established frequencies – it is said that the tide has a line spectrum. The examples given in these figures were obtained using an algorithm called a fast Fourier transform (FFT), but it is actually a rapid algorithm of a discrete Fourier transform (DFT).

Readers requiring further details on fundamental elements of Fourier transforms and series should refer to Appendix D, especially to gain greater insight into the role played by sampled data distributions (Dirac pulse or rectangular distribution).

1.1 • Overview of spectral analysis of tide

At a given location and at time t, $h(t)$ represents the tidal height above its average level. The harmonic tidal equation is represented by the sum of its constituents i:

$$h(t) = \sum_i h_i \cos(\mathrm{V}_{0i} + q_i t - g_i) \tag{6.1a}$$

where here the value of i is considered as a sequence number ($i \in \mathrm{N}^*$) according to the angular velocities q_i (positive). Note that parameter V_{0i} is the cosine argument in the development of the potential at time zero ($t = 0$) and g_i is the phase lag of the tide at the considered site (this parameter is dependent on the temporal reference frame used: LT is the standard or local civil time).

Assuming that

$$\eta_i = h_i e^{-j(g_i - \mathrm{V}_{0i})}$$

and

$$\nu_i = \frac{q_i}{2\pi} \tag{6.2}$$

equation (6.1a) becomes:

$$h(t) = \frac{1}{2} \sum_{i \in \mathrm{N}^*} \left(\eta_i e^{j2\pi\nu_i t} + \eta_i^* e^{-j2\pi\nu_i t} \right) \tag{6.1b}$$

In practice, observations are recorded at a regular interval, with measurements obtained every t_e. Where M is the number of samples, the useful observation period is $\mathrm{T} = \mathrm{M}t_e$.

Where $\Pi_{\mathrm{T},t_e}(t)$ is the rectangular distribution, it is defined by:

$$\Pi_{\mathrm{T},t_e}(t) = t_e \sum_{m=0}^{m=\mathrm{M}-1} \delta(t - mt_e)$$

The part of the $h(t)$ record sampled by the rectangular distribution $\frac{1}{\mathrm{T}}\Pi_{\mathrm{T},t_e}(t)$ is represented by the distibution in figure 6.4:

$$h_{\mathrm{T},t_e}(t) = \frac{1}{\mathrm{T}}\Pi_{\mathrm{T},t_e}(t)\ h(t) = \frac{1}{\mathrm{M}} \sum_{m=0}^{m=\mathrm{M}-1} h(mt_e)\ \delta(t - mt_e) \tag{6.3}$$

For a Fourier transform $\mathrm{F}_{\mathrm{T},t_e}(\upsilon)$, a continuous function of the frequency, this distribution assumes:

$$\mathrm{F}_{\mathrm{T},t_e}(\upsilon) = \int h_{\mathrm{T},t_e}(t)\, e^{-j2\pi\upsilon t} = \frac{1}{\mathrm{M}} \sum_{m=0}^{m=\mathrm{M}-1} h(mt_e)\, e^{-j2\pi\upsilon m t_e} \tag{6.4}$$

Expressing $h(mt_e)$ according to equation (6.1b) reveals geometric series of ratios $e^{i2\pi(\upsilon_i-\upsilon)t_e}$ and $e^{-i2\pi(\upsilon_i+\upsilon)t_e}$. This therefore becomes:

$$\mathrm{F}_{\mathrm{T},t_e}(\upsilon) = \frac{1}{2}\sum_i \left[\eta_i \Lambda^*_{\mathrm{T},t_e}(\upsilon - \upsilon_i) + \eta_i^* \Lambda_{\mathrm{T},t_e}(\upsilon + \upsilon_i)\right] \tag{6.5}$$

an expression in which $\Lambda_{\mathrm{T},t_e}(x) = \dfrac{\sin(\pi x \mathrm{M}\, t_e)}{\mathrm{M}\sin(\pi x t_e)} e^{-j\pi x(\mathrm{M}-1)t_e}$

Note that $\Lambda_{\mathrm{T},t_e}(\upsilon)$ is the FT of the rectangular function $\frac{1}{\mathrm{T}}\Pi_{\mathrm{T},t_e}(t)$, which enables us to obtain equation (6.5) directly by the convolution product

$$\mathrm{F}_{\mathrm{T},t_e}(\upsilon) = \Lambda_{\mathrm{T},t_e}(\upsilon) * \mathrm{F}(\upsilon) \tag{6.6}$$

where υ_e is the sampling frequency ($\upsilon_e = 1/t_e$), the periodic character of $\mathrm{F}_{\mathrm{T},t_e}(\upsilon)$ in the frequency domain ($\mathrm{F}_{\mathrm{T},t_e}(\upsilon) = \mathrm{F}_{\mathrm{T},t_e}(\upsilon + k\upsilon_e)$), associated with its Hermitian character for the real temporal function ($\mathrm{F}_{\mathrm{T},t_e}(\upsilon) = \mathrm{F}^*(-\upsilon)$), thus giving equation:

$$\mathrm{F}_{\mathrm{T},t_e}(\upsilon_e/2 - \Delta\upsilon) = \mathrm{F}^*_{\mathrm{T},t_e}(\upsilon_e/2 + \Delta\upsilon + k\upsilon_e)$$

which leads to aliasing, with $\Delta\upsilon$ being any frequency deviation. Frequency $\upsilon_{\mathrm{N}} = \upsilon_e/2$ is called the Nyquist frequency. Spectrum $\left|\mathrm{F}_{\mathrm{T},t_e}\right|$ thus has two symmetry axis families: $\upsilon = k\upsilon_e$ and $\upsilon = \upsilon_{\mathrm{N}} + k\upsilon_e$.

Consequently, the spectrum derived from the sampling function of a real signal is only representative of a real spectrum if the external constituents

at frequency interval $[0, \upsilon_N]$ can be overlooked (Shannon's theorem). For a complex signal, the Hermitian character is not verified, so the interval becomes $[-\upsilon_N, \upsilon_N]$. If necessary, prefiltering may be performed to get to these cases.

There are nevertheless situations in which the sampling frequency is such that constituents detected in the useful observation period are not representative of the real spectrum but instead derived from a number of aliasing distortions. This is the case, for instance, with respect to tidal heights determined by spatial altimetry, where the acquisition period is a few days. Then it is still possible to use DFT but, for each spectral constituent detected with a frequency of υ_d, a k value must be attributed in order to clarify $\upsilon = \pm\upsilon_d + k\upsilon_e$. This is possible for tidal constituents, since they have perfectly established frequencies.

Based on

$$\Lambda_{T,t_e}(\upsilon) = \frac{\sin(\pi\upsilon M t_e)}{M \sin(\pi\upsilon t_e)} e^{-j\pi\upsilon(M-1)t_e}$$

(FT of the rectangular function $\frac{1}{T}\Pi_{T,t_e}(t)$), discretized according to the frequency step $\upsilon_T = 1/T$, which gives:

$$\Lambda_{T,t_e}(\upsilon) \sum_{n=-M/2}^{n=M/2-1} \delta(\upsilon - m\upsilon_T) = \sum_{n=-M/2}^{n=M/2-1} \frac{\sin n\pi}{M \sin(n\pi/M)} e^{-jn\pi\frac{M-1}{M}} \quad (6.7)$$
$$= \delta(n)$$

All the terms are thus zero, except that for which $n = 0$, which corresponds to the Dirac pulse $\delta(\upsilon)$.

To the normalized rectangular distribution, a discrete series of time steps t_e,

$$\frac{1}{T}\Pi_{T,t_e}(t) = \frac{1}{M} \sum_{m=0}^{m=M-1} \delta(t - mt_e)$$

may be mapped with a discrete transform (line spectrum every $\upsilon_T = 1/T$) in the symmetrical rectangular frequency distribution of width υ_e.

Let $\upsilon_T = 1/T$.

The symmetrical rectangular frequency distribution

$$\Pi_{\upsilon_e,\upsilon_T}(\upsilon) = \sum_{n=-M/2}^{n=M/2-1} \delta(\upsilon - n\upsilon_T) \quad (6.8)$$

enables mapping, at the sample distribution $h_{T,t_e}(t)$, of the DFT defined by:

$$F_{\upsilon_e,\upsilon_T}(\upsilon) = \Pi_{\upsilon_e,\upsilon_T}(\upsilon) F_{T,t_e}(\upsilon) \quad (6.9)$$

In other words, $F_{\upsilon_e,\upsilon_T}(\upsilon)$ is the sampling of $F_{T,te}(\upsilon)$ by the symmetrical rectangular distribution $\Pi_{\upsilon_e,\upsilon_T}(\upsilon)$ having width υ_e with the elementary interval υ_T.

According to equations (6.5) and (6.8),

$$F_{\upsilon_e,\upsilon_T}(\upsilon) = \sum_{n=-M/2}^{n=M/2-1} \sum_i \left[\eta_i \Lambda^*_{T,t_e}\left(\frac{n}{T} - \upsilon_i\right) + \eta_i^* \Lambda_{T,t_e}\left(\frac{n}{T} + \upsilon_i\right)\right] \delta\left(\upsilon - \frac{n}{T}\right) \quad (6.10)$$

DFTs represent a series of distributions that are spaced regularly on the frequency axis. They thus have a line spectrum. In Appendix D (part 4.2), it is shown that, based on $F_{\nu_e,\nu_T}(\nu)$, the inverse DFT again gives us the initial series $h_{T,t_e}(t)$. Hence, there is a total correspondence between the sample distribution and its DFT, with each series bearing M elements:

$$h_{T,t_e}(t) \Longleftrightarrow F_{\nu_e,\nu_T}(\nu)$$

Hereafter we will mainly use the acronym FFT since, in practice, it is more commonly used than DFT.

1.2 • Tidal spectrum features

Shannon's theorem cannot be satisfied with the selected sampling because of the range of the tidal spectrum. It is therefore not possible to determine whether or not a value calculated via the FFT at a given frequency is actually due to spectral constituents that are symmetrical in relation to one of the axes of equation $\nu = k\nu_e/2$ (aliasing).

We will, for the moment, only apply these results qualitatively to determine the tidal spectrum trend. It is interesting to study the behaviour of tidal constituents. Figure 6.1 illustrates the application of FFT results to constituent i (assuming $h_i = 1$ and $V_{0i} - g_i = 0$), where $h_i(t) = \cos(2\pi\nu_i t)$, with period $T_i = 1/\nu_i = 3.23t_e$, and where the sampling interval t_e is taken for the unit time over a duration of $T = 40t_e$. Shannon's theorem is satisfied with the sampling selected in this case ($\nu_i < \nu_N = \nu_e/2$). In the positive frequency domain, a continuous spectrum is a representative curve of the function $\left|\Lambda^*_{T,t_e}(\nu_i - \nu) + \Lambda_{T,t_e}(\nu_i + \nu)\right|$.

This example shows the bias that this technique introduces in the detection of periodic signal constituents. In the domain $(0, \nu_N)$, around 20 vertical bars appear with a maximum length of less than 1 (value of the sought-after constituent). The signal frequency value ν_i, corresponding to the first peak of the continuous spectrum (red curve), is located between the first two

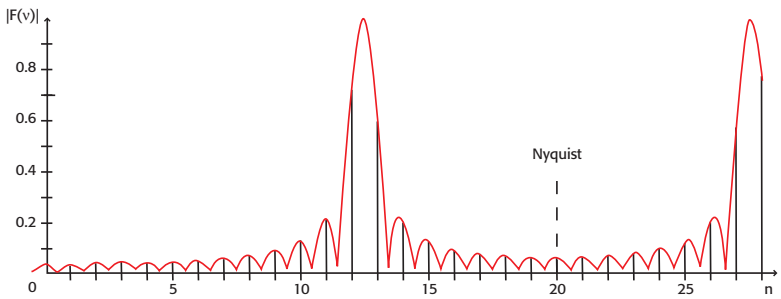

Figure 6.1: The two spectra (continuous and discrete) are established on the basis of a function $\cos(2\pi\nu_i t)$ with a period of $T_i = 1/\nu_i = 3.23t_e$, sampled over a duration of $T = 40t_e$ with a time step t_e taken for the unit time. The x-axis is graduated in 1/40 frequency units $\nu_e = 1/t_e$; the values are from coefficient n of $\nu_n = n/T$. The red curve represents the continuous spectrum of the sampled signal. Black segements over the entire x-axis represent the corresponding line spectrum. Beyond the Nyquist frequency ($\nu_N = 20/T$), the plot highlights the symmetry relative to axis $\nu = \nu_N$ of the sampled function spectrum.

of the highest vertical bars. When duration T is exactly equal to a multiple n_i of the period of constituent i, the spectrum will then reveal a single line of unit length corresponding to the constituent's value at frequency $\nu_i = n_i/T$.

The most unfavourable situation is when $\nu_i = (n \pm 1/2)\nu_T$. Even in this case, a constituent may still be revealed by the presence of two neighbouring lines of the same amplitude of $1/[M \sin(\pi/2M)] \approx 2/\pi$ with $M \gg 1$. The presence of secondary peaks could, however, impede the detection of low amplitude constituents.

Since the tide is not a periodic phenomenon, no duration T that generates a single spectral line for each constituent – T would have to increase to infinity to achieve this. It is nevertheless possible, at least for main waves, to get close to this ideal situation by choosing an observation time that is around an integral number of solar days, lunar days and lunations. Moreover, the resolution increases as the duration of the signal to be processed increases. Figure 6.2 shows the results obtained for the same constituent i examined above, and sampled with the same time step but over twice the period. The spectral line close to the sought-after frequency has a greater signature than in the previous treatment.

When Shannon's theorem is not satisfied, sampling a constituent $\cos(2\pi\nu_j t)$ where $\nu_j = 2\nu_N - \nu_i > \nu_N$ would reveal, within the interval $(0, \nu_N)$, a constituent at frequency ν_i that is not present in the real signal. In figure 6.2, constituent j is represented by the second peak, close to the line corresponding to coefficient $n = 55$.

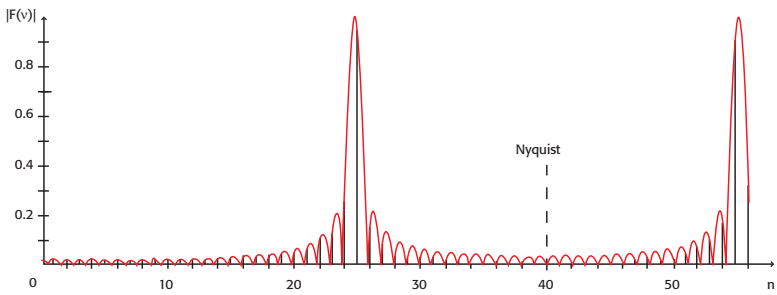

FIGURE 6.2: Here the two spectra (continuous and discrete) of the same constituent i are obtained by sampling over twice as long a period, i.e. $T = 80t_e$. The x-axis is graduated in 1/80 frequency units (coefficient n of $\nu_n = n/80t_e$). Here the Nyquist frequency ($\nu_N = \nu_e/2$) corresponds to $n = 40$. Note that the highest vertical bar is close to the continuous spectrum peak.

Experience proves that an observation duration of more than 30 years is required to obtain a sufficiently high resolution to be able to detect all significant tidal constituents. A step-by-step process is still possible if the observation period is insufficient. By this strategy, the predominant constituents are subtracted from the signal since their secondary peaks could hamper detection of more minor constituents, and the FFT of the resulting signal is then calculated.

Figure 6.3 presents common tidal characteristics in this type of representation, showing groups of lines, called species, separated by domains in which only noise prevails. This noise – generally of meteorological origin – is mainly detectable at low frequencies (less than 1-2 cpd). The frequency domain of the swell and waves was filtered out of the records upon which these results were based (filtering due to a stilling well, with an additional digital filter sometimes also applied).

The x-axis is graduated in cycles/day (cpd of the mean time), with integer values giving the order number of each species. The gradual shift in the mean frequency of each species towards values below the x-axis integers (figure 6.3) highlights that the species are centred on lunar day harmonics $T_L = 24.841\,2$ h (24 h 50 min 28.3 s). Hence, for instance, a so-called 12^{th} diurnal species would have a centre frequency of about 11.6 cycles, which corresponds to 12 cycles/lunar day. Figure 6.3 is a spectral image derived from an FFT (or DFT).

We have seen that the temporal series of sampled observations and the associated Fourier series (distribution that gives a line spectrum) are closely matched, with each containing exactly the same amount of information.

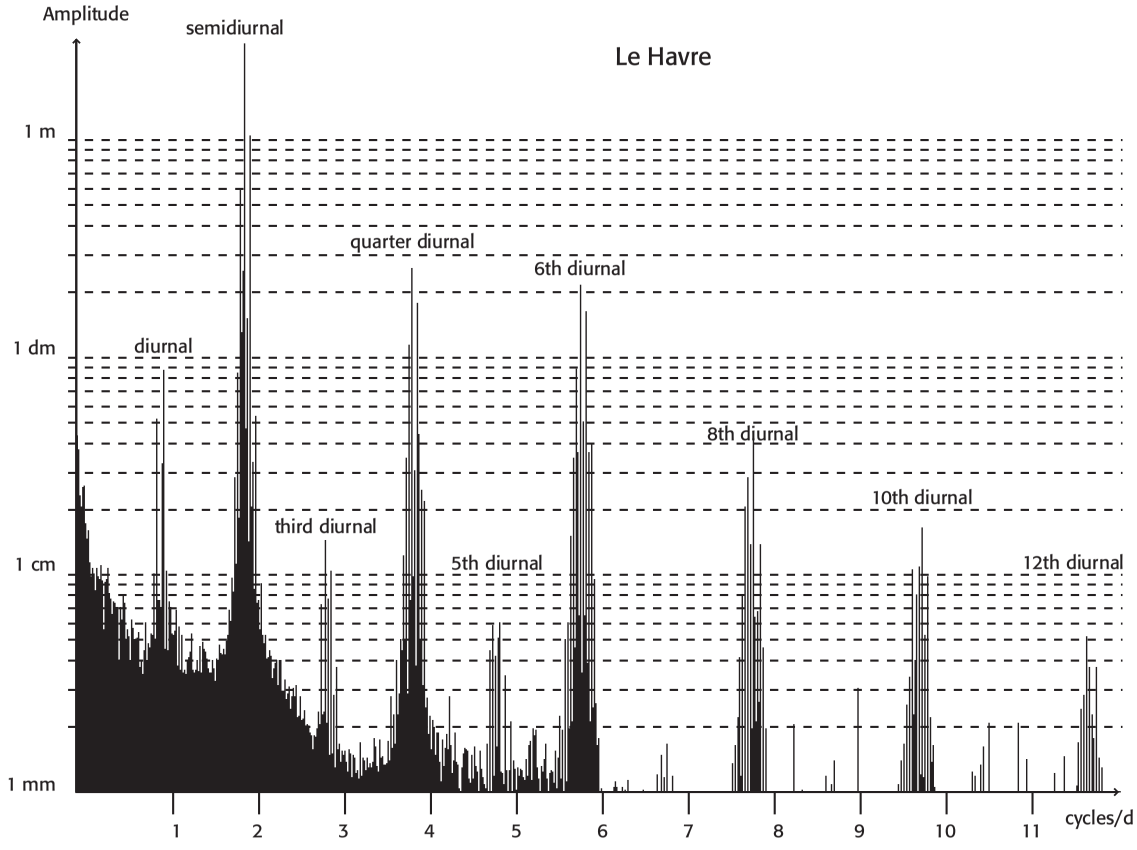

Figure 6.3: A so-called low resolution spectrum obtained by FFT (Le Havre, France). The x-axis represents the angular velocity expressed in cycles/day (1 cpd = 360° / 24 h). The main feature of this spectrum is its structure of groups of clearly separated frequencies which represent tidal species. This spectrum spans around 12 species. Note that the frequency bands for each species are relatively narrow.

It is thus very important to note that FFT accurately represents an observed signal, irrespective of the procedure used to compute it. For the harmonic analysis of tides, only frequency domains containing spectral lines of species are of interest for tidal prediction. Hence, there is relatively little useful spectral information despite the breadth of the spectrum and, because of the equivalence principle discussed above, this could also be applied in the temporal domain to reduce the number of data.

These considerations are especially interesting with respect to long-term observations. In such cases, the very high data quantity can hamper processing, especially due to the substantial number of cumulated rounding errors that occur during computation. This same approach encourages separate processing of species. A global problem consisting of many operations is thus split up into several partial problems that are easier to solve, thus enabling us to obtain more accurate solutions for each species.

Each species actually has quite a high number of spectral lines, as shown in figure 6.4, which represents the semidiurnal domain shown in figure 6.3, but with better definition.

The phase and amplitude of a constituent are unknowns in harmonic analysis. Frequencies derived from the the potential or from compound waves are obviously assumed to be known (see Appendix D). Restricting the problem solving process, by always just focusing on single species, considerably reduces the number of unknowns and consequently the difficulty of the overall operation. Since with this operation a linear system has to be solved (see Chapters IV and V), it is not always easy to properly condition a system that takes all species into account.

2 • Reduced-height method

For the reasons discussed above, it would seem more suitable to perform band-pass filtering so as to be able to deal with each species separately. We have seen that the error $\nu_{T_L} = 1/T_L$ between centre frequencies of neighbouring species corresponds to an angular velocity error of one cycle/lunar day, or 14.492 05°/h. Moreover, the half band width for each k species (relative to the centre frequency $k\nu_{T_L}$) is not more than ±2.5°/h, or around 20% of the base error ν_{T_L}. In figure 6.4 for instance, we may note that for semidiurnal species at Le Havre (France) all constituents of over a few millimetres are included in this interval.

Moreover, we know that a frequential convolution corresponds to a temporal filtering and that, conversely, a temporal convolution corresponds to a

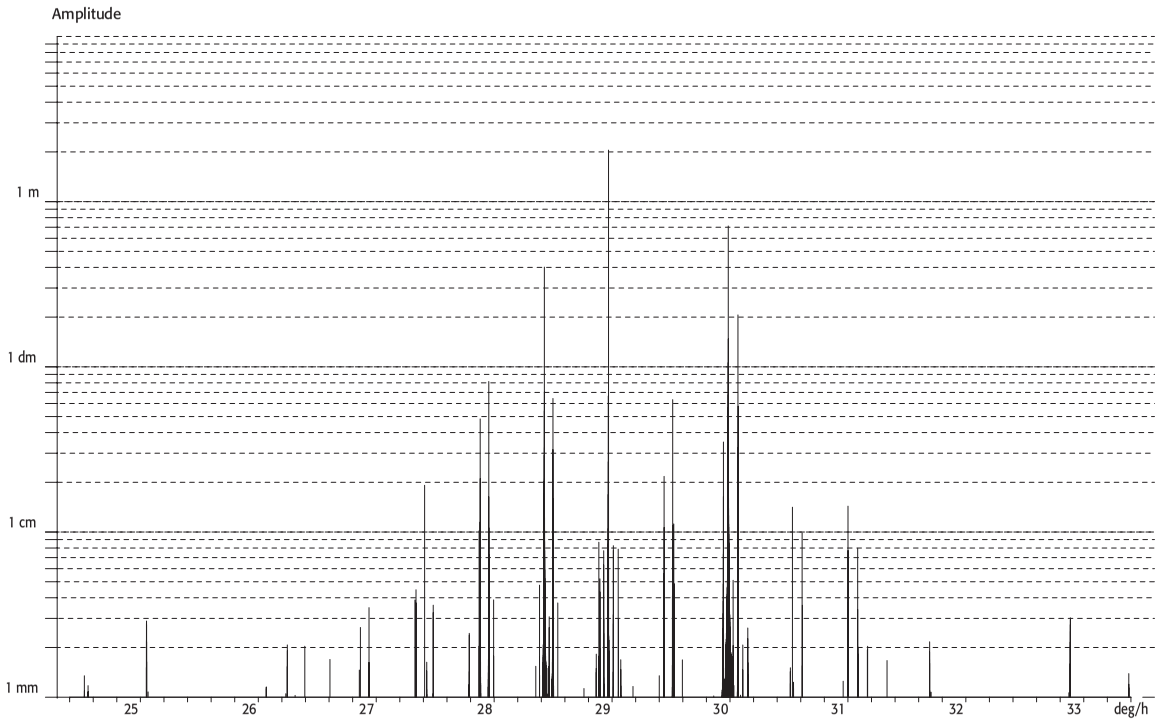

Figure 6.4: A so-called medium resolution spectrum (Le Havre, France): semidiurnal species as a function of the angular velocity expressed here in degrees/hour (30°/h = 2 cpd). Each segment represents the amplitude of a semidiurnal tide harmonic constituent. Note that amplitudes of over a few millimetres are all within an interval of ±2.5°/h relative to the M_2 wave (28.984 1°/h).

frequency filtering. For tidal analysis, we normally have access to a temporal representation, so a specific temporal filter thus has to be built with a frequential convolution (often called a transfer function) having a half-width of around 20% of the error ν_{T_L}. From a physical standpoint, it is not possible to build a perfect filter. However, several filters specifically tailored for tidal harmonic analysis have been developed. This is the focus of the current chapter, which will cover the definition of 'reduced height', and harmonic analysis by species based on the corresponding 'reduced vector' method. Harmonic constituents have been obtained within each species by solving a system of equations (with reduced vectors) using the least-squares method to eliminate noise, or directly by FFT, depending on the case. These techniques have been used by the French Hydrographic Service since 1974.

In practice, we have seen that the Fourier series of a sampled curve is determined using an FFT algorithm. The FFT computation time on a computer is thus minimized when the number of samples is a power of 2 (2^p). Based on measurement readings, which are generally logged hourly, a new sampling is often carried out by parabolic interpolation in order to obtain $M = 2^5 = 32$ values/lunar day ($T_L = 24.841\,2$ h). Data recomputed in this way are used for harmonic analysis by the so-called 'reduced heights' by reduced vectors at a given time method. For tidal analysis, this method is equivalent to applying a temporal filter to isolate the estimator of the global constituent of each species at a given time. To ensure that the filter is well adapted to the problem at hand, the estimator of this global amplitude (which will be translated here in its complex form) should represent the sum of waves forming the species at the considered time.

2.1 • Definition of reduced vectors

To get back to the harmonic tidal equation where the tidal height $h(t)$ can be formulated by highlighting species that are designated here by the subscript k (equivalent to the value of parameter m_τ in Chapter V):

$$h(t) = \sum_k \sum_i h_{ki} \cos(V_{0ki} + q_{ki}t - g_{ki}) \tag{6.11a}$$

or even:

$$h(t) = \frac{1}{2} \sum_k \sum_i h_{ki} \left[e^{j(V_{0ki} + q_{ki}t - g_{ki})} + e^{-j(V_{0ki} + q_{ki}t - g_{ki})} \right] \tag{6.11b}$$

where:

h_{ki} and q_{ki} are the amplitude and angular velocity of constituent i of species k;

V_{0ki} is the argument at time zero ($t = 0$; subscript 0) of this constituent, which can be of astronomical origin (argument of the cosine of the tide-generating potential) or be the result of a combination of astronomical arguments that give an interaction constituent in species k;

g_{ki} is the phase lag of the constituent; this parameter is always associated with the reference time used (local time, UT or time zone).

By introducing the frequency error υ_{ki} between $q_{ki}/2\pi$ the centre frequency k/T_L of species k (i.e. T_L, lunar day length), we have:

$$\upsilon_{ki} = q_{ki}/2\pi - k/T_L \tag{6.12}$$

Then let $C_k(t)$ be the complex value (representing a vector) given by the equation:

$$C_k(t) = \sum_i h_{ki} e^{j(V_{0ki} + 2\pi\upsilon_{ki}t - g_{ki})} \tag{6.13}$$

Equation (6.11b) for the tidal height thus becomes:

$$h(t) = \frac{1}{2} \sum_k \left[C_k(t) e^{j2\pi \frac{k}{T_L} t} + C_k^*(t) e^{-j2\pi \frac{k}{T_L} t} \right] \tag{6.14}$$

where $C_k(t)$ is a complex number called the reduced vector of species k at time t.

We have seen that the half band width associated with each species is relatively narrow ($\leq 2.5°/h$) in comparison to $360°/T_L \approx 14.5°/h$, i.e. the interval between the centre frequencies of two neighbouring species ($T_L\,|\upsilon_{ki}| < 0.2$). Hence, the reduced vectors $C_k(t)$ vary slowly with respect to the tidal height $h(t)$. We can interpret them as slow variations in amplitude and in the phase associated with each species.

These reduced vectors all contain information relative to each species as long as they can be isolated by a specially adapted filter. The following advantages could be expected if an optimal temporal filter is available:

• for astronomical tide analysis, the data are processed more efficiently because the spectrum, excluding frequency bands associated with species, is disregarded

• each species can also be treated individually, and in this way a difficult overall problem can be transformed into several easier to solve subproblems.

2.2 • Definition of reduced heights

Note that equation (6.14) resembles a Fourier series. It is obviously not a Fourier series because the coefficients are time dependent, but their slow

variation reflects the fact that the tide is almost periodic with a period T_L. This finding provides a guide for defining a temporal filter tailored to tidal observations.

Interestingly, the reduced height method resembles the British Admiralty semi-graphic analysis method. From this standpoint, it could be considered as a formalisation and generalisation.

Let us consider a time t_0 in the vicinity of the time of a measurement $h(t)$, such that the maximum error $|t - t_0|$ is around a lunar day. We call function $H(t_0, t)$ the 'tidal height' at time t reduced at time t'_0, as formulated by the equation:

$$H(t_0, t) = \frac{1}{2} \sum_k \left[C_k(t_0)\, e^{j2\pi \frac{k}{T_L} t} + C_k^*(t_0)\, e^{-j2\pi \frac{k}{T_L} t} \right] \tag{6.15}$$

Because of the low frequency error $\upsilon_{k,i}$ values, the reduced vectors vary slowly, as does the reduced height $H(t_0, t)$ relative to t_0.

The centre frequencies k/T_L of each species were naturally selected as centre frequencies of band pass filters that we are going to build. However, as the observation data sampling frequencies are always a fraction of the solar day (usually 1 h), the observations must be resampled for a strict application of the method. However, it is possible to avoid this resampling by using filters $k/25\,h^{-1}$, close to k/T_L, as centre frequencies. In this case, the practical application is substantially simplified and leads to what can be called 'reduced heights at midday', as the times t_0 are set daily at midday. Errors between centre frequencies of filters built in this way and k/T_L do not really have a significant impact if $k \leq 12$, i.e. throughout the accessible spectrum using hourly observations. This is no longer true with respect to fluvial tides where the energy may still be detected beyond the 30^{th} diurnal.

The following considerations will be as general as possible.

Reduced heights $H(t_0, t)$ have the following properties:

• because of the low frequency error υ_{ki} values, the reduced vectors vary slowly. This is also the case for reduced heights with respect to $\theta = t_0 - t$

• because of the periodicity of the complex exponents $e^{j2\pi \frac{k}{T_L} t}$ and $e^{-j2\pi \frac{k}{T_L} t}$, the reduced heights are periodic, with a period of T_L relative to their second argument:

$$\begin{aligned} H(t, t) &= h(t) \\ H(t - T_L, t) &= H(t - T_L, t - T_L) = h(t - T_L) \\ H(t + T_L, t) &= H(t + T_L, t + T_L) = h(t + T_L) \end{aligned}$$

Determination of reduced heights is clearly of interest because the reduced

vectors $C_k(t_0)$, which are periodic with a period of T_L, are coefficients of the associated Fourier series. They are computed on the basis of the previously described properties.

The slow variation in reduced heights as a function of the initial argument *a priori* enables us to approximate them using a limited development:

$$\begin{aligned} H(t_0, t) &= H(t + \theta, t) \\ &= H(t, t) + \theta \frac{\partial H(\tau = t, t)}{\partial \tau} + \frac{1}{2}\theta^2 \frac{\partial^2 H(\tau = t, t)}{\partial \tau^2} + \dots \end{aligned} \quad (6.16)$$

The accuracy of the result obviously depends on the degree of development, but also on the possibility of calculating the successive derivatives of $H(\tau, t)$ on the basis of available observations $h(t)$.

The best approximations that can be achieved for these derivatives, assuming that observations are available for the interval between days $t - T_L$ and $t + T_L$, are obtained by the following equations, where the derivatives are approximated via finite differences:

$$\begin{aligned} \frac{\partial H(\tau = t, t)}{\partial \tau} &\approx \frac{1}{2}\left[\frac{H(t, t) - H(t - T_L, t)}{T_L} + \frac{H(t + T_L, t) - H(t, t)}{T_L}\right] \\ &= \frac{h(t + T_L) - h(t - T_L)}{2T_L} \end{aligned} \quad (6.17)$$

$$\begin{aligned} \frac{\partial^2(\tau = t, t)}{\partial \tau^2} &\approx \frac{1}{T_L}\left[\frac{H(t + T_L, t) - H(t, t)}{T_L} - \frac{H(t, t) - H(t - T_L, t)}{T_L}\right] \\ &= \frac{h(t + T_L) + h(t - T_L) - 2h(t)}{T_L^2} \end{aligned} \quad (6.18)$$

Thus giving the limited second-order development:

$$\begin{aligned} H(t_0, t) \approx h(t) &+ (t_0 - t)\frac{h(t + T_L) - h(t - T_L)}{2\,T_L} \\ &+ (t_0 - t)^2 \frac{h(t + T_L) + h(t - T_L) - 2h(t)}{2\,T_L^2} \end{aligned} \quad (6.19)$$

2.3 • Reduced vector computation

Because of the periodicity of $H(t_0, t)$ with respect to the second argument, the reduced vectors $C_k(t_0)$ are coefficients of the Fourier series of this tidal height sampled over a duration of T_L. In practice, when calculating reduced vectors, the observations (initially often hourly) can be resampled to obtain a number of tidal heights per lunar day equal to a power of 2, and then the very efficient Tuley-Tukey FFT computation algorithm can be used.

However, to be able to calculate the transfer function while still remaining general, t_0 can be used as the temporal reference point. Morover, it is recommended that the computations be performed symmetrically with respect to this time zero in order to avoid introducing a phase lag. In the following equation, we have $M = 2N + 1$ (odd number) reduced heights separated by a time interval $t_e = T_L/M$.

$$C_k(0) = \frac{2}{M} \sum_{n=-N}^{n=N} H(0, nt_e)\, e^{-j2\pi \frac{kn}{T_L} t_e} \tag{6.20}$$

Reduced vectors are thus obtained by temporal filtering while taking the observation data around time zero into account.

The transfer function of this filter depends on the extension of equation (6.16). It is obtained (like all transfer functions) by filtering the complex exponent $e^{j2\pi\upsilon t}$. This computation is based on the expression of a geometrical series and on its successive derivatives according to the filtering degree. Let us call FT0, FT1, FT2, ... the filtering degrees 0, 1, 2, ...

$$\begin{aligned} FT0(\upsilon) &= \frac{1}{M} \frac{\sin(\pi\upsilon T_L)}{\sin(\pi\upsilon\, te)} \\ FT1(\upsilon) &= FT0(\upsilon)^2 \left[M \sin \pi\upsilon T_L \sin \pi\upsilon\, t_e + \cos \pi\upsilon T_L \cos \pi\upsilon\, t_e\right] \\ FT2(\upsilon) &= FT0(\upsilon)^3 \left[1 + \frac{M^2 - 1}{2} \sin^2(\pi\upsilon t_e)\right] \end{aligned} \tag{6.21}$$

Based on the fact that the angular velocities of tidal constituents are 2.5°/h on both sides of the centre frequency of each species, the filter resulting from the second-order polynomial development is clearly very efficient (FT2 curve in figure 6.5). Almost all constituents of each species are thus preserved and, because of the low transfer function values at points located at n/T_L frequencies, this filter almost completely suppresses the effects of constituents associated with other species. This latter point is especially important and overcomes the FT0 filter, which allows the contamination of a given species by neighbouring species. The FT1 filter is not too bad from this standpoint, but it is markedly less good in the [-2.5°/h, 2.5°/h] interval and, since it must take just as many observations as required for FT2 into account (from $t_0 - (3/2)T_L$, to $t_0 + (3/2)T_L$), this FT1 filter is of limited interest.

The FT3 filter is slightly better than FT2, but an additional day has to be taken into account (from $t_0 - 2T_L$ to $t_0 + 2T_L$) for very little improvement in performance. However, since it is able to diminish noise between tidal frequencies, it has been beneficially applied for the analysis of tidal current observations that are regularly hampered by considerable noise. In this case, the loss of 2 days at the beginning and end of the observation period

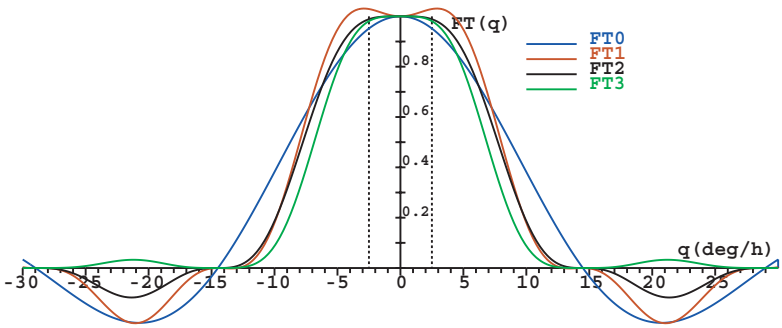

FIGURE 6.5: Graphical representation of filters FT0, FT1 end FT2.

(which is often short) can turn out to be an impediment. A special end-point treatment can be applied to overcome this problem.

Consider a time t_0, in the vicinity of the measurement time $h(t)$ such that the maximum error $|t_0 - t|$ is around a lunar day. When $t_0 = t + \theta$, we thus obtain: $|\theta| \leq T_L$. Note that other limit options are possible depending on the filter to be used. The 'tidal height' at time t, reduced at time t_0' is what we call function $H(t_0, t)$ given by equation (6.16).

This tidal height is often simply called the 'reduced height'. Due to the low frequency error υ_{ki} values, the reduced vectors vary slowly, as does the variation in the reduced height $H(t_0, t)$ relative to $\theta = t_0 - t$.

Based on a series of measurements, the reduced vectors C_k are generally calculated with a regular time step t_c. This interval t_c should be selected such that Shannon's theorem, concerning the sampling, is respected. For all errors υ_{ki} relative to the corresponding centre frequency k/T_L, condition $|\upsilon_{ki}| \leq 1/2t_c$ must be fulfilled.

As we have: $\max |\upsilon_{ki}| \approx \dfrac{2.5°/h}{360°} = \dfrac{1}{144h}$, we thus require: $t_c \leq 72$ h.

For each species, computing a reduced vector every 72 h is sufficient to avoid aliasing errors in the tidal frequency domain. We thus have considerable liberty concerning the choice of sampling interval t_c in the determination of reduced vectors. This feature facilitates the use of an FFT algorithm. A time step of under 72 h should be chosen, while making sure that the number of reduced vectors calculated over the observation period is a power of 2, and also that the maximum amount of available data is taken into consideration. When there are measurement errors, the FFT cannot be applied – then a reduced vector is computed per lunar day to ensure that a maximum number of observations are taken into consideration.

We will see later that harmonic analysis based on a series of reduced vectors obtained in this way simply involves solving a number of linear equations equal to the number of species considered. Although the noise issue has already been pointed out, it is important to examine this perturbation on the basis of a few examples before dealing with solving 'normal' equations of the harmonic analysis by species.

3 • Noise in tidal analysis

The previous developments dealt especially with theoretical tides just involving harmonic constituents. In real situations, the sea level, as recorded by instruments, is the result of tidal contributions (astronomical and radiational (solar)), as well as meteorological effects (especially pressure and wind). Errors inherent in all measurement systems and to stilling wells also have an influence. A tide level measurement error relative to a theoretical tide is thus considered as noise in any harmonic analysis of tide.

It is essential to assess the nature of noise to determine the impact of meteorological conditions and detect the presence of residual periodic constituents, which could be natural or the result of systematic errors caused by measuring systems. There are clearly only two main causes underlying all periodic elements of noise, i.e. the omission of a tidal constituent, or the presence of a cyclical anomaly in the functioning of one or several constituents of the measuring system (gauge, decoder, transmitter, recorder or power supply).

The chances are high that noise will have daily, weekly or even seasonal periods because of the impact of human activities and meteorological conditions on these different instruments. Some of the main factors include line voltage or air temperature variations on the measuring devices. Spectral analysis of noise or of a 'difference tide' (difference between the measured tidal height and an approximated theoretical tide) can be a very useful tool to complete a list of constituents or detect potential instrument malfunctions.

A float gauge malfunction at Brest between 1953 and 1978 is an illustrative case. The drum drive mechanism was not rotating in a perfectly uniform manner, which led to a cyclical daily modulation in the tide curve time scale (same type of graphs as shown in figure 6.6). This defect was revealed by the appearance of spectral lines at frequencies having valid Doodson numbers. This type of defect introduces changes in the M_2 tidal constituent, generating angular velocities identical to $q_{M_2} \pm q_{S_1}$, which are allocated Doodson numbers of 364 555 and 146 554, respectively. However, it was not possible to

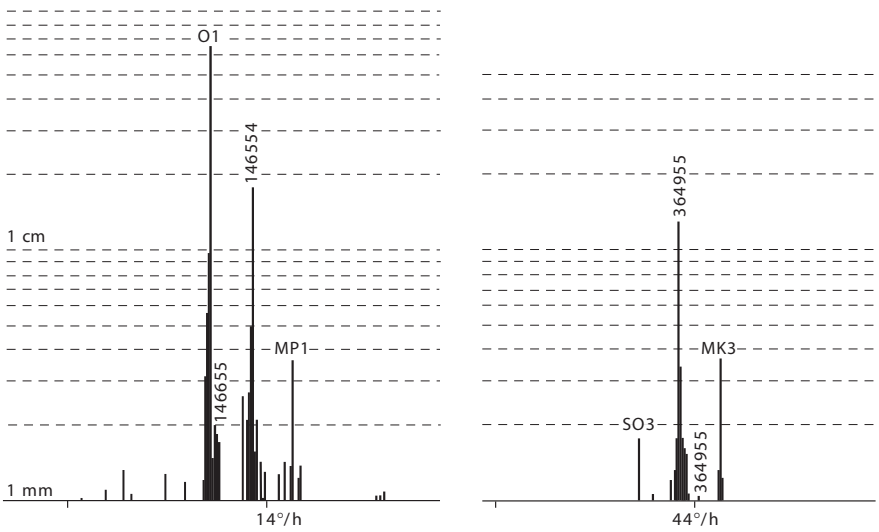

Figure 6.6: Detection of anomalies in flood gauge measurements at Brest (France) from 1953 to 1978: spectral lines with Doodson numbers of 146 554 and 364 555 were due to a defect in the drum drive mechanism (daily cyclical variation in the chart paper speed).

interpret such cyclical variations, especially by the size of the corresponding amplitudes, or as waves from the tide-generating potential, or as nonlinear interaction constituents. These calculations also revealed abnormally high amplitudes at frequencies corresponding to S_1 and S_3 waves. These latter results are likely due to the same modulation effects induced by the drum rotation speed on the S_2 constituent.

In the low frequency domain, figure 6.7 gives an especially interesting illustration of the nature of noise. Without conducting a quantitative estimation, the amplitudes of the harmonic constituents Sa, Ssa and Mf can be clearly distinguished from the background noise and are significantly high in this part of the spectrum. All the others, even though they are present in the tide-generating potential, are mixed with the noise.

Note that, in the development of the tide-generating potential, the bimonthly constituent Mf has the highest coefficient in this long-period domain. However, because of their low coefficient in the potential, Sa (annual) and Ssa (semi-annual) waves appear with unexpected amplitudes. Their presence is mainly associated with 'solar radiational' effects. Note that seasonal variations, i.e. solar radiation and meteorological conditions (wind fields and atmospheric pressure), have an impact on the tide level either directly (pressure) or indirectly (variation in the coastal tide level according

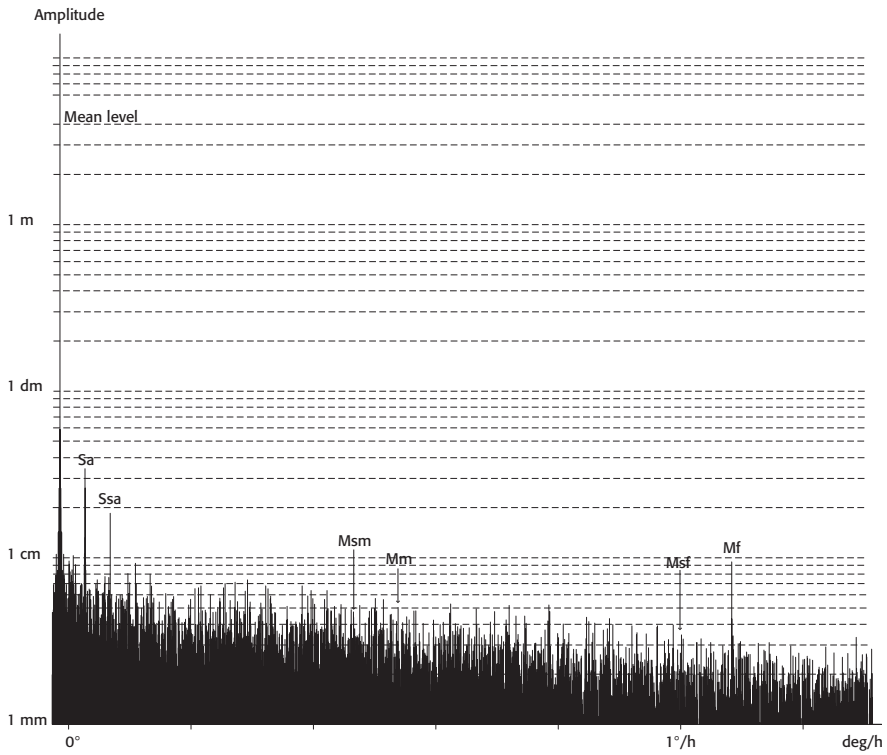

FIGURE 6.7: Tide spectrum at Brest in the long period domain: the highly noisy structure of this spectrum highlights how hard it is to detect tidal harmonic constituents that are present in this frequency band, especially those corresponding to Msm, Mm and Msf. Only Sa (annual), Ssa (semiannual) and Mf (bimonthly) waves have significant constituents.

to the wind conditions; expansion of the surface water layer). These effects are generally minor along North Atlantic coasts, but are greater in areas influenced by monsoon conditions. These influences are much more noticeable in seas with very low amplitude tides, e.g. along the French Mediterranean coast, the Sa wave is the same magnitude as the M_2 wave (around 10 cm).

Sa and Ssa waves have amplitudes that are not constant from year to year because of the nature of their origins. This is shown by spectral noise in the vicinity of the corresponding frequencies. Many years of observations are required to be able to accurately determine their amplitude and mean phase. These two waves, which correspond to nontrivial tide level variations, should be taken into account in accurate tidal computations. Note that they are the dominant solar radiational tide constituents (included in the theoretical tide definition) and are thus included in the list of harmonic

constituents like those derived from the tide-generating potential. Of the other existing and detectable radiational constituents, the mean diurnal solar constituent S_1, which is derived from the action of thermal winds, stands out particularly, along with the diurnal surface water dilation effect on the tide level. The main S_2 solar semidiurnal wave likely has a very weak radiational constituent, but it is hard to distinguish from the generally dominant gravitational part.

Note finally that these radiational waves can involve nonlinear interactions with major gravitational constituents, thus especially inducing annual M_2 wave amplitude modulations. In such cases, this modulation contributes to the two spectral lines of the angular velocities $q_{M_2} \pm q_{Sa}$, to the nearest angular velocity at solar perigee. These constituents, which are located on both sides of M_2 (sometimes designated as MA_2 and MB_2), are denoted $M(KS)_2$ and $M(SK)_2$ by the French Hydrographic Service, with Doodson numbers of 256 554 and 254 556, respectively. These waves are some of the constituents whose origins should be clearly defined since they are inseparably linked to tide-generating potential constituents. Modulations in M_2 due to meteorological noise or cyclical measurement errors sometimes seriously hamper clear determination of the gravitational portion of these interaction waves.

The mean annual tide level variation pattern reveals another aspect of noise in the very low frequency domain. Most records of very long duration T (several decades) show a secular variation trend in the mean annual level, especially at the Brest (France) site. This trend is reflected in FFT by spectral constituents corresponding to the frequency 1/T and its harmonics, whereas FFT provides a consistent representation of the analysed signal over this interval. However, this is a Fourier series with a built-in assumption that the T value is the signal period. When this mean level varies linearly over the measurement time, this trend is reflected by a Fourier series of the 'sawtooth' function with the measurement interval as period. These constituents obviously represent artefacts that have to be eliminated prior to performing the FFT. One technique involves, for instance, correcting the measured tidal heights by removing the tide level trend. This is generally calculated by applying a linear regression to the mean annual measured levels.

Another source of noise, which is very problematic since it is often hard to distinguish from the actual tide, concerns systematic errors due to poor tidal time and height calibrations, especially for float gauges (Chapter II: part 3.2).

Time calibration errors are quite easily detected. According to the theoretical tide, which represents a very accurate clock, a temporal representation can be drawn up which should quite closely match the observed tide. It is thus possible to correct obvious errors, for instance, on the basis of differences in daily phases of reduced vectors of both theoretical and measured tides. Although the technique is perfectly adjusted, it would be unsuitable to systematically adjust observations according to a theoretical tide for at least two reasons: firstly, because the theoretical tide is itself established on the basis of observations and, secondly, because there is a random constituent that should not be overlooked with respect to tide level variations.

Conversely, tidal height calibration errors are harder to detect. Tide level variations associated with meteorological conditions (wind and atmospheric pressure) are sometimes substantial, thus masking this type of error (usually a few centimetres). Studies (which are seldom carried out) based on correlations between the observed tide level and meteorological conditions recorded at the site, or between simultaneous measurements obtained at the monitored site and in a neighbouring port, would be required to detect such errors.

These sources of noise, which concern the entire measurement system, are problematic because of their systematic nature. However, random errors (generally centred) associated with the determination of an individual measurement value usually do not markedly upset the results. For instance, automatically logged measurements are hampered by the problem of noise introduced by measurement digitisation. It was shown (Y. Desnoës, 1977) that the harmonic constant evaluation inaccuracy resulting from automatic recording was around $A/\sqrt{3M}$, where A denotes the numerical resolution interval and M denotes the sample number. With a minimum of 24 measurements/day, the M value quickly rises to a very high value and the corresponding error becomes negligible.

4 • Analysis by the least-squares method

We have seen that the structure of a frequential filter $FT_2\nu$ (6.21), resulting from a second-order approximation of the reduced tidal height, gives reduced vectors that contain all information relative to each species. Hence, each k species can be analysed separately on the basis of the series of corresponding reduced vectors. These vectors, as described by equation (6.20), are generally calculated at regular time intervals t_c, but at most 72 h in order to avoid aliasing. In this part of the chapter, we will deal with just one species

at a time so as to be able (without any possible confusion) to get rid of each species' k index, thus simplifying the equations.

We obtain a limited series of reduced vectors for each species. The harmonic analysis can then be performed by two main methods, i.e. the least-squares method which accounts for the presence of noise, or FFT.

Harmonic analysis by the least-squares method mainly involves solving a system of so-called 'normal' equations after conditioning them well to ensure that the answer will not be indeterminate. The frequencies of constituents of the potential or interaction waves (see Appendix C) are the problem's input data, with the unknowns being the respective amplitudes and phases.

4.1 • System of normal equations

By omitting the k index, the reduced vector given by equation (6.9) can be formulated for time t_m as:

$$\mathrm{C}(t_m) = \sum_i h_i e^{j(\mathrm{V}_{0i} - g_i)} e^{j2\pi \upsilon_i t_m} \tag{6.22}$$

For a given species, consider the series of reduced vectors calculated every t_c over an interval of $\mathrm{T} = \mathrm{M}t_c$, and let:

$$\begin{aligned} t_m &= (m-1)t_c & \mathrm{C}(t_m) &= c_m \\ a_{m,i} &= e^{j2\pi \upsilon_i t_m} & x_i &= h_i e^{j(\mathrm{V}_{0i} - g_i)} \end{aligned} \tag{6.23}$$

Equation (6.22) then becomes:

$$c_m = \sum_i a_{m,i} x_i \tag{6.24}$$

Until now, reduced vector equations have been formulated based on the assumption that tidal height measurements are perfect. However, tidal measurements are actually riddled with errors. After eliminating known systematic errors and periodic terms other than those associated with tide, the reduced vectors c_n, calculated from data corrected in this way, take into account, besides tidal constituents of the considered species, a random term that we symbolise by:

$$b(t_m) = b_m \tag{6.25}$$

Based on the above-mentioned preliminary precautions, the noise features that we assume are stationary, centred and Gaussian are allocated to this random term. Although not absolutely necessary, we will simplify the discussion by considering this to be 'white noise'– its correlation function is a Dirac pulse (to the nearest variance factor), i.e. nil for all time errors except

for the zero error where it has the variance value. The hypothesis set out for this noise is readily acceptable for reduced vectors whose temporal sampling step t_c is much higher than that of the original observations t_e. This is an additional advantage in favour of the reduced heights method.

Let M denote the number of reduced vectors c_m (n.b. $\mathrm{T} = \mathrm{M}t_c$) and N represent the number of harmonic constituents x_i(complex) to compute. When the noise is taken into account (6.25), we thus have a system of M equations with N unknowns of the following type:

$$c_m = \left(\sum_{i=1}^{i=\mathrm{N}} a_{m,i} x_i \right) + b_m \tag{6.26a}$$

where obviously $\mathrm{N} < \mathrm{M}$. The least-squares method involves looking for a solution that assigns a minimum modulus to the noise. Using a matrix calculus, let:

$$\mathrm{C} = \begin{bmatrix} c_1 \\ . \\ . \\ . \\ . \\ . \\ c_{\mathrm{M}} \end{bmatrix} \quad \mathrm{A} = \begin{bmatrix} a_{1,1} & \cdots & a_{1,\mathrm{N}} \\ . & . & . \\ . & . & . \\ . & . & . \\ . & . & . \\ . & . & . \\ a_{\mathrm{M},1} & \cdots & a_{\mathrm{M},\mathrm{N}} \end{bmatrix} \quad \mathrm{X} = \begin{bmatrix} x_1 \\ . \\ . \\ . \\ . \\ . \\ x_{\mathrm{M}} \end{bmatrix} \quad \mathrm{B} = \begin{bmatrix} b_1 \\ . \\ . \\ . \\ . \\ . \\ b_{\mathrm{M}} \end{bmatrix}$$

and the system of equations (6.26a) can thus be formulated as:

$$\mathrm{AX} - \mathrm{C} = -\mathrm{B} \tag{6.26b}$$

To overcome the problem of minimising the noise, the value of the matrix product $\mathrm{B}^*\mathrm{B}$ must be minimised, where the superscript $*$ applied to a matrix indicates that it is the adjoint matrix, i.e. transposed and conjugate.

With this being the case, the matrix product $\mathrm{B}^*\mathrm{B}$ is expressed by:

$$\mathrm{B}^*\mathrm{B} = (\mathrm{AX} - \mathrm{C})^* (\mathrm{AX} - \mathrm{C}) = \mathrm{X}^*\mathrm{A}^*\mathrm{AX} - \mathrm{C}^*\mathrm{AX} - \mathrm{X}^*\mathrm{A}^*\mathrm{C} + \mathrm{C}^*\mathrm{C} \tag{6.27}$$

and the noise minimum is thus obtained for:

$$\mathrm{d}\left(\mathrm{B}^*\mathrm{B}\right) = \left(\mathrm{X}^*\mathrm{A}^*\mathrm{A} - \mathrm{C}^*\mathrm{A}\right) \mathrm{dX} - \mathrm{dX}^* \left(\mathrm{A}^*\mathrm{AX} - \mathrm{A}^*\mathrm{C}\right) = 0 \tag{6.28}$$

By noting the equivalence of the following matrices:

$$\left(\mathrm{X}^*\mathrm{A}^*\mathrm{A} - \mathrm{C}^*\mathrm{A}\right) = \left(\mathrm{A}^*\mathrm{AX} - \mathrm{A}^*\mathrm{C}\right)^*$$

we obtain a system of so-called normal equations that minimise the product B^*B. This system of normal equations is formulated as follows:

$$A^*AX - A^*C = 0 \tag{6.29}$$

where X represents the matrix solution of the system of N linear equations with N unknowns.

Hereafter we will explain the formulation of matrix equation (6.29). The equation solving problem will not be discussed in detail, but the question of properly conditioning the system warrants special attention.

4.2 • System conditioning criteria

In system (6.29), we have matrix A (M lines, N columns) of the general term $a_{m,n}$ and its adjoint term A^* (N lines, M columns) of the general term $a^*_{m,i}$. Their product gives matrix A^*A (N lines, N columns) whose general term (nth line, ith column) is expressed as:

$$\sum_{m=1}^{m=M} a^*_{m,i} a_{m,n} = \sum_{m=1}^{m=M} e^{-j2\pi(\upsilon_i - \upsilon_n)t_m} \tag{6.30}$$

while keeping in mind that we set out $a_{m,n} = e^{j2\pi\upsilon_n t_m}$.

Matrix A^*A is thus Hermitian, i.e. equal to its adjoint matrix $\left(A^*A\right)^*$, and all terms of its diagonal ($\upsilon_i - \upsilon_n = 0$) have value M.

Hence, where Λ denotes matrix A^*A normalised by M:

$$\Lambda = \frac{1}{M} A^*A \tag{6.31}$$

this matrix, which is obviously Hermitian, has all the diagonal terms of unit value. Considering (6.32), its general term $\lambda_{n,i}$ (nth line, ith column) is thus expressed as:

$$\lambda_{n,i} = \frac{1}{M} \sum_{m=1}^{m=M} e^{-j2\pi(\upsilon_n - \upsilon_i)t_m} \tag{6.32}$$

We have often seen that a series of reduced vectors represents a series of complex values every t_c. As we already defined $t_m = (m-1)t_c$, equation (6.32) thus represents the FFT of the normalised rectangular function by its width $T = Mt_c$ for frequency $\upsilon_n - \upsilon_i$. Hence, the term $\lambda_{n,i}$ can be expressed by:

$$\lambda_{n,i} = \Lambda_{T,t_c}(\upsilon_n - \upsilon_i) = \frac{\Lambda_T(\upsilon_n - \upsilon_i)}{\Lambda_{t_c}}(\upsilon_n - \upsilon_i) \tag{6.33}$$

which is the ratio of FFTs of rectangular functions of respective widths T and t_c at frequency $\upsilon_n - \upsilon_i$. This simplification can only be adopted if there are no errors in the observation data.

Moreover, when $\Phi = (1/\mathrm{M})\mathrm{A}^*\mathrm{C}$, the general term of this matrix or vector (N lines, one column) is expressed by:

$$\frac{1}{\mathrm{M}} \sum_{m=1}^{m=\mathrm{M}} a^*_{m,n} c_m = \frac{1}{\mathrm{M}} \sum_{m=1}^{m=\mathrm{M}} c_m e^{-j2\pi\sigma_n t_m} \tag{6.34}$$

which is the FFT value of the series of reduced vectors c_m at frequency σ_n.

With the elements defined above, the matrix equation (6.31) becomes:

$$\Lambda \mathrm{X} = \Phi \tag{6.35a}$$

which represents the system of N linear equations with N unknowns, with the general equation expression being:

$$\sum_{n=1}^{n=\mathrm{N}} \lambda_{i,n} x_n = \frac{1}{\mathrm{M}} \sum_{m=1}^{m=\mathrm{M}} c_m e^{-j2\pi\upsilon_i t_m} \tag{6.35b}$$

Note that for a given k species, parameters c_m, x_i and υ_i respectively represent:

- the reduced vector at time t_m of this species: $c_m \Rightarrow \mathrm{C}_k(t_m)$
- the vector (amplitude and phase) of its corresponding constituent i: $x_i \Rightarrow h_{ki} e^{i(\mathrm{V}_{0ki} - g_{ki})}$
- the error between the frequency of constituent i and the centre frequency of the considered species $k/\mathrm{T_L} : \upsilon_i \Rightarrow (q_{ki}/2\pi) - (k/\mathrm{T_L})$.

Within each species k (0, long period; 1, diurnal; 2, semidiurnal; 3, third-diurnal, etc.), determining the harmonic constants by the least-squares method thus involves solving the system of linear equations (6.35b), where N is the number of constituents x_i to calculate and M is the number of reduced vectors c_m. Equation system (6.35b) could be better explained by highlighting the Hermitian character of matrix Λ with $\lambda_{m,i} = \lambda^*_{i,m}$, or:

$$
\begin{aligned}
&x_1 + \lambda_{1,2}x_2 + \cdots + \lambda_{1,n}x_n \\
&\qquad + \cdots + \lambda_{1,\mathrm{N}-1}x_{\mathrm{N}-1} + \lambda_{1,\mathrm{N}}x_{\mathrm{N}} = \frac{1}{\mathrm{M}}\sum_{m=1}^{m=\mathrm{M}} c_m e^{-j2\pi\upsilon_1 t_m} \\
&\lambda^*_{1,2}x_1 + x_2 + \cdots + \lambda_{2,n}x_n \\
&\qquad + \cdots + \lambda_{2,\mathrm{N}-1}x_{\mathrm{N}-1} + \lambda_{2,\mathrm{N}}x_{\mathrm{N}} = \frac{1}{\mathrm{M}}\sum_{m=1}^{m=\mathrm{M}} c_m e^{-j2\pi\upsilon_2 t_m} \\
&\lambda^*_{1,n}x_1 + \lambda^*_{2,n}x_2 + \cdots + x_n \\
&\qquad + \cdots + \lambda_{n,\mathrm{N}-1}x_{\mathrm{N}-1} + \lambda_{n,\mathrm{N}}x_{\mathrm{N}} = \frac{1}{\mathrm{M}}\sum_{m=1}^{m=\mathrm{M}} c_m e^{-j2\pi\upsilon_n t_m} \\
&\qquad\qquad \cdots\cdots\cdots\cdots\cdots\cdots = \cdots \\
&\lambda^*_{1,\mathrm{N}-1}x_1 + \lambda^*_{2,\mathrm{N}-1}x_2 + \cdots + \lambda^*_{n,\mathrm{N}-1}x_n \\
&\qquad + \cdots + x_{\mathrm{N}-1} + \lambda_{\mathrm{N}-1,\mathrm{N}}x_{\mathrm{N}} = \frac{1}{\mathrm{M}}\sum_{m=1}^{m=\mathrm{M}} c_m e^{-j2\pi\upsilon_{\mathrm{N}-1} t_m} \\
&\lambda^*_{1,\mathrm{N}}x_1 + \lambda^*_{2,\mathrm{N}}x_2 + \cdots + \lambda^*_{m,\mathrm{N}}x_m \\
&\qquad + \cdots + \lambda^*_{\mathrm{N}-1,\mathrm{N}}x_{\mathrm{N}-1} + x_{\mathrm{N}} = \frac{1}{\mathrm{M}}\sum_{m=1}^{m=\mathrm{M}} c_m e^{-j2\pi\upsilon_{\mathrm{N}} t_m}
\end{aligned}
$$

In solving this system of equations, note that if two constituents have the same frequency, this system is completely indeterminate. Errors excepted, this situation should not arise. However, if two frequencies are closely adjacent, the situation is close to indeterminacy and the results will not be very accurate, and the question arises as to whether the system is properly conditioned.

The graphs (figures 6.1 and 6.2) of the spectrum of function $h_i(t) = \cos(2\pi\nu_i t)$, sampled with the same time step but different intervals, provide an intuitive way to deal with this problem. Let us thus consider two sinusoidal waves with distinct frequencies ($\nu_i \neq \nu_n$), sampled over a time interval T with time step t_e. These two waves take the respective 'vectors' $a_i e^{j2\pi\nu_i t}$ and $a_n e^{j2\pi\nu_n t}$. In the domain delimited by the Nyquist frequency ($0 < \nu < \nu_{\mathrm{N}}$), the respective spectra of these vectors are represented by $a_i \left|\Lambda_{\mathrm{T},t_e}(\nu - \nu_i)\right|$ and $a_n \left|\Lambda_{\mathrm{T},t_e}(\nu - \nu_n)\right|$, which are continuous functions of the frequency. When there is a frequency deviation where $|\nu_i - \nu_n|$ is a multiple of $1/\mathrm{T}$, the two constituents are clearly separated. The position of the spectral peak of one of the signals corresponds to a zero position of the other and vice versa. However, when the error is below the frequency $1/\mathrm{T}$, the two main peaks tend to overlap, so it could be hard to differentiate them.

The so-called Rayleigh criterion is often selected to avoid these latter situations when solving a system of normal equations. For all pairs of constituents i and n belonging to a given k species (n.b. index k is omitted here in the subscripts), when applying this criterion, one of the respective frequency constituents ν_i and ν_n (corresponding to frequencies υ_i and υ_n relative to the centre frequency of the considered species) is overlooked, if they do not fulfil the condition:

$$|\nu_i - \nu_n| = |\upsilon_i - \upsilon_n| > \frac{1}{\mathrm{T}} \tag{6.36}$$

This criterion is actually very restrictive since we have seen that the error $|\upsilon_i - \upsilon_n| = 1/\mathrm{T}$ corresponds to zero values of spectra $\left|\Lambda_{\mathrm{T},t_c}(\upsilon - \upsilon_i)\right|$ or $\left|\Lambda_{\mathrm{T},t_c}(\upsilon - \upsilon_m)\right|$. Besides, for errors $|\upsilon - \upsilon_i|$ of around 1/T, we have:

$$\left|\Lambda_{\mathrm{T},t_c}(\upsilon - \upsilon_i)\right| = \left|\frac{\mathrm{sinc}\,[(\upsilon - \upsilon_i)\mathrm{T}]}{\mathrm{sinc}\,[(\upsilon - \upsilon_i)t_c]}\right| \approx |\mathrm{sinc}\,[(\upsilon - \upsilon_i)\mathrm{T}]| \tag{6.37}$$

since $\mathrm{sinc}[(\upsilon - \upsilon_i)t_c] \approx 1$ when $t_c = \mathrm{T/M} \ll 1$.

When $\sigma = (\upsilon - \upsilon_i)\mathrm{T}$, a frequency normalised by $\nu_\mathrm{T} = 1/\mathrm{T}$ centred on υ_i, we obtain the spectrum of the normalised rectangular function $|\mathrm{sinc}(\sigma)|$. The Rayleigh criterion then gives $|\sigma| = |\upsilon - \upsilon_i|\,\mathrm{T} > 1$. Beyond the error $|\sigma| = 1$, the value of the first two secondary peaks of the spectrum of this rectangular function is 0.217; these peaks are reached for $|\sigma| \approx 1.430$ (value of around 1.5 for which $|\sin \pi\sigma| = 1$).

If we accept the errors $|\sigma| > 1$, there would be no reason to prohibit errors below 1 and giving values of $|\mathrm{sinc}(\sigma)|$ below the two secondary peaks at 0.217. Besides, this latter value is also achieved by $|\mathrm{sinc}(\sigma)|$ within the interval $(-1, +1)$ for $|\sigma| \approx 0.813$.

The Rayleigh criterion can be tempered by rounding off this latter value to 0.8. We therefore do not try to solve the system of equations for all pairs of constituents i and n of each species that does not satisfy the condition:

$$|\upsilon_i - \upsilon_n| = |\nu_i - \nu_n| > \frac{0.8}{\mathrm{T}}, \text{ ou } \mathrm{T} > \frac{0.8}{|1/\mathrm{T}_i - 1/\mathrm{T}_n|} \tag{6.38}$$

where T is the duration of the series of reduced vectors, and $\mathrm{T}_i = 1/\nu_i$ and $\mathrm{T}_n = 1/\nu_n$ are periods of the two unseparated constituents. When this condition is fulfilled, there will be a dominant diagonal of at least 80 % and a system of equations that could be considered as being well conditioned.

Note finally that this criterion is not very stringent. It can be more or less effectively interpreted depending on the noise level in the analysed frequency domain. It should still be kept in mind that, where possible, it would be

best to select observation periods close to multiples of periods of the most important constituents.

5 • FFT analysis

The series of M reduced vectors of species k can be dealt with directly via FFT. Let us get back to equation (6.9) for reduced vectors C_k relative to species k. With each species being treated separately, we can remove subscript k to simplify the equations. By using the same convention as previously for defining x_i, i.e. $x_i = h_i e^{j(V_{0i}-g_i)}$, it becomes:

$$C(t) = \sum_i h_i e^{j(V_{0i}+2\pi\upsilon_i t-g_i)} = \sum_i x_i e^{j2\pi\upsilon_i t}$$

We will select a time such as $t = mt_c$ (note the convention change with respect to equation 6.23), where t_c still represents the time interval for computation of two consecutive reduced vectors of the same species k, and with m being the sequence number of samples ranging from 0 to $M - 1$. Moreover, where T is the series interval, the time step t_c is selected such that Shannon's theorem is satisfied and the number $M = T/t_c$ is a power of 2.

Applying FFT to a series of M vectors $C(mt_c)$ generates $M/2$ complex amplitudes corresponding to frequencies n/T with $0 \leq n < M/2$, or:

$$F_{T,t_c}\left(\frac{n}{T}\right) = \frac{t_c}{T}\sum_{m=0}^{m=M-1} C(mt_c)e^{-j2\pi\frac{n}{T}mt_c} \tag{6.39}$$

With the definition of $C(mt_c)$, this latter equation becomes:

$$F_{T,t_e}\left(\frac{n}{T}\right) = \frac{1}{M}\sum_i x_i \sum_{m=0}^{m=M-1} e^{-j2\pi\left[\left(\frac{n}{T}\right)-\upsilon_i\right)]mt_c} \tag{6.40a}$$

Considering that summmations in m, normalised by M, are FFRs of cyclical functions of angular velocities $2\pi\upsilon_i$ sampled within the range T, we deduce:

$$F_{T,t_c}(n/T) = \sum_i x_i \Lambda^*_{T,t_c}(\upsilon_i - n/T) \tag{6.40b}$$

where function $\Lambda_{T,t_c}(\sigma)$ is the Fourier transform (continuous function of σ) of the normalised rectangular function of width T, and sampled every $t_c = T/M$. This latter equation should be matched with the complete expression (6.5) of the FFT of $h(t)$ sampled over interval T with a time step of t_e.

Hence, with n values ranging from 0 to $M/2 - 1$, we obtain a system of $M/2$ equations whose unknowns are amplitudes and phases of harmonic constituents i of species k.

The least-squares method would not be useful for solving this system. When N is the number of unknowns, i.e. necessarily equal to or below M/2, in the system of equations that is to be solved for the considered species k, we will only deal with N equations corresponding to n values such that, for all constituents i, we have:

$$\left|\upsilon_i - \frac{n}{T}\right| < \frac{1}{T} \tag{6.41}$$

This system does, however, have a restriction. If two constituents are related to the same n value, the system will have two identical lines, which will lead to indeterminacy. This could be avoided by making sure that all pairs (υ_i, υ_j) of species k satisfy the Rayleigh criterion (6.36), or:

$$\left|\upsilon_i - \upsilon_j\right| > \frac{1}{T} \tag{6.42}$$

This method is only applicable with a regular series of reduced vectors calculated with a constant time step t_c. It especially cannot be used if the observation data have errors. The advantage is that an FFT can be applied, thus substantially reducing the processing time. Note that the separation criterion is more restrictive than with the least-squares method. However, this restriction is more technical than fundamental, and programming tools could be designed to make it possible to apply the same criterion as used for the least-squares method.

6 • Separation conditions

The impacts of tidal constituent separation conditions should be assessed before dealing with the overall problem concerning harmonic analysis of tide. To be able to solve this first aspect of the problem, unseparated constituent phases should be expressed in the form of explicit functions of fundamental variables used in the harmonic development of the tide-generating potential. Note, however, that this is just a tentative procedure meant only to provide an indication of the orders of magnitude involved.

In the definition of Doodson's harmonic development (5.7), the astronomical argument V_i (of a tidal constituent i) is expressed as a function of coefficients to be assigned to fundamental variables and the number of '$\pi/2$' to add (or delete) so that V_i will only be present in the form of its cosine in (5.7), or:

$$V_i = \overbrace{\overbrace{m_{\tau,i}\tau}^{\text{species}}}^{\text{group}} + m_{s,i}s + m_{h,i}h + m_{p,i}p + m_{N,i}N + m_{p_1,i}p_1 + m_{\pi/2,i}\frac{\pi}{2} \quad (6.43)$$

Moreover, we have seen that Tables 5.3 and 5.4 give the astronomical origin and format of the fundamental variables in equation (6.45) as a function of the decreasing order of respective angular velocities (increasing order of periods). Table 5.4 also shows the magnitude of these angular velocities relative to that of the civil lunar hour angle τ.

Note that the main elements of these astronomical parameters (notations Æ and ML correspond to the hour angle and mean longitude, respectively):

N°	Parameter origin	Symbol	Period
1.	Civil lunar HA	$\tau^\circ = 15^{(\circ/h)}t^{(h)} + h^\circ - s^\circ$	24.841 2 hours 1.035 050 days
2.	ML of the Moon	s	27.321 582 days
3.	ML of the Sun	h	365.242 199 days 1 year
4.	ML of lunar perigee	p	8.847 309 years
5.	Opposite of ML of the ascending lunar node	$N' = -N$	18.612 904 years
6.	ML of solar perigee	p_1	20 940.2 years 209.402 centuries

The difference in magnitudes of these fundamental periods (hours, days, years, centuries) enables us to draw up a number of rules for separating tidal constituents.

Concerning harmonic analysis by the least-squares method, the criterion given by equation (6.40) enables us to set the minimum observation interval T_{min} required to separate two constituents. This interval is:

$T_{min} = 22$ days (rounded value of $27.321 \times 0.8 \approx 21.9$) for constituents belonging to two neighbouring groups, as differentiated by the 2nd digit in their Doodson number;

$T_{min} = 292$ days ($365.242 \times 0.8 \approx 292.2$) when they belong to two neighbouring groups, as differentiated by the 3rd digit in their Doodson number;

$T_{min} = 7$ years ($8.847 \times 0.8 \approx 7.1$), if the constituents only differ by the 4th digit in their Doodson number;

$T_{min} = 15$ years ($18.613 \times 0.8 \approx 14.9$), for those that only differ by the 5th digit in their Doodson number.

For example, we may examine separation conditions for a few main waves (see Table 5.1 or Appendix D), with the constituent angular velocities expressed here in cycles/day (cpd):

Constituents M_2 (mean lunar) and N_2 (major lunar ellipsoid) have the following respective arguments $V_{M_2} = 2\tau$ and $V_{N_2} = 2\tau - s + p$, with an angular velocity error of $q_{M_2} - q_{N_2} = 1/27.32 - 1/(8.85 \times 365.24)$, or 1/27.57 cpd; so $T_{min} = 22$ days ($27.57 \times 0.8 \approx 22.05$) is required to separate these two waves;

- For M_2 and S_2 waves (mean solar: $V_{S_2} = 2\tau + 2s - 2h$), the corresponding error is $q_{S_2} - q_{M_2} = 2/27.32 - 2/365.24$, or 1/14.16 cpd; a minimum interval of $T_{min} = 12$ days ($14.16 \times 0.8 \approx 11.32$) is required for their separation;
- For S_2 and K_2 (lunisolar declinational: $V_{K_2} = 2\tau + 2s$), the difference in angular velocities is $q_{K_2} - q_{S_2} = 2/365.2$, or 1/182.6 cpd; so a minimum record of $T_{min} = 146$ days ($182.6 \times 0.8 \approx 146.09$) is required to separate them;
- Constituents S_2 and T_2 (major solar ellipsoid: $V_{T_2} = 2\tau + s + p_1$) present, when disregarding the corresponding angular velocity at p_1, an error of $q_{S_2} - q_{T_2} \approx 1/365.24$ cpd; a minimum interval of $T_{min} = 292$ days ($365.24 \times 0.8 \approx 292.19$) is required to separate these two elements.

Each subgroup is generally assigned the name of the most important constituent. A minimum interval of 292 tide monitoring days is required to separate two neighbouring subgroups.

For separation conditions involving mean longitudes of lunar perigee (p) and of the ascending node ($N' = -N$), it is necessary to assess series of measurements with a much longer observation interval (several years). Obviously, this type of observation data series is seldom available. Since it is essential to have access to very long-term observation data and also since Darwin's development was incomplete when the harmonic analysis method was created, the problem of separating the concerned constituents is presented in a different setting. This problem was thus not dealt with in the same way, but for no really fundamentally important reason.

Since separation involving solar perigee (p_1) is not common practice,

we will not say much about these conditions. Constituents that could be concerned have very low amplitudes. Moreover, the mean longitude of solar perigee is considered as constant in many applications since it does not vary markedly.

However, because of some nonlinear interactions, there are constituents for which the difference in astronomical arguments just involves lunar parameters p and N, with a value of $|p - 2\mathrm{N}|$. This corresponds to an error of: $1/8.84 - 2/18.61 = 1/176.89$ cycles/year – separation of the concerned constituents then requires a minimal interval of $\mathrm{T_{min}} = 142$ years ($176.89 \times 0.8 = 141.5$). This is an exceptionally long tide observation interval, but such records are available for the Brest (France) site.

7 • Conditioning the equation system

The system of normal equations must be well conditioned to ensure its solution, which is an essential condition for application of the least-squares method for harmonic analysis.

Since poorly separated tidal frequencies introduce major errors in the resulting solutions, at first only constituents that have the highest coefficients, and which fulfil the separation criteria for the interval of the available observation data, are computed. Other constituents that are considered as perturbations are evaluated later.

Take, for instance, a major constituent r that is poorly separated from its minor neighbour i which is considered as a perturbation of the first consituent. In terms of the order number, we assume that $i = r + 1$. In the complete linear system which is deduced from (6.35b) for each k species, on line r we obtain:

$$\lambda^*_{1,r}x_1 + \lambda^*_{2,r}x_2 + \cdots + x_r + \lambda_{r,i}x_i + \cdots + \lambda_{r,\mathrm{N}-1}x_{\mathrm{N}-1} + \lambda_{r,\mathrm{N}}x_{\mathrm{N}} = \frac{1}{\mathrm{M}}\sum_{m=1}^{m=\mathrm{M}} c_m e^{-j2\pi\upsilon_r t_m}$$

In this form, constituents r and i cannot be separated, so the system is obviously poorly conditioned. By removing these constituents, it is replaced by a system where line r becomes:

$$\lambda^*_{1,r}x_1 + \lambda^*_{2,r}x_2 + \cdots + x'_r + \cdots + \lambda_{r,\mathrm{N}-1}x_{\mathrm{N}-1} + \lambda_{r,\mathrm{N}}x_{\mathrm{N}} = \frac{1}{\mathrm{M}}\sum_{m=1}^{m=\mathrm{M}} c_m e^{-j2\pi\upsilon_r t_m} \quad (6.44)$$

Solving this system will not provide the value of the sought-after unknown x_r but rather that of $x'_r = x_r + \lambda_{r,i} x_i$, by taking into account the conventions adopted in (6.23) and equation (6.33) defining coefficients $\lambda_{r,i} = \lambda^*_{i,r}$:

$$\frac{x'_r}{x_r} = 1 + \frac{x_i}{x_r}\lambda_{r,i} = 1 + \frac{h_i e^{j(\mathrm{V}_{0i} - g_i)}}{h_r e^{j(\mathrm{V}_{0r} - g_r)}} \times \Lambda^*_{\mathrm{T},t_c}(\upsilon_i - \upsilon_r) \tag{6.45}$$

According to the notations used in (6.11a), (6.11b) and (6.8), the astronomical argument $\mathrm{V}_j(t)$ at time t for constituent j belonging to species k (excluded here in the subscripts) has the following vector:

$$\mathrm{V}_j(t) = \mathrm{V}_{0j} + q_j t = \mathrm{V}_{0j} + 2\pi(k/\mathrm{T}_\mathrm{L} + \upsilon_j)t = \mathrm{V}_{0j} + 2\pi\nu_j t \tag{6.46}$$

where ν_j represents the frequency $q_j/2\pi$

Recall that $\Lambda_{\mathrm{T},t_c}(\upsilon_r - \upsilon_i) = \Lambda_{\mathrm{T},t_c}(\nu_r - \nu_i)$ and let $t_{\mathrm{T}/2}$ denote the time defined by $t_{\mathrm{T}/2} = (\mathrm{T} - t_c)/2$, then equation (6.45) may be formulated as:

$$\frac{x'_r - x_r}{x_r} = \frac{h_i}{h_r} e^{-j(g_i - g_r)} \frac{\mathrm{sinc}\,[(\nu_i - \nu_r)\mathrm{T}]}{\mathrm{sinc}\,[(\nu_i - \nu_r)t_c]} e^{j[\mathrm{V}_i(t_{\mathrm{T}/2}) - \mathrm{V}_r(t_{\mathrm{T}/2})]} \tag{6.47}$$

This example involves only one perturbation, so the equation can be readily generalised to any number of constituents *i* that are unseparated from a major constituent *r* belonging to a given species *k*. Then:

$$\frac{x'_r - x_r}{x_r} = \sum_i \frac{h_i}{h_r} e^{-j(g_i - g_r)} \frac{\mathrm{sinc}\,[(\nu_i - \nu_r)\mathrm{T}]}{\mathrm{sinc}\,[(\nu_i - \nu_r)t_c]} e^{j[\mathrm{V}_i(t_{\mathrm{T}/2}) - \mathrm{V}_r(t_{\mathrm{T}/2})]} \tag{6.48}$$

Hypotheses are required to evaluate the relative perturbation value expressed by the right side of (6.48), first on the value of the amplitude ratio h_i/h_r, and secondly on the phase lag difference $(g_i - g_r)$.

When no other information is available, the most natural and commonly accepted hypothesis is that the amplitude ratio h_i/h_r is equal to the ratio of the corresponding coefficients $\mathrm{A}_i/\mathrm{A}_r$ of the tide-generating potential:

$$\frac{h_i}{h_r} = \frac{\mathrm{A}_i}{\mathrm{A}_r}. \tag{6.49}$$

However, if accurate harmonic constants calculated over a longer period are available for a neighbouring site, it is best to consider that the amplitude ratios are equal at both sites.

Concerning hypotheses on the phase lag error $(g_i - g_r)$, note that the phase lag represents the lag in a tidal constituent with respect to the corresponding potential element. As the frequencies are very close, it makes sense to consider that the corresponding tidal waves have errors, often quite near and, in practice, considered as nil $(g_i - g_r \approx 0)$. However, when frequency errors are substantial, e.g. when the separation problem concerns constituents

belonging to different subgroups, it is preferable to consider the phase lag difference as proportional to the frequency error. This gives:

$$\frac{g_i - g_r}{\nu_i - \nu_r} = \mathrm{Q} \tag{6.50}$$

The Q coefficient is first estimated on the basis of results concerning directly computed constituents. We sometimes try to enhance the accuracy via successive approximations. However, it is often the case that there is no benefit in going beyond the initial estimate as any improvement is hard to achieve and is often insignificant.

8 • Computation of nodal factors

In Chapter V, because of the effect of the Sun's attraction on the lunar orbit, it was noted that – in his development of the tide-generation potential – Darwin introduced nodal factors for each constituent that was considered in his day. For tidal prediction, software is available that uses tables of nodal factors that have been determined at the mid-point of the year and are considered to be constant throughout this interval. With current computation tools, this method is no longer warranted since instantaneous nodal factor data can now be used.

We will focus specifically on the case of constituents whose Doodson number differs with respect to the 5th digit. This case is very important because it concerns the main lunar constituents that undergo cyclical modulation over a period of 18.61 years (revolution of the ascending lunar node).

Let us now refer to Appendix D and consider, for instance, constituent M_2 of the tide-generating potential, whose arguments (angular and literal) are $\mathrm{V}_{\mathrm{M}_2} = 2\tau$ and B ZZZ ZZZ. In the latter, the 7th letter (Z) indicates that the $\mathrm{V}_{\mathrm{M}_2}$ value is associated with a cosine ($m_{\pi/2,\mathrm{M}_2} = 0$). The corresponding potential coefficient (column PL in Appendix D) is thus assigned a positive sign ($\mathrm{A}_{\mathrm{M}_2} = 0.908\ 120$). The constituent, which is denoted by m_2 in this appendix, has a literal argument of B ZZZ YZB, so it is very close to M_2. The last letter (B) corresponds to a negative cosine coefficient ($m_{\pi/2,m_2} = 2$). Hence, for this consitutent m_2, we have: $\mathrm{V}_{m_2} = 2\tau - \mathrm{N}$ and $\mathrm{A}_{m_2} = -0.033\ 830$.

Equation (6.47) has to be applied if the 15 years of observation data required ($18.61 \times 0.8 \approx 14.9$) to separate the two constituents M_2 and m_2 are not available. In such cases, we can adopt the following conventions:

• the phase lags are considered to be equal ($g_{\mathrm{M}_2} - g_{m_2} \approx 0$) because of the extremely close frequency values;

• by expressing the time in days (with T being the duration of the series of M reduced vectors: $T = Mt_c$), $T_{M/2}$ denotes the elapsed time between 1st January 2000 at midday (Greenwich Civil Time) and the half-series time; the beginning of the series is thus at time $T_{M/2} - T/2$.

Moreover, the angular velocity error, calculated in radians/day (rad/d), is:

$$2\pi(\nu_{m_2} - \nu_{M_2}) \approx -6.28/(18.61 \times 365.24) \approx -0.924 \cdot 10^{-5} \text{ rad/d}$$

According to hypothesis (6.51) on the corresponding tidal wave amplitudes, it becomes:

$$\frac{h_{m_2}}{h_{M_2}} = \frac{A_{m_2}}{A_{M_2}} = -\frac{0.033\ 830}{0.908\ 120} \approx -0.037$$

Equation (6.48) is then expressed by (n.b. it is the half-error of the angular velocities that is considered in the sine computations):

$$\frac{x'_{M_2} - x_{M_2}}{x_{M_2}} = -\frac{0.037}{M} \frac{\sin\left(0.462 \cdot 10^{-3} T\right)}{\sin\left(0.462 \cdot 10^{-3} t_c\right)} e^{-j(4.09 + 0.924 \cdot 10^{-3} T_{M/2})} \quad (6.51)$$

Note that t_c is around unity and that the denominator sine can be treated as its argument, which reveals the product $Mt_c = T$ and eliminates the sampling effect.

If the observation interval is short enough (in practice, a year or less), the numerator sine can also be treated as its argument, thus giving:

$$\frac{x'_{M_2}}{x_{M_2}} \approx 1 - 0.037 \cdot e^{-j(4.09 + 0.924 \cdot 10^{-3} T_{M/2})} = f_{M_2} e^{j u_{M_2}} \quad (6.52)$$

Parameters f_{M_2} (always positive) and u_{M_2} are what could be called Darwin's 'nodal corrections' (see equation 5.1) of tidal wave M_2. They correspond to the amplitude factor (f_{M_2}) and the phase lag (u_{M_2}) to apply to constituent M_2 to account for the presence of wave m_2. With this often adopted approximation, the perturbation is treated as the instantaneous perturbation corresponding to the center observation of the measurement series (time $T_{M/2}$). This result is only acceptable for harmonic analyses data with a sampling duration of a year or less. Beyond this time period, the accuracy deteriorates and the equation is not applicable.

With current computational tools, this approximation is no longer of interest, even for short series. In all situations, it is thus preferable to use the complete formula which gives the mean perturbation throughout the observation interval.

Conversely, it is preferable to calculate instantaneous nodal factors for predictions. This may seem obvious, however there are still software pro-

grammes that use Darwin's tables for tide table computation, which give nodal factors corresponding to the mid-point of each year.

9 • Computation of nonlinear interaction waves

The problem concerning the determination of tidal waves, which are the result of nonlinear interactions, is harder to solve. This difficulty is due to the fact that there are no corresponding constituents in the tide-generating potential that could provide support for the amplitude ratio hypothesis.

The following approach is used in this case. Assume that two tidal waves A and B are respectively perturbed by constituents a and b. Nonlinear hydraulic interactions generate the AB wave, as well as waves Ab, aB and ab.

Using the same notations as in the previous parts, the relative error (complex value) of the perturbed total constituent x_{AB} with respect to the most important interaction waves present, e.g. x_{AB}, can be expressed as:

$$\frac{x'_{AB} - x_{AB}}{x_{AB}} = \frac{x_{Ab}}{x_{AB}} + \frac{x_{Ba}}{x_{AB}} + \frac{x_{ab}}{x_{AB}} \tag{6.53}$$

An additional hypothesis is still required to solve the problem. From a hydrodynamic standpoint, it is generally acknowledged that the amplitudes of interaction waves are proportional to the amplitudes of the constituents involved. With the amplitude term, considered here in a broad sense, this concerns the complex amplitude, i.e. the product of the modulus and the complex exponent of the phase. Where the symbol $\propto$ indicates the proportionality (real or complex), this additional hypothesis enables us to formulate the four following equations:

$$\begin{aligned} x_{AB} &=\propto x_{A}\cdot \propto x_{B} \\ x_{Ab} &=\propto x_{A}\cdot \propto x_{b} \\ x_{Ba} &=\propto x_{B}\cdot \propto x_{a} \\ x_{ab} &=\propto x_{a}\cdot \propto x_{b} \end{aligned} \tag{6.54}$$

By taking this proportionality into account, we deduce (6.55):

$$\frac{x'_{AB}}{x_{AB}} = 1 + \frac{x_a}{x_A} + \frac{x_b}{x_B} + \frac{x_a x_b}{x_A x_B}$$

or even:

$$\frac{x'_{AB}}{x_{AB}} = \left(1 + \frac{x_a}{x_A}\right)\left(1 + \frac{x_b}{x_B}\right) \tag{6.55}$$

This latter equation is very important because it provides a basis for analysing interaction waves. The correction applied for an interaction constituent is thus the product of the corrections to apply to the interacting constituents. With the same notations as used for the nodal corrections, we obtain the amplitude factor and phase of the correction to apply, or:

$$f_{\mathrm{AB}} e^{ju_{\mathrm{AB}}} = f_{\mathrm{A}} f_{\mathrm{B}} e^{j(u_{\mathrm{A}}+u_{\mathrm{B}})}$$

Based on the hypotheses put forward, this rule can be applied regardless of the degree of interactions (double, triple, etc.). It is also used for high-order harmonics and for interactions wherein the same constituent is involved several times. We have, for instance:

$$f_{\mathrm{M}_4} e^{ju_{\mathrm{M}_4}} = f_{\mathrm{M}_2}^2 e^{j2u_{\mathrm{M}_2}}$$

$$f_{\mathrm{M}_6} e^{ju_{\mathrm{M}_6}} = f_{\mathrm{M}_2}^3 e^{j3u_{\mathrm{M}_2}}$$

$$f_{2\mathrm{MS}_6} e^{ju_{2\mathrm{MS}_6}} = f_{\mathrm{M}_2}^2 f_{\mathrm{S}_2} e^{j(2u_{\mathrm{M}_2}+u_{\mathrm{S}_2})}$$

The analysis of available long observation data series enabled us to verify the accuracy of the results obtained by this procedure. This direct determination of interaction waves thus *a posteriori* confirms hypothesis (6.54) on the proportionality of complex amplitudes.

VII

Nonharmonic analysis methods

1 • Introduction

The harmonic tidal equation has prevailed chiefly because of its high analytical accuracy and the fact that it can deal with any type of tide, except estuarine tides. It is, however, not very satisfactory because of the substantial computations that it requires using a high number of harmonic constants, in addition to the long recording times.

Accuracy is obviously a key asset, but it should still be kept in mind that tide tables, drawn up on the basis of a small number of parameters, existed before the harmonic analysis method was developed. One example of this is the Laplace tidal equation. Before the advent of computers, this Laplace equation was more accurate for computing tide tables for French coastal regions than the harmonic tidal equation.

Other procedures are also available and a few examples are discussed in this chapter. These methods are mainly used when the harmonic analysis method turns out to be unsuitable, particularly in the following cases:

• For short-term observations, hypotheses on amplitude ratios and phase lag differences for constituents with close periods are required to be able to apply the tidal harmonic constituent separation criterion. These hypotheses only partially reflect the actual situation, which means that the accuracy declines as the observation interval shortens due to the increase in the number of unseparated constituents. A minimum observation interval equal to the semi-lunation (approximately 15 days) is required to apply the harmonic

analysis method, but the accuracy is not optimal. One year is generally considered to be a reasonable observation period for an analysis that would generate accurate enough predictions to meet maritime navigation requirements.

• For estuarine tides, a spectral analysis of observed upstream water heights shows that, because of the proliferation of interaction constituents beyond the twelfth diurnals, it is impossible to identify individual constituents and to apply the harmonic analysis method.

• For some observations, the recording frequency is unsuitable for application of the harmonic analysis method, e.g. tide pole readings around high and low waters, or tide logs obtained to fulfil special harbour project requests (channel maintenance and building, buoying, dredging, rock clearing, etc.).

Besides cases where the harmonic analysis method is hard to apply, there are situations for which the studied parameters, such as tidal constants from reference stations, can be more readily obtained by other procedures. When studying a new site, these procedures generally benefit from previous tide records obtained from a nearby port, or so-called 'reference station' which, for estuaries, is preferably located close to the mouth. Otherwise, we call the study site the 'secondary port'.

2 • Concordance method

2.1 • Concordance in high and low waters

The concordance method is based on a common sense rule – an amplitude and a phase lag at a secondary port correspond to a given amplitude at the reference station.

The geographical proximity of the two ports is not a prerequisite condition for applying this method, but both must have the same type of tide. It is essential to be able to clearly correlate the high water (HW) and low water (LW) parameters at the reference station with the corresponding HW and LW parameters at the secondary port. The ages of the tide have an important role in each port because their difference roughly corresponds to the phase lag between the two tides and helps to determine the associated extremes. This is not problematic for strictly diurnal or semidiurnal tides. However, for highly imbalanced diurnal tides, or mixed tides, the different errors for the diurnal and semidiurnal constituents can lead to confusion, thus making this method inapplicable.

The 'concordance conditions' can normally be assessed on the basis of the harmonic constants. These constants are generally not available for

secondary ports (which is mainly why this method was developed). Direct and empirical comparison of tide graph data available for a secondary port with that of the reference station is generally satisfactory. Moreover, the uncertainty in the results can be estimated by this procedure.

This method thus involves graphically assessing relations between HW and LW tidal times and heights for the two ports. A few examples are described below (figures 7.1, 7.2 and 7.3).

The first example concerns a study of concordances between tidal heights at two quite remotely separated ports (Brest and Le Havre, which are located several hundreds of kilometres apart along the French coasts). Tides at both sites are semidiurnal, whereas there are many nonlinear interactions at Le Havre (secondary port, spectrum in figure 6.3) but not at Brest (reference station).

On the first graph (figure 7.1), the x-axis for each dot represents a HW or LW height at the reference station, while the y-axis represents the associated HW or LW height for the secondary port. Each intersection gives the centroid of dots calculated at height intervals (for the reference station) selected by the operator. The dot distribution around these centroids enables estimation of confidence levels for HW or LW heights at the secondary port as a function of the corresponding elements at the main port. The statistical parameters can be obtained by a routine computation procedure, but it is often just as efficient to estimate them directly on the graph. Indeed, some tidal observation anomalies may not be revealed by automated computations. These anomalies are hard to detect without visual inspection of the graph. This concordance in tidal heights is very easy to implement: for each HW or LW height at the reference station there is a better corresponding HW or LW height at the secondary port. Moreover, this type of graph is useful for correlating mean spring and neap tide HW or LW heights at the reference station with the corresponding levels at the secondary port.

This concordance should facilitate tidal predictions at a secondary port on the basis of heights at the reference station. It would thus be relevant to ask whether the concordance method could be performed via predictions rather than on the basis of observations at the reference station. The answer to this question should account for the need to minimize meteorological noise, which is partially responsible for the uncertainty in the concordance results. This noise has an impact especially in the low frequency range, mainly leading to variations in the daily mean tidal level.

The treatment will differ depending on whether the ports are located close to each other or far apart, and operators mainly make common sense choices. For two ports that are sufficiently close together, the meteorological effects

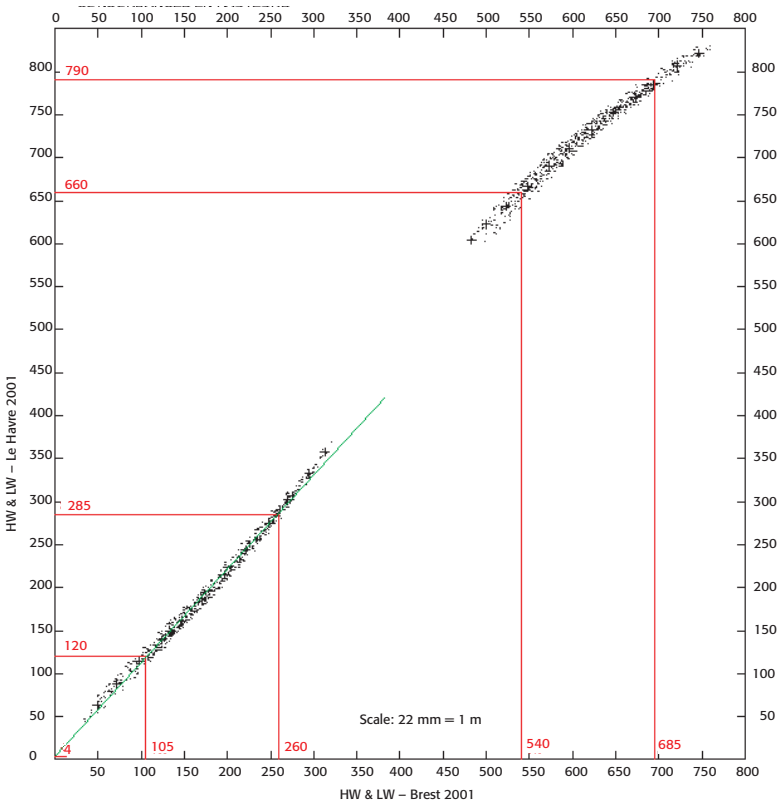

Figure 7.1: Concordance in tidal heights (cm). The x-axis represents the HW or LW heights at the reference station (Brest) in 2001, while the corresponding heights at the secondary port (Le Havre) are given on the y-axis. The standard heights at Brest enable determination of the corresponding values at Le Havre (red lines).

could be considered as identical. In such cases, raw observation data can be used. Otherwise, it is better to prefilter the dataset to eliminate low frequency data. The following operations can be performed on the observations logged at each port:

- Calculating the series of daily mean levels focused on each observed height (see 4.1);
- Calculating the mean level over the measurement time at the secondary port (the mean level at the reference port is already known);
- Correcting each observed height by the difference between the mean level over the measurement time and the daily mean level corresponding to this observation;
- Plotting a graph of concordances in tidal heights (HW and LW).

When simultaneous observations are not available (e.g. due to reference tide-gauge breakdown), the HW and LW heights predicted for the reference station can still be used, while making sure to eliminate long-period constituents (mainly S*a* and S*sa*). This precautionary measure is essential because measurements at the secondary port are obtained over a relatively short interval (but still over a minimum of 15 days), and they should be prefiltered to eliminate low frequency constituents (mainly S*a* and S*sa*). In this case, the concordance method is unable to predict long-period constituents. These constituents can nevertheless be introduced later by simply appropriating those of the reference station when the secondary port is located nearby. Otherwise this gap must be taken into account when estimating the uncertainty in the measurement data.

Note that this procedure, which involves using a reference station prediction, should not be applied in the following situations:

- Reference station observations are unavailable;
- Simultaneous observations are available, but the variations in the two series of daily mean levels are not correlated.

Where possible, to obtain the best estimate of the mean level at a secondary port (over the sampling time) when the two ports are located quite close together, it is best to compute the concordances on the basis of observations recorded at the two ports, while potentially filtering out long-period constituents of the reference station.

2.2 • Concordance by time for semidiurnal tide cycles

Under a semidiurnal tide cycle, spring tide (ST) and neap tide (NT) high and low waters always occur around the same time. This property is utilized in the concordance by time method.

Concordances by HW and LW times at Brest and Le Havre ports, over the same observation period as that considered to establish the concordances in tidal heights (figure 7.1), are represented by scatter plots in figures 7.2 (HW) and 7.3 (LW).

In this type of graph, the x-axis for each dot has a reference station HW or LW time value within the 0 h to 12 h range, while the time difference between associated extremes is represented on the y-axis. As previously, the centroids of dots obtained in predefined intervals are represented by plus signs.

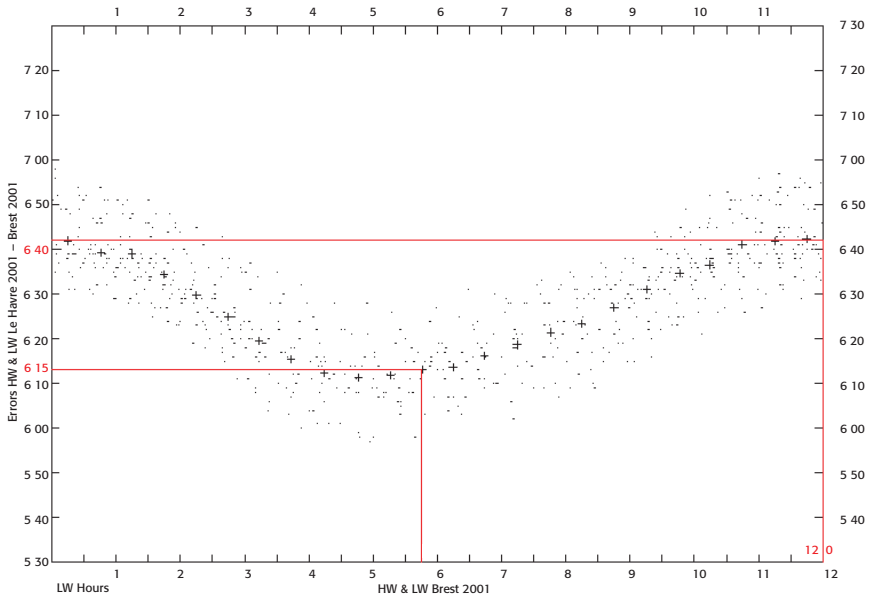

Figure 7.2: Concordances in low water times (Brest and Le Havre).

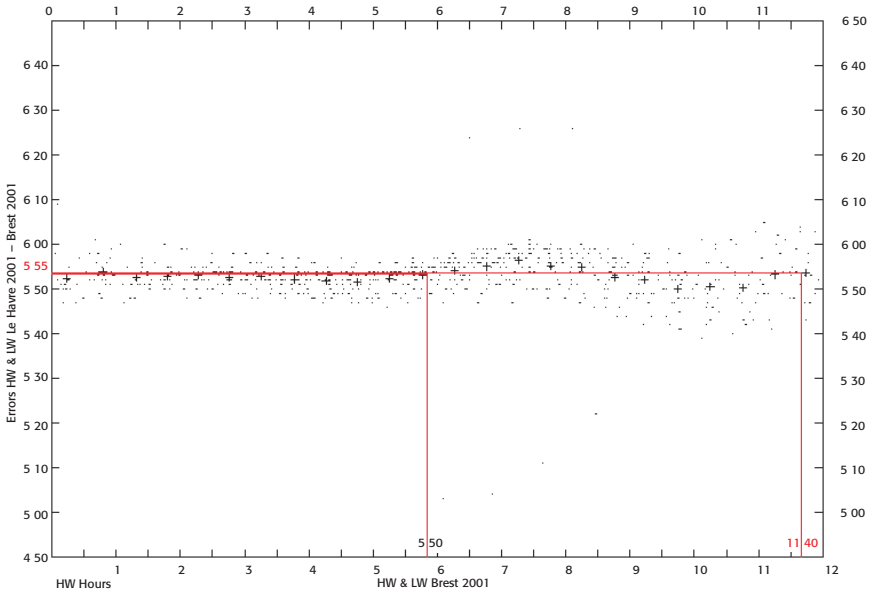

Figure 7.3: Concordances in high water times (Brest and Le Havre).

Note that here the dot dispersion is greater than for tidal heights. This dispersion is partially associated with the fact that a visual reading at an extreme time is always tainted by error on an experimental curve (more or less long slack water duration), while an extreme height reading is easier to establish. The dispersion remains substantial even when this cause of error is taken into account. Moreover, there is no simple relationship between the HW or LW hours at the reference station and the corresponding errors with respect to the reference station.

For spring and neap tide HW or LW times at a reference station, this representation has the advantage of facilitating determination of the corresponding errors for the secondary port. These are indicated by dots at the intersections of red lines on the graphs. Such treatments generate tide table indicators for all ports linked with a reference station. This method enables HW and LW predictions for secondary ports on the basis of predictions of the corresponding elements in main ports. No rules of thumb apply for intermediate times other than those corresponding to ST and NT. For want of more percise indications, the ST or NT error should be used if it is under 2 h, while using the mean when the error is greater.

2.3 • Concordance by time for other types of tide

A phase lag cannot be associated with a reference station HW or LW time when the tidal cycle is not completely semidiurnal. For application of the concordance method, the ratios between HW or LW heights at the reference station and the corresponding extremes at the secondary port must be clearly determined. When the ratio between extremes at the two ports can be established, it is then possible (sometimes through a graphic representation) to associate the corresponding time errors with these heights. For tables of tide corrections, in most cases the HW and LW time errors for the secondary port are only indicated without taking the tidal heights into account.

2.4 • Tide curve

So far the concordance method has only been applied to HW and LW heights and times. If tidal data acquired at faster rates are available, other concordance-related analytical treatments can be applied to encompass all dots on a secondary port tide curve.

Standard curves* can thus be plotted when, for instance, hourly records are available for the secondary port. On a graph, this involves plotting a line whose y-axis is a reference station HW (or LW) height. On this line,

at an hourly interval, dots are plotted whose x-axes are secondary port tidal heights relative to the corresponding reference station extremes (HW or LW). For a semidiurnal tide cycle, these dots are thus distributed between −6 h and +6 h around the associated extreme at the secondary port.

This procedure may only be applied if a sufficient number of tidal measurements are available to ensure relatively accurate predictions. In this case, however, better results can be obtained by plotting standard tide curves using harmonic constants.

3 • Response method

In the harmonic analysis of tide, only the tidal line spectrum, i.e. a distribution of constituents with known and clearly determined frequencies, is sought. All other parts of the signal associated with the action of other meteorological or oceanographic phenomena have a continuous spectrum, which is disregarded.

The so-called response method developed by Munk and Cartwright (1965) involves an analysis of the tide level overall. Here the tide height $h(t)$ is treated as a signal representing the response of the sea surface (excluding swells and waves) to an excitation function $\mathrm{U}(t)$ which accounts for all physical factors that could impact the tide level (tide-generating potential, solar radiation, atmospheric pressure, wind, etc.).

Due to the nonlinearity of the response to the excitation function, the tide height $h(t)$ is reflected by a series of convolution integrals of the following type:

$$h(t) = \sum_{n=1}^{n=\mathrm{N}} \int_{\tau_1} \dots \int_{\tau_n} w_n(\tau_1, \dots, \tau_n)\mathrm{U}(t-\tau_1)\dots \times \mathrm{U}(t-\tau_n)\mathrm{d}\tau_1 \dots \mathrm{d}\tau_n \quad (7.1)$$

w_n are characteristic functions of the considered point and are relatively small in number in comparison to analyses using the harmonic method. The first $w_1(t) * \mathrm{U}(t)$ term of this equation corresponds to the linear part of the response, while the others account for the nonlinear aspects.

In signal theory, the $w_1(t)$ term represents the pulsed response of a linear system. Its Fourier transform $a_1(\nu)$ may be called the system transfer function, or admittance (complex):

$$a_1(\nu) = \int w_1(t)e^{-j2\pi\nu t}\mathrm{d}t$$

By extension, the admittances a_n are defined by:

$$a_n(\nu_1, \cdots, \nu_n) = \int_{\tau_1} \cdots \int_{\tau_n} w_n(\tau_1, \cdots, \tau_n) e^{-j2\pi\nu_1\tau_1} \cdots \times e^{-j2\pi\nu_n\tau_n} \mathrm{d}\tau_1 \cdots \mathrm{d}\tau_n$$

The admittance concept thus provides a new approach for tidal prediction. Summation of a high number of constituents via application of the harmonic method is replaced here by application of a response function that links the cause (i.e. tide-generating potential, radiational potential, various meteorological-oceanographic actions) with the effect (tidal height variations).

The response function is computed from the admittances. Munk and Cartwright (1965) showed that the response method can account for radiational effects and the results are generally better than can be obtained with the harmonic method. However, this is only possible when the nonlinear effects are minor and substantial computation is necessary, thus neutralizing the slight improvement achieved by applying this method.

The response method has never been used for tide table computation. However, the admittance concept, whose physical significance is fully accounted for in signal processing, is still favoured by some specialists.

Finally, it should be noted that this method is a generalization of the Laplace method. From a formal standpoint, results obtained by the Laplace method are similar to the linear approximations applied to the first three species ($k = 0$, 1 and 2). This prompted us to assess the widely used species concordance method.

4 • Species concordance method

The Munk and Cartwright method is hampered mainly by the fact that it attempts to deal with the entire tidal spectrum. Many operations thus have to be performed, which soon becomes impossible, especially with respect to overcoming the problem of nonlinear interactions. This concept is still quite interesting though, since it involves assessing cause-effect relationships, with the possibility of characterizing a site according to a small number of parameters, i.e. much smaller than required for harmonic analysis.

As already mentioned, in this sense the method resembles the Laplace method, which involves determining the species transfer function relating the tide-generating potential with the tidal height. The fact that Laplace restricted application of his equation to three species, each representing a

narrow frequency domain, explains why it is efficient for tide prediction at the port of Brest (France). The Laplace equation was thus found to generate good results with minimal computation resources. It cannot, however, be applied under all conditions because the transfer function characterizes linear systems, so no interaction constituents are involved.

The species concordance method takes up the idea underlying the response method, beginning with the same fundamental equation (7.1) in the form of multiple convolution integrals. However, its efficiency, i.e. it performs better for computing multiple convolutions, is due to the fact that it deals only with narrow frequency bands containing all of the tidal energy. This procedure is actually not restrictive since these are the only frequency bands useful for prediction. The remaining frequency domain just contains noise which, by definition, is unpredictable.

Another essential difference with respect to the response method is the choice of input function. Munk and Cartwright very logically selected the tide-generating force in order to be able to come up with general equations. However, this choice is also a source of difficulty because the complexity of the ocean's response to the excitation of the force is reflected in the response function. It would thus be more suitable to select an input function that is as close as possible to the response.

Based on these choices, the species concordance method turns out to be effective for dealing with estuarine tides. This procedure is currently being used to compute tide tables for the Gironde River estuary (France), from the mouth at Verdon to Bordeaux, 90 km upstream (see figure 1.8).

4.1 • Species concordance: formulation of the method

This method was designed especially for estuarine tide prediction since the harmonic analysis method is not able to predict such tides correctly.

The basic concept is based on two features:

• The tide at the estuary mouth is not very deformed and can be readily predicted with the harmonic method;

• There is a relation between the estuary mouth tide and the upstream tide.

Therefore let:

• $h_R(t)$ denote the tidal height observed at time t at a reference station (R) located close to the mouth;

• and $h_S(t)$ denote the level observed at the same time at a specific upstream site which we call the 'secondary port' (S).

Apart from other external contributions (fluvial or atmospheric), the most general relation between these two tides is given by a multiple convolu-

tion equation similar to (7.1), where $U(t)$ is replaced by $h_R(t)$:

$$h_S(t) = \sum_{n=1}^{n=N} \int_{\tau_1} \dots \int_{\tau_n} w_n(\tau_1, \dots, \tau_n) h_R(t - \tau_1) \dots \times h_R(n = t - \tau_n)\, d\tau_1 \dots d\tau_n$$

Let us use the approach that gave rise to the reduced heights method. We have seen that the results obtained were very effective for harmonic analysis. This procedure is based mainly on the following points:

- Because of the equivalence of the spectral and temporal signal distributions, focusing only on narrow tidal frequency bands makes it possible to consider only a small quantity of temporal data;
- Moreover, by dealing with species separately, the global problem which is hard to completely solve can be transformed into several much simpler computations.

The concept of reduced vectors of species k at time t was defined in Chapter VI by equation (6.10) as follows:

$$h(t) = \frac{1}{2} \sum_k \left[C_k(t) e^{j2\pi \frac{k}{T_L} t} + C_k^*(t) e^{-j2\pi \frac{k}{T_L} t} \right]$$

where T_L is the lunar day duration. Constituents of the same k species (long periods, diurnal, semidiurnal, etc.) are all represented by the complex expression vector $C_k(t)$ whose modulus and phase vary slowly over time.

Let $R_k(t)$ and $S_k(t)$ denote reduced vectors of k species at time t at the reference station (R) and secondary port (S), respectively. In case of an estuarine tide, if $\max k_R + 1$ is the number of species detected by the harmonic method at the reference station located at the estuary mouth, the $\max k_S + 1$ number at the secondary port is still much higher ($\max k_S > \max k_R$). For instance, around 12 species are present in the tidal spectrum at Verdon (Gironde River mouth), but a threefold higher number of species were detected at Bordeaux (90 km upstream).

The multiple convolution formulation in terms of reduced vectors and the identification (term by term) of coefficients relative to exponents (complex) leads us to an equation that gives us $S_k(t)$. This relation represents the sum of the following elements that are classified according to the number m of reduced vectors $R_{n_i}(t)$ which interact, such that:

$$\sum_{i=1}^{i=m} n_i = k \tag{7.2}$$

So the terms of this sum representing $S_k(t)$ are:

$m = 1$: a single reduced vector ($n_1 = k$; no interaction: $m - 1 = 0$):

$$\int w_1(\tau)\mathrm{R}_k(t-\tau)e^{-j2\pi\frac{k\tau}{\mathrm{T_L}}}\mathrm{d}\tau$$

$m = 2$: all pairs such that $n_1 + n_2 = k$ (single interaction):

$$\sum_{n_1+n_2=k}\iint_{\tau_1\tau_2} w_2(\tau_1,\tau_2)\mathrm{R}_{n_1}(t-\tau_1)\mathrm{R}_{n_2}(t-\tau_2)e^{-j2\pi\frac{n_1\tau_1+n_2\tau_2}{\mathrm{T_L}}}\mathrm{d}\tau_1\mathrm{d}\tau_2$$

$m = 3$: all double interactions such that $n_1 + n_2 + n_3 = k$:

$$\sum_{n_1+n_2+n_3=k}\iiint w_3(\tau_1,\tau_2,\tau_3)\mathrm{R}_{n_1}(t-\tau_1) \times \mathrm{R}_{n_2}(t-\tau_2)\mathrm{R}_{n_3}(t-\tau_3)e^{-j2\pi\frac{n_1\tau_1+n_2\tau_2+n_3\tau_3}{\mathrm{T_L}}}\mathrm{d}\tau_1\mathrm{d}\tau_2\mathrm{d}\tau_3$$

The series continues by taking all possible interactions into account. The reduced vector $\mathrm{S}_k(t)$ of the secondary port can then be expressed in a more compact form by:

$$\mathrm{S}_k(t) = \sum_{m=1}^{\mathrm{M}}\sum_{\Sigma n_i=k}\int_{\overrightarrow{\tau}}\left[\prod_{i=1}^{m}\mathrm{R}_{n_i}(t-\tau_i)\right]w_m(\overrightarrow{\tau})e^{-j2\pi\frac{\overrightarrow{n}\,\overrightarrow{\tau}}{\mathrm{T_L}}}\mathrm{d}\overrightarrow{\tau} \qquad (7.3)$$

In this equation (7.3), note that the m parameter represents the number of interacting reduced vectors $\mathrm{R}_{n_i}(t)$, with the sum of n_i indices satisfying equation (7.2).

Moreover, when $\mathrm{K_R} = \{-\max k_\mathrm{R}, \ldots, 0, \ldots, \max k_\mathrm{R}\}$ denotes all relative integers (corresponding to positive or negative centre frequencies of reference station species), for all n_i, we have: $n_i \in \mathrm{K_R}$.

The reduced vectors $\mathrm{S}_k(t)$ are computed for all $k \in [0, \max k_\mathrm{S}]$. Hence, to obtain all interactions of all groups of m vectors $\mathrm{R}_{n_i}(t)$, we calculate the sum of all possible products of m reduced vectors of the main port whose n_i indices fulfill the conditions of equation (7.2). Finally, for each set $\{n_i\}$ satisfying these latter conditions, the $\overrightarrow{n}$ and $\overrightarrow{\tau}$ vectors are defined by the following respective constituents: $\overrightarrow{n} \Rightarrow (n_1, \ldots, n_m)$ and $\overrightarrow{\tau} \Rightarrow (\tau_1, \ldots, \tau_m)$.

4.2 • Species concordance: simplifying hypotheses

These equations formulated for computation of reduced vectors $\mathrm{S}_k(t)$ at the secondary port cannot be used without applying some simplifying hypotheses.

A first hypothesis, which was called the 'credo of smoothness' by the authors of the response method, assumes that the relationship between

the tide at the reference station and that at the secondary port is a slowly varying function of the frequency. It thus involves highly accurate w_m pulse functions. For a reduced pulse at a complex constant (constant amplitude and phase), we obtain a Dirac pulse $\delta(t - \mathrm{d}_{i,m})$ weighted by a complex constant coefficient. d_{im} represent the signal lag times (reduced S vector) for the different causes (all reduced R vectors). Due to the slow variation in the reduced vectors, the $\mathrm{R}_{n_i}(t - \tau_{i,m})$ vectors can be considered as constant in the definition range of pulse responses $w_m(\ldots, \tau_{i,m}, \ldots)$. These vectors can thus be derived from convolution integrals.

For the reduced vector of the k species at the secondary port S, we obtain:

$$\mathrm{S}_k(t) = \sum_{m=1}^{\mathrm{M}} \mathrm{Q}_{m,k} \sum_{\Sigma n_i = k} \prod_{i=1}^{m} \mathrm{R}_{n_i}\left(t - \mathrm{d}_{im}\right) \tag{7.4}$$

with:

$$\mathrm{Q}_{m,k} = \int_{\vec{\tau}} w_m(\vec{\tau}) e^{-j2\pi \frac{\vec{n}\,\vec{\tau}}{\mathrm{T_L}}} \mathrm{d}\vec{\tau}$$

Now the second simplifying hypothesis is based on the physical significance of the lag times d_{im}. These could be considered as propagation times of the different waves. Wave propagation is actually dispersive in estuaries, and the apparent propagation velocity is frequency dependent. However, accurate d_{im} values are unnecessary because of the slowly varying reduced vectors. It is generally admitted that they are all equal to a constant lag d_{RS}, for a pair of ports (R, S), and are evaluated by averaging the approximate propagation times of tidal extremes between ports R and S. A comparison of measurements and predictions for S, based on $\mathrm{R}_{n_i}(t - \mathrm{d}_{\mathrm{RS}})$, shows that an accurate value of this duration d_{RS} is unnecessary, thus confirming the relevance of this second hypothesis.

On the basis of these two hypotheses, the final expression of the reduced vector $\mathrm{S}_k(t)$ of species k at the secondary port at time t can be formulated as follows:

$$\mathrm{S}_k(t) = \sum_{m=1}^{\mathrm{M}} \mathrm{Q}_{m,k} \sum_{\Sigma n_i = k} \prod_{i=1}^{i=m} \mathrm{R}_{n_i}\left(t - \mathrm{d}_{\mathrm{RS}}\right) \tag{7.5}$$

First, computation of reduced vectors derived from measurements at the two ports generates a system of equations that can be used to determine the $\mathrm{Q}_{m,k}$ coefficients by the least squares method.

Once calculated, these $\mathrm{Q}_{m,k}$ coefficients can be applied to more accurately determine the reduced vectors $\mathrm{S}_k(t)$ for the secondary port so as to come up with the requisite predictions. Recall that the underlying hypothesis of

this species concordance method is based on the possibility of having a very good tidal prediction for the reference station, and thus of computing the reduced vectors $R_{n_i}(t - d_{RS})$ involved in equation (7.5).

This method enables the use of additional input data so as to be able to take, for instance, the stream discharge $D_0(t)$, which here is considered as a long-period constituent ($k = 0$), into account.

4.3 • Species concordance: applications

We will now examine the two main applications of this method by the French Hydrographic Service, i.e. for estuarine tidal prediction and processing short-term observations in the vicinity of sounding areas.

In order to make the $Q_{m,k}$ coefficients adimensional in such applications, the reduced vectors (of the parameters taken into account: tidal height, stream discharge, etc.) are related to their mean modulus over the total sampling time (operator $\overline{|x(t)|_T}$) considered. The following correspondences are used to simplify the equations:

$$\begin{aligned} S_k &\Rightarrow S_k(t)/\overline{|S_k(t)|_T} \\ R_n &\Rightarrow R_n(t - d_{RS})/\overline{|R_n(t)|_T} \\ D_0 &\Rightarrow D_0(t)/\overline{|D_0(t)|_T} \end{aligned}$$

The reduced vectors at the secondary port are calculated for time t and those at the reference station for time $t - d_{RS}$, while d_{RS} is the tide propagation time from the reference station R to the secondary port S. An accurate value is generally not required and an error of around 1 h does not lead to marked variations in the results.

4.3.1 • Estuarine tides

The following examples only apply to semidiurnal tides. The maximum number M of interacting reduced vectors R_n is obtained through a spectral analysis at the secondary port.

Let us consider the case of the Seine River (France). The port of Le Havre is the reference station and Rouen is the secondary port where tidal consituents are detectable up to the 36th diurnals. The formulation therefore must include interactions up to the 18th order for R_2.

In the following equations, note that the subscript allocated to all reduced vectors represents the number of the considered species. For the $Q_{m,k}$ coefficient, the first subscript represents the number of interacting vectors, while the second is equal to the value of the k species of the S_k vector to be computed. Note also that each interaction of the reduced vector R_2 with

its conjugate R_2^* introduces a contribution proportional to $R_2^* R_2$ of the zero species ($k = 0$).

It thus becomes:

$$S_0 = Q_{0,0} R_0 + Q_{1,0}^{(D)} D_0 + \sum_{m=1}^{9} Q_{2m,0} |R_2|^{2m}$$

$$S_1 = \left[Q_{0,1} + Q_{2,1} |R_2|^2 \right] R_1$$

$$S_2 = \left[Q_{1,2} R_0 R_2 + \left(Q_{1,2}^{(D)} D_0 + \sum_{m=1}^{9} Q_{2m+1,2} |R_2|^{2m} \right) \right] R_2$$

$$S_3 = \left[Q_{0,3} + Q_{2,3} |R_2|^2 \right] R_3$$

$$S_{2n} = \left[Q_{1,2n}^{(D)} D_0 + \sum_{m=0}^{9} Q_{2m+n,2n} |R_2|^{2m} \right] R_2^n \quad (n > 1)$$

In this Seine River example, only first-order river discharge D_0 interactions apply to the reduced vectors R_2^n, whereas third-order discharge interactions have to be taken into account when using this method to assess tides propagating up the Loire River.

Many coefficients that are often hard to determine must be calculated when applying this method upstream of the estuary. The complete equation should not be used when the higher order terms are not very accurate.

All possible situations should be taken into account to obtain good analytical results. The observational data to be analysed should include all amplitude domains associated with the different discharge values. Observations that include extreme discharge values (flooding and minimum flow) are especially interesting. In practice, at least 1 year of measurements (tide and discharge) are required, but a sampling period of several years would be better.

4.3.2 • Analysis of series of short-term measurements

For open sea observations in the vicinity of coasts or estuaries, harmonic constituents are seldom detected beyond the 10th diurnals. The formulation is thus simplified and tailored to the type of tide.

The development presented hereafter on the basis of equation (7.5) is used for semidiurnal tides. It is largely based on experience. Only vectors whose interactions involve known constituents are taken into account. Amongst

all of the potential reference stations near the study site (S), the one that has constituents that will enable the best tidal prediction is selected. The river discharge is no longer involved in this application. It is, however, still possible to modify the equations to account for meteorological parameters, e.g. wind and atmospheric pressure. Note that the normalized reduced vectors S_k and R_n are considered at times t and $t - d_{RS}$, respectively, with the d_{RS} term being the tide propagation time from R to S. For a semidiurnal tide, this gives:

$$\begin{aligned}
S_0 &= Q_{0,0} + Q_{1,0}R_0 + Q_{2,0}R_2^*R_2, \\
S_1 &= Q_{1,1}R_1 + Q_{2,1}R_2R_1^* + Q_{3,1}R_2^*R_2R_1 \\
S_2 &= Q_{1,2}R_2 + Q_{2,2}R_0R_2 + Q_{3,2}R_2^*R_2^2 \\
S_3 &= Q_{1,3}R_3 + Q_{2,3}R_2R_1 + Q_{3,3}R_2^*R_2R_3 \\
S_4 &= Q_{1,4}R_4 + Q_{2,4}R_2^2 + Q_{4,4}R_2^*R_2^3 \\
S_6 &= Q_{1,6}R_6 + Q_{2,6}R_2R_4 + Q_{3,6}R_2^3 + Q_{5,6}R_2^*R_2^4 \\
S_8 &= Q_{1,8}R_8 + Q_{2,8}R_4^2 + Q_{4,8}R_2^4 + Q_{6,8}R_2^*R_2^5 \\
S_{10} &= Q_{1,10}R_{10} + Q_{2,10}R_4R_6 + Q_{5,10}R_2^5 + Q_{7,10}R_2^*R_2^6
\end{aligned} \tag{7.6}$$

This method has turned out to be especially efficient for handling mesurements spanning a period of around a month. It is routinely used by the French Hydrographic Service to deal with observations sampled around hydrographic sounding areas. Note, however, that there is an operational constraint to this usage, i.e. this method should not be applied when there is a diurnal or semidiurnal amphidromic point located nearby, since they are incompatible with the credo of smoothness.

Concerning predictions at the secondary port, we have seen that application of this method requires accurate preliminary knowledge of the harmonic constants at the reference station. The reduced vectors $R_n(t)$ can be determined via these elements.

Based on measurements obtained at site S, the reduced vectors are determined from the observed heights (see Chapter VI). The equations (7.6) formulated above can first be used to calculate the $Q_{m,k}$ coefficients (adimensional) by the least squares method. The $Q_{m,k}$ coefficients obtained in this way are reinstated in their respective dimensions (new $Q_{m,k}$ coefficients have $L^{-(m-1)}$ dimensions, i.e. inverse powers of the length). The same equations (7.6) are used again to calculate the reduced vectors $S_k(t)$ directly for the secondary port on the basis of those of the main port $R_n(t - d_{RS})$. As each step is reversible, it is now possible to draw up predictions for the study site.

The reduced tidal heights at site S are calculated using an inverse FFT from $S_k(t)$. Note that the TFR efficiency is maximal when the number of M values is a power of 2. Usually $M = 2^7 = 128$ values per lunar day $T_L = 24.8412$ h are selected, which gives a computation time step of $t_c = 11.64$ min.

At the secondary port, the tidal height at time $t = mt_c$, reduced at time t_o (see Chapter VI, equation (6.22), is expressed as:

$$H(t_o, mt_c) = S_0(t_o) + \frac{1}{2}\sum_{k=1}^{k=M/2-1}\left[S_k(t_o)e^{j2\pi\frac{k}{T_L}mt_c} + S_k(t_o)e^{-j2\pi\frac{k}{T_L}mt_c}\right]$$

The predicted heights are finally obtained by parabolic interpolation (7.7):

$$\begin{aligned} h(mt_c) = {} & H(t_o, mt_c) \\ & + \frac{t_o - mt_c}{2T_L}[H(t_o + T_L, mt_c) - H(t_o - T_L, mt_c)] \\ & + \frac{(t_o - mt_c)^2}{2T_L^2}[H(t_o + T_L, mt_c)] \\ & + [H(t_o - T_L, mt_c) - 2H(t_o, mt_c)] \end{aligned} \quad (7.7)$$

We thus obtain 128 predicted tidal heights per lunar day, i.e. a height every 11.64 min, which means that tidal heights for a given hour can readily be obtained by interpolation, along with HW and LW hours and heights.

This procedure is used for harmonic constant based predictions. It is very efficient because the harmonic constant contribution is only calculated once per lunar day (at times t_o and $t_o \pm T_L$), rather than 128 times if the same result were sought simply by application of the harmonic method.

Note finally that the $Q_{m,k}$ coefficients (reinstated in their actual dimension) can be used to compute harmonic constants of the secondary port. This is obviously interesting for $Q_{1,k}$ coefficients that are related to the linear correspondence between the same tidal waves at the two ports.

We present a simple example to illustrate how it is possible to utilize other $Q_{m,k}$ coefficients. Let us consider a case in which the MS_4 constituent is to be determined for the secondary site S. The $Q_{2,4}$ coefficient can be used to compute the contribution of the semidiurnal constituents (lunisolar) of the main port at the quarter-diurnal constituent of the study site.

Where the pair (h_i, g_i) denotes the harmonic constants (amplitude and phase lag) of wave i at the reference station and (h_j^S, g_j^S) denotes those of wave j at the secondary port, the MS_4 constituent in the latter port is determined by the following equation:

$$h^S_{MS_4} e^{-jg^S_{MS_4}} = Q_{1,4} h_{MS_4} e^{-jg_{MS_4}} + Q_{2,4} h_{M_2} e^{-jg_{M_2}} h_{S_2} e^{-jg_{S_2}}$$

All harmonic constants for the secondary port can be readily calculated when the $Q_{m,k}$ coefficients and harmonic constants for the reference station are known.

VIII

Characteristic values and tidal constituents

In addition to tidal height predictions, harbour users often require information on other basic characteristics for specific applications. These characteristics used to be conventionally computed with data collected by very simple means. Nowadays, thanks to our greater understanding of harmonic constants and their use, these characteristic parameters can be determined with greater accuracy.

We have seen in Chapter V that the main semidiurnal (M_2, S_2, N_2 and K_2) and diurnal (K_1, O_1, P_1 and Q_1) harmonic constituents encompass most of the tidal signal (80-90 %). The fundamental tidal characteristics sought for a given port can be quite accurately determined simply by taking these waves into account.

1 • Study of tidal characteristics of a port

1.1 • Main semidiurnal tidal characteristics

Table 8.1 gives the characteristics of the main semidiurnal tidal constituents. The tide-generating potential coefficients are presented relative to the highest one, i.e. that of the mean lunar constituent M_2.

The cosine arguments of the harmonic tidal equation are given. For clarity, we used the absolute phase lags κ_i for each constituent i, which are conventionally expressed in degrees whereas the times t are always expressed in hours. Note that the local civil time t (in hours) is implemented when absolute phase lags are used.

Table 8.1: Main semidiurnal tidal constituents.

Constituent symbol	Relative coefficient of the potential	Argument number of the tidal wave	Argument in degrees (t in hours)
M_2	1.000	B ZZZ ZZZ	$2\tau - \kappa_{M_2} = 30t + 2(h - s) - \kappa_{M_2}$
S_2	0.466	B BXZ ZZZ	$2\tau + 2s - 2h - \kappa_{S_2} = 30t - \kappa_{S_2}$
N_2	0.192	B YZA ZZZ	$2\tau - s + p - \kappa_{N_2} = 30t + 2(h - s) - s + p - \kappa_{N_2}$
K_2	0.127	B BZZ ZZZ	$2\tau + 2s - \kappa_{K_2} = 30t + 2h - \kappa_{K_2}$

Parameters h, s and p are conventional notations for mean longitude (in angular degrees, unless indicated otherwise) of the Sun, Moon and lunar perigee, respectively, with the mean lunar time expressed in degrees by the equation: $\tau^\circ = 15^{\circ/h} t^h + h^\circ - s^\circ$. The angular velocities of these different parameters are as follows:

$$\begin{aligned} \mathrm{d}\tau/\mathrm{d}t &= q_{\mathrm{M}_2}/2 \approx 14.492^\circ/h \\ \mathrm{d}s/\mathrm{d}t &\approx 0.549^\circ/h \\ \mathrm{d}h/\mathrm{d}t &= q_{\mathrm{S}a} \approx 0.041^\circ/h \\ \mathrm{d}p/\mathrm{d}t &\approx 0.004^\circ/h \end{aligned}$$

where q_i is the angular velocity (expressed here in °/h) of constituent i. For semidiurnal tides, we will thus define a number of characteristics, particularly the mean establishment, age of tide, establishment of the port (which should not be mistaken for the mean establishment) and equinoctial spring tide.

1.1.1 • Mean semidiurnal tide: mean establishment

Tidal potential coefficients have a hierarchical arrangement reflected in the amplitude range of tidal constituents, except in the vicinity of amphidromic points. The functional traits of semidiurnal tides are thus dictated by the M_2 wave, which generally has a dominant amplitude. This tidal wave is generated by the mean Moon which, as noted earlier, is the fictional celestial body having a circular orbit on the equatorial plane at constant velocity, while the radius and period are the mean distance and orbital period of the true Moon, respectively. Its contribution to the total tide is:

$$h_{\mathrm{M}_2}(t) = h_{\mathrm{M}_2} \cos(2\tau - \kappa_{\mathrm{M}_2}) \tag{8.1}$$

which can also be expressed by:

$$h_{\mathrm{M}_2}(t) = h_{\mathrm{M}_2} \cos\left[30t + 2(h - s) - \kappa_{\mathrm{M}_2}\right]$$

According to the civil lunar hour angle definition, transits of the mean Moon over the upper and lower branches of the meridian of the place correspond to τ values that are multiples of 180°, or $\tau = 180^\circ k$ where k is the relative integer. Equation (8.1) gives the maximum M_2 wave for $\tau = (\kappa_{\mathrm{M}_2}/2) + 180^\circ k$, i.e. with a lag, or so-called mean establishment (symbolized by E_m and equal to $\kappa_{\mathrm{M}_2}/q_{\mathrm{M}_2}$), after the Moon's meridian transit. When taking the q_{M_2} value into account, we obtain the mean establishment (in hours) by:

$$\mathrm{E}_m = \kappa_{\mathrm{M}_2}/28.984 \text{ hours} \tag{8.2}$$

Note that only the M_2 constituent is involved in the mean establishment E_m. However, since this wave is dominant, the E_m parameter is quite representative of the lag of the true semidurnal high water with respect to the Moon's meridian transit (upper or lower branches). This very practical lag concept was developed much before the harmonic method – here it is presented as a ramification of this method.

1.1.2 • Semidiurnal spring tide, age of tide, establishment of the port

The mean solar constituent S_2, like the mean lunar constituent M_2, represents the tide generated by the mean Sun, i.e. a fictional celestial body with a circular orbit on the equatorial plane at constant velocity, but at the mean distance and with the same orbital period as the true Sun.

Its contribution to the total tide is:

$$h_{S_2}(t) = h_{S_2} \cos(30t - \kappa_{S_2}) \tag{8.3}$$

The Sun transits over the upper branch of the meridian of a place at noon ($t = 12$ h) and over the lower meridian at midnight ($t = 0$). The high water of this wave of amplitude h_{S_2} follows these transits of $\kappa_{S_2}/30$ h. Hence, the two daily high waters of the S_2 wave occur daily at $\kappa_{S_2}/30$ and $\kappa_{S_2}/30 + 12$ local times, while the low waters occur at $\kappa_{S_2}/30 + 6$ and $\kappa_{S_2}/30 + 18$ local times. As the amplitude of the S_2 wave is substantially lower than that of the M_2 wave, its action can be interpreted as a modulaton of the mean lunar constituent. Their superposition peaks when they are in phase, i.e. when:

$$30t + 2(h - s) - \kappa_{M_2} = 30t - \kappa_{S_2} \qquad \text{(modulo } 360°\text{)}$$

which gives:

$$s - h = \frac{\kappa_{S_2} - \kappa_{M_2}}{2} \qquad \text{(modulo } 180°\text{)} \tag{8.4}$$

The mean longitude difference of the Moon and Sun that verify equation (8.4) define the semidiurnal spring tides. Moreover, when $s = h$ (modulo 180°), the Sun and Moon are located on the same meridian plane. These times are called syzygies and correspond to full Moons (opposition) and new Moons (conjuction). Spring tides thus follow syzygies with a T_2 lag, which is called the age of semidiurnal tide. When considering the fact that $2\mathrm{d}(s - h)/\mathrm{d}t = 1.016$, the age of semidiurnal tide can be expressed in hours as follows:

$$T_2 \approx \frac{\kappa_{S_2} - \kappa_{M_2}}{1.016} \text{ hours}$$

Semidiurnal neap tides occur when M_2 and S_2 are in opposition, i.e. when:

$$s - h = \frac{\kappa_{S_2} - \kappa_{M_2}}{2} + 90° \qquad \text{(modulo 180°)}$$

Neap tides are at quadrature (first and last quarters) with the same T_2 lag. Spring and neap tides thus successively occur at regular intervals of:

$$\frac{180}{\mathrm{d}(s-h)/\mathrm{d}t} = \frac{180}{0.508} = 354.37 \text{ hours} \Rightarrow 14.77 \text{ days}$$

Establishment of the port is, by definition, the high water time on days of full and new Moons (syzygy). This time is computed in local true times and is extended to the high water following true noon, i.e. the evening high water. Depending on whether syzygy takes place at 0 h in the morning or at 24 h in the evening, the high water time differs with respect to the mean value. We thus define the establishment of a syzygy that occurs at true noon. However, the high water does not coincide with the S_2 high water. It is close to that of M_2, but the fact that the phase lags of M_2 and S_2 vary extremely slowly ($q_{s_2} - q_{M_2} \approx 1.016°/\text{h}$) indicates that these two waves are almost in phase at the HW time. The HW time is thus very similar to the S_2 wave HW time.

Where $h(t)$ is the tide reduced to the M_2 and S_2 waves, we have:

$$h(t) = h_{M_2} \cos(q_{M_2} t - \kappa_{M_2}) + h_{S_2} \cos(q_{S_2} t - \kappa_{S_2})$$

High water occurs at t_{pm}, such that:

$$\sin(q_{M_2} t_{pm} - \kappa_{M_2}) + \frac{q_{S_2} h_{S_2}}{q_{M_2} h_{M_2}} \sin(q_{S_2} t_{pm} - \kappa_{S_2}) = 0 \qquad (8.5)$$

As the S_2 high water time is $\frac{\kappa_{S_2}}{q_{S_2}}$, let:

$$t_{pm} = \kappa_{S_2}/q_{S_2} + \delta t_0. \qquad (8.6)$$

Based on the approximation:

$$q_{M_2} \delta t_0 \approx q_{S_2} \delta t_0$$

we deduce equation (8.5):

$$\tan q_{S_2} \delta t_0 \approx \frac{\sin\left[\kappa_{M_2} - (q_{M_2}/q_{S_2})\kappa_{S_2}\right]}{(q_{S_2} h_{S_2}/q_{M_2} h_{M_2}) + \cos\left[\kappa_{M_2} - (q_{M_2}/q_{S_2})\kappa_{S_2}\right]} \qquad (8.7)$$

We have $h = s$ (modulo 180°) on the day of syzygy. The Moon and Sun together cross the meridian of the place (upper and/or lower branches). We have seen that the approximate high water time (8.6) is $t_{HW} \approx \kappa_{S_2}/q_{S_2} = \kappa_{S_2}/30$, give or take δt_0. E_P, which denotes the establishment of port P, is thus considered to be the high water time on a day of syzygy taking place at

true noon. This parameter is expressed in hours by equation (8.6), with δt_0 given by the approximation (8.7), or:

$$E_P \approx \frac{1}{q_{S_2}} \left\{ \kappa_{S_2} + \arctan \frac{\sin[\kappa_{M_2} - (q_{M_2}/q_{S_2})\kappa_{S_2}]}{(q_{S_2} h_{S_2}/q_{M_2} h_{M_2}) + \cos[\kappa_{M_2} - (q_{M_2}/q_{S_2})\kappa_{S_2}]} \right\} \quad (8.8)$$

Laplace's approximation is generally used to compute E_P, or: $q_{M_2}/q_{S_2} \approx 29/30$. The definition of E_p differs from that of E_m given in 8.6, but their values are close.

1.1.3 • Semidiurnal spring tide at lunar perigee

Recall that tidal wave N_2 is called the major elliptic constituent. It is in phase with the M_2 wave when (see Table 8.1):

$$s - p = \kappa_{M_2} - \kappa_{N_2} \qquad \text{(modulo 360°)}$$

While $d(s-p)/dt \approx 0.545°/h$, this event occurs with a lag of $(\kappa_{M_2} - \kappa_{N_2})/0.545$ h after the Moon's transit at perigee ($s = p$ modulo 360°). These two waves are in phase opposition with the same time lag with reference to its transit at apogee ($s - p = 180°$ modulo 360°). The modulation period is:

$$\frac{360}{d(s-p)/dt} \approx \frac{360}{0.545} = 660.6 \text{ hours} \Rightarrow 27.5 \text{ days}$$

This value can be compared to the fortnightly spring-neap tidal cycle (14.77 days). Hence, when the N_2 wave increases the spring tide amplitude, the following spring tide will be reciprocally reduced to about the same extent. The M_2, S_2 and N_2 waves will be in phase if the following conditions are simultaneously fulfilled:

$$s - h = \frac{\kappa_{S_2} - \kappa_{M_2}}{2} \qquad \text{modulo } 180° \qquad (8.9a)$$

$$s - p = \kappa_{M_2} - \kappa_{N_2} \qquad \text{modulo } 360° \qquad (8.9b)$$

Strictly speaking, such an event is impossible because the differences in mean logitudes $s - h$ and $s - p$ have no common period. Were this situation to occur at a given date, an infinite amount of time would be required for it to occur again. Note, however, that $h - p$, whose period is around 412 days, varies slowly in comparison to $s - h$, whose period is around a month (29.531

days). The system of equations (8.9a 8.9b) can be reformulated to specifically highlight $h - p$ as follows:

$$h - p = \frac{3\kappa_{M_2} - \kappa_{S_2} - 2\kappa_{N_2}}{2} \qquad \text{modulo } 180°. \tag{8.10a}$$

$$s - p = \kappa_{M_2} - \kappa_{N_2} \qquad \text{modulo } 360° \tag{8.10b}$$

This new system (8.10a and 8.10b) could be interpreted as follows. Let us consider the time when the Sun transits in the vicinity of perigee or apogee in the Moon's orbit, the difference $h - p$ satisfies equation (8.10a). The time of the spring tide closest to this date corresponds to a maximum spring tide amplitude. The Moon then transits in the vicinity of its perigee and the difference $s - p$ satisfies equation (8.10a). These events define perigean spring tides with a period of:

$$\frac{180}{\mathrm{d}(h-p)/\mathrm{d}t} = \frac{180}{0.036426} = 4941.43 \text{ hours } \Rightarrow 205.89 \text{ days}$$

1.1.4 • Equinoctial spring tides

The contribution of the K_2 tidal wave can be expressed on the basis of elements presented in Table 8.1, as follows:

$$h_{K_2}(t) = h_{K_2} \cos\left(30t + 2h - \kappa_{K_2}\right) \tag{8.11a}$$

or:

$$h_{K_2}(t) = h_{K_2} \cos\left(2\tau + 2s - \kappa_{K_2}\right) \tag{8.11b}$$

The cosine argument of K_2 may be formulated and interpreted in two different ways:

• According to (8.11a), the K_2 wave is considered as a semiannual modulation, which varies with the solar declination (periodicity of the $2h$ parameter) of the S_2 wave

• According to (8.11b), the K_2 wave is a modulation of the M_2 constituent, which varies with the lunar declination and has a period of 13.66 days (periodicity of the $2s$ parameter).

The K_2 wave therefore has two different origins, i.e. solar and lunar, which explains why it is called the 'lunisolar declinational constituent'. This K_2 wave is also called a sidereal wave because it consists of two high waters and two low waters per sidereal day (Earth's rotation period).

It is in phase with the M_2 wave when:

$$s = \frac{\kappa_{K_2} - \kappa_{M_2}}{2} \qquad \text{modulo } 180°$$

Contrary to similar situations, this occurs when the Moon transits in the vicinity of the Equator. When the Sun is also in the vicinity of the Equator,

i.e. at equinox, the corresponding spring tides are more substantial. Then we have:

$$h = \kappa_{K_2} - \kappa_{S_2} 2 \qquad \text{modulo } 180°$$

These are equinoctial spring tides. Note that since the K_2 and S_2 constituents have very close periods, their phase lags κ_{K_2} and κ_{S_2} are generally quite close. Moreover, the Moon and Sun never transit simultaneously over the Equator. The mean longitude of the Sun h, which has a period of 1 year, i.e. 13.36-fold greater than that of s, does not markedly vary between two lunations. The spring tide closest to equinox thus has an amplitude a very similar to that of a spring tide occurring right at equinox.

1.1.5 • Perigean equinoctial spring tide

An exceptional so-called perigean equinoctial spring tide takes place when M_2, S_2, N_2 and K_2 waves are in phase (this situation can only be approximated). Its amplitude is the sum of the following amplitudes:

$$h_{M_2} + h_{S_2} + h_{K_2} \cos\left(2h + \kappa_{S_2} - \kappa_{K_2}\right) \pm h_{N_2} \cos\left\{p - h + \left[(3\kappa_{M_2} - \kappa_{S_2} - 2\kappa_{N_2})/2\right]\right\}$$

The plus or minus sign preceding the contribution of the N_2 constituent means that this constituent has a positive or negative contribution from one spring tide to the next.

1.2 • Main diurnal tide characteristics

The main diurnal tide constituents are given in Table 8.2. The coefficients are those of the tide-generating potential relative to the highest one associated with the K_1 constituent.

The argument numbers are those of the cosine in the harmonic tidal equation. As is the case for semidiurnal tidal waves, the absolute phase lags κ_i are used in association with the local civil time t.

The tidal contribution of the K_1 wave is:

$$h_{K_1} \cos(15t + h + 90 - \kappa_{K_1}) = h_{K_1} \cos(\tau + s + 90 - \kappa_{K_1}) \qquad (8.12)$$

It has one high water and one low water per sidereal day (23 h 56 min). As is the case for the K_2 wave, two interpretations are possible based on the two argument expressions. This wave is the result of the superposition of a solar constituent and a lunar constituent induced by the respective declination variations of the Moon and Sun – the so-called 'lunisolar declinational'.

TABLE 8.2: Main diurnal tide constituents (n.b. $\tau° = 15^{°}/_{h} t^{h} + h° - s°$).

Constituent symbol	Relative coefficient of the tidal potential	Argument number	Argument in degrees of the tidal wave (n.b. t in hours)
K_1	1.000	A AZZ ZZA	$\tau + s + 90 - \kappa_{K_1} = 15t + h - \kappa_{K_1} + 90$
O_1	0.710	A YZZ ZZY	$\tau - s - 90 - \kappa_{O_1} = 15t + h - 2s - \kappa_{O_1} - 90$
P_1	0.331	A AXZ ZZY	$\tau + s - 2h - 90 - \kappa_{P_1} = 15t - h - \kappa_{P_1} - 90$
Q_1	0.138	A XZA ZZY	$\tau - 2s + p - 90 - \kappa_{Q_1} = 15t + h - 3s + p - \kappa_{Q_1} - 90$

The tidal contribution of the O_1 wave, or so-called 'principal lunar wave', can be formulated as:

$$h_{O_1} \cos\left(15t + h - 2s - \kappa_{O_1} - 90\right) = h_{O_1} \cos\left(\tau - s - 90 - \kappa_{O_1}\right). \quad (8.13)$$

The cosine argument formulations on the right side of equations (8.12) and (8.13) clearly highlight the symmetry of the K_1 and O_1 wave potential constituents relative to the mean diurnal lunar constituent M_1 (generally very low). Like the K_1 lunar constituent, the O_1 wave is induced by lunar declination variations.

Note also that the P_1 constituent, whose tidal contribution is $h_{P_1} \cos(15t - h - 90 - \kappa_{P_1})$, is symmetrical to K_1 with respect to the mean solar constituent S_1. The P_1 wave is induced by solar declination variations, like the K_1 solar constituent.

Declinations of the Moon and Sun are responsible for diurnal tides. Declinations of the Sun vary between virtually constant extremes $-23°26'21''$ and $+23°26'21''$.

However, maximum declinations of the Moon vary markedly according to the position of the ascending node N. The inclination of the lunar orbit at the Equator is maximal (28°36) when the ascending node is around vernal equinox and minimal (18°20) when it is around autumnal equinox. The amplitudes of the lunar diurnal constituents are thus modulated for an 18.613 year period, i.e. the time required for the ascending node to complete a full elliptical orbit, from one vernal equinox to the next (see Appendix B §2).

1.2.1 • Diurnal spring tide characteristics

Due to the importance of the K_1 and O_1 wave constituent coefficients (see Table 8.1), diurnal spring tides occur when K_1 and O_1 waves are in phase. The arguments of the corresponding tidal waves thus give the following condition:

$$s = \frac{\kappa_{K_1} - \kappa_{O_1}}{2} - 90 \qquad \text{modulo } 180°$$

Depending on the phase lag, the diurnal spring tide therefore occurs around the time when the Moon transits at its absolute maximum declination ($s = 90$ modulo 180°).

Conversely, the diurnal neap tide occurs around the time when the Moon transits over the Equator.

Diurnal spring tides successively occur every:

$$\frac{180}{ds/dt} = \frac{180}{0.549} = 327.85 \text{ hours} \Rightarrow 13.66 \text{ days}$$

They take place around the time when the Moon transits at its maximum declination over a time interval T_1, or the so-called 'age of diurnal tide', of

$$T_1 = \frac{\kappa_{K_1} - \kappa_{O_1}}{2ds/dt} = \frac{\kappa_{K_1} - \kappa_{O_1}}{1.098} \text{ hours}$$

HW generally does not coincide with the time of the diurnal spring tide, but the gap between these two events is 12 h at most. The phase difference between the K_1 and O_1 waves, which is zero at the diurnal spring tide time, is still relatively low at the time of the nearest high water. The high water time t_{HW} (local civil time) thus does not differ markedly from the K_1 high water time:

$$t_{HW} \approx \frac{\kappa_{K_1} - h}{15} - 6 \text{ hours}$$

As the interval between two successive diurnal spring tides is 13.661 days (327.859 h) and the angular velocity dh/dt is 0.041°/h (0.985°/d), the high water times thus advance by $327.859 \times 0.041/15 \approx 0.90$ h, or 54 min between two spring tides. Based on equations (8.12) and (8.13), the tide reduced to the two waves K_1 and O_1 at the diurnal spring tide times t_{ved} (waves in phase) can be expressed by (n.b. cosine argument in degrees):

$$h(t_{ved}) = (h_{O_1} + h_{K_1}) \cos\left\{\tau - \left[(\kappa_{K_1} + \kappa_{O_1})/2\right] + k \times 180\right\}$$

where the coefficient is $k = 0$ for the northern tropic and $k = 1$ for the southern tropic.

Parameter $E = (\kappa_{K_1} + \kappa_{O_1})/2$ is sometimes called the 'diurnal establishment'.

1.2.2 • Solstitial diurnal spring tide characteristics

The contribution of the P_1 tidal wave can be espressed by:

$$h_{Pr_1}(t) = h_{P_1} \cos(15t - h - \kappa_{P_1} - 90)$$

Hence, the K_1 and P_1 waves are in phase when

$$h = \frac{\kappa_{K_1} - \kappa_{P_1}}{2} - 90 \qquad \text{modulo } 180°$$

Contrary to similar phase lags, which are generally small for these two constituents with close periods, this occurs around the solstices, or:

- $h = 90°$ for the summer solstice
- $h = 270°$ for the winter solstice.

These two waves are out of phase at equinox ($h = 0°$ at spring equinox and $h = 180°$ at autumn equinox).

Diurnal spring tides are thus higher around the solstices and lower around the equinoxes.

Note that relative amplitude variations are greater around equinox so the diurnal tide can disappear completely at neaps.

1.2.3 • Perigean spring tide characteristics

The Q_1 wave is a major diurnal elliptical constituent. It is in phase with O_1 when:

$$s - p = \kappa_{O_1} - \kappa_{Q_1} \qquad \text{modulo } 360°$$

or: $\dfrac{\kappa_{O_1} - \kappa_{Q_1}}{\mathrm{d}(s-p)/\mathrm{d}t} = \dfrac{\kappa_{O_1} - \kappa_{Q_1}}{0.545}$ hours after the Moon's transit at perigee ($s - p = 0°$ modulo 360°). These two waves are out of phase with the same time lag after this celestial body transits at apogee ($s - p = 180°$ modulo 360°). Like the N_2 wave (major semidiurnal ellipsoid) with respect to the mean lunar wave M_2 (8.10b), the Q_1 wave appears as a modulation of O_1, i.e. the main lunar wave, with a period of:

$$360/\left[\mathrm{d}(s-p)/\mathrm{d}t\right] \approx 360/0.545 = 660.6 \text{ hours} \Rightarrow 27.52 \text{ days}$$

and this value can be compared to the spring-neap tidal period (13.66 days). Although the Q_1 wave tends to increase the amplitude of a diurnal spring tide, the following spring tide will be diminished to almost the same extent, and inversely.

Let us now consider a case where the three K_1, O_1 and Q_1 waves are in phase. We thus have:

$$s = (\kappa_{K_1} - \kappa_{O_1})/2 + 90 \qquad \text{modulo } 360° \qquad (8.14a)$$

$$p = (\kappa_{K_1} + 2\kappa_{Q_1} - 3\kappa_{O_1})/2 + 90 \qquad \text{modulo } 360° \qquad (8.14b)$$

Strictly speaking, this situation is impossible because the main longitudes s and p have no common period. If such an event were to occur at a given date, it would take an infinite amount of time for it to reoccur. However, $\mathrm{d}p/\mathrm{d}t \ll \mathrm{d}s/\mathrm{d}t$, i.e. the mean longitude of lunar perigee p (period: 8.847 years) changes very slowly with respect to that of the Moon s (period: 27.321 days).

Equations (8.14a) and (8.14b) could thus be interpreted as follows. When lunar perigee is around the summer solstice ($p \approx h = 90°$) and winter solstice ($p \approx h = 270°$), which occurs with a periodicity of around 4.424 years, the solstitial diurnal spring tides are stronger. These events are typical of diurnal spring tides at perigee.

1.2.4 • Diurnal spring tide amplitude

With all of the previously described elements, the following is a first-order formulation for the total diurnal spring tide amplitude (the Moon's transit at

maximal declination) reduced to its four main constituents (K_1, O_1, P_1, and Q_1):

$$h_{K_1} + h_{O_1} - h_{P_1} \cos(2h + \kappa_{P_1} - \kappa_{K_1}) \pm h_{Q_1} \sin\left\{p - \left[(\kappa_{K_1} + 2\kappa_{Q_1} - 3\kappa_{O_1})/2\right]\right\}$$

The $\pm$ sign before the contribution of the Q_1 wave indicates that the effect of this constituent is to increase and decrease, by turns, successive spring tides.

1.3 • Nonlinear interaction waves

It would be impossible to conduct an in-depth study on the impact of interaction waves on tidal extremes. Complex factors are involved because of the lack of linearity, so general rules cannot be formulated. However, it is still possible to at least qualitatively assess the influence of often paramount quarter diurnal waves.

Tide is the result of the superposition of a high number of harmonic constituents. However, over a relatively short timespan (e.g. a day), the tidal process seems to be the sum of different species, with each species represented by a sine function. Based on this hypothesis, we can look at the case of a semidiurnal tide in the presence of quarter diurnal interaction constituents and, for instance, examine the tide reduced to M_2 and M_4 waves, which are representative of mean tides relative to these species, or:

$$h(t) = h_{M_2} \cos(2\tau - \kappa_{M_2}) + h_{M_4} \cos(4\tau - \kappa_{M_4}) \tag{8.15}$$

The extremes are reached for τ values such that $\mathrm{d}h(t)/\mathrm{d}t = 0$, or:

$$h_{M_2} \sin(2\tau - \kappa_{M_2}) + 2h_{M_4} \sin(4\tau - \kappa_{M_4}) = 0 \tag{8.16}$$

We can procede by a first-order approximation on the basis of the assumption that the amplitude $h_{M_4} \ll h_{M_2}$. According to this hypothesis, the extreme of the tide reduced to the M_2 and M_4 waves is close to that of the $M_2(\pm h_{M_2})$ tide.

Where τ_{ex} is the τ value corresponding to an extreme of the M_2 constituent, we then have:

$$\tau_{ex} = (\kappa_{M_2}/2) + k \times 90°$$

with the k coefficient being even for high waters and odd for low waters.

The reduced tidal extreme time (8.15) is such that $\tau = \tau_{ex} + \vartheta$. Equation (8.16) thus becomes:

$$(-1)^k h_{M_2} \sin 2\vartheta + 2h_{M_4} \sin(4\vartheta + 2\kappa_{M_2} - \kappa_{M_4}) = 0 \tag{8.17a}$$

According to the initial hypothesis, the error ϑ should be small and, as a first-order approximation, equation (8.17a) becomes (with ϑ expressed in radians):

$$\vartheta[(-1)^k \frac{h_{M_2}}{h_{M_4}} + 4\cos(2\kappa_{M_2} - \kappa_{M4})] + \sin(2\kappa_{M_2} - \kappa_{M4}) \approx 0 \qquad (8.17b)$$

which gives the approximate equation, for ϑ expressed in degrees:

$$\vartheta = -\frac{\sin(2\kappa_{M_2} - \kappa_{M_4})}{(-1)^k \frac{h_{M_2}}{h_{M_4}} + 4\cos(2\kappa_{M_2} - \kappa_{M_4})} \times \frac{180°}{\pi} \qquad (8.17b)$$

We verify *a posteriori* that hypothesis $h_{M_2} \gg h_{M_4}$ confirms the approximation on the lowness of the error ϑ. This latter equation (8.17b) shows that quarter-diurnal waves can modify the semidiurnal tidal extreme times. The HW correction applied (k even) is contrary to the LW correction (k odd).

This correction also depends on $\sin(2\kappa_{M_2} - \kappa_{M_4})$, and the HW time is advanced ($\vartheta < 0$) or delayed ($\vartheta > 0$) depending on whether the sign of $2\kappa_{M_2} - \kappa_{M_4}$ is positive or negative. For tidal height extremes $h(t)$ given by equation (8.15), we can consider as a first-order approximation that:

$$h(\tau_{ex} + \vartheta) \approx h(\tau_{ex})$$

which gives:

$$h(\tau_{ex} + \vartheta) \approx (-1)^k h_{M_2} + h_{M_4} \cos(2\kappa_{M_2} - \kappa_{M_4})$$

It should be noted that the height correction $h_{M_4} \cos(2\kappa_{M_2} - \kappa_{M_4})$ has the same sign for the M_2 wave HW and LW. This is an important point because it indicates that the mean tidal height $\overline{h(t)}$ cannot be determined on the basis of the mean observed tidal extremes.

1.4 • Different types of tide

In Chapter I on general features of tides, we presented tide graphs (figure 1.6) based on the French classification of four types of tide: semidiurnal, mixed semidiurnal, mixed and diurnal. There are also other classifications since this French classification is somewhat arbitrary. The tide-generating force essentially consists of diurnal and semidiurnal tidal terms that are found in the form of corresponding constituents with different amplitudes and phases.

For simplicity, let us consider the case of a tide reduced to its diurnal and semidurnal constituents. Based on the hypothesis (confirmed here) that tidal amplitudes and phases vary slowly during a diurnal tidal cycle, these parameters can be considered constant over this timespan.

Where the pairs (h_1, φ_1) and (h_2, φ_2) represent the amplitudes and phases of diurnal and semidiurnal constituents, then:

$$h(t) = h_1 \cos(\tau - \varphi_1) + h_2 \cos(2\tau - \varphi_2)$$

and, let: $r = h_1/h_2$, $\theta = \tau - (\varphi_2/2)$, $\alpha = \varphi_1 - (\varphi_2/2)$, which becomes:

$$h(t) = h_2 \left[r \cos(\theta - \alpha) + \cos 2\theta\right]$$

It can then be demonstrated that:

- if $r \geq 4$, there is always one daily high water and low water;
- if $r \leq 2$, there are always two daily high and low waters;
- if $r \geq 4$, the daily number of high and low waters (two or four) depends on α.

Mathematical developments (not outlined here) are required to demonstrate these results, which are not fundamental. r and θ must be computed to determine the number of high and low waters per day. These highly variable parameters are therefore hard to use for a classification. A less stringent but easier to use criterion is preferred. The classification adopted in France (F) includes four types according to the value of the R_F coefficient, the ratio of the sums of the amplitudes of the two main diurnal waves (K_1 and O_1) and semidiurnal waves (M_2 and S_2), or:

$$R_F = \frac{h_{K_1} + h_{O_1}}{h_{M_2} + h_{S_2}}$$

We therefore have:

- the semidiurnal type for: $R_F < 0.25$
- the mixed semidiurnal type for: $0.25 \leq R_F < 1.5$
- the mixed type for: $1.5 \leq R_F < 3$
- the diurnal type for: $R_F \geq 3$

In Great Britain (GB), the M_2 constituent is not taken into account and the R_{GB} coefficient is given by:

$$R_{GB} = \frac{\pi}{2} \times \frac{h_{S_2}}{h_{K_1} + h_{O_1}}$$

The GB classification only includes two types of tide:

- the semidiurnal type for: $R_{GB} > 1$
- the diurnal type for: $R_{GB} < 1$

Three types are often adopted in other countries (semidiurnal, mixed and diurnal), but the criteria sometimes vary between countries.

2 • Typical extreme levels

Before considering extreme HW conditions, recall that the harmonic tidal equation (see Chapter V) can be formulated as a function of the local civil time t, as follows:

$$h(t) = Z_{00} + \sum_{i=1}^{i=N} h_i \cos(V_i - \kappa_i) \tag{8.18}$$

In this equation, Z_{00} is the mean level, while parameters h_i, V_i and κ_i respectively represent the amplitude, cosine argument (in the development of the tide-generating potential) and the absolute phase lag of constituent i. The absolute phase lag κ_i and the local civil time are used here to be in line with the options selected at the beginning of this chapter. Recall that parameter κ_i represents the wave lag (in degrees) relative to the constituent associated with the potential. κ_i can be divided by the angular velocity dV_i/dt (in degrees/hour) in order to obtain this wave lag expressed in time. All of the elements Z_0, h_i and κ_i are constant at a given place. Only the V_i argument is time dependent and expressed via the fundamental variables (τ, s, h, p N and p_1) by equation (see 6.2):

$$V_i = m_{\tau,i}\tau + m_{s,i}s + m_{h,i}h + m_{p,i}p + m_{N',i}N' + m_{p_1,i}p_1 + m_{\pi/2,i}\frac{\pi}{2}$$

where the angular unit is the radian and element $m_{\pi/2,i}$ represents the number of $\pi/2$ radians to add to ensure that the cosine coefficient will be positive.

This argument can thus be formulated as:

$$V_i = \vec{M}_i \times \vec{X} + m_{\pi/2,i}\frac{\pi}{2} \tag{8.19}$$

with the $\times$ symbol representing the scalar product.

The result is that the i wave is characterized by the $\vec{M}_i$ vector having $\left[m_{\tau,i}, m_{s,i}, m_{h,i}, m_{p,i}, m_{N,i}, m_{p_1,i}\right]$ as constituents and the V_i argument can be considered as a linear function of the $\vec{X}$ vector having the fundamental variables $\left[\tau,\ s,\ h,\ p,\ N',\ p_1\right]$ as constituents. This formulation will enable us to study extreme tidal heights.

2.1 • The extreme tide problem

In the light of the latter equation (8.19), the height $h(t)$ given by equation (8.18), can be considered as a function Ψ of vector $\vec{X}$. Although this function Ψ has a period of 2π relative to each fundamental variable (constituents of vector $\vec{X}$), it is not a periodic function since the fundamental variables have incommensurable periods. Hence, a given vector $\vec{X}$ cannot materialize in finite time. We therefore will not seek a solution to the problem as an

explicit temporal function, but rather as a function of each of these independent variables, which represent as many degrees of freedom of the system. The extreme height values are obtained when $\overrightarrow{grad}\,\Psi = 0$.

This condition can still be represented by the following equations:

$$\frac{\partial\Psi}{\partial\tau} = \frac{\partial\Psi}{\partial s} = \frac{\partial\Psi}{\partial h} = \frac{\partial\Psi}{\partial p} = \frac{\partial\Psi}{\partial \mathrm{N}'} = \frac{\partial\Psi}{\partial p_1} = 0$$

These equalities constitute a system of equations that cannot be directly solved due to their paramount character. With the x symbol denoting a fundamental variable, based on an approximate solution $\overrightarrow{\mathrm{X}}_0$, it is necessary to make a series of first-order approximations, such that:

$$\frac{\partial\Psi\left(\overrightarrow{\mathrm{X}}\right)}{\partial x} \approx \frac{\partial\Psi\left(\overrightarrow{\mathrm{X}}_0\right)}{\partial x} + \left(\overrightarrow{\mathrm{X}} - \overrightarrow{\mathrm{X}}_0\right)\frac{\partial^2\Psi\left(\overrightarrow{\mathrm{X}}_0\right)}{\partial x^2} \tag{8.20}$$

The new vector $\overrightarrow{\mathrm{X}}$ obtained by eliminating the right side of equation (8.20) provides a better approximation:

$$\overrightarrow{\mathrm{X}} = \overrightarrow{\mathrm{X}}_0 - \frac{\partial\Psi\left(\overrightarrow{\mathrm{X}}_0\right)}{\partial x} \Big/ \frac{\partial^2\Psi\left(\overrightarrow{\mathrm{X}}_0\right)}{\partial x^2}$$

but as long as there is a suitable choice of $\overrightarrow{\mathrm{X}}_0$ to ensure the consistency of the successive approximations.

The idea is thus to come up with an approximate solution $\overrightarrow{\mathrm{X}}_0$ by determining the values of constituents $\left[\tau,\ s,\ h,\ p,\ \mathrm{N}',\ p_1\right]$ that are close enough to the extreme height to ensure that the convergence to this solution will be achieved.

2.2 • Finding the approximate solution

Because of the complexity of the problem, the semidiurnal and diurnal tidal types should first be separated so that they can be processed individually. Questionable cases, generally concerning mixed tides and mixed semidiurnal tides, are examined by applying the two previous treatments (diurnal and semidiurnal) in order to come up with the best solution.

This question is dealt with on the basis of the fact that the amplitudes of tidal constituents are generally increasing functions of the corresponding tide-generating potential coefficients with a time lag with respect to the age of tide. This rule always applies when nonlinear interaction constituents are low or negligible. Tides that fulfil these conditions are treated separately. Solar perigee is considered constant since its movement is very slow ($\mathrm{d}p_1/\mathrm{d}t < 2°$/century). We thus adopt the constant value $p_1 = 283°$ that

applied at the beginning of the 21st century. Its movement could still be taken into account despite a slight increase in computation time, but the extreme values calculated in this way would not be reached for around 40 centuries, so this calculation is of no current interest.

2.2.1 • Extreme diurnal tide levels

The ascending lunar node has a different role for diurnal and semidiurnal constituents. As already noted, the inclination of the lunar orbit at the Equator is maximal (28°36) when the ascending node is at vernal equinox (N = 0°) and minimal (18°20) at autumnal equinox (N = 180°). However, diurnal waves are greater as the declination increases. A baseline N value of 0° is thus used for the maximum diurnal. The maximal action of the diurnal tide is obtained when the celestial bodies meet the following conditions (fundamental variables expressed here in radians):

- The two declinations are maximal, or: $s = h = \frac{\pi}{2} + k\pi$
- The Moon is at perigee (see 1.2.3): $p = s + 2k\pi$
- The Moon transits over the meridian of the place: $\tau = 2k\pi$ (high water), $\tau = \pi + 2k\pi$ (low water).

However, the maximum amplitude of the diurnal tide is not reached at the same time because of the age of this species, as reflected by a certain degree of tidal lag with respect to the action of the celestial bodies. The previous equations must be modified in order to take this lag into account, which is possible via the harmonic constants of the place. The arguments of the four main diurnal constituents (K_1, O_1, P_1 and Q_1) provide the four equations required to find the τ, s, h, and p values fulfilling the baseline conditions given above. By taking the argument expression in equation 8.1 into account and assuming $\phi_i = V_i - \kappa_i$ (cosine argument of the i wave), we get the following system of equations:

$$\begin{aligned}
\phi_{K_1} &= \tau + s - \kappa_{K_1} + \pi/2 \\
\phi_{O_1} &= \tau - s - \kappa_{O_1} - \pi/2 \\
\phi_{P_1} &= \tau + s - 2h - \kappa_{P_1} - \pi/2 \\
\phi_{Q_1} &= \tau - 2s + p - \kappa_{Q_1} - \pi/2
\end{aligned}$$

We can obtain a first approximate solution through this system. Two subscripts are attached to the corresponding parameter values, i.e. 0 for the baseline value and 1 for the diurnal tide:

$$
\begin{aligned}
\tau_{0,1} &= \frac{\kappa_{O_1} + \kappa_{K_1}}{2} + k_\tau \pi \\
s_{0,1} &= \frac{\kappa_{K_1} - \kappa_{O_1}}{2} - \frac{\pi}{2} + k_s \pi \\
h_{0,1} &= \frac{\kappa_{K_1} - \kappa_{P_1}}{2} - \frac{\pi}{2} + k_h \pi \\
p_{0,1} &= \frac{2\,\kappa_{Q_1} + \kappa_{K_1} - 3\,\kappa_{O_1}}{2} - \frac{\pi}{2} + k_p \pi
\end{aligned}
\tag{8.21}
$$

where all k_j type coefficients are relative integers.

To determine extreme high and low waters, an iterative process is used alternately with the eight baseline conditions (number of arrangements with replication: $2^3 = 8$, corresponding to the attribution of 0 or 1 values to the three coefficients k_τ, k_s and k_h, while noting:

- that the k_τ value is even for high waters and odd for low waters
- and that the action peaks around the time of the Moon's transit at perigee, so $k_p = k_s$ can be used.

2.2.2 • Extreme semidiurnal tide levels

Concerning the semidiurnal constituents, it is not easy to choose a baseline condition for the mean longitude of the ascending node $N = -N'$. Since the sought-after extreme spring tide occurs around the time of the Moon's transit at the Equator, the orbital inclination value is not necessarily as high. However, because of tidal propagation irregularities, the maximum amplitude does not correspond exactly to the Moon's transit at the Equator and the semidiurnal constituents are thus higher when the declination is low. For the semidiurnal maximum, we thus select a baseline N value of 180° (autumnal equinox node) corresponding to the slightest lunar declination variations. The maximum semidiurnal tidal action thus corresponds to the following conditions:

- celestial bodies at the Equator: $h = s + k\pi$
- the Moon at perigee: $p = s + 2k\pi$
- the Moon on the meridian (HW): $\tau = k\pi$
- the Moon at maximum declination (LW): $\tau = \pi/2 + k\pi$.

Like the diurnal tide, the sought-after baseline conditions are deduced from the arguments ϕ_i of the four main semidiurnal tidal constituents (M_2,

S_2, N_2, K_2). Table 8.1 gives:

$$\begin{aligned}
\phi_{M_2} &= 2\tau - \kappa_{M_2} \\
\phi_{S_2} &= 2\tau + 2s - 2h - \kappa_{S_2} \\
\phi_{N_2} &= 2\tau - s + p - \kappa_{N_2} \\
\phi_{K_2} &= 2\tau + 2s - \kappa_{K_2}
\end{aligned}$$

When applying the same conventions as those used for the diurnal tide, but with a subscript of 2 for semidiurnal tides, the following baseline conditions can be deduced:

$$\begin{aligned}
\tau_{0,2} &= \frac{\kappa_{M_2}}{2} + k_\tau \frac{\pi}{2} \\
s_{0,2} &= \frac{\kappa_{K_2} - \kappa_{M_2}}{2} + k_s \pi \\
h_{0,2} &= \frac{\kappa_{K_2} - \kappa_{S_2}}{2} + k_h \pi \\
p_{0,2} &= \frac{2\,\kappa_{N_2} + \kappa_{K_2} - 3\,\kappa_{M_2}}{2} + k_p \pi
\end{aligned} \tag{8.22}$$

Recall:

- that the k_τ value is even for high waters and odd for low waters
- and that the action peaks around the time of the Moon's transit at perigee, so the $k_p = k_s$ equality can be adopted.

As for diurnal tides, an iterative process is implemented alternately with the eight baseline conditions, corresponding to k_τ, k_s and k_h values of 0 or 1.

2.2.3 • Extreme mixed semidiurnal and mixed tidal levels

In this case, the risk is that an extreme tidal level may not lead to a convergence point in the iterative process.

Recall that the height, expressed in the form Ψ (a function of $\overrightarrow{X}$), is periodic with respect to each fundamental variable (period 2π). As an example, consider the case of h, i.e. the mean solar longitude. During spring tide periods, the semidiurnal tide peaks around the time of equinox ($h \approx k\pi$), whereas the diurnal tide peaks around solstice ($h \approx \pi/2 + k\pi$). By setting the other astronomic variables at their baseline value, superposition of the diurnal and semidiurnal tides is reflected by the sum of two sinusoids (a function of h) approximately in phase opposition. The maximum of this sum is for $h \approx k\pi$, or for $h \approx \pi/2 + k\pi$, depending on the relative size of the diurnal and semidiurnal amplitudes around their respective maximal values. Hence, for h, by selecting baseline conditions around $k\pi/2$ with k successively taking the four values 0, 1, 2 and 3, it is certain that all possibilities will be covered. The same rationale could be applied to s, i.e.

the mean lunar longitude. For the τ variable (civil lunar time), the number of baseline values to assign to it will be 2 if ratio $r = h_1/h_2 \geq 4$ (diurnal tide, see §1.4 above) and 4 in other cases. Concerning p (mean lunar perigean longitude), it should be noted that the two tidal constituents (diurnal and semidiurnal) are both subjected to maximum action at the time of the Moon's transit at perigee. The fact that the ages of the tide (diurnal T_1 and semidiurnal T_2, which are about a few days) are different is not important in practice, since T_1 and T_2 are negligible with respect to the period of p ($\approx$ 8.85 years). A baseline p value close to s could be chosen without problem. Concerning mixed semidiurnal or mixed tides, based on the above considerations, this tide will have to be separated into its two constituents (diurnal and semidiurnal) for individual treatment in order to obtain the sought-after extreme.

2.2.4 • Extreme shallow water tidal levels

Double high or low waters are generally present when there are substantial quarter and sixth diurnal tides. The iterative process can give a result that does not necessarily correspond to an extreme high or low water. In such cases, a procedure should first be implemented to detect situations in which this type of phenomenon is likely to occur. Then, where relevant, the number of baseline values for the τ variable is increased.

The procedure is identical to that whereby the number of high and low waters is sought according to the value of the ratio $r = h_1/h_2$ (see 1.4), where h_1 and h_2 respectively represent the diurnal and semidiurnal tide amplitudes.

Based on the same conventions, where h_n denotes the amplitude of the *n-th* diurnal constituent, we systematically look for 8 high and low waters if $h_4/h_2 > 0$, 25 and 16 high and low waters if $h_6/h_2 > 0.0625$.

2.3 • Mean spring tide

According to a generally adopted standard, the mean spring tide is often defined, especially for ports where there are few tidal records, using the two main semidiurnal constituents on one hand, and diurnal consituents on the other.

Here the following abbreviations denote the high water (HW) and low water (LW) spring (ST) or neap (NT) tide heights:

- HWST: spring tide high water height
- HWNT: neap tide high water height
- LWNT: neap tide low water height
- LWST: spring tide low water height.

Where Z_0 denotes the mean level, we thus obtain:

- for the semidiurnal tide:
  - HWST $= Z_0 + (h_{M_2} + h_{S_2})$
  - HWNT $= Z_0 + (h_{M_2} - h_{S_2})$
  - LWNT $= Z_0 - (h_{M_2} - h_{S_2})$
  - LWST $= Z_0 - (h_{M_2} + h_{S_2})$
- for the diurnal tide:
  - HWST $= Z_0 + (h_{K_1} + h_{O_1})$
  - LWST $= Z_0 - (h_{K_1} + h_{O_1})$

For mixed semidiurnal and mixed tides, the formulation is slightly more complicated. It includes the phase lag between the mean semidiurnal constituent and the diurnal constituent during spring tide periods.

These equations have the advantage of being simple and may be considered as blanket definitions. However, the values obtained are unsatisfactory, at least for representing the mean of these specific heights. These equations do not give the same results as those obtained when the mean high and low water heights during spring and neap tides are calculated on the basis of recorded data. For instance, the fact that HWST, which is defined as a mean, is not identical to the mean spring tide high water height is often a source of confusion. Let us examine, for instance, the case of Le Havre where semidiurnal tides prevail. The following results are obtained for this port:

$$\left.\begin{aligned} Z_0 &= 487.7 \text{ cm} \\ h_{M_2} &= 261.6 \text{ cm} \\ h_{S_2} &= 87.6 \text{ cm} \end{aligned}\right\} \Rightarrow \left\{\begin{aligned} &\text{HWST} \approx 837 \text{ cm} \\ &\text{LWST} \approx 139 \text{ cm} \end{aligned}\right.$$

The mean spring tide high and low water heights are actually 790 cm and 120 cm, respectively. The 47 cm and 19 cm errors for spring tide high and low waters, respectively, are too high to claim that these two determination methods can generate similar results.

There is a real risk of confusion. The simplified equation is unsuitable in ports where there are marked nonlinear interactions. For Le Havre port, for instance, we have HWST $\approx$ 837 cm, i.e. very close to the maximal theoretical height (842 cm), which obviously is out of line with the actual situation (790 cm).

The main reason for the inadequacy of the simplified equation for defining a mean spring tide is that the nonlinear interaction constituents have a relatively important role that is not taken into account. Moreover, simplicity is no longer an advantage with current computation technology. All harmonic constituents for a port, which are required to be able to quickly come up with an accurate forecast, can now be readily taken into account. However, one

important aspect should be mentioned concerning the spring and neap tide definitions.

Recall that semidiurnal spring tides occur around the time when the difference is $s - h = (\kappa_{S_2} - \kappa_{M_2})/2 + k\pi$ (see 1.1.3). The mean spring tide high and low waters are thus mean high and low water heights around these times. If the mean is calculated for a sufficiently long period, all constituents whose astronomical argument is not of the form $k_1\tau + k_2\left(s - h\right)$ are eliminated (k_1 and k_2 are relative integers). Obviously M_2 and S_2 remain, along with all nonlinear interaction constituents with which these latter constituents are involved, e.g. MS_f, $2MS_2$, $2SM_2$, M_4 and MS_4, which are compound waves that are not accounted for in the simple equations presented above. The same applies (see 1.2.1) for diurnal spring tides, which occur around the time when the mean lunar longitude fulfils the following condition:

$$s = \frac{\kappa_{K_1} - \kappa_{O_1}}{2} - \frac{\pi}{2} + k\pi$$

All constituents with an astronomical argument that is not of the form $k_1\tau + k_2 s$ are cancelled out in the mean. The principal constituents K_1 and O_1, along with the compound waves OQ_2, K_2, MK_3, etc., naturally remain.

The computations can thus be conducted in exactly the same way as for extreme tides. However, it is essential to only take constituents that are not cancelled out in the mean into account, i.e. those with an astronomical argument of the form $k_1\tau + k_2\left(s - h\right)$ for semidiurnal tides, or $k_1\tau + k_2 s$ for diurnal tides.

In the iterative process, high and low waters are calculated at the same time as the maximum amplitude. Since this is a mean computation, it is essential to take $s - h$ variations into account for semidiurnal tides and s variations into account for diurnal tides during a half tidal cycle on both sides of high and low waters.

We have:

- for a semidiurnal tide, a cycle time of $T_{M2} = 12.42$ h, with: $\mathrm{d}(s - h)/\mathrm{d}t = 0.5079479°/\mathrm{h}$
- for a diurnal tide, a cycle time of $T_{M1} = 24.84$ h, with: $\mathrm{d}s/\mathrm{d}t = 0.5490165°/\mathrm{h}$.

Assuming that there is a sinusoidal amplitude variation on both sides of the maximum, correction factors can be applied for each type of tide:

- for semidiurnal tides:

$$c_2 = \frac{1}{T_{M2}} \int_{-T_{M2}/2}^{T_{M2}/2} \cos\left\{\left[\mathrm{d}(s - t)/\mathrm{d}t\right] t\right\}\, \mathrm{d}t = 0.9995 \approx 1$$

- for diurnal tides:

$$c_1 = \frac{1}{T_{M1}} \int_{-T_{M1}/2}^{T_{M1}/2} \cos\left[(ds/dt)t\right] \, dt = 0.9976 \approx 1$$

These corrections, which are very close to unity, are overlooked in practice.

2.4 • Extreme neap tides

The baseline conditions used for approximating extreme neap tide levels are contrary to those used for standard spring tides.

For diurnal tides, we focus on the vicinity of the phase opposition of the K_1 and O_1 waves at the time of zero declination of the two celestial bodies ($h = s = k\pi$) and the Moon's transit at apogee ($p = s + \pi + 2k\pi$), which is reflected by the following baseline conditions (to be compared with the equation system 8.21):

$$\begin{aligned}
\tau_{0,1} &= \frac{\kappa_{O_1} + \kappa_{K_1}}{2} + \frac{\pi}{2} + k_\tau \pi \\
s_{0,1} &= \frac{\kappa_{K_1} - \kappa_{O_1}}{2} + k_s \pi \\
h_{0,1} &= \frac{\kappa_{K_1} - \kappa_{P_1}}{2} + k_h \pi \\
p_{0,1} &= \frac{2\,\kappa_{Q_1} + \kappa_{K_1} - 3\,\kappa_{O_1}}{2} + k_p \pi
\end{aligned} \tag{8.23}$$

N is of little importance because the lunar declination is near zero. However, a baseline value of around N = 180° should be chosen, corresponding to the minimum inclination of the lunar orbit.

For semidiurnal tides, we focus on the vicinity of the phase opposition of M_2 and S_2 waves at the time:

- of the maximum lunar declination, or: $s = \pi/2 + k\pi$ and N= 0
- of the minimum solar declination, or: $h = k\pi$
- of the Moon's transit at apogee, or: $p = s + \pi + 2k\pi$.

This celestial body arrangement is reflected by the following baseline conditions:

$$\begin{aligned}
\tau_{0,2} &= \frac{\kappa_{M_2}}{2} + k_\tau \frac{\pi}{2} \\
s_{0,2} &= \frac{\kappa_{K_2} - \kappa_{M_2}}{2} + \frac{\pi}{2} + k_s \pi \\
h_{0,2} &= \frac{\kappa_{K_2} - \kappa_{S_2}}{2} + k_h \pi \\
p_{0,2} &= \frac{2\,\kappa_{N_2} + \kappa_{K_2} - 3\kappa_{M_2}}{2} - \frac{\pi}{2} + k_s \pi
\end{aligned} \tag{8.24}$$

These conditions (8.24) can be compared with those of equation (8.22) corresponding to extreme spring tide levels. Algorithms developed for spring tides can thus be used for neap tides, sometimes with a few modifications to account for the fact that extreme neaps can be of zero amplitude.

2.5 • Mean neap tides

The rationale outlined above concerning spring tides can be applied without modification for calculating typical mean neap tide levels by simply modifying the baseline $s - h$ values for semidiurnal neap tides and s for diurnal neap tides. We have seen (1.1.2) that semidiurnal neap tides occur around the time when the mean longitudes of the Moon and Sun are in phase quadrature, contrary to similar $\kappa_{S_2} - \kappa_{M_2}$ situations, or:

$$s - h = \frac{\kappa_{S_2} - \kappa_{M_2}}{2} + \frac{\pi}{2} + k\pi$$

In neap tide situations, the mean high water and low water heights are thus the mean heights of high and low waters close to these times. If the mean of these heights is computed over a sufficiently long time, all constituents whose astronomical argument is not of the form $k_\tau\tau + k_{s-h}(s - h)$ are eliminated (k_j are relative integers). There are naturally also M_2 and S_2 main waves, along with all the nonlinear interaction constituents that bring these two main semidiurnal waves into play (e.g. MS_f, $2MS_2$, $2SM_2$, M_4, MS_4), which are not accounted for in the simplified equations that give the HW and LW and NT values presented in 2.3. Diurnal neap tides occur around the time when:

$$s = \frac{\kappa_{K_1} - \kappa_{O_1}}{2} + k\pi$$

All constituents whose argument is not of the form $k_\tau\tau + k_s s$ are cancelled out in the diurnal neap tide mean. As for semidiurnal tides, there are two main diurnal waves K_1 and O_1, along with all the corresponding compound waves: OQ_2, K_2, MK_3, etc.

2.6 • Tidal coefficient

For the comparison of tidal coefficients of different ports (see 3.2), Laplace characterized each port by a tidal height unit: "the height unit is the mean amplitude (half-range of tide) of the highest tide following the moment of the full or new moon, around equinoctial syzygy."

The coefficient concept is directly derived from this definition. Note that, by convention, the mean amplitude of the spring tide that follows the syzygy

closest to equinox is given a coefficient of 100, as represented by the following equation:

$$C = 100 \frac{h_{pm} - N_{mm}}{U}$$

in which we have:

- the tidal coefficient: C
- the high water height: h_{HW}
- the half-tide level: N_{ht}
- the height unit: U

In practice, the coefficient is calculated just from the semidiurnal constituents. The popularity of this coefficient concept in France may be explained by the fact that it provides a very quick indication on the tidal amplitude. Obviously it is only a relative indication, but it is very widely used by people visiting and active in the Channel and Atlantic coastal regions of France. The coefficient also has the advantage of facilitating rapid calculation of tidal heights and currents. Tables of tide corrrection used for calculating tidal heights in secondary ports, and current atlases providing elements for mean spring tide and neap tide situations that correspond to coefficients of 95 and 45, respectively. It is very easy, based on knowledge of the current tidal coefficient, to perform a rule of three to obtain a good estimate of tidal heights or corresponding currents.

Mariners are aware of the fact that these values are approximate. They may apply this coefficient (which is only calculated for the port of Brest) for the entire French Atlantic coast, but possibly not for North Sea ports. In this latter region, relative tidal amplitude variations are much lower than at Brest. However, for navigational purposes, it would not be reasonable to apply this Brest-based coefficient to areas that are too remotely located with respect to this port. It also does not make sense to apply it for ports that do not have semidiurnal tides. Since this type of coefficient is very practical, it may be given a more universal scope based on the harmonic equation, i.e. applicable for all types of tide.

2.7 • Coefficient calculation based on the harmonic tidal equation

According to Laplace's highly relevant concept, the tidal coefficient is a measurement of tidal amplitude in reference to the height unit U. We have just seen that this reference is the mean equinoctial spring tide amplitude. The term 'mean' essentially refers to the range that the mean encompasses. This is *a priori* based on the assumption that all extreme contributions due to movements of lunar perigee (p) and of the ascending node (N) should cancel

each other out. This implies that the mean is calculated over a sufficiently long period (saros is optimal). Hence, in the harmonic tidal equation, all tidal waves whose astronomical argument depends on p or N are cancelled out in the mean.

To make this coefficient more widely applicable, it is necessary to determine the height unit U that could be applied to all tidal types rather than just for semidiurnal tides and equinoctial spring tides. The extreme tide computation method naturally lends itself to a height unit that is defined according to constituents whose astronomical arguments are not dependent on the mean longitudes p and N.

By applying a calculation method that is identical to that used for computing extreme tides, we look for the maximum Ψ_{U}, i.e. the value of the Ψ function for $\overrightarrow{\mathrm{X}} = \overrightarrow{\mathrm{X}}_{\mathrm{U}}$, where $\overrightarrow{\mathrm{X}}_{\mathrm{U}}$ is the vector of the $[\tau,\ s,\ h]$ constituents.

Beyond simply being a tidal height indicator, the coefficient defined by Laplace relates more to the amplitude of the tide $h_{\mathrm{HW}} - \mathrm{N}_{\mathrm{HT}}$. However, this amplitude concept, which can be readily understood for essentially diurnal or semidiurnal tides, is harder to apply for mixed semidiurnal tides. In order to avoid defining a coefficient that could undergo substantial variations within a day, the height or amplitude notions are replaced by the notion of 'variability', whose value is deemed to be statistically proportional to the standard deviation (square root of the variance).

Where $h_{k,\mathrm{U}}$ denotes the amplitude of the k species, which corresponds to the maximum Ψ_{U} ($k = 1$ for diurnal constituents, $k = 2$ for semidirunal constituents, etc.), the height unit U can be formulated as follows:

$$\mathrm{U} = \sqrt{\sum_k h_{k,\mathrm{U}}^2}$$

When h_k denotes the amplitude of the k species at a given time, the C coefficient at the same time can be formulated as follows:

$$\mathrm{C} = 100 \frac{\sqrt{\sum_k h_k^2}}{\mathrm{U}}. \tag{8.25}$$

This definition is not exactly the same as that used for calculating the Laplace coefficient. For the port of Brest, the amplitudes of diurnal waves and interactions are relatively low as compared to that of semidiurnal species. Results obtained via the two equations for this port are very similar: different tests carried out on coefficients within the extreme value range did not reveal any errors of over 1. Since equation (8.25) is very widely applicable, it can be used to define a universal tidal coefficient. Note that the h_k amplitudes are simply moduli of the reduced vectors C_k.

2.8 • Examples of applications for different types of tide

Four ports (Brest, Honolulu, Do-Son and Nagasaki) were selected to provide examples of calculation results for certain tidal parameters that are outlined in this chapter.

2.8.1 • Brest: 48° 23′ N , 4°30′ W

Type:	**Semidiurnal tide**		
Mean level:	402.0 cm		
Diurnal age:	97.3 h		
Semidiurnal age:	381 h		
High water		**Low water**	
Highest:	779.1 cm	Lowest:	17.0 cm
Coef. 100:	720.8 cm	83.3 cm	
mean ST:	690.9 cm		109.4 cm
mean NT:	521.0 cm		278.4 cm
Lowest:	457.3 cm	Highest:	342.9 cm
Hours (UT+1.0 h):			
HWST:	05 h 33 min	LWST: 00 h 13 min	
HWNT:	23 h 42 min	LWNT: 17 h 40 min	

2.8.2 • Honolulu: 21° 18′ N, 157° 52′ W

Type:	**Mixed semidiurnal tide**		
Mean level:	24.0 cm		
Diurnal age:	10.8 h		
Semidiurnal age:	−4.0 h		
High water		**Low water**	
Highest:	80.0 cm	Lowest:	−13.7 cm
Coef. 100:	71.4 cm	−8.9 cm	
mean ST:	61.5 cm	−1.0 cm	
mean NT:	28.7 cm	22.5 cm	
Lowest:	24.0 cm	Highest:	24.0 cm
Hours (UT-10.0 h):			
HWST:	04 h 11 min	LWST:	20 h 28 min

2.8.3 • Do-Son: 20° 40′ N, 106° 48′ E

Type:	**Diurnal tide**
Mean level:	186.0 cm
Diurnal age:	50.2 h
Semidiurnal age:	51.4 h

High water		**Low water**	
Highest:	408.8 cm	Lowest:	−24.5 cm
Coef. 100:	364.4 cm	18.3 cm	
mean ST:	333.7 cm	39.7 cm	
mean NT:	186.1 cm	185.5 cm	
Lowest:	186.0 cm	Highest:	186.0 cm

2.8.4 • Nagasaki: 32° 44′ N, 129° 52′ E

Type:	**Mixed semidiurnal tide**		
Mean level:	164.0 cm		
Diurnal age:	18.0 h		
Semidiurnal age:	25.5 h		
High water		**Low water**	
Highest:	337.4 cm	Lowest:	−48.6 cm
Coef. 100:	317.0 cm	−19.4 cm	
mean ST:	286.2 cm	39.9 cm	
mean NT:	206.2 cm	142.6 cm	
Lowest:	164.0 cm	Highest:	164.0 cm
Hours (UT+9.0 h):			
HWST:	08 h 58 min	LWST:	15 h 02 min

3 • Extreme tidal heights

Sea level variations on time scales ranging from a few hours to a few years are the result of two overlapping phenomena:

• random movements, mainly of meteorological origin (but sometimes tectonic, e.g. tsunamis), which are surges and negative surges that are usually symbolized by: $\mathrm{SD}(t)$

• astronomical tides, which are deterministic phenomena whose $h_a(t)$ predictions are listed in tide tables; with Z_{00} being the mean sea level (international convention) relative to the hydrographic datum (see Chapter IX for the definition of the different mean levels), and its prediction is expressed by:

$$h_a(t) = \mathrm{Z}_{00} + \sum_i h_i \cos(\mathrm{V}_i - \kappa_i)$$

The observed sea level is usually expressed by:

$$h(t) = \mathrm{Z}_{00} + \sum_i h_i \cos(\mathrm{V}_i - \kappa_i) + \mathrm{SD}(t)$$

Consequently, the highest tidal height, which has a random constituent, is a factor that only makes sense if evaluated in terms of probability. We thus have to look for the mean time interval, or so-called return period*, that separates two rare events in which the tidal heights are above a certain threshold.

When expressed in this way, the problem seems to be limited to a simple mean calculation. However, to get a significant mean, the observation time has to be much longer than the sought-after return periods. Considering the extent of available records, return periods of more than 2 or 3 years could not be estimated in most cases.

This problem can still be efficiently dealt with for ports where over 10 years of tide records are available by benefitting from the fact that surges, negative surges and tides are very independent phenomena. If many tidal data are available, it should be easy to calculate the probability laws governing rare but unexceptional events such as high spring tides or very substantial positive surges. Two such events may never have been previously observed to occur simultaneously, but the return period corresponding to this type of uncommon phenomenon can be computed with a high degree of confidence by combining probability laws associated with the tide and also with positive surges. As an example, figures 8.1 and 8.2 (a and b) show results obtained for Brest. Figure 8.1 gives the level of probability that a predicted high water height will be equal to a given value (to the nearest centimetre).

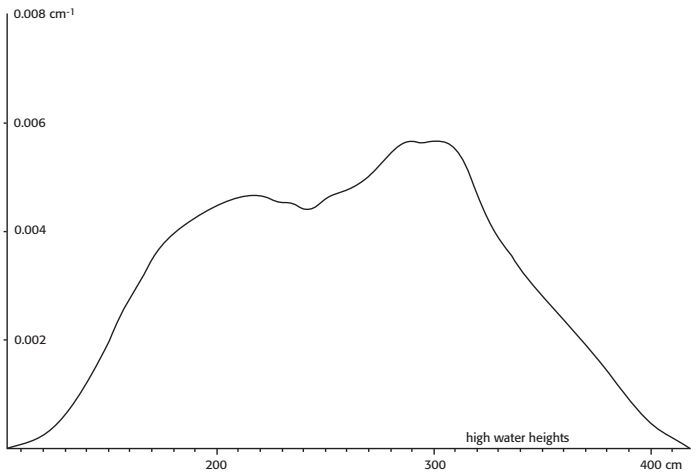

Figure 8.1: Brest, France: Curve representing the function $f(s)$, the probability density function for high water heights s (x-axis). It gives the probability (y-axis) that a high water will have a height ranging from s to $s + \delta s$, with $\delta s = 1$ cm.

With positive surges, it may be hard to calculate the probability associated with a positive surge that is greater than a given value. One difficulty concerns the fact that very substantial, but uncommon, positive surges cannot be overlooked. These never previously observed events should be taken into account via an extrapolation model. The chosen model is called 'Gumbel's law', which is widely used for estimating river and stream floods. Application of this model to the longest available series of tidal height measurements (120 years at Brest) demonstrated that this law is very suitable for estimating tide levels.

Gumbel's law was formulated on the basis of a study of extreme values attained by a random variable through independent samplings. Fisher and Tuppet, followed by Gumbel, first analysed this type of variable or those concerning the overshooting of various thresholds. The adopted law is just one special case of those deduced from probability theory. It was found to be very suitable for the analysis of flood phenomena, thus explaining its success. Recall that if $F(\varsigma)$ is the distribution function of the positive surge ς, which is considered as a random variable, this function represents the probability (Pr) that the random variable values will be lower than a given value ς_0, or: $F(\varsigma) = Pr(\varsigma < \varsigma_0)$.

If for all values of ς (given variable of $-\infty$ to $+\infty$), function $F(\varsigma)$ has a derivative $f(\varsigma)$, such that

$$F(\varsigma_0) = \int_{-\infty}^{\varsigma_0} f(\varsigma) d\varsigma$$

where function $f(\varsigma)$ defines the probability density function, i.e. the probability that the positive surge value will range from ς to $\varsigma + d\varsigma$.

Gumbel's law is expressed by the function:

$$F(\varsigma) = \exp\left[-\exp(a\varsigma + b)\right]$$

where a and b are the parameters to be determined.

Hence, where $S(\varsigma_0)$ denotes the probability of observing a positive surge of over ς_0, we have: $S(\varsigma_0) = Pr(\varsigma > \varsigma_0) = 1 - F(\varsigma_0)$, or

$$S(\varsigma) = 1 - \exp\left[-\exp(a\varsigma + b)\right] \tag{8.26}$$

For experimental validation of this law, the observed points are plotted in a system of so-called Gumbel coordinates (ς, Y), where the ordinate Y is linked to ς by the following equation:

$$Y(\varsigma) = \log\left\{-\log\left[1 - S(\varsigma)\right]\right\} \tag{8.27}$$

It also turns out that, since the tide and positive surges are treated separately, the choice of extrapolation model is not very critical for the estimation of extreme height return periods.

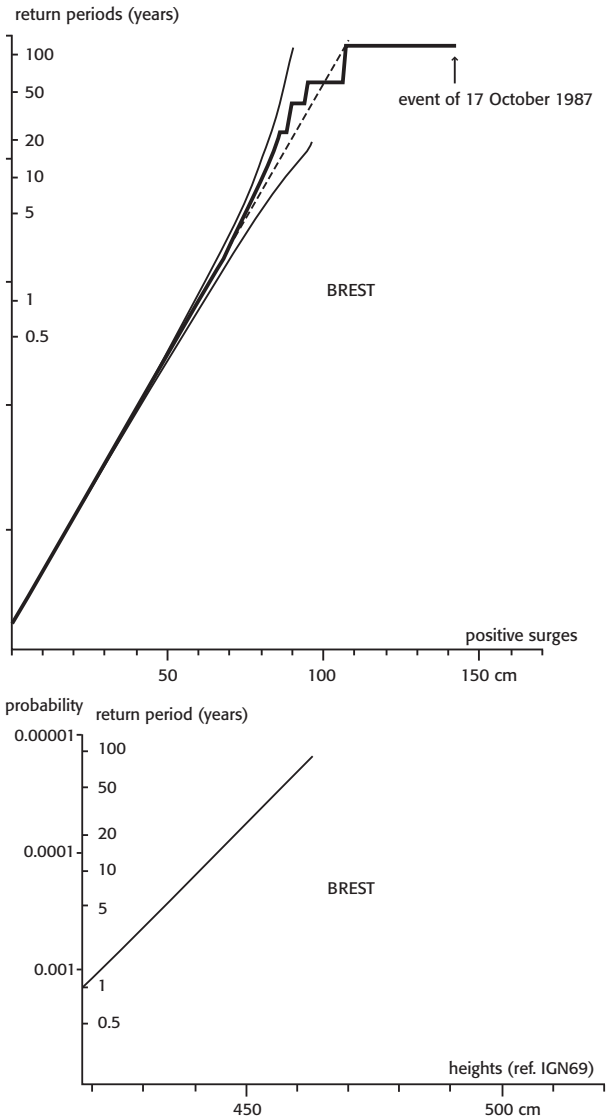

Figure 8.2: Brest, France: These two graphs present, in a Gumbel coordinate system, probabilities (with associated return periods) that a positive surge (top) and an extreme height (high water + positive surge)(bottom) will exceed a given value.

Figure 8.2 (top) shows the probability $S(\varsigma_0) = Pr(\varsigma > \varsigma_0)$ that a positive surge ς will exceed a given value ς_0 in the coordinate system (8.27) described by Gumbel. The experimental points, which follow a stepped curve, would be aligned in case of compliance with the law defined by equation (8.26). The dashed line shows the best fit in the experimental point cloud. The two thin line curves on both sides of the dashed line define the zone where 90% of the experimental points would be located if the extrapolation model used is suitable.

Figure 8.2 (bottom) shows the results obtained when applying a combination of probability laws concerning predicted positive surges and high waters (tidal). Where $f(z)$ denotes the density function for the probability that the predicted high water height z will have a value ranging from z to $z + dz$, as expressed by: $f(z)\,dz$. Note also that the z domain is bounded by the values z_{min} and z_{max}, which represent the predicted HW extremes.

As the positive surges ς are *a priori* independent of the predicted heights z, the probability $Pr(\eta_0)$ of observing a sea level of over η_0 is thus obtained via the convolution product:

$$P_n(\eta_0) = \int_{z_{min}}^{z_{max}} f(z)S(\eta_0 - z)dz$$

There are 705.8 high waters a year on average under a semidiurnal tidal regime. Hence, the mean number of observed high waters above the η_0 value is $705.8 \times P(\eta_0)$ per year. The return period $T_R(\eta > \eta_0)$, expressed in years, of an observed extreme tide $\eta > \eta_0$ is therefore:

$$T_R(\eta > \eta_0) = \frac{1}{705.8 \times Pr(\eta_0)} \text{ years}$$

Function $P_n(\eta)$ gives the probabilities of observing high water heights above a given value, which can then be expressed in terms of associated return periods. We have decided to just present heights above the maximum astronomical tide (thus avoiding the problem of dealing with negative surges).

It should be noted that under certain conditions return periods can be estimated on the basis of height measurements covering a period of more than a month. Bottom pressure gauges have now been installed at chart sounding points where such series of measurements. Relationships between these measurements may obtained and heights recorded simultaneously at the nearest reference station can be established and used to estimate probability laws required for calculating extreme tide return periods at these points. Due to spatial variability patterns in the studied phenomena, there should be

enough of these sites in the sampling area to be able to interpolate these values for places throughout the study area. In some areas, charts are available that present lines of equal extreme tidal heights.

An example of tidal height patterns for a 75 year return period is presented for the Aroise Sea and the roadstead of Brest (figure 8.3). In this example, all data available for this zone were processed for the purposes of mapping extreme heights corresponding to the given return period.

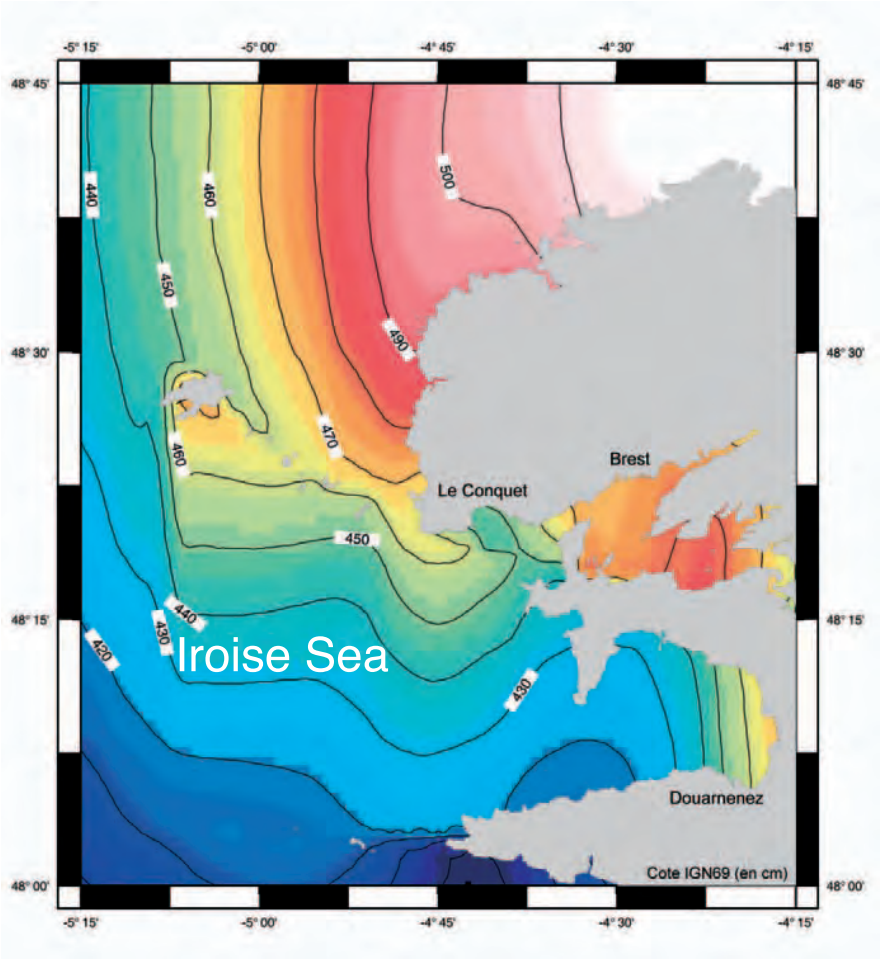

Figure 8.3: Iroise Sea and the roadstead of Brest (France): chart of extreme tidal heights corresponding to a 100 year return period. Heights are given relative to the IGN 69 zero mark (in cm).

Errors associated with obtained tidal height values can also be computed. The results often highlight defects in tide recording networks and areas where additional tidal measurements could be necessary.

4 • Different mean tidal heights

The mean level (often denoted ML) of the observed height $h(t)$ is a rather vague concept. Intuitively, it refers to a supposedly constant characteristic quantity. However, by definition, ML values are fundamentally variable because they depend on the centre time t_n of the chosen timespan and the duration T of the latter:

$$\mathrm{NM}_{t_n,\mathrm{T}} = \frac{1}{\mathrm{T}} \int_{t_n-\mathrm{T}/2}^{t_n+\mathrm{T}/2} h(t)\mathrm{d}t \tag{8.28}$$

Moreover, concerning tides, this ambiguity is accentuated by the fact that the term 'mean level' is not attributed to the mean (8.28) of observed heights $h(t)$. The term is mainly applicable for data filtering and more complex than the mathematical mean (8.28), which represents a special case of filtering $h(t)$ by the symmetrical rectangular frequency distribution of breadth T.

According to a well established tide monitoring practice, the mean level can apply to the result of an operation on measured heights aimed at eliminating the astronomical tide. This practice is used especially for determining different mean levels, including the daily mean height. The duration of a mean solar day (24 h) is not exactly the tidal period ($\mathrm{T}_{\mathrm{M}_1} \approx 2\mathrm{T}_{\mathrm{M}_2} \approx 24.84$ h), as the simple mean of 24 hourly measurements leaves a residual containing tidal constituents that are very problematic for statistical analysis of the daily mean level.

4.1 • Daily mean level

To gain insight into slow sea level variations, digital filtering of $h(t_n + mt_e)$ measurements, sampled over a time step t_e(on each side of a time t_n), involves carrying out a so-called filtering operation, by:

$$\overline{h}(t_n) = \sum_{m=\mathrm{M}_i}^{m=\mathrm{M}_j} w(mt_e)h(t_n - mt_e) \tag{8.29}$$

where $w(mt_e)$ is the filter $w(t)$ sampled every t_e by the rectangular distribution of width $(\mathrm{M}_j - \mathrm{M}_i)t_e$ centred on time $(\mathrm{M}_j + \mathrm{M}_i)t_e/2$, which is generally different from zero.

By applying this filter to the exponent $e^{-j2\pi\nu t}$, we directly obtain the transfer function $\mathrm{FT}(\nu)$:

$$\mathrm{FT}(\nu) = \sum_{m=\mathrm{M}_i}^{m=\mathrm{M}_j} w(mt_e) e^{-j2\pi\nu(t_n - mt_e)}$$

The transfer function $\mathrm{FT}(\nu)$ should be true. This will only be the case if the filter $w(t)$ is symmetrical (even function) and sampled by a rectangular distribution centred at the origin. This requires:

- firstly: $w(mt_e) = w(-mt_e)$
- secondly: $\mathrm{M}_i = -\mathrm{M}_j = \mathrm{M}$, $t_n = 0$

Where $w(mt_e)$ and $w(-mt_e)$ are respectively denoted by a_m and a_{-m} (n.b. $a_m = a_{-m}$), the transfer function of a symmetrical digital filter may be formulated as:

$$\mathrm{FT}(\nu) = a_0 + 2 \sum_{m=1}^{m=\mathrm{M}} a_m \cos(2\pi\nu m t_e) \tag{8.30}$$

As this involves a mean level calculation, the filter should accurately restore a height that is constant (not time-dependent). The transfer function must therefore be unity for zero frequency, or:

$$a_0 + 2 \sum_{m=1}^{m=\mathrm{M}} a_m = 1$$

The filter can theoretically be attributed desired characteristics through the choice of a_m coefficients. Let us assume, for instance, that we want a filter whose transfer function (8.30) value is imposed at M points. One solution would be to solve the system of $\mathrm{M} + 1$ equations with $\mathrm{M} + 1$ unknowns so as to be able to calculate a_m coefficients. However, this procedure is not realistic for calculating mean levels. The ideal filter would be a low pass filter whose transfer function is a symmetrical rectangular frequency distribution of width $2\nu_0$ in the freqency domain ($\nu_0 > 0$).

Clearly, to dampen oscillations introduced by such a transfer function between the imposed frequencies, the corresponding frequency can only be approximated by a very high number of coefficients. However, each of these coefficients is given an observed size. This means that to obtain an ideal filter, it is necessary to take into account many observations on both sides of time t_n to which the filter is applied. A tradeoff is clearly required. First, we will not necessarily attempt to approximate the ideal filter, but will preferentially try to give it certain key features for the problem to solve. Eliminating tidal constituents is one of our top priorities. Secondly, an upper limit is set for the number of coefficients to take into account. An assessment of the filters

proposed by different authors reveals an implicit consensus: the maximum number of coefficients $a_m(t_e = 1h)$ is set at $M_{max} + 1 = 36$. Like $a_m = a_{-m}$, this number of values enables filtering with the mean daily height being attributed at noon of a given day, by taking measurements available for three days into account (previous day, the current day, and the next day, or 72 h).

Table 8.3 gives the coefficients of different filters commonly used for the computing main daily levels (n.b. these filters are symmetrical). The W_{25} filter is the mean of 25 hourly values. For the tidal period, which is closer to 25 h than to 24 h, this filter is more efficient than the mean of 24 hourly heights. Moreover, the calculation can be focused on noon every day. This very easy to use filter is still less efficient than that of Doodson, which is just as simple. Nowadays, with computer technology, the simplicity factor is no longer important for calculating mean daily heights.

The efficiency of these filters is generally assessed on the basis of their ability to offset the tidal constituents. The main wave residual coefficients are presented in Table 8.4. A comparison the these results with those deduced from the reduced height method (RH, last column on Table 8.4) is instructive. This latter method is the only one to give residual coefficients of zero for the main wave M_2 and subsequent waves (M_3, M_4, M_6, M_8).

4.2 • Mean monthly and annual levels

Calculations of mean monthly and annual levels are simply derived from arithmetic means of mean daily levels. These means are new filters that dampen residue coefficients resulting from daily level filters. The new residue coefficients are given in Table 8.4, (except for Sa and Mf) multiplied by the corresponding factors that are listed in Table 8.5, according to the duration in days (d) of the month (28, 29, 30 or 30 d) or of the year (365 or 366 d).

As the means are established on an integer number of days, the solar constituents are not dampened. However, since their phase at noon does not vary, their residual is simply a constant term.

5 • Long-term mean level variations

Variations in the mean annual tidal level are the focus of very progressive studies aimed at determining the long-term trends and relating them to observed climate change patterns. This brief presentation is limited to discussing the problem of observations and prediction, while examining the possible causes and consequences.

Table 8.3: The main digital filters used for calculation of mean daily levels from hourly tide levels. The number of values taken into consideration for each filter is always odd, i.e. $1 + 2m_{\max}$.

hour	W_{25}	Doodson	Munk	Godin	Demerliac
m	$25a_m$	$30a_m$	$10^7 a_m$	$14\,400a_m$	$24\,576a_m$
0	1	0	395 287	444	768
1	1	2	386 839	443	766
2	1	1	370 094	440	762
3	1	1	354 118	435	752
4	1	2	338 603	428	738
5	1	0	325 633	419	726
6	1	1	314 959	408	704
7	1	1	300 054	395	678
8	1	0	278 167	380	658
9	1	2	251 492	363	624
10	1	0	234 033	344	586
11	1	1	219 260	323	558
12	1	1	208 050	300	512
13		0	195 518	276	465
14		1	180 727	253	435
15		0	165 525	231	392
16		0	146 225	210	351
17		1	122 665	190	325
18		0	101 603	171	288
19		1	85 349	153	253
20			72 261	136	231
21			60 772	120	200
22			47 028	105	171
23			30 073	91	153
24			13 307	78	128
25				66	105
26				55	91
27				45	72
28				36	55
29				28	45
30					32
31				15	21
32				10	15
33				6	8
34				3	3
35				1	1

TABLE 8.4: Residual coefficients for the main tidal waves obtained via the different filters used for computation of the mean daily level.

waves	W_{25}	Doodson	Munk	Godin	Demerliac	RH
Q_1	0.074 31	0.010 41	0.007 40	0.001 03	0.001 62	0.002 76
O_1	0.032 80	0.002 99	0.001 41	0.000 19	0.000 43	0.003 38
P_1	−0.037 38	−0.000 13	−0.000 96	0.000 00	0.000 00	−0.000 19
K_1	−0.042 60	0.000 15	−0.000 74	0.000 00	0.000 00	−0.000 30
N_2	−0.012 79	0.001 71	0.000 89	0.000 04	−0.000 16	−0.000 14
M_2	0.006 42	-0.000 58	0.000 02	0.000 01	−0.000 04	0.000 00
S_2	0.040 00	0.000 00	−0.000 20	0.000 00	0.000 00	0.000 84
K_2	0.042 55	0.000 33	−0.000 15	0.000 00	0.000 00	0.001 06
M_3	−0.006 50	−0.009 09	−0.000 08	0.000 01	0.000 04	0.000 00
M_4	0.006 62	0.002 59	0.000 30	0.000 01	0.000 00	
MS_4	0.021 16	0.004 84	0.000 00	0.000 01	0.000 42	
M_6	0.006 99	−0.001 98	−0.000 39	0.000 01	−0.000 07	0.000 00
M_8	0.007 55	−0.003 84	−0.000 06	0.000 01	−0.003 63	0.000 00

TABLE 8.5: Factors applied to daily residual coefficients (Table 8.4) of main waves (except Sa and Mf) to obtain those corresponding to mean monthly levels (28, 29, 30 or 31 days) and annual levels (365 or 366 days).

waves	28 d	29 d	30 d	31 d	365 d	366 d
Sa	0.990 4	0.989 7	0.989 0	0.988 2	0.000 7	0.002 1
M f	0.024 3	0.057 0	0.084 5	0.105 9	0.009 3	0.007 3
Q_1	0.003 7	0.031 1	0.060 2	0.081 0	0.000 9	0.001 9
O_1	0.013 8	0.021 4	0.053 2	0.080 4	0.009 6	0.007 6
P_1	0.990 4	0.989 7	0.989 0	0.988 2	0.000 7	0.002 1
K_1	0.990 4	0.989 7	0.989 0	0.988 2	0.000 7	0.002 1
N_2	0.030 2	0.005 6	0.038 4	0.065 2	0.000 9	0.001 9
M_2	0.054 1	0.018 4	0.015 7	0.047 0	0.010 0	0.008 0
S_2	1.000 0	1.000 0	1.000 0	1.000 0	1.000 0	1.000 0
K_2	0.961 8	0.959 1	0.956 2	0.953 3	0.000 7	0.002 1
M_3	0.053 4	0.018 6	0.015 8	0.046 4	0.002 1	0.004 7
M_4	0.052 4	0.018 7	0.016 0	0.045 7	0.006 5	0.006 4
MS_4	0.054 1	0.018 4	0.015 7	0.047 0	0.010 0	0.008 0
M_6	0.049 7	0.019 2	0.016 5	0.043 7	0.002 2	0.004 2
M_8	0.045 8	0.020 0	0.017 2	0.040 7	0.001 3	0.001 7

5.1 • Observations

Long-term tidal observations are essential for climate studies, especially those that have been recorded at Brest since 1806.

Tide levels have been measured for almost 200 years at the Brest tide monitoring station, which is a long enough period to document long-term sea level variations (figure 8.4).

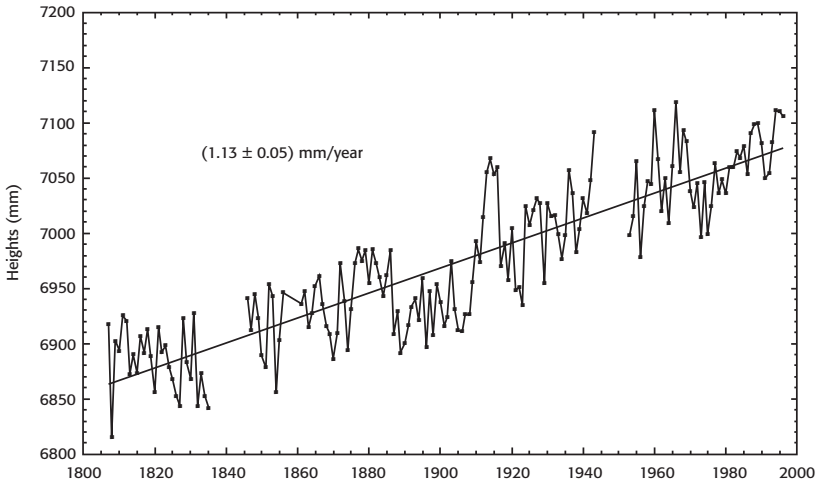

Figure 8.4: Evolution of the mean annual sea level at Brest between 1806 and 1997. Each point represents a mean annual level. Over this period of almost two centuries, a regular trend of 1.13 ± 0.05 mm/year is noted, but without any obvious acceleration.

This example shows that there are relatively marked local variations in the mean annual level, i.e. as high as or over ±5 cm between years. This is why at least a century of observations are necessary to be able to evaluate trends with a good degree of accuracy.

At Brest, the mean level increased by 25 cm in 200 years. This example is, however, not representative of all long-term observations available worldwide. In most cases, these observations actually reveal a mean increase of around 1-2 mm/year, with about the same extent of scatter around these values as that documented at Brest. There are sites, especially in Scandinavia, where the reverse trend has been noted.

Otherwise, available observations do not provide an accurate indication of the overall trends because of the very irregular distribution of tide monitoring stations, which are mostly located in temperate regions in the Northern Hemisphere. The variability in the trend between sites is mainly due to vertical crustal movements that tide gauges obviously cannot detect

(measurement of relative levels). Tectonic movements can now be measured by spatial imaging techniques, which are effective for monitoring levels of various elements in marine or terrestrial environments relative to an absolute reference frame.

Data logged by many satellites equipped with altimetric radar (especially Topex-Poseidon since October 1992, and Jason since 2003) provide close to centimetre measurement accuracy. The findings indicate that there has been almost the same extent of increase in ocean levels as that mentioned above for Brest. However, because of interannual variations, many years of altimetric radar data collection would be required worldwide to reduce the estimation error. The satellite data collected so far indicate very high spatial variability in trends for periods of around a decade. Satellite-borne radar altimeters have proven their reliability and the quality of the acquired data has been improving year by year. Moreover, spatial geodesy techniques make it possible to position (with centimetre accuracy) specific points on the Earth's surface via the International Terrestrial Reference System (ITRS), which was adopted by the International Union of Geodesy and Geophysics (IUGG). Tide gauge reference levels can be pegged to the ITRS through operational systems such as GPS and Doris.

Sea level variations can now be monitored within an absolute reference frame. International and national programmes are currently under way to improve the precision of geodetic datums and models through spatial imaging techniques. For the same reasons as those mentioned for altimetric radar data, it will be several years before minable results will be obtained (for the purposes of studying long-term sea level variations).

Finally, vertical crustal movements can also be detected on the basis of measurements of gravity acceleration on the Earth's surface. Devices have been designed to detect gravity variations equivalent to height variations of a few millimetres.

5.2 • Causes of long-term tidal variations

Altimetruc radar data currently indicate that the global sea level is rising, but these measurements have not been obtained over a sufficiently long period and they are not accurate enough to confirm any acceleration trends. While awaiting further and more accurate measurement data, an analysis of possible causes could help us gain insight into the phenomenon and eventually predict how it will evolve.

The rise in sea level is generally attributed to global warming due to the greenhouse effect, with atmospheric carbon dioxide being the main

greenhouse gas. However, an analysis of Brest tidal records did not highlight any acceleration in this trend associated with industrial development.

An analysis of data recorded on different paramters came up with the following findings:

- the carbon dioxide concentration has increased by 25% since the beginning of the industrial revolution, and it is currently increasing at a rate of 0.4-0.5% a year.
- the mean air temperature has risen by 0.5°C over the last century.

This warming impacts the sea level via different processes, especially glacier and polar ice cap melting and the expansion of ocean surface layers. Land movements also have an effect on ocean levels.

5.2.1 • Ice cap melting and thermal expansion of oceans

We make a distinction between mountain glaciers and ice caps (Antarctica and Greenland) because of the differences in volume. The volume of water retained in mountain glaciers is the equivalent of 30-50 cm in sea level. Their melting has been responsible for boosting the sea level by 1-4 cm over the last century, and could reach around 10 cm in the 21st century.

The ocean level would rise by around 87 m if all the ice caps were to melt completely (80 m for Antarctica and 7 m for Greenland). The extent of responsibility of the greenhouse effect in accelerating this phenomenon is a highly controversial issue.

For Antarctica, following the catastrophic scenarios that were put forward in the 1980s and widely covered in the media, estimated mean annual melting rates have been regularly declining. The possibility that the Western Antarctic Ice Sheet will disappear, which fuelled this debate, is no longer expected to occur before several centuries. Conversely, the volume of the Antarctic ice cap seems to be increasing. This ice cap is generally subjected to extreme negative temperatures during both winter and summer, so slight warming of the atmosphere in this region would not induce substantial melting. Instead, a temperature increase would boost the humidity which in turn would lead to more abundant snowfalls, thus increasing water storage in the form of ice to the detriment of the ocean.

The atmosmhere above the Greenland ice cap is much colder than in Antarctica. The northern ice cap should contribute positively to the evolution of the sea level despite the presence of a few stabilizing factors. However, the budget of contributions of the two ice caps would likely be slightly negative.

Thermal expansion of the oceans (which oceanographers also call the 'steric effect') contributes to sea level variations. Atmospheric warming

affects the ocean temperature by various physical processes, which are often pooled under the term ocean-atmosphere interactions (radiation, evaporation, precipitation, thermal conduction, etc.). An increase in temperature in a 1 000 m thick marine water column of 1°C to 15°C would lead to a sea level rise of around 16 cm. Homogenous warming of such a layer is, however, unrealistic. Heat diffusion from the surface to the ocean depths is a complex nonlinear process that should be considered in a broader framework of thermohaline circulation on a World Ocean scale. This phenomenon could, for instance, reduce deep-water production at high latitudes (Weddell Sea in the Southern Ocean; Labrador and Greenland Seas in the Northern Hemisphere).

Ocean warming is estimated to have been responsible for a 4 ± 2 cm level rise over the last century.

5.2.2 • Crustal movements

Ground movements are of isostatic, tectonic and anthropogenic origin.

These vertical movements due to the ice weight or melting, which have been documented on a scale of several thousands of years (corresponding to glaciation/deglaciation cycles at high latitudes), have reached amplitudes of several hundreds of metres. Even today it is very obvious that the 'elastic rebound' following the last deglaciation (which ended over 7 000 years ago) is under way. In the Gulf of Bothnia (Baltic Sea), the apparent sea level has been declining by around a metre per century. An analysis of mean levels seems to indicate a shift around a pivot running from Scotland to southern Scandinavia. France could thus be faced with subsidence as a backlash to this elastic rebound.

Human activities may also have very marked local impacts. This is the case, for instance, in the Gulf of Mexico due to petroleum development, which is inducing subsidence. Tapping of aquifers and river sediment compaction has aggravated the problem in the Mississippi Delta region.

5.3 • Forecasts and impacts

Forecasting of sea-level rises must be preceded by modelling studies that take climate change patterns and especially air temperature increases into account. There are, however, substantial uncertainties at this stage concerning the estimation of the evolution of some factors (especially greenhouse gas emissions) in the coming years.

Modelling development must be further pursued because current models do not accurately account for past patterns. In fact, there is no real evidence that current warming trends correspond to the onset of the greenhouse effect

as predicted by present models. These models also foresee a certain degree of polar warming, which has not been clearly documented. Conversely, some circumpolar regions seem to be cooling off.

Predictions of an overall rise in sea level vary depending on when they were published. Concerning forecasts for the year 2100, catastrophic scenarios were predicted in the early 1980s, with some published simulations forecasting an overall rise of 3.5 m, but since then there has been a regular downward adjustment in these estimates. Paradoxically, in the early 1990s a quite marked increase in prediction uncertainty was noted, i.e. the discrepancy between the highest and lowest predictions. It nevertheless seems that this gap is narrowing, with a sea-level rise of around 50 cm now being predicted for 2100.

The conseqences of this sea-level rise are extremely wide ranging, and it would be impossible to make an exhaustive assessment. Depending on the amplitude of the phenomenon, these consequences will depend on the type of coast, its topography and especially the population density along the coastal fringe.

Severe erosion and groundwater salination can be expected to take place, in addition to the submersion of currently out of reach areas.

We should nevertheless be wary of simplistic predictions because the coast does not respond passively to sea-level rises. Coastal marshland vegetation and mangroves promote sedimentary accretion and may offset the trends in some areas. Moreover, climate change can modify river flow regimes and the sediment balance in coastal zones.

Dams and river flow management projects also often have serious impacts on this balance. Beach recession, which is a common phenomenon, often turns out to be the result of a sediment deficit, sometimes of natural origin, but too often due to human activities. Finally, it is important to be cautious about blaming uncontrolled constructions and resource extractions for causing sea-level rises.

IX

Tidal datums and chart soundings

Selection and determination of vertical datums and their corresponding levels is a key problem in hydrography.

These are conventional problems, but the advent of associated new technologies, especially satellite monitoring and computer development, has substantially changed the ways of dealing with them.

New datums are now being considered as a result of the development of satellite geopositioning systems (GPS/Glonass/*Galileo*), satellite altimetry, recognition of the International Terrestrial Reference Frame (ITRF) by the entire geodetic research community, determination of the Earth's global gravity field with ever higher spatial resolution, and the development of increasingly efficient computation of hydrodynamic models.

However, conventional tidal datums are still in use and their levels have to be accurately referenced with respect to other datums.

Chart sounding reduction involves the correction of depths measured by sounding systems with modeled but accurately determined depth, which can be tied to the nautical chart datum, or so-called chart datum, with enough accuracy to be suitable for navigational purposes. Two problems are overcome in this operation:

- determining the chart datum for the geographical area of the survey with respect to the selected datum.
- determining, relative to this datum, the sea surface elevation, which varies according to the geographical position and time of sounding.

These problems are generally independent (even though the levels are determined by the same measurement and processing methods – especially

conventional and spatial methods which are both based on tidal analysis and prediction) and are solved by different techniques.

1 • Definitions

The principles underlying sounding reduction are simple but can lead to misinterpretation because the exact meanings of some of the terms are unclear. Specifically, several different tidal datums are used in practice, and must be clearly defined so as to be able to reference their levels with respect to the others.

As measurements obtained by spatial techniques may differ from those obtained by standard techniques, it is essential to define the datums and rigorous reduction processes used in their determination.

1.1 • Chart datum characteristics

The chart datum, which is jointly used in nautical charts and tide tables, has two basic characteristics:

It is defined on the basis of tide monitoring criteria to ensure the safest possible navigation conditions: it is an estimation of the lowest possible astronomical tide, according to recommendations of the International Hydrographic Organization (IHO), and its level is referenced relative to a benchmark, or (conventionally) relative to a stable landmark located in the vicinity of a tide gauge, or (henceforth) relative to a datum plane, so as to ensure that it will remain valid in the long term, thus enabling consistent use of readings obtained during different periods. The level of this datum plane should be determined relative to an international reference frame such as ITRF.

In the vicinity of coastal tide stations, these two problems are overcome via tidal data analysis and by the fact that their levels can be determined relative to benchmarks located near tide gauges. The levels of these benchmarks are in turn referenced with respect to terrestrial benchmark networks.

Offshore, tide models are required, which must be evaluated on the basis of the ability to provide (for the chart datum) results that meet the quality criteria required of all reference frames, i.e. accuracy, accessibility, stability and accuracy.

1.2 • Lowest astronomical tide

According to the International Hydrographic Organization (IHO), the chart datum should be as close as possible to the lowest astronomical tide

level. The term 'astronomical' means that it is not a directly measured level, but rather a level calculated from the tide-generating force due to the gravitational attraction of the Moon and Sun. However, this astronomical or predicted tide is generally calculated by an equation based on harmonic constants determined by the analysis of preliminary tidal measurements. There are two problems with this.

First, the computational accuracy varies markedly depending on the quality and duration of the observed measurement data, the correction (or not) of meteorological and oceanographic effects, the computation methods and means, and the tidal type and range.

Secondly, over and above this astronomical tide, tidal height variations induced by other phenomena (non-astronomical, but meteorological and oceanographical, for instance), as well as long-term sea level trends, come into play during the measurement period. Hence, calculating it on the basis of measurements obtained during different periods will give different results with a significant rate of error.

Note that the idea of a lowest low water is intrinsically approximate and directly linked with the mean sea level concept, as discussed hereafter. Since the lowest LW is not accurate or stable, it cannot serve as an exact tidal height reference for hydrographic applications. However, once calculated by the harmonic equation, it can be used to determine the chart datum, which will thus be 'approximately' the lowest astronomical tide level.

1.3 • Mean sea level (MSL) and mean sea surface (MSS)

The term 'mean sea level' (MSL) is ambiguous. It intuitively suggests a constant level, whereas it is fundamentally variable because it depends on the period of time for which it has been calculated. It is actually a mean that is obtained by the following equation, where t_1 and t_N are dates of the beginning and end of the tide recording period and $h(t_n)$ is the measured sea level at time t_n, with the height reference origin being fixed and the time interval between measurements generally being constant and short in comparison to the interval between successive HW and LW.

$$\mathrm{NM}_{t_1}^{t_N} = \frac{1}{N} \sum_{n=1}^{n=N} h(t_n)$$

In practice (see Chap. VIII, §4), in the discussions on tides, MSL does not refer to the true mean of the measured levels, but instead is the result of a digital filtering operation (where the mean is just one particular aspect). According to the established custom, the 'instantaneous MSL' is the result of

an operation whereby the astronomical tide is subtracted from the measured heights.

$$\text{Instantaneous MSL}(t) = (\text{measured height at time t}) - \sum A_i \cos(q_i t - \alpha_i)$$

By this definition, for statistical applications, the instantaneous MSL can be considered as a random variable representing the free surface height without periodic oscillations due to astronomical effects. The mean instantaneous MSL is more accurate than the simple tidal height mean because it minimises periodic constituent residuals, which in any case are low over long periods. The MSL for long periods is thus generally calculated on the basis of the instantaneous MSL. The problem, however, is that regardless of the time scale, even quite long (a few years), this random variable is not static because the mean depends on the sample under consideration. This is clearly illustrated in figure 8.4, which shows the long-term rise in mean annual tide levels at Brest.

The MSL (for which the initial and final recording dates, and the computation method should be indicated) and the instantaneous MSL relative to a benchmark, vary over time. Because of this variability, neither of these levels can be taken as a vertical datum, which must be stable.

For tide forecasts, the MSL is calculated over the longest possible period and is referenced to the terrestrial reference system and benchmarks. In French this is referred to as the 'nominal MSL' (no distinction from MSL in English). This calculation is done for sites where long-term tidal measurements are recorded (several years if possible). These sites are called reference stations.

When the harmonic equation is applied for sounding reduction, it is assumed that the instantaneous MSL and the MSL, and thus also all other mean levels, define parallel surfaces, whereas the instantaneous MSL is a function of time, and the MSL relative to a terrestrial datum is constant.

The mean sea surface (MSS) is regularly mentioned hereafter, and this level is calculated on the basis of satellite altimetry measurements. The ellipsoidal height of the sea surface is averaged for each tracking position (after applying various corrections, especially to eliminate the astronomical tide). After interpolation to account for gaps in the satellite tracking coverage, the result is presented as a mean surface, which is representative of the mean sea level at each tracking position (at a resolution that depends on gaps in the satellite tracks) during the monitoring period.

MSS cannot currently be measured in coastal areas by satellite altimetry. The resolution is only a few dozens of kilometres, which still limits the use of

this technology for hydrographic purposes.

1.4 • Geoids

A geoid is an equipotential surface in the gravity field of the Earth. It is determined on land by geodetic levelling along with gravimetric measurements. Tide gauge benchmarks are, when possible, related to a geoid, in practice the land levelling network, which we call here the 'on-land geoid'.

In oceans, the same geoid can be extended via gravimetric measurements. A good argument in favour of using a geoid as tidal datum is that the vertical datum of mathematical models used to simulate the dynamics of oceans is an equipotential in the gravity field of the Earth. At any position, the local vertical is perpendicular to the geoid. One very common error is to confuse it with the MSS. These two surfaces should be differentiated because, relative to the geoid, MSS is affected by phenomena that we refer to as 'meteorological and oceanic'. This includes, for instance, the general ocean circulation (hence, at a latitude of 45°, a current of 1 m/s over a breadth of 10 km creates a height difference of 10 cm perpendicular to the current), the mean density distribution, atmospheric pressure gradients and nonlinear tide propagation effects in shallow areas. The nonlinear effects (e.g. in the Channel) alone can induce errors of as much as 10 cm (figure 9.1).

The geoid used as the initial surface in simulation models also differs from the on-land geoid. The geoid at sea is an equipotential of the gravity field that closely corresponds to a homogeneous ocean surface at rest, with a density equivalent to the mean density of the ocean at time zero, and subjected to an atmosphere, which is also homogeneous and at rest. We will call this the 'ocean geoid', which is determined almost like the on-land geoid, which is usually calibrated with respect to the mean sea level, but sometimes measured at a past date and a remote position. However, it does not coincide with it (if only because of secular evolution of the sea level), and the errors, which cannot currently be accurately measured, could be as much as several tens of centimetres, which is excessive for hydrographic applications and for studying ocean circulation.

Using the harmonic tidal equation, it is possible to determine the lowest astronomical tide level, and thus the chart datum, relative to the mean sea level over the considered period. In practice, and in models, variations in harmonic constants as a function of variations in the mean sea level are negligible. This is essential for chart datum determination and sounding reduc-

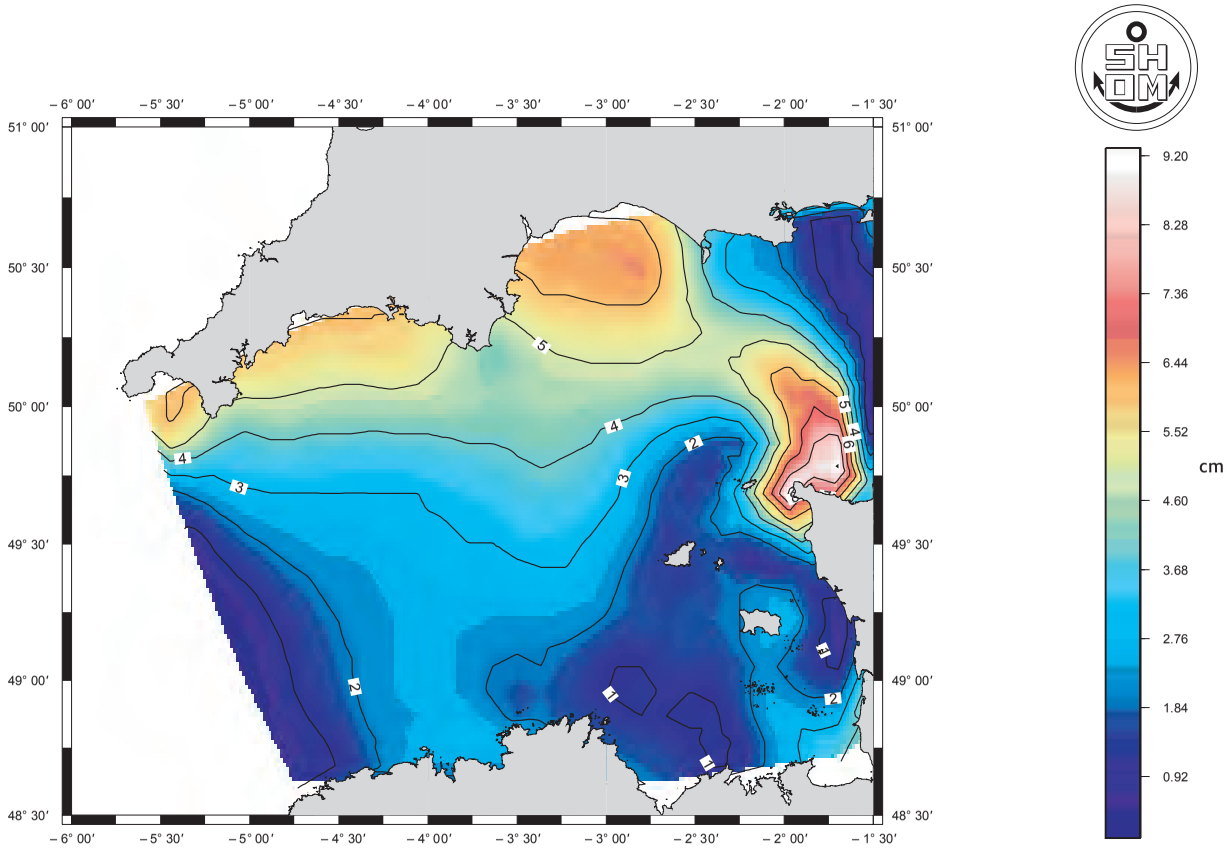

Figure 9.1: Influence of nonlinear effects of tides on the error between the MSS and the geoid (in cm, calculated by Shom using a sounding reduction model).

tion by the so-called conventional method because it almost completely overcomes mean sea level errors.

A complete digital model should make it possible to determine the chart datum relative to the ocean geoid, which is the vertical reference of the model. In practice, however, this is hard to do because it requires a simulation spanning several years while taking the external meteorological and oceanographic effects noted above into account (excluding nonlinear tidal effects that are readily taken into account by models). Moreover, relative differences in the mean sea level and geoid are not clearly defined at the open boundaries of models, thus hampering simulation of induced residual circulation and corresponding height variations.

To be able to apply such models to vast areas using the ocean geoid as benchmark, this geoid must be accurately calibrated in a terrestrial (or spatial) reference frame, and all MSS variations relative to the ocean geoid must be accurately (cm) determined. We are still far from having this knowledge, although progress has been achieved through spatial techniques (including gravimetric analysis) and modelling.

1.5 • Ellipsoid and ITRF

A reference ellipsoid is a mathematical surface defining a geodetic system from relative positions of points located on the Earth's surface. The stability of this reference, like any other geodetic datum, depends on the number and geographical distribution of points that define it and on the range of techniques used to locate these points. The advantage of an ellipsoid is that it is a practical datum, especially for certain satellite techniques, i.e. in altimetry. According to 1991 IUGG and IAG recommendations, the International Terrestrial Reference System (ITRS), from which the International Terrestrial Reference Frame (ITRF) was created, should be used for all applications requiring better than metre accuracy. Although WGS84, the reference coordinate system used by GPS, is more popular, the 1991 recommendations are still relevant because ITRS is implemented from a very dense geographic coverage of several hundreds of points, as compared to around 20 for WGS84, and using different techniques (VLBI, SLR, GPS, Doris), as compared to a single one for WGS84 (GPS). In practice, the results of applying the two systems are quite similar, but ITRS is conceptually independent of the technique and all performance-proven techniques can contribute. Please note that this text is additional to the French but provides a pertinent update. Future advances and new positioning systems (Galileo, etc.) should not be overlooked. Another argument in favour of ITRS (as if another were needed) concerns the fact that it is maintained and improved

by the international community and is therefore independent of organizations and countries but dependent on an internatinal scientific association, i.e. the International Association of Geodesy (IAG), and benefits from its scientific seal of approval.

1.6 • Terrestrial reference frames and levelling

In ports, the chart datum and MSL are represented by their levels relative to benchmarks. These benchmarks are located in the vicinity of the tide gauge, and there are enough marks, and marks spaced far enough apart, to ensure that they could not all be destroyed at once, e.g. during harbour work. The elevations of these benchmarks are ranked with respect to other benchmarks by geodetic levelling and, if possible, tied to the national levelling network. Note that the chart datum is not defined by its level in the national levelling network. The chart datum cannot be put in question by successive levelling operations, which may generate different results because of changes in measurement techniques, as well as vertical (tectonic or seismic) movements of the Earth. Moreover, the tidal load itself may induce vertical movements (periodic, like the tide) of reference frames (e.g. relative to the geoid) of over 20 cm. These movements are not very significant locally for hydrographic applications since they involve movement of the entire seabed, which is naturally accounted for in tide measurements and models, but for some applications these movements have to be taken into account to ensure centimetre accuracy when spatial techniques are used.

2 • Accuracy

There are two aspects to the accuracy concept. A distinction must be made between accuracy resulting from relatively close compliance with the definition (lowest low water), and the accuracy of the level in a reference frame.

There is an arbitrary aspect to the definition of the chart datum, which gives some degree of freedom, as shown by the range of definitions currently in use. Adopting the lowest low water level is basically a facility to enable navigators to readily determine the charted depth that has to be taken into account for tidal purposes, but the accuracy of the chart datum determination relative to the lowest low water is not a crucial criterion, i.e. it may be acceptible that the charted depth is 'approximately' related to the lowest low water, as often noted on navigational charts.

The second aspect of the accuracy concept concerns determining the chart datum. Once adopted, it should be referenced in an accessible stable datum. This is very important because a chart datum must be absolutely stable to qualify as a recognized vertical datum. Levels of coastal tide stations must be determined very carefully with respect to datums so as not to be challenged in successive levelling operations. Millimetre accuracy, which is usually authorized in conventional levelling operations, should be targeted. This extent of accuracy is obviously unnecessary for maritime navigation, but essential for evaluating the datum stability, and especially for some studies on sea level variations.

3 • Accessibility

Access to a vertical datum is the main problem encountered far from coastal tide stations.

3.1 • Conventional method

The surface and seabed are the two immediately accessible surfaces for conventional chart sounding. The seabed can be used, but minimally, to find the chart datum in the vicinity of a tide gauge whose benchmarks have disappeared. In practice, for conventional soundings, the surface is the only accessible reference, which obviously has the drawback of not being stable, so it can only serve as a temporary datum.

The conventional procedure is based on the concordance method (see Chap. VII,2), which models the correspondence between tides at two adjacent points by linear regression. It can also be accomplished with geometric levelling in order to relate the sea level to the tidal heights to known benchmarks that are generally installed on the coast in the vicinity of tide gauges. This involves locating the chart datum relative to the sea surface at the measurement site and time using harmonic constants derived from a tidal model and the lag which is assumed to be constant in the space between the MSL and the intantaneous MSL. An improved procedure, but not implemented in practice (soundings are generally acquired in calm weather), would be to use a model that includes meteorological effects. This would also certainly enhance the accuracy at sites remote from a reference station, e.g. mean instantaneous currents generated by the wind can induce substantial surface slopes (1 cm/10 km is quite common, see 1.4). This reasoning could also apply for density variations, which can be quite marked, especially at river mouths.

Modelling[1] is used to first calculate an instantaneous astronomical tidal height at sounding points relative to the mean sea level.

$$A_S(L, G, t) = \sum_i A_{si} \cos[q_i t - \alpha_{si}(L, G)]$$

It is also used to determine the nominal mean height $N_S(L, G)$ relative to the lowest LW. As this height is constant at a given point, it is calculated initially on the basis of the charted lowest LW relative to the mean sea level, obtained by digital modelling, as exemplified in figure 9.8.

Hence, at the sounding point, we obtain the astronomical tidal height relative to the lowest LW:

$$H_{AS}(L, G, t) = N_S(L, G) + A_S(L, G, t)$$

To determine the surface level relative to the chart datum, this value must be corrected to account for errors in tide prediction due to meteorological and oceanographic effects, and for a potential error between the chart datum and the lowest LW at the nearest reference station. This latter correction is applied to avoid irregularities in the sounding values on charts as the offshore distance from the reference station increases.

δh_R is the tide prediction error at the reference station. This is the error between the measured and predicted tides. Because of the process used to compute the instantaneous MSL, it is also the error between the instantaneous MSL and the MSL and, as noted earlier, this error is assumed to be spatially constant. This correction is thus applied at the sounding point and symbolised by δh.

Otherwise δZ_R is the level of the lowest LW at the reference station relative to the chart datum. A non-zero value is generally the result of a previous (and possibly not very accurate) determination and of a secular change in the MSL. $\delta Z_S(L, G)$, i.e. the hydrographic lowest LW level at a sounding point, is often determined using an agreement in height, which comes to almost the same result when solving:

$$\frac{\delta Z_S}{\delta Z_R} = \frac{N_S}{N_R}$$

where N_R is the MSL relative to the lowest LW at the reference station, or

$$A_R(t) = \sum_i A_{Ri} \cos(q_i t - \alpha_{Ri})$$

1. Le Shom currently (2005) uses the Telemac model, which is described in *Hydrodynamique des écoulements à surface libre (Modélisation numérique avec la méthode des éléments finis)*, Jean-Michel Hervouet, Presses de l'ENPC, 2003.

is the astronomical tidal level at the reference station R, relative to the MSL, and $M_M(t)$ is the height measured at the tide gauge relative to the chart datum.

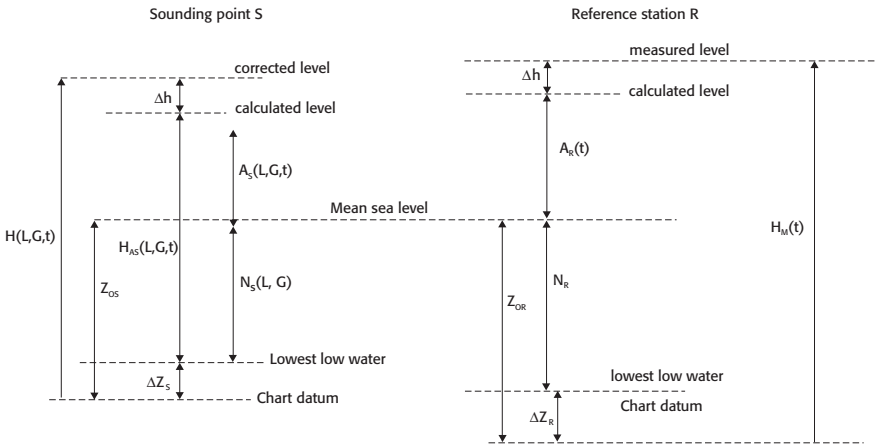

FIGURE 9.2: Conventional sounding correction method.

Based on the notations given in figure 9.2, sounding reduction is done by calculating the sea level $H(L, G, t)$ at the sounding point S by the following equation:

$$H(L, G, t) = H_{AS}(L, G, t) + H_M(t) - [A_R(t) + N_R + \delta Z_R] + \delta Z_R \frac{N_S(L, G)}{N_R}$$

Where S is the sounding measurement (height), the level Z to be indicated on the chart (reduced height) is:

$$Z = S - H(L, G, t)$$

Note that A_S, A_R, N_S, and N_R are related to the mean sea level (MSL), which can thus be considered as a datum. However, the absolute positioning of this datum has little impact on the soundings because the MSL is used to determine the position of the chart datum relative to the lowest astronomical tidal level and to calculate the astronomical tide in R, as well as the effects of lags in S on these levels are almost cancelled out. If MSL is shifted by a magnitude ΔN, the level of the lowest astronomical LW shifts to the same extent, while δz_R is increased by the same quantity and δh, measured in R, varies by $-\Delta N$. In S, the chart datum is shifted by $\Delta N \cdot (N_S/N_R)$. The shift in $H_{AS}(L, G, t)$, thus in the sounding height Z (N.b. δh in S and in R are equal to $-\Delta N$), is thus $\Delta N(N_S - N_R)/N_R$. This lag is negligible if the tidal ranges in R and S are close. However, if these ranges are not close, the

error remains low as long as we do not stray too far from the true values (unknown) and the selected chart datum is close to the lowest astronomical LW, e.g. for $\Delta N = 20$ cm, which is substantial[2], and for a relative variation of $(N_S - N_R)/N_R$ of 10 %, then $\Delta H = 2$ cm, which is acceptible.

A major effect of this practice should be noted, i.e. a potential error between the chart datum and the lowest LW for a reference station may be related to the sounding point. There is no problem if this error is low, but if it is high difficulties could arise when there is a change of reference station. SHOM has thus set up 'tide zones' for the main coastal ports of France. Another problem concerns the possible remoteness from the reference station, which may markedly reduce the accuracy of the method in correcting meteorological and oceanographic effects relative to δh.

The procedure could be improved by using tide pressure gauges that are set on the seabed in the sounding area. If a month of tidal observations are available, the so-called species concordance method can be used to obtain an astronomical tide that is accurate enough for this offshore sounding point to serve as a reference station and thus, because of its nearness, to obtain a better correction for meteorological and oceanographic effects. First, however, it is necessary to determine the chart datum at the sounding point relative to the instrumental datum of the submerged tide gauge.

As the above-described method enables determination of the chart datum relative to the MSL, its level must be determined with respect to the instrumental datum. This is done by using an approximation of the parallelism of various mean surfaces between the reference station and the submerged tide gauge. This is better verified for an MSL calculated over a defined time period than for an instantaneous MSL (there may be bias that is undetectable over this period). Submerged tide gauges also make it possible to ensure the validity of the tide model used. Once the instrumental MSL of a submerged tide gauge is calculated during the sampling period, it is corrected for the error between the MSL during the same period and the MSL of the reference station.

The use of submerged tide gauges therefore does not overcome the need for tidal observations at reference stations. They do not solve the problem of tidal zones, but they do partially offset the meteorological and oceanographic effects.

2. The low relative variations in MSL for close by ports in relation to the terrestrial geoid (a few centimetres) confirms that achieving only a 20 cm error is very unlikely, especially since many of these levels were determined for very different periods.

3.2 • Spatial techniques

Spatial techniques offer a different solution to the sounding reduction problem.

First, it is now possible to accurately determine the level of the seabed in a terrestrial reference frame without considering the sea level, and therefore without using a tidal model. This means that it is an absolute and permanent determination, which is a key advantage of using spatial techniques. This determination currently cannot be performed in real time in a global reference frame (e.g. ITRS) but, when located in the in the vicinity of an on-land reference station, it is possible to make an accurate determination relative to this station.

For accuracy, seabed movements also have to be taken into account. These movements can be considered as identical within an area of a few tens of kilometers for Earth tides, but not for seabed movements induced by oceanic loading, for which gradients of around 1 cm/10 km have already been noted[3]. Contrary to the conventional method where the tidal model (calibrated on the basis of measurements along the coast and offshore, which encompass movements on the sea surface as well as seabed movements) also compensates for seabed movements, the spatial method, even in some small areas, must take these into account to remain accurate.

It is also possible to accurately position the mean sea surface (MSS) obtained by altimetry in a geodetic reference frame (ellipsoid). Satisfactory results have already been obtained with *Topex-Poseidon* data, and further progress should be possible with *Jason* altimetry. The accuracy degrades in the vicinity of coasts because of the low resolution (10 km) and unaccounted for consideration of land masses in the computations. However, it is possible to overcome these drawbacks by benefitting from tidal measurements obtained in these coastal areas and pegging them to an accurate geodetic datum. As for the conventional method, the chart datum should also be determined in current local reference frames (tidal zones) on the basis of the MSL. This involves correcting the MSS for errors between the calculated MSL of the reference tide gauge during the altimetric sampling period and MSL and applying the tide modelling correctors in order to position the chart datum at all points in the tidal zone. The ellipsoidal height of chart datum is deduced from the known ellipsoidal height of the MSS. The baseline datum is always the chart datum of the reference station.

3. cf. *La surcharge océanique*, by Françoise Duquenne, ESGT, January 2001.

Note that, at the current state of the knowledge and as mentioned with respect to the conventional method, the tidal model used should be calibrated relative to data on sea surface and seabed movement so as to guarantee the sounding accuracy. This is the simplest method. For maximum accuracy, all surface and seabed movements must be modelled by taking all the effects into account: astronomical tides, meteorological and oceanographic conditions.

It could be quite possible to achieve continuous determination of the chart datum over broad surface areas by increasing the measurement and modelling accuracy. However, we are obliged to work in the current cartographic reference frame, which is based on tidal zones. All charts would have to be updated to have a continuous chart datum, but this task would likely take decades to achieve because it is very complex and no hydrographic service has sufficient resources to be able to conduct a substantially quicker update.

Based on the notations in figure 9.3: E_{MSS} = MSS ellipsoidal level determined by altimetry. The problem is to determine the seabed ellipsoidal level E_F (one of the IHO recommendations), as well as the depth of the seabed below chart datum Z.

On the basis of figure 9.3, the following results can be readily obtained:

$$E_F = E_{GPS} - S$$

$$Z = E_{MSS} - E_F - (\delta Z_S + N_S + \delta N_S)$$

E_{GPS}, S and E_{MSS} are measured values. Figure 9.5 gives an example of E_{MSS} values for French coastal regions obtained from *Topex-Poseidon* altimetry data.

One key advantage of this method is that the sea surface height in a terrestrial reference frame is not part (even implicitly) of the previous equation, thus eliminating problems associated with tide forecasting (except with respect to determination of the lowest LW and substantial seabed movements) and with meteorological and oceanographic effects.

As noted in the previous chapter, δZ_S is obtained by the following equation:

$$\delta Z_S = \delta Z_R \frac{N_S}{N_R}$$

N_S and N_R are obtained using harmonic constants derived from marine tidal models and observations at the reference station. Figure 9.8 gives an example for the Channel. δN_S is the difference between the MSL and MSS at the sounding point. With the mean surfaces being approximately parallel to one another, then $\delta N_S = \delta N_R$ where δN_R, at the reference station, is the error between the mean sea level calculated from observations covering the period

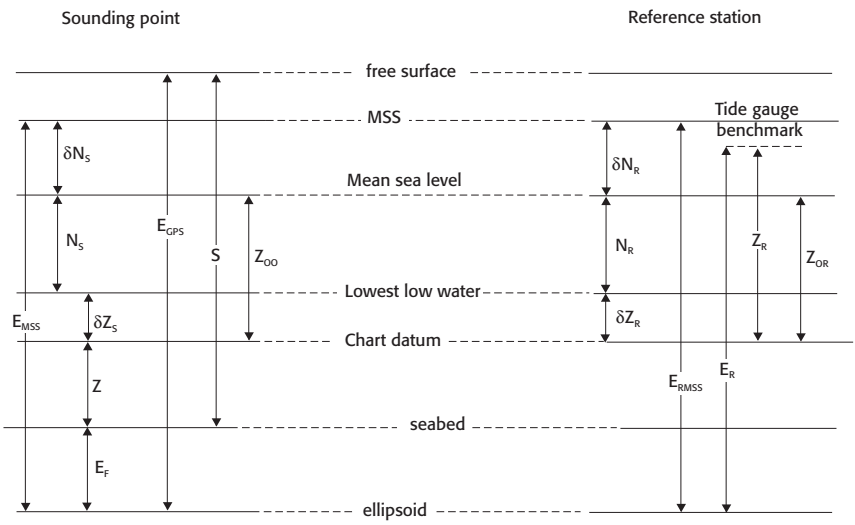

FIGURE 9.3: Sounding correction–spatial technique.
δN_S: difference between the MSL and MSS at the sounding point
N_S: MSL relative to the lowest LW at the sounding point
δZ_S: lowest LW level below chart datum at the sounding point
Z: seabed depth below chart datum at the sounding point
E_F: seabed ellipsoidal level
E_{GPS}: sea surface ellipsoidal level as measured by GPS
S: depth measured by the depth finder
δN_R: difference beween the MSL and MSS at the reference station
N_R: MSL relative to the lowest LW at the reference station
δZ_R: lowest LW level below chart datum at the reference station
E_{RMSS}: MSS ellipsoidal level at the reference station
E_R: tide gauge benchmark ellipsoidal level
Z_R: tide gauge benchmark level below chart datum
Z_{00}: MSL below chart datum.

from which the MSS was determined, and the MSL. All elements included in the equation for determining Z are thus available.

There is still one problem due to the inaccuracy of altimetric measurements close to coasts, but it can be overcome by also using accurate tide station geodetic measurements, thus offering the possibility of interpolation. Because of this inaccuracy, for instance, the E_{RMSS} ellipsoidal level at the reference station cannot be obtained by altimetry, but the tide gauge benchmark ellipsoidal level E_R can be determined via geodetic measurements obtained at the tide station, and then the following equation may be applied:

$$E_{RMSS} = E_R - Z_R + \delta Z_R + N_R + \delta N_R$$

4 • Stability

The question that comes to mind when considering the stability of benchmarks is, 'stability relative to what'? The answer generally depends on the problem at hand. Concerning stability in hydrographical applications, although there may be some differences in sounding values, they cannot be questioned since they may be the result of changes made to the reference level. This applies especially to the stability of physical benchmarks whose level relative to the chart datum is accurately established.

We have seen earlier that excellent accuracy in determining the lowest low water is not essential, but once it is set, the chart datum defines it very precisely and (excluding an unusual accidental event) definitively, independently of a subsequent and potentially more accurate determination of the lowest low water. It is important that a more permanent charting be carried out to avoid successive subsequent determinations. However, this stability rule is often disobeyed with the seemingly commendable aim of improving the accuracy.

To ensure datum stability, the lowest astronomical tide level should not be calculated when new observations are obtained, but should rather be determined via permanent global charting, even though it can be determined through harmonic constants. However, this rule is seldom respected due to the lack of confidence in the quality of models, and especially since it is generally acknowledged that this quality is rapidly improving with advances in computation methods. There is also a problem of compatibility with neighbouring countries. Ideally, a common model should be adopted, but attempts in this direction by the Tidal Working Group of the North Sea Hydrographic Commission revealed the many stumbling blocks in the way to reaching a trade off. Meanwhile, the best short- to medium-term option would likely be to make adjustments at the boundaries of areas of responsibility. The lowest astronomical tide level is charted relative to the mean modelled level which, as noted previously and within the true value range, has little impact on harmonic constants (which are used to calculate the lowest astronomical tide level).

4.1 • Conventional methods

Through conventional chart datum positioning procedures, the mean sea level (MSL) has taken on the status of vertical datum. For its offshore accessibility, a model is used to calculate its level relative to the sea surface at the place and at the sounding time (based on the assumption that δh is spatially constant at the sounding time).

The stability of the MSL as vertical datum does not concern the accuracy of its level relative to the sea level (which actually reflects the extent of sounding reduction uncertainty), but instead concerns the relevance of the choice of this reference surface for solving sounding reduction problems. Note first that tide gauge benchmarks serve as vertical datums for coastal tide stations. This is suitable because potential vertical movements are likely to closely match those affecting nearby coastal areas. This also applies to the MSL whose level relative to coastal benchmarks is constant.

Note, however, that due to reduction procedures, potential tide gauge vertical movements have an impact on the stability of the vertical datum at remote points where vertical seabed movements may not be identical to those of the tide gauge. This problem can only be properly solved by taking the geodetic positioning of coastal tide gauges around the sounding area into account and by modelling potential movements offshore and on land. Finally, when submerged tide gauges are used, another stability problem concerns a possible slow change in the mean slope of the water column between the sounding area and the reference station, which is not detected during the sampling period. Future systems (as a follow up to ongoing research) for coastal modelling of combined meteorological and oceanographic impacts should make it possible to quantify this slope.

Chart sounding correction is the only issue dealt with here, but it should be kept in mind that the ultimate goal is to fulfil navigators' needs since they usually only have access to tidal predictions relative to the MSL not to the instantaneous MSL. Using the so-called 'inverse barometer correction' recommended in tide tables makes it possible to improve the accuracy, but it would be better to have access to the δh value (difference between the instantaneous MSL and the MSL) measured by the tide gauge, as carried out by pilotage services in certain ports.

4.2 • Spatial techniques

As demonstrated above with respect to spatial geodetic datums, ITRS is preferred over WGS 84 due to the enhanced reference ellipsoid stability. To establish the chart datum, it is still necessary to have access to a local MSL (extended via the MSS, and translated to fit the MSL at the reference station), as long as current tidal zones apply, and the MSS (determined over a long and well chosen period) when a general continuous chart datum comes into effect. However the MSL is now losing its datum status because the lowest low water – after having been situated within the ellipsoidal reference frame – acquires the status of chart datum with a permanently set ellipsoidal

height, thus overcoming the datum stability problem. Then the question of the validity of the selected ellipsoidal datum arises because, contrary to the MSL which is based on benchmarks, ellipsoid datums are unaffected by potential vertical benchmark movements, which in turn can bias the sounding values. When possible, a geodetic survey of nearby vertical tide gauge benchmark movements (which should be accounted for in different ITRS operations) should be undertaken, while also modelling seabed movements, when this technique is adopted.

5 • Conclusion: modelling implementation recommendations

Chart sounding reduction problems arise mainly when coastal tide stations are not nearby. Tide modelling is necessary in this case. Modelling helps to situate the chart datum within an on-land reference frame. Once this datum is fixed, other techniques can be used to determine tidal heights, e.g. kinematic GPS (with its accurate ephemeris) or other more specific models.

In the vicinity of tide gauges, the chart datum relative to benchmarks is seldom challenged, even after a potentially more accurate determination of the lowest low water. This avoids having to add the uncertainty concerning the datum position to the tidal height uncertainty (relative to benchmarks). Offshore, depending on the technique used, the mean sea level or ellipsoid are fundamental reference levels. For the same reason as put forward with respect to establishing the chart datum of coastal tide stations, the zero mark should be permanently set relative to these datums. The problem is presented in this way because of the current performaces of digital models, i.e. it is possible to determine the lowest low water accurately enough to define the chart datum. Hence, the question arises as to the performance required to be able to use the model for this purpose.

Determination of the chart datum also obviously depends on its definition, i.e. normally the lowest astronomical tide level. There are two options:

- either the model provides the low water level for various spring tide situations and the lowest low water is extrapolated
- or the model provides harmonic constants to enable calculation of the extreme lowest low water.

These two solutions are not equivalent because, for the first option, the lowest low water related to the model datum, i.e. a geoid if a mathematical model is involved, while the harmonic equation is the reference for the latter option, i.e. the mean sea level.

Note: as discussed in section 1.4, variations in harmonic constants as a function of variations in the mean sea level are insignificant in practice, so it is not possible to have access to an accurately determined mean sea level.

The second option is the only applicable approach nowadays because extrapolations are sometimes risky, the marine geoid is not very accurately determined and meteorological and oceanographic effects have yet to be sufficiently accurately modelled.

It is not necessary to know the exact 'true' mean sea level when determining the reduction by the conventional method. Moreover, computations by the spatial method can be based on absolute MSS measurements (models of meteorological and oceangographic effects can help in solving interpolation problems in the vicinity of coasts, while also enhancing MSS validation).

Previous experience with modelling tides in the Channel indicates the type of information that can be obtained via such techniques, i.e. harmonic constants can be calculated from a standard list at each of the 25 000 (approx.) grid points of the model based on 1-year tidal simulations. These constants are corrected so as to closely correspond to already established constants, according to their degrees of confidence.

The lowest astronomical tides are calculated for each grid point of the model using the harmonic method.

The level of accuracy that may be achieved by this technique is around 1% of the tidal range. This magnitude seems reasonable and should be adopted as the standard, based on the following rule: if the lowest low water cannot be determined closer than N cm (typical value: 10 cm), the chart datum will be lowered to a level that (considering the extent of uncertainty in its determination) is at least as low as the lowest astronomical tide. The mean sea level is generally rising along the French coasts, so the safety margin cannot be any broader.

6 • Methods

In this chapter, we only describe the principles of the chart sounding reduction methods, since their practical use is described in hydrography manuals.

6.1 • Cotidal range charts

Figure 9.4 shows a chart that can be used for offshore sounding correction, with a grid of lines of equal high water ranges and times in the Channel. This type of chart is used in addition to tidal observations in reference stations. Where K(L, G) represents the ratio of ranges on the tidal chart

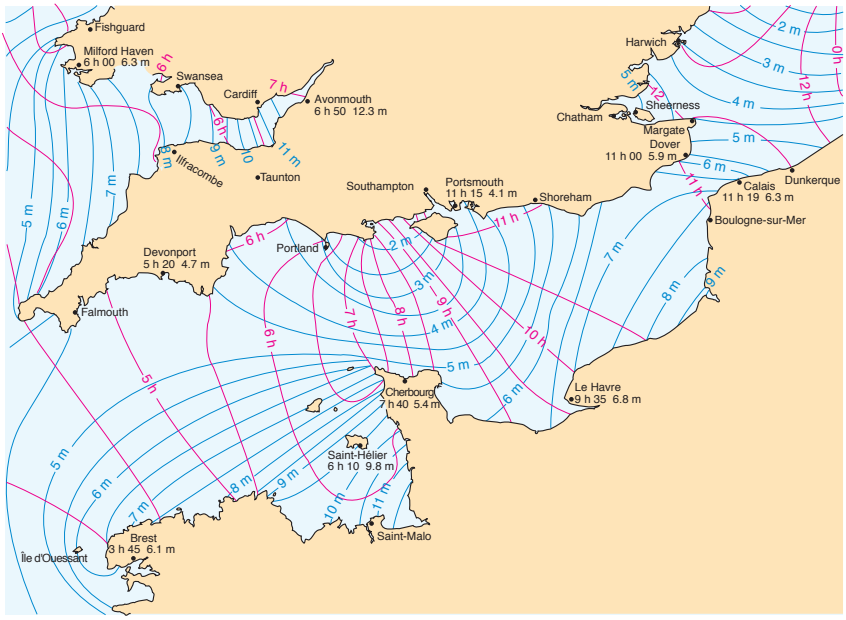

Figure 9.4: Cotidal chart for the English Channel. Blue co-range lines run between points of equivalent tidal ranges (spring tide here), while red co-time lines run between points where high waters are reached at the same time.

at point (L, G) and at the reference station, and $\theta(L, G)$ is the lag, which is also deduced from reading the chart. The method involves applying the following equation:

$$h(t, L, G) = K(L, G)[h_R(t - \theta(L, G))] + C(L, G)$$

C(L, G) is a constant lag when the sounding datums are all in agreement (see Chap. VII, § 2.1). It is zero if they are in agreement with the chart datum of the reference station.

This process is based on the assumption that tides are similar at all points in the sounding area, so it cannot be applied in areas far from the reference station where there may be substantial nonlinear effects. The method is improved by using different cotidal range charts, e.g. a mean spring tide chart and a mean neap tide chart. Better results can also be obtained when tidal stations are located close to the sounding area.

One drawback of this method is that it requires slow and tedious manual processes, and the results are not always sufficiently accurate, especially for sounding in shallow areas with a substantial tidal fall.

6.2 • Harmonic method

The harmonic method tailored for sounding reduction involves applying the following equation:

$$h(t, \mathrm{L}, \mathrm{G}) = \mathrm{NM}(\mathrm{L}, \mathrm{G}) + \sum_{i=1}^{i=\mathrm{N}} h_i(\mathrm{L}, \mathrm{G}) \cos[\mathrm{V}_i(t) - \mathrm{G}_i(\mathrm{L}, \mathrm{G})]$$

$h_i(\mathrm{L}, \mathrm{G})$ $\mathrm{G}_i(\mathrm{L}, \mathrm{G})$	harmonic constants
$\mathrm{Z}_0(\mathrm{L}, \mathrm{G})$	mean sea level
$\mathrm{V}_i(t)$	astronomical argument
N	number of harmonic constituents

The problem is thus to determine the harmonic constants for all points.

Two methods are used: having a sufficiently dense network of tidal stations in the area and, when possible, calculating the constants for all points simply by spatial interpolation; or modelling the area so as to be able to calculate the constants for all points.

6.2.1 • Spatial interpolation

Figure 9.5 shows tide recording points along the coasts of France. Most offshore recording points do not store more than a month of tidal records. However, it is possible to take full advantage of these data by using the species concordance method based on harmonic constants and simultaneous observations from the nearest reference station. Considering the spatial variability in the constants, the density of recording points is generally considered to be suitable enough to, by interpolation, generate the harmonic constants required for accurate astronomical tide calculation. Figure 9.7 shows the results obtained by this method for the M_2 wave.

6.2.2 • Modelling

Dealing with the problem from a strictly physical standpoint, whereby hydrodynamic equations are solved directly in a tidal wave propagation environment, is not a new concept. However, it was not until the advent of high-performance computers that it could be applied in practice. It involves dividing the domain into geometrically simple elements called grids, and then applying the following basic principles to them:

• the conservation principle, whereby water height variations in a grid are the result of the difference between the quantity of water entering the

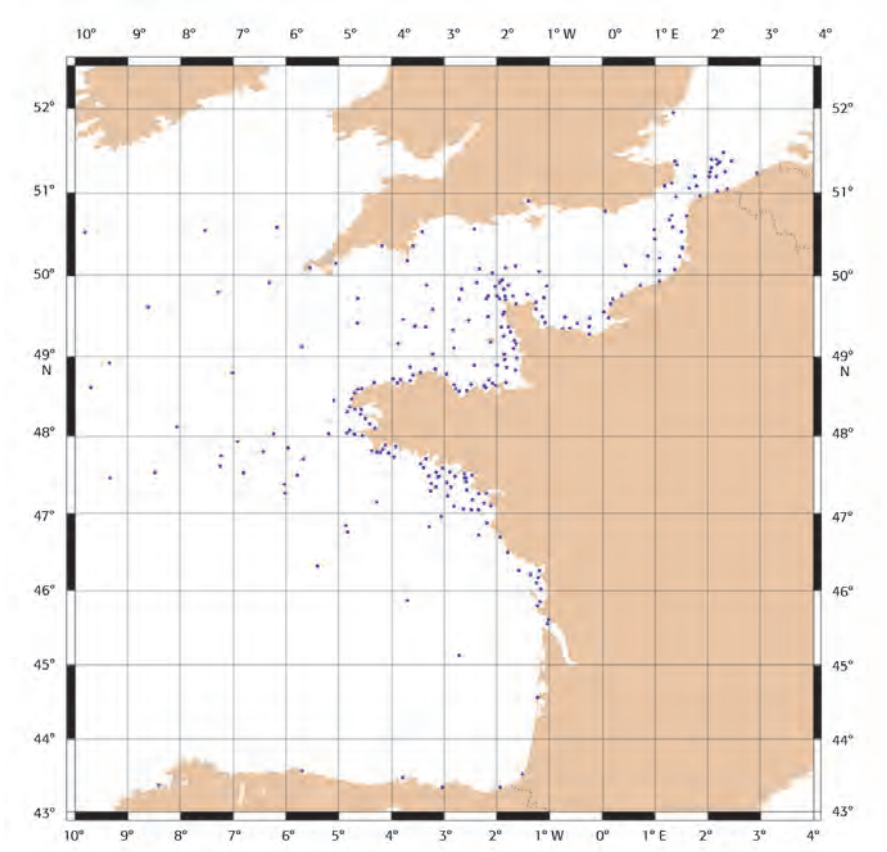

Figure 9.5: Position of tide recording points.

grid and that which exits through the sides. This difference depends only on currents passing through the grid

- the fundamental principle of dynamics, whereby current velocity variations in a grid depend on external forces affecting a continuous water column in the grid. There are three types of such forces:
  - — pressure forces due to differences in water height in neighbouring grids
  - — Coriolis forces due to the Earth's rotation which tend, in the Northern Hemisphere, to deflect the current to the right
  - — braking forces, similar to friction, which affect movement near the grid bottom and walls.

The result of applying these principles is that water height and current velocity variations in a grid depend on the water heights and currents in

neighbouring grids. All grids are interdependent, so the problem of height and current variations should be solved globally in the entire study domain.

Movements cannot occur, however, unless there is a driving force, i.e. the tide at the model open boundaries, i.e. where there is no coastline. This imposed movement propagates between grids throughout the domain.

Calculations are done at regular intervals, or so-called time steps, starting from a steady state. The results can only be used after a stabilization period which, in practice, corresponds to two to three tidal cycles.

In practice, grids are square, rectangular or triangular. The choice of grid size is crucial, i.e. the smaller it is, the higher the resolution and thus the higher the accuracy in the results. On the other hand, the smaller the grids, the more numerous they are within a given domain.

The time step is not independent of the grid size, i.e. digital instability may occur when the time step is too long. A reduction in the grid size can thus considerably increase the computation time, so a reasonable trade off is generally sought.

Depth information is another major restriction. It would be unreasonable to wish to enhance the resolution of a model if the description of the environment is not done on an equivalent scale. From this standpoint, navigational charts do not supply bathymetric information suitable for hydrodynamic modelling. This depends on the choice of depth finders, whose main function is to generate information useful for navigational safety. Information density is often sacrificed to enhance the clarity of the charts, while highlighting topographical features that could be dangerous for navigation, which may distort the seabed representation.

Figure 9.6 shows an example of a grid used for modelling tides in the western Channel region.

It should be noted that despite the progress achieved through high-performance computers, the level of accuracy obtained by digital models is not sufficient to meet chart sounding reduction needs. The results often have to be fitted to the observation data. Marked progress should be achieved in this field through assimilation techniques.

The theoretical tide at all grid points can be readily determined through 1-year tidal simulations, followed by calculation of harmonic constants at all grid points.

Figure 9.7 provides an example of results obtained for the M_2 wave in the Channel. Charts on the left represent situations in degrees (relative in reference to Universal Time), while those on the right show tidal ranges (in cm). The top charts were obtained by simulation, the middle charts represent interpolations, while those on the bottom are the result of a model fit.

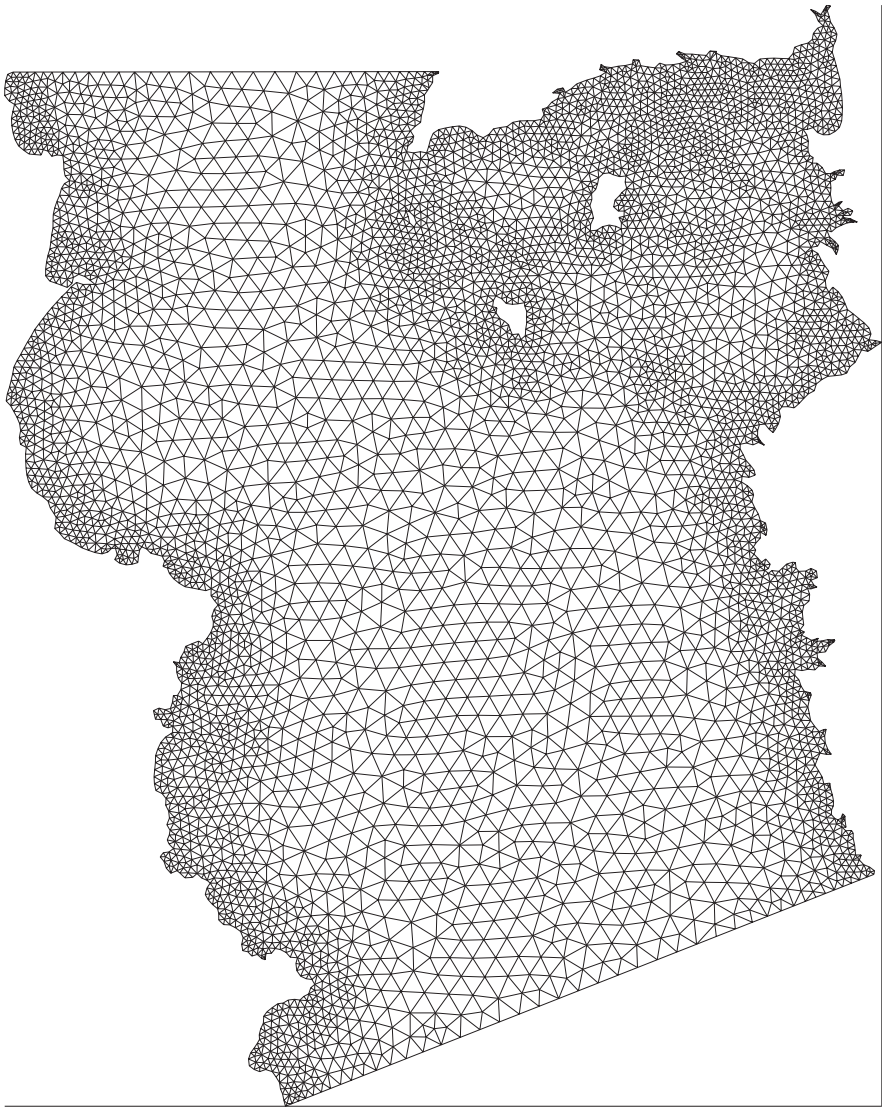

Figure 9.6: Western Channel grid. This so-called finite elements grid can improve computations where necessary.

All harmonic constituents that are usually calculated for a year can be obtained in this way.

6.2.3 • Mean sea level

$Z_0(L, G)$ is the mean sea level (MSL) as discussed earlier (see 1.3). It depends on the datum, which is theoretically the lowest low water but actu-

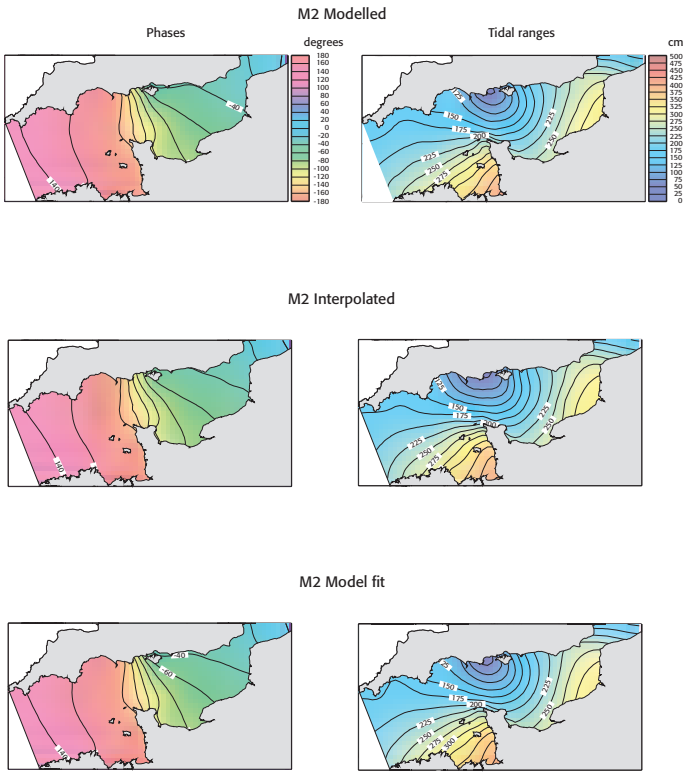

FIGURE 9.7: Modelling the M2 wave in the Channel.

ally a level close to this. In order to adopt a datum in line with that of the reference station, at the sounding point, the difference δZ between the lowest low water and the chart datum of the reference station is carried forward to the sounding point. One way of doing this is to apply the harmonic equation for the lowest theoretical tide time, i.e. $t_{bm}(\mathrm{L},\mathrm{G})$ at the sounding point and $t_{bm}(\mathrm{L_R},\mathrm{G_R})$ at the reference station.

$$
\begin{aligned}
&z_0(\mathrm{L},\mathrm{G}) \\
&= \underbrace{z_0(\mathrm{L_R},\mathrm{G_R}) + \sum_{i=1}^{i=\mathrm{N}} \mathrm{A}_i(\mathrm{L_R},\mathrm{G_R}) \cos\left\{\mathrm{V}_i[t_{bm}(\mathrm{L_R},\mathrm{G_R}) - \mathrm{G}_i(\mathrm{L_R},\mathrm{G_R})]\right\}}_{\delta z} \\
&\qquad - \sum_{i=1}^{i=\mathrm{N}} \mathrm{A}_i(\mathrm{L},\mathrm{G}) \cos\{\mathrm{V}_i[t_{bm}(\mathrm{L},\mathrm{G}) - \mathrm{G}_i(\mathrm{L},\mathrm{G})]\}
\end{aligned}
$$

A 19-year tidal prediction is often used to determine the time of the lowest theoretical tide. This method is not accurate because, contrary to common opinion, the lunar node rotation period is not the tidal period. Rather than looking for the time of the minimum tide, it would be preferable to determine the value of the astronomical parameters corresponding to this minimum using the method described in Chapter VIII, 2.

$$z_0(\mathrm{L},\mathrm{G}) = \underbrace{z_0(\mathrm{L_R},\mathrm{G_R}) + \sum_{i=1}^{i=\mathrm{N}} \mathrm{A}_i(\mathrm{L_R},\mathrm{G_R}) \cos\{\mathrm{V}_{imin}(\mathrm{L_R},\mathrm{G_R}) - \mathrm{G}_i(\mathrm{L_R},\mathrm{G_R})\}}_{\delta z} - \sum_{i=1}^{i=\mathrm{N}} \mathrm{A}_i(\mathrm{L},\mathrm{G}) \cos\{\mathrm{V}_{imin}(\mathrm{L},\mathrm{G})\}$$

6.2.4 • Tide prediction errors

Meteorological conditions can cause marked differences between the theoretical tide and the true tidal height. Since no model is available to estimate this error, the method used involves carrying forward errors measured at the reference station to the sounding point. Obviously, by this method, the results obtained for sounding points far from the reference station may not be very accurate. This problem can be quite effectively overcome by using tide pressure gauges. They are submerged in the sounding area for long enough to calculate reliable harmonic constants, and can be used as intermediary reference stations to obtain more reliable estimations of tidal prediction error corrections to be applied.

Figure 9.2 illustrates how procedures for computing the mean sea level and tidal prediction error corrections are applied. It implies that the chart datum correction and the tidal prediction error correction are included in the same operation. This apparent simplification gives rise to a fundamental problem of stability of the vertical reference since a potentially variable water column slope between the reference station and the sounding point is reflected in the mean sea level.

7 • Digital models and spatial techniques

The conventional methods described in the previous chapters are not fully satisfactory. There are some practical drawbacks (setting up tide gauges), along with other more fundamental drawbacks concerning the accuracy of the results. Particularly, the fact that the chart datum is determined for each

point according to the measured data raises a question as to the permanence of the datum.

7.1 • Digital models

A very important hydrological application of digital modelling concerns charting of the lowest low water relative to the MSL, as exemplified in figure 9.8.

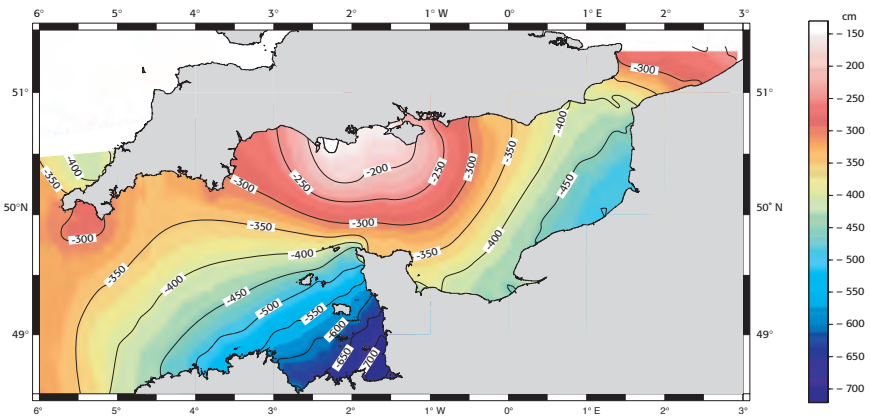

FIGURE 9.8: Lowest low water relative to the mean sea level.

Even the most complex digital model is not perfect, but the inaccuracy can be acceptable if it is calculated and disseminated. This type of charting can then be used to set the chart datum zero mark and thus ensure its appropriate stability. The mean sea level (see 1.3) is then implicitely the fundamental datum. The fact that the tidal prediction error correction is independent of the chart datum determination is a major advance with respect to conventional methods, for which the zero mark inaccuracy is part of the error budget.

7.2 • Spatial techniques: kinematic GPS and the mean sea surface

Research to take advantage of the possibilities offered by spatial techniques has facilitated the development of new chart sounding correction techniques. Kinematic GPS can be used to measure height in the ITRS (with 10 cm accuracy) on a moving platform, which is in line with standards required for bathymetric surveys. Moreover, spatial altimetry provides the mean sea surface (MSS), which can also be referenced to the ITRS (figure 9.9). When the the chart datum is determined relative to the mean sea

level through hydrodynamic modelling (figure 9.8), it is possible to position the chart datum in the ITRS (figure 9.10), and thus determine the position of the moving platform relative to the chart datum. Once this principle is established, a few implementation problems arise, mainly due to the inaccuracy of the MSS close to the coast. The best is to take the geodetic position of the tide gauges into account so as to facilitate interpolation.

Various studies have confirmed the validity of this approach, while highlighting the progress that could be expected in improving the MSS and in setting up tide stations so as to bridge certain gaps.

Note however that high accuracy is not required when positioning the chart datum in the ITRS. It just has to be situated in the vicinity of the lowest low water, but it is important that:

- this datum be jointly used in tide tables and navigational charts
- its level cannot be changed once it is set.

These techniques have been perfected and represent substantial progress, but they can only be gradually adopted for operational applications because of the need to develop complex digital models, to gain skills in operating the appropriate equipment, and to encourage changes in fixed habits.

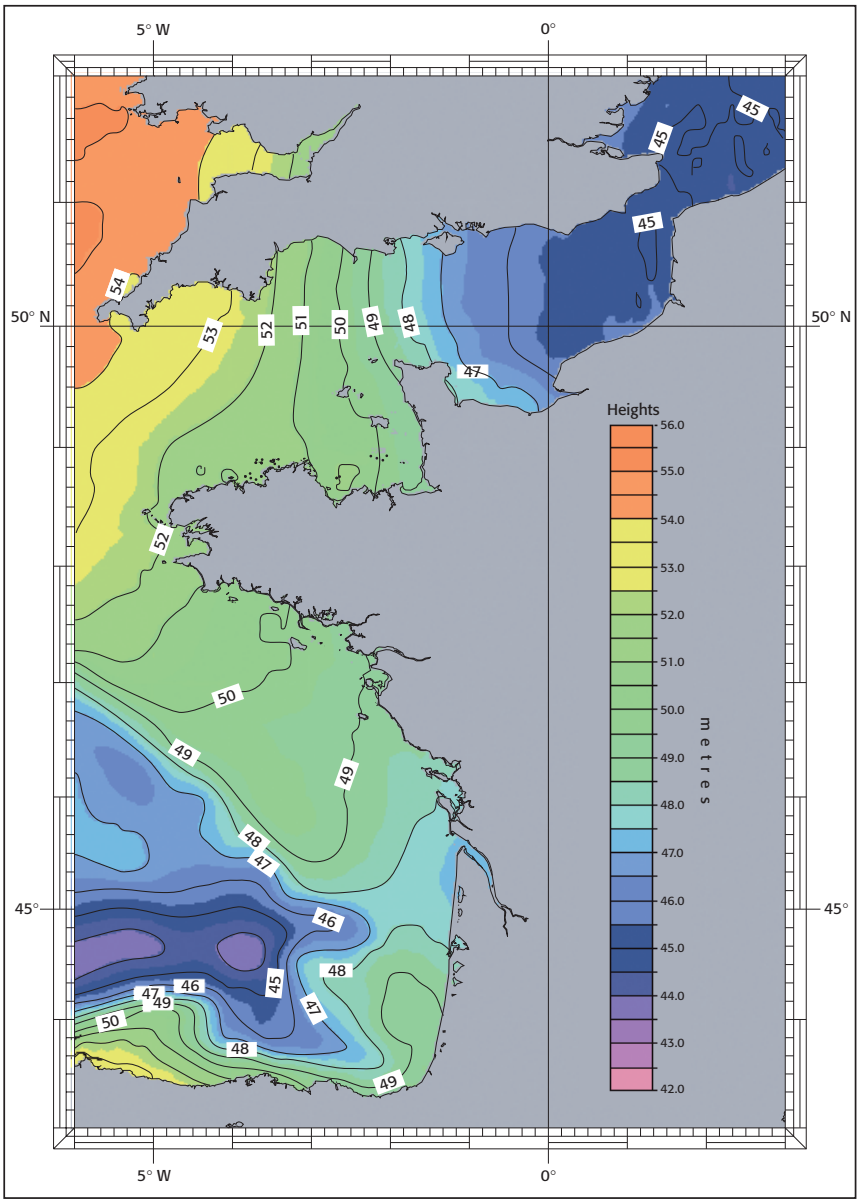

FIGURE 9.9: Mean sea surface obtained by spatial altimetry and referenced to the IRTS.

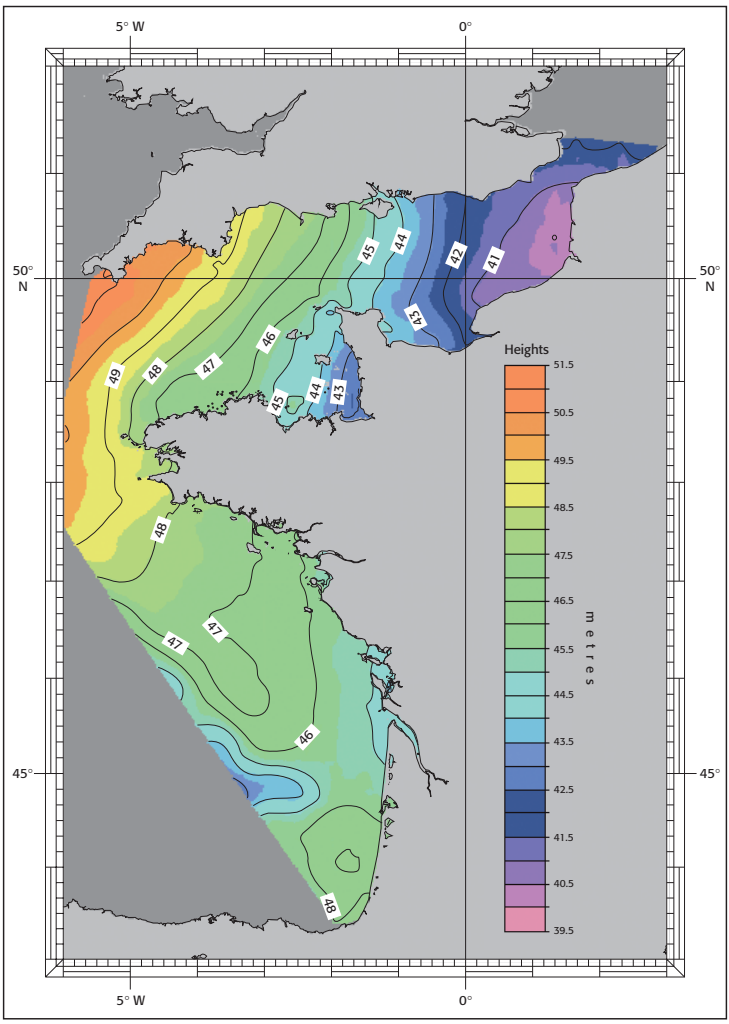

Figure 9.10: Lowest low water referenced to the ITRS.

X

Tidal streams

Some water movements in ocean coastal regions have the same frequencies as constituents of the tide-generating potential. They are called tidal streams. Note however that, like the tidal height, these streams have two distinct origins:

- so-called 'gravitational' tidal streams: these are derived from the tide-generating force, which is mainly caused by Newtonian attraction
- so-called 'radiational' currents: these are the result of the effects of solar radiation on daily or seasonal cycles through all ocean-atmosphere interactions (pressure field, wind conditions, density of the sea surface layers).

1 • General features

Here we have limited the study of tidal streams to coastal regions based, in principle, on the assumption that the water density is identical from the surface to the seabed. It is also assumed that the stream velocity is constant throughout the water column, except in the layer at the sea bed where friction reduces the velocity. Note also that the issue of internal waves with the same frequency as the tides is not covered in this manual.

1.1 • Radiational currents

These currents can be subdivided into three principal constituents:

- a 'permanent' constituent resulting from the mean distribution of meteorological and oceanic systems on the Earth's surface; this permanence is relative as it is based on a mean that depends on the measurement period

• a periodic constituent due to the succession of seasons, which can be interpreted as a cyclic modulation (of solar origin) of the permanent constituent

• a more or less random but sometimes predictable (via observations and models) nonperiodic constituent that is driven by meteorological events or ocean dynamics (topographic Rossby waves).

Ocean currents are weak in the vicinity of coasts. However, those influenced by bathymetric features (straits and oceanic channels) can be as strong as 5 knots, for example the Gulf Stream between Florida and the Bahama Grand Banks. In this tidal manual, these residual currents are just mentioned for the record. Note simply that they impact tidal stream measurements (as they seldom last more than a few months) by fluctuations with sometimes substantial residual constituents, and several ocean dynamics processes must be considered in the interpretation. In the absence of other information, it is difficult to determine whether a measured residual current is permanent, due to a seasonal variations or to temporary meteorological and oceanographic effects. The wind especially has a marked local effect. It accounts for around 3% of the current velocity and, a few kilometres from the coast in the presence of a seasonal thermocline, produces so-called inertial currents whose period is a function of the latitude L and equal to $T_{In} = 12/\sin L$ sidereal hours. The wind action induces considerable noise which, considering the short duration of measurements that are generally available, can considerably hamper detection of tidal constituents on the continental plate (e.g. in the North Sea).

1.2 • Tidal streams

The velocity of tidal streams is often extreme and sometimes very high near coasts, i.e. 10 knots or more in some areas with a marked tidal range and very rough seabed. This tidal phenomenon has a clearly identified gravitiational origin and is caused by variations in the tide-generating force due to relative motions of the Earth, Moon and Sun.

This action of celestial bodies can be identified and analysed according to current measurements recorded at one place over a sufficiently long period (at least 15 days). Since the causes always generate the same effects, and based on knowledge of celestial body movements, tidal streams can be calculated and predicted from the results of this analysis. For a long time, many documents on tidal streams for navigators focused on this technique, and it is still the main source of information for tidal stream tables on navigational charts.

However, for this procedure, good quality measurements are required over a sufficiently long period to be able to identify and eliminate meteorological effects and evaluate the gravitational constituents as accurately as possible. It is often hard and costly to acquire such measurements in places of interest for marine navigation, such as navigation channels or zones with strong currents. Current meters are expensive, hard to anchor and recover, so the write-off rate is often high. Hence there are often not enough measurement data or tidal stream sampling points, and there is little hope that this situation will improve in the immediate future at the present tidal stream monitoring rate.

1.3 • Tidal stream measurements and use

Navigators nevertheless had to rely on this source of information for a very long time. Past publications pooled knowledge gained over the years, often conveyed by navigators. This knowledge is presented in the form of texts describing tidal stream flow patterns in specific areas, and charts on which these streams are indicated by arrows. This information is mainly qualitative but still valuable, and most of it has been reviewed in recent publications.

The oldest known book published on tidal streams is the *Thresoor der Zeevaert* ('Treasure of Navigation'), which was published in 1590 by Lucas Waghenaër, marine pilot for the town of Enchuysen. According to Keller (in a document on tidal stream flow patterns, 1855), "this remarkable book, which is much better than anything present day pilots would be capable of writing", must have been written at a time then there was Spanish shipping in the region because of the Spanish rule over Holland.

Halley's work on tidal streams in the Channel was of high quality for the time (18th century), but not popular amongst navigators. No further studies were published until around 1830, when observations from previous centuries had been completely forgotten. Since no instruments were available for recording tidal stream measurements, these works were based mainly on the analysis of slack water patterns relative to reference station high waters.

Thereafter, especially as of the end of the 19th century, various types of instruments were used. These were generally equipped with a compass and a propeller-driven revolution counter, e.g. the device of E. Mayer (1877) for which the revolution counter was blocked at the end of the measurement by a messenger dispatched along the cable supporting the current meter. The best known and most commonly used instrument is that developed by Ekman in 1932. Two messengers dispatched along the support cable controlled the

beginning and end of the measurement, while the measurement duration was determined by a timer. This instrument included a stock of small metal beads that were released every 33 propeller turns and channelled by a small trough supported by the compass. These metal beads ended up in one of the 36 slots regularly distributed along a circular support under the compass (angular slot width: 10°). This instrument generated very high quality measurements, with a mean measurement vector and a crosscheck of the number of propeller turns (counter and number of beads). However, with these manual devices, a boat and an operator were required at the measuring site, so they were hard to implement for long-term measurements.

A very broad range of measurement techniques were used and it would be irrelevant here to draw up an exhaustive list. We should nevertheless mention the Pitot tube, which was first used in 1932. At that time the most widely used method involved a rotor associated with a compass, but it is hard to determine the exact date when the first recording instrument was developed based on this principle. One of the most efficient instruments designed is called a 'Doppler profiler'. Depending on the power of its transducer, this device can measure the velocities and directions of various ocean layers from the surface to depths of several hundreds of metres.

Several recording systems have also been used, but it is only highly self-sufficient instruments that are capable of logging long-term current measurements. This includes the electric recording device of Sverdrup and Dahl (1918-1925), the vertical log current metre of Carruthers (1933) and photographic recording instruments, which were relatively reliable. These streamlined devices, which were naturally oriented in the set of the current, were fitted with a camera that photographed the compass direction and the propeller revolution count at regular intervals. However, the individual measurement quality was not as good as could be obtained with an Ekman current meter. These techniques are now obsolete. Modern instruments rely on sophisticated electronic and computer technology for measurement and recording, with a power capacity that can sometimes enable them to remain self-sufficient for over a year.

For many years, current measurement processing was quite rudimentary, with information supplied to navigators consisting of hourly indications of tidal stream velocities and directions at mean spring and neap tides relative to HW at a reference station. Such information can be readily obtained from measurements recorded around mean spring and neap tides to meet this need. Computer progress did not markedly modify these methods.

Figure 10.1 shows an example of a tidal stream chart drawn up on the basis of such measurements. Tidal streams are represented by arrows emanating

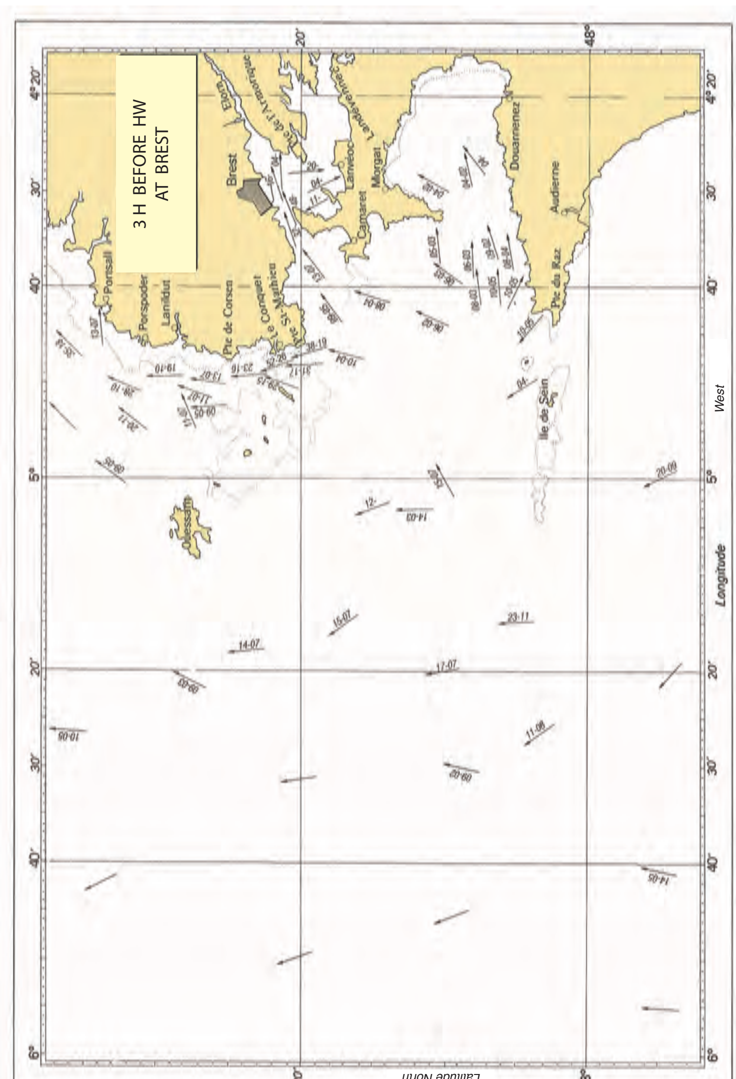

FIGURE 10.1: Brest Roadstead/Iroise Sea: excerpt from a current atlas. Each arrow represents a measurement point. Tidal stream velocities at mean spring and neap tide conditions are shown above each arrow (expressed in tenths of a knot).

from the measurement point. The two values shown above each arrow represent velocities (expressed in tenths of a knot) corresponding to mean spring tide and mean neap tide conditions, respectively. For a given area, 13 values are presented, corresponding to hourly values from 6 h before to 6 h after HW (sometimes LW) at a reference station.

Spatiotemporal interpolations are required for tidal stream evaluation (velocity and direction) at a given point from a set of such charts. It seems obvious, especially when comparing these charts with the more recent ones presented later (figure 10.3), that such interpolations do not always generate accurate results. Dead reckoning navigation on the basis of such data could be extremely risky.

1.4 • Present trends: hydrodynamic modelling

Shortcomings in conventional documents on tidal streams have never been overlooked, but ways to remedy them have only recently been developed thanks to advances in hydrodynamic modelling using computer computation technology. Tidal streams can thus be directly calculated by hydrodynamic equations through digital modelling. The capacity of a model to calculate tidal streams in an area is limited almost only by the power of the computer used, the accuracy of the bathymetry and the information on boundary conditions in the target area.

The hydrodynamic modelling principles are discussed in Chapter IX, 6.2.2. Figure 10.2 shows the resolution that can be achieved using finite element models. It should be noted, however, that it would be of little interest to use a high-resolution grid if the environmental and bathymetric features, in particular, have not been determined on the same scale. Recall, for instance, that navigational charts are unsuitable for digital modelling because they mainly contain information that is useful for navigational safety without an objective representation of the seabed.

Atlases drawn up using this type of model provide more information than conventional atlases drawn up only on the basis of occasional measurements.

Figure 10.3 clearly shows, by comparison with figure 10.1 (in which only measurement results are represented), the improvements that can be achieved by digital modelling. Because of the strong tidal streams around the islands of Sein and Ouessant, it is impossible to obtain direct measurments, so no information is shown on the conventional chart (figure 10.1). In contrast, the modelling results clearly show the strength of the tidal streams, especially in Fromveur Channel (SE of Ouessant) and Sein Strait (figure 10.3). Digital modelling is therefore essential for charting tidal streams in such areas.

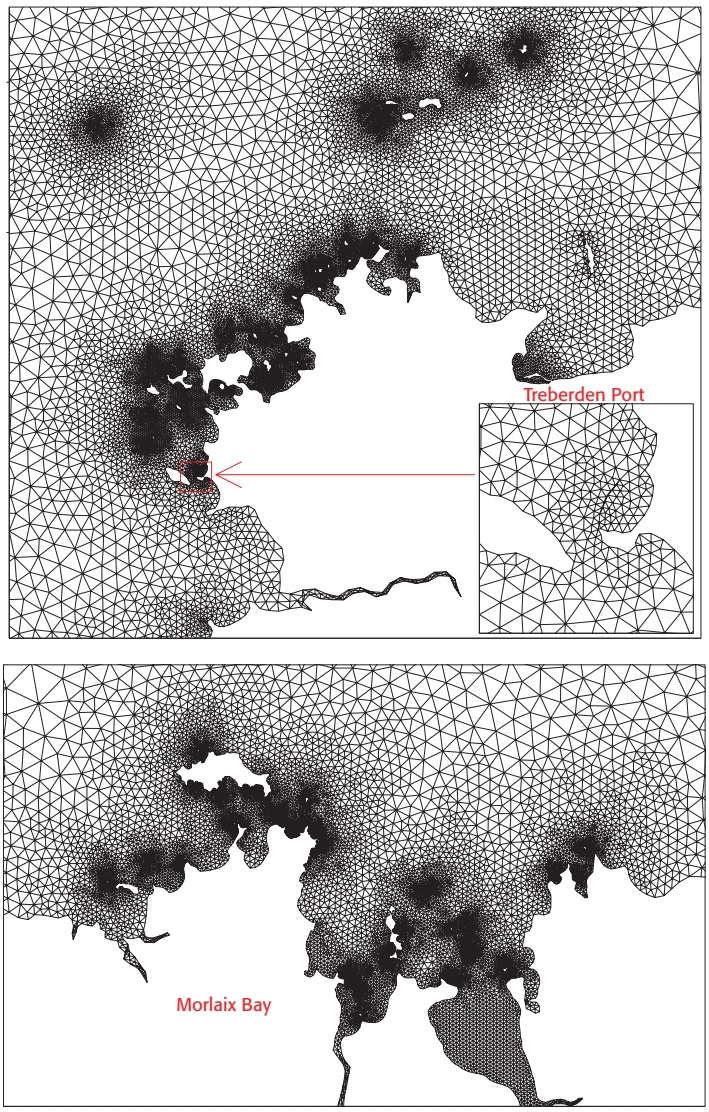

FIGURE 10.2: Examples of grids used to draw up a current atlas in studied regions with digital models. These charts represent two coastal areas along the Brittany coast of France: the Granit Rose coast (top) and Morlaix Bay (bottom). The grid segment sizes range from a few tens to several hundreds of metres.

The development of digital models has led to higher spatial resolution which allows the bathymetry to be taken into full account. This procedure has considerably improved the accuracy of the results. Direct measurements are still necessary, but they are mainly only used to calibrate the models.

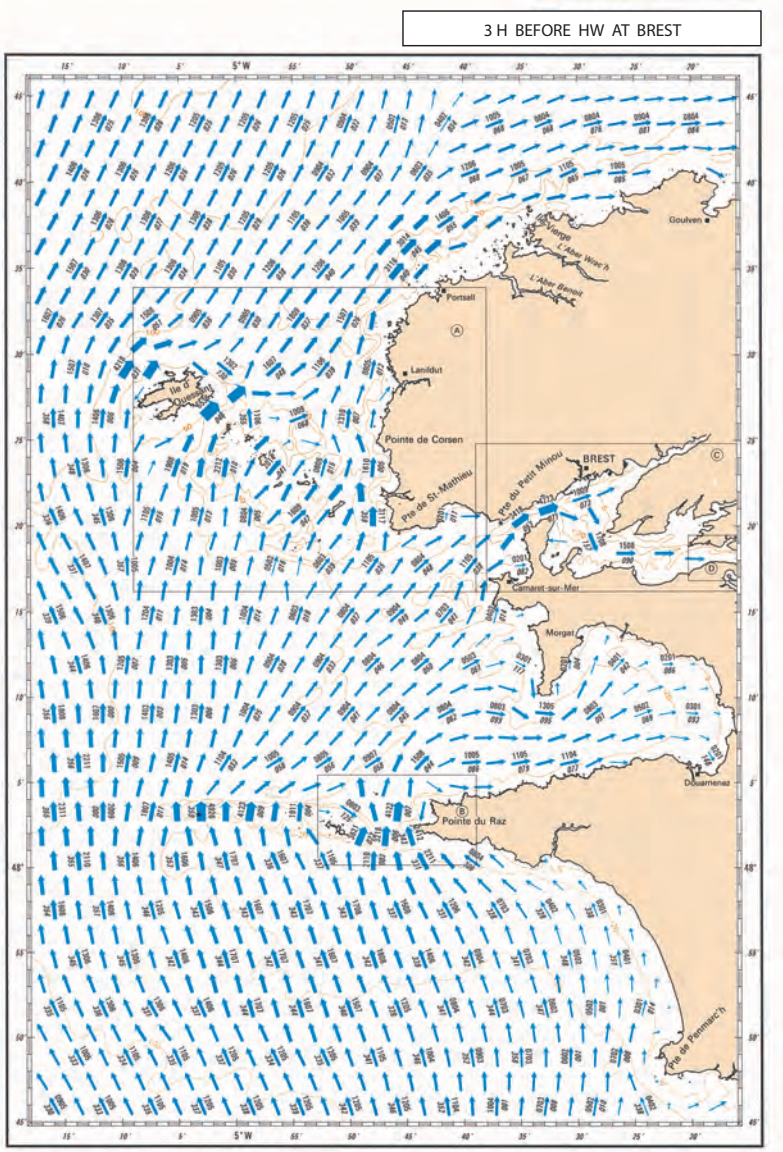

Figure 10.3: Tidal stream charts generated by digital modelling for the tip of Brittany (France): areas concerning the islands of Ouessant (chart A) and Sein (chart B).

Moreover, with recent models, subsequent fitting of measured data and modelling data is no longer as crucial as it was for the initial models.

1.5 • Digital tidal stream data

The models generate data on all hydrodynamic parameters (especially tidal streams and heights) for each grid point. For obvious reasons of clarity, all calculated values cannot be presented on tidal stream charts. There is an inevitable loss of information in some zones even when navigational charts on different scales are proposed.

The use of these documents is markedly simplified, but information pertaining to given times is not shown. Spatial interpolations are almost useless because of the density of arrows presented on the charts, but temporal interpolations are still necessary to be able to calculate tidal streams at given times.

The procedure can presently be accelerated thanks to advanced computer technology. Data on parameters derived from digital tidal stream models can now be processed on ships to obtain specific information using tailored software.

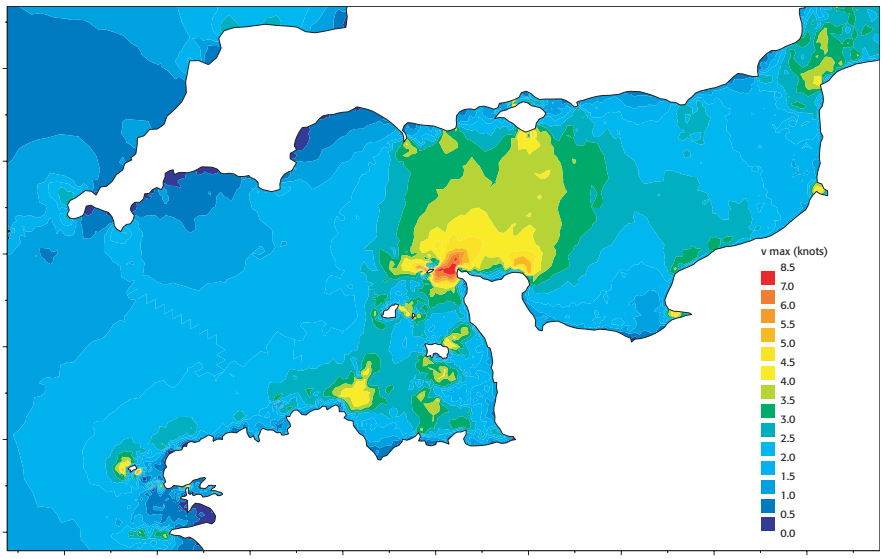

FIGURE 10.4: The Channel: maximum velocity field of tidal streams at mean spring tide.

A basic software program that simulates the tidal stream velocity and direction at all places and times can be supplemented with other specific software programs in order to fulfil various needs, e.g. routeing. Figure 10.4 shows an example of a by-product chart that has no specific application, but which could be of interest for various marine activities.

2 • Tidal streams: definitions and features

Flood and ebb tidal streams can be differentiated in vertical oscillations of the sea level during a tidal cycle. Moreover, the flood stream, or flood tide* and the ebb stream, or ebb tide*, can be identified in horizontal oscillations in water particles.

Tidal streams are either either reversing (rectilinear) or turning (rotatory). In the former case, the flood stream direction is almost constant throughout its duration (about a half tidal cycle). This direction is almost the opposite of that of the ebb stream throughout its duration. In the latter case, the current vector is gyratory during a tidal cycle. Its velocity never declines to zero and may vary over a broad range.

In cases when the extreme velocities vary markedly, there is often a slight variation in direction when the tidal stream velocity is relatively high and a high variation in direction when the velocity is relatively low. These are intermediary streams that are called 'almost reversing' or 'slightly turning' depending on the situation.

The tide occurs in the form of a progressive wave when no obstacles are in the way: high waters (or low waters) advance at velocity c, depending on the depth H, according to the equation $c = \sqrt{g\mathrm{H}}$, where g represents the acceleration of gravity. In the presence of an obstacle (e.g. a coast), the constituent of the wave perpendicular to the obstacle gives rise to a reflected wave that, by interferring with the incident part, generates a stationary constituent. The HW time relative to a pure stationary wave (velocity perpendicular to the coast) is identical over a broad area, and only the amplitude varies according to the site.

With progressive waves, the flood stream accompanies the HW and flows in the direction of tidal wave propagation. It begins at half flood tide, reaches maximum at HW and ends at half ebb tide when flood tide slack water (stream reversal) takes place. The ebb stream is the prevailing reverse stream. It begins at half ebb tide, peaks at LW, and ends at half flood tide when ebb tide slack water (stream reversal) takes place.

With stationary waves, the flood stream accompanies the flood tide. It reaches maximum at half flood tide and ends at HW when flood tide slack water (stream reversal) takes place. The ebb stream accompanies the ebb tide and reaches maximum at half ebb tide and ends at LW when ebb tide slack water (stream reversal) takes place. These tidal stream features are generally noted in the vicinity of coasts.

The hydraulic tidal stream phenomenon that accompanies height variations in bays and estuaries resembles a stationary wave: the flood stream flows upstream and corresponds to the filling. It is maximum around half

flood tide, when the flood rate is highest. The ebb stream is the reverse phenomenon. The flood tide slack water occurs around HW and the ebb tide slack water occurs around LW.

A good example of a progressive wave is in the Channel where the tidal wave propagates from west to east. At Cherbourg, half way between the two coasts, the maximum eastward flow stream occurs almost simultaneously with HW time at Cherbourg while the maximum ebb stream occurs around LW. However, closer to the coast, stream reversals tend to be near slack water.

These stationary and progressive waves generally tend to overlap and may flow in different directions. In such conditions, the streams are sometimes turning, where:

- the flood stream, which flows in the direction of incident wave propagation, begins between LW and half flood tide, and then peaks between half flood tide and HW
- the flood stream, which flows in the reverse direction, begins between HW and half ebb tide, and then peaks between half ebb tide and LW.

Stream reversals tend to occur around flood tide slack water, marking the end of the flood tide. They also take place around ebb tide slack water, marking the end of the ebb tide. Considering the term 'slack water', a distinction should be made between stream slack waters (end of flood or ebb streams) and tidal slack waters (high and low waters).

Times of stream reversals and maximum flood and ebb streams are respectively staggered by clearly determined time intervals relative to the HW time at a suitably chosen reference station. In other words, the tidal stream is in the same phase at different times relative to the HW time at the reference station.

There is sometimes a slight stream phase lag at the seabed relative to the surface stream. However, this phenomenon does not apply in the vicinity of the mouth of tidal rivers where the flood stream at the seabed is generally established before the surface stream.

During both spring and neap tides, tidal stream directions usually have identical values for the same reference station tidal times. However, this does not always apply around stream reversal, when the stream direction changes very quickly. If only one tidal stream direction is referred to in a document, unless otherwise indicated, it refers to the direction of the mean spring tide.

In terms of tide monitoring, the amplitude of a tidal stream is the maximum velocity reached during a tidal cycle. This velocity varies depending on the depth and height of tide. Its variation with respect to depth is especially marked near the seabed because of the turbulent flow induced by friction, which leads to a decrease in the mean velocity.

Depending on the tidal wave propagation mode, i.e. progressive wave, stationary wave or a basin hydraulic filling/emptying phenomenon, the tidal stream amplitude will not vary to the same extent at different tidal heights. It would also be hard to describe a general rule to correlate the stream amplitude with the tidal height. However, for navigational needs, experience has shown that the amplitude of the stream V_C, corresponding to the tidal coefficient C, can be obtained on the basis of data on spring tide V_{ST} and neap tide V_{NT} stream amplitudes by the following first-order approximation:

$$V_C = V_{NT} + \frac{C - 45}{50} (V_{ST} - V_{NT})$$

In case of reversing streams, the modulus of stream $V(t)$ can be estimated at a given time t by applying the so-called rule of sixths, which is analogous to the rule of twelfths for tidal heights. This rule of sixths is based on the implicit assumption that velocity variations are sinusoidal. For semidiurnal tides, where V_C denotes the amplitude (maximum velocity of the reversing stream during a semidiurnal cycle) and the stream slack water time ($t = 0$) is the reference time, we thus obtain:

- 3 h before slack water ($t = -3$ h), the velocity is maximum: $V(-3) = V_C$
- 2 h before ($t = -2$ h), $V(-2) = (5/6)V_C$, or $(1/6)V_C$ less than $V(-3)$
- 1 h before ($t = -1$ h), $V(-1) = (1/2)V_C$, or $(2/6)V_C$ less than $V(-2)$
- at slack water ($t = 0$), the stream is zero before reversal (change of stream direction), $V(0) = 0$, or $(3/6)V_C$ less than $V(-1)$
- 1 h after slack water ($t = 1$ h), $V(1) = (1/2)V_C$, or $(3/6)V_C$ more than $V(0)$
- 2 h after ($t = 2$ h), $V(2) = (5/6)V_C$, or $(2/6)V_C$ more than $V(1)$
- 3 h after ($t = 3$ h), the stream is again at maximum velocity, but in the opposite direction from that at $t = -3$ h, $V(3) = V_C$, or $(1/6)V_C$ more than $V(2)$.

3 • Tidal streams: analytical approach

Movements associated with tides comply with fundamental laws of ocean dynamics. For fluids, these include:

- laws of thermodynamics with respect to salt and heat conservation
- an equation of state, with the sea water density depending on the salinity, temperature and pressure
- the principle of conservation of mass

- and, finally, the principle of conservation of momentum.

3.1 • The linear approach: long-wave equation

For a simple analytical approach to the behaviour of tidal waves, salt and heat flows which are the source of so-called thermohaline streams are disregarded. The sea water density ρ is also considered to be constant (HW $\rho \approx 1.03$ t/m^3), and the fluid is assumed to be incompressible. According the these hypotheses, the law of conservation of mass, which is formulated as:

$$\partial\rho/\partial t + \vec{\nabla} \cdot (\rho \vec{V}) = \partial\rho/\partial t + \rho \vec{\nabla} \cdot \vec{V} = 0$$

is reduced to the simple equation:

$$\vec{\nabla} \cdot \vec{V} \equiv \text{div}\, \vec{V} = 0 \tag{10.1}$$

where $\vec{V}$ is the velocity of the fluids, of constituents (u, v, w) in an orthonormal system Oxyz (with axis Oz being oriented according to the local vertical of the place)

$\vec{\nabla}$ is the gradient operator vector of constituents

$$\left(\frac{\partial}{\partial x}, \frac{\partial}{\partial y}, \frac{\partial}{\partial z}\right)$$

$\vec{\nabla} \cdot \vec{V}$ is their scalar product expressing the divergence of $\vec{V}$.

In our tide-generating force computation (Chap. III § 1.1), we formulated an equation for the absolute acceleration $\vec{\gamma_S}(M)$ of a liquid object M of unit mass located on the Earth's surface. Moreover, when disregarding the viscosity (turbulence and bottom friction) and the advection and vertical acceleration terms (hydrostatic pressure hypothesis), we get back to Laplace's equations (4.1 and 4.2a or the equivalent 4.2.b), which we recall hereafter.

The first one (4.1) represents the continuity equation (10.1) of a water column H(x, y) at level $\eta(x, y, t)$ of the ocean surface (with $\eta \ll$ H), or:

$$\vec{\nabla}_h \cdot (H\vec{V}_h) + \partial\eta/\partial t = 0 \tag{10.2}$$

where

$\vec{V}_h$ is the horizontal part of $\vec{V}$, which is the same throughout the entire depth (as the vertical constituent w is negligible, the velocity $\vec{V}_h$ is identical from the surface to the seabed at a given place)

$\vec{\nabla}_h$ the vector of the horizontal gradient operator of constituents $(\partial/\partial x, \partial/\partial y)$.

The second equation expresses the horizontal movement of a liquid, or:

$$\frac{\partial \overrightarrow{V_h}}{\partial t} + 2\overrightarrow{\omega_T} \wedge \overrightarrow{V_h} = \nabla_h(U - g\eta) \tag{10.3}$$

where

$\overrightarrow{\omega_T}$ is the Earth rotation vector

∇_h is the horizontal gradient operator of a scalar $(\partial/\partial x + \partial/\partial y)$

U is the tide-generating potential of a unit mass

$p/\rho = g\eta$ is the pressure disturbance on a particle of unit mass induced by variations in $\eta(x, y, t)$.

In 1879, Kelvin used the system of equations (10.2) and (10.3) to study long wavelength free waves in an ocean basin while disregarding the potential ($U = 0$).

Were $\overrightarrow{\zeta_M}$ denotes the unit vector of the upward vertical at point M (latitude L), we have seen that the Coriolis parameter f can be expressed by:

$$f = 2\overrightarrow{\omega_T} \cdot \overrightarrow{\zeta_M} = 2\omega_T \sin L$$

where ω_T is the Earth rotation vector modulus (f takes the sign of the latitude, i.e. positive in the Northern and negative in the Southern Hemispheres).

For information only, internal waves at tidal frequencies are only involved in the dissipation process if $q_i \geq |f|$. This process is not present throughout the World. Hence, for internal waves associated with the major constituents M_2 and K_1, dissipative zones are defined by specific latitudes:

- $L_{M2} = \pm 74°28 (f = \pm q_{M2})$
- $L_{K1} = \pm 30°00 (f = \pm q_{K1})$

Based on Kelvin's hypotheses, equation (10.3) then becomes:

$$\frac{\partial \overrightarrow{V_h}}{\partial t} + f\overrightarrow{\zeta_M} \wedge \overrightarrow{V_h} = -g\nabla_h \eta \tag{10.4}$$

In the orthonormal reference frame described above, and based on the assumption that f and H are constant, the free wave motion factor could be explained by the following system of equations:

$$\frac{\partial u}{\partial t} - fv = -g\frac{\partial \eta}{\partial x} \tag{10.5a}$$

$$\frac{\partial v}{\partial t} - fu = -g\frac{\partial \eta}{\partial y} \tag{10.5b}$$

$$\frac{\partial u}{\partial x} + \frac{\partial v}{\partial y} + \frac{1}{H}\frac{\partial \eta}{\partial t} = 0 \tag{10.5c}$$

By differentiating (10.5a) relative to x, (10.5b) relative to y, and (10.5c) relative to z, we obtain:

$$\frac{\partial^2 \eta}{\partial t^2} + fH\left(\frac{\partial v}{\partial x} + \frac{\partial u}{\partial y}\right) + gH\left(\frac{\partial \eta^2}{\partial x^2} + \frac{\partial \eta^2}{\partial y^2}\right) \tag{10.5d}$$

Based on various simplifying hypotheses, these equations – even when they have no nonlinear terms – can only be solved when there are simple geometric configurations. They can still, nevertheless, generate some general information.

3.2 • Simplified model: narrow channel of infinite length

A narrow channel of constant depth and infinite length is oriented in the direction Ox. Equation (10.5) is reduced to:

$$\frac{\partial^2 \eta}{\partial t^2} - c^2 \frac{\partial^2 \eta}{\partial x^2} = 0 \tag{10.6}$$

where:

$$c = \sqrt{gH}$$

The solutions are independent of coordinate y and the Coriolis force. When function $\eta(x,t) = \eta(x)e^{jqt}$ is a specific solution of equation (10.6), and the height $\eta(x)$ depends only on the x-axis, and where $k = q/c$, we have:

$$\frac{\partial^2 \eta(x)}{\partial x^2} + k^2 \eta(x) = 0 \tag{10.7}$$

The general solution of this latter second-order differential equation can be formulated as:

$$\eta(x) = \eta_d\left(e^{-jkx} + re^{jkx}\right) \tag{10.8}$$

where η_d is the amplitude of the height of the direct wave ($x = ct$) and the dimensionless parameter r is the reflection coefficient (which can be a complex number). Equation (10.8) can also be formulated in the following form:

$$\eta(x) = \eta_d\left[(1-r)e^{-jkx} + 2r\cos kx\right] \tag{10.9}$$

When taking equation (10.5a) into account with $f = 0$, the following expression is obtained for the velocity:
$u(x,t) = c\frac{\eta_d}{H}\left[(1-r)\,e^{-jkx} - j2r\sin kx\right]e^{jqt}$, and the amplitude at point x is:

$$u(x) = c\frac{\eta_d}{H}\left[(1-r)\,e^{-jkx} - j2r\sin kx\right] \tag{10.10}$$

For a progressive wave ($r = 0$) propagating at velocity $c = \sqrt{gH}$, we thus obtain:

$$r = 0 \Rightarrow \frac{u(x)}{\eta(x)} = \frac{c}{H} = \sqrt{\frac{g}{H}}$$

Note that the previous equation gives the equality:

$$u(x)/c = \eta(x)/H$$

Progressive waves thus have the following features (figure 10.5):

- the tidal stream and height are in phase
- the flood stream is maximum at HW and flows in the tidal wave propagation direction
- the ebb stream is maximum at LW and flows in the opposite direction
- stream reversals occur at half-tide times.

This is of interest in terms of setting so-called 'radiational conditions' at open boundaries of digital models in order to avoid noise created by reflection from these boundaries.

3.3 • Stationary waves

$$\Omega = 1 \Rightarrow \frac{u(x)}{\eta(x)} = -i\sqrt{\frac{g}{H}} \tan kx$$

The tidal stream and height are in quadrature:

- The flood stream flowing in the incident wave direction is maximum at half flood tide.
- The ebb stream flowing in the reflected wave direction is maximum at half ebb tide.

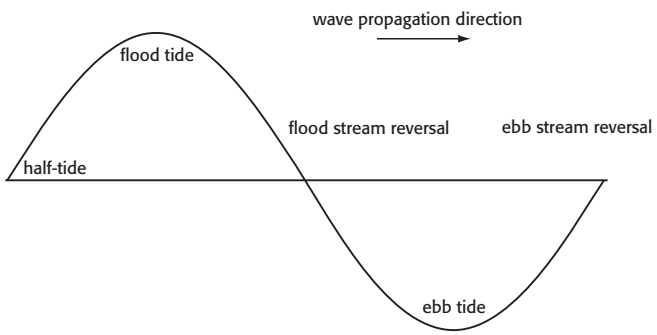

Figure 10.5: A progressive wave: the maximum stream that accompanies the HW in the tidal wave propagation direction, and that accompanies the LW in the reverse direction.

- Flood stream reversal occurs at HW.
- Ebb stream reversal occurs at LW.

3.4 • True tidal streams

Tidal waves are obviously never strictly progressive or stationary, but this simple approach can still help explain certain observed phenomena of considerable practical interest. When tidal wave propagation has been clearly identified, as is generally possible far from the coasts, the flood stream accompanies the HW and the ebb stream accompanies the LW. Near coasts, however, stream reversals tend to be around HW and LW slack waters, with the maximum flood stream occurring around half flood tide and the maximum ebb stream taking place around half ebb tide.

The two constituents can coexist far from the coasts and the tidal stream is generally not strictly a reversing stream–the stream vector describes a hodograph that is called a 'current rose'.

4 • Current roses and harmonic constants

As tidal streams have the same origin as the tide itself, analytical methods described for tidal heights can be applied without modification. However, stream measurements have specific features that have to be taken into account. In particular, they are often noisier than height measurements, and measurement periods are seldom longer than 15 days. However, it is generally not as important to achieve high accuracy.

4.1 • Data analysis

The tidal stream vector can be represented by a complex number. Apart from this difference, methods designed for the analysis of tide levels can be applied without modification. However, the short measurement time is detrimental to the data analysis, i.e. there are too few observations to be able to reliably determine the harmonic constants, which are always calculated by the least squares method. A negligible redundancy level will generate excessive degrees of freedom for the system to resolve and boost the susceptibility to noise, thus upsetting the tidal stream measurements to a greater extent than the height measurements.

The easiest way to limit the impact of noise is to reduce the number of degrees of freedom by setting additional constraints on the harmonic constants. These constraints – although not directly derived from the tide measurements – should be important from a physical standpoint to enhance

the relevance of the results. The species concordance method disucussed in Chapter VII § 3 is especially well adapted for this, and the following two points should be mentioned:

- tidal heights and streams are correlated
- long-term tide measurements are easier to carry out and suitable for standard data analysis procedures.

To take advantage of these observations, we assume that the tidal stream is in concordance with the tide in the spectral domain. This is in line with the species concordance technique used for analysis of short tide monitoring periods. To tailor this technique for tidal streams, it would nevertheless be preferable to slightly modify the reduced height computations (Chap. VI, § 2) in order to reduce the impact of noise between tidal frequencies, i.e. parabolic interpolation on tidal heights is replaced by third-degree polynomial interpolation on tidal stream vectors.

4.2 • Tidal stream harmonic constants

A tidal stream harmonic constituent can be represented by a complex number:

$$\Gamma = u \cos(V - G_u) + jv \cos(V - G_v) \tag{10.11}$$

where u, G_u, v, and G_v are the amplitudes and phase lags of east-west and south-north constituents of a tidal stream harmonic constant.

The hodograph of Γ is an ellipse.

What are called tidal stream harmonic constants are typical elements of this ellipse:

- half major axis a
- half minor axis b
- major axis orientation β_c
- phase lag G.

Navigators generally measure the orientation of the major axis clockwise starting from the north. In compliance with mathematical practices, in the following computations we assume:

$$\varphi = \frac{\pi}{2} - \beta_c$$

We can state:

$$\Gamma = e^{j\varphi} \left[a \cos(V - G) + jb \sin(V - G) \right] \tag{10.12}$$

where we recognise the parametric representation of an ellipse in a complex plane, and a rotation of a φ angle is applied.

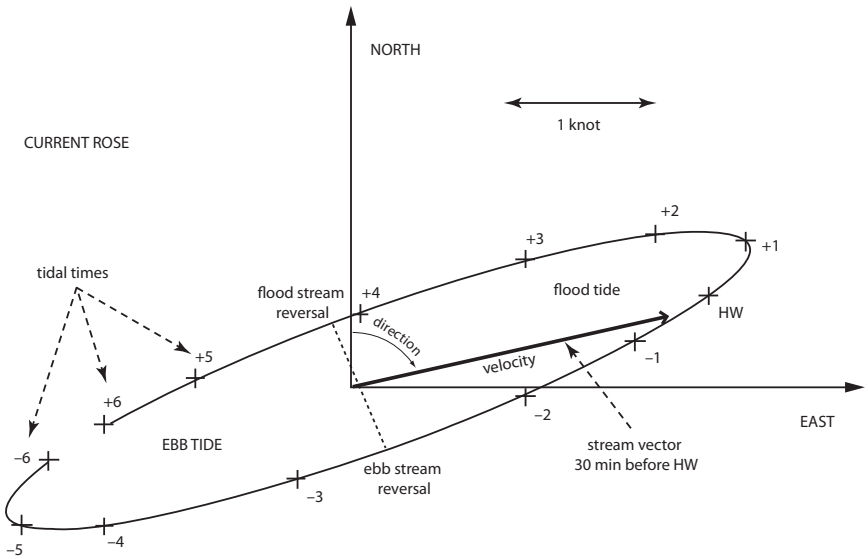

FIGURE 10.6: Hodograph of the tidal stream vector, called a current rose. The tidal times are rounded off to the hour relative to the HW.

G is the phase lag of the wave. It is the maximum stream lag relative to the maximum of the corresponding potential constituent. However, there is one ambiguous aspect, i.e. since the stream modulus passes through two maxima during a cycle, the major axis must be oriented so as to select one of them.

The following conditions apply to this formulation:

$$-\frac{\pi}{2} < \varphi < \frac{\pi}{2}$$
$$a > 0$$
$$a > |b|$$

As the hodograph can turn in a clockwise direction, b can be negative.
The problem is to identify equations (10.13) and (10.14).
Expansion of equation (10.13) gives the following result:

$$\Gamma = \frac{1}{2}\left\{u\left[e^{j(\mathrm{V}-\mathrm{G}_u)} + e^{-j(\mathrm{V}-\mathrm{G}_u)}\right] + jv\left[e^{j(\mathrm{V}-\mathrm{G}_v)} + e^{-j(\mathrm{V}-\mathrm{G}_v)}\right]\right\}$$
$$= \frac{1}{2}\left[\left(ue^{-j\mathrm{G}_u} + j\,ve^{-j\mathrm{G}_v}\right)e^{j\mathrm{V}} + \left(ue^{j\mathrm{G}_u} + jve^{j\mathrm{G}_v}\right)e^{-j\mathrm{V}}\right] \quad (10.13)$$

and expansion of equation (10.14) gives:

$$\Rightarrow \Gamma = \frac{e^{j\varphi}}{2}\left\{a\left[e^{j(\mathrm{V}-\mathrm{G})}+e^{-j(\mathrm{V}-\mathrm{G})}\right]+b\left[e^{j(\mathrm{V}-\mathrm{G})}-e^{-j(\mathrm{V}-\mathrm{G})}\right]\right\}$$
$$= \frac{1}{2}\left[(a+b)\,e^{j(\varphi-\mathrm{G})}e^{j\mathrm{V}}+(a-b)\,e^{j(\varphi+\mathrm{G})}e^{-j\mathrm{V}}\right] \quad (10.14)$$

This expression is interesting because it shows that C can be interpreted as the superposition of two circular hodographs at the same angular velocity, with one turning counterclockwise and the other clockwise.

The identification of factors of $e^{j\mathrm{V}}$ and $e^{-j\mathrm{V}}$ gives:

$$(a+b)\,e^{j(\varphi-\mathrm{G})} = ue^{-j\mathrm{G}_u}+jve^{-j\mathrm{G}_v}$$
$$(a-b)\,e^{j(\varphi+\mathrm{G})} = ue^{j\mathrm{G}_u}+jve^{j\mathrm{G}_v}$$

or by identifying complex and imaginary parts:

$$(a+b)\cos(\varphi-\mathrm{G}) = u\cos\mathrm{G}_u+v\sin\mathrm{G}_v$$
$$(a+b)\sin(\varphi-\mathrm{G}) = -u\sin\mathrm{G}_u+v\cos\mathrm{G}_v$$
$$(a-b)\cos(\varphi+\mathrm{G}) = u\cos\mathrm{G}_u-v\sin\mathrm{G}_v$$
$$(a-b)\sin(\varphi+\mathrm{G}) = u\sin\mathrm{G}_u+v\cos\mathrm{G}_v$$

such that:

$$a+b = \pm\sqrt{u^2+v^2+2uv\sin(\mathrm{G}_u-\mathrm{G}_v)}$$
$$a-b = \pm\sqrt{u^2+v^2-2uv\sin(\mathrm{G}_u-\mathrm{G}_v)}$$

The signs are clarified by the following conditions:

$$\begin{cases} a > 0 \\ a > |b| \end{cases}$$

which require that + signs be shown in front of radicals (square roots).

Recall that b can be negative:

- if b is positive, the ellipse turns counterclockwise
- if b is negative, the ellipse turns clockwise.

$$a = \frac{1}{2}\left[\sqrt{u^2+v^2+2\,u\,v\sin(\mathrm{G}_u-\mathrm{G}_v)}+\sqrt{u^2+v^2-2\,u\,v\sin(\mathrm{G}_u-\mathrm{G}_v)}\right]$$

$$b = \frac{1}{2}\left[\sqrt{u^2+v^2+2\,u\,v\sin(\mathrm{G}_u-\mathrm{G}_v)}-\sqrt{u^2+v^2-2uv\sin(\mathrm{G}_u-\mathrm{G}_v)}\right]$$

The major axis orientation and phase lag are deduced from the following equations:

$$\tan(\varphi - \mathrm{G}) = \frac{v\cos \mathrm{G}_v - u \sin \mathrm{G}_u}{u\cos \mathrm{G}_u + v \sin \mathrm{G}_v} = \tan(t_1)$$
$$\tan(\varphi + \mathrm{G}) = \frac{v\cos \mathrm{G}_v + u \sin \mathrm{G}_u}{u\cos \mathrm{G}_u - v \sin \mathrm{G}_v} = \tan(t_1)$$

Note that t_1 and t_2 are defined to within 2π since the sine and cosine values are known.

$$\begin{cases} \varphi - \mathrm{G} = t_1 + 2k_1\pi \\ \varphi + \mathrm{G} = t_2 + 2k_2\pi \end{cases} \Rightarrow \begin{cases} \varphi = \dfrac{t_1 + t_2}{2} + (k_1 + k_2)\,\pi \\ \mathrm{G} = \dfrac{t_2 - t_1}{2} + (k_2 - k_1)\,\pi \end{cases}$$

The φ and G values can be clarified by applying the following condition:

$$-\frac{\pi}{2} < \varphi < \frac{\pi}{2}$$

which imposes the even or odd values of $k_1 + k_2$ and thus of $k_2 - k_1$ (if $k_1 + k_2$ is even then $k_2 - k_1$ is too, and vice-versa).

Note that what we call the 'major axis direction' is

$$\beta_c = \frac{\pi}{2} - \varphi.$$

The condition applied to the φ value imposes an east-west orientation of the major axis.

The significance of phase lag G resembles that concerning tidal heights (maximum wave lag at the maximum action of the harmonic constituent), i.e. the maximum stream lag in the east-west direction relative to the maximum action of the constituent.

Hence, all of the tidal stream ellipse elements are defined.

A

Astronomical factors considered in tidal studies

Studies of ocean tides on Earth involve the positioning of tide-generating celestial bodies and all liquid elements affected by their gravitational forces. In order to understand the basis of such studies, it would be useful to review a few elements of astronomy, especially spherical coordinate systems, celestial body motions and their frequencies. This will help to more accurately determine the relationships between the characteristics of motions and tidal harmonic constituents.

Concerning the positioning (celestial body or place on Earth), only the usual spherical coordinate systems and the conventional method for switching from one coordinate system to another are described. When a celestial body is mentioned this usually refers to its centre. Theoretically, the gravitational effect of the entire solar system has an influence on the tides, however those planets outside of the Sun-Earth-Moon system have little effect and can be ignored. While describing their relative motions, we will see how the different time bases are determined on the basis of orbital periods, associated with the Earth's rotation, thus allowing us to define various time bases.

1 • Spherical coordinate systems

Coordinate systems are selected according to the type of phenomenon or motion to be studied. Note however that a reference is said to be Galilean

when a point mass unaffected by any forces maintains its velocity. In such a reference frame, this point is either immobile or in uniform translational motion. The Copernician reference frame, which is based on the centroid of the solar system, with axes oriented towards fixed stars, is a Galilean reference frame (even though this is likely not perfectly exact if galactic rotation is taken into account), as well as all other reference frames in uniform translational motion relative to the Copernician reference frame.

For tidal studies, the primary references used are derived from geometric characteristics associated with the shape and movements of our planet:

• Ellipsoidal rotation around a so-called polar axis or Earth axis (northern and southern), with the Equator being the great circle.

• Two separate movements, including the rotation around the polar axis and the orbital movement around the Sun, according to Kepler's laws, which have an ecliptic trajectory.

To determine astronomical directions, we use a sphere whose centre is defined as required, with an infinite radius: a celestial sphere.

Two types of reference frame are used:

• Coordinate systems of the first type have the centre of the Earth as origin and they rotate with it; these are used to determine the position of a place on Earth and the direction of a celestial body relative to this place. The celestial sphere used in such cases, which is fixed with respect to the observer, is called a local celestial sphere.

• Coordinate systems of the second type also have the centre of the Earth as origin, but their axes are oriented towards points that are quite fixed with respect to the stars. They are used to determine the position of a celestial sphere that is not fixed with respect to the observer. The celestial body used here is called a fixed sphere which, relative to the local celestial sphere, has a rotational movement around the polar axis, i.e. a so-called diurnal movement.

Note that a reference frame associated with the Earth and having rotational movements around the polar axis and following an orbit that is governed by laws of gravitation, is not Galilean. This gives rise to the Coriolis force and the tide-generating force.

1.1 • Spherical coordinates on a local celestial sphere

In a precise geodetic system, the ellipsoidal shape of the Earth must be taken into account. However, for tidal studies, the hypothesis of a spherical Earth with a centre T and a mean radius a_T is sufficient for first-order approximations.

Under this hypothesis, the vertical at a place M is determined by a plumb-line whose direction follows that of the Earth's radius of the place. The direction of the upward vertical indicates the zenith, as symbolised by the letter M (like the place) on the local celestial sphere, with nadir being in the opposite direction. The polar axis and vertical also determine the meridian of the place. More generally, the meridian is a plane that contains the polar axis. The great circle of a celestial sphere, which passes through the zenith and the celestial poles, is called the celestial meridian of the place. Note however that several different meanings of the word 'meridian' are accepted. We adopt the most common meaning: the meridian of a point (place, celestial body or star) is a semicircle (terrestrial or celestial) delimited by the polar axis and the point. In this case, the term 'upper meridian' of the point (terrestrial or celestial) is sometimes used, while the 'lower meridian' is the antipodal meridian.

The equatorial plane and polar axis provide a practical basis for determining the references, which are centred on T and linked with the globe (rotating with it). Two systems correspond to this first type of reference, with the first providing the geographical coordinates of a place on Earth, and the second giving the equatorial coordinates of a celestial body for a given place. These two orthonormal reference frames have a common polar axis $\overrightarrow{TP}$. However, the meridian used as origin (its intersection with the equatorial plane is the zero axis of the latter) will differ depending on whether it is used to determine the position of a place or the direction of a celestial body.

1.1.1 • Geographical coordinates of a place

It is assumed that the zero axis is arbitrarily determined on the equatorial plane. The Greenwich meridian (UK) was established as the zero meridian at an international conference held in Washington in 1884, and it defines the equatorial zero axis.

In these conditions, the geographical coordinates of place M are (figure A.1):

• longitude G, angle of the hemisphere of place M relative to the Greenwich meridian, measured anticlockwise (in an orthonomal reference frame, while adopting the axis of positive z northward), positive eastward and negative westward, from 0° to ±180°;

• latitude L, angle of the zenith direction in M relative to the equatorial plane, measured as positive in the northern hemisphere and negative in the southern hemisphere, from 0° to ±90°.

Note that for the complete determination of a place on the real Earth, the altitude z must be known with respect to the reference ellipsoid, which

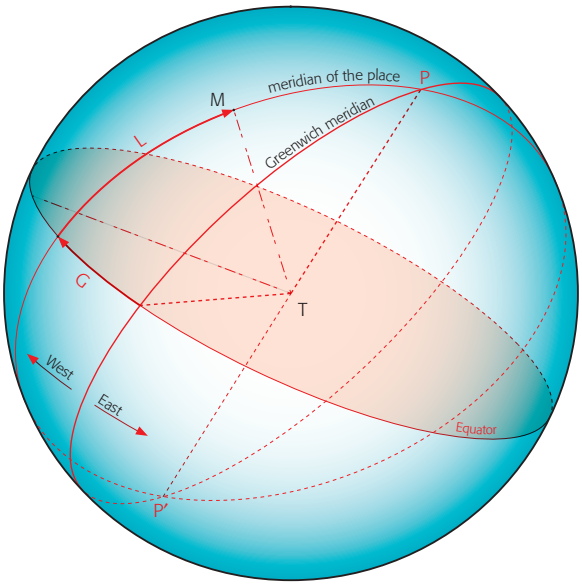

Figure A.1: Geographical coordinates of point M on the surface of the globe: longitude G and latitude L.

here is considered as the spherical surface of radius a_T, while the altitude is measured positively according to the upward vertical.

1.1.2 • Equatorial coordinates of celestial bodies

As previously, the bases are the polar axis $\overrightarrow{TP}$ and the equatorial plane, but here the meridian of point M is selected as origin.

In this reference frame, the two spherical coordinates of a celestial body A are (figure A.2):

• the hour angle $\mathcal{H}$, the angle of the hemisphere of celestial body A relative to that of point M, calculated positively in a westerly direction. This convention may be explained by the fact that the Earth rotates eastward (anticlockwise with respect to the axis $\overrightarrow{TP}$), while the apparent motion of celestial bodies is westward. The hour angle is always positive and usually expressed in hours (360° $\Rightarrow$ 24 h, or 15° $\Rightarrow$ 1 h).

• the declination δ, i.e. the angle of the direction of celestial body A (axis $\overrightarrow{TA}$) relative to the equatorial plane, calculated (like the latitude of a place) positively northward and negatively southward. The complement of the declination is the polar distance which is given by $\pi/2 - \delta$ with respect to the north celestial pole and $\delta + \pi/2$ from the south celestial pole.

Figure A.2 shows the geocentric zenithal distance θ, i.e. the angle of $\overrightarrow{TM}$

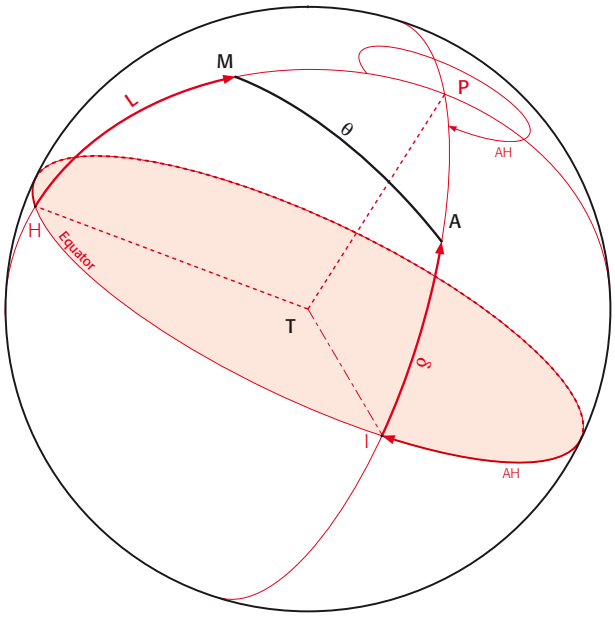

FIGURE A.2: Equatorial coordinates of a celestial body: hour angle Æ H and declination δ. Angle θ is the geocentric zenithal distance of celestial body A with respect to the zenith M of the place.

relative to $\overrightarrow{TA}$ and ranging from 0° to 180°, involved in the tide-generating potential equation. The half-plane delimited by the direction of zenith $\overrightarrow{TM}$ and passing through the centre of the celestial body defines the vertical of the celestial body.

1.2 • Spherical coordinates on fixed spheres

These coordinates are independent of the place. The ecliptic is the plane containing the Earth's orbit. The trigonometric convention adopted for the ecliptic is determined by a person who is standing on the side of the ecliptic that encompasses the Earth's North Pole. This person can thus see the Earth's orbit as it moves in an anticlockwise direction.

The ecliptic and the equatorial planes form an angle ε of $23°26'21''$, called the obliquity of the ecliptic, and their intersection defines the line passing through the spring and autumn equinoctial points. The spring equinoctial point, which is also called vernal equinox γ, is determined by the position of the Sun during its apparent motion as it passes northward through the celestial equator. The thus defined direction of point γ is a reference axis common to the ecliptic and the equator for a fixed sphere. The position

of a celestial body, irrespective of the observation site, can thus be readily obtained in reference frames based on the equatorial or ecliptic plane, with $\overrightarrow{T\gamma}$ as common axis, thus giving the two following coordinate systems:

- celestial equatorial coordinates,
- ecliptic coordinates.

1.2.1 • Celestial equatorial coordinates

The polar axis $\overrightarrow{TP}$ and equatorial plane are the reference frame bases, but here the meridian of point γ serves as the origin (figure A.3). The two celestial equatorial coordinates of a celestial body are thus defined by:

- the right ascension α, the angle of the half plane TPA with respect to that of point γ, calculated in an easterly direction from 0° to 360°;
- the declination δ, the angle already determined in the equatorial coordinate system from the Equator, thus positive northwards and negative southwards, from 0° to ±90°.

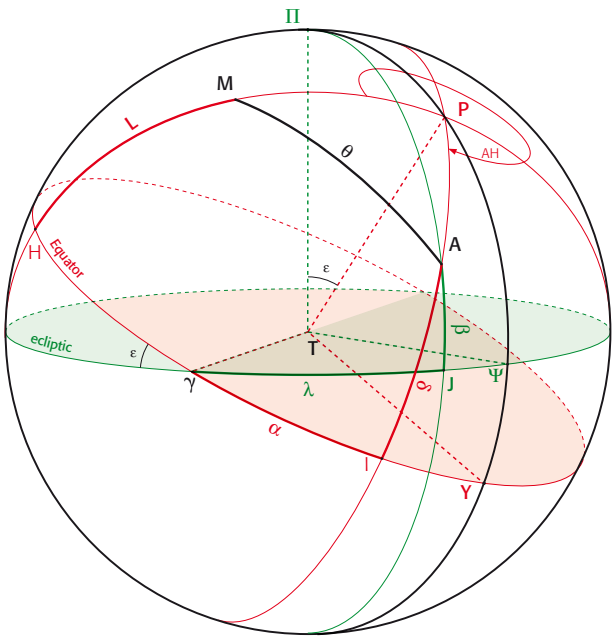

Figure A.3: Celestial body coordinates on a fixed sphere: a) celestial equatorial: right ascension α and declination δ; ecliptics: longitude λ and latitude β.

1.2.2 • Ecliptic coordinates

The reference of this coordinate system (figure A.3) has the ecliptic and its orthogonal $\overrightarrow{T\Pi}$ as base, with axis $\overrightarrow{T\gamma}$ being the origin axis in the ecliptic. The

orientation of point Π, i.e. the ecliptic north pole, is determined by the angle between the two polar axes $\overrightarrow{TP}$ and $\overrightarrow{T\Pi}$, which is equal to ε, the obliquity of the ecliptic. This reference can be represented by the orthonormal axis system $T\gamma\Psi\Pi$.

The ecliptic coordinates of celestial body A are thus:

• the ecliptic longitude λ: angle of the half-plane $T\Pi A$ (delimited by axis $\overrightarrow{T\Pi}$ and containing celestial body A) relative to that of the origin $T\Pi\gamma$, calculated in a westerly direction from 0° to 360°;

• the ecliptic latitude β: the angle of the direction of celestial body A (axis $\overrightarrow{TA}$) relative to the ecliptic, which is positive northward of the ecliptic Π and negative southward, ranging from 0° to ±90°.

As no confusion is possible with longitudes and latitudes on Earth, these coordinates are usually simply called longitude and latitude of a celestial body.

As, by definition, the apparent motion of the Sun occurs in the ecliptic, its latitude is zero. Its longitude is given by Newcomb's model (1895), which also gives the variations in the Earth-Sun distance relative to the mean (149.6 million km).

Later (in § 3.3) the mean celestial body notion will be introduced in the mean time definition. The 'mean Sun' is a fictional celestial body with a constant angular velocity in the ecliptic, with the same apparent period (vernal equinox to vernal equinox) as the true Sun. It should be pointed out that the longitude of this fictional celestial body, whose value varies uniformly over time, is incorrectly called the 'mean longitude' of the celestial body rather than the 'longitude of the mean celestial body'.

Similarly, in his lunar orbit model, Brown (1896) also used ecliptic coordinates, which gave the variations in the Earth-Moon distance relative to the mean (384 400 km). In his last model tailored for digital computation, Brown provided astronomic precision for this orbit, thus enabling a very good tidal prediction over several centuries.

1.3 • The geocentric zenithal distance of a celestial body

For a given place, the tide-generating force and potential are calculated in the the vertical plane of the celestial body, and the geocentric zenithal distance θ[1] of the celestial body is the key parameter in determining these two quantities. The tide-generating potential, which is the result of a so-called meridian field revolving around the axis $\overrightarrow{TA}$, see Appendix B), is

1. In astronomy, the term 'distance' may be applied to an angle.

expressed especially by a series of Legendre polynomials as a function of $\cos\theta$. It is also useful to know the expressions of cosine $\cos\theta$ as a function of the hour angle $\measuredangle H$ of the celestial body in the different coordinate systems.

1.3.1 • Formulation of θ in equatorial systems

By assigning a celestial sphere a radius of 1 (this assumption will be adopted hereafter), we have: $\cos\theta = \overrightarrow{TM} \times \overrightarrow{TA}$.

In the two reference frames based on the equatorial plane (equatorial and celestial coordinates), the geocentric zenithal distance of celestial body θ is more readily obtained by the cosine equation in the PAM spherical triangle:

$$\cos\theta = \sin L \sin\delta + \cos L \cos\delta \cos \measuredangle H \tag{A.1}$$

This angle depends only on the equatorial coordinates $(\measuredangle H, \delta)$ of celestial body A and latitude L of zenith M.

In an equatorial coordinate system (meridian of M as origin), the constituents (here equal to direction cosines) of vectors $\overrightarrow{TM}$ and $\overrightarrow{TA}$ take the form of two column matrices (subscript *t* for 'time'):

$$M_t = \begin{bmatrix} \cos L \\ 0 \\ \sin L \end{bmatrix} \qquad A_t = \begin{bmatrix} \cos\delta \cos \measuredangle H \\ \cos\delta \sin \measuredangle H \\ \sin\delta \end{bmatrix}$$

It is readily confirmed that their scalar product gives equation A.1.

Where $\measuredangle H_\gamma$ denotes the hour angle of point γ, which is often called 'sidereal time'[2] ż :

$$\measuredangle H_\gamma = \measuredangle H + \alpha.$$

In a celestial equatorial coordinate system:

$$M_q = \begin{bmatrix} \cos L \cos \measuredangle H_\gamma \\ \cos L \sin \measuredangle H_\gamma \\ \sin L \end{bmatrix}$$

1.3.2 • Formulation of θ in an ecliptic system

The cosine of the θ angle in the ecliptic reference frame $T\gamma\Psi\Pi$ can also be expressed using several spherical trigonometry equations, but the choice of different spherical triangles to obtain the sought-after result is somewhat arbitrary. It would make more sense to calculate it directly from the scalar

2. Note that this name is incorrect, i.e. depending on the usage adopted for names such as 'tropical year' and 'tropical revolution', the name 'tropical time' would be prefereable, but it is still an ambiguous time base.

product $\overrightarrow{TM} \times \overrightarrow{TA}$, as the constituents of these vectors are expressed in this reference system.

If subscript e is added to the ecliptic reference frame, the constituents of vector $\overrightarrow{TA}$ take the following column matrix form:

$$A_e = \begin{bmatrix} \cos\beta \cos\lambda \\ \cos\beta \sin\lambda \\ \sin\beta \end{bmatrix} \tag{A.2}$$

In the same reference frame, the direction cosines of $\overrightarrow{TM}$ have slightly more complex expressions, but can be readily obtained by using the coordinate transformation matrix C_{eq}, so as to be able to derive the ecliptic constituents from the equatorial constituents:

$$C_{eq} = \begin{bmatrix} 1 & 0 & 0 \\ 0 & \cos\varepsilon & \sin\varepsilon \\ 0 & -\sin\varepsilon & \cos\varepsilon \end{bmatrix}$$

Matrix M_e, corresponding to the constituents of vector $\overrightarrow{TM}$ in an ecliptic system, can be obtained via the matrix product: $M_e = C_{eq} \times M_q$

Considering the previous equation for the M_q matrix, then:

$$M_e = \begin{bmatrix} \cos L \cos(\alpha + \text{Æ}) \\ \cos L \sin(\alpha + \text{Æ}) \cos\varepsilon + \sin L \sin\varepsilon \\ -\cos L \sin(\alpha + \text{Æ}) \sin\varepsilon + \sin L \cos\varepsilon \end{bmatrix}$$

With A_e obtained by equation (A.2), $\cos\theta$ can be expressed as a function of the hour angle and ecliptic coordinates of the celestial body as follows:

$$\overrightarrow{TM} \times \overrightarrow{TA} = \cos\theta = \sin L \times f(\beta, \lambda) + \cos L \times g(\beta, \lambda, \text{Æ}) \tag{A.3}$$

where:

$$f(\beta, \lambda) = \cos\varepsilon \sin\beta + \sin\varepsilon \cos\beta \sin\lambda$$

$$g(\beta, \lambda, \text{Æ}) = \cos\beta \cos\lambda \cos(\alpha + \text{Æ}) + (\cos\varepsilon \cos\beta \sin\lambda - \sin\varepsilon \sin\beta) \sin(\alpha + \text{Æ})$$

As equations (A.1) and (A.3) are equivalent, then:

$$\sin\delta = \cos\varepsilon \sin\beta + \sin\varepsilon \cos\beta \sin$$

an equality which can be deduced from the equation of cosines in the spherical triangle APΠ, and also:

$$\cos\delta\cos\text{Ĥ} = \cos\beta\cos\lambda\cos(\alpha+\text{Ĥ}) + (\cos\varepsilon\cos\beta\sin\lambda - \sin\varepsilon\sin\beta)\sin(\alpha+\text{Ĥ})$$

This much more complex latter equation can also be obtained through spherical trigonometry equations. As pointed out above, and since we have several possibilities when selecting spherical triangles to achieve this result, direct determination of the scalar product $\overrightarrow{TM} \times \overrightarrow{TA}$ by the coordinate transformation matrix would seem to be the most sensible option in this case.

2 • Celestial bodies, typical motions and times

We described the ecliptic as the Earth's orbit around the Sun when defining the different spherical coordinate systems. Actually, it is the Earth-Moon centroid that, according to Kepler's laws, describes the ecliptic, with one of the focal points being the barycentre of the solar system.

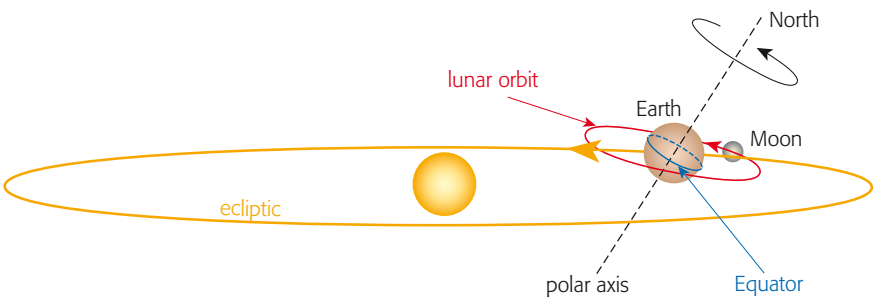

Figure A.4: Movements of celestial bodies.

The Sun, Earth and Moon are the only celestial bodies taken into account in tidal predictions (figure A.4 and table 1.1). The Earth-Sun distance and the respective masses of these two celestial bodies indicates that their centroid is very close to the centre of the sun (450 km), a distance that is less than 0.1% of the Sun's equatorial radius. However, the centroid of the Earth-Moon is 4 700 km from the Earth's centre, or 75 % of the Earth's radius, 1.2 % of the distance between these two celestial bodies, but only 0.003 % of the Earth-Sun distance. This very low percentage explains why the ecliptic is usually defined as the Earth's orbit around the Sun, whereas it is actually the orbit of the centroid of the Earth-Moon system.

TABLE 1.1: Features of celestial bodies relative to the Earth's features (mass: $5.98 \cdot 10^{24}$ kg; equatorial radius: 6 378 km).

	Mass	Mean distance (km)	Equatorial radius
Sun	333 946	$1.496 \cdot 10^{8}$	109.125
Earth	1	0	1
Moon	0.0123	384 400	0.272 5

Note that the lunar orbit is not completely elliptic around the Earth-Moon centroid as it is very markedly disturbed by solar attraction.

2.1 • Earth: typical motions and times

We have seen that the different spherical coordinate systems used to locate a place or a celestial body are selected on the basis of the Earth's specific characteristics (ellipsoidal rotation, gravity, orbital plane). However, the time bases are determined from the periods of the Earth's motions: orbital rotation around the Sun and its rotation around its own axis.

Its ellipsoidal rotation pattern has an excentricity of 0.082 and the two poles are 12 714 km apart; the circumference of the Equator, i.e. the great circle of this ellipsoid, is 40 075 km (equatorial diameter 12 756 km).

As mentioned above, the angle between the ecliptic and equatorial planes is $\varepsilon = 23°26'21''$, and their intersection defines the line of the spring and autumn equinoctial points. These points, which are reached around 21 March (ascending solar node or vernal equinox) and 23 September (descending node), respectively, move westward at an extremely slow angular velocity relative to stars – this is the precession of the equinoxes.

Precession consists of a motion of the equatorial pole around the ecliptic pole, with a period of around 26 000 years, associated with a slight variation in obliquity ε. Vernal equinox moves around the Equator in a westward direction at a rate of about $50''$ a year.

With the chosen orientation conventions, the Earth's orbital rotation is in an anticlockwise direction (this also applies for the apparent motion of the Sun in the ecliptic). The duration of this rotation, i.e. the time interval between two transits of the Sun at vernal equinox, defines the tropical or equinoctial year, as usually symbolized by T_A, during which the Earth's meridian undergoes 365.242 2 rotations relative to the Sun. During this orbital rotation, the time interval between two transits of the Sun over the Earth's meridian varies around a mean value, i.e. the mean solar day which, when divided into 24 h, served as the fundamental time base prior to the

advent of the atomic clock. The duration of a tropical year is thus 365.242 2 days (in mean solar time) or 365 d 5 h 48 min 45 s. This time base was adopted because it is in line with the continuous cycle of seasons, and it is used for tidal computations.

A sidereal year, or the time between two transits of the Sun at a specific point in the sky (fixed sphere), is 365.256 4 days – this value is 20 min 25 s greater than the tropical year T_A following the precession of the equinoxes.

Moreover, in astronomy, apsides are the extremities of the great axis of the elliptic orbit of a cellestial body. For the ecliptic (celestial eccentricity 0.016 7), the closest apsis to the Sun, i.e. periapsis or perihelion, is at $147.1 \cdot 10^6$ km and the furthest, i.e. apoapsis or aphelion, is at $152.1 \cdot 10^6$ km. From the point of view of tidal studies (as observed on land), the apparent motion of the Sun is considered to be that of a satellite of Earth. Relative to the vernal equinox, it takes 209.4 centuries for a complete rotation of solar perigee in anticlockwise direction. Because of this slow movement, the Earth's path passes perihelion every 365.2594 days – this is an anomalistic year which is 24 min 46 s longer than a tropical year. Note also that the Sun achieves maximum declination $\max|\delta_S| = \varepsilon$ at solstice (from the Latin *sol*, Sun, and *stare*, stop). The positive declination corresponds to summer solstice in the Northern Hemisphere and winter in the Southern Hemisphere (around 21 June), while the negative declination corresponds to the opposite situation (around 22 December). It should be noted that the respective directions of these extremes do not correspond to those of apsides. The Earth reaches perihelion around 3 January and aphelion around 5 July. During past centuries, these transit points were earlier, with a drift of around 1.74 days per century.

We have already seen that the Earth rotates anticlockwise (eastward) on its axis. A complete revolution of an Earth meridian relative to vernal equinox is 23 h 56 min 4 s (23.934 470 h), which is the length of a sidereal day (the term commonly used, but it is actually a tropical or equinoctial day) of close to 24 h. This difference could be explained by the fact that, when orbiting, the Earth completes an extra rotation relative to the vernal equinox as compared to that relative to the Sun, i.e. 366.242 2 sidereal rotations in 365.242 2 days. Actually, the rotational velocity varies very slowly, like the polar axis, which behaves like the axis of a spinning top, but it does not maintain a constant spatial orientation. Nevertheless, as pointed out above, the precession of equinoxes, i.e. a high amplitude but very slow motion, is not taken into consideration in tidal computations, nor is the very minor decrease in rotation velocity, i.e. around 2 ms/day over a century.

However, there are also fluctuations of minor amplitude in these two

elements (polar rotation and direction), but with shorter periods (nutation). These fluctuations have several causes, with the most important being impulse exchanges between the different Earth envelopes made up of geophysical fluids: atmosphere, hydrosphere, cryosphere, lithosphere and magmatic mantle. Earth rotation velocity measurements thus indicate, for instance, variations due to atmospheric motions of around a millisecond per day. Ocean tides induce only slight day length variations, i.e. a maximum of 0.1 ms (figure A.5).

Similarly, the poles have more or less periodic gyratory motions, with one of the most important being Chandler wobble. It has a period of 434.3 days (±2 days) with an amplitude of around 0.2 to 0.3 arc seconds. This period, which has been identified by a few authors in sea level measurements in the North Sea, has never been detected in the series of over 150 years of tidal records available for Brest (France).

Due to the very low variation in these parameters, studies of tides could be conducted with the factors indicated above with records spanning several centuries: a fixed polar axis direction with a uniform Earth rotation, thus with a constant angular velocity, symbolized by ω_T and equal to 15.041 068°/h.

2.2 • The Moon and its motions

The Moon, which is subjected to the attraction of the Earth and Sun, follows an almost elliptical orbit anticlockwise with a mean excentricity of 0.054 9, with the Earth-Moon centroid (4 700 km from the Earth's centre) being one of the foci. Under the gravitational force of the Sun, the eccentricity ranges from 0.044 to 0.067 (2.5-4-fold that of the ecliptic). The Moon's mass is thus 81.3-fold less than that of Earth and it orbits at a mean distance of 384 400 km from Earth (around 60.3 Earth radii), with the range being roughly 356 000 to 410 000 km.

Relative to the vernal equinox meridian, the Moon completes its orbit in a mean time of 27.321 581 6 days (27 d 7 h 43 min 4.7 s), i.e. its tropical revolution time. This revolution corresponds to a mean angular velocity (derived relative to its right ascension time) of 0.549 016 521 °/h, with the same sign as the Earth's rotation. An Earth meridian, in phase with the Moon at a given time, should thus complete more than one rotation (relative to the vernal equinox meridian) for this celestial body to pass over again. The time interval between these two transits of the Moon over the meridian of the place is a lunar day. The mean angular velocity of an Earth meridian relative to the Moon's meridian corresponds to the deviation between the

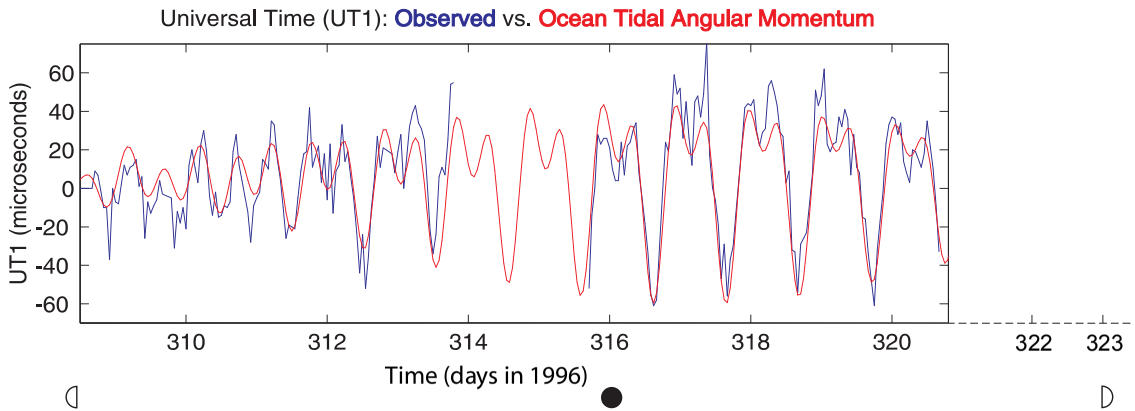

Figure A.5: Impact of the world ocean tide on the Earth's rotation (expressed in variations in day length, with the magnitude expressed in microseconds). Comparison of direct VLBI measurements (blue curve) with predictions of the angular momentum of the world ocean tide, derived from model simulations based on *TOPEX-Poseidon* satellite altimetry data (red curve). The response is a diurnal inequality (B.F. Chao, *EOS* vol. 84, n° 16, 2003).

two above mentioned angular velocities, so the mean duration of a lunar day is 24 h 50 min 28.3 s.

The mean time interval between two successive conjunctions of the Moon and Sun (new moons) is called a synodical month, which has a duration of 29.530 588 1 days (29 d 12 h 44 min), i.e. lunation, which represents a month on ancient lunar calendars.

Moreover, the position of perigee varies over time and completes a revolution in an eastward direction (from vernal equinox to vernal equinox) in 8.8475 years. An anomalistic month (27.554 550 2 days, or 27 d 13 h 18.5 min) corresponds to two successive transits of the Moon at perigee. The direction of this rotation, which is the same as that of the Moon on its orbit, explains why its duration is longer than a tropical period.

The ascending node N is the point at which the Moon's orbit crosses the ecliptic in northward direction. This point gradually shifts westward along the ecliptic, i.e. so-called regression motion, with a complete revolution taking 18.613 3 years relative to the vernal equinox. Two successive transits of the Moon at its ascending node represents a draconic month, with a period of 27.212 217 8 days (27 d 05 h 05.6 min), which is shorter than a tropical month because of the regression. It should be mentioned here that the Sun crosses the Moon's ascending node every 346.6 days, and this period represents a draconic year.

Note also that solar attraction induces periodic oscillations in the Moon's motion relative to its mean orbit around Earth. The two major perturbations in its orbital velocity are evection (period 31.8 days) and variation (period 14.8 days). The inclination of the Moon's orbit ranges from 05°00′ to 05°17′ on the ecliptic (mean 05°07′47″), and from 18°30′ (ascending node N at vernal equinox) to 28°30′ (N at the autumnal equinoctial point) on the Equator.

The description of celestial body motions thus reveals many different periodicities, but these motions occur independently. However, at around 10 centuries BC, Chaldeans already knew about the eclipse recurrence interval (around 18 years and 11 days), or the so-called saros cycle.

The following correspondences may be noted:

- for the Moon:
  - — 223 lunations representing 6 585.321 1 days,
  - — 239 anomalistic months (perigee): 6 585.537 5 days,
  - — 242 draconic months (ascending node): 6 585.356 7 days,
  - — 241 sidereal months (fixed stars): 6 584.520 3 days,
  - — 241 tropical years (vernal equinox): 6 584.501 1 days.
- for the Sun:

— 18 tropical years: 6 574.359 6 days,
— 18 sidereal years: 6 574.614 6 days,
— 18 anomalistic years: 6 574.669 2 days,
— 19 draconic years: 6 585.400 0 days.

After one saros, the Earth, Moon and Sun are thus in around the same relative configuration, but deviations relative to the initial configuration increase during successive saros cycles. It would thus be incorrect to state that saros represents an absolute period of the system. The fact that the durations of the different months of the system are not the same is sufficient to conclude that the relative motions of the three celestial bodies (Earth, Moon and Sun) are not periodic.

3 • Time considerations for tidal studies

Since the beginning of life on Earth, the diurnal cycle has been considered as the most natural time base due to its impact on biorhythms. However, for the purposes of organizing their activities, human civilizations have for thousands of years been focusing on defining more precise time units, as well as conventions so as to be able to apply a common time system to larger and larger geographical sectors.

The primary time bases for tidal studies are defined chiefly on the basis of the rotation period of each celestial body. Items described earlier are necessary to examine these different times and relationships between them, so some repetition is inevitable.

For tidal studies, minute accuracy is generally considered sufficient in dating specific events, thus warranting the approximations made in the following sections.

3.1 • Sidereal time

Sidereal time is directly associated with the Earth's rotation around its polar axis $\overrightarrow{TP}$, whose anticlockwise (eastward) angular velocity ω_T is considered constant (see 2.1) for the purposes of tidal studies. For a given place, we have seen that the hour angle $\text{Æ}H_\gamma$ of point γ defines the local sidereal time.

A sidereal day T_γ (n.b. the term commonly used in reference to a tropical or equinoctial day) is the time required for $\text{Æ}H_\gamma$ to increase by 2π, i.e. 360° or 24 sidereal hours (hs), which corresponds to $\omega_T = 2\pi/T_\gamma$, i.e. 360°/24 hs or 15°/hs. Variations in ΔT_γ relative to the mean $\overline{T}_\gamma$ are very slight, with $\max |\Delta T_\gamma / T_\gamma| \approx 10^{-7}$. For tidal studies, this time is therefore considered as being mechanically constant. The mean angular velocity ω_T is 15.041 068

degrees per hour (from the mean solar time; see 3.2), thus giving a mean sidereal day time of 23 h 56 min 04.09 s, with variations of less than 0.01 s in absolute value, which is very negligible for tidal studies.

3.2 • True and mean lunar times

The lunar time concept is applied only for tidal studies since the Moon is the main driving force of tides. It is actually a uniform time, derived from the mean time, and defined by the motion of the mean Moon (n.b. fictional celestial body), whose orthogonal projection on the ecliptic involves uniform motion with the same apparent orbital period (from vernal equinox to vernal equinox) as the true Moon. Recall that the longitude of this projection, which varies uniformly over time, is incorrectly called the 'mean longitude' of the celestial body, rather than the 'mean Moon'.

The time interval between two consecutive transits of the Moon over the meridian of the place is called the true lunar day, with the mean lunar day denoted T_L. In mean time, we have $T_L = 24\text{h } 50 \text{ min } 28.3 \text{ s}$. This is a first-order approximation of the fundamental period of the so-called 'diurnal' lunar tide. The term lunar hour is sometimes used ($T_L/24$), where 1 lunar hour = 1.035 050 101 h of mean time.

3.3 • True and mean solar times; equation of time

The tropical year T_A, which governs the seasonal cycle and the rhythm of human activities, was selected as the principal time base. Although the Earth's motion may at first seem to be circular and heliocentric, its orbit is actually elliptical, whereby the Earth transits along this orbit sweeping out equal areas in equal intervals of time, in compliance with Kepler's laws. This gives an orbital angular velocity of the Earth relative to the Sun (located in one of the foci) that varies around a mean value, with a maximum at perihelion and a minimum at aphelion. In other words, the hour angle of the Sun $\text{Æ}H_{S\nu}$, which defines the true solar time (where subscript $S\nu$ denotes the true Sun), has the drawback of varying irregularly. The true solar day, symbolized here by $T_{S\nu}$, is thus determined by the time between two successive transits of the Sun over the meridian of a given place. It begins at true midday, at the time of the upper meridian transit. This time, which in ancient times was measured with a gnomon, was subsequently more accurately determined using sundials fitted with a style oriented parallel to the Earth's axis. These instruments were used for a very long time to determine the local time in use. This time base was used especially for the first tidal measurements recorded at Brest from 1806 to 1897.

During the year, the true solar day undergoes fluctuations $\Delta T_{S\nu}$ with respect to its mean $\overline{T_{S\nu}}$, with $\max |\Delta T_{S\nu}/\overline{T_{S\nu}}| \approx 0.5 \cdot 10^{-3}$, which are much greater than those of the sidereal day T_γ (n.b. $\max |\Delta T_\gamma/\overline{T_\gamma}| \approx 10^{-7}$). The range is from 23 h 59 min 39 s to 24 h 00 min 30 s.

If we overlook these variations (derived from the laws of mechanics) in the true solar time obtained via observations, we get the the mean local time (denoted t) whose corresponding unity is the mean day, a mean value $\overline{T_{S\nu}}$ established on the basis of the duration of a tropical year T_A. The mean local time runs from 0 to 24 h, beginning at midday. The deviation between the two solar times (i.e. 'mean' minus 'true') is called the equation of time.

Below we formulate an equation where $T_{S\nu}$ is considered as a function of the mean longitude of the Sun, a parameter that is defined has having a uniform variation pattern. For a given place, we obtain the following hour angle equation:

$$\text{Æ}H_\gamma = \alpha_{S\nu} + \text{Æ}H_{S\nu}$$

where

$\text{Æ}H_\gamma$ is the hour angle at vernal equinox (local sidereal time),

$\alpha_{S\nu}$ is the right ascension,

$\text{Æ}H_{S\nu}$ is the hour angle of the Sun.

When this equation is derived as a function of time, we obtain:

$$\frac{\partial \text{Æ}H_\gamma}{\partial t} = \frac{\partial \alpha_{S\nu}}{\partial t} + \frac{\partial \text{Æ}H_{S\nu}}{\partial t}$$

The derivative of the local sidereal time $\partial \text{Æ}H_\gamma/\partial t$ is simply the angular velocity of the Earth's rotation $\omega_T = 2\pi/T_\gamma$, which is considered constant. However, this does not apply for the derivative of $\partial \text{Æ}H_{S\nu}/\partial t$, which varies continuously but slowly around the mean. With a very accurate approximation, we have, by assimilating the derivative $\partial \text{Æ}H_{S\nu}/\partial t$ to the increment $\delta \text{Æ}H_{S\nu}/\delta t$, with $\delta \text{Æ}H_{S\nu} = 2\pi$ and the corresponding time δt, which is simply $T_{S\nu}$, we obtain:

$$\frac{2\pi}{T_\gamma} \approx \frac{\partial \alpha_{S\nu}}{\partial t} + \frac{2\pi}{T_{S\nu}}$$

and also:

$$T_{S\nu} \approx \frac{2\pi}{\frac{2\pi}{T_\gamma} - \frac{\partial \alpha_{S\nu}}{\partial t}}$$

To simplify the formulation, the subscript $S\nu$ will be omitted for the celestial equatorial coordinates (α, β) and ecliptic coordinates $(\lambda, 0)$ of the

true Sun. As the value of $\partial\alpha/\partial t$ is small with respect to $\omega_T = 2\pi/T_\gamma$ (around 1/366), we can also write, with a good degree of approximation:

$$T_{S\nu} \approx T_\gamma \left[1 + \frac{\frac{\partial\alpha}{\partial t}}{\omega_T} \right]$$

Moreover, the relationships between ecliptic and celestial equatorial coordinates give:

$$\tan\alpha = \cos\varepsilon \tan\lambda \Rightarrow \frac{\partial\alpha}{\partial t} = \frac{\cos\varepsilon}{\cos^2\lambda + \sin^2\lambda\cos^2\varepsilon} \times \frac{\partial\lambda}{\partial t}$$

Hence, when taking Kepler's area law into account, we have:

$$\frac{r_{S\nu}^2 \partial\lambda}{\partial t} = ab\left(\frac{2\pi}{T_{An}}\right)$$

where:

$r_{S\nu}$ is the Earth-true Sun distance at time t,

a and b are the semi-major axis and semi-minor axis of the ecliptic,

T_{An} is the duration of an anomalistic year (time between two successive passages at solar perigee, i.e. 365.259 4 days).

The true solar day $T_{S\nu}$, can be expressed with a very good degree of approximation as a function of polar coordinates of the apparent Sun $r_{S\nu}$ by:

$$T_{S\nu} \approx T_\gamma \left(1 + \frac{\cos\varepsilon}{\cos^2\lambda + \sin^2\lambda\cos^2\varepsilon} \times \frac{ab}{r_{S\nu}^2} \times \frac{T_\gamma}{T_{An}} \right)$$

To obtain the equation of time, we have to formulate equations for $r_{S\nu}$ and λ as a function of the mean time t (expressed in mean days).

When taking the direction of perihelion of longitude λ_{ps} as reference axis in the ecliptic, the position of the apparent Sun with respect to the centre of the Earth is given by the equation in polar coordinates $[r_{S\nu}, (\lambda - \lambda_{ps})]$ of the ellipse:

$$r_{S\nu} = a\frac{1 - e^2}{1 + e\cos(\lambda - \lambda_{ps})} \tag{A.4}$$

where e is the eccentricity of the orbit (recalling that perihelion moves slowly in anticlockwise direction and completes a revolution in 209.4 centuries). The angle $(\lambda - \lambda_{ps})$ of the Sun's direction relative to that of its perihelion is called the true anomaly. As it varies irregularly over time, the mean anomaly (as symbolized by the letter M, which always represents the value of this angle if the variation in the Sun's longitude were uniform) is defined, while the perhelion transit times remain constant. It can be expressed as a function

of time as: $M = h - p_1$, where h is the mean longitude of the Sun (symbol h for *helios*), and p_1 is the mean longitude of perihelion.

Let t_0 denote the time of the Earth's transit at perihelion and t denote the number of days since 1st January 2000 at 0 h. The value of the anomaly M in arc degrees is determined by:

$$M° \approx \frac{360(t - t_0)}{T_{An}} = 357.036\,3 + 0.985\,60t$$

Now the parameters $(r_{S\nu}, \lambda)$ of the apparent Sun can be expressed as a function of M. Because of the low value of excentricity e (0.016 73), equation A.4 gives a first-order approximation of the value of $r_{S\nu}$ in metres:

$$r_{S\nu} \approx a(1 - e\cos M) = 149.6 \cdot 10^9 \times (1 - 0.016\,73\cos M).$$

Note that, with this approximation, the semi-major axis of the Earth's orbit defines the mean Earth-Sun distance. The longitude λ can be obtained in degrees by: $\lambda° \approx 282.94 + M + 1.917\sin M$.

In a first-order approximation, the duration of the true solar day $T_{S\nu}$ thus has cyclical variations of period T_A. The equation of time $E(t)$ below, provided by the Bureau des Longitudes (Paris, France), is valid for the 1900 to 2100 period. It can be used to compute the deviation $E(t)$ in minutes between the mean time and the mean solar time by expressing the values of time t in this equation in mean days:

$$\begin{aligned} E(t)\ \text{min} = {} & 7.362\sin M - 0.144\cos M + 8.955\sin 2M \\ & + 4.302\cos 2M + 0.288\sin 3M + 0.133\cos 3M + 0.131\sin 4M \\ & + 0.167\cos 4M + 0.009\sin 5M + 0.011\cos 5M + 0.001\sin 6M \\ & + 0.006\cos 6M - 7.064 \cdot 10^{-5} t\sin 2M + 1.46 \cdot 10^{-5} t\cos 2M \end{aligned}$$

The extremes are reached in February (+14 min) and November (−16 min). This difference is balanced out four times a year (around mid-April, mid-June, early September and late December).

Note, finally, that the mean day is the result of a uniform variation (from 0 to 24 h) counted from midday. To avoid the drawback of a date change occurring in the middle of the day (between sunrise and sunset), the civil time is defined, which is equal to the mean time plus 12 h.

3.4 • Universal time in common use

The civil time of the place is no longer used because, by definition, it changes from one place to another, which is inconvenient. The advent of the railroad in the 19th century prompted the need for a common time to

encompass large areas (e.g. in France, the Law of 14 March 1891 established the mean civil time of Paris for all of metropolitan France and Algeria). At even earlier times and in remote areas, prior to the advent of radio transmission, the local civil time or, when there was no public clock available, the sundial time was generally used. Hence, from the outset in 1806, tidal measurements at Brest were read or recorded first in true time, then in local civil time, in Paris civil time, and finally in universal time.

After the International Meridian Conference that was held in Washington in 1884, the Greenwich civil time became the legal universal time, which is generally just called universal time and symbolized by UT. Note that the Greenwich mean time (GMT), which is often provided instead of UT, is unsuitable because it refers to the mean time, not the civil time.

Times used throughout the world are directly derived from UT. The surface of the globe is divided into 24 time zones having as median lines the 24 meridians whose longitudes occur every 15°. These time zones are numbered from 0 to 23 eastward, beginning at the Greenwich meridian. Based on mariners' usage, they have been assigned letters of the alphabet, beginning with the letter A representing time zone 1 and, in alphabetical order, finishing with letter Z for time zone 0. By convention, the time corresponding to each one is the UT plus the number of the time zone. The lower Greenwich meridian, which is in the 12th time zone, is the international date line. When the time zone number is above 12, one day must be deleted from the date. For the 12th time zone, this day is deleted only if the place is east of the international date line.

Note however that the dispositions imposed by the Washington Conference in 1884 included several exceptions. Many countries have two legal times, i.e. daylight savings time and standard time. In some regions, the legal time differs by 30 min from that of the time zone, but sometimes there is very little difference.

The universal time defines the time scale as published on calendars and as expressed by a time unit, i.e. the mean second. However, this definition of a fundamental unit turned out to be too inaccurate for certain modern physics applications. This led to the development of ephemeris time (ET) and International Atomic Time (IAT), which are only mentioned here for information – such high accuracy would be unwarranted for tidal applications.

3.5 • Calendars

The time interval since an initial time is required when calculating astronomic elements for a given date. This is a chronology issue. The dates are

obtained from calendars with a clearly defined baseline day numbering system. However, for tradition and convenience reasons, these calendars are in the form of a complex partitioning in years and months. Each civilization has created its own calendar, e.g. Julian, Gregorian, Coptic, Muslim, Israelian, Republican, Hellenistic, Indian, Tamil, Cambodian, Chinese, etc.

The earliest calendars were lunar calendars or almanacs (from the Arabic *al* and *mene*, i.e. lunation) that were based on lunations or time intervals between consecutive new moons. This was the case with the Chaldean calendar, and with the Muslim calendar (Hijri calendar), which is the official calendar in some Persian Gulf countries. The first day of the first year on the Hijri calendar is the day that Muhammad left Mecca for Medina, i.e. 17 July 622. Most Muslim countries have, however, now adopted the Gregorian calendar and only use the Hijri calendar for religious purposes.

Lunation thus serves as a time unit on these calendars. This may seem surprising, but at a time when the mechanical concept of 'uniform time' was meaningless, the lunar cycle seemed more regular than diurnal cycles in which the lengths of days and nights vary between seasons. However, this dating approach, which is not dependent on the rhythm of life (days, seasons, years), clearly has major shortcomings. As there are also marked variations in lunation (ranging from 29 days and 6 h to 29 days and 20 h), its use as a time unit is incompatible with clockwork. It is thus necessary to introduce the notion of mean lunation, which is equivalent to 29.530 588 1 days (29 d 12 h 44 min) of mean time.

The Gregorian calendar, which has now been universally adopted, includes two types of year, i.e. 'common years' divided into 12 months of 31, 28, 31, 30, 31, 30, 31, 31, 30, 31, 30 and 31 days, respectively, and 'leap years' in which the second month has 29 days. Leap years are those whose year is a multiple of 4, except those whose year is a multiple of 100, but not of 400. Hence, 1900 was a common year whereas 2000 (divisible by 400) was a leap year. The mean year length obtained in this way – called the Gregorian year – is 365.242 5 days of mean time, which is close to the tropical year length (365.242 2 days).

The Gregorian calendar was designed with respect to the Julian calendar, which was created in 45 BC. In the Julian calendar, all years whose millenium is a multiple of 4 (including multiples of 100), are leap years. The mean length of a Julian year is thus 365.25 days, which differs markedly from the length of a tropical year (a time unit that is often used in astronomy is the Julian century of 36 525 days of mean time). Due to this difference, over the centuries, there was a lag in the dates of solstices and equinoxes, which was only partially corrected by the adoption of the Gregorian calendar through

the elimination of 10 days in October 1582: the day after Thursday 4 October 1582 (Julian calendar) was thus Friday 15 October 1582 (Gregorian calendar). The Gregorian calendar was immediately adopted in four Catholic countries: Italy, Spain, Portugal and the Netherlands. In France, the reform was only applied in December of the same year, when the day after Sunday 9 December 1582 became Monday 20 December 1582. In Great Britain, the reform was not applied until 1752, when 2 September was followed immediately by 14 September. The Gregorian calendar was gradually adopted by different countries up until the early 20th century, and it is now used throughout the world (except for the celebration of certain religious holidays).

These are important considerations for astronomic and tidal computations which are sometimes performed for the reenactment of historical events. In such cases, it is necessary to be able to transcribe a date – after checking the calendar from which it derives – into a chronologically consistent system.

According to a convention that was adopted by astronomers to facilitate chronological numbering, mean days, beginning at midday UT, are numbered as of a prehistoric period. The day number, beginning from the original prehistorical date, is the Julian date, i.e. 1st January 4713 BC on the Julian calendar. The Julian date thus represents the interval of time since midday UT on that day. Note that historians use the Julian celendar for dates prior to its creation (-45) and that the year preceding 1 AD on the Christian calendar is denoted 1 BC, which is a leap year. Years 1, 5, 9, etc., BC are thus leap years. Astronomers use the algebraic notation: year 1 BC corresponds to the astronomical year number 0, with 2 BC being year -1, and so on.

B
Force and potential fields

In many problems involving vector fields (forces or currents), the concept of potential can be introduced to enable substantial simplifications and clarify the physical aspects of the phenomenon. Concerning tides (Chapter III), we have analysed the spatial distribution of the tide-generating force on Earth at a given time. This distribution is representative of a force field with a meridional structure with the direction of the celestial body-Earth centres as axis of revolution. It is essential to know whether this force distribution derives from a potential in order to be able to assess the structure.

This appendix provides a brief review of vector and potential fields, whose concepts are common to many physical phenomena: electricity, magnetism, hydrodynamics, gravitation, etc. Hereafter, by preference, the term 'force' is used instead of 'vector' or 'velocity'. The main definitions required to understand the concepts of force and potential fields are first outlined. Plane fields are then examined to facilitate the understanding of so-called meridional fields in 3D space.

1 • Force fields: terminology and definitions

Let us consider an orthonormal reference frame Oxyz. It is assumed that there is a simply connected spatial region where a force field is defined by regular functions (uniform, non-zero, continuous and accepting continuous partial derivatives). These conditions give rise to lines and tubes of force.

One feature of lines of force is that they accept as tangent the force applied at each of their M points of coordinates (x, y, z). While the force vector

$\overrightarrow{F}(M)$ characterizing the studied field accepts the regular functions of constituents $[F_{(x)}, F_{(y)}, F_{(z)}]$, lines of force verify the two differential equations:

$$\frac{dx}{F_{(x)}} = \frac{dy}{F_{(y)}} = \frac{dz}{F_{(z)}} \tag{B.1}$$

Hence, only one line runs through each point M in this space (application of Cauchy's theorem on solutions for differential equation systems).

A tube of force is a surface consisting of a set of lines of force that is dependent on a closed curve and completely contained in the associated space considered. This curve cannot have any crunodes or arcs in common with a line of force.

A force field with the above described properties is said to be 'solenoidal' if the divergence of the force $\overrightarrow{F}(M)$ is zero at all M points, i.e. if:

$$\overrightarrow{\nabla} \times \overrightarrow{F}(M) = \frac{\partial F_{(x)}}{\partial x} + \frac{\partial F_{(y)}}{\partial y} + \frac{\partial F_{(z)}}{\partial z} = 0 \tag{B.2}$$

where $\overrightarrow{\nabla}$ is the vectorial operator of constituents $\left(\partial/\partial x, \partial/\partial y, \partial/\partial z\right)$ in Cartesian coordinates, while $\times$ denotes the scalar product. This latter property results in the conservation of flows through tubes of force. In hydrodynamics, the equivalent is the conservation of incompressible fluid flow in a stream tube.

Force $\overrightarrow{F}(M)$ derives from a scalar potential U(M) if its constituents satisfy the following equation:

$$\overrightarrow{F}(M) = \overrightarrow{\nabla} U(M) \tag{B.3a}$$

where $\overrightarrow{\nabla}$ is the previously described vectorial operator. In a matrix representation, this equality gives the Cartesian constituents of the force:

$$\overrightarrow{F}(M) \Rightarrow \begin{bmatrix} F_{(x)} \\ F_{(y)} \\ F_{(z)} \end{bmatrix} = \begin{bmatrix} \partial U/\partial x \\ \partial U/\partial y \\ \partial U/\partial z \end{bmatrix} \tag{B.3b}$$

A force will derive from a potential if and only if the rotational (or whirl) is zero, or:

$$\overrightarrow{\nabla} \wedge \overrightarrow{F}(M) = 0 \tag{B.4}$$

Note that in some applications (especially in electricity and magnetism) U(M) often denotes the force function, whereas the potential is defined as the opposite, i.e. $-U(M)$.

For a solenoidal field deriving from a scalar potential, force $\overrightarrow{F}(M)$ satisfies the two conditions B.2 and B.3, thus giving the following equation:

$$\overrightarrow{\nabla} \times \overrightarrow{\nabla} U(M) = \frac{\partial^2 U}{\partial^2 x} + \frac{\partial^2 U}{\partial^2 y} + \frac{\partial^2 U}{\partial^2 z} = \Delta U = 0 \qquad (B.5)$$

where Δ is the Laplace operator. Function U(M), which is both regular (definite, continuous, and derivable) and the solution of the Laplace equation when the right-hand side happens to be zero, is said to be 'harmonic'.

2 • Plane fields

Concerning certain physical phenomena, the force $\overrightarrow{F}(M)$ has the following two properties: it remains parallel to a fixed plane, and also its intensity and direction remain the same while its origin M moves perpendicular to this plane. This results in a plane force field. With an orthonormal trihedral O*xyz*, where the force field is identical in all planes parallel to O*xy*, it is possible to determine the entire field in the considered space by assessing what is taking place on this latter plane. In this section, coordinate *z* is not involved ($z = 0$).

2.1 • Lines of force on a plane solenoidal field

When using O*xy* as Cartesian reference frame, the differential equation for such a line of force is:

$$-F_{(y)} \cdot dx + F_{(x)} \cdot dy = 0 \qquad (B.6)$$

In the case of a solenoidal field (zero divergence), the first side of equation B.6 is a total differential $d\Lambda$. Then at all points $M(x, y)$, there exists a flow or discharge function that satisfies equation:

$$\Lambda(x, y) = \lambda$$

where λ is constant. The corresponding line of force is denoted by Λ_λ. The matrix representation of constituents of $\overrightarrow{F}(M)$ is as follows:

$$\overrightarrow{F}(M) \Rightarrow \begin{bmatrix} F_{(x)} \\ F_{(y)} \end{bmatrix} = \begin{bmatrix} +\partial\Lambda/\partial y \\ -\partial\Lambda/\partial x \end{bmatrix} \qquad (B.7)$$

Let us consider the variation in function $\Lambda(x, y)$ along a pathway that links

any point P on line Λ_p with any point Q on line Λ_q. Along the pathway PQ, $\overrightarrow{ds}$ is the elementary displacement defined by its constituents:

$$\overrightarrow{ds} \Rightarrow \begin{bmatrix} dx \\ dy \end{bmatrix}$$

and $\overrightarrow{n}$ is the unit vector of the orthogonal at each of its points, which is obtained by an anticlockwise rotation of $\pi/2$ from $\overrightarrow{\mathrm{d}s}$. At each point on the curve PQ, we thus have the constituents of vector $\overrightarrow{n}\,ds$:

$$\overrightarrow{n}\,\mathrm{d}s \Rightarrow \begin{bmatrix} -dy \\ +dx \end{bmatrix}$$

with $ds = \|\overrightarrow{ds}\|$.

We can thus write:

$$\begin{aligned} \Lambda(\mathrm{Q}) - \Lambda(\mathrm{P}) &= \int_{\mathrm{P}}^{\mathrm{Q}} \left[\frac{\partial \Lambda}{\partial x}\, dx + \frac{\partial \Lambda}{\partial y}\, dy \right] \\ &= \int_{\mathrm{P}}^{\mathrm{Q}} \left(-\mathrm{F}_{(y)}\, dx + \mathrm{F}_{(x)}\, dy \right) \end{aligned}$$

or:

$$\Lambda(\mathrm{Q}) - \Lambda(\mathrm{P}) = -\int_{\mathrm{P}}^{\mathrm{Q}} \overrightarrow{\mathrm{F}}\,(\mathrm{M}) \times \overrightarrow{n}\, ds.$$

This is, to the closest sign, the flow of force $\overrightarrow{\mathrm{F}}\,(\mathrm{M})$ along pathway PQ. From a hydrodynamic standpoint, this corresponds to the flow of a fluid between the two corresponding stream lines Λ_p and Λ_q.

2.2 • Plane solenoidal fields: complex potential

A force $\overrightarrow{\mathrm{F}}\,(\mathrm{M})$ can derive from a scalar potential U(M) if and only if the rotational of this force is zero.

In the light of equation B.7, this rotational may be formulated as:

$$\frac{\partial \mathrm{F}_{(y)}}{\partial x} - \frac{\partial \mathrm{F}_{(x)}}{\partial y} = -\left(\frac{\partial^2 \Lambda}{\partial^2 x} + \frac{\partial^2 \Lambda}{\partial^2 y} \right) = -\Delta_h \Lambda$$

where Δ_h is the Laplace operator in the plane Oxy, which is assumed to be horizontal (subscript h), or:

$$\Delta_h = \frac{\partial^2}{\partial^2 x} + \frac{\partial^2}{\partial^2 y}$$

Hence, for a plane solenoidal field, this necessary and sufficient condition indicates that the function of flow $\Lambda(M)$ confirms, as does the scalar potential $U(M)$, the Laplace equation.

2.2.1 • Associative relations between the potential and lines of force

Based on the properties described above, we may formulate the following association equations representing relations between functions representing a solenoidal potential plane and those representing flow lines:

$$F_{(x)} = \frac{\partial U}{\partial x} = \frac{\partial \Lambda}{\partial y} \tag{B.8a}$$

$$F_{(y)} = \frac{\partial U}{\partial y} = -\frac{\partial \Lambda}{\partial x} \tag{B.8b}$$

As for $\Lambda(x, y)$, consider the variation in function $U(x, y)$ along a pathway linking any point P on line U_p with any point Q on line U_q. On the curve PQ, $\overrightarrow{ds}\,(dx, dy)$ denotes the elementary displacement along the pathway.

The potential difference is therefore as follows:

$$\begin{aligned} U(Q) - U(P) &= \int_P^Q \left[\frac{\partial U}{\partial x}\, dx + \frac{\partial U}{\partial y}\, dy \right] \\ &= \int_P^Q (F_{(x)}\, dx + F_{(y)}\, dy) \\ &= \int_P^Q \overrightarrow{F} \times \overrightarrow{ds} \end{aligned}$$

It represents the work of force $\overrightarrow{F}\,(M)$ along curve PQ, regardless of the pathway chosen to link these two points.

When one of the two functions $U(x, y)$ or $\Lambda(x, y)$ is known, the other may be determined to the closest additive constant. Moreover, the equipotential lines U_u and flow lines Λ_λ are orthogonal.

By orienting the equipotential lines U_u in increasing order with respect to the flow lines Λ_λ, and the latter in decreasing order with respect to the equipotential lines, i.e. in the direction of force $\overrightarrow{F}\,(M)$, at all points M, we obtain $(\overrightarrow{ds_\Lambda}, \overrightarrow{ds_U}) = \pi/2$, where $\overrightarrow{ds_\Lambda}$ and $\overrightarrow{ds_U}$ are the elementary vectorial displacements on the corresponding lines indicated by the subscripts.

The sum $\Phi = U + j\Lambda$ then becomes a regular function of the complex variable $\zeta = x + jy$, while function Φ represents the complex potential of the solenoidal field derived from potential U.

It should be noted that, due to the linearity of the gradient operator, any linear combination of elementary complex potentials (representing plane solenoidal fields derived from a potential) is in turn a complex potential

function. Note also that the associated equations B.8a and B.8b enable permutation of the roles of the two functions. If we consider lines Λ_λ as being equipotential, U_u are the corresponding flow lines.

2.2.2 • Examples of complex potentials

Let us consider the following very simple examples:

The parallel complex potential. The complex function $\Phi_{(p)} = \zeta = x + jy = U_{(p)} + j\Lambda_{(p)}$ is representative of a plane parallel field, as denoted by subscript (p). The equipotentials and flow lines are $x = u$ and $y = \lambda$, respectively, with u and λ being constant. The lines of force are thus parallel to the Ox axis and the equipotentials are parallel to Oy. The constituents of force $\overrightarrow{F}_{(p)}(M)$ are:

$$\overrightarrow{F}_{(p)}(M) \Rightarrow \left| \begin{array}{l} F_{(x)} = 1 \\ F_{(y)} = 0 \end{array} \right.$$

The work required to get from any point of equipotential $x = u$ to any point of equipotential $x = u + k$ is equal to k, and the flow between any point of $y = \lambda$ and $y = \lambda + \nu$ is equal to ν, where k and ν are arbitrary constants.

The radial complex potential. With $\zeta = re^{j\varphi}$, function $\Phi_{(r)} = (\kappa/2\pi)\log\zeta = (\kappa/2\pi)\log(re^{j\varphi})$, where κ is a positive or negative constant, represents the plane field with radial lines of force, as denoted by subscript (r). This potential may be formulated as follows: $\Phi_{(r)} = (\kappa/2\pi)(\log r + j\varphi) = U_{(r)}(r) + j\Lambda_{(r)}(\varphi)$

To the closest coefficient $\kappa/2\pi$, the equipotentials are concentric circumferences $\log r \propto u$ with, as centre, the origin of axes from which stem lines of force according to radii $\varphi \propto \lambda$ (n.b. u and λ are constant).

Force $\overrightarrow{F}_{(r)}(M)$ on radius $\overrightarrow{OM}$ of the unit vector $\overrightarrow{v}$ is:

$$\overrightarrow{F_{(r)}}(M) = \frac{\partial U_{(r)}}{\partial r}\overrightarrow{v} = \frac{\kappa}{2\pi}\frac{1}{r}\overrightarrow{v}$$

The force flow through each circumference remains steady and equal to κ. This flow can also be obtained by: $\Lambda(\varphi = 2\pi) - \Lambda(\varphi = 0) = \kappa$. The origin behaves as a source if constant κ is positive, but as a sink if it is negative.

The hyperbolic complex potential. The complex function $\Phi_{(h)} = \zeta^2 = (x + jy)^2$ can also be expressed by the following equation:

$$\Phi_{(h)} = (x^2 - y^2) + j2xy = U_{(h)} + j\Lambda_{(h)}$$

This is a flat plane with hyperbolic lines of force, as denoted by (h). The equation for the equipotentials is $U_{(h)} = x^2 - y^2 = u$ and that for the flow lines is $\Lambda_{(h)} = 2xy = \lambda$, with u and λ being constant. These equations define two orthogonal hyperbola families. The equipotential asymptotes are

bisectors (lines $y = \pm x$) of axes Ox and Oy, and those of lines of force are the axes themselves.

The constituents of force $\overrightarrow{\mathrm{F}}_{(h)}(\mathrm{M})$ are thus:

$$\overrightarrow{\mathrm{F}}_{(h)}(\mathrm{M}) \Rightarrow \begin{bmatrix} \mathrm{F}_{(x)} = \partial \mathrm{U}_{(h)}/\partial x = +2x \\ \mathrm{F}_{(y)} = \partial \mathrm{U}_{(h)}/\partial y = -2y \end{bmatrix}$$

The origin is a specific but non-unique point. Derivative $\mathrm{d}\Phi_{(h)}/\mathrm{d}\zeta = 2\zeta$ is definite and continuous and is cancelled out. On each axis of reference frame Oxy, the force changes direction as it passes the origin, which is a flow stagnation point, i.e. a convergence point on Oy and divergence point on Ox.

3 • Meridional fields

Fields are said to be 'meridional' when the lines of force and equipotential lines are encompassed in hemispheres delimited by a line, i.e. the field's axis of revolution. In other words, the equipotential surfaces and associated flux tubes rotate around this axis. We will assess the different properties of these fields using the same approach as that used for plane fields.

Let us consider the orthonormal reference frame Oxyz. Ox is the axis of revolution that can generate equipotential surfaces and flows from the corresponding lines occurring on the half-plane $y \geq 0$ of Oxy. The properties of the meridional fields are also studied, as for plane fields, on the basis of the functions of flows and potential, but the association equations (B.8a and B.8b) are different.

3.1 • Associative relations between flows and meridional potentials

On the half-plane $y \geq 0$ of Oxy, where the force constituents and coordinates of the point of application are:

$$\overrightarrow{\mathrm{F}}(\mathrm{M}) \Rightarrow \begin{vmatrix} \mathrm{F}_{(x)} \\ \mathrm{F}_{(y)} \end{vmatrix} \qquad \mathrm{M} \Rightarrow \begin{vmatrix} x \\ y \end{vmatrix}$$

Force $\overrightarrow{\mathrm{F}}$ is tangential to the flow line Λ_λ at point M. In the trihedron Oxyz, ϖ denotes the longitude of the field whose origin meridian is the upper meridian of axis Oy, where the axis of revolution Ox is considered as a polar axis of the studied field.

Let $\partial\Lambda = d\Lambda\partial\varpi$ be the variation in flow corresponding to the differential $d\Lambda = (\partial\Lambda/\partial x)dx + (\partial\Lambda/\partial y)dy$ at point M along the element of circumference $y\overrightarrow{\partial\varpi}$. This corresponds to the flux of the force $\overrightarrow{\mathrm{F}}(\mathrm{M})$ through a conical

element whose sides are the portion of arc $y\overrightarrow{\partial\varpi}$ and the portion of curve $\overrightarrow{ds_U}(dy, -dx)$ orthogonal to the force $\overrightarrow{F}$ (M). The flow through the annular surface generated by a complete rotation around Ox of element $\overrightarrow{ds_U}$ can be formulated by the following equation:

$$2\pi d\Lambda = 2\pi y(-F_{(y)}dx + F_{(x)}dy)$$

At the considered point M, we thus have:

$$d\Lambda(x, y) = -yF_{(y)}dx + yF_{(x)}dy$$

and the consituents of $\overrightarrow{F}$ (M) may be expressed in the Oxy plane by:

$$\overrightarrow{F}(M) \Rightarrow \left| \begin{array}{l} F_{(x)} = +\dfrac{1}{y} \cdot \dfrac{\partial\Lambda}{\partial y} \\ F_{(y)} = -\dfrac{1}{y} \cdot \dfrac{\partial\Lambda}{\partial x} \end{array} \right.$$

Moreover, if $U(x, y)$ is the function representing the equipotential line passing through M, we obtain the following association equations:

$$F_{(x)} = \frac{\partial U}{\partial x} = +\frac{1}{y} \cdot \frac{\partial\Lambda}{\partial y} \tag{B.9a}$$

$$F_{(y)} = \frac{\partial U}{\partial y} = -\frac{1}{y} \cdot \frac{\partial\Lambda}{\partial x} \tag{B.9b}$$

These equations may be compared to those formulated for plane fields (B.8a and B.8b). Lines U_u and Λ_λ cross at a right angle, but are not interchangeable.

Based on equations B.9a and B.9b, and by crossed derivation in order to successively eliminate functions Λ and U, we obtain:

$$\partial^2 U/\partial^2 x + \partial^2 U/\partial^2 y + y^{-1}\partial U/\partial y = 0 \tag{B.10a}$$

$$\partial^2\Lambda/\partial^2 x + \partial^2\Lambda/\partial^2 y - y^{-1}\partial\Lambda/\partial y = 0 \tag{B.10b}$$

It is possible to verify the equivalence of equation (B.10a) and the Laplace equation. Let us consider the trihedron OXYZ obtained by considering $X = x$, $Y = y\cos\varpi$ and $Z = y\sin\varpi$ (plane OXY coincides with Oxy for $\varpi = 0$). This gives us, first:

$$y^2 = Y^2 + Z^2 \Rightarrow y \cdot dy = Y \cdot dY + Z \cdot dZ$$

where

$$\frac{\partial y}{\partial Y} = \frac{Y}{y} = \cos\varpi$$

and

$$\frac{\partial y}{\partial \mathrm{Z}} = \frac{\mathrm{Z}}{y} = \sin \varpi$$

and, secondly:

$$\tan \varpi = \mathrm{Z}/\mathrm{Y} \Rightarrow y \cdot d\varpi = -\sin \varpi \cdot d\mathrm{Y} + \cos \varpi \cdot d\mathrm{Z}$$

where $\partial\varpi/\partial \mathrm{Y} = -y^{-1} \sin \varpi$ and $\partial\varpi/\partial \mathrm{Z} = y^{-1} \cos \varpi$

Then we obtain:

$$\begin{aligned}
\frac{\partial \mathrm{U}}{\partial \mathrm{X}} &= \frac{\partial \mathrm{U}}{\partial x} \\
\frac{\partial \mathrm{U}}{\partial \mathrm{Y}} &= \frac{\partial \mathrm{U}}{\partial y} \cos \varpi - \frac{\partial \mathrm{U}}{\partial \varpi} \frac{\sin \varpi}{y} \\
\frac{\partial \mathrm{U}}{\partial \mathrm{Z}} &= \frac{\partial \mathrm{U}}{\partial y} \sin \varpi + \frac{\partial \mathrm{U}}{\partial \varpi} \frac{\cos \varpi}{y}
\end{aligned}$$

When considering the fact that the flow is meridional (potential U is independent of ϖ, thus $\partial \mathrm{U}/\partial\varpi = 0$), then by a second derivation we get:

$$\begin{aligned}
\frac{\partial^2 \mathrm{U}}{\partial^2 \mathrm{X}} &= \frac{\partial^2 \mathrm{U}}{\partial^2 x} \\
\frac{\partial^2 \mathrm{U}}{\partial^2 \mathrm{Y}} &= \frac{\partial^2 \mathrm{U}}{\partial^2 y} \cos^2 \varpi + \frac{\partial \mathrm{U}}{\partial y} \frac{\sin^2 \varpi}{y} \\
\frac{\partial^2 \mathrm{U}}{\partial^2 \mathrm{Z}} &= \frac{\partial^2 \mathrm{U}}{\partial^2 y} \sin^2 \varpi + \frac{\partial \mathrm{U}}{\partial y} \frac{\cos^2 \varpi}{y}
\end{aligned}$$

By addition, we note the equivalence with equation (B.10a):

$$\Delta \mathrm{U} = \frac{\partial^2 \mathrm{U}}{\partial^2 \mathrm{X}} + \frac{\partial^2 \mathrm{U}}{\partial^2 \mathrm{Y}} + \frac{\partial^2 \mathrm{U}}{\partial^2 \mathrm{Z}} = \frac{\partial^2 \mathrm{U}}{\partial^2 x} + \frac{\partial^2 \mathrm{U}}{\partial^2 y} + \frac{1}{y}\frac{\partial \mathrm{U}}{\partial y} = 0 \qquad \text{(B.11a)}$$

The fact that the two equations B.10a and B.11a are identical indicates that the flux of the force is constant between two tubes rotating around axis Ox. When parameters x and y are constant, function U(X, Y, Z) does not vary when point M of coordinates (X $=$ x, Y, Z) describes a parallel of radius y around Ox. U is called a zonal harmonic function, which means that it satisfies the Laplace equation with no right side and its value is independent of angle ϖ, i.e. the longitude of the field.

However, the associated function Λ(X, Y, Z) is not harmonic because, by affecting Λ in the same way, it becomes:

$$\Delta\Lambda = \frac{\partial^2 \Lambda}{\partial^2 \mathrm{X}} + \frac{\partial^2 \Lambda}{\partial^2 \mathrm{Y}} + \frac{\partial^2 \Lambda}{\partial^2 \mathrm{Z}} = \frac{\partial^2 \Lambda}{\partial^2 x} + \frac{\partial^2 \Lambda}{\partial^2 y} + \frac{1}{y}\frac{\partial \mathrm{U}}{\partial y} \qquad \text{(B.11b)}$$

If we then take equation B.10b into account:

$$\Delta\Lambda = \frac{2}{y}\frac{\partial U}{\partial y} \neq 0$$

The Laplace operator of Λ is thus not zero, but the flow function Λ is independent of ϖ, like U.

Hence, for functions U and Λ to form a joint set $(U;\Lambda)$ of a meridional field such that U is a zonal harmonic function and Λ is a flow function, they must be associated via equations B.9a and B.9b.

The linearity of equations B.10a and B.10b gives rise to the following property: if sets $(U_A;\Lambda_A)$ and $(U_B;\Lambda_B)$ are two distinct meridional fields, the linear combination of these fields $(U_A + cU_B;\Lambda_A + c\Lambda_B)$, where c is a positive or negative constant, also represents a meridional field $(U_C;\Lambda_C)$. This property is especially useful for determining a potential from the elementary fields of the different forces present.

3.2 • Meridional fields and Legendre polynomials

A meridional field $(U;\Lambda)_n$ is said to be homogeneous and of degree n if potential U is a homogeneous function of x and y, and of degree n. Because of the linear association equations B.9a and B.9b, function Λ is obviously of degree $n+1$.

Generally, when $\mu = x/r$, the homogeneous zonal harmonic functions of degee n are of the form $U = r^n f_n(\mu)$.

If we take equations $r^2 = x^2 + y^2$ and $\mu = x/r$ into account, then:

$$dr = \mu dx + \sqrt{1-\mu^2}\, dy$$

$$d\mu = \frac{dx}{r} - \frac{x}{r^2}dr = \frac{1}{r^3}\left(y^2 dx - dy \cdot dy\right)$$

Association equations B.9a and B.9b, expressed as a function of r and μ, may be formulated as:

$$\frac{\partial U}{\partial r}\mu + \frac{\partial U}{\partial \mu}\frac{y^2}{r^3} = \frac{1}{y}\left(\frac{\partial \Lambda}{\partial r}\sqrt{1-\mu^2} - \frac{\partial \Lambda}{\partial \mu}\frac{xy}{r^3}\right)$$

$$\frac{\partial U}{\partial r}\sqrt{1-\mu^2} - \frac{\partial U}{\partial \mu}\frac{xy}{r^3} = -\frac{1}{y}\left(\frac{\partial \Lambda}{\partial r}\mu + \frac{\partial \Lambda}{\partial \mu}\frac{y^2}{r^3}\right)$$

By solving the system with $\partial U/\partial r$ and $\partial U/\partial \mu$, we obtain:

$$r^2 \frac{\partial U}{\partial r} = -\frac{\partial \Lambda}{\partial \mu} \tag{B.12a}$$

$$(1-\mu^2)\frac{\partial U}{\partial \mu} = +\frac{\partial \Lambda}{\partial r} \tag{B.12b}$$

By cross derivations and eliminating Λ, we obtain the following Legendre differential equation, which is equivalent to that of Laplace for homogeneous functions (B.11a):

$$(1-\mu^2)\frac{d^2 f_n}{d^2\mu} - 2\mu\frac{df_n}{d\mu} + n(n+1)f_n = 0 \tag{B.13}$$

The general solution may be obtained by knowing the particular solution of this equation. This is the case when n is an integer, and then the integral is a so-called Legendre polynomial of degree n and generally denoted by $P_n(\mu)$.

The first polynomials are cumulatively formulated. For the first ones, we obtain:

$$\begin{aligned}
P_0(\mu) &= 1 \\
P_1(\mu) &= \mu \\
P_2(\mu) &= (3\mu^2 - 1)/2 \\
P_3(\mu) &= (5\mu^3 - 3\mu)/2 \\
P_4(\mu) &= (35\mu^4 - 30\mu^2 + 3)/8 \\
\cdots &= \cdots
\end{aligned}$$

It may be noted that they obey the following recurrence equation:

$$(n+1)\cdot P_{n+1}(\mu) - (2n+1)\cdot\mu\cdot P_n(\mu) + n\cdot P_{n-1}(\mu) = 0$$

One important feature of meridional fields, assuming that the axis of revolution Ox is the stream line, is that they may be determined from plane fields when axis Ox is recognized as both the stream line and the symmetry axis. It is demonstrated that transformation of the plane potential, as represented by a complex function $\Phi(\zeta)$ with $\zeta = x + jy$, into a meridional potential U occurs via the integral:

$$U = \frac{1}{\pi}\int_0^{\pi} \Phi(x + jy\cos\varpi)\,d\varpi \tag{B.14a}$$

In the case of a plane field defined by a homogeneous function $\Phi(\zeta)$ of degree n relative to ζ, the integral equation B.14a necessarily determines a homogeneous meridional field of the same degree. When taking, for

instance, the flat field represented by the complex function $\Phi(\zeta) = \zeta^n$, where n is an integer, with $\mu = x/r$ we obtain the meridional field:

$$\begin{aligned} U_{(n)} &= \frac{1}{\pi}\int_0^{\pi} \left(x + jy\cos\varpi\right)^n \mathrm{d}\varpi \\ &= \frac{r^n}{\pi}\int_0^{\pi} \left(\mu + j\sqrt{1-\mu^2}\cos\varpi\right)^n \mathrm{d}\varpi \end{aligned} \tag{B.14b}$$

The latter term is the product of r^n via a μ polynomial which turns out to be the Legendre polynomial of degree n, i.e. the only integral polynomial of the Legendre differential equation (A2.13), hence the $P_n(\mu)$ integral equation:

$$P_{n,}(\mu) = \frac{1}{\pi}\int_0^{\pi} \left(\mu + j\sqrt{1-\mu^2}\cos\varpi\right)^n \mathrm{d}\varpi \tag{B.15}$$

It is thus possible to demonstrate that the entire potential of a meridional field can be developed in a series of homogeneous functions in the vicinity of an ordinary point on the axis of revolution. In other words, in a connected space around a point (which is not unique on the axis of the meridional field, e.g. source or sink), all zonal harmonic functions can be expanded from Legendre polynomials. This property may be demonstrated on the basis of a number of hypotheses (in particular, the symmetry axis should be the line of force and the reference frame origin cannot be a unique point) and of the Legendre polynomial integral equation B.15.

Where $\Phi(\zeta = x + jy)$ is the analytic function defining the field in plane Oxy ($y \geq 0$), which is true when variable ζ is true. Potential $\Phi(\zeta = 0)$ is considered as the unity of the potential with a true value. The expansion of function $\Phi(\zeta)$ around origin O, which is an ordinary point of the field, may be expressed by:

$$\Phi(\zeta) = 1 + \sum_{n=1}^{n=N} b_n \zeta^n \tag{B.16a}$$

where N is the integer whose value can range from unity to infinity depending on the nature of function $\Phi(\zeta)$, with b_n being the constants.

The corresponding meridian potential is expressed by:

$$U(r, \mu) = 1 + \sum_{n=1}^{n=N} b_n r^n P_n(\mu) \tag{B.16b}$$

As the potential at origin O was selected as the unity of the potential,

equation B.16b may also be formulated as:

$$U(M)/U(O) = 1 + \sum_{n=1}^{n=N} b_n r^n P_n(\mu) \qquad \text{(B.16c)}$$

This result is essential for understanding the role of Legendre polynomials in studies on homogeneous meridian fields.

4 • Examples of meridional fields

As for plane fields, a practical representation of sets $(U; \Lambda)$ is obtained by plotting curves U_u and Λ_λ on the half-plane Oxy ($y \geq 0$). The difference with respect to plane fields is due to factor y^{-1}, which is present in association equations (A2.09.a and b). This factor hampers permutation of roles between force and equipotential lines, as in plane fields.

We will now provide examples related to the potential of the tide-generating force, corresponding to a given celestial body.

4.1 • Parallel meridional fields

The lines of force are parallel to the axis of revolution. As for plane fields, the corresponding meridional fields are also represented by subscript (p). We have seen that a plane field with lines of force parallel to axis Ox is expressed by the complex potential on plane Oxy:

$$\Phi_{(p)} = \zeta = x + jy = re^{j\varphi}$$

A meridional field accepting the same lines of force is obtained with functions $\Lambda_{(p)}$ and only depends on y on the Oxy plane, and equation B.9b gives:

$$F_{(y)} = -\frac{1}{y}\frac{\partial \Lambda_{(p)}}{\partial x} = \frac{\partial U_{(p)}}{\partial y} = 0 \Rightarrow \Delta U_{(p)} = \frac{\partial^2 U_{(p)}}{\partial^2 x} = 0$$

where:

$$U_{(p)} = x = r\cos\varphi \Rightarrow F_{(x)} = \partial U_{(p)}/\partial x = 1$$

For associated lines of force $\Lambda_{(p)}$, we thus have:

$$d\Lambda_{(p)} = y(-F_{(y)}dx + F_{(x)}dy) = ydy \Rightarrow \Lambda_{(p)} = y^2/2 = (r\sin\varphi)^2/2$$

A meridional field whose lines of force are parallel to the axis is thus represented in Oxy by the set: $(U_{(p)}; \Lambda_{(p)}) = (x; y^2/2)$.

This meridional field accepts planes $x = u$ as equipotential surfaces, and cylindrical surfaces with axis Ox and radius $y = \sqrt{2\lambda}$ as tubes of force, while u and λ are constant.

The work of the force between any two points located on planes $x = u_0$ and $x = u_1$, respectively, is equal to $u_1 - u_0$. The flow between two tubes of force of radius $y = \sqrt{2\lambda_0}$ and $y = \sqrt{2\lambda_1}$, respectively, is equal to $2\pi(\lambda_1 - \lambda_0)$.

Here a homogeneous first-order function represents the potential:

$$U_{(p)}(M) = x = r\mu \tag{B.17a}$$

The integral equation B.14b representing this meridional field in the Legendre polynomial can be immediately verified:

$$U_{(p)} = \frac{r}{\pi}\int_0^{\pi}(\mu + j\sqrt{1-\mu^2}\cos\varpi)\mathrm{d}\varpi = r\mu = rP_1(\mu) \tag{B.17b}$$

4.2 • Radial meridional fields: force source or sink

In a plane field, we have seen an example of a radial complex potential, as denoted by subscript (r) $\Phi_{(r)} = U_{(r)}(r) + j\Lambda_{(r)}(\varphi) = (\kappa/2\pi)(\log r + j\varphi)$

This plane potential is representative of a source if $\kappa > 0$, or of a sink if $\kappa < 0$. Circumferences centred on the origin are equipotential and their radii are lines of force (radial force).

For symmetry reasons, the comparable radial meridional field accepts concentric spheres around the origin as equipotential surfaces, and half-lines deriving from the centre (anticlockwise from the origin at the point of force application) as lines of force. In the half-plane Oxy ($y \geq 0$), where the complex coordinates of point M are $x + jy = re^{j\varphi}$ with φ ranging from 0 to π, the potential U_r is only a function of r and Λ_r or of φ.

The flow, which must remain the same through all spheres centred on the origin, involves a normal force at the sphere that is inversely proportional to the square of the radius of this sphere. Where κ is the value of this flow, we thus have:

$$\overrightarrow{F}_{(r)}(M) = \frac{dU_{(r)}}{dr}\overrightarrow{\nu} = \frac{\kappa}{4\pi r^2}\overrightarrow{\nu} \Rightarrow U_{(r)} = -\frac{\kappa/4\pi}{r}$$

$$F_{(x)} = F_{(r)}\cos\varphi; F_{(y)} = F_{(r)}\sin\varphi \Rightarrow d\Lambda = -F_{(r)}y(\sin\varphi\, dx - \cos\varphi\, dy)$$

with $F_{(r)} = \| \overrightarrow{F}_{(r)} \|$ and $\overrightarrow{\nu}$ as unit vector of $\overrightarrow{OM}$

Since:

$$dx = \cos\varphi dr - r\sin\varphi d\varphi$$
$$dy = \sin\varphi dr + r\cos\varphi d\varphi$$

then:

$$d\Lambda_{(r)} = (\kappa/4\pi)\sin\varphi d\varphi \Rightarrow \Lambda_{(r)} = -(\kappa/4\pi)\cos\varphi$$

Hence, to the closest factor $\kappa/4\pi$, we obtain the representation of the radial meridional field by the pair of functions:

$$(U_{(r)}; \Lambda_{(r)}) \propto (-1/r; -\cos\varphi)$$

As for the corresponding plane field, there will be a source when κ is positive and a sink if it is negative. In 3D space, tubes of force are rotating conical surfaces having origin O as apex and φ as half angle. All of these cones therefore cross the equipotential spheres at a right angle.

In many applications, it is often easier to study the structure of this type of field in the vicinity of a singular point in the field (source or sink). Here we will alter the conventions in order to examine the formulation of the field around point T. The reference frame that has so far been represented by O*xyz* will now be denoted OXYZ; reference frame T*xyz* will be that which has point T as origin, with its axes parallel to those of OXYZ; and the direction $\overrightarrow{TO}$ will be the axis of revolution of this radial field.

Where $r_O = \|\overrightarrow{OT}\|$, i.e. the distance between the two origins, the value of the x-axis of point T on OX is considered to be $-r_O$.

In the half-plane common to T*xy* ($y \geq 0$) and OXY ($Y \geq 0$), with a point M being distances *r* and *a* from points O and T, respectively, and with $a/r \ll 1$, we have:

- in OXY ($Y \geqslant 0$) : $\overrightarrow{OM} \Rightarrow X + jY = re^{j\varphi}$
- in T*xy* ($y \geqslant 0$) : $\overrightarrow{TM} \Rightarrow x + jy = ae^{j\theta}$

The matrix equation of constituents of vector $\overrightarrow{MO}$ in the two reference frames and its complex representation in T*xy* may be formulated as follows:

$$\overrightarrow{MO} \Rightarrow \begin{bmatrix} -X \\ -Y \end{bmatrix} = \begin{bmatrix} r_O - x \\ 0 - y \end{bmatrix} \Rightarrow (r_O - x) - jy = r_O(1 - \zeta)$$

where

$$\zeta = \alpha e^{j\theta} \text{ with } \alpha = a/r_O \ll 1 \tag{B.18}$$

When $\mu = x/a = \cos\theta$, distance *r* is thus given by:

$$r^2 = (x - r_0)^2 + y^2 = r_0^2(1 - 2\alpha\mu + \alpha^2)$$

Potential $U_{(r)}(M)$ at point M, relative to that at point T, which is non-zero and equal to $U_{(r)}(T) = \kappa/4\pi r_O$, can be expressed as:

$$\frac{U_{(r)}(M)}{U_{(r)}(T)} = \frac{1}{\sqrt{1 - 2\alpha\mu + \alpha^2}} \tag{B.19a}$$

Note that, as the computations are done in the reference frame of origin T,

there is an inversion of the sign of parameter κ in its relation with the singular point of the radial field (positive sign for a sink, negative for a source).

As point T is on the axis of revolution $\zeta(\mathrm{T}) = 0$, its complex potential is true with $\Phi_{(r)}(\mathrm{T}) = \mathrm{U}_{(r)}(\mathrm{T})$. When taking the complex expression of vector $\overrightarrow{\mathrm{MO}}$ in (A2.18) into account, the complex potential $\Phi_{(s)}(\mathrm{M})$ in the Txy plane may be expressed in the following form:

$$\frac{\Phi_{(r)}(\mathrm{M})}{\mathrm{U}_{(r)}(\mathrm{T})} = \frac{1}{1-\zeta} = 1 + \sum_{n=1}^{n\to\infty} \zeta^n$$

Because of the property summarized by equations (B.16a) and (B.16c), potential $\mathrm{U}_{(r)}(\mathrm{M})$ relative to that of T is thus expressed in Txyz by the following Legendre polynomial series:

$$\frac{\mathrm{U}_{(r)}(\mathrm{M})}{\mathrm{U}_{(r)}(\mathrm{T})} = 1 + \sum_{n=1}^{n\to\infty} \alpha^n \mathrm{P}_n(\mu) \tag{B.19b}$$

As B.19a and B.19b are equivalent equations, we may deduce:

$$\frac{1}{\sqrt{1-2\alpha\mu+\alpha^2}} = 1 + \sum_{n=1}^{n\to\infty} \alpha^n \mathrm{P}_n(\mu)$$

where

$$|2\alpha\mu - \alpha^2| \ll 1 \tag{B.20}$$

All radial meridional fields – thus with spherical equipotential surfaces – generated by a sink (or a source), thus develops from an ordinary point in the space by a harmonic Legendre polynomial series (B.19b), where the line joining the ordinary point to the singular point is the axis of the field.

4.3 • A meridional field of hyperbolic $a^2\mathrm{P}_2(\mu)$ shape

Recall that, for a given celestial body A (Moon or Sun), the tide-generating force at a point M is the difference in gravitational attraction exerted by this celestial body at point M (radial force of direction $\overrightarrow{\mathrm{MA}}$, therefore depending on the position of the point on Earth) and at the Earth's centre T (force of constant intensity at all M points and with a fixed direction parallel to TA). The fields of these two forces have $\overrightarrow{\mathrm{TA}}$ as symmetry axis.

The tide-generating potential associated with a given celestial body is thus the difference between a radial field $\mathrm{U}_{(r)}$ and a parallel field $\mathrm{U}_{(p)}$.

For any radial meridional field $\mathrm{U}_{(r)}$, we have just seen that equation B.19b may be applied to express the potential of any point M in the vicinity of any ordinary point on the axis of revolution. As the Earth's centre T is an

ordinary point of the gravitational field generated by celestial body A (force sink), its potential $U_{(r)}(T)$ may be expressed by:

$$U_{(r)}(T) \equiv V_A(T) = km_A/r_A$$

where $V_A(T)$ is the attraction potential at T generated by celestial body A, where k is the universal gravitation constant, m_A is the mass of the celestial body, and r_A is the distance between the centres of the Earth and the celestial body. For a point M on the Earth's surface ($a = a_T$, Earth's radius), equation B.19b becomes:

$$\frac{U_{(r)}(M)}{V_A(T)} = 1 + \sum_{n=1}^{n\to\infty} \alpha^n P_n(\mu) \tag{B.21}$$

where α and μ have the same definitions, distances r_O and a have been respectively replaced by r_A (origin O at the centre of celestial body A) and by a_T, the Earth's radius.

With respect to the parallel meridional field, with a force equal to unity and parallel to the axis of the field, the corresponding potential $U_{(p)}$ is given by equation B.17a. When considering that the conventions applied to work in the reference frame of origin T, and also that the second force applied in M is constant (km_A/r_A^2) and of fixed direction $\overrightarrow{TA}$ (tractive force of reference body Txyz), the potential of the corresponding parallel field $U_{(p)}(M)$ can be expressed as:

$$U_{(p)}(M) - U_{(p)}(T) = \frac{km_A}{r_A^2}x = \frac{km_A}{r_A}\frac{a_T}{r_A}\cos\theta$$

where:

$$U_{(p)}(M) - U_{(p)}(T) = V_A(T)\alpha P_1(\mu) \tag{B.22}$$

As the potentials are defined to the nearest constant, then let:

$$U_{(p)}(T) = V_A(T) = \frac{km_A}{r_A}$$

The last relation of B.22 can thus be expressed by:

$$U_{(p)}(M)/V_A(T) = 1 + \alpha P_1(\mu) \tag{B.23}$$

The difference between the two elementary fields B.21 and B.23 hence gives the tide-generating potential at the Earth's surface generated by celestial body A, as:

$$\frac{U_{(s)}(M) - U_{(p)}(M)}{V_A(T)} = \sum_{n=2}^{n\to\infty} \alpha^n P_n(\mu) \tag{B.24}$$

The terms of series B.24 rapidly decrease with $\alpha \ll 1$, and it is also relevant to study the meridional field relative to the terms in $\alpha^2 P_2(\mu)$.

Hereafter, distance r_A is assumed to be constant, but we consider that the distance TM is variable. In order to avoid confusing it with the Earth's radius a_T, we will switch back to the initial designation a. Then, where subscript m denotes the tide, let:

$$U_{(m)} = r_A^2 \alpha^2 P_2(\mu) = a^2 P_2(\mu)$$

With multiplicative factor $k m_A r^{-3}$, U_m represents the tide potential generated by celestial body A.

Note that, via the integral B.14b, this meridional field corresponds to the plane hyperbolic field $\Phi(\zeta) = \zeta^2$. This field $U_{(m)}$ can be readily studied by examining the intersections of the equipotential surfaces and tubes of force with the plane Txy. Let us recall the relations between the Cartesian and polar coordinates of a point M on this plane:

$$x/a = \cos\theta = \mu \text{ avec } a^2 = x^2 + y^2$$

The part of the field represented in figure B.1 is that of the quadrant with coordinates x and y being positive, i.e. corresponding to $0 \leq \theta \leq 90°$. Traces in plane Txy of equipotential surfaces correspond to lines in equation:

$$U_{(m)} = a^2 P_2(\mu) = a^2 (3\cos^2\theta - 1)/2 = u$$

with u being constant, is:

$$U_{(m)} = \frac{2x^2 - y^2}{2} = u$$

Equipotential surfaces generated by the rotation of these lines around Tx form two rotational hyperboloid families having the same asymptotic cone of apex T. This conical surface is therefore at the same potential as point T, which was adopted here as the reference potential, with $u = 0$. The traces of this conical surface in Txy are the lines of equation $y = \pm x\sqrt{2}$. The half-angle at apex θ_0 is determined by:

$$\cos\theta_0 = 1/\sqrt{3} \Rightarrow \theta_0 = 53°44$$

In the box in figure B.1, this pair of lines corresponds to traces whose colour is referenced by $p(0)$, i.e. a potential of zero value $u = 0$. This is the location of points where the flow (or force) lines are tangential to spheres centred on T.

When $u < 0$, equation $y^2 = 2(x^2 - u)$ is always positive and the first family of equipotential surfaces is made up of one-sheeted rotational hyperboloids.

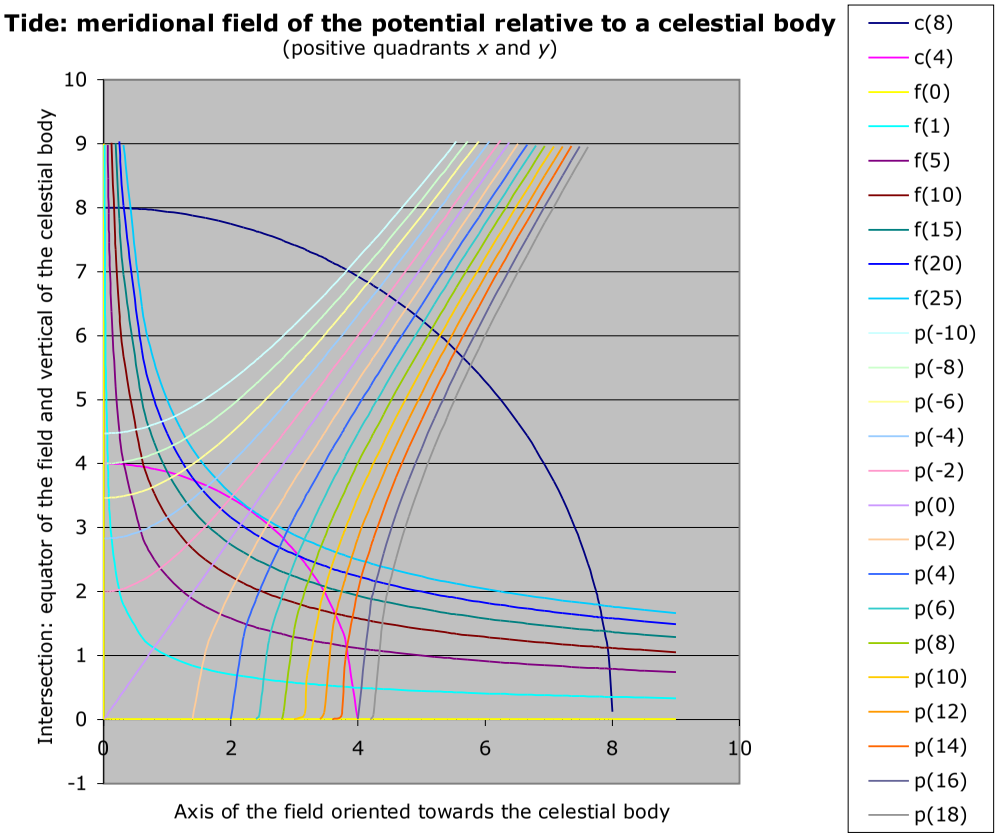

FIGURE B.1: Potential field generated by a celestial body. To the closest constant, it corresponds to the limited approximation of the Legendre polynomial $P_2(\cos\theta)$. In the positive x and y quadrants, lines $c(a)$, $f(\lambda)$ and $p(n)$ represent the traces of spheres of radius a, flow lines of value λ and equipotentials of value u.

The corresponding traces shown in figure B.1 are curves $p(u)$, where u is negative.

When $u > 0$, the values of function $y^2 = 2(x^2 - u)$ are only positive for $x^2 > u$. The second family of equipotential surfaces is made up of two-sheeted rotational hyperboloids. In figure B.1, their corresponding traces are curves $p(u)$, where u is positive.

In plane Txy, the coordinates of M and the constituents of force $\overrightarrow{\mathrm{F}}_{(m)}(\mathrm{M})$ may be expressed by:

$$\mathrm{M} \Rightarrow \left| \begin{array}{l} x \\ y \end{array} \right. \qquad \overrightarrow{\mathrm{F}}_{(m)}(\mathrm{M}) \Rightarrow \left| \begin{array}{l} \mathrm{F}_{(x)} = \partial \mathrm{U}_{(m)}/\partial x = 2x \\ \mathrm{F}_{(y)} = \partial \mathrm{U}_{(m)}/\partial y = -y \end{array} \right.$$

Noting that $\mathrm{F}_{(x)}$ is twice the x value of M, i.e. the point of application of the force, and $\mathrm{F}_{(y)}$ is minus the y value of M, we obtain the result of Proctor's rule, with the celestial body at infinity.

The modulus of $\overrightarrow{\mathrm{F}}_{(m)}$ is thus $a\sqrt{3\cos^2\theta + 1}$.

With $a = a_\mathrm{T}$ and to the nearest multiplicative factor, $g(m_\mathrm{A}/m_\mathrm{T})(a_\mathrm{T}^2/r_\mathrm{A}^3)$ is the equation formulated by Proctor. Proctor's rule thus corresponds to the expression of the tide-generating potential limited to the first term in $\mathrm{P}_2(\cos\theta)$.

Decomposition of force $\overrightarrow{\mathrm{F}}_{(m)}$ according to $\overrightarrow{\mathrm{TM}}$ and the tangent at the circumference passing by M (which corresponds to a rotation θ of reference frame Txy) gives the vertical constituent $\mathrm{F}_{(\zeta)}$ and horizontal constituent $\mathrm{F}_{(\xi)}$, respectively, or:

$$\mathrm{F}_{(\xi)} = \frac{1}{a}\frac{\partial \mathrm{U}_{(m)}}{\partial \theta} = -3a\cos\theta\sin\theta = -\frac{3}{2}a\sin 2\theta$$

$$\mathrm{F}_{(\zeta)} = \frac{\partial \mathrm{U}_{(m)}}{\partial a} = 2a\mathrm{P}_2(\cos\theta) = a(3\cos^2\theta - 1)$$

The absolute value of the horizontal constituent $\mathrm{F}_{(\xi)}$ (which affects the tide) is zero on axis Tx ($\theta = 0°$ and 180°) and on the equatorial plane of the field ($\theta = 90°$); it is maximum for $\theta = 45°$ and 135°.

The vertical constituent $\mathrm{F}_{(\zeta)}$, like $\mathrm{P}_2(\cos\theta)$, is zero on the asymptotic cone $\cos\theta_0 = 1/\sqrt{3} \Rightarrow \theta_0 = 53°44$. The absolute value has two maximums, i.e. a main one on axis Tx ($\theta = 0°$ and 180°) and a secondary one on the equatorial plane of the field, which is that of the great circle where the celestial body can be seen on the horizon ($\theta = 90°$). For this second maximum, the force is always directed towards the centre T (zero horizontal constituent).

Flux tubes rotating around Tx can be studied in the same way as equipotential surfaces. Equations of their traces in Txy are deduced from associa-

tion equations B.9a and B.9b to the nearest constant:

$$\frac{\partial \Lambda_{(m)}}{\partial y} = +y\frac{\partial U_{(m)}}{\partial x} = 2xy \Rightarrow \Lambda_{(m)=} = xy^2$$

or

$$\frac{\partial \Lambda_{(m)}}{\partial x} = -y\frac{\partial U_{(m)}}{\partial y} = y^2 \Rightarrow \Lambda_{(m)=} = xy^2$$

In Txy, the equations for the lines of flow are thus: $\Lambda_{(m)} = xy^2 = \lambda$, where λ is constant.

In Txy, the lines of force are of the 3rd degree and have a hyperbolic shape. The structure of the corresponding tubes resembles a family of two-sheeted rotational hyperboloids which have axis Tx, i.e. the flow line ($\lambda = 0$, with $y = 0$), and the equatorial plane of the field, i.e. the flow surface ($\lambda = 0$, with $x^2 = 0$), as asymptotes. The flow sheets λ and $-\lambda$ are symmetrical with respect to the plane $x = 0$, i.e. the equatorial plane of the field. Hence, when the absolute values of the respective x-axes cross, the flow lines are oriented in opposite directions. In positive quadrants x and y (see figure B.1), the lines of force correspond to positive values of λ. Curve $f(\lambda)$ represents the flow line for the corresponding positive value λ.

The quarter circumferences, with radii $a = 4$ and $a = 8$, respectively, may be plotted to obtain a clearer view of the structure of this 'tidal' meridional field associated with celestial body A, relative to spheres of centre T.

C

Stilling wells

Studying an entire stilling well system is a highly complex process. The response of the well depends on the dimensions and forms of its different elements (well, intake opening and pipe), as well as on the internal and external hydrodynamic conditions (viscosity, head loss, waves, currents, density differences). Moreover, because of environmental conditions at the well site, problems of fouling, concretions or silting around the intake or the pipe often arise.

Very few authors have focused on this issue, apart from O'Brien (1950), Lennon (1967), Cross (1968), and especially Noye (1968, 1970, 1972, 1974a, b & c). A stilling well equation will first be formulated to represent the response of the well (internal water level) in its simplest configuration (pipeless well with an intake and assuming zero viscosity for sea water). Then the equation will be extended to represent wells equipped with a pipe (so-called 'pipe wells') and taking into account the liquid viscosity and the roughness of the pipe surface. A very simple digital model of the response of a well of clearly defined dimensions will then be applied to two cases (a pipeless well with an intake and a pipe well), while assuming that the external excitation (tide or swell) is completely sinusoidal.

1 • Stilling well equation

The equation formulated below is based on Noye's first work on wells with an intake directly interconnected with the sea – this is the most common type of stilling well.

Let us consider a coastal site where the depth is H (relative to the mean level) and where $h(t)$ represents the sea level variation (from zero mean: $\overline{h(t)} = 0$), with the variation being positive according to the upward vertical.

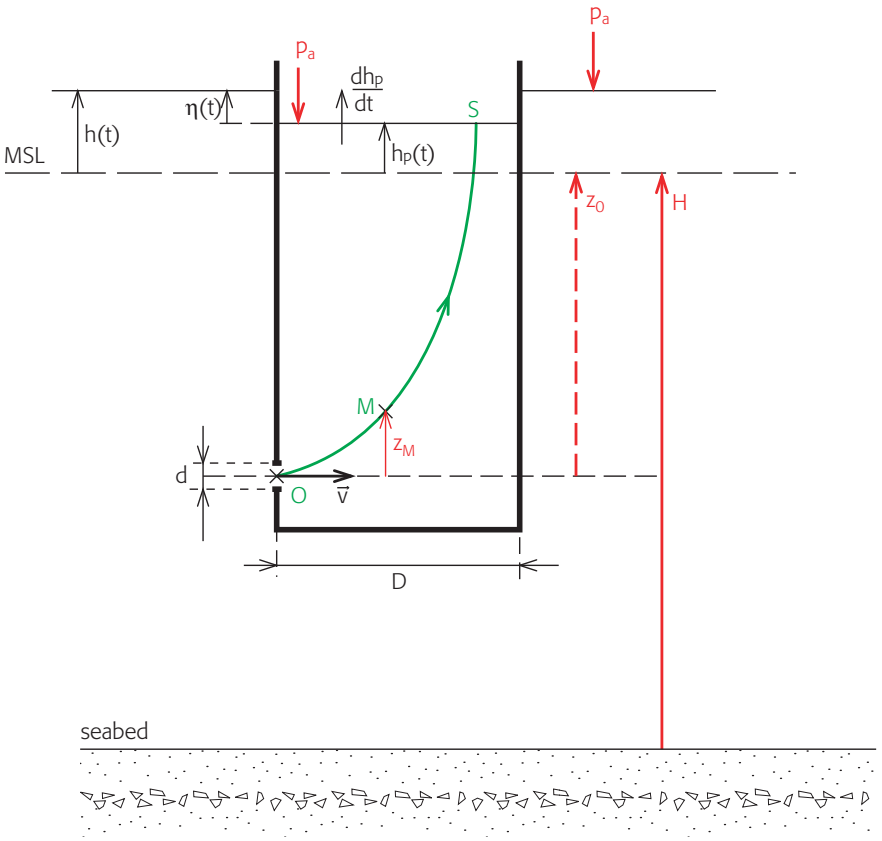

Figure C.1: Diameter of a pipeless stilling well of diameter D, where the intake opening O (diameter d) is directly connected with the sea. The notations are outlined in the text. MSL: mean sea level $\overline{h(t)} = 0$.

A cylindrical well of diameter D has a circular intake opening of centre O and diameter d located at a mean depth of z_0 (fig. C.1), which is below the lowest low water. Hence, the mean sea level is at the z_0 mark (always a positive value) relative to point O. Let $\eta(t)$ denote the error in $h(t)$ relative to $h_p(t)$, i.e. the level in the well at time t, or:

$$\eta(t) = h(t) - h_p(t) \tag{C.1}$$

We also assume that sea water is a perfect, incompressible and isothermal liquid, therefore of constant density ρ and zero viscosity ($\upsilon = 0$).

Within the well, at all points M of height z_M relative to the intake and subjected to pressure p_M, velocity v_M derived from potential Φ_M along

the stream line and running through M (flow thread OMS in figure C.1, with point S being at the water surface in the stilling well), the generalised Bernoulli equation may be formulated as:

$$\frac{\partial \Phi_M}{\partial t} + \frac{1}{2} v_M^2 + g z_M + \frac{p_M}{\rho} = f(t) \tag{C.2}$$

As function $f(t)$ is the same along this line, equation (C.2) applied at points S and O, respectively, gives equation:

$$\frac{\partial \Phi_S}{\partial t} + \frac{1}{2}\left(\frac{dh_p}{dt}\right)^2 + g(z_0 + h_p) + \frac{p_a}{\rho} = \frac{\partial \Phi_O}{\partial t} + \frac{1}{2} v_O^2 + \frac{p_O}{\rho} \tag{C.3}$$

In this latter equation, p_a is the atmospheric pressure at S, with p_O and v_O respectively representing the liquid pressure and velocity (positive direction towards the well) at the intake O.

Further hypotheses must be put forward to determine pressure p_O. We assume that currents around the well do not induce a Venturi effect and that only the variable constituent of p_O is associated with the surface wave h (which is assumed to be sinusoidal: waves, swells, seiches, tides). The pressure associated with this gravitational wave is a function of the immersion of intake O. In addition to this immersion, equal to z_0, the transmission factor k_O (while taking the exponential attenuation of the pressure into account) is also a function of the number κ of the wave, or:

$$\begin{aligned} k_O &= \frac{\cosh[\kappa(H - z_0)]}{\cosh(\kappa H)} \approx \exp(-\kappa^2 z_0 H) \\ k_O &\approx 1 - \kappa^2 z_0 H \end{aligned} \tag{C.4}$$

with $\kappa^2 z_0 H \ll 1$.

This coefficient is equal to 1 for very long wavelengths (e.g. tidal).

The pressure around the intake can thus be expressed by:

$$p_O = p_a + \rho g(z_0 + k_O h) \tag{C.5}$$

Considering the convention chosen for the sign of velocity v_O, the continuity equation is formulated as:

$$D^2(dh_p/dt) = d^2 \cdot v_O \Rightarrow v_O = (dh_p/dt)/r^2 \tag{C.6}$$

where $r = d/D$.

Equation (C.3) then becomes:

$$\frac{\partial(\Phi_S - \Phi_O)}{\partial t} = g(k_O h - h_p) + \frac{1}{2}\left[\frac{dh_p/dt}{m}\right]^2 \tag{C.7}$$

where

$$m^2 = r^4/(1 - r^4) \tag{C.8}$$

The left side of equation (C.7) may be estimated by integration of velocity v_M along the stream line (line OMS). If the well is long and narrow ($D \ll z_0$), the first-order velocity in the well is dh_p/dt and the distance OS can be assimilated to $z_0 + h_p$. With these approximations, we have:

$$\Phi_S - \Phi_O \approx (z_0 + h_p)(dh_p/dt) \tag{C.9}$$

and equation (C.7) is expressed by:

$$\left(\frac{dh_p}{dt}\right)^2 = g\frac{2m^2}{1 - 2m^2}(k_p h_p - k_O h) \tag{C.10}$$

where

$$k_p = 1 + \frac{z_0}{g}\frac{d^2h_p/dt^2}{h_p} \tag{C.11}$$

Equation (C.10) is the so-called 'stilling well equation' for a liquid of zero viscosity that is directly connected with the sea.

Coefficient k_p represents the inertia of the well. For a sinusoidal wave with angular velocity ω and wave number κ , the two coefficients k_p and k_O are the same magnitude. Based on the hypotheses put forward and the Laplace dispersion equation, for gravitational waves expressed by:

$$\omega^2 = g\kappa \tanh(\kappa H) \tag{C.12}$$

it turns out that:

$$k_p \approx 1 - (z_0/g)\omega^2 = 1 - \kappa z_0 \tanh(\kappa H) \approx 1 - \kappa^2 z_0 H \tag{C.13}$$

Based on the definition (C.4) of k_O, for a completely sinusoidal wave we thus obtain:

$$k_p \approx k_O \tag{C.14}$$

Since it is not easy to model equation (C.10) (difficulty in determining coefficients k_p and k_O), we accept that $k_p = k_O = 1$ and $r = d/D \ll 1$ (and thus $m \approx r^2$), and therefore the well equation (C.10) may be simplified to:

$$\frac{dh_p}{dt} = \frac{d(h - \eta)}{dt} = m\eta\sqrt{\frac{2g}{|\eta|}} \tag{C.15}$$

and:

$$\frac{d\eta}{dt} + m\eta\sqrt{\frac{2g}{|\eta|}} = \frac{dh}{dt} \tag{C.16}$$

where η is the error defined in (C.1).

This latter equation may also be obtained by assuming that velocity v_O, as defined by the continuity equation (C.6), is at all times equal to velocity v given by Torricelli's equation:

$$v^2/2 = g|\eta| \tag{C.17}$$

This means that the hydrostatic hypothesis is satisfied while disregarding the inertia in the well (thus the immersion of the intake opening).

Sea water is actually not a perfect liquid. When taking the kinematic viscosity coefficient into account, Noye (1974,b) demonstrated that it is possible to build a well with a pipe of length l and having a linear response. For relatively low frequencies (especially tidal frequencies), the response time is dependent only on the well characteristics. The subsequent phase lag correction required for each tidal constituent is not problematic when using modern computation methods. To build such a system, however, a perfectly smooth (no roughness) pipe of very long length l relative to its diameter d ($l > 10^2 d$) would be necessary to preserve the flow, which is always laminar. Maintenance of this system would also not be easy due to fouling and silting problems.

Flow through the intake is often turbulent even in pipeless wells. Hence, when the error value $|\eta|$ is constant, depending on whether we are considering inflow or outflow, the turbulence is not the same and the intake cross section is modified in all cases. The result is that the corresponding velocity moduli differ. This can be explained by the fact that part of the kinetic energy is lost via heat dissipation. To simplify the equations representing energy conservation along a stream line, this effect is generally represented by a decrease in the theoretical pressure gradient (obtained for the flow of a perfect liquid). The integral for this gradient error throughout the stream line reflects a drop in potential, or 'head loss' in the well. It is also essential to ensure that the geometry of the intake connected with the sea (directly or via a tube) promotes flow with minimal turbulence.

Hereafter we will assess digital model results applied to a well with clearly defined features (with a pipe or pipeless), while taking the type of flow into account. The flow will be considered as being laminar for pipeless wells. For pipe wells, the pipe roughness will be taken into account, and the regime will be laminar or turbulent, depending on the flow velocity.

2 • Digital modelling of the system

A simple but adequate digital model of a well's response to clearly defined characteristics can be developed in order to quantify and possibly reduce the error (by changing the well characteristics) so as to obtain satisfactory results for tidal constituents.

Assessment of the head loss that may occur when water passes through the intake or pipe is a complex problem to solve. It involves the turbulence of liquid flows whose physical aspects can only be partially controlled in real situations. It is however still possible to draw on empirical (but experimentally based) results, which are widely accepted for solving this type of problem. We will briefly look a these results, which will be used in the models presented.

2.1 • A brief review of liquid flows through tubes

Dimensional analysis methods provide a basis for formulating parameters whose values are involved in laminar (Poiseuille flow) or turbulent (hydraulic flow) flow equations. Newton (1713) was the first to study the viscosity μ of a liquid. He came up with the idea of an internal resistance proportional to the relative velocity of liquid elements sliding over each other (for water at 20°C: $\mu \approx 10^{-3}$kg/ms). The ratio $\upsilon = \mu/\rho$ is involved in equations that express the acceleration of a liquid with laminar flow. This ratio defines the kinematic viscosity ($\upsilon \approx 10^{-6} m^2/s$ for water at 20°). This is sometimes called the 'molecular kinematic viscosity' in order to differentiate it from the 'turbulent kinematic viscosity', which can reach values of around $10^{11}\upsilon$, especially for oceanic flows. This turbulence considerably increases the head loss, which is hereafter denoted p_c.

For a given pipe (tube of constant diameter) with smooth walls (zero roughness), it is logical, from a hydrodynamic standpoint, to assume that the gradient of head loss per length unit and per mass unit, denoted $\Gamma = (\mathrm{d}p_c/\mathrm{d}l)/\rho$, which has the dimensions of an acceleration, is a function of:

- d, the tube diameter,
- ρ, the liquid density,
- υ, the kinematic viscosity coefficient, and
- v, the flow velocity.

All of these quantitative factors are combined in the following equation:

$$\mathrm{F}(\Gamma, d, \rho, \upsilon, v) = 0 \tag{C.18a}$$

This equation is relevant irrespective of the units selected (in a consistent system). With d for length, ρ for density, and v for velocity as fundamental

units, equation (C.18a) leads to an equation between two dimensionless ratios:

$$F(\Gamma d/v^2, 1, 1, \upsilon/vd, 1) = 0 \tag{C.18b}$$

According to hydraulic conventions, the 'head loss coefficient λ' is defined by:

$$\lambda = \frac{\Gamma d}{(v^2/2)} = \frac{1}{\rho}\frac{dp_c}{dl}\frac{d}{(v^2/2)} \tag{C.19}$$

and the Reynolds number Re is defined by:

$$\mathrm{Re} = \frac{vd}{\upsilon} = \frac{\rho vd}{\mu}$$

From equation (C.18b), we deduce that the head loss coefficient is a function of the Reynolds number:

$$\lambda = f(\mathrm{Re}) \tag{C.20}$$

The Hagen-Poiseuille law, as experimentally determined for the laminar flow regime, gives:

$$\lambda = 64/\,\mathrm{Re} \tag{C.21}$$

When log(Re) is on the x-axis and log(λ) is on the y-axis, the curve plotted for (C.21) is a straight line up to a certain Re value at which there is turbulence onset (see figure C.2: Moody diagram). This critical value, which is dependent on the agitation of the liquid when it penetrates the tube, increases and the agitation decreases. It is never lower than $2.4 \cdot 10^3$, but it may be over 10^4 when there is extreme flow regulation at the tube intake. Beyond this critical Re value, the curve rises sharply and then slowly declines. Many authors have studied turbulent flow regimes in smooth tubes. These experimental results are represented by the lowest curve on the Moody diagram, and corresponds to the interval $(3 \cdot 10^3, 10^7)$ of the Reynolds number. The equation formulated by Karman for this curve is:

$$\lambda[\log_{10}(\mathrm{Re}\sqrt{\lambda}) - 0{,}40]^2 = 0{,}25 \tag{C.22}$$

In practice, for modelling purposes, it is generally considered that the flow regime is respectively:

- laminar if $\mathrm{Re} < 2 \cdot 10^3$,
- turbulent if $\mathrm{Re} > 4 \cdot 10^3$.

The regime is transitional between these two values. The following rule is often adopted for computations of hydraulic systems. A laminar flow whose velocity increases as of zero stays in this state until $\mathrm{Re} = 4 \cdot 10^3$. Conversely,

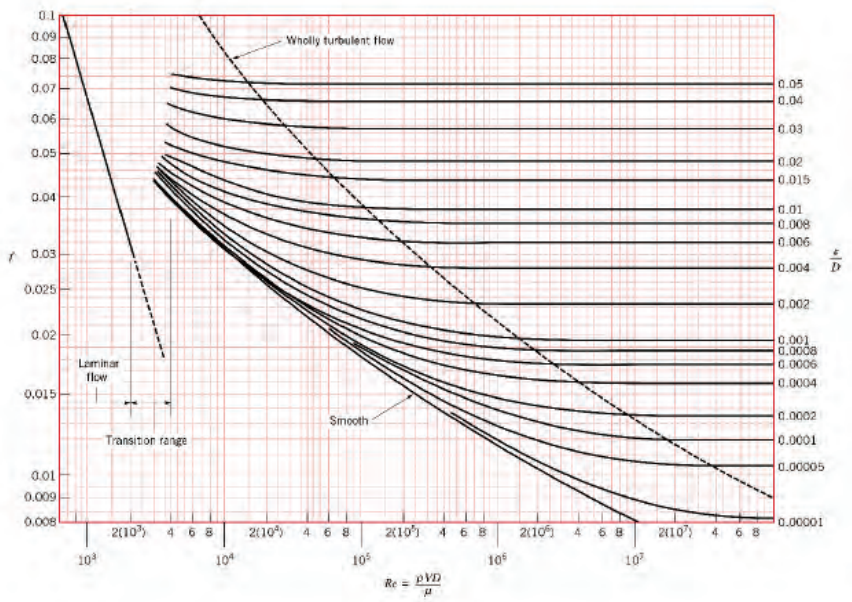

FIGURE C.2: The Moody diagram (log-log scale) giving the head loss coefficient λ as a function of the Reynolds number Re and the roughness ε/d (where f, V and D are changed to λ, ν and d, respectively)

when a regime is completely turbulent at the outset, it remains so as long as $\mathrm{Re} \geq 2 \cdot 10^3$.

The behaviour is more complex when the pipe walls are rough. When ϵ denotes the characteristic dimension of the pipe roughness, the pipe roughness can be represented by the ϵ/d ratio. The magnitude ϵ is another hard to evaluate parameter. The millimetre is adopted as the magnitude for measurements in new stilling well pipes, but it turns out to be too small when the pipe becomes fouled over time. However, as long as condition $\epsilon/d \ll 1$ is fulfilled, a highly accurate value is not required for parameter ϵ since roughness has been found to only have detectable effects after a specific Re value has been reached, which decreases as the roughness increases. Beyond this value, the head loss coefficient λ rapidly increases to a value, which is independent of Re and only a function of the roughness ϵ/d. All of these results are summarized in the Moody diagram (figure C.2).

2.2 • Digital application to stilling wells with specific characteristics

We have established that a stilling well hydraulic system is a nonlinear filter. It would be of interest to study variations in the internal level in a well corresponding to the overlapping of several sinusoidal waves in the external ocean environment. Unfortunately such a study would require preselection of critical representative cases, which has yet to be done. Here we will just present the response of a well to a sinusoidal wave of clearly defined frequency. The two most common situations (pipeless well and pipe well) are presented while examining the response of each type to a semidiurnal wave and then to swells. The well equation is digitally solved in the spectral domain using the Runge-Kutta method. In the case of a well equipped with a pipe of constant diameter, the head loss coefficient λ is fitted at each integration step on the basis of the Moody diagram.

Pipeless stilling wells. Stilling wells with an intake connected directly to the sea (without a pipe) is the most common type. It generally consists of a single pipe (made of stainless steel or a synthetic material such as PVC), and the simple first-order equation (C.16) may be applied (the intake immersion is not taken into account). It is assumed that there is no turbulence effect around the intake and that the sea water behaves like a perfect liquid.

The only characteristic to account for is the ratio of the diameter of the intake opening to that of the well ($r = d/\mathrm{D}$). The responses to semidiurnal waves, which are completely sinusoidal and with amplitudes ranging from 1 m to 7 m, were calculated as a function of the diameter ratio $r = d/\mathrm{D}$. Figures C.3a and C.3b, which respectively concern the admittances and phases of the response as a function of the ratio $r = d/\mathrm{D}$, summarize all of the results of calculations conducted at this frequency.

These results show that with a ratio $d/\mathrm{D} > 1/25$ (4 %) the phase lag and attenuation are negligible for possible extreme amplitudes (7 m in the examples shown). For a semidiurnal constituent, it is thus considered that a phase lag of less than 30 s and an attenuation of less than 0.1 % are negligible. This conclusion also applies to the diurnal constituent because of its higher period and to interaction species (quarter-diurnal, sixth-diurnal, etc.) due to their lower amplitude. However, it is quite likely that the high number of high-frequency interaction species (present in estuaries) affects the well response at low frequencies.

The same calculation procedure was applied to assess the impacts of very high frequency gravitational waves (waves, swells, seiches) on the well level at different amplitudes (10 cm to 1 m) and periods (1-30 s). The surface wave is assumed to be completely sinusoidal. As the intake immersion

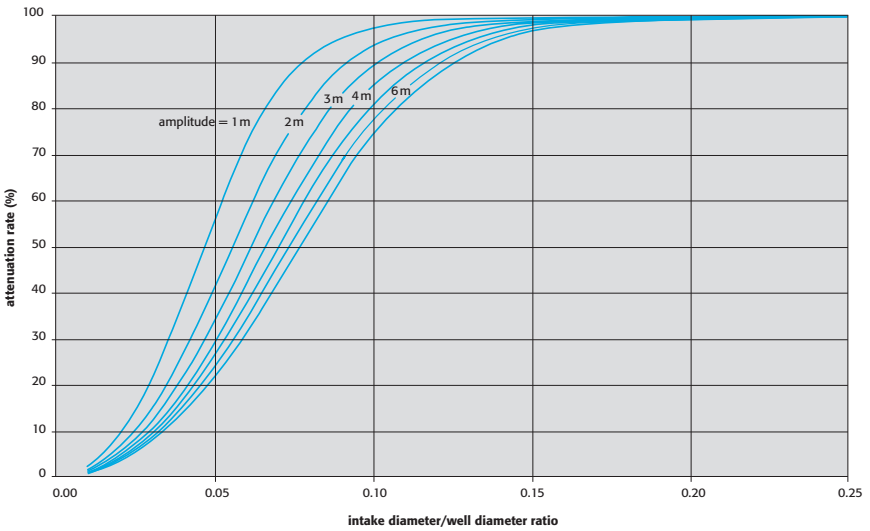

Figure C.3a: Well admittance for a semidiurnal constituent. A pipeless well with an intake: amplitude of the response to a semidiurnal wave. Each curve corresponds to a specific tidal amplitude (1-7 m) and gives the well response, which is expressed as a percentage of the input signal as a function of the intake to well diameter ratio $r = d/\mathrm{D}$.

value was not taken into consideration, the effect of the exponential pressure attenuation (as a function of the immersion) induced by the wave was not accounted for. The results obtained likely represent an increase in possible errors. Because of the nonlinear features, the model shows that the well response reflects a variation in the mean level in addition to the presence of an internal oscillation of the same frequency as the external wave.

The model results concerning the oscillation constituent of the response of a pipeless well (ratio $d/\mathrm{D} = 4$ %) are summarized on the graph in figure C.4.

Concerning the error in the mean levels, the model shows a decrease within the well which, with a swell of 1 m amplitude, reaches a maximum of 2 cm for a 2 min period. This is an extreme case. This error seldom excedes 5 mm in regular situations.

Pipe stilling wells. Pipe stilling well systems are less common. This type of well is generally found at permanent tide stations, often very old ones (e.g. Brest, France).

With this type of well, it is necessary to take into account the head loss coefficient λ and the there are too many parameters to consider to be able to draw up general laws. The d/D ratio, as well as the ratio of the diameter d

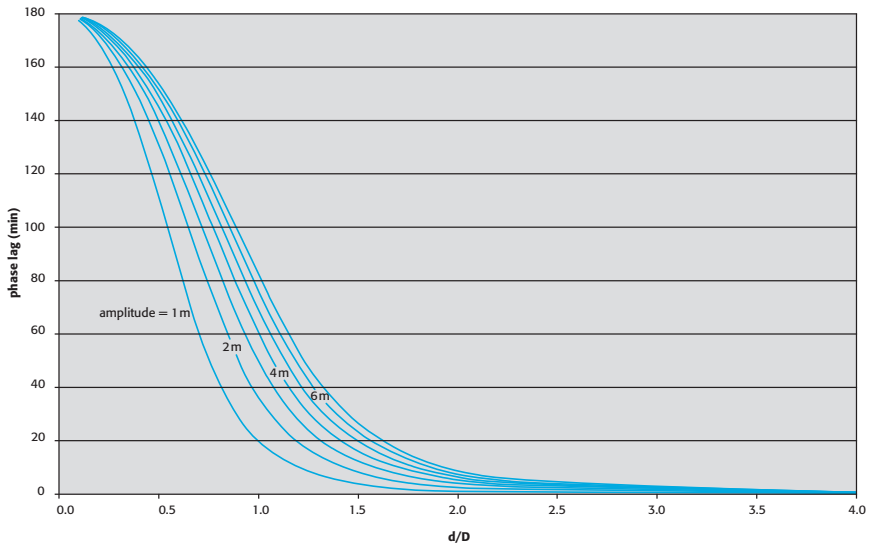

FIGURE C.3B: A pipeless well with an intake: phase lag in the response to a semidiurnal wave. Each curve corresponds to a specific tidal amplitude (1-7 m) and gives the phase lag in the well response (in degrees) as a function of the intake to well diameter ratio $r = d/\mathrm{D}$.

to the length l of the pipe, and the size ϵ of the roughness all have an impact. The well modelling is complicated because of the need to digitize the Moody diagram so as to be able to perform calculations according to the flow regime in the pipe.

The pipe well equation is formulated by introducing the head loss coefficient λ which, for a pipe of diameter d and length l, is as follows:

$$\lambda = \frac{\Gamma d}{(v^2/2)} = \frac{d}{\rho(v^2/2)} \cdot \frac{\mathrm{d}p_c}{\mathrm{d}l} \tag{2.19}$$

The integral of the head loss gradient over the entire length l gives the total head loss for pipe p_c. Note that the opposite of $p_c/\rho g$ reflects the decrease in the efficient height reduction. Hence, for the head loss per mass unit:

$$p_c/\rho = \lambda \frac{l}{d} \frac{v^2}{2} \tag{C.23}$$

This head loss results in reducing the velocity given by the Torricelli equation (C.17). The equivalent, which is called the Darcy-Weisbach equation, is as follows:

$$v^2/2 = g|\eta| - (p_c/\rho) \tag{C.24}$$

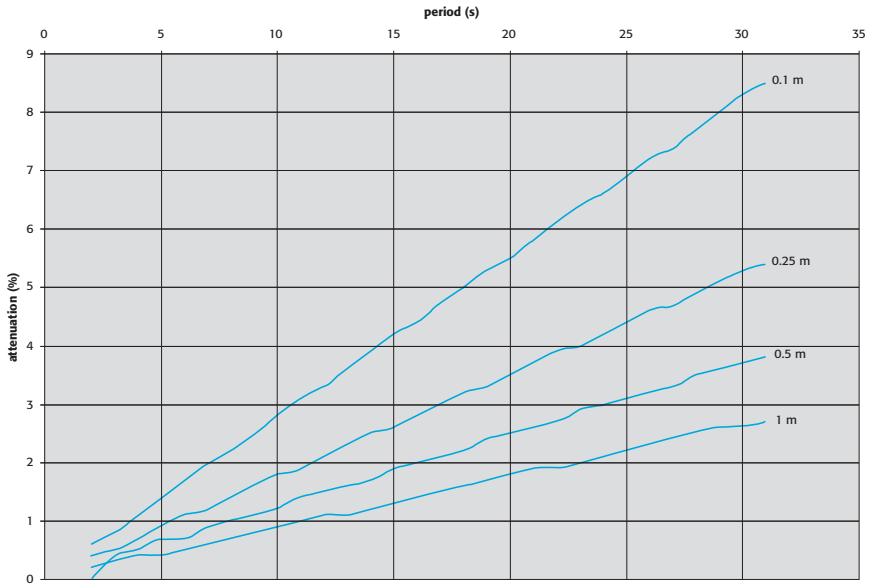

Figure C.4: Case of a pipeless well with an intake to well diameter ratio of $r = d/\mathrm{D} = 4$ %: well response at the external signal frequency. Each curve corresponds to a constant swell amplitude and gives the amplitude of the oscillation constituent of the response (as a percentage of that of the input signal)as a function of the swell period.

and when taking (C.23) into account, we obtain:

$$\frac{v^2}{2} = \frac{g|\eta|}{1 + (\lambda l/d)} \tag{C.25}$$

The well equation thus has the same form as equation (C.16), or:

$$\frac{\mathrm{d}\eta}{\mathrm{d}t} + m_c \eta \sqrt{\frac{2g}{|\eta|}} = \frac{\mathrm{d}h}{\mathrm{d}t}$$

with

$$m_c = \frac{r^2}{\sqrt{1 + (\lambda l/d)}} \tag{C.26}$$

Figure C.5 shows an example of the impact of the pipe characteristics (length l and diameter d) on the phase lag (expressed in minutes of mean time) of the well response in the case of a semidiurnal sinusoidal wave. In this example, a well diameter of $\mathrm{D} = 150$ cm and signal amplitude of $\max |h| = 5$ m were taken into account.

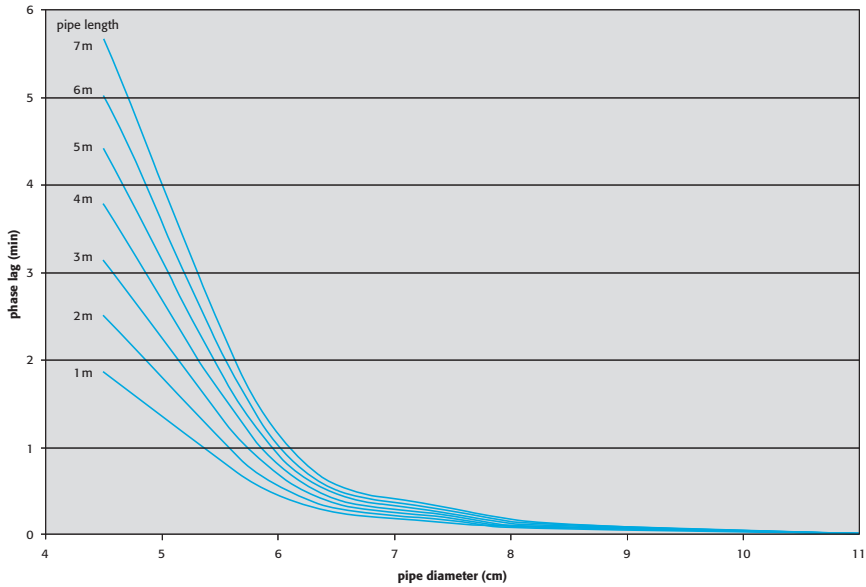

FIGURE C.5: Case of a well of diameter D $= 150$ *cm* with a pipe of diameter *d* and length *l*: well response to a semidiurnal wave of 5 m amplitude. Each curve corresponds to a constant pipe length *l* (values: 1-7 m) and gives the phase lag (min of mean time) of the response as a function of the pipe diameter *d* (in cm).

The results would differ with other values. The dimensions used here, however, correspond to realistic values for old existing stilling wells, so the results represent magnitudes that could be applicable to similar or more favourable situations.

It should be noted especially that the empirical rule that is often applied, whereby a $r = d/\mathrm{D}$ value of over 1/10 (here d $>$ 15 cm) is acceptable, is satisfied with respect to the phase lag, regardless of the pipe length. However, a value of 1/25, or $d = 6$ cm ($r = 4$ %), which is acceptable for a pipeless well intake, is not acceptable for a pipe length of $l = 100$ cm – the phase lag would be around 30 s.

Results concerning the response admittance are not presented, but calculations show that the signal attenuation is negligible when the phase lag is negligible.

This model of a pipe well response to a semidiurnal wave gives satisfactory results with respect to the performance of regular stilling wells at low wave frequencies. However, its capacity to attenuate the swell reveals that the performances are not as good as those of pipeless wells with an intake having

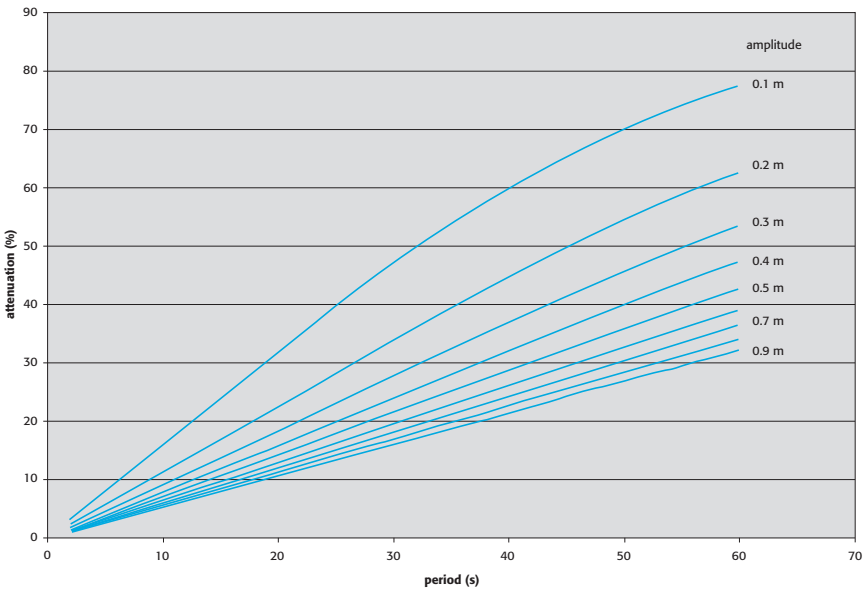

Figure C.6a: Well of diameter D $=$ 150 cm with a pipe of length l $=$ 400 cm and diameter d $=$ 15 cm $\Rightarrow$ r $=$ 10 %: well response at the same frequency as the swell. At a constant swell amplitude, the amplitude of the response (in %) is calculated as a function of the period (in s). As compared to the results shown in figures C.4 a and b (pipeless well r $=$ 4 % , without stress on D), the curves in figure C.6a clearly show the poor performances of the pipe well (r $=$ 10 %, but with D $=$ 150 cm).

the same parameter r $=$ d/D. When the r $=$ 1/10 value is adopted for a pipe well (here d $=$ 15 cm), the response gives the different tidal species correctly, but the swell attenuation rate turns out to be markedly lower than that obtained with a pipeless well – for which it is possible to adopt r $=$ 1/25 (or d $=$ 6 cm). Due to nonlinear features in the system, we obtain a response in which several frequencies appear along with a variation in the mean level. The curves in figure C.6a summarize results concerning the well response at the same frequency as the external sinusoidal wave.

Constituents with frequencies other than that of the input signal were noted in the response, but they were of low amplitude. However, modifications in the mean level in the presence of swells were sometimes significant (figure C.6b).

These calculations were done with a characteristic pipe roughness dimension of ϵ $=$ 1 mm. On condition that the roughness ϵ is low at the given pipe diameter d, the results obtained above were not markedly different. However, concretions and fouling that build up in the pipe over time make it harder to

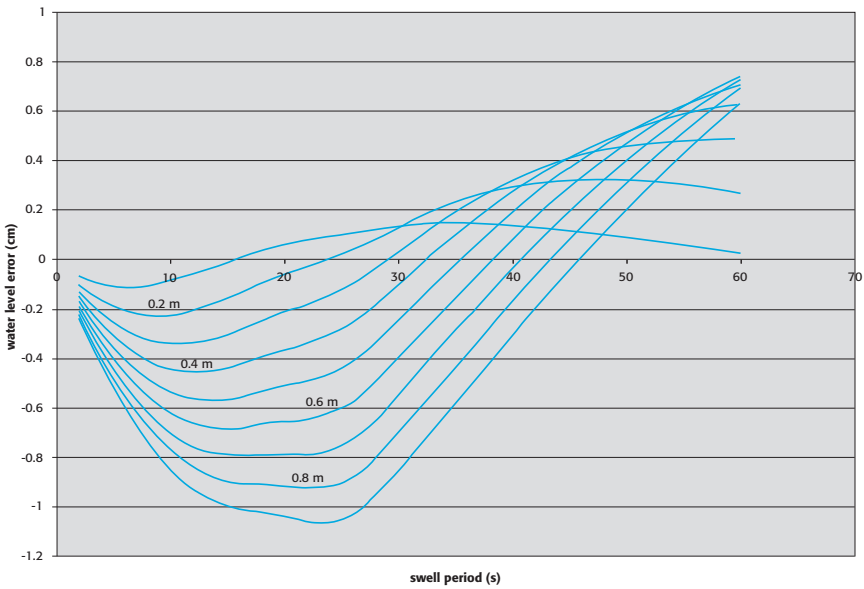

FIGURE C.6B: Well of diameter D $=$ 150 cm with a pipe of length $l = 400$ cm and diameter $d = 15$ cm $\Rightarrow r = 10$ %: effect of swells on the mean level in the well. For a given swell amplitude, each curve represents the variation in the mean level (in cm) in the well as a function of the external signal period.

accurately assess this parameter, which is generally not clearly defined when the well is put into operation. In practice, it is generally more a problem of pipe narrowing (due to silting or fouling) than an increase in roughness that alters the well performance.

The previous results show that efficient attenuation of unwanted high frequency signals (swell, waves harbour seiches) and efficient preservation of low frequency signals (tide, storm waves, tsunamis) are the result of tradoffs which should be sought for a given site, depending on the tidal amplitude, swell exposure and the well installation possibilities.

Concerning the error associated with the hydraulic response of the well to external signals, no general rules can be formulated, but a preliminary digital simulation, in which the characteristics of the place are accounted for, should help avoid unsuitable installations.

D

Development of the potential, harmonic constituents

The computations are based on the general formulation of the potential:

$$U = \frac{k\, m_A}{r_A}\left(\frac{1}{\sqrt{1 - 2\alpha_A \cos\theta + \alpha_A^2}} - 1 - \alpha_A \cos\theta\right)$$

$k = 6.670\ \ 10^{-11}$ SI units

$m_A =$ celestial body mass

$r_A =$ distance from the celestial body

$\alpha_A = \frac{a_T}{r_A}$, where a_T is the Earth's radius

Based on the notations used in Chapter III: $\cos\theta$, i.e. the cosine of the geocentric zenithal distance, is calculated with the following equations:

$$\cos\theta = \sin L \sin\delta + \cos L \cos\delta \cos AH$$

$$\sin\delta = \sin\epsilon \cos\beta \sin\lambda + \cos\epsilon \sin\beta$$

$$\cos\delta \cos AH = \cos\beta \cos\lambda \cos\alpha + (\cos\epsilon \cos\beta \sin\lambda - \sin\epsilon \sin\beta) \sin\alpha$$

where:

$$\begin{aligned}
\mathrm{L} &= \text{latitude of the observer}\\
\delta &= \text{declination of the celestial body}\\
\epsilon &= \text{inclination of the ecliptic}\\
\beta &= \text{latitude of the ecliptic of the celestial body}\\
\lambda &= \text{longitude of the ecliptic of the celestial body}\\
\alpha &= \text{hour angle of vernal equinox}\\
\mathrm{N} &= \text{ecliptic longitude of the ascending lunar node}
\end{aligned}$$

If t is the number of mean days since 1 January 2000 at 12 h UT, with angles expressed in decimal degrees, then:

$$\begin{aligned}
\epsilon &= 23.439\,29 - 3.56\,10^{-7}t\\
\alpha &= 280.466\,448\,5 + 360.985\,647\,360\,t\\
&\quad - 11.99\,10^{-13}t^2 - 4.785\,9\,10^{-3}\sin\mathrm{N}\cos\epsilon - \mathrm{G}\\
\mathrm{N}' &= -\mathrm{N} = 234.955 + 1\,934.136\,3\,t + 0.002\,1\,t^2
\end{aligned}$$

1 • Lunar potential

For the lunar potential, the $\sin\delta$, $\sin\beta$ and i values are obtained at any time using Brown's expansion, as given in the following tables. The sine and cosine arguments are obtained by the method described in Chapter V using Doodson numbers.

1.0.1 • Brown's expansion

Ecliptic longitude λ		Ecliptic latitude β		$(r_0/r)\ i_\mathrm{L}$	
arg.	sin *coeff*. × 10^6	arg.	sin *coeff*. × 10^6	arg.	cos *coeff*. × 10^6
55 654	5	55 566	−4	55 555	10^6
55 753	1	55 665	−4 847	56 455	4
55 775	6	56 444	−25	56 554	−117
56 356	−12	56 466	4	57 355	−89
56 455	90	56 565	23	57 553	−3
56 554	−3 243	56 664	−27	57 575	−31
56 576	7	57 245	−1	58 354	−6
57 355	−1 026	57 465	−808	58 574	−2
57 553	−37	57 685	1	61 657	14
57 575	−267	58 464	−36	61 855	2

Ecliptic longitude λ		Ecliptic latitude β		$(r_0/r)\ i_L$	
58 354	−42	59 463	−1	62 656	422
58 574	−11	61 547	5	62 755	−3
59 353	−1	61 745	3	63 435	−14
60 658	1	62 546	144	63 457	6
61 635	1	62 645	−2	63 655	10 025
61 657	36	63 545	3 024	64 456	337
61 855	6	63 765	−8	64 555	−285
62 436	−2	64 346	1	64 654	−66
62 535	−1	64 445	−3	65 455	54 501
62 656	1 000	64 544	−59	65 554	44
62 755	−6	64 566	24	65 653	−6
63 435	−31	65 345	154	65 675	−209
63 457	13	65 565	89 504	66 355	5
63 556	−3	66 344	−2	66 454	−278
63 655	22 236	66 465	2	66 575	2
64 456	717	66 564	−31	67 255	−35
64 555	−605	67 365	−75	67 453	−3
64 654	−138	67 585	−11	67 475	−24
65 356	−2	68 364	−3	68 254	−1
65 455	109 760	70 646	3	70 756	9
65 554	87	71 645	32	71 557	27
65 653	−12	71 667	2	71 755	109
65 675	−192	72 446	9	72 556	561
66 355	9	72 545	−2	72 655	−11
66 454	−532	72 666	43	73 335	−1
66 575	3	73 445	162	73 555	8 249
67 255	−64	73 665	967	73 775	−4
67 453	−6	74 444	−4	74 356	37
68 254	−2	74 466	33	74 455	−32
70 558	2	74 565	−26	74 554	−88
70 756	13	74 664	−6	75 355	2 970
71 557	40	75 245	8	75 454	5
71 656	−1	75 465	4 897	75 575	−4
71 755	149	75 564	4	76 354	−30

Ecliptic longitude λ		Ecliptic latitude β		$(r_0/r)\ i_L$	
72 556	802	75 685	−14	77 155	−4
72 655	−16	76 464	−26	77 375	−3
72 754	−2	77 265	−7	81 855	1
73 335	−2	77 485	−2	80 656	20
73 357	1	80 546	2	81 457	3
73 555	11 490	80 766	1	81 655	176
73 654	1	81 545	18	82 456	67
73 775	−3	81 567	2	82 654	−3
74 356	47	81 765	12	83 455	902
74 455	−41	82 566	39	83 675	−3
74 554	−119	82 665	−1	84 256	4
75 355	3 728	83 345	10	84 355	−3
75 454	6	83 565	568	84 454	−14
75 575	−1 996	84 366	4	85 255	182
76 354	−37	84 465	−3	86 254	−3
76 574	2	84 564	−6	91 755	3
77 155	−5	85 365	300	90 556	10
77 375	3	85 585	−31	91 555	76
81 657	2	86 364	−3	92 356	6
81 855	1	90 666	2	92 554	−1
80 656	21	91 445	2	93 355	83
81 457	4	91 665	15	94 354	−1
81 655	186	92 466	6	95 155	12
82 456	71	93 465	73	101 655	3
82 555	2	93 685	−1	100 456	2
82 654	−3	94 464	−1	101 455	13
82 676	−2	95 265	19	103 255	7
83 455	931	95 485	−5	111 355	1
83 675	−46	101 565	6		
84 256	3	103 365	7		
84 355	−3	105 165	1		
84 454	−14	111 464	1		
84 476	−1				
84 575	1				

Ecliptic longitude λ		Ecliptic latitude β	$(r_0/r)\ i_L$
85 255	175		
85 475	−219		
86 254	−3		
91 755	3		
90 556	9		
91 555	67		
92 356	6		
92 554	−1		
92 576	−2		
93 355	70		
93 575	−28		
94 354	−1		
95 155	9		
95 375	−19		
95 595	2		
101 655	2		
100 456	1		
101 455	10		
101 675	−1		
103 255	5		
103 475	−5		
105 275	−2		
111 355	1		

2 • Solar potential

The development is much simpler for the Sun. Its latitude may be disregarded and the longitude and parallax expansions contain many fewer terms:

$$\cos\theta = \sin L \sin\delta + \cos L \cos\delta \cos AH$$
$$\sin\delta = \sin\epsilon \sin\lambda$$
$$\cos\delta \cos AH = \cos\lambda \cos\alpha + \sin\lambda \sin\alpha \cos\epsilon$$

Based on the notations used in Chapter V, where h denotes the mean

longitude of the Sun and p_1 is the mean longitude of perihelion:

$$\lambda = h + 3.3501 \cdot 10^{-3} \sin\left(h - p_1\right) + 3.51 \cdot 10^{-4} \sin 2\left(h - p_1\right) + 5 \cdot 10^{-6} \sin 3\left(h - p_1\right) + \ldots$$

$$i = 1 + 1.6750 \cdot 10^{-2} \cos\left(h - p_1\right) + 2.81 \cdot 10^{-4} \cos 2\left(h - p_1\right) + 5 \cdot 10^{-6} \cos 3\left(h - p_1\right) + \ldots$$

h and p_1 can be calculated at all times using the equations set down in Chapter V.

3 • Harmonic analysis of the potential, species separation

Based on the previous equations, it is possible to calculate the tide-generating potential at regular intervals and to perform a harmonic analysis.

However, as the potential is dependent on the latitude, it is convenient to adopt Doodson's presentation, where the latitude is involved in the geodesic coefficients in the form of factors of variable terms, as presented in table 5.2.

For comparison with Doodson's development, the potential was calculated at latitudes 0°, 26.5650°[1], 45° and 90°.

By adopting the notations of table 5.2 and assuming $C_{n,m} = G_{n,m}/C_L$, we obtain:

L	$C_{2.0}$	$C_{3.0}$	$C_{2.1}$	$C_{3.1}$	$C_{2.2}$	$C_{3.2}$	$C_{3.3}$
0°	0.5	0	0.0	0.726 18	1	0	1
26.565 0°	0.2	1	0.8	0	0.8	0.929 5	0.715 5
45°	0.2	0.395 28	1.0	−0.770 23	0.5	0.918 56	0.353 55
90°	−1	−2.236 06	0.0	0	0	0	0

When the different latitude values are taken into account, the contributions of the different terms of the potential expansion can be clearly separated into Legendre polynomials.

By adopting the notations $U_{n,m}$ for the constituent of the potential of species m derived from the P_n term of the Legendre polynomial development ($n = 2$ or $n = 3$), and where U(L) is the potential calculated at latitude L, the following table indicates the different combinations required to calculate the terms of the potential.

1. $\sin^2(26.5650°) = 0.2$

$U_{2.0}$	$2U(0)$
$U_{3.0}$	$\dfrac{-[2U(0)+U(90)]}{2.236\,06}$
$U_{2.1}$	$U(45)+1.060\,6\,U(0)$
$U_{3.1}$	$1.37707\,U(0)$
$U_{2.2}$	$U(0)$
$U_{3.2}$	$\dfrac{[2U(45)-U(0)]}{1.837\,12}$
$U_{3.3}$	$U(0)$

Other combinations are possible and were used for verification purposes.

The different potential values were computed hourly over a period spanning eight ascending lunar node rotation periods, or approximately 150 years beginning on 1 January 1950.

For the solar potential, as the P_3 term of the Legendre polynomial development is negligible, the results are obtained directly through the analysis of $U(0)$ and $U(45)$.

4 • Nonlinear interactions

The constituents generated by nonlinear interactions were calculated via harmonic analysis of series obtained from the following products:

$U_{2.2}^2$: quarter diurnal and long period constituents D22

$U_{2.2}^3$: sixth diurnal and semidiurnal constituents T23

$U_{2.2}^4$: eigth diurnal and quarter diurnal constituents Q24

$U_{2.2}^5$: tenth diurnal, sixth diurnal and semidiurnal constituents C25

$U_{2.2}^6$: twelfth diurnal, eigth diurnal and quarter diurnal constituents S26

$U_{2.1}^2$: semidiurnal and long period constituents D11

$U_{2.1}U_{2.2}$: diurnal and terdiurnal constituents D12

$U_{2.1}^3$: diurnal and terdiurnal constituents T11

$U_{2.1}U_{2.2}^2$: terdiurnal and fifth diurnal constituents T122

$U_{2.1}U_{2.2}^3$: seventh diurnal constituents Q123

Note that nonlinear interactions involving semidiurnal constituents are given more weight than diurnal constituents. It may be necessary to compute other combinations in regions were diurnal constituents prevail.

Combinations involving the P_3 constituent of the potential are legitimately disregarded.

5 • Harmonic developments

The results of the above-described calculations are presented in the following tables.

The potential term coefficients (PL, PS and P3) are directly derived from the potential equation and are comparable to those of Doodson.

The interaction constituent coefficients were calculated by arbitrarily attributing the value of 1,000 to the highest coefficient listed in the same column. Only their relative importance in the same column should be considered. A comparison of coefficients of constituents of different origins, and thus from different columns, would not make sense.

Constituents derived directly from the potential (PL and PS) are generally the most important, and the interaction constituents decrease with their degree beyond second-order interactions. Second-order interactions (T11, T23, T123) are mainly derived from friction terms in propagation equations. Their origin differs from that of first-order interactions (D22, D11, D12), which are mainly derived from advection terms. In principle, their relative importance cannot be determined, and neither can the relative importance of interactions involving diurnal and semidiurnal constituents, which depend on the type of tide.

5.1 • Long period

NAME	deg/hour	ARGUMENT NUM	ALPHA	PL	PS	D22	D11
Mean level	0.00000000	055555	ZZZZZZ|Z	50458|Z	23411|Z	1000|Z	1000|
	0.00220641	055565	ZZZZAZ|B	6553|-	-----|B	18|Z	6|
	0.00441283	055575	ZZZZBZ|Z	70|-	-----|-	-----|-	-----|
Sa	0.04106864	056555	ZZAZZZ|-	-----|-	-----|-	-----|-	-----|
Ssa	0.08213728	057555	ZZBZZZ|-	-----|Z	7245|Z	32|B	9|
	0.08434369	057565	ZZBZAZ|B	186|-	-----|Z	9|B	1|
Sta	0.12320396	058554	ZZCZZY|-	-----|Z	423|Z	2|-	-----|
	0.46931466	063645	ZAXAYZ|B	112|-	-----|B	1|-	-----|
MSm	0.47152108	063655	ZAXAZZ|Z	1581|-	-----|Z	12|Z	1|
	0.47372749	063665	ZAXAAZ|B	100|-	-----|-	-----|-	-----|
	0.54216827	065445	ZAZYYZ|B	544|-	-----|B	3|Z	1|
Mm	0.54437468	065455	ZAZYZZ|Z	8253|B	2|Z	91|Z	6|
	0.54658110	065465	ZAZYAZ|B	538|-	-----|B	3|Z	1|
	0.55365836	065655	ZAZAZZ|B	444|-	-----|Z	2|B	1|
	0.55586477	065665	ZAZAAZ|B	182|-	-----|Z	1|-	-----|
	0.62651196	067455	ZABYZZ|B	112|-	-----|Z	2|B	1|
Msf	1.01589576	073555	ZBXZZZ|Z	1367|-	-----|Z	268|Z	7|
	1.08874937	075355	ZBZXZZ|Z	677|-	-----|Z	11|Z	1|
Mf	1.09803304	075555	ZBZZZZ|Z	15640|-	-----|Z	70|B	19|
	1.10023945	075565	ZBZZAZ|Z	6487|-	-----|Z	18|B	6|
	1.10244587	075575	ZBZZBZ|Z	608|-	-----|Z	1|-	-----|
SN	1.56027044	083455	ZCXYZZ|Z	216|-	-----|Z	52|Z	1|
MStm	1.56955412	083655	ZCXAZZ|Z	568|-	-----|Z	3|B	1|
	1.57176053	083665	ZCXAAZ|Z	234|-	-----|Z	1|-	-----|
Mfm	1.64240772	085455	ZCZYZZ|Z	2984|-	-----|Z	17|B	5|
	1.64461414	085465	ZCZYAZ|Z	1237|-	-----|Z	5|B	2|
	1.64682055	085475	ZCZYBZ|Z	116|-	-----|-	-----|-	-----|
MSqm	2.11392880	093555	ZDXZZZ|Z	474|-	-----|Z	3|B	1|
	2.11613521	093565	ZDXZAZ|Z	198|-	-----|Z	1|-	-----|

5.2 • Diurnal

			ARGUMENT							
NAME	deg/hour	NUM	ALPHA	PL	PS	D12	T11	P3		
				|	|	|	|	|	|	
	12.30991155	115855	AVZCZZ	Y 107	-----	Y 5	Y 8	-----		
				|	|	|	|	|	|	
	12.38055874	117645	AVBAYZ	Y 52	-----	Y 1	Y 16	-----		
	12.38276515	117655	AVBAZZ	Y 275	-----	Y 12	Y 44	-----		
	12.45561876	119455	AVDYZZ	Y 54	-----	Y 2	Y 8	-----		
				|	|	|	|	|	|	
	12.84964440	125655	AWZAZZ	-----	-----	-----	A 2	Z 67		
	12.85207982	125745	AWZBYZ	Y 180	-----	Y 3	Y 19	-----		
2Q1	12.85428623	125755	AWZBZZ	Y 952	-----	Y 39	Y 53	-----		
				|	|	|	|	|	|	
	12.92493342	127545	AWBZYZ	Y 217	-----	Y 5	Y 43	-----		
SIGMA1	12.92713984	127555	AWBZZZ	Y 1148	-----	Y 43	Y 120	-----		
				|	|	|	|	|	|	
	12.96820652	128554	AWCZZY	Y 78	-----	Y 2	Y 7	-----		
				|	|	|	|	|	|	
	13.39181267	135545	AXZZYZ	-----	-----	-----	-----	Z 89		
	13.39401908	135555	AXZZZZ	-----	A 3	-----	-----	Z 225		
q1	13.39645450	135645	AXZAYZ	Y 1360	-----	Y 28	Y 82	-----		
Q1	13.39866092	135655	AXZAZZ	Y 7206	-----	Y 246	Y 265	-----		
				|	|	|	|	|	|	
	13.43972759	136654	AXAAZY	Y 66	-----	-----	Y 5	-----		
				|	|	|	|	|	|	
	13.46930811	137445	AXBYYZ	Y 258	-----	Y 5	Y 16	-----		
RHO1	13.47151452	137455	AXBYZZ	Y 1368	-----	Y 48	Y 50	-----		
	13.48079819	137655	AXBAZZ	A 79	-----	A 66	A 57	-----		
				|	|	|	|	|	|	
	13.51258120	138454	AXCYZY	Y 63	-----	Y 2	Y 2	-----		
				|	|	|	|	|	|	
	13.87018199	143755	AYXBZZ	A 113	-----	Y 1	Y 11	-----		
				|	|	|	|	|	|	
	13.90196892	144556	AYYZZA	A 130	-----	Y 5	Y 11	-----		
				|	|	|	|	|	|	
	13.93862277	145535	AYZZXZ	A 217	-----	A 7	Y 9	-----		
o1	13.94082919	145545	AYZZYZ	Y 7110	-----	Y 101	Y 258	-----		
O1	13.94303560	145555	AYZZZZ	Y 37689	-----	Y 1000	Y 881	-----		
	13.94767744	145655	AYZAZZ	-----	-----	-----	Y 1	Z 104		
	13.95231927	145755	AYZBZZ	A 243	-----	A 12	A 27	B 3		
				|	|	|	|	|	|	
	13.98410228	146554	AYAZZY	Y 109	-----	-----	Y 15	Y 1		
				|	|	|	|	|	|	
MP1	14.02517288	147555	AYBZZZ	A 492	-----	A 341	A 231	-----		
	14.02737929	147565	AYBZAZ	Y 107	-----	-----	A 30	-----		
				|	|	|	|	|	|	
	14.41235026	153645	AZXAYZ	A 63	-----	Y 6	Y 13	-----		
	14.41455668	153655	AZXAZZ	A 278	-----	Y 30	Y 73	-----		
				|	|	|	|	|	|	
	14.48520387	155445	AZZYYZ	A 197	-----	Y 7	Y 27	-----		
	14.48741028	155455	AZZYZZ	A 1064	-----	Y 33	Y 87	-----		
	14.48984571	155545	AZZZYZ	-----	-----	-----	-----	B 98		
	14.49205212	155555	AZZZZZ	B 1	-----	-----	-----	Z 661		
	14.49448754	155645	AZZAYZ	Y 86	-----	Y 7	A 23	-----		
M1	14.49669396	155655	AZZAZZ	A 2961	-----	A 100	A 180	-----		
KHI1	14.49890037	155665	AZZAAZ	A 595	-----	A 18	A 54	B 1		
				|	|	|	|	|	|	
	14.56954756	157455	AZBYZZ	A 567	-----	A 12	A 44	-----		

```
           14.57175397 157465 AZBYAZ|A   125|- -----|A     4|A    13|- -----|
                                    |      |       |      |      |       |
PI1        14.91786468 162556 AAWZZA|Y     1|Y   984|Y    30|Y    32|- -----|
           14.95672495 163545 AAXZYZ|A   198|- -----|Y    60|Y    58|- -----|
P1         14.95893136 163555 AAXZZZ|Y    30|Y 16817|Y   466|Y   465|- -----|
                                    |      |       |      |      |       |
S1         15.00000000 164555 AAYZZZ|- -----|- -----|- -----|- -----|- -----|
                                    |      |       |      |      |       |
           15.03886223 165545 AAZZYZ|Y  1049|- -----|Y    42|A   108|- -----|
K1         15.04106864 165555 AAZZZZ|A 36232|A 16124|A   742|A  1000|- -----|
k1         15.04327505 165565 AAZZAZ|A  7186|A     1|A   100|A   260|- -----|
           15.04548147 165575 AAZZBZ|Y   154|- -----|Y     7|A     8|- -----|
                                    |      |       |      |      |       |
PSI1       15.08213532 166554 AAAZZY|Y     6|A   409|A     6|A    20|- -----|
                                    |      |       |      |      |       |
PHI1       15.12320592 167555 AABZZZ|- -----|A   714|A    41|Y   118|- -----|
                                    |      |       |      |      |       |
THETA1     15.51258972 173655 ABXAZZ|A   566|- -----|A    12|A    44|- -----|
           15.51479613 173665 ABXAAZ|A   112|- -----|A     3|A    15|- -----|
                                    |      |       |      |      |       |
           15.58323691 175445 ABZYYZ|Y    86|- -----|Y     7|A    23|- -----|
J1         15.58544332 175455 ABZYZZ|A  2959|- -----|A   100|A   182|- -----|
           15.58764974 175465 ABZYAZ|A   587|- -----|A    17|A    56|- -----|
           15.59008516 175555 ABZZZZ|- -----|- -----|- -----|- -----|Z   247|
                                    |      |       |      |      |       |
S01        16.05696440 183555 ACXZZZ|A   489|- -----|A   341|A   224|- -----|
           16.05917081 183565 ACXZAZ|A    96|- -----|A    64|A    70|- -----|
                                    |      |       |      |      |       |
           16.12981801 185355 ACZXZZ|A   241|- -----|A    12|A    26|- -----|
O01        16.13910168 185555 ACZZZZ|A  1615|- -----|A    87|Y   256|- -----|
oo1        16.14130809 185565 ACZZAZ|A  1034|- -----|A    42|Y   108|- -----|
           16.14351451 185575 ACZZBZ|A   217|- -----|A     7|Y     9|- -----|
                                    |      |       |      |      |       |
           16.60133908 193455 ADXYZZ|A    77|- -----|A    65|A    55|- -----|
           16.61062276 193655 ADXAZZ|A    58|- -----|A     4|Y    16|- -----|
                                    |      |       |      |      |       |
KQ1        16.68347636 195455 ADZYZZ|A   308|- -----|A    22|Y    77|- -----|
```

5.3 • Semidiurnal

```
                          ARGUMENT
NAME         deg/hour    NUM  ALPHA     PL      PS     D11     T23     C25
                                    |      |       |      |      |       |
2MN2S2     26.40793803 209655 BUDAZZ|Z    18|- -----|- -----|Z     9|Z    63|
                                    |      |       |      |      |       |
3M(SK)2    26.87017544 217555 BVBZZZ|- -----|- -----|B    25|Z     7|Z    57|
2NS2       26.87945911 217755 BVBBZZ|Z   110|- -----|Z     1|Z    30|Z    73|
                                    |      |       |      |      |       |
3M2S2      26.95231272 219555 BVDZZZ|Z    68|- -----|- -----|Z    24|Z   122|
2NK2S2     26.96159639 219755 BVDBZZ|- -----|- -----|- -----|- -----|Z     4|
                                    |      |       |      |      |       |
           27.33949010 225645 BWZAYZ|- -----|- -----|B    49|Z     9|Z    18|
OQ2        27.34169652 225655 BWZAZZ|- -----|- -----|B   132|Z    36|Z    83|
           27.35098019 225855 BWZCZZ|Z   258|- -----|Z     5|Z     9|Z    19|
```

Semidiurnal (cont'd)

NAME	deg/hour	NUM	ARGUMENT ALPHA	PL	PS	D11	T23	C25
				|	|	|	|	|
	27.42162738	227645	BWBAYZ|B	25|-	-----|Z	2|B	9|B	23|
MNS2	27.42383379	227655	BWBAZZ|Z	667|-	-----|Z	13|Z	132|Z	253|
				|	|	|	|	|
	27.46490047	228654	BWCAZY|Z	51|-	-----|-	-----|Z	9|Z	19|
				|	|	|	|	|
MNK2S2	27.50597107	229655	BWDAZZ|-	-----|-	-----|-	-----|-	-----|Z	15|
MNUS2	27.49668740	229455	BWDYZZ|Z	129|-	-----|Z	2|Z	25|Z	46|
				|	|	|	|	|
2MS2K2	27.80393392	233555	BXXZZZ|-	-----|-	-----|-	-----|Z	2|Z	11|
				|	|	|	|	|
	27.88386479	235545	BXZZYZ|-	-----|-	-----|B	129|Z	19|Z	34|
2MK2	27.88607120	235555	BXZZZZ|-	-----|-	-----|B	348|Z	85|Z	162|
	27.89314846	235745	BXZBYZ|B	86|B	1|Z	7|B	4|B	8|
2N2	27.89535487	235755	BXZBZZ|Z	2300|-	-----|Z	40|Z	57|Z	101|
				|	|	|	|	|
	27.96600206	237545	BXBZYZ|B	103|-	-----|Z	7|B	25|B	47|
MU2 2MS2	27.96820848	237555	BXBZZZ|Z	2777|-	-----|Z	43|Z	351|Z	529|
				|	|	|	|	|
	28.00927515	238554	BXCZZY|Z	188|-	-----|Z	2|Z	23|Z	41|
				|	|	|	|	|
SNK2	28.35759228	243655	BYXAZZ|-	-----|-	-----|B	56|Z	19|Z	61|
	28.36687595	243855	BYXCZZ|B	56|-	-----|-	-----|Z	2|Z	9|
				|	|	|	|	|
	28.39866288	244656	BYYAZA|B	147|-	-----|Z	1|Z	1|Z	7|
				|	|	|	|	|
	28.42603306	245435	BYZYXZ|B	67|Y	1|-	-----|B	1|B	2|
	28.43288131	245545	BYZZYZ|Y	3|-	-----|-	-----|-	-----|-	-----|
	28.43508772	245555	BYZZZZ|-	-----|-	-----|-	-----|-	-----|-	-----|
n2	28.43752314	245645	BYZAYZ|B	648|-	-----|Z	40|B	18|B	30|
N2	28.43972956	245655	BYZAZZ|Z	17391|-	-----|Z	246|Z	298|Z	403|
				|	|	|	|	|
	28.47615636	246555	BYAZZZ|B	94|-	-----|-	-----|B	2|B	3|
	28.48079623	246654	BYAAZY|Z	163|-	-----|Z	3|Z	5|Z	14|
				|	|	|	|	|
nu2	28.51037675	247445	BYBYYZ|B	123|-	-----|Z	8|B	2|B	10|
NU2	28.51258316	247455	BYBYZZ|Z	3302|-	-----|Z	48|Z	45|Z	119|
	28.52186683	247655	BYBAZZ|Z	14|-	-----|-	-----|Z	20|Z	61|
				|	|	|	|	|
	28.55364984	248454	BYCYZY|Z	152|-	-----|Z	2|Z	3|Z	8|
				|	|	|	|	|
2KN2S2	28.60400411	249655	BYDAZZ|-	-----|-	-----|-	-----|-	-----|Z	1|
				|	|	|	|	|
	28.89976055	253545	BZXZYZ|-	-----|-	-----|B	56|Z	20|Z	38|
MSK2	28.90196696	253555	BZXZZZ|-	-----|-	-----|B	317|Z	76|Z	159|
gamma2	28.91125063	253755	BZXBZZ|B	272|-	-----|Z	1|Z	16|Z	54|
				|	|	|	|	|
M(SK)2	28.94303756	254556	BZYZZA|B	313|-	-----|-	-----|Z	12|Z	27|
				|	|	|	|	|
m2	28.98189783	255545	BZZZYZ|B	3383|-	-----|Z	163|B	56|B	70|
M2	28.98410424	255555	BZZZZZ|Z	90812|-	-----|Z	1000|Z	1000|Z	1000|
	28.98631065	255565	BZZZAZ|B	5|-	-----|Z	131|B	19|B	34|
	28.98874608	255655	BZZAZZ|-	-----|-	-----|-	-----|-	-----|Z	1|
				|	|	|	|	|
M(KS)2	29.02517092	256554	BZAZZY|Z	277|-	-----|Z	11|Z	18|Z	34|

Semidiurnal (cont'd)

		ARGUMENT											
NAME	deg/hour	NUM	ALPHA	PL		PS		D11		T23		C25	
MKS2	29.06624152	257555	BZBZZZ	Z	104	-----	Z	1	Z	82	Z	167
	29.06844793	257565	BZBZAZ	B	51	-----	Z	1	Z	23	Z	44
2SM2K2	29.14837880	259555	BZDZZZ	-----		-----	-----		-----		Z	5	
LAMBDA2	29.45562532	263655	BAXAZZ	B	669	-----	Z	30	Z	121	Z	254
2SN(MK)2	29.37348804	261655	BAVAZZ	-----		-----	Z	2	Z	1	Z	18
	29.52627251	265445	BAZYYZ	Z	94	-----	Z	4	B	7	B	17
L2 2MN2	29.52847892	265455	BAZYZZ	B	2567	-----	Z	34	Z	108	Z	233
	29.53312076	265555	BAZZZZ	-----		-----	-----		-----		-----		
NKM2	29.53776260	265655	BAZAZZ	Z	642	-----	B	69	Z	39	Z	86
	29.53996901	265665	BAZAAZ	Z	283	-----	B	22	Z	12	Z	23
	29.61061620	267455	BABYZZ	Z	122	-----	B	14	Z	10	Z	43
2SK2	29.91786272	271555	BBVZZZ	-----		-----	B	74	Z	16	Z	63
T2	29.95893332	272556	BBWZZA	Z	3	Z	2472	Z	29	Z	45	Z	60
	29.99779359	273545	BBXZYZ	Z	94	-----	B	12	B	20	B	39
S2	30.00000000	273555	BBXZZZ	Z	73	Z	42286	Z	454	Z	710	Z	816
	30.00220641	273565	BBXZAZ	-----		-----	Z	62	B	20	B	39
R2	30.04106668	274554	BBYZZY	-----		-----	B	437	-----		-----		-----
	30.07993087	275545	BBZZYZ	B	147	-----	Z	33	B	8	B	17
K2	30.08213728	275555	BBZZZZ	Z	7852	Z	3643	B	637	Z	207	Z	279
k2	30.08434369	275565	BBZZAZ	Z	3423	Z	1	B	166	Z	56	Z	70
	30.08655011	275575	BBZZBZ	Z	371	-----	B	5	Z	5	Z	5
	30.12320396	276554	BBAZZY	B	1	Z	91	B	11	Z	3	Z	9
	30.16427456	277555	BBBZZZ	-----		Z	76	B	19	Z	7	Z	22
MSnu2	30.47152108	281655	BCVAZZ	-----		-----	Z	5	Z	18	Z	79
MSN2	30.54437468	283455	BCXYZZ	Z	9	-----	Z	26	Z	104	Z	225
XI2	30.55365836	283655	BCXAZZ	Z	122	-----	B	14	Z	10	Z	43
KJ2	30.62651196	285455	BCZYZZ	Z	640	-----	B	70	Z	39	Z	85
	30.62871838	285465	BCZYAZ	Z	279	-----	B	26	Z	12	Z	22
2KM(SN)2	30.70864924	287455	BCBYZZ	B	1	-----	B	2	Z	1	Z	6
	30.97482712	290555	BDUZZZ	Y	2	-----	-----	-----	-----		-----		-----
2SM2	31.01589576	291555	BDVZZZ	Z	1	-----	Z	4	Z	154	Z	304
	31.05696440	292555	BDWZZZ	-----		-----	-----		-----	A	8	A	16
	31.08874937	293355	BDXXZZ	-----		-----	Z	2	Z	12	Z	42
	31.10023945	293565	BDXZAZ	Z	45	-----	Z	4	Z	22	Z	41

Semidiurnal (cont'd)

NAME	deg/hour	NUM	ARGUMENT ALPHA	PL	PS	D11	T23	C25
SKM2	31.09803304	293555	BDXZZZ	Z 105	- -----	- -----	Z 82	Z 169
	31.18017032	295555	BDZZZZ	Z 165	- -----	B 41	Z 14	Z 30
	31.18237673	295565	BDZZAZ	Z 144	- -----	B 31	Z 8	Z 17
	31.18458315	295575	BDZZBZ	Z 47	- -----	B 9	Z 2	Z 4
2SNU2	31.48741684	2X*655	BETAZZ	Y 1	- -----	- -----	Z 6	Z 18
2SN2	31.56027045	2X1455	BEVYZZ	- -----	- -----	Z 1	Z 30	Z 98
SKN2	31.64240772	2X3455	BEXYZZ	Z 16	- -----	- -----	Z 20	Z 61
3S2M2	32.03179152	2E*555	BFTZZZ	- -----	- -----	- -----	Z 4	Z 49
3SK2M2	32.11392880	2E1555	BFVZZZ	- -----	- -----	- -----	Z 3	Z 38

5.4 • Terdiurnal

NAME	deg/hour	NUM	ARGUMENT ALPHA	PL	D12	T11	P3
	41.29401579	315855	CVZCZZ	- -----	Y 21	Y 17	- -----
	41.36686939	317655	CVBAZZ	- -----	Y 37	Y 27	- -----
	41.83618406	325745	CWZBYZ	- -----	Y 7	Y 30	- -----
	41.83839047	325755	CWZBZZ	- -----	Y 110	Y 84	- -----
	41.91124408	327555	CWBZZZ	- -----	Y 91	Y 65	- -----
	42.38055874	335645	CXZAYZ	- -----	Y 31	Y 110	- -----
MQ3	42.38276515	335655	CXZAZZ	- -----	Y 431	Y 326	- -----
	42.45561876	337455	CXBYZZ	Z 1	Y 83	Y 63	- -----
	42.85428623	343755	CYXBZZ	- -----	Y 31	Y 23	- -----
	42.84500256	343555	CYXZZZ	- -----	Y 40	A 227	- -----
	42.92493342	345545	CYZZYZ	- -----	Y 68	Y 253	- -----
2MK3	42.92713984	345555	CYZZZZ	- -----	Y 1000	Y 753	- -----
	42.93178167	345655	CYZAZZ	Z 329	- -----	Y 1	Z 158
2NKM3	42.93642351	345755	CYZBZZ	- -----	A 45	A 59	- -----
2MS3	42.96820848	346555	CYAZZZ	B 2	- -----	- -----	B 1
2MP3	43.00927712	347555	CYBZZZ	Z 1	A 353	A 47	- -----
	43.39866092	353655	CZXAZZ	- -----	Y 221	Y 162	- -----
m3	43.47394994	355545	CZZZYZ	B 66	Y 1	- -----	B 32
M3	43.47615636	355555	CZZZZZ	Z 1188	Y 1	B 1	Z 569

Terdiurnal (cont'd)

NAME	deg/hour	NUM	ARGUMENT ALPHA	PL	D12	T11	P3
NK3	43.48079819	355655	CZZAZZ	-	A 226	A 300	-
	43.55365180	357455	CZBYZZ	-	A 29	A 60	-
	43.90196892	362556	CAWZZA	-	Y 56	Y 40	-
SO3	43.94303560	363555	CAXZZZ	-	Y 905	Y 662	-
MS3	43.98410424	364555	CAYZZZ	-	B 11	-	-
	44.02296646	365545	CAZZYZ	X 1	Y 85	A 134	-
MK3	44.02517288	365555	CAZZZZ	-	A 762	A 1000	-
	44.02737929	365565	CAZZAZ	-	A 66	A 257	-
	44.06623956	366554	CAAZZY	-	A 15	A 19	-
	44.10731016	367555	CABZZZ	-	A 84	A 14	-
	44.48741028	373455	CBXYZZ	-	Y 28	Y 22	-
	44.49669396	373655	CBXAZZ	-	A 106	A 64	-
2MQ3	44.56954756	375455	CBZYZZ	-	A 85	A 95	-
	44.57418940	375555	CBZZZZ	Z 144	-	-	Z 69
	44.57883123	375655	CBZAZZ	-	A 36	Y 58	-
	44.58103765	375665	CBZAAZ	Z 1	A 18	Y 24	-
SP3	44.95893136	381555	CCVZZZ	-	Y 215	Y 152	-
S3	45.00000000	382555	CCWZZZ	-	-	-	-
SK3	45.04106864	383555	CCXZZZ	-	A 609	A 437	-
	45.04327505	383565	CCXZAZ	-	A 91	A 115	-
K3	45.12320592	385555	CCZZZZ	-	A 192	Y 369	-
	45.12541233	385565	CCZZAZ	-	A 85	Y 138	-
	45.58544332	393455	CDXYZZ	-	A 92	A 49	-
	45.66758060	395455	CDZYZZ	Y 1	A 37	Y 60	-
	45.66978701	395465	CDZYAZ	-	A 19	Y 31	-
2SO3	46.05696440	3X1555	CEVZZZ	-	A 159	A 5	-

5.5 • Quarter diurnal

NAME	deg/hour	NUM	ARGUMENT ALPHA	D22	Q24	S26
	55.86356335	417755	DVBBZZ	Z 7	Z 58	Z 112
4M2S4	55.93641695	419555	DVDZZZ	Z 3	Z 37	Z 120

Quarter diurnal (cont'd)

NAME	deg/hour	ARGUMENT NUM	ALPHA	D22	Q24	S26
	56.32580075	425655	DWZAZZ	- -----Z	46Z	99
	56.33508443	425855	DWZCZZ	Z 15Z	26Z	44
2MNS4	56.40793803	427655	DWBAZZ	Z 27Z	183Z	306
2MnuS4	56.48079164	429455	DWDYZZ	Z 5Z	33Z	55
3MK4	56.87017544	435555	DXZZZZ	- -----Z	75Z	149
N4	56.87945911	435755	DXZBZZ	Z 86Z	128Z	180
3MS4	56.95231272	437555	DXBZZZ	Z 74Z	340Z	488
mn4	57.42162738	445645	DYZAYZ	B 28B	41B	55
MN4	57.42383379	445655	DYZAZZ	Z 381Z	465Z	548
Mnu4	57.49668740	447455	DYBYZZ	Z 71Z	73Z	130
2MSK4	57.88607120	453555	DZXZZZ	- -----Z	96Z	179
	57.89535487	453755	DZXBZZ	Z 14Z	66Z	125
MA4	57.92713984	454555	DZYZZZ	- ------ ----- -----
m4	57.96600206	455545	DZZZYZ	B 73B	87B	97
M4	57.96820848	455555	DZZZZZ	Z 1000Z	1000Z	990
2MRS4	58.00927515	456554	DZAZZY	Z 8Z	27Z	42
2MKS4	58.05034576	457555	DZBZZZ	Z 11Z	114Z	201
SN4	58.43972956	463655	DAXAZZ	Z 161Z	326Z	451
ML4	58.51258316	465455	DAZYZZ	B 22Z	111Z	231
NK4	58.52186683	465655	DAZAZZ	Z 61Z	110Z	169
nk4	58.52407325	465665	DAZAAZ	Z 20Z	33Z	46
MT4	58.94303756	472556	DBWZZA	Z 50Z	64Z	76
ms4	58.98189783	473545	DBXZYZ	B 32B	58B	74
MS4	58.98410424	473555	DBXZZZ	Z 915Z	995Z	1000
mK4	59.06403510	475545	DBZZYZ	B 12B	23B	34
MK4	59.06624152	475555	DBZZZZ	Z 249Z	314Z	374
Mk4	59.06844793	475565	DBZZAZ	Z 74Z	87Z	96
2SNM4	59.45562532	481655	DCVAZZ	B 7Z	82Z	189
2MSN4	59.52847892	483455	DCXYZZ	B 26Z	118Z	249
2MKN4	59.61061620	485455	DCZYZZ	Z 8Z	52Z	107
ST4	59.95893332	490556	DDUZZA	Z 25Z	49Z	67
S4	60.00000000	491555	DDVZZZ	Z 211Z	403Z	524

Quarter diurnal (cont'd)

NAME	ARGUMENT deg/hour	NUM	ALPHA	D22	Q24	S26
SK4	60.08213728	493555	DDXZZZ	Z 117	Z 224	Z 306
	60.08434369	493565	DDXZAZ	Z 35	Z 61	Z 76
	60.16427456	495555	DDZZZZ	Z 20	Z 38	Z 59
	60.16648097	495565	DDZZAZ	Z 13	Z 23	Z 34

5.6 • Fifth diurnal

NAME	ARGUMENT deg/hour	NUM	ALPHA	T122
	70.27812003	515855	EVZCZZ	Y 32
	70.35097363	517655	EVBAZZ	Y 47
	70.82028830	525745	EWZBYZ	Y 15
	70.82249471	525755	EWZBZZ	Y 137
	70.89534831	527555	EWBZZZ	Y 96
	71.36466298	535645	EXZAYZ	Y 49
2MQ5	71.36686939	535655	EXZAZZ	Y 431
	71.43972300	537455	EXBYZZ	Y 78
	71.83839047	543755	EYXBZZ	Y 75
	71.90903766	545545	EYZZYZ	Y 84
4MK5	71.91124408	545555	EYZZZZ	Y 766
	71.92052775	545755	EYZBZZ	A 94
	71.95231075	546554	EYAZZY	Y 11
4MP5	71.99338135	547555	EYBZZZ	A 77
	72.38276515	553655	EZXAZZ	Y 368
	72.46490243	555655	EZZAZZ	A 365
	72.88607316	562556	EAWZZA	Y 52
2MP5	72.92713984	563555	EAXZZZ	Y 1000
	73.00707070	565545	EAZZYZ	Y 123
2MK5	73.00927712	565555	EAZZZZ	A 846
	73.01148353	565565	EAZZAZ	A 85
	73.05034379	566554	EAAZZY	A 13
	73.09141439	567555	EABZZZ	A 29

Fifth diurnal (cont'd)

NAME	deg/hour	ARGUMENT NUM	ALPHA	T122
			|	|
	73.39866092	571655	EBVAZZ|Y	75|
			|	|
	73.47151452	573455	EBXYZZ|A	39|
	73.48079819	573655	EBXAZZ|A	188|
			|	|
	73.55365180	575455	EBZYZZ|A	38|
	73.56293547	575655	EBZAZZ|A	85|
	73.56514189	575665	EBZAAZ|A	41|
			|	|
	73.94303560	581555	ECVZZZ|Y	464|
			|	|
2SK5	74.02517288	583555	ECXZZZ|A	773|
	74.02737929	583565	ECXZAZ|A	78|
			|	|
	74.10731016	585555	ECZZZZ|A	284|
	74.10951657	585565	ECZZAZ|A	122|
			|	|
	74.56954756	593455	EDXYZZ|A	25|
			|	|
	74.65168484	595455	EDZYZZ|A	27|
	74.65389125	595465	EDZYAZ|A	12|
			|	|
	74.95893136	5X*555	EETZZZ|Y	72|
			|	|
	75.04106864	5X1555	EEVZZZ|A	181|
			|	|
	75.12320592	5X3555	EEXZZZ|A	143|

5.7 • Sixth diurnal

NAME	deg/hour	ARGUMENT NUM	ALPHA	T23	C25
			|	|	|
2(MN)K6	84.76553031	615755	FVZBZZ|-	-----|Z	18|
			|	|	|
5MKS6	84.83838391	617555	FVBZZZ|-	-----|Z	11|
2(MN)S6	84.84766759	617755	FVBBZZ|Z	16|Z	75|
			|	|	|
	84.92052119	619555	FVDZZZ|Z	7|Z	42|
			|	|	|
	85.30990499	625655	FWZAZZ|-	-----|Z	43|
	85.31918867	625855	FWZCZZ|Z	32|Z	48|
			|	|	|
3MNS6	85.39204227	627655	FWBAZZ|Z	48|Z	189|
3NKS6	85.40132594	627855	FWBCZZ|-	-----|Z	6|
			|	|	|
3MnuS6	85.46489588	629455	FWDYZZ|Z	9|Z	34|
			|	|	|
4MK6	85.85427968	635555	FXZZZZ|-	-----|Z	57|
2NM6	85.86356335	635755	FXZBZZ|Z	138|Z	183|
			|	|	|

Sixth diurnal (cont'd)

NAME	deg/hour	ARGUMENT NUM	ALPHA	T23	C25
4mS6	85.93421054	637545	FXBZYZ	11|B	38|
4MS6	85.93641695	637555	FXBZZZ	97|Z	278|
	85.97748363	638554	FXCZZY	7|Z	21|
2MSNK6	86.32580075	643655	FYXAZZ	----|Z	53|
2mn6	86.40573162	645645	FYZAYZ	47|B	61|
2MN6	86.40793803	645655	FYZAZZ	432|Z	510|
2Mnu6	86.48079164	647455	FYBYZZ	78|Z	82|
2MNKS6	86.49007531	647655	FYBAZZ	10|Z	68|
3mSk6	86.86796902	653545	FZXZYZ	----|Z	17|
3MSK6	86.87017544	653555	FZXZZZ	----|Z	88|
	86.87945911	653755	FZXBZZ	75|Z	140|
MA6	86.91124408	654555	FZYZZZ	----|-	----|
m6	86.95010630	655545	FZZZYZ	83|B	95|
M6	86.95231272	655555	FZZZZZ	764|Z	812|
3MKS6	87.03444999	657555	FZBZZZ	25|Z	119|
3MkS6	87.03665641	657565	FZBZAZ	5|Z	33|
MTN6	87.38276712	662656	FAWAZA	18|Z	29|
MSN6	87.42383379	663655	FAXAZZ	368|Z	492|
	87.49448099	665445	FAZYYZ	1|B	11|
2ML6	87.49668740	665455	FAZYZZ	11|Z	107|
MNK6	87.50597107	665655	FAZAZZ	120|Z	173|
MKnu6	87.57882468	667455	FABYZZ	23|Z	34|
2(MS)K6	87.88607120	671555	FBVZZZ	----|Z	57|
	87.89535487	671755	FBVBZZ	3|Z	42|
2MT6	87.92714180	672556	FBWZZA	52|Z	65|
2mS6	87.96600206	673545	FBXZYZ	72|B	89|
2MS6	87.96820848	673555	FBXZZZ	1000|Z	1000|
2MK6	88.05034576	675555	FBZZZZ	277|Z	338|
2Mk6	88.05255217	675565	FBZZAZ	83|Z	95|
	88.13248303	677555	FBBZZZ	4|Z	23|
2SN6	88.43972956	681655	FCVAZZ	74|Z	204|
3MTN6	88.47151648	682456	FCWYZA	1|Z	8|
3MSN6	88.51258316	683455	FCXYZZ	39|Z	108|
	88.52186683	683655	FCXAZZ	62|Z	130|

Sixth diurnal (cont'd)

NAME	deg/hour	NUM	ALPHA	T23	C25
				ARGUMENT	
3MKN6	88.59472044	685455	FCZYZZ	12|Z	57|Z
	88.59692685	685465	FCZYAZ	5|Z	17|Z
MST6	88.94303756	690556	FDUZZA	52|Z	70|Z
2SM6	88.98410424	691555	FDVZZZ	459|Z	585|Z
	89.02517288	692555	FDWZZZ	21|A	28|A
MSK6	89.06624152	693555	FDXZZZ	252|Z	335|Z
MSk6	89.06844793	693565	FDXZAZ	76|Z	92|Z
	89.14837880	695555	FDZZZZ	39|Z	59|Z
	89.15058521	695565	FDZZAZ	24|Z	35|Z
2MSTN6	89.48741224	6XO456	FEUYZA	2|B	8|Z
2(MS)N6	89.52847892	6X1455	FEVYZZ	12|B	72|Z
2MSKN6	89.61061620	6X3455	FEXYZZ	8|Z	58|Z

5.8 • Seventh diurnal

NAME	deg/hour	NUM	ALPHA	Q123
				ARGUMENT
	99.26222426	715855	GVZCZZ	54|Y
	99.33507787	717655	GVBAZZ	68|Y
	99.40793147	719455	GVDYZZ	12|Y
	99.80439253	725745	GWZBYZ	14|Y
	99.80659895	725755	GWZBZZ	185|Y
	99.87945255	727555	GWBZZZ	113|Y
	99.92051923	728554	GWCZZY	8|Y
	100.34876722	735645	GXZAYZ	34|Y
3MQ7	100.35097363	735655	GXZAZZ	456|Y
	100.39204031	736654	GXAAZY	10|Y
	100.42382724	737455	GXBYZZ	80|Y
	100.82249471	743755	GYXBZZ	170|Y
	100.89314190	745545	GYZZYZ	45|Y
5MK7	100.89534831	745555	GYZZZZ	624|Y
	100.90463199	745755	GYZBZZ	126|A

Seventh diurnal (cont'd)

NAME	ARGUMENT deg/hour	NUM	ALPHA	Q123
	100.93641499	746554	GYAZZY	Y 14
	100.97748559	747555	GYBZZZ	A 86
	101.36686939	753655	GZXAZZ	Y 560
	101.43972300	755455	GZZYZZ	Y 45
	101.44900667	755655	GZZAZZ	A 359
	101.87017740	762556	GAWZZA	Y 51
	101.91124408	763555	GAXZZZ	Y 1000
3MS7	101.95231272	764555	GAYZZZ	B 6
	101.99117494	765545	GAZZYZ	Y 127
3MK7	101.99338135	765555	GAZZZZ	A 591
	101.99558777	765565	GAZZAZ	A 45
	102.03444803	766554	GAAZZY	A 13
	102.07551863	767555	GABZZZ	A 41
	102.38276515	771655	GBVAZZ	Y 241
	102.45561876	773455	GBXYZZ	A 34
	102.46490243	773655	GBXAZZ	A 327
	102.53775604	775455	GBZYZZ	A 50
	102.53996245	775465	GBZYAZ	A 6
	102.54703971	775655	GBZAZZ	A 143
	102.92713984	781555	GCVZZZ	Y 683
3SK7	103.00927712	783555	GCXZZZ	A 764
	103.01148353	783565	GCXZAZ	A 58
	103.09141439	785555	GCZZZZ	A 299
	103.09362081	785565	GCZZAZ	A 124
	103.55365180	793455	GDXYZZ	A 18
	103.63799549	795465	GDZYAZ	A 14
	103.94303560	7X*555	GETZZZ	Y 211
	104.02517288	7X1555	GEVZZZ	A 351
	104.10731016	7X3555	GEXZZZ	A 272

5.9 • Eighth diurnal

		ARGUMENT					
NAME	deg/hour	NUM	ALPHA	Q24		S26	
	113.83177183	817755	HVBBZZ	Z	27	Z	95
2MNS8	114.37614651	827655	HWBAZZ	Z	69	Z	199
5MK8	114.83838391	835555	HXZZZZ	-	-----	Z	47
	114.91831478	837545	HXBZYZ	B	16	B	42
2(MN)8	114.84766759	835755	HXZBZZ	Z	187	Z	245
5MS8	114.92052119	837555	HXBZZZ	Z	114	Z	250
3MSNK8	115.30990499	843655	HYXAZZ	-	-----	Z	64
	115.38983586	845645	HYZAYZ	B	65	B	83
3MN8	115.39204227	845655	HYZAZZ	Z	458	Z	553
3Mnu8	115.46489588	847455	HYBYZZ	Z	79	Z	89
	115.85207326	853545	HZXZYZ	-	-----	Z	13
4MSK8	115.85427968	853555	HZXZZZ	-	-----	Z	82
	115.86356335	853755	HZXBZZ	Z	170	Z	243
	115.93421054	855545	HZZZYZ	B	88	B	105
M8	115.93641695	855555	HZZZZZ	Z	624	Z	708
	115.97748363	856554	HZAZZY	Z	14	Z	31
4MKS8	116.01855423	857555	HZBZZZ	Z	42	Z	129
	116.02076065	857565	HZBZAZ	Z	11	Z	36
2MSN8	116.40793803	863655	HAXAZZ	Z	560	Z	657
3ML8	116.48079164	865455	HAZYZZ	Z	45	Z	117
2MNK8	116.49007531	865655	HAZAZZ	Z	176	Z	242
	116.56292892	867455	HABYZZ	Z	33	Z	45
3M2SK8	116.87017544	871555	HBVZZZ	-	-----	Z	68
	116.87945911	871755	HBVBZZ	Z	43	Z	109
3MT8	116.91124604	872556	HBWZZA	Z	51	Z	66
	116.95010630	873545	HBXZYZ	B	108	B	120
3MS8	116.95231272	873555	HBXZZZ	Z	1000	Z	1000
	117.03224358	875545	HBZZYZ	B	35	B	49
3MK8	117.03444999	875555	HBZZZZ	Z	290	Z	363
	117.03665641	875565	HBZZAZ	Z	86	Z	103
	117.11658727	877555	HBBZZZ	Z	8	Z	31
2SMN8	117.42383379	881655	HCVAZZ	Z	240	Z	382

Eighth diurnal (cont'd)

NAME	deg/hour	ARGUMENT NUM	ALPHA	Q24	S26
				| |	| |
	117.49668740	883455	HCXYZZ	B 34	Z 110
	117.50597107	883655	HCXAZZ	Z 160	Z 241
				| |	| |
4MSN8	117.57882468	885455	HCZYZZ	Z 23	Z 69
				| |	| |
2MST8	117.92714180	890556	HDUZZA	Z 40	Z 44
				| |	| |
2(MS)8	117.96820848	891555	HDVZZZ	Z 677	Z 749
				| |	| |
2MSK8	118.05034576	893555	HDXZZZ	Z 373	Z 442
	118.05255217	893565	HDXZAZ	Z 113	Z 124
				| |	| |
	118.13248303	895555	HDZZZZ	Z 58	Z 82
				| |	| |
3SN8	118.43972956	8X*655	HETAZZ	Z 30	Z 112
				| |	| |
	118.51258316	8X1455	HEVYZZ	B 30	Z 80
	118.52186683	8X1655	HEVAZZ	Z 41	Z 107
				| |	| |
3M2SN8	118.59472044	8X3455	HEXYZZ	Z 8	Z 72
				| |	| |
	118.98189783	8E*545	HFTZYZ	B 6	B 18
3SM8	118.98410424	8E*555	HFTZZZ	Z 203	Z 303
				| |	| |
2SMK8	119.06624152	8E1555	HFVZZZ	Z 170	Z 256
	119.06844793	8E1565	HFVZAZ	Z 51	Z 70

5.10 • Tenth diurnal

NAME	deg/hour	ARGUMENT NUM	ALPHA	C25
				| |
	142.81587606	X17755	JVBBZZ	Z 42
				| |
5MNS10	143.36025075	X27655	JWBAZZ	Z 91
				| |
	143.82956541	X35745	JXZBYZ	B 43
3M2N10	143.83177183	X35755	JXZBZZ	Z 243
6MS10	143.90462543	X37555	JXBZZZ	Z 129
				| |
4MN10	144.37614651	X45655	JYZAZZ	Z 492
				| |
4Mnu10	144.44900011	X47455	JYBYZZ	Z 83
				| |
5MSK10	144.83838391	X53555	JZXZZZ	B 4
				| |
	144.91831478	X55545	JZZZYZ	B 97
M10	144.92052119	X55555	JZZZZZ	Z 557
				| |
	144.96158787	X56554	JZAZZY	Z 17

Tenth diurnal (cont'd)

NAME	deg/hour	ARGUMENT NUM	ALPHA	C25
	145.00265847	X57555	JZBZZZ|Z	61
	145.00486488	X57565	JZBZAZ|Z	16
3MSN10	145.39204227	X63655	JAXAZZ|Z	746
4ML10	145.46489588	X65455	JAZYZZ|Z	79
3MNK10	145.47417955	X65655	JAZAZZ|Z	238
	145.54703315	X67455	JABYZZ|Z	45
	145.86356335	X71755	JBVBZZ|Z	137
	145.93421054	X73545	JBXZYZ|B	143
4MS10	145.93641695	X73555	JBXZZZ|Z	1000
	146.01634782	X75545	JBZZYZ|B	47
4MK10	146.01855423	X75555	JBZZZZ|Z	311
	146.10069151	X77555	JBBZZZ|Z	14
2(MS)N10	146.40793803	X81655	JCVAZZ|Z	476
	146.48079164	X83455	JCXYZZ|B	17
	146.49007531	X83655	JCXAZZ|Z	297
5MSN10	146.56292892	X85455	JCZYZZ|Z	42
3M2S10	146.95231272	X91555	JDVZZZ|Z	870
3MSK10	147.03444999	X93555	JDXZZZ|Z	487
	147.03665641	X93565	JDXZAZ|Z	147
	147.11658727	X95555	JDZZZZ|Z	78
3SMN10	147.42383379	XX*655	JETAZZ|Z	133
	147.49668740	XX1455	JEVYZZ|B	43
	147.50597107	XX1655	JEVAZZ|Z	138
4M2SN10	147.57882468	XX3455	JEXYZZ|Z	13
	147.96600206	XE*545	JFTZYZ|B	26
3S2M10	147.96820848	XE*555	JFTZZZ|Z	388
2(MS)K10	148.05034576	XE1555	JFVZZZ|Z	322
	148.05255217	XE1565	JFVZAZ|Z	97

5.11 • Twelfth diurnal

NAME	ARGUMENT deg/hour	NUM	ALPHA	S26
	171.79998030	T17755	LVBBZZ|Z	63
	171.87283391	T19555	LVDZZZ|Z	21
	172.27150138	T25855	LWZCZZ|Z	121
4MNS12	172.34435499	T27655	LWBAZZ|Z	118
	172.41720859	T29455	LWDYZZ|Z	18
	172.81366965	T35745	LXZBYZ|X	62
4M2N12	172.81587606	T35755	LXZBZZ|Z	297
	172.88652326	T37545	LXBZYZ|X	31
4M2N12	172.88872967	T37555	LXBZZZ|Z	145
	172.92979635	T38554	LXCZZY|Z	11
	173.28739714	T43855	LYXCZZ|Z	153
	173.35804433	T45645	LYZAYZ|X	107
5MN12	173.36025075	T45655	LYZAZZ|Z	519
	173.40131742	T46654	LYAAZY|Z	20
	173.43089794	T47445	LYBYYZ|X	17
5Mnu12	173.43310435	T47455	LYBYZZ|Z	82
	173.83177183	T53755	LZXBZZ|Z	444
	173.90021260	T55535	LZZZXZ|Z	8
	173.90241902	T55545	LZZZYZ|X	106
M12	173.90462543	T55555	LZZZZZ|Z	518
	173.91611552	T55765	LZZBAZ|Z	46
	173.94569211	T56554	LZAZZY|Z	20
	173.98676271	T57555	LZBZZZ|Z	84
	173.98896912	T57565	LZBZAZ|Z	24
	174.33507983	T62656	LAWAZA|Z	42
4MSN12	174.37614651	T63655	LAXAZZ|Z	895
	174.40793344	T64456	LAYYZA|Z	10
	174.44679370	T65445	LAZYYZ|X	16
4ML12	174.44900011	T65455	LAZYZZ|Z	102
4MNK12	174.45828379	T65655	LAZAZZ|Z	298
	174.46049020	T65665	LAZAAZ|Z	91
	174.53113739	T67455	LABYZZ|Z	53
	174.84766759	T71755	LBVBZZ|Z	290

Twelfth diurnal (cont'd)

NAME	deg/hour	ARGUMENT NUM	ALPHA	S26
			|	|
5MT12	174.87945451	T72556	LBWZZA|Z	54|
			|	|
	174.91831478	T73545	LBXZYZ|X	172|
5MS12	174.92052119	T73555	LBXZZZ|Z	967|
			|	|
	175.00045206	T75545	LBZZYZ|X	61|
5MK12	175.00265847	T75555	LBZZZZ|Z	331|
	175.00486488	T75565	LBZZAZ|Z	99|
	175.00707130	T75575	LBZZBZ|Z	11|
			|	|
	175.04372515	T76554	LBAZZY|Z	10|
			|	|
	175.08479575	T77555	LBBZZZ|Z	24|
			|	|
3M2SN12	175.39204227	T81655	LCVAZZ|Z	745|
			|	|
	175.46489588	T83455	LCXYZZ|Z	19|
	175.47417955	T83655	LCXAZZ|Z	454|
			|	|
5MSN12	175.54703315	T85455	LCZYZZ|Z	64|
	175.54923957	T85465	LCZYAZ|Z	20|
			|	|
	175.86356335	T9*755	LDTBZZ|Z	84|
			|	|
4MST12	175.89535028	T90556	LDUZZA|Z	109|
			|	|
	175.93421054	T91545	LDVZYZ|X	143|
4M2S12	175.93641695	T91555	LDVZZZ|Z	1000|
			|	|
	176.01634782	T93545	LDXZYZ|X	91|
4MSK12	176.01855423	T93555	LDXZZZ|Z	575|
	176.02076065	T93565	LDXZAZ|Z	175|
	176.02296706	T93575	LDXZBZ|Z	18|
			|	|
	176.05962091	T94554	LDYZZY|Z	8|
			|	|
	176.10069151	T95555	LDZZZZ|Z	98|

Twelfth diurnal (cont'd)

	176.95010630	TE*545	LFTZYZ|X	61|
3(MS)12	176.95231272	TE*555	LFTZZZ|Z	587|
			|	|
	177.03224358	TE1545	LFVZYZ|X	60|
3M2SK12	177.03444999	TE1555	LFVZZZ|Z	492|
	177.03665641	TE1565	LFVZAZ|Z	150|

E

Fourier transforms and series

There are two types of signal representation:

• temporal representation $f(t)$ in which the independent variable is time t;

• a frequency representation $\mathrm{F}(\nu)$ in which the independent variable is the frequency ν, i.e. time^{-1}, measured in hertz: 1 Hz = 1 cycle/second.

The switch from one to the other is done via the so-called Fourier (1768-1830) transform. This transform can be extended to combinations other than time-frequency. When the independent variable is a length, then we may have the length-wave number combination, for instance. This appendix summarises a number of definitions, general aspects and properties of Fourier transforms and series, while also reviewing the role of distributions in the analysis of sampled measurements with a regular time interval. In the last part, as a supplement to Chapter VI, two examples are presented that highlight the impact of the tide monitoring period (month and year) on the number of tidal constituents that can be separated.

1 • Definitions and general aspects

Where the real function $f(t)$ is representative of a physical phenomenon, let us consider the two following cases:

• first case: function $f(t)$ is a Fourier series of period T (corresponding frequency $\nu_{\mathrm{T}} = 1/\mathrm{T} > 0$), i.e. the value of the function is the same for t and $t \pm k\mathrm{T}$, irrespective of the value of $k \in \mathrm{N}^*$, i.e. a set of positive integers.

The Fourier transform of the periodic function $f(t)$ at frequency $\nu_m = m\nu_\mathrm{T}$, where $m \in \mathrm{Z}$ is a set of relative integers, is formulated as follows:

$$\mathrm{F}(\nu_m) = \frac{1}{\mathrm{T}} \int_{-\mathrm{T}/2}^{+\mathrm{T}/2} f(t) e^{-j2\pi m \nu_\mathrm{T} t} \mathrm{d}t \tag{E.1a}$$

• second case: with any function $f(t)$, the aperiodic character can be considered as an extension of period T to infinity. Depending on the existing conditions, the Fourier transform (FT) at frequency ν of a function $f(t)$, is defined by:

$$\mathrm{F}(\nu) = \mathrm{FT}\left[f(t)\right] = \int_t f(t) e^{-j2\pi\nu t} \mathrm{d}t \tag{E.1b}$$

where the letter t under the integral symbol indicates that the integration takes place throughout the $-\infty$ to $+\infty$ domain. The inverse Fourier transform, denoted FT^{-1}, is then obtained by:

$$f(t) = \mathrm{FT}^{-1}\left[\mathrm{F}(\nu)\right] = \int_\nu \mathrm{F}(\nu) e^{+j2\pi\nu t} \mathrm{d}\nu \tag{E.2}$$

The amplitude spectrum of $f(t)$ represents the absolute value $|\mathrm{F}(\nu)|$ as a function of the frequency. For a periodic function, this spectrum is defined for discrete frequencies $\nu_m = m\nu_\mathrm{T}$. It is called the line spectrum with a minimum error on the frequency axis of $\nu_\mathrm{T} = 1/\mathrm{T}$. For any function accepting a transform, the frequency interval ν_T then tends towards zero and the spectrum becomes continuous, but only if function $f(t)$ does not contain any periodic constituents (e.g. turbulence). We demonstrate that a nonperiodic real function $f(t)$ must meet the following three conditions in order to accept a Fourier transform $\mathrm{FT}\left[f(t)\right]$:

• function $f(t)$ should be bounded (no infinite values),

• its integral between $-\infty$ and $+\infty$ should have a finite value,

• its potential discontinuities and maxima and minima should be finite throughout its domain.

The two functions $f(t)$ and its transform $\mathrm{F}(\nu)$ represent the same phenomenon in their respective domains (time, frequency). We demonstrate that a number of properties are attached to these functions. If function $f(t)$ is considered real, thus Hermitian (formed with two complex conjugate elements), then equations (E.1a) and (E.1b) show that the transform preserves this property, and thus:

$$\mathrm{F}(\nu) = \mathrm{F}^*(-\nu) \tag{E.3}$$

Moreover, the two functions are linked by Poisson's equation:

$$\sum_{m \in \mathrm{Z}} f(m) = \sum_{n \in \mathrm{Z}} \mathrm{F}(n) \tag{E.4}$$

where the terms m or $n \in \mathrm{Z}$ under the sum symbol indicate that the sum concerns the entire set **Z**. The crucial Plancherel theorem states that the Fourier transform of a convolution product ($*$) of two functions is the simple product ($\times$) of the corresponding products, and reciprocally. When:

$$\mathrm{FT}\left[f(t)\right] = \mathrm{F}(\nu) \quad \text{and} \quad \mathrm{FT}\left[g(t)\right] = \mathrm{G}(\nu)$$

this fundamental property is summarised by the following equations:

$$\begin{aligned} \mathrm{FT}\left[f(t) * g(t)\right] &= \mathrm{F}(\nu) \times \mathrm{G}(\nu) \\ \mathrm{FT}\left[f(t) \times g(t)\right] &= \mathrm{F}(\nu) * \mathrm{G}(\nu) \end{aligned} \tag{E.5a}$$

and reciprocally:

$$\begin{aligned} \mathrm{FT}^{-1}\left[\mathrm{F}(\nu) \times \mathrm{G}(\nu)\right] &= f(t) * g(t) \\ \mathrm{FT}^{-1}\left[\mathrm{F}(\nu) * \mathrm{G}(\nu)\right] &= f(t) \times g(t) \end{aligned} \tag{E.5b}$$

This theorem simplifies the calculations in many cases.

In the real environment, a quantifiable phenomenon is always observed over a finite timespan T since the representative function of its temporal change generally meets the existing transform conditions. However, it is hard to apply the Fourier transform in studies focused on a continuous but changing phenomenon due to the problem of sampling the representative curve. In most cases, an analog signal $f(t)$ (thus continuous) is sampled over a regular time interval t_e between two consecutive readings – it is said that the signal is sampled every t_e or at the frequency (or rate) of a value by $t_e(\nu_e = 1/t_e)$. We obtain a series with a general term $f(mt_e)$ having the value $m \in \mathrm{Z}$ as sequence number (assuming that the representative function can be sampled throughout its existing domain). Several sampling techniques are available for the same signal, but there are two overall types:

- point sampling: the data are values of the continuous function $f(t)$, sampled at times $t = mt_e$;
- mean sampling: the sample every t_e is the result of the simple or weighted (filtering) mean of $f(t)$ calculated for all or part of the intervals $[mt_e, (m+1)t_e[$.

Here we will only deal with regular point sampling. The continuous function $f(t)$ becomes a series of discrete values $f(mt_e)$ and the question then arises as to how the real transform $\mathrm{F}(\nu)$ can be extracted from this series. It is nevertheless possible to determine $\mathrm{F}(\nu)$ from the sampled series by applying the distribution theory (especially Dirac combs and rectangular distributions) to solve this problem, provided that certain conditions are fulfilled. Before dealing with this issue, it would be useful to review a few points concerning distributions and their transforms.

2 • Distributions and their transforms

Here we will summarise aspects concerning Dirac distributions and combs, as well as rectangular distributions and the corresponding Fourier transforms.

2.1 • Dirac distributions

A Dirac distribution $\delta(x-x_i)$ is a linear form equal to unity for $x = x_i$ and zero elsewhere in the domain of the independent variable ($x \in \mathrm{R}$). We adopt the symbolism $\delta(x - x_i)$, despite the fact that it is an improper notation (δ_{x_i} is the correct one). Hence, we have:

$$\delta(x - x_i) = \begin{cases} 1 & \text{si } x = x_i \\ 0 & \text{si } x \neq x_i, \end{cases} \tag{E.6}$$

Note that for $x_i = 0$, with our convention, the distribution is formulated as $\delta(x)$. At frequency ν, the Dirac transform $\delta(t - t_i)$ is perfectly defined by:

$$\mathrm{FT}\left[\delta(t - t_i)\right] = \int_t \delta(t - t_i) e^{-j2\pi\nu t} \mathrm{d}t = e^{-j2\pi\nu t_i} \tag{E.7}$$

As this transform is complex, the amplitude spectrum is then equal to the norm $\left\| e^{-j2\pi\nu t_i} \right\|$, of unit value regardless of the frequency, but its phase spectrum is a linear function of the frequency ($\varphi = 2\pi\nu t_i$). However, the temporal function having a Dirac distribution $\delta(\nu - \nu_i)$ as spectrum is obtained via the inverse transform, which gives:

$$\mathrm{FT}^{-1}\left[\delta(\nu - \nu_i)\right] = \int_\nu \delta(\nu - \nu_i) e^{+j2\pi\nu t} \mathrm{d}t = e^{j2\pi\nu_i t} \tag{E.8}$$

This complex exponent can be interpreted as the representative cyclic function (in terms of polar coordinates) of a moving platform describing a circumference with a radius of 1 at a constant angular velocity of $2\pi\nu_i$, except for $\nu_i = 0$, a value for which $\mathrm{FT}^{-1}\left[\delta(\nu)\right] = 1$. When considering Poisson's equation and equations (E.7) and (E.8), we deduce the equality:

$$\sum_{m \in \mathrm{Z}} \delta(t - m) = \sum_{n \in \mathrm{Z}} e^{j2\pi nt}$$

This latter equation defines the two forms of the Dirac comb distribution at unit rate, which we denote by $\mathrm{X}_1(t)$, or:

$$\mathrm{X}_1(t) = \sum_{m \in \mathrm{Z}} \delta(t - m) = \sum_{m \in \mathrm{Z}} e^{j2\pi mt} \tag{E.9}$$

The subscript (1) attached here to X represents the time interval between two successive Dirac distributions of the series. We will now examine the

properties of the comb distribution $\mathrm{X}_{t_e}(t)$, which has a more general scope with an interval t_e between two successive Dirac distributions.

2.2 • Dirac comb distributions

A Dirac comb distribution $\mathrm{X}_{t_e}(t)$ is a periodic distribution, of period t_e, defined by the following equation:

$$\mathrm{X}_{t_e}(t) = \sum_{m\in\mathrm{Z}} \delta(t - mt_e) \tag{E.10}$$

This distribution represents the mathematical operator for sampling all continuous functions $f(t)$ with a time step t_e. Hence:

$$f(t)\cdot \mathrm{X}_{t_e}(t) = \sum_{m\in\mathrm{Z}} f(t)\delta(t - mt_e) = \sum_{m\in\mathrm{Z}} f(mt_e) \tag{E.11}$$

If we apply $\mathrm{X}_1(t)$, as defined by equation (E.9), to a regular function $h(t)$, then:

$$\int_t h(t) \sum_{m\in\mathrm{Z}} \delta(t - m)\cdot \mathrm{d}t = \sum_m h(m) = \sum_m \int_t h(t) e^{j2\pi mt}\mathrm{d}t \tag{E.12}$$

When changing the variable such that $h(t) = \mathrm{H}(t/a)$, with $a > 0$, the last equality of equation (E.12) may be formulated as:

$$\sum_{m\in\mathrm{Z}} \mathrm{H}(m/a) = a\sum_m \int_t \mathrm{H}(t/a) e^{j2\pi ma(t/a)}\mathrm{d}t/a \tag{E.13}$$

This leads to an equation similar to (E.9) defining $\mathrm{X}_1(t)$, but with a separate scale:

$$\frac{1}{a}\sum_{m\in\mathrm{Z}} \delta\left(t - \frac{m}{a}\right) = \sum_{n\in\mathrm{Z}} e^{j2\pi nat} \tag{E.14}$$

Therefore, by taking $a = 1/t_e$, we obtain:

$$t_e \mathrm{X}_{t_e}(t) = \sum_{m\in\mathrm{Z}} e^{j2\pi m\frac{t}{t_e}} \tag{E.15}$$

Moreover, by taking equation (E.7) into account, the transform of comb $\mathrm{X}_{t_e}(t)$ is formulated as:

$$\mathrm{FT}\left[\mathrm{X}_{t_e}(t)\right] = \sum_{k\in\mathrm{Z}} e^{j2\pi\nu kt_e} \tag{E.16}$$

When equation (E.14) is applied to ν, we deduce from equation (E.16) that the transform of a comb is a comb to the closest constant. Then:

$$\mathrm{FT}\left[\mathrm{X}_{t_e}(t)\right] = \frac{1}{t_e}\cdot \mathrm{X}_{1/t_e}(\nu)$$

where, with $\nu_e = 1/t_e$:

$$\mathrm{FT}\left[t_e \mathrm{X}_{t_e}(t)\right] = \mathrm{X}_{\nu_e}(\nu) \tag{E.17}$$

This very important latter result is the basis for the entire sampling theory. Hence, the transform $\mathrm{X}_{\nu_e}(\nu)$, which also has a periodic distribution, corresponds to the comb $t_e \mathrm{X}_{t_e}(t)$ of period t_e, and this introduces the period $\nu_e = 1/t_e$ in the frequency domain. We find this sequential repetition ν_e in all transforms of functions 'combed' by $t_e \mathrm{X}_{t_e}(t)$.

2.3 • Rectangular functions and distributions

A regular function $f(t)$, representing a physical phenomenon, is only known over a limited time interval. Sampling $f(t)$ over a duration T naturally leads us to define the rectangular distribution from the rectangular function.

2.3.1 • Rectangular functions

The rectangular function is also an important signal processing tool. This function, which is also called a 'window' or 'slot' function, is defined by its width T on the time axis. It is equal to unity over the interval $\left[t_i, t_j\right]$, edges included, such that $t_j - t_i = \mathrm{T}$, and zero elsewhere. As a signal is generally studied from a temporal origin over a given time T, we let $\Pi_{\mathrm{T}}(t)$ denote the rectangular function defined according to the following elements:

$$\Pi_{\mathrm{T}}(t) = \begin{cases} 1 & \text{si } t \in [0, \mathrm{T}] \\ 0 & \text{si } t \notin [0, \mathrm{T}] \end{cases} \tag{E.18}$$

The rectangle is considered to be symmetrical when it is centred on the zero mark of the variable (time or frequency). In a time domain, it is the result of the convolution of Dirac $\delta(t + \mathrm{T}/2)$ with $\Pi_{\mathrm{T}}(t)$, which translates the beginning of the new rectangle at time $t = -\mathrm{T}/2$:

$$\int_{\tau} \delta(\tau + \mathrm{T}/2)\Pi_{\mathrm{T}}(t - \tau)\mathrm{d}\tau = \Pi_{\mathrm{T}}(t + \mathrm{T}/2). \tag{E.19}$$

The transform of this symmetrical rectangle normalised by its width T is expressed by:

$$\mathrm{FT}\left[\frac{1}{\mathrm{T}}\Pi_{\mathrm{T}}(t + \mathrm{T}/2)\right] = \frac{1}{\mathrm{T}}\int_{t} \Pi_{\mathrm{T}}(t + \mathrm{T}/2)e^{-j2\pi\nu t}\mathrm{d}t = \frac{1}{\mathrm{T}}\int_{-\mathrm{T}/2}^{\mathrm{T}/2} e^{-j2\pi\nu t}\mathrm{d}t$$

The last integral of the previous equation thus gives:

$$\mathrm{FT}\left[\frac{1}{\mathrm{T}}\Pi_{\mathrm{T}}(t + \mathrm{T}/2)\right] = \frac{\sin \pi\nu\mathrm{T}}{\pi\nu\mathrm{T}} \tag{E.20}$$

This transform is even and its representative curve is symmetrical with respect to axis $\nu = 0$. It is maximal and equal to unity for $\nu = 0$ and it reaches relative extremes for frequencies $\nu = (1/2 + k)\nu_T$ with $k \in Z$ and $\nu_T = 1/T$. The amplitudes of these extremes tend towards zero when $|\nu| \to \infty$. This function is cancelled out for frequencies of $\nu = k\nu_T$, here with $k \in Z^*$ (set of relative integers, excluding zero). Note that when T tends towards infinity, equation E.20 tends towards the distribution $\delta(\nu)$. We have seen that $FT^{-1}[\delta(\nu)] = 1$ for all t. The rectangular function $\Pi_T(t)$, which is considered as a convolution of $\Pi_T(t + T/2)$ with $\delta(t - T/2)$, enables us to obtain its transform via the simple product of the respective transforms. As this transform normalised by the width T is a continuous function which keeps returning, we denote it by $\Lambda_T(\nu)$, where:

$$\Lambda_T(\nu) = FT\left[\frac{1}{T}\Pi_T(t)\right] = FT\left[\frac{1}{T}\Pi_T(t + T/2) * \delta(t - T/2)\right] = \frac{\sin \pi\nu T}{\pi\nu T} e^{-j\pi\nu T} \tag{E.21}$$

This gives rise to a phase lag that is a linear function of the frequency ($\pi\nu T$), while the modulus preserves the same characteristics as in (E.20), i.e. the spectrum is identical. This transform $\Lambda_T(\nu)$ is one of the basic functions used in studying any signal over a limited duration ($0 \leq t \leq T$).

2.3.2 • Rectangular distributions

A rectangular distribution of width T sampled by the comb $t_e X_{t_e}(t)$ defines this distribution, but the term 'rectangle' often refers to the function or distribution, depending on the setting. For the distribution, the width T and the sampling interval t_e are always linked by $T = Mt_e$, with M being an integer representing the number of samples (for simplification, M values are always considered to be even in this appendix). Hence, $\Pi_{T,t_e}(t)$ is the rectangular distribution resulting from the sampling of function $\Pi_T(t)$ by the comb $t_e X_{t_e}$, with $T = Mt_e$. It may be expressed by:

$$\Pi_{T,t_e}(t) = t_e X_{t_e} \cdot \Pi_T(t) = t_e \sum_{m=0}^{m=M-1} \delta(t - mt_e) \tag{E.22}$$

It is important to note that the sampling is done from time $t = 0$ until time $t = (M - 1)\, t_e$. We obtain a series of M values equal to t_e and, since $T = Mt_e$, then:

$$\frac{1}{Mt_e} \sum_{m=0}^{m=M-1} t_e \delta(t - mt_e) = 1 = \frac{1}{T}\int_0^T \Pi_T(t)dt \tag{E.23}$$

The sum of the series sampled in this way is equal to the integral of the corresponding rectangular function, i.e. the sum of the series is identified with the integral of the function when t_e tends towards zero. When considering the normalised rectangular distribution (E.22), its Fourier transform is formulated as:

$$\mathrm{FT}\left[\frac{1}{\mathrm{T}}\Pi_{\mathrm{T},t_e}(t)\right] = \mathrm{FT}\left[\frac{t_e}{\mathrm{T}}\sum_{m=0}^{m=\mathrm{M}-1}\delta(t-mt_e)\right] = \frac{1}{\mathrm{M}}\sum_{m=0}^{m=\mathrm{M}-1}e^{-j2\pi\nu mt_e} \tag{E.24a}$$

Note that the series of the right hand side of equation (E.24a) represents a geometric sequence ratio $e^{-j2\pi\nu t_e}$. We denote this transform by $\Lambda_{\mathrm{T,M}}(\nu)$, and it thus becomes:

$$\Lambda_{\mathrm{T,M}}(\nu) = \mathrm{FT}\left[\frac{1}{\mathrm{T}}\Pi_{\mathrm{T},t_e}(t)\right] = \frac{1}{\mathrm{M}}\cdot\frac{e^{-j2\pi\nu\mathrm{M}t_e}-1}{e^{-j2\pi\nu t_e}-1}$$

where:

$$\Lambda_{\mathrm{T,M}}(\nu) = \frac{\sin(\pi\nu\mathrm{T})}{\mathrm{M}\sin(\pi\nu\mathrm{T}/\mathrm{M})}e^{-j\pi\nu\mathrm{T}(1-1/\mathrm{M})} \tag{E.24b}$$

A third expression of $\Lambda_{\mathrm{T},t_e}(\nu)$ may be obtained via the convolution product:

$$\Lambda_{\mathrm{T,M}}(\nu) = \Lambda_{\mathrm{T}}(\nu) * \mathrm{FT}\left[t_e\mathrm{X}_{t_e}(t)\right] = \frac{\sin(\pi\nu\mathrm{T})}{\pi\nu\mathrm{T}}e^{-j\pi\nu\mathrm{T}} * \mathrm{X}_{\nu_e}(\nu)$$

which can be formulated, while recalling that:

$$\mathrm{X}_{\nu_e}(\nu) = \sum_{k\in\mathrm{Z}}\delta(\nu-k\nu_e)$$

with $\nu_e = \mathrm{M}/\mathrm{T}$:

$$\Lambda_{\mathrm{T,M}}(\nu) = \sum_{k\in\mathrm{Z}}\frac{\sin\left[\pi(\nu+k\nu_e)\mathrm{T}\right]}{\pi(\nu+k\nu_e)\mathrm{T}}e^{-j\pi(\nu+k\nu_e)\mathrm{T}} \tag{E.24c}$$

A comparison of $\Lambda_{\mathrm{T}}(\nu)$, i.e. the transform of the normalised rectangular function E.24, with $\Lambda_{\mathrm{T,M}}(\nu)$, given in the three forms (E.24a), (E.24b) and (E.24c), demonstrates that the sampling leads to a very clearcut modification in the nature of the spectrum:

- the spectrum of the rectangular distribution is regenerated every $k\nu_e$ (periodicity) with $\Lambda_{\mathrm{T,M}}(\nu) = \Lambda_{\mathrm{T,M}}(\nu+k\nu_e)$; it is not possible to obtain the exact sepctrum of the rectangular function by sampling; note that in equation (E.24b), the denominator is equal to $\mathrm{M}\sin(\pi\nu\mathrm{T}/\mathrm{M})$, which converges around $\pi\nu\mathrm{T}$ when M tends towards infinity ($t_e \to 0$);

• we have seen that the spectrum of $\Lambda_T(\nu)$ has an absolute maximum equal to unity for $\nu = 0$; because of the periodicity, the spectrum of $\Lambda_{T,M}(\nu)$ reaches these absolute maxima, also equal to unity, for all $\nu = k\nu_e$;

• as the two transforms are Hermitian with $\Lambda_T(\nu) = \Lambda_T^*(-\nu)$ and $\Lambda_{T,M}(\nu) = \Lambda_{T,M}^*(-\nu)$, the two spectra are symmetrical with respect to axis $\nu = 0$; however, due to the seqential repetition of $\Lambda_{T,M}(\nu)$, $\nu = k\nu_e$ are also symmetry axes for the rectangular distribution spectrum;

• when $\Delta\nu$ represents any positive or negative frequency error, the periodic and Hermitian character of $\Lambda_{T,M}(\nu)$ leads to the following equality:

$$\Lambda_{T,M}(\nu_e/2 - \Delta\nu) = \Lambda_{T,M}^*(\nu_e/2 + \Delta\nu + k\nu_e)$$

This equation can be readily verified through the different equations for $\Lambda_{T,M}(\nu)$ and generates the spectrum with an additional property, i.e. the axes $\nu = (1/2 + k)\,\nu_e$ are also symmetry axes of this spectrum. This phenomenon is called aliasing. $\nu_N = \nu_e/2$ is called the Nyquist frequency.

A good image of the transform $\Lambda_T(\nu)$ is thus obtained by $\Lambda_{T,M}(\nu)$ while restricting it to the frequency interval $(-\nu_N, \nu_N)$, but this image does not retrieve the constituents of $\Lambda_T(\nu)$ outside of this domain. However, if we integrate the two intervals, i.e. temporal T and frequential $\nu_e = 2\nu_N$, each in its domain at the periods, we have:

$$M = \frac{T}{t_e} = \frac{\nu_e}{\nu_T} \tag{E.25}$$

At the normalised rectangular distribution (discrete series of time step t_e):

$$\frac{1}{T}\Pi_{T,t_e}(t) = \frac{t_e}{T}X_{t_e} \cdot \Pi_T(t) = \frac{1}{M}\sum_{m=0}^{m=M-1} \delta(t - mt_e) \tag{E.26}$$

we can thus map a discrete transform (line spectrum every $\nu_T = 1/T$) in the symmetrical rectangular frequency distribution of width ν_e, having the same number of terms M. Indeed, from $\Lambda_{T,M}(\nu)$ defined by equation E.24b) and noting that $\nu_N = \nu_e/2 = M\nu_T/2$, we then obtain the following series:

$$\Lambda_{T,M}(\nu) \cdot \sum_{n=-M/2}^{n=M/2-1} \delta(\nu - n\nu_T) = \sum_{n=-M/2}^{n=M/2-1} \frac{\sin n\pi}{M \sin(n\pi/M)} e^{-jn\pi(1-1/M)} = \delta(n) \tag{E.27}$$

All of the terms of this transform discretised to values $\nu = n\nu_T$ are zero, apart from the term for which $n = 0$, which corresponds to the Dirac $\delta(\nu)$ whose inverse transform has unit value. Note that the discretisation of

$\Lambda_T(\nu)$ expressed by equation (E.21) gives the same result. We thus obtain the same image for the respective discrete spectra of the function and of the normalised rectangular distribution in the frequency interval $(-\nu_N, \nu_N)$. As the inverse transform of (E.27) is equal to unity, its sampling within the interval (0, T) again clearly gives the rectangular distribution (E.26). There is complete correspondence between the two equations. We will see that this correspondence is a property common to all functions that accept a Fourier transform and that are sampled over a given time interval. Note that these discrete Fourier transforms (DFT), which are more often called Fourier series, are the result of the 'sampling-periodisation' duality in the two domains, i.e. temporal and frequential. These tools facilitate the analysis of series of data representing discrete values of a signal sampled regularly over a given time interval.

3 • Real periodic functions

Recall that a real function f of a real variable t is considered to be periodic, i.e. of period T (positive number), if the function value is the same for t and $t \pm k\mathrm{T}$ ($k \in \mathrm{N}^*$).

3.1 • Periodic series

Let us consider the complex exponential series

$$\sum_{m\in\mathrm{Z}} \lambda_m e^{j2\pi\nu_m t}$$

where the frequencies ν_m are defined by $\nu_m = m\nu_\mathrm{T} (m \in \mathrm{Z})$ and $\nu_\mathrm{T} = 1/\mathrm{T} > 0$), with the complex coefficients ($\lambda_m \in \mathrm{C}$) satisfying equation $\lambda_m = \lambda^*_{-m}$. This series thus defines a real trigonometric series, expressed in complex notation. On condition that the sum is bounded, this series is representative of a real periodic function of period T and is defined for all t. Its value is the same for all points $t \pm k\mathrm{T}$ and does not depend on $k \in \mathrm{N}^*$. It is thus a function $f(t)$, defined for all t values, and of period T. If there is a trigonometric series for which $f(t)$ is the sum, it would define the Fourier series of the function, which in complex notation is:

$$f(t) = \sum_{m\in\mathrm{Z}} \lambda_m e^{j2\pi m\nu_\mathrm{T} t} \tag{E.28a}$$

This Fourier series can be formulated in different forms, here with $\nu_n = n\nu_T$ ($n \in N$):

$$f(t) = \lambda_0 + \sum_{n\in N^*} \left[\lambda_n e^{+j2\pi n\nu_T t} + \lambda_n^* e^{-j2\pi . n\nu_T t}\right] \tag{E.28b}$$

$$f(t) = \frac{c_0 e^{-j\varphi_0}}{2} + \sum_{n\in N^*} \frac{c_n}{2}\left(e^{+j(2\pi n\nu_T t-\varphi_n)} + e^{-j(2\pi n\nu_T t-\varphi_n)}\right) \tag{E.28c}$$

$$f(t) = \frac{a_0}{2} + \sum_{n\in N^*} c_n \cos(2\pi n\nu_T t - \varphi_n) \tag{E.28d}$$

$$f(t) = \frac{a_0}{2} + \sum_{n\in N^*} \left[a_n \cos(2\pi n\nu_T t) + b_n \sin(2\pi n\nu_T t)\right] \tag{E.28e}$$

Thus, for $n \in N^*$ ($\lambda_n \in C$); $c_n \in R^+$; $a_n, b_n \in R$), as $f(t)$ is a real function, the different coefficients are linked by the following equations:

$$\lambda_n = \frac{c_n}{2} e^{-j\varphi_n} = \frac{a_n - jb_n}{2} \tag{E.29}$$

The following equations are deduced:

$$a_n^2 + b_n^2 = c_n^2 = 4\lambda_n\lambda_n^*$$
$$a_n = c_n \cos\varphi_n = \lambda_n + \lambda_n^*$$
$$b_n = c_n \sin\varphi_n = j\left(\lambda_n - \lambda_n^*\right)$$

For $n = 0$, the mean λ_0 of the function over a period T (or an integer multiple) is real, and hence $2\lambda_0 = c_0 e^{j\varphi_0} = a_0$, with $\varphi_0 = 0$ if $\lambda_0 > 0$ and $\varphi_0 = \pi$ if $\lambda_0 < 0$, where b_0 is obviously zero. Hence, when a real periodic function $f(t)$ of period T is known, the question is to know:

- firstly, the conditions under which this function can be represented by a Fourier series,
- secondly, how to calculate the coefficients of this series.

3.2 • Fourier transform of a periodic function

In order to be able to expand a periodic function $f(t)$ in a Fourier series, the function has to be bounded, continuous and integrable. This is Jordan's theory, which states that "If (a function) $f(x)$ is periodic with the variation bounded within all finite intervals, its Fourier series is uniformly convergent within all intervals where $f(x)$ is continuous." Let us suppose that the conditions of a Fourier series for the periodic function $f(t)$ of period T are fulfilled. We have seen at the beginning of this appendix that the Fourier transform of a periodic function $f(t)$, at frequency $\nu_m = m\nu_T$ (with $m \in$

Z and $\nu_T = 1/T$), is defined by the integral (E.1a). When function $f(t)$ is replaced by its form (E.28a), it becomes:

$$F(m\nu_T) = \frac{1}{T}\int_{-T/2}^{+T/2} \sum_{\mu\in Z} \lambda_\mu e^{j2\pi(\mu-m)\nu_T t} dt$$

$$= \sum_{\mu\in Z} \lambda_\mu \left(\frac{1}{T}\int_{-T/2}^{T/2} e^{j2\pi(\mu-m)\nu_T t} dt \right) \quad \text{(E.30)}$$

Integration of the bracketed part in the general term of the second series in the above equation gives:

$$\frac{1}{T}\int_{-T/2}^{+T/2} e^{j2\pi(\mu-m)\frac{t}{T}} dt = \frac{e^{i\pi(\mu-m)} - e^{-i\pi(\mu-m)}}{2j\pi(\mu-m)}$$

$$= \frac{\sin[\pi(\mu-m)]}{\pi(\mu-m)} = \delta(\mu-m) \quad \text{(E.31)}$$

where:

$$F(m\nu_T) = \sum_{\mu\in Z} \lambda_\mu \delta(\mu-m) \quad \text{(E.32a)}$$

All terms of the series (E.32a) are zero except that of rank $\mu = m$. The transform $F(\nu)$ at frequency $\nu = m\nu_T$ of the periodic function $f(t)$ of period T is only the Fourier coefficient λ_m, or:

$$\lambda_m = F(\nu) \cdot \delta(\nu - m\nu_T) \quad \text{(E.32b)}$$

For $m = 0$, we obtain the value λ_0, i.e. the mean of the considered periodic function $f(t)$. We have just seen how it is possible to determine the Fourier series of a real periodic function that is continuous and bounded within all finite intervals. Note that equation (E.42) can be interpreted as the frequential sampling of a transform $F(\nu)$ every $\nu_T = 1/T$. The periodic series (E.28a) can then be assimilated to the inverse transform of $F(\nu)$ sampled by the comb $X_{\nu_T}(\nu)$:

$$f(t) = FT^{-1}\left[F(\nu)\cdot X_{\nu_T}(\nu)\right] = FT^{-1}\left[F(\nu)\right] * T.X_{T(t)}$$

Hence, since the transform of a comb is a comb to the closest constant (E.17), the convolution of the inverse transform with $X_T(t)$ results in function $f(t)$ being periodic of period T with: $f(t) = f(t + kT)$ $k \in Z^*$. Moreover, it is important to note that the spectrum of the periodic function $f(t)$ of period T is not a continuous spectrum. It consists of **lines** with an elementary error on the frequency axis being ν_T. As the function is real, its ampli-

tude spectrum is completely defined for discrete frequencies $\nu = n\nu_T \geq 0$ ($n \in N$), with:

$$|F(\nu)| = \frac{c_0}{2}\delta(\nu) + \sum_{n\in N^*} c_n \delta(\nu - n\nu_T) \tag{E.33}$$

where the coefficients c_n are defined by equation (E.29). Let us now look at the general case of a real function that is representative of the temporal pattern of a quantifiable and continuous phenomenon sampled at a regular interval every t_e over a period T.

4 • Sampled real functions

Recall that only the point sampling situation is studied here (as we also did for the rectangular function, see § 3.2), i.e. that of the function sampled by the comb $t_e X_{t_e}(t)$, which can be defined under these two forms with $\nu_e = 1/t_e$:

$$t_e X_{t_e} = t_e \sum_{m\in Z} \delta(t - mt_e) = \sum_{m\in Z} e^{j2\pi m\nu_e t} \tag{E.34}$$

4.1 • Sampling throughout the existing domain

Let us consider a continuous and integrable real function $f(t)$ accepting the transform $F(\nu)$ defined by (E.1b). Let $f_{t_e}(t)$ denote the sampled function throughout its existing domain by (E.34). This latter can be expressed by the following equivalent equations:

$$f_{t_e}(t) = t_e X_{t_e} f(t) = t_e \sum_{m\in Z} f(t)\delta(t - mt_e) \tag{E.35a}$$

where

$$f_{t_e}(t) = t_e X_{t_e} f(t) = \sum_{m\in Z} f(t) e^{j2\pi m\nu_e t} \tag{E.35b}$$

Note that we have:

$$\sum_{m\in Z} t_e f(mt_e) \xrightarrow[t_e\to 0]{} \int_t f(t)\mathrm{d}t$$

Therefore, when the sampling interval t_e tends towards zero, the limit of the sum of the series is the integral of the continuous function $f(t)$. The question arises as to how to recover this transform $F(\nu)$ from this sampled series. For the rectangular function, we have seen that it is not possible to reconstruct its continuous spectrum by sampling, except when T tends towards infinity. However, an identical image of the spectrum

has been obtained via discrete transforms (or Fourier series) by taking the sampling-periodisation duality into account in both the time and frequency domains. Let us thus consider the sampled function $f_{t_e}(t)$, which satisfies the conditions set out at the beginning (bounded, integrable function with a finite number of discontinuities in its existing domain). It also accepts a Fourier transform: $\mathrm{F}_{(t_e)}(\nu) = \mathrm{FT}\left[f_{t_e}(t)\right]$, where the subscript (t_e) in $\mathrm{F}_{(t_e)}(\nu)$ means that it is the transform of a function sampled at the rate t_e. $\mathrm{F}_{(t_e)}(\nu)$ can be calculated directly on the basis of the transform definition. When taking expression (E.35a) of $f_{t_e}(t)$, we obtain a first equation that defines the transform which is a continuous function of frequency ν:

$$\mathrm{F}_{(t_e)}(\nu) = t_e \int_t \sum_{m\in\mathrm{Z}} \delta(t - mt_e) f(t) e^{-j2\pi\nu t} \mathrm{d}t$$
$$= t_e \sum_{m\in\mathrm{Z}} f(mt_e) e^{-j2\pi\nu m t_e} \quad \text{(E.36a)}$$

By using the properties of the transforms summarised in equation (E.6), we also have:

$$\mathrm{F}_{(t_e)}(\nu) = \mathrm{FT}\left[t_e \mathrm{X}_{t_e}\right] * \mathrm{FT}\left[f(t)\right] = \mathrm{X}_{\nu_e}(\nu) * \mathrm{F}(\nu)$$

or a second equivalent equation, while recalling that:

$$\mathrm{X}_{\nu_e}(\nu) = \sum_{k\in\mathrm{Z}} \delta(\nu - k\nu_e)$$

$$\mathrm{F}_{(t_e)}(\nu) = \sum_{k\in\mathrm{Z}} \delta(\nu - k\nu_e) * \mathrm{F}(\nu) = \sum_{k\in\mathrm{Z}} \mathrm{F}(\nu - k\nu_e) \quad \text{(E.36b)}$$

This result means that the spectrum of $f_{t_e}(t)$ is that of $f(t)$, but 'periodised', i.e. that this latter regenerates itself on the frequency axis with a period of $\nu_e = 1/t_e$, as for the 'rectangle'. It is thus not possible to reconstruct the functions $f(t)$ or $\mathrm{F}(\nu)$ solely based on knowledge of $f_{t_e}(t)$ or of $\mathrm{F}_{(t_e)}(\nu)$. Generally there is an infinite number of solutions. Recall that, as the sampled function $f_{t_e}(t)$ is real and thus Hermitian, its transform preserves this property: $\mathrm{F}_{(t_e)}(\nu) = \mathrm{F}^*_{(t_e)}(-\nu)$. We thus find the two families of spectrum symmetry axes, as for the rectangle. The spectrum of the sampled real function $f_{t_e}(t)$ is symmetrical in the frequency domain relative to all axes of equation $\nu = k\nu_e$, with $k \in \mathrm{Z}$. Moreover, the periodisation ν_e (induced by the sampling) and the Hermitian trait lead to the equality:

$$\mathrm{F}_{(t_e)}(\nu_\mathrm{N} - \Delta\nu) = \mathrm{F}^*_{(t_e)}(\nu_\mathrm{N} + \Delta\nu + k\nu_e)$$

where $\nu_\mathrm{N} = \nu_e/2$ is the Nyquist frequency, $\Delta\nu$ any frequency error, and $k \in \mathrm{Z}$. This latter equality gives rise to a second family of spectrum

symmetry axes with the equation $\nu = \nu_N + k\nu_e$ (with here $k \in Z^*$). This type of symmetry introduces aliasing, as with the rectangular distribution. If precautionary measures are not taken during the sampling, aliasing of high frequency constituents ($\nu > \nu_N$) of the true spectrum will occur at low frequencies of the $f_{t_e}(t)$ spectrum. Let us suppose, however, that $f(t)$ has a transform $F(\nu)$ whose maximum frequency in absolute value is $\nu_M > 0$, i.e. $F(\nu)$ is zero for all frequencies with absolute values being $|\nu| \geq \nu_M > 0$. The spectrum of the real function $f(t)$ will then stretch over a width of $2\nu_M$ from $-\nu_M$ to ν_M.

To ensure that the true spectrum pattern is not modified by the periodic repetition introduced by the comb $X_{t_e}(t)$, the sampling frequency ν_e must be above or equal to $2\nu_M$ (Shannon's theorem):

$$\nu_e \geq 2\nu_M \Rightarrow t_e = \frac{1}{\nu_e} \leq \frac{1}{2\nu_M} \tag{E.37}$$

When the signal has frequencies $|\nu| \geq \nu_e$, frequencies whose absolute values are at least twofold higher than that of the sampling should be filtered. Hence, for any real function $f(t)$, and assuming a Fourier transform $F(\nu)$ and sampling throughout the existing domain at a rate that is in line with Shannon's condition ($\nu_e \geq 2\nu_M$), the transform $F_{(t_e)}(\nu)$ limited to the frequency interval ($-\nu_e/2 < \nu < \nu_e/2$), i.e. corresponding to the term $k = 0$ of the equation (E.36b), is then equal to $F(\nu)$:

$$\delta(k) \cdot F_{(t_e)}(\nu) = F(\nu) \tag{E.38}$$

As the functions considered here are real, their transforms are Hermitian and, when the spectrum in the domain $(0, \nu_e/2)$ is known, the total spectrum in ($-\nu_e/2 < \nu < \nu_e/2$) will be known.

4.2 • Sampling over a limited period

In practice, signals are studied over a limited period T. The continuous real function $f(t)$ is therefore not known throughout its existing domain, but it is perceived through the rectangle $\Pi_T(t)$. The Fourier transform $F_T(\nu)$ of the known part of the function is thus expressed by:

$$F_T(\nu) = FT\left[\frac{1}{T}\Pi_T(t)f(t)\right] = \frac{1}{T}\int_0^T f(t)e^{-j2\pi\nu t}dt = \Lambda_T(\nu) * F(\nu) \tag{E.39}$$

$\Lambda_T(\nu)$ is given in equation (E.21).

Once a signal has been identified in this way it may be interpreted in two ways:

• either its representative function is periodic and of period T, and the signal may be known for all t;

• or it is aperiodic and the transform of its known part is the convolution product of $\Lambda_T(\nu)$, i.e. the transform of the rectangle normalised by its width T, with the transform of the entire signal; the complete spectrum then cannot be obtained.

To be able to process the signal on a computer, the sampling must be done at a time frequency t_e over a given duration T, which results in broadening the initial signal by introducing period ν_e in the frequency domain. Similarly, we have seen that sampling a continuous spectrum (every $\nu_T = 1/T$) generates a discrete spectrum (or line spectrum) and a signal of period T.

We have already examined the effect of sampling on the rectangular function. This first example will enable us to quickly detect the impact of this discretisation on simple periodic functions, i.e. the complex cyclic function $e^{j2\pi\nu_i t}$ and the cosine function.

4.2.1 • Complex cyclic functions

We have already seen (2.1) that the Fourier transform of the complex exponential cyclic function $e^{j2\pi\nu_i t}$, with $\nu_i \in= \lim \mathrm{R}e$, is the Dirac $\delta(\nu-\nu_i)$:

$$\mathrm{FT}^{-1}\left[\delta(\nu-\nu_i)\right] = \int_t \delta(\nu-\nu_i)e^{j2\pi\nu t}\mathrm{d}t = e^{j2\pi\nu_i t}$$

Let us therefore consider the distribution defined by equation (E.26) with $T = Mt_e$. Sampling $e^{j2\pi\nu_i t}$ in this rectangle provides M readings. It is obviously assumed that the sampling interval t_e is in line with Shannon's criterion, i.e. $\nu_e = 1/t_e > 2|\nu_i|$. We thus have the sampled function: $\left(e^{j2\pi\nu_i t}\right)_{T,t_e} = e^{j2\pi\nu_i t}\cdot\dfrac{1}{T}\Pi_{T,t_e}(t)$

Since $\Lambda_{T,M}(\nu)$, as defined by (E.24a), is the transform of the considered rectangle, then:

$$\mathrm{FT}\left[\left(e^{j2\pi\nu_i t}\right)_{T,t_e}\right] = \delta(\nu-\nu_i) * \Lambda_{T,M}(\nu) = \Lambda_{T,M}(\nu-\nu_i) \qquad \text{(E.40a)}$$

or when specifying from equation (E.24b):

$$\Lambda_{T,M}(\nu-\nu_i) = \frac{\sin\left[\pi(\nu-\nu_i)T\right]}{M\sin\left[\pi(\nu-\nu_i)T/M\right]}e^{-j\pi(\nu-\nu_i)T(1-1/M)} \qquad \text{(E.40b)}$$

It can be noted that:

$$\Lambda_{T,M}(\nu_i-\nu) = \Lambda^*_{T,M}(\nu-\nu_i) \qquad \text{(E.40c)}$$

Hence, the transform of the function $e^{j2\pi\nu_i t}$, sampled by the normalised rectangular distribution is no longer the Dirac distribution $\delta(\nu-\nu_i)$ but rather the periodic continuous function $\Lambda_{T,M}(\nu-\nu_i) = \Lambda_{T,M}(\nu-\nu_i+k\nu_e)$

of period $\nu_e = \mathrm{M/T}$. Its spectrum is that of the normalised rectangular distribution, translated to all frequencies $\nu = \nu_i + k\nu_e$ ($k \in \mathrm{Z}$), with the spectrum value being equal to unity.

All axes $\nu = \nu_i + k\nu_e$ are obviously spectrum symmetry axes. As the initial function $e^{j2\pi\nu_i t}$ is complex, the transform of the sampled function is therefore not Hermitian and the axes $\nu = k\nu_e$ are not spectrum symmetry axes. Aliasing is thus not possible from axes $\nu = \nu_\mathrm{N} + k\nu_e$ (n.b. $\nu_\mathrm{N} = \nu_e/2 = \mathrm{M/2T}$, the Nyquist frequency). For a complex function, only the periodicity ν_e holds for the transform. When the width of rectangle T is a multiple of the cyclic function period, its frequency can be formulated as $\nu_i = k_i\nu_\mathrm{T}$, with $k_i \in \mathrm{Z}$ contained within the interval $(-\mathrm{M}/2, \mathrm{M}/2)$, excluding boundaries. When $\Lambda_{\mathrm{T,M}}(\nu - k_i\nu_\mathrm{T})$ is sampled by the discrete spectral rectangle within the interval $(-\nu_\mathrm{N}, \nu_\mathrm{N})$ with a step ν_T, we obtain a discrete spectrum formed only by the Dirac distribution $\delta(\nu - k_i\nu_\mathrm{T})$. The calculation is similar to that done for the rectangle (E.27).

Hence, by double sampling:

• temporal sampling at step t_e and duration T of the initial continuous function (here the complex exponent $e^{j2\pi\nu_i t}$),

• frequential sampling at step ν_T in the limited interval $(-\nu_\mathrm{N}, \nu_\mathrm{N})$ of the continuous transform of the sampled signal,

we find a complete correspondence between the two series, with each containing M terms and the image of the true spectrum can be obtained on condition that the width T of the rectangle is a multiple of the period of the studied function. Clearly, if the frequency ν_i is higher in absolute value than the Nyquist frequency ν_N, the problem cannot be solved (out of line with Shannon's theorem). The spectral peak obtained within the interval $(-\nu_\mathrm{N}, \nu_\mathrm{N})$ corresponds to a specific value $k = k_n \in \mathrm{Z}$, such that: $-\nu_\mathrm{N} < \nu_i + k_n\nu_e < \nu_\mathrm{N}$

Hence, because of the periodicity, sampling of an HF signal (high frequency: $|\nu_i| > \nu_\mathrm{N}$) will reveal, within the interval $(-\nu_\mathrm{N}, \nu_\mathrm{N})$, LF energy which actually does not exist in the true spectrum (stroboscopic effect).

4.2.2 • Cosine functions

Let us consider the following cosine function, with $\nu_i > 0$:

$$\mathrm{C}_i(t) = 2\cos(2\pi\nu_i t) = e^{j2\pi\nu_i t} + e^{-j2\pi\nu_i t} \tag{E.41}$$

Its Fourier transform is:

$$\mathrm{FT}\left[\mathrm{C}_i(t)\right] = \delta(\nu - \nu_i) + \delta(\nu + \nu_i) \tag{E.42}$$

When taking the previous results into account, the continuous transform

$\chi_{\mathrm{T,M},i}(\nu)$ of the function sampled in the rectangle of width $\mathrm{T} = \mathrm{M}t_e$, is formulated as:

$$\chi_{\mathrm{T,M},i}(\nu) = [\delta(\nu - \nu_i) + \delta(\nu + \nu_i)] * \left[\Lambda_{\mathrm{T,M}}(\nu)\right]$$

or:

$$\chi_{\mathrm{T,M},i}(\nu) = \Lambda_{\mathrm{T,M}}(\nu - \nu_i) + \Lambda_{\mathrm{T,M}}(\nu + \nu_i) \tag{E.43}$$

or, when accounting for equation (E.40b):

$$\chi_{\mathrm{T,M},i}(\nu) = \Lambda^*_{\mathrm{T,M}}(\nu_i - \nu) + \Lambda_{\mathrm{T,M}}(\nu_i + \nu)$$

Besides the periodicity $\nu_e = \mathrm{M}/\mathrm{T}$, which is common to all transforms of functions combed by $t_e \mathrm{X}_{t_e}$, and as the cosine function is real and therefore Hermitian, its transform preserves this property, and we have:

$$\chi_{\mathrm{T,M},i}(\nu) = \chi^*_{\mathrm{T,M},i}(-\nu) \tag{E.44}$$

$$\chi_{\mathrm{T,M},i}(\nu_\mathrm{N} - \Delta\nu) = \chi^*_{\mathrm{T,M},i}(\nu_\mathrm{N} + \Delta\nu + k\nu_e) \tag{E.45}$$

This leads to the symmetry property of the amplitude spectrum $\left|\chi_{\mathrm{T,M},i}(\nu)\right|$ relative to the two axis families of equations: $\nu = k\nu_e$ and $\nu = \nu_\mathrm{N} + k\nu_e$, with $k \in \mathrm{Z}$.

This property, which has already been noted on several occasions, is specific to all real functions accepting a transform, with aliasing relative to the Nyquist frequency ($\nu_\mathrm{N} = \nu_e/2 = 1/2t_e$). If the duration T is a multiple of the period of the considered function, by performing double sampling, i.e. temporal t_e over the duration $\mathrm{T} = \mathrm{M}t_e$ and frequential ν_T within the interval $(-\nu_\mathrm{N}, \nu_\mathrm{N})$, we obtain an image of the true spectrum given by equation (E.42).

In summary, if the sampling theory is respected, the combined effect of the periodicity (symmetry relative to the axes $\nu = k\nu_e$) and the aliasing (symmetry relative to $\nu = \nu_\mathrm{N} + k\nu_e$) is that the spectrum of a real function is here completely defined in the positive frequency domain $(0, \nu_\mathrm{N})$. However, for complex magnitudes, only the periodicity and the spectrum should be defined in the frequency domain $(-\nu_\mathrm{N}, \nu_\mathrm{N})$.

Figure E.1 highlights the different spectrum symmetries depending on whether the continuous transform of a sampled cyclic function is taken into account or that of the cosine function, i.e. the sum of two cyclic functions of opposite angular velocities.

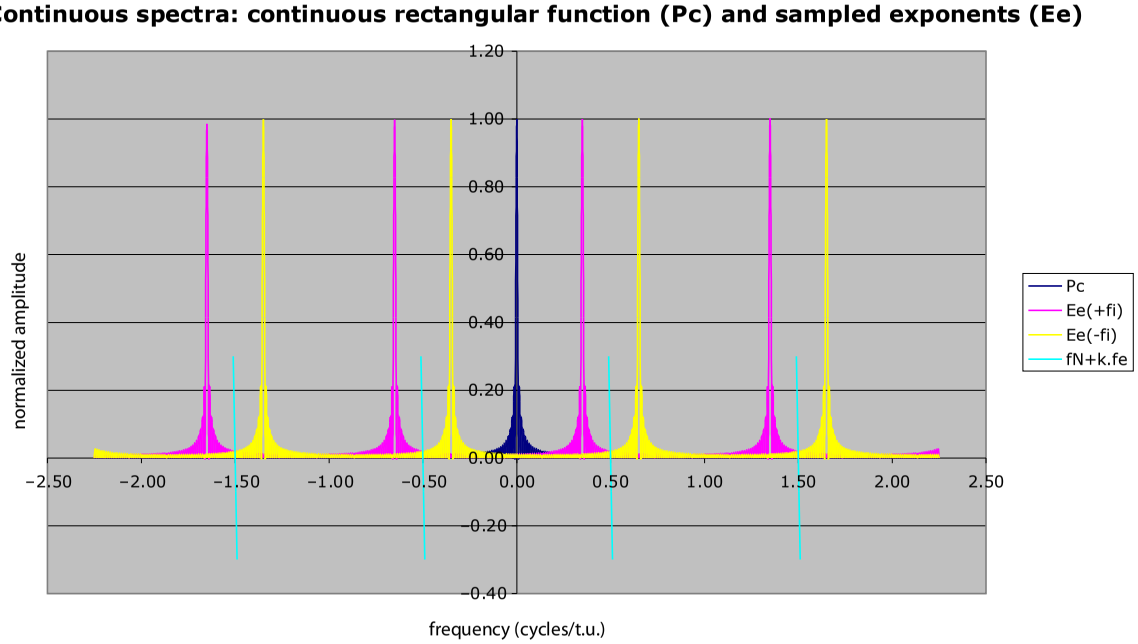

FIGURE E.1: The rectangle has a width T equal to 100 time units (t.u.). This unit was selected as the sampling interval (fe=1 cycle/t.u., with the Nyquist frequency: $f\mathrm{N} = fe/2 = 0.5$ cycle/t.u.). Only the two cyclic functions are sampled (complex exponents of opposite angular velocities: $\pm fi = \pm 0.35$ cycle/t.u.).

a. The Pc curve (blue) is the continuous spectrum of the rectangular function (normalised by T and not sampled); there is only one absolute maximum for zero frequency.

b. The Ee(+fi) end Ee(-fi) curves represent the respective continuous spectra of the sampled exponents (purple for the positive frequency, yellow for the negative frequency). Note the repetition of peaks at frequencies $\pm fi + kfe$, where $k \in \mathrm{Z}$.

c. The spectrum of the cosine function (to the closest factor of 2) is the sum of the two last spectra, and it accepts two symmetry axis families: kfe and $f\mathrm{N} + kfe$. This second family results in aliasing.

5 • Application to tides

The tidal phenomenon is a very special situation. Although the tide is viewed as being a regular movement phenomenon, it is not periodic. Even saros is not a period for tide (see Appendix A, 2.2). It is, however, the sum of a certain number of periodic constituents and its Fourier transform is a sum of Dirac distributions weighted by the amplitudes of corresponding waves. It thus has a line spectrum but its frequential sampling by a larger common denominator is not possible. The absence of periodicity is due solely to the fact that the frequencies of the different tidal constituents are not measurable. Hence, $h(t)$ is the tidal height at time t supposedly reduced to its constituents i–the value of i is considered here to be a number of around ($i \in \mathrm{N}^*$) according to increasing (positive) frequencies. Each constituent is defined by three elements: the amplitude a_i, frequency ν_i (≥ 0)) and phase φ_i at time zero $t = 0$. Function $h(t)$ can thus be formulated (for simplification, it can at first be assumed that the mean level is zero):

$$h(t) = \sum_{i \in \mathrm{N}^*} h_i(t) = \sum_{i \in \mathrm{N}^*} a_i \cos(2\pi\nu_i t - \varphi_i) \tag{E.46}$$

Where the complex conjugate amplitudes are denoted by $\eta_i = a_i e^{-j\varphi_i}/2$ and $\eta_i^* = a_i e^{j\varphi_i}/2$, then:

$$h_i(t) = \eta_i e^{j2\pi\nu_i t} + \eta_i^* e^{-j2\pi\nu_i t} \tag{E.47}$$

The Fourier transform $h_i(t)$ is thus the sum of two Dirac distributions with opposite frequencies (ν_i and $-\nu_i$), weighted by complex conjugate amplitudes (η_i and η_i^*):

$$\mathrm{FT}\left[h_i(t)\right] = \eta_i \delta(\nu - \nu_i) + \eta_i^* \delta(\nu + \nu_i) \tag{E.48}$$

Where $\mathrm{F}(\nu)$ denotes the transform of $h(t)$ throughout its existing domain, the tide has a line spectrum with a unique distribution, i.e. these lines are distributed around each species ($\approx \pm 2.5°/\mathrm{h}$) and the species are separated by $14.492°/\mathrm{h}$ ($= 360°/\mathrm{T_L}$, where $\mathrm{T_L} = 24.841\,2$ h is a lunar day):

$$\mathrm{F}(\nu) = \mathrm{FT}\left[h(t)\right] = \sum_{i \in \mathrm{N}^*} \left[\eta_i \delta(\nu - \nu_i) + \eta_i^* \delta(\nu + \nu_i)\right] \tag{E.49}$$

In practice, tidal sampling (E.45) by the normalised rectangular distribution gives us the series $h_{\mathrm{T},t_e}(t)$ of M values with $\mathrm{T} = \mathrm{M}t_e$. Its Fourier

transform $F_{T,M}(\nu)$, as a continuous function of ν, is thus given by the series:

$$F_{T,M}(\nu) = FT\left[\frac{1}{T}\Pi_{T,t_e}(t)h(t)\right] = FT\left[h_{T,t_e}(t)\right] = \frac{1}{M}\sum_{m=0}^{m=M-1} h(mt_e)e^{-j2\pi\nu mt_e} \quad \text{(E.50a)}$$

or even by the convolution:

$$F_{T,M}(\nu) = FT\left[\frac{1}{T}\Pi_{T,t_e}(t)h(t)\right] = \Lambda_{T,M}(\nu) * F(\nu)$$

When taking equations (E.40b) and (E.49) into account, which define $\Lambda_{T,M}(\nu)$ and $F(\nu)$, respectively, this latter form of the transform $F_{T,M}(\nu)$ can also be expressed by:

$$F_{T,M}(\nu) = \sum_{i\in N^*}\left[\eta_i\Lambda^*_{T,M}(\nu_i - \nu) + \eta^*_i\Lambda_{T,M}(\nu_i + \nu)\right] \quad \text{(E.50b)}$$

Like all real functions sampled with a time t_e and accepting a transform, we have:

- the periodicity ν_e: $F_{T,M}(\nu) = F_{T,M}(\nu + k\nu_e)$, with $k \in Z$,
- the Hermitian character: $F_{T,M}(\nu) = F^*_{T,M}(-\nu)$, which results in the symmetry of the spectrum relative to the axes $\nu = k\nu_e$;
- the symmetry of the spectrum relative to the axes $\nu = \nu_N + k\nu_e$ (aliasing, as a consequence of the two previous properties, where $\nu_N = \nu_e/2$ is the Nyquist frequency) with the equation:

$$F_{T,M}(\nu_N - \Delta\nu) = F^*_{T,M}(\nu_N + \Delta\nu + k\nu_e)$$

On condition that Shannon's theorem is applied, the complete definition of the spectrum can be obtained in the window $(-\nu_N, \nu_N)$. Recall that the transform $F_{T,M}(\nu)$ is a continuous function of the frequency ν. It is possible to determine the corresponding discrete Fourier transform (DFT)(or Fourier series) by considering the symmetrical spectral rectangle $[-\nu_N, \nu_N]$ of width ν_e. It is represented by the part of comb $X_{\nu_T}(\nu)$ which consists of the sequence of M frequencies $\nu_k = k\nu_T$, with $\nu_T = 1/T$ and k ranging from $-M/2$ to $(M/2-1)$. This gives us the relations between the different parameters: $M = T/t_e = \nu_e/\nu_T$. The continuous transform $F_{T,M}(\nu)$ becomes the Fourier series (or DFT): $\delta(\nu - k\nu_T).F_{T,M}(\nu) = F_{T,M}(k\nu_T)$ which is expressed

from equation (E.50a) by:

$$\mathrm{F}_{\mathrm{T,M}}\left(k\nu_{\mathrm{T}}\right) = \frac{1}{\mathrm{M}} \sum_{m=0}^{m=\mathrm{M}-1} h(mt_e) e^{-j2\pi \frac{k}{\mathrm{T}} m \frac{\mathrm{T}}{\mathrm{M}}}$$

$$= \frac{1}{\mathrm{M}} \sum_{m=0}^{m=\mathrm{M}-1} h(mt_e) e^{-j2\pi \frac{k}{\mathrm{M}} m} \quad \text{(E.51)}$$

Based on equation (E.50b), it is also possible to obtain another form of the series. The inverse relation of the DFT described by equation (E.51) gives the series of $h(mt_e)$ values. It is obtained by:

$$h(mt_e) = \sum_{k=-\mathrm{M}/2}^{k=\mathrm{M}/2-1} \mathrm{F}_{\mathrm{T,M}}\left(k\nu_{\mathrm{T}}\right) e^{j2\pi \frac{k}{\mathrm{T}} m \frac{\mathrm{T}}{\mathrm{M}}}$$

$$= \sum_{k=-\mathrm{M}/2}^{k=\mathrm{M}/2-1} \mathrm{F}_{\mathrm{T,M}}\left(k\nu_{\mathrm{T}}\right) e^{j2\pi \frac{m}{\mathrm{M}} k} \quad \text{(E.52a)}$$

The last series of equation (E.52a) can also be formulated by taking equation (E.51) into account:

$$\sum_{k=-\mathrm{M}/2}^{k=\mathrm{M}/2-1} \mathrm{F}_{\mathrm{T,M}}\left(k\nu_{\mathrm{T}}\right) e^{j2\pi \frac{m}{\mathrm{M}} k}$$

$$= \sum_{k=-\mathrm{M}/2}^{k=\mathrm{M}/2-1} \left(\frac{1}{\mathrm{M}} \sum_{\mu=0}^{\mu=\mathrm{M}-1} h(\mu t_e) e^{-j2\pi \frac{k}{\mathrm{M}} \mu} \right) e^{j2\pi \frac{m}{\mathrm{M}} k} \quad \text{(E.52b)}$$

or:

$$\sum_{k=-\mathrm{M}/2}^{k=\mathrm{M}/2-1} \mathrm{F}_{\mathrm{T,M}}\left(k\nu_{\mathrm{T}}\right) e^{j2\pi \frac{m}{\mathrm{M}} k}$$

$$= \sum_{\mu=0}^{\mu=\mathrm{M}-1} h(\mu t_e) \left(\frac{1}{\mathrm{M}} \sum_{k=-\mathrm{M}/2}^{k=\mathrm{M}/2-1} e^{-j2\pi \frac{(\mu-m)}{\mathrm{M}} k} \right) \quad \text{(E.52c)}$$

while the bracketed part on the right side of the equation gives:

$$\frac{1}{\mathrm{M}} \sum_{k=-\mathrm{M}/2}^{k=\mathrm{M}/2-1} e^{-j2\pi \frac{(\mu-m)}{\mathrm{M}} k} = \frac{\sin \pi(\mu - m)}{\mathrm{M} \sin\left[\pi(\mu - m)/\mathrm{M}\right]} e^{j\pi(\mu-m)} = \delta(\mu - m)$$

Equation (E.52c) then becomes:

$$\sum_{k=-\mathrm{M}/2}^{k=\mathrm{M}/2-1} \mathrm{F}_{\mathrm{T,M}}\left(k\nu_{\mathrm{T}}\right) e^{j2\pi \frac{m}{\mathrm{M}} k} = \sum_{\mu=0}^{\mu=\mathrm{M}-1} h(\mu t_e)\delta(\mu - m) = h(mt_e) \quad \text{(E.52d)}$$

Hence, the M values of the discrete Fourier series, as defined by equation (E.51), enable complete reconstruction of the initial sampled signal. There is a complete equivalence between the signal $h(mt_e)$, with m ranging from 0 to $(M-1)$ and its transform $F_{T,M}(k\nu_T)$, with k ranging from $-M/2$ to $(M/2-1)$.

When taking the Hermitian character of the DFT into account, let:

$$F_{T,M}(n\nu_T) = F^*_{T,M}(-n\nu_T) = \frac{c_n}{2}e^{-j\phi_n}$$

with $n \geq 0$ and $c_n \in R^+$ (ϕ_0 is zero, and here we assume the mean level $F_{T,M}(0) = c_0/2 \geq 0$). While respecting Shannon's theorem, at the Nyquist frequency $\nu_N = M\nu_T/2 > 2\nu_M$, the corresponding constituent is zero. Then equation E.52d) giving $h(mt_e)$ can still be formulated as (n.b. $T = Mt_e$):

$$h(mt_e) = \frac{c_0}{2} + \sum_{n=1}^{n=M/2-1} c_n \cos(2\pi\frac{n}{T}mt_e - \phi_n) \qquad \text{(E.52e)}$$

This latter result should be compared to the periodic function (E.28d). Moreover, as long as several conditions are fulfilled, especially:

- respecting the sampling theorem;
- T, being a multiple of a period of a constituent i of the signal ($\nu_i = n_i/T$);
- frequency errors $(\nu_i - \nu_{i-1})$ and $(\nu_{i+1} - \nu_i)$ of over $\nu_T = 1/T$ (Rayleigh's criterion; so the characteristics of constituent i may be deduced from equations (E.45) and (E.52e):

$$\nu_i = n_i\nu_T \Rightarrow a_i = c_{n_i}$$

and

$$\varphi_i = \phi_{n_i}$$

If the two latter conditions are not fulfilled, the value of the c_n term will then represent a linear combination of several constituents, with each being weighted by a function coefficient of the error $|\nu_i - \nu_n|$.

To optimise the DFT computation time, Cooley and Tuckey developed the first elaborate algorithm, i.e. the so-called fast Fourier transform (FFT) by utilising symmetries present in complex exponential series. Although they were incorrectly called fast Fourier transforms (FFT), the distribution theory demonstrated that they are true transforms. The name FFT is currently more common than DFT (for discrete Fourier transform). The efficiency of computational algorithms increases as the power of the first factors derived from

the M value (sample number) increases. Maximum efficiency is obtained when the number M is a power of 2.

6 • Constituents separated according to the observation period

As an example of a harmonic analysis application, which is the focus of Chapter VI, the following two lists were drawn up on the basis of observations of semidiurnal tides. These lists highlight the impact of the measurement period (month and year) on the fineness of the analysis for separating neighbouring constituents within each species. For a given observation period, each line is relative to a tidal constituent (which can be separated over this duration) with its name and extended literal argument (seven letters), as well as the elements required for calculating disturbances due to constituents that cannot be separated. These elements are, for each of these latter constituents, the extended literal argument and the amplitude (expressed in mils of the amplitude of the main constituent. For other types of tide, a few modifications are required to account for nonlinear interactions responsible for getting certain diurnal constituents more involved. It is thus useful to refer to the development of the potential and the list of compound waves presented in Appendix D. When all species up to the twelfth diurnals are taken into account, an examination of the two lists shows that with 1 year of observations it is possible to separate nearly 350 constituents, and that with 1 month of observations only around a hundred can be identified.

6.1 • Observation period: a month

Niv Moy	ZZZZZZZ										
Mm	ZAZYZZZ	ZAXAZZZ	191	ZAZYAZB	65	ZAZAZZB	53	ZAZAAZB	22	ZABYZZB15	
Mf	ZBZZZZZ	ZBZZAZZ	414	ZBXZZZZ	88	ZBZXZZZ	43	ZBZZBZZ	38		
Mfm	ZCZYZZZ	ZCZYAZZ	416	ZCXAZZZ	188	ZCXAAZZ	74	ZCZYBZZ	40		
MSqm	ZDXZZZZ	ZDXZAZZ	417								
	AVBAZZY	AVZCZZY	393	AVDYZZY	179						
SIGMA1	AWBZZZY	AWZBZZY	826	AWBZYZY	191	AWZBYZY	157	AWCZZYY	70		
Q1	AXZAZZY	AXBYZZY	190	AXZAYZY	188	AXBYYZY	36	AXBAZZA	11	AXAAZYY10	
O1	AYZZZZY	AYZZYZY	189	AYBZZZA	13	AYZBZZA	6	AYZZXZA	6	AYYZZAA	3
M1	AZZAZZA	AZZYZZA	361	AZZAAZA	199	AZBYZZA	193	AZXAZZA	95	AZZYYZA	68
K1	AAZZZZA	AAXZZZY	331	AAZZAZA	136	AAZZYZY	20	AAWZZAY	19	AABZZZA	14
J1	ABZYZZA	ABZYAZA	199	ABXAZZA	193	ABXAAZA	37	ABZYYZY	30		
OO1	ACZZZZA	ACZZAZA	636	ACXZZZA	302	ACZXZZA	148	ACZZBZA	136	ACXZAZA	62

KQ1	ADZYZZA	ADXYZZA	400	ADXAZZA	300						
2MN2S2	BUDAZZZ										
2NS2	BVBBZZZ	BVDZZZZ	636	BVBZZZZ	545						
MNS2	BWBAZZZ	BWZAZZZ	537	BWZCZZZ	388	BWDYZZZ	194	BWBAYZZ	134	BWCAZYZ	75
MU2 2MS2	BXBZZZZ	BXZBZZZ	830	BXZZZZZ	235	BXXZZZZ	108	BXCZZYZ	69	BXBZYZB	36
N2	BYZAZZZ	BYBYZZZ	190	BYZAYZB	37	BYAAZYZ	9	BYCYZYZ	9	BYBYYZB	7
M2	BZZZZZZ	BZZZYZB	37	BZXZZZZ	4	BZYZZAB	3	BZAZZYZ	3	BZXBZZB	3
L2 2MN2	BAZYZZB	BAXAZZB	262	BAZAZZZ	250	BAZAAZZ	109	BABYZZZ	47	BAZYYZZ	35
S2	BBXZZZZ	BBZZZZZ	272	BBZZAZZ	81	BBWZZAZ	58	BBYZZYB	10	BBZZBZZ	9
MSN2	BCXYZZZ	BCZYZZZ	557	BCZYAZZ	243	BCXAZZZ	104				
2SM2	BDVZZZZ	BDXZZZZ	810	BDXZAZZ	246	BDZZZZZ	204	BDZZAZZ	141	BDUZZZA	120
SKN2	BEXYZZZ										
3SK2M2	BFVZZZZ										
	CVBAZZY	CVZCZZY	545								
	CWZBZZY	CWBZZZY	853	CWZBYZY	147						
MQ3	CXZAZZY	CXBYZZY	185	CXZAYZY	149						
2MK3	CYZZZZY	CYZZYZY	149	CYBZZZA	56	CYZBZZA	51	CYZAZZB	18	CYXBZZY	15
M3	CZZZZZZ	CZZZYZB	56								
MK3	CAZZZZA	CAXZZZY	725	CAZZAZA	119	CAZZYZY	81	CAWZZAY	40	CABZZZA	19
2MQ3	CBZYZZA	CBXAZZA	939	CBZAZZA	636	CBXYZZA	606	CBZZZZB	394	CBZAAZA	364
SK3	CCXZZZA	CCZZZZA	376	CCVZZZZ	331	CCZZAZA	170	CCXZAZA	121	CCWZZZB	62
	CDXYZZA	CDZYZZA	741	CDZYAZA	407						
2SO3	CEVZZZA										
	DVBBZZZ	DVDZZZZ	429								
2MNS4	DWBAZZZ	DWZCZZZ	536	DWDYZZZ	179						
N4	DXZBZZZ	DXBZZZZ	872								
MN4	DYZAZZZ	DYBYZZZ	186	DYZAYZB	73						
M4	DZZZZZZ	DZZZYZB	74	DZXBZZZ	15	DZBZZZZ	11	DZAZZYZ	8		
SN4	DAXAZZZ	DAZAZZZ	379	DAZYZZB	137	DAZAAZZ	124				
MS4	DBXZZZZ	DBZZZZZ	273	DBZZAZZ	81	DBWZZAZ	55	DBXZYZB	34	DBZZYZB	13
2MSN4	DCXYZZB	DCZYZZB	308								
S4	DDVZZZZ	DDXZZZZ	555	DDXZAZZ	166	DDUZZAZ	118	DDZZZZZ	95	DDZZAZZ	62
	EVBAZZY	EVZCZZY	633								
	EWZBZZY	EWBZZZY	708	EWZBYZY	117						
2MQ5	EXZAZZY	EXBYZZY	181	EXZAYZY	114						
4MK5	EYZZZZY	EYZBZZA	123	EYZZYZY	110	EYXBZZY	99	EYBZZZA	97	EYAZZYY	13
	EZXAZZY	EZZAZZA	997								
2MP5	EAXZZZY	EAZZZZA	848	EAZZYZY	124	EAZZAZA	84	EAWZZAY	53	EABZZZA	30
	EBXAZZA	EBZAZZA	457	EBVAZZY	399	EBZAAZA	218	EBXYZZA	213	EBZYZZA	202
2SK5	ECXZZZA	ECVZZZY	601	ECZZZZA	369	ECZZAZA	161	ECXZAZA	98		
	EEVZZZA	EEXZZZA	790	EETZZZY	398	EDZYZZA	155	EDXYZZA	133	EDZYAZA	88

2(MN)S6	FVBBZZZ	FVDZZZZ	438								
3MNS6	FWBAZZZ	FWZCZZZ	667	FWDYZZZ	188						
2NM6	FXZBZZZ	FXBZZZZ	703	FXBZYZB	80	FXCZZYZ	51				
2MN6	FYZAZZZ	FYBYZZZ	181	FYZAYZB	109	FYBAZZZ	23				
M6	FZZZZZZ	FZZZYZB	108	FZXBZZZ	98	FZBZZZZ	33	FZBZAZZ	7		
MSN6	FAXAZZZ	FAZAZZZ	326	FABYZZZ	63	FAWAZAZ	49	FAZYZZZ	30	FAZYYZZ	3
2MS6	FBXZZZZ	FBZZZZZ	277	FBZZAZZ	83	FBXZYZB	72	FBWZZAZ	52	FBBZZZZ	4
2SN6	FCVAZZB	FCXAZZZ	838	FCXYZZB	527	FCZYZZB	162	FCZYAZB	68	FCWYZAB	14
2SM6	FDVZZZZ	FDXZZZZ	549	FDXZAZZ	166	FDUZZAZ	113	FDZZZZZ	85	FDZZAZZ	52
2(MS)N6	FEVYZZB	FEXYZZZ	667	FEUYZAB	167						
	GVBAZZY	GVZCZZY	794	GVDYZZY	176						
	GWZBZZY	GWBZZZY	622	GWZBYZY	76	GWCZZYY	43				
3MQ7	GXZAZZY	GXBYZZY	173	GXZAYZY	75	GXAAZYY	20				
5MK7	GYZZZZY	GYXBZZY	272	GYZBZZA	202	GYBZZZA	139	GYZZYZY	72	GYAZZYY	22
	GZXAZZY	GZZAZZA	641	GZZYZZY	80						
	GAXZZZY	GAZZZZA	591	GAZZYZY	128	GAWZZAY	51	GAZZAZA	45	GABZZZA	42
	GBXAZZA	GBVAZZY	741	GBZAZZA	436	GBZYZZA	152	GBXYZZA	101	GBZYAZA	18
3SK7	GCXZZZA	GCVZZZY	894	GCZZZZA	388	GCZZAZA	162	GCXZAZA	77		
	GDXYZZA	GDZYAZA	737								
	GEVZZZA	GEXZZZA	775	GETZZZY	604						
	HVBBZZZ										
2MNS8	HWBAZZZ										
2(MN)8	HXZBZZZ	HXBZZZZ	610	HXBZYZB	86						
3MN8	HYZAZZZ	HYBYZZZ	172	HYZAYZB	142						
M8	HZZZZZZ	HZXBZZZ	272	HZZZYZB	141	HZBZZZZ	67	HZAZZYZ	22	HZBZAZZ	18
2MSN8	HAXAZZZ	HAZAZZZ	314	HAZYZZZ	80	HABYZZZ	59				
3MS8	HBXZZZZ	HBZZZZZ	290	HBXZYZB	108	HBZZAZZ	86	HBWZZAZ	51	HBVBZZZ	43
2SMN8	HCVAZZZ	HCXAZZZ	667	HCXYZZB	142	HCZYZZZ	96				
2(MS)8	HDVZZZZ	HDXZZZZ	551	HDXZAZZ	167	HDZZZZZ	86	HDUZZAZ	59		
3M2SN8	HEXYZZZ										
3SM8	HFTZZZZ	HFVZZZZ	272	HFVZAZZ	80	HFTZYZB	38				
	JVBBZZZ										
5MNS10	JWBAZZZ										
3M2N10	JXZBZZZ	JXBZZZZ	531	JXZBYZB	177						
4MN10	JYZAZZZ	JYBYZZZ	169								
M10	JZZZZZZ	JZZZYZB	174	JZBZZZZ	110	JZAZZYZ	31	JZBZAZZ	29	JZXZZZB	7
3MSN10	JAXAZZZ	JAZAZZZ	319	JAZYZZB	106	JABYZZZ	60				
4MS10	JBXZZZZ	JBZZZZZ	311	JBXZYZB	142	JBVBZZZ	136	JBZZYZB	47	JBBZZZZ	14
2(MS)N10	JCVAZZZ	JCXAZZZ	624	JCZYZZZ	88	JCXYZZB	36				
3M2S10	JDVZZZZ	JDXZZZZ	560	JDXZAZZ	169	JDZZZZZ	90				
	JEVAZZZ	JETAZZZ	964	JEVYZZB	326	JEXYZZZ	94				
3S2M10	JFTZZZZ	JFVZZZZ	830	JFVZAZZ	250	JFTZYZB	67				

	LVBBZZZ	LVDZZZZ	323								
4MNS12	LWBAZZZ	LWDYZZZ	149								
4M2N12	LXZBZZZ	LXBZZZZ	493	LXZBYZX	208	LXBZYZX	97	LXCZZYZ	40		
5MN12	LYZAZZZ	LYXCZZZ	293	LYZAYZX	209	LYBYZZZ	159	LYAAZYZ	40	LYBYYZX	34
M12	LZZZZZZ	LZXBZZZ	857	LZZZYZX	204	LZBZZZZ	166	LZZBAZZ	91	LZBZAZZ	46
4MSN12	LAXAZZB	LAZAZZZ	336	LAZYZZB	115	LAZAAZZ	101	LABYZZZ	59	LAWAZAZ	46
5MS12	LBXZZZZ	LBZZZZZ	344	LBVBZZZ	302	LBXZYZX	177	LBZZAZZ	103	LBZZYZX	64
3M2SN12	LCVAZZZ	LCXAZZZ	609	LCZYZZZ	87	LCZYAZZ	28				
4M2S12	LDVZZZZ	LDXZZZZ	575	LDXZAZZ	174	LDVZYZX	142	LDUZZAZ	109	LDZZZZZ	100

6.2 • Observation period: a year

Niv Moy	ZZZZZZZ										
Sa	ZZAZZZY										
Ssa	ZZBZZZZ	ZZBZAZB	25								
Sta	ZZCZZYY										
MSm	ZAXAZZZ	ZAXAYZB	76	ZAXAAZB	63						
Mm	ZAZYZZZ	ZAZYAZB	65	ZAZAZZB	53	ZAZAAZB	22				
	ZABYZZB										
Msf	ZBXZZZZ										
Mf	ZBZZZZZ	ZBZZAZZ	414	ZBZXZZZ	43	ZBZZBZZ	38				
MStm	ZCXAZZZ	ZCXAAZZ	393								
Mfm	ZCZYZZZ	ZCZYAZZ	416	ZCZYBZZ	40						
MSqm	ZDXZZZZ	ZDXZAZZ	417								
	AVZCZZY										
	AVBAZZY	AVBAYZY	179								
	AVDYZZY										
2Q1	AWZBZZY	AWZBYZY	189								
SIGMA1	AWBZZZY	AWBZYZY	191								
	AWCZZYY										
	AWDZZZY										
	AXXAZZY										
Q1	AXZAZZY	AXZAYZY	188								
RHO1	AXBYZZY	AXBYYZY	190	AXBAZZA	58	AXAAZYY	51				
	AXCYZYY										
	AXDYZZY										
	AYXBZZA										
	AYYZZAA										
O1	AYZZZZY	AYZZYZY	189	AYZBZZA	6	AYZZXZA	6				
	AYAZZYY										
MP1	AYBZZZA	AYBZAZY	224								
	AYCZZZY										
	AZXAZZA	AZXAYZA	214								
M1	AZZAZZA	AZZYZZA	361	AZZAAZA	199	AZZYYZA	68	AZZAYZY	37		
	AZBYZZA	AZBYAZA	228								

PI1	AAWZZAY						
P1	AAXZZZY	AAXZYZA	11				
S1	AAYZZZA						
K1	AAZZZZA	AAZZAZA	136	AAZZYZY	20	AAZZBZY	3
PSI1	AAAZZYA						
PHI1	AABZZZA						
THETA1	ABXAZZA	ABXAAZA	193				
J1	ABZYZZA	ABZYAZA	199	ABZYYZY	30		
	ACWZZZA						
SO1	ACXZZZA	ACXZAZA	204				
OO1	ACZZZZA	ACZZAZA	636	ACZXZZA	148	ACZZBZA	136
	ADXYZZA	ADXAZZA	750				
KQ1	ADZYZZA						
2MN2S2	BUDAZZZ						
2NS2	BVBBZZZ	BVBZZZZ	545				
3M2S2	BVDZZZZ						
OQ2	BWZAZZZ	BWZCZZZ	722	BWZAYZZ	250		
MNS2	BWBAZZZ	BWBAYZZ	134				
	BWCAZYZ						
MNUS2	BWDYZZZ						
2MS2K2	BXXZZZZ						
2N2	BXZBZZZ	BXZZZZZ	283	BXZBYZB	39		
MU2 2MS2	BXBZZZZ	BXBZYZB	36				
	BXCZZYZ						
	BYXCZZB						
	BYYAZAB	BYZYXZB	467				
N2	BYZAZZZ	BYZAYZB	37				
	BYAAZYZ	BYBYYZB	750	BYAZZZB	625		
NU2	BYBYZZZ						
	BYCYZYZ						
2KN2S2	BYDAZZZ						
MSK2	BZXZZZZ	BZXBZZB	818				
M(SK)2	BZYZZAB						
M2	BZZZZZZ	BZZZYZB	37				
M(KS)2	BZAZZYZ						
MKS2	BZBZZZZ						
2SM2K2	BZDZZZZ						
LAMBDA2	BAXAZZB						
2SN(MK)2	BAVAZZZ						
L2 2MN2	BAZYZZB	BAZAZZZ	250	BAZAAZZ	109	BAZYYZZ	35
	BABYZZZ						
2SK2	BBVZZZZ						
T2	BBWZZAZ						
S2	BBXZZZZ	BBXZAZZ	7	BBXZYZZ	2		
R2	BBYZZYB						

K2	BBZZZZZ	BBZZAZZ	298	BBZZBZZ	32	BBZZYZB	13
	BBAZZYZ						
	BBBZZZZ						
MSnu2	BCVAZZZ						
MSN2	BCXYZZZ	BCXAZZZ	104				
KJ2	BCZYZZZ	BCZYAZZ	438				
2KM(SN)2	BCBYZZZ						
	BDUZZZA						
2SM2	BDVZZZZ						
	BDWZZZA						
SKM2	BDXZZZZ	BDXZAZZ	304	BDXXZZZ	122		
	BDZZZZZ	BDZZAZZ	690	BDZZBZZ	276		
2SNU2	BETAZZZ						
2SN2	BEVYZZZ						
SKN2	BEXYZZZ						
3S2M2	BFTZZZZ						
3SK2M2	BFVZZZZ						
	CVZCZZY						
	CVBAZZY						
	CWZBZZY	CWZBYZY	147				
	CWBZZZY						
MQ3	CXZAZZY	CXZAYZY	149				
	CXBYZZY						
	CYXBZZY						
2MK3	CYZZZZY	CYZZYZY	149	CYZBZZA	51	CYZAZZB	18
2MS3	CYAZZZB						
2MP3	CYBZZZA						
	CZXAZZA						
M3	CZZZZZZ	CZZZYZB	56				
	CZBYZZZ						
	CAWZZAY						
SO3	CAXZZZY						
MS3	CAYZZZB						
MK3	CAZZZZA	CAZZAZA	119	CAZZYZY	81		
	CAAZZYA						
	CABZZZA						
	CBXAZZA	CBXYZZA	645				
2MQ3	CBZYZZA	CBZAZZA	636	CBZZZZB	394	CBZAAZA	364
SP3	CCVZZZZ						
S3	CCWZZZB						
SK3	CCXZZZA	CCXZAZA	121				
K3	CCZZZZA	CCZZAZA	452				
	CDXYZZA						
	CDZYZZA	CDZYAZA	550				
2SO3	CEVZZZA						

	DVBBZZZ				
4M2S4	DVDZZZZ				
	DWZCZZZ				
2MNS4	DWBAZZZ				
2MnuS4	DWDYZZZ				
N4	DXZBZZZ				
3MS4	DXBZZZZ				
MN4	DYZAZZZ	DYZAYZB	73		
Mnu4	DYBYZZZ				
	DZXBZZZ				
MA4	DZYZZZZ				
M4	DZZZZZZ	DZZZYZB	74		
2MRS4	DZAZZYZ				
2MKS4	DZBZZZZ				
SN4	DAXAZZZ				
NK4	DAZAZZZ	DAZYZZB	361	DAZAAZZ	328
MT4	DBWZZAZ				
MS4	DBXZZZZ	DBXZYZB	34		
MK4	DBZZZZZ	DBZZAZZ	295	DBZZYZB	48
2SNM4	DCVAZZB				
2MSN4	DCXYZZB				
2MKN4	DCZYZZB				
ST4	DDUZZAZ				
S4	DDVZZZZ				
SK4	DDXZZZZ	DDXZAZZ	299		
	DDZZZZZ	DDZZAZZ	650		
	EVZCZZY				
	EVBAZZY				
	EWZBZZY	EWZBYZY	117		
	EWBZZZY				
2MQ5	EXZAZZY	EXZAYZY	114		
	EXBYZZY				
	EYXBZZY				
4MK5	EYZZZZY	EYZBZZA	123	EYZZYZY	110
	EYAZZYY				
4MP5	EYBZZZA				
	EZXAZZY				
	EZZAZZA				
	EAWZZAY				
2MP5	EAXZZZY				
2MK5	EAZZZZA	EAZZYZY	146	EAZZAZA	99
	EAAZZYA				
	EABZZZA				
	EBVAZZY				

	EBXAZZA	EBXYZZA	213		
	EBZAZZA	EBZAAZA	477	EBZYZZA	442
	ECVZZZY				
2SK5	ECXZZZA	ECXZAZA	98		
	ECZZZZA	ECZZAZA	435		
	EDXYZZA				
	EDZYZZA	EDZYAZA	571		
	EETZZZY				
	EEVZZZA				
	EEXZZZA				
2(MN)K6	FVZBZZZ				
2(MN)S6	FVBBZZZ				
	FVDZZZZ				
	FWZCZZZ				
3MNS6	FWBAZZZ				
3MnuS6	FWDYZZZ				
2NM6	FXZBZZZ				
4MS6	FXBZZZZ	FXBZYZB	113		
	FXCZZYZ				
2MSNK6	FYXAZZA				
2MN6	FYZAZZZ	FYZAYZB	109		
2Mnu6	FYBYZZZ	FYBAZZZ	128		
	FZXBZZZ				
MA6	FZYZZZZ				
M6	FZZZZZZ	FZZZYZB	108		
3MKS6	FZBZZZZ	FZBZAZZ	200		
MTN6	FAWAZAZ				
MSN6	FAXAZZZ				
MNK6	FAZAZZZ	FAZYZZZ	92	FAZYYZZ	8
MKnu6	FABYZZZ				
	FBVBZZB				
2MT6	FBWZZAZ				
2MS6	FBXZZZZ	FBXZYZB	72		
2MK6	FBZZZZZ	FBZZAZZ	300		
	FBBZZZZ				
2SN6	FCVAZZB				
3MTN6	FCWYZAB				
SNK6	FCXAZZZ	FCXYZZB	629		
3MKN6	FCZYZZB	FCZYAZB	417		
MST6	FDUZZAZ				
2SM6	FDVZZZZ				
	FDWZZZA				
MSK6	FDXZZZZ	FDXZAZZ	302		
	FDZZZZZ	FDZZAZZ	615		
2MSTN6	FEUYZAB				

2(MS)N6	FEVYZZB				
2MSKN6	FEXYZZZ				
	GVZCZZY				
	GVBAZZY				
	GVDYZZY				
	GWZBZZY	GWZBYZY	76		
	GWBZZZY				
	GWCZZYY				
3MQ7	GXZAZZY	GXZAYZY	75		
	GXAAZYY				
	GXBYZZY				
	GYXBZZY				
5MK7	GYZZZZY	GYZBZZA	202	GYZZYZY	72
	GYAZZYY				
	GYBZZZA				
	GZXAZZY				
	GZZAZZA	GZZYZZY	125		
	GAWZZAY				
	GAXZZZY				
3MS7	GAYZZZB				
3MK7	GAZZZZA	GAZZYZY	217	GAZZAZA	76
	GAAZZYA				
	GABZZZA				
	GBVAZZY				
	GBXAZZA	GBXYZZA	101		
	GBZAZZA	GBZYZZA	350	GBZYAZA	42
	GCVZZZY				
3SK7	GCXZZZA	GCXZAZA	77		
	GCZZZZA	GCZZAZA	418		
	GDXYZZA				
	GDZYAZA				
	GETZZZY				
	GEVZZZA				
	GEXZZZA				
	HVBBZZZ				
2MNS8	HWBAZZZ				
5MK8	HXZZZZZ				
	HXBZYZB				
2(MN)8	HXZBZZZ				
5MS8	HXBZZZZ				
3MSNK8	HYXAZZB				
3MN8	HYZAZZZ	HYZAYZB	142		
3Mnu8	HYBYZZZ				
	HZXBZZZ				

M8	HZZZZZZ	HZZZYZB	141		
	HZAZZYZ				
4MKS8	HZBZZZZ	HZBZAZZ	262		
2MSN8	HAXAZZZ				
2MNK8	HAZAZZZ	HAZYZZZ	256		
	HABYZZZ				
	HBVBZZZ				
3MT8	HBWZZAZ				
3MS8	HBXZZZZ	HBXZYZB	108		
3MK8	HBZZZZZ	HBZZAZZ	297	HBZZYZB	121
	HBBZZZZ				
2SMN8	HCVAZZZ				
	HCXAZZZ	HCXYZZB	213		
4MSN8	HCZYZZZ				
2MST8	HDUZZAZ				
2(MS)8	HDVZZZZ				
2MSK8	HDXZZZZ	HDXZAZZ	303		
	HDZZZZZ				
3SN8	HETAZZZ				
	HEVAZZZ				
3M2SN8	HEXYZZZ				
3SM8	HFTZZZZ	HFTZYZB	38		
2SMK8	HFVZZZZ	HFVZAZZ	296		
	JVBBZZZ				
5MNS10	JWBAZZZ				
3M2N10	JXZBZZZ	JXZBYZB	177		
6MS10	JXBZZZZ				
4MN10	JYZAZZZ				
4Mnu10	JYBYZZZ				
5MSK10	JZXZZZB				
M10	JZZZZZZ	JZZZYZB	174		
	JZAZZYZ				
	JZBZZZZ	JZBZAZZ	262		
3MSN10	JAXAZZZ				
3MNK10	JAZAZZZ	JAZYZZB	332		
	JABYZZZ				
	JBVBZZZ				
4MS10	JBXZZZZ	JBXZYZB	142		
4MK10	JBZZZZZ	JBZZYZB	151		
	JBBZZZZ				
2(MS)N10	JCVAZZZ				
	JCXAZZZ	JCXYZZB	57		
5MSN10	JCZYZZZ				
3M2S10	JDVZZZZ				
3MSK10	JDXZZZZ	JDXZAZZ	302		

	JDZZZZZ						
3SMN10	JETAZZZ						
	JEVAZZZ	JEVYZZB	326				
4M2SN10	JEXYZZZ						
3S2M10	JFTZZZZ	JFTZYZB	67				
2(MS)K10	JFVZZZZ	JFVZAZZ	301				
	LVBBZZZ						
	LVDZZZZ						
	LWZCZZZ						
4MNS12	LWBAZZZ						
	LWDYZZZ						
4M2N12	LXZBZZZ	LXZBYZX	208				
4M2N12	LXBZZZZ	LXBZYZX	197				
	LXCZZYZ						
	LYXCZZZ						
5MN12	LYZAZZZ	LYZAYZX	209				
	LYAAZYZ	LYBYYZX	857				
5Mnu12	LYBYZZZ						
	LZXBZZZ						
M12	LZZZZZZ	LZZZYZX	204	LZZBAZZ	91	LZZZXZZ	17
	LZAZZYZ						
	LZBZZZZ	LZBZAZZ	279				
	LAWAZAZ						
4MSN12	LAXAZZB						
	LAYYZAZ						
4MNK12	LAZAZZZ	LAZYZZB	342	LAZAAZZ	302	LAZYYZX	50
	LABYZZZ						
	LBVBZZZ						
5MT12	LBWZZAZ						
5MS12	LBXZZZZ	LBXZYZX	177				
5MK12	LBZZZZZ	LBZZAZZ	300	LBZZYZX	186	LBZZBZZ	36
	LBAZZYZ						
	LBBZZZZ						
3M2SN12	LCVAZZZ						
	LCXAZZZ	LCXYZZZ	46				
5MSN12	LCZYZZZ	LCZYAZZ	323				
	LDTBZZZ						
4MST12	LDUZZAZ						
4M2S12	LDVZZZZ	LDVZYZX	142				
4MSK12	LDXZZZZ	LDXZAZZ	303	LDXZYZX	158	LDXZBZZ	31
	LDYZZYZ						
	LDZZZZZ						
3(MS)12	LFTZZZZ	LFTZYZX	105				

References

Accad Y. & Pekeris C.L. — The K_2 tide in oceans bounded by meridians and parallels. *Proc. R. Soc.* London, A, 278, 110-128, 1964.

Accad Y. & Pekeris C.L. — Solution of Laplace's equations for M_2 and S_2 in the World Ocean from knowledge of the tidal potential alone. *Phil. Trans. R. Soc.* London, 290, 235-266, 1978.

Andersen O.B. Woodworth P.L. & Flather R.A. — Intercomparison of recent ocean tide models. *J. Geophys. Res.,* 100, (C12), 25, 261-282, 1995.

Brown E.W. — *An Introductory Treatise on Lunar Theory*. Cambridge Univ. Press, XVI, 1896.

Cartwright D.E. — Tides, A Scientific History. Cambridge University Press, 1999.

Cassini J. — Articles on tidal rises and falls in different ports . *Mém. Acad. Roy. des Sciences,* 1710-1714 and 1720.

Chabert-d'Hières G. & Le Provost C. — Détermination des caractéristiques d'ondes de marée dans la Manche sur modèle réduit hydraulique. *C.R. Acad. Sci.*, Paris, 270, 1703-1706, 1970.

Chandler S.C. — On the variation of latitude. *Astron. J.,* 277, 97-101, 1892.

Courtier M.A. — *Données numériques concernant les marées des côtes de France.* Service Hydrographique de la Marine, Paris, Imprimerie nationale, 1934.

Chazallon. — *Annuaire des marées des côtes de France.* Dépôt des Cartes et Plans, Paris, 1839.

Darwin G.H. — On the dynamic theory of tides of long period. *Proc. R. Soc.* London, 41, 337-342, 1886.

Darwin G.H. — *The harmonic analysis of tidal observations*. Scientific papers, 1, 1-70, Cambridge Univ. Press, 463 pp., 1907.

Darwin G.H. — *The tides and Kindered Phenomena in the Solar System.* 3rd edition, Murray, London, 437 pp.,1911.

Descartes, R. — *Pincipes de la philosophie,* (1647) œuvres. ed. V. Cousin, 3, 371-377, 1824.

Desnoë Y. — Le bruit dans l'analyse de marée. *Annales hydrographiques* 5^{e} série, vol. 5, fasc. 2 - 1977 n^{o} 747 Service hydrographique et océanographique de la Marine, Paris.

Doodson A.T. — Harmonic development of the tide-generating potential. *Proc.R. Soc.* London A, 100, 305-329, 1921. Republished in 1954 (with some modifications) in the *International Hydrographic Review*.

Doodson A.T. — The analysis of high and low water. *International Hydrographic Review,* 28, 13-77, 1951.

Dronkers J.J. — *Tidal computations in rivers and coastal waters.* North-Holland Publishing Company, Amsterdam, 1964.

Duhem Pierre. — *Le Système du Monde - (Histoire des doctrines cosmologiques de Platon à Copernic).* Paris 1913-1917, vol. 2, ch. 13 sec. 14: La théorie des marées selon les Arabes-Abou Masar; vol. 3, ch. 3, sec.10/ La théorie es marées au xii^{e} siècle . . . , Giraud de Barri.

Franco A.S. & Harari J. — Tidal analysis of long series. *International Hydrographic Review,* Monaco LXV (1), 1988.

Georges K. & Simon B. — La méthode de concordances par espèce de prédiction de la marée dans les estuaires. *International Hydrographic Review* , 61(1), Monaco, January 1984.

Godin G. — The analysis of tides and currents (review). *Tidal Hydrodynamics,* Parker ed., Washington D.C., 1991.

Gonella J. — A rotary-component method for analysing meteorological and oceanographic vector time series. *Deep-Sea Research,* vol. 19, pp 833-846, 1972.

Halley, E. — The true theory of tides, extracted from that admired treatise of Mr Isaac Newton.*Phil. Trans. R. Soc.*, London 19, 445-457, 1696.

Hansen W. — *The reproduction of the motion in the sea by means of hydrodynamical numerical methods.* Mitteilung Inst. Meereskünde, Univ. Hamburg, Pub. N^{o} 5, 1-57, 1966.

Harris, R.A. — *Manual of Tides*, Book 1. Gov. Printing Office, Washington D.C, 1897.

Intergovernmental Oceanographic Commission. — Manuals and guides 14 – *Manual on sea-level measurements and interpretation,* Volumes I, II and III – Unesco, 2002.

Intergovernmental Oceanographic Commission. — Global Sea Level Observing System (GLOSS) Implementation Plan 1997. *Intergovernmental Oceanographic Commission Technical Series* N° 50, 1997.

International Association of Physical Oceanography (IAPO-IUGG). — Scientific publication n° 15: bibliography on tides. 1665-1939, Bergen, 1955.

Kepler, Johanes. — *De fundamentalis astrologiae certioribus*. Prague, Boemorum, 1602.

Lalande. — *Astronomie*, (4 volumes) *Traité du flux et du reflux de la mer*. In volume 4, 1-348, 1781.

Lambeck K., Cazenave A. & Balmino G. — Solid earth and ocean tide estimates from satellite orbit analyses. *Rev. Geophys. and Space Phys.,* 12, (3), 421-434, 1974.

Landau & Lifchitz. — *Mécanique*. Ed. Mir, Moscow 1966.

Laplace, P.S. — Mémoire sur le flux et le reflux de la mer. *Mém. de l'Acad. des Sciences*, 45-181, 1790.

Laplace, P.S. — *Traité de mécanique céleste*, 2, Livre 4, 1799 and 5 Livre 13, 1825.

Lennon G.W. — A critical examination of the conventional tide gauge. Proceedings of the Symposium on Tides organized by the International Hydrodynamics Bureau, Monaco, 28-29 April 1967.

Le Provost C., Genco M.L., Lyard F. & Canceil P. — Spectroscopy of the world ocean tides from a finite element hydrodynamic model. *J. Geophys Res.,* 99, (C12), 24, 777-797, 1994.

Lubbock J.W. — On the tides. *Phil. Trans. R. Soc.* London, 127, 97-104, 1837.

Mazzega P. — The M_2 ocean tide recovered from Seasat altimetry in the Indian Ocean. *Nature*, 302, 514-516, 1983.

Munk W.H. & MacDonald G.J.F. — *The rotation of the earth - a geophisical discussion.* Cambridge Univ. Press, 323 pp., 1960.

Newton, Sir I. — *Principia* (1687). Univ. California Press, Berkeley, 1962.

Parke M.E. and Hendershott M.C. — M_2, S_2, K_1 models of the global ocean tide on an elastic earth. *Marine Geodesy*, 3, 379-408, 1981.

Parker B.B. — The relative importance of the various nonlinear mechanisms in a wide range of tidal interactions (review). *Tidal Hydrodynamics*, Parker ed. Washington D.C., 1991.

Patullo J.G., Munk W., Revelle R. & Strong E. — The seasonal oscillation in sea level. *J. Marine Res.,* 14, 88-156, 1955.

Pekeris C.L. & Accad Y. — Solution of the Laplace's equation for the M_2 tide in the world ocean. *Phil. Trans. R. Soc.* London, A, 265, 413-426, 1969.

Marchuk, GI & Kagan. — *Dynamics of Ocean Tides.* Kluwer Acad. Pub. Dordrecht, 327 pp., 1989.

Mink W.H. & Cartwright D.E. — Tidal spectroscopy and prediction. *Phil. Trans. R. Soc.* London, A, 259, 533-581, 1966.

Poincaré, H. — *Leçons de mécanique céleste*, Tome III *Théorie des marées*. Gauthier-Villar, Paris, pp. 469, 1910.

Proudman J. — On the dynamic equations of the tides, Parts 1-3. *Proc. London Math. Soc.,* 18, 1-68, 1917.

Rossiter J.R. — On the application of the relaxation method to oceanic tides. *Proc. R. Soc.* London, A, 348, 482-498, 1958.

Schuremann P. — *Manual of harmonic analysis and prediction of tides*. USCGS Special Pub. N^{o} 98, Washington D.C. 1940.

Schwiderski E.W. — Ocean tides; 1- Global ocean tide equations; 2- A hydrodynamic interpolation model. *Marine Geodesy*, 3, 161-217 and 219-255, 1980.

Schwiderski E.W. — *Atlas of ocean tidal charts and maps.* Naval Surface Weapons Center, Dahlgren, Virginia, 1983.

Simon B. — Calcul de la marée au large pour la correction des sondages. *Revue hydrographique internationale* 51(2), July 1990.

Simon B. — The species concordance method of tide prediction. *Tidal Hydrodynamics*, Parker ed. Washington D.C. 1991.

Thomson, W. — On gravitational oscillations of rotating water. *Proc. R. Soc.* Edinburgh, 10, 92-100, 1879.

Thomson, Sir W. — The tide gauge, tidal harmonic analyser and tide predictor. *Proc. Civil Engineers,* London, 65, 4-74, 1881.

Wallis J. — Hypothesis on the flux and refux of the sea. *Phil. Trans. R. Soc.* London, 1, 263-289, 297-298, 1966.

Woodworth P.L. & Cartwright D. — Extraction of the M_2 ocean tide from Seasat altimeter data. *Geophys. J. Res. Astr. Soc.*, 84, 227-255, 1986.

Wunsch C. — The long-period tides. *Rev. Geophys.*, 5, (4), 447-475, 1967.

Zetler B., Cartwright D. & Berkman S. — Some comparisons of response and harmonic tide predictions. *International Hydrographic Review*, 56, (2), 105-115, 1979.

Glossary

Absolute reference frame: inertial reference frame (without acceleration)

Admittance: frequency-dependent response of the ocean to the tide-generating force.

Age of the tide: time lag of the highest spring tides after syzygy.

Altimetry: sea level measurement using spatial techniques.

Amphidromic point: point located offshore around which the tidal wave seems to gyrate.

Amplitude: difference between the high water height (HWH) or low water height (LWH) and the mean level. This term is often wrongly used in reference to tidal range.

Ascending node: point at which the Moon's orbit intersects the ecliptic at the time when the Moon crosses the equatorial plane from the south into the Northern Hemisphere.

Chart datum: synonym for hydrographic datum.

Civil time: mean time advanced by 12 h.

Coastal circulation: resultant of the slope current and drift current close to the coast.

Coastal slope current: strengthening coastal current in near geostrophic balance with the sea-level slope generated by the wind, exclusive of the tide current.

Concordance; Species concordance: tidal analysis and prediction technique that focuses on relations between reduced vectors from a reference port and a secondary port.

Cotidal line: curve on a chart passing through all points having the same high water time.

Current amplitude: maximum current velocity intensity during a tidal cycle.

Current atlas: cartographic representation of tidal current fields at different hours.

Declination: angle between the position of a celestial body and the equatorial plane.

Doodson number: method for determining tidal constituents using a six-digit number to identify the astronomical parameters from which they are derived and to deduce their period.

Drift current: wind-generated current.

Ebb: period during which the water level decreases.

Ebb current, or ebb: current that accompanies a falling tide.

Ecliptic: Earth's orbit around the Sun, or the apparent orbit of the Sun as viewed from Earth.

Ecliptic latitude: angle between the position of a celestial body and the ecliptic plane.

Ecliptic longitude: angle between the orthogonal projection on the ecliptic of the celestial body position and the vernal equinox position.

Ellipsoid: in geodesy, a mathematical figure formed according to the relative positions of points located on the Earth's surface.

Equation of time: difference between the mean and actual solar time.

Equator: great circle on the Earth's surface that is perpendicular to the polar axis.

Equinoctial point: point where the ecliptic plane intersects the equator.

Equinoctial spring tide: maximum amplitude of a semidiurnal tide that occurs around equinox.

Establishment of the port: actual time of high water of spring tide that occurs after the actual midday at the site, considered as the reference time, on days of the new and full moon.

Exceptional spring tide: semidiurnal equinoctial spring tide at perigee.

Extended Doodson number: Doodson number to which a seventh digit has been added to determine whether the angular argument is associated with a positive or negative sine or cosine.

FFT: Fast Fourier transform. A technique used to represent a temporal signal in the spectral domain.

Fixed sphere: representation system in which celestial bodies are located by their position on a fixed sphere relative to stars.

Flood current, or flood: current that accompanies a rising tide.

Flood tide: time between the low water level and the following high water level.

Geocentric zenithal distance: angular distance between the Earth's radius at a site (zenith direction or ascending vertical) and the direction of the celestial body with respect to the Earth's mass centre.

Geodesic coefficient: latitude-dependent element of the tide-generating potential.

Geographical coordinates: latitudinal and longitudinal quantities defining a point on the surface of the Earth.

Geoid: equipotential surface of terrestrial gravity.

Grid: division of an area into single geometric elements for mathematical modelling purposes, e.g. 2D or 3D grid.

Harmonic analysis: calculation of harmonic tidal constants.

Harmonic constant: the amplitude and situation of a harmonic constituent are harmonic constants of this constituent.

Harmonic constituent: elementary tidal wave, defined by its frequency, amplitude and phase.

High and low water heights: tidal curve extremes (maxima and minima).

High water height: tidal curve maxima.

High water spring tide: spring tide maxima.

Hour angle: angle, expressed in hours and measured westward, of the meridian half-plane of a celestial body with respect to that of the site.

Hydrographic datum: also called chart datum, a standard reference provided on marine maps and tide tables used by navigators.

International Terrestrial Reference System (ITRS): geodesic system of coordinates.

Interaction constituent: harmonic constituent generated by nonlinear effects of the ocean's response to the tide-generating force.

Intertidal zone: coastal zone that lies between the highest high tide level and the lowest low water height.

Keel clearance: safety margin that accounts for random water level variations.

Lag: period during which the tidal amplitude declines.

Latitude: angle between the vertical of the site and the equatorial plane.

Least squares method: calculation technique to obtain an optimal estimate of a deterministic signal in the presence of noise.

Legendre polynomials: orthogonal polynomials. The tide-generating potential is expressed as a series of Legendre polynomials.

Light probe: usually a metallic graduated band equipped with a device that emits a light signal when its tip comes in contact with the water surface.

Literal argument: Doodson number in which figures are replaced by letters.

Local apparent time: or LAT, the hour angle of the true Sun.

Longitude: angle between the meridian half-plane of a site and the prime meridian (Greenwich meridian).

Low water height: minimum water height reached during a tidal cycle.

Low water neaps: minimum tidal range.

Lunar month: time interval between two full moons and two new moons, also called synodical month.

Lunisolar potential: potential from which the sum of the lunar and solar tide-generating forces is derived.

Mean anomaly: angle, measured counter-clockwise in the ecliptic, between the mean Sun position with respect to the perihelion.

Mean establishment: mean lag from high water time relative to the time of the Moon's crossing of the meridian; also called the lunitidal interval.

Mean level: result of digital filtering of observed water heights which tends to eliminate sinusoidal components.

Mean longitude: ecliptic longitude of a celestial body. This is a time-honoured yet unsuitable term (i.e. it does not represent the mean longitude).

Mean sea surface: ocean area determined by spatial altimetry.

Mean solar time: uniform time scale defined by the mean Sun. By definition, a mean solar day is 24 h.

Mean sun: imaginary celestial body having the same apparent revolution period as the real sun, but whose movement is uniform. The mean time ranges from 0 to 24 h from the passage of the mean Sun across the superior meridian.

Mean tide level: arithmetic mean of mean high water and mean low water.

Meridian plane: plane that includes the polar axis.

Nadir: a point in the vertical downward direction; directly opposite the zenith.

Nodal correction: correction applied to harmonic constants to account for variations in lunar orbit elements.

Noise: an observed magnitude component that cannot be measured by harmonic analysis.

Periapsis: closest point of an orbit to a focus.

Perigean spring tide: maximum tidal amplitude that occurs around the time of lunar perigee.

Phase lag: measured as the angle between the constituent maximum of the constituent and the maximum action of the element corresponding to the tide-generating potential. This concept was generalized for interaction constituents.

Polar axis: rotational axis of the Earth.

Polar distance: complementary angle of the declination.

Priming of tide: period during which the tidal amplitude increases between neap and spring tides.

Proctor's rule: geometrical model for the tide-generating force.

Quadrature: position of the Moon and Sun when their positions relative to the Earth form a right angle (general term for first quarter and last quarter).

Radiational constituent: element derived from the radiational effects of the Sun, contrary to gravitational constituents.

Reduced heights: periodic magnitudes resulting from an interpolation of observed heights for the calculation of reduced vectors.

Reduced vector: complex number representative of species elements (module and phase) at a given time.

Response analysis: tidal analysis and prediction technique based on the system's admittances.

Right ascension: angle between the meridian plane of the celestial body and the vernal equinox, measured eastward with respect to the vernal equinox.

Rule of sixty: quick method for calculating a current on the basis of its amplitude maxima time.

Saros: a period of 6 585.322 days, corresponding to 223 lunations. At the end of this period, the Moon, Sun, lunar orbit node and lunar perigee are roughly in the same relative position.

Sidereal day: time interval between two successive transits of the vernal equinox during a terrestrial rotation; the right ascension of the Greenwich zenith.

Sidereal period: time necessary for the mean longitude of the Moon, measured from a fixed equinox, to increase by 360°. Equal to 27 days 7 h 43 min.

Slack water: time at low or high water height when the water level is essentially stationary; this is called low-tide slack water and high-tide slack water.

Solar day: time interval between two successive upper transits of the Sun's centre.

Solstices: maxima declinations of celestial bodies.

Species: term coined by Laplace in reference to a set of constituents whose frequencies are close to a full number (including zero) of cycles per lunar day. The principal species are long-period, diurnal, semidiurnal, etc.

Spectral analysis: energy (or amplitude) distribution of a time variable signal on a frequency scale (or domain).

Spectrum: graphic representation of spectral component modules.

Stilling well: tidal observatory device designed to dampen the water column and rapid movements caused by waves and swell.

Synodical month: time between two full Moons and two new Moons, also called lunar month.

Syzygy: moment when the meridian planes of the Moon and Sun are lined up. This corresponds with the full Moon and new Moon.

Tidal bore: collapsing wave accompanying a tidal flow that propagates up some estuaries.

Tidal coefficient: measurement of the tidal amplitude in reference to the height unit.

Tidal current: horizontal component of a tidal wave induced by gravitational interactions between the Sun and Moon.

Tidal fall: falling (or ebbing) part of the tidal cycle.

Tidal height unit: half range of mean spring tide at equinox (semidiurnal tide) or solstice (diurnal tide).

Tidal observatory: tide-monitoring site that it is equipped with a tide gauge to record water heights, a tidal scale and benchmarks located within the vicinity.

Tidal range: difference in water height between successive low and high water heights.

Tidal rise: rising (or flowing) part of the tidal cycle.

Tide scale: a board with linear.

Tide: periodic rise and fall of sea water levels due to the gravitational effects of the Sun and Moon.

Tide curve: graphical representation of the tide-gauge record at a given site, or the tide prediction computed from site harmonic constants.

Tide graph: graphic record of sea water level variations at a given site over a time course.

Tide recorder: device used to record the vertical rise and fall of sea water levels; also called a sea-level recorder.

Tide-generating force: resultant of the gravitational attraction exerted by celestial bodies at a point on Earth and that which would be exerted at the centre of the Earth.

Tide-generating potential: scalar quantity from which the tide-generating force is derived.

Tropical year: time interval between two consecutive passages of the Sun at the vernal equinox.

True anomaly: angle, measured counter-clockwise in the ecliptic, between the real Sun position with respect to the perihelion.

Types of tide:

- diurnal tide: only one high and one low water height each day; the semidiurnal constituents are insignificant.
- mixed semidiurnal tide: two daily high and low water heights; the semidiurnal constituents are dominant.
- mixed tide: sometimes two daily high and low water heights, sometimes just one; the diurnal constituents are dominant.
- semidiurnal tide: two daily high and low water heights; the diurnal constituents are insignificant.

Universal time: or UT, is same as the Greenwich mean time.

Vernal equinox: spring equinoctial point.

Vertical: a plumb line. It is assumed (with an acceptable degree of leeway for tidal issues) that the vertical crosses the polar axis at the centre of the Earth.

Wave velocity: tidal wave propagation velocity.

Zenith: a point in the vertical upward direction; directly opposite the nadir).

Bernard Simon

with the participation of Joseph Gonella
Professor at the Muséum national d'histoire naturelle, Paris
Translation by David Manley

Coastal Tides

Synthèses

• AMPHIDROMIC POINTS • COTIDAL LINES • DECLINATION • DOODSON NUMBER • ECLIPTIC LONGITUDE • GEODESY • HARMONIC ANALYSIS •

• INTERTIDAL ZONE • LEGENDRE POLYNOMIALS • OCEAN CIRCULATION • SIDEREAL MONTH • STILLING WELL • TIDAL STREAMS • UNIVERSAL TIME •

This book presents the cornerstones of ocean tide studies and applications in coastal regions.
The author first reviews some of the basic concepts before describing, in Chapter 2, the different tide monitoring techniques, focusing on issues of tidal measurement accuracy. In subsequent chapters, he offers an in-depth discussion on the tide-generating force, its effects in terms of tidal height variations, as well as the different analytical techniques used for tide forecasting and the calculation of standard tide levels. Tidal datums and tidal streams are covered in Chapters 9 and 10. The highly comprehensive appendices presented at the end of the book will enable serious readers to gain further insight into the theoretical concepts and specific technical points outlined in the book.
This book will be useful for anyone interested in the monitoring, analysis and prediction of tide level variations for the purposes of marine navigation, hydrography and coastal planning and development.
Bernard Simon was an engineer for the French Service hydrographique et océanographique de la marine, where he was responsible for coastal hydrodynamics research at the Centre d'hydrographie. He taught the Science of Tides at the French École nationale supérieure des techniques avancées, the École nationale d'ingénieurs des études et des techniques de l'armement and the École navale.
The International Hydrographic Organization, the French Service hydrographique et océanographique de la marine and the Government of the Principality of Monaco provided financial support for the publication of this book.

Members of the IHO Tidal and Water Level Working Group (TWLWG) are thanked for their valuable support during the translation process

ISSN : 1272-0763
ISBN : 978-2-903581-83-1